SF 17

Forschungszentrum Karlsruhe
Technik und Umwelt

Wissenschaftliche Berichte
FZKA 6420

Long-Term Safety of Radioactive Waste Disposal: Source Term for Performance Assessment of Spent Fuel as a Waste Form

Final report

B. Grambow, A. Loida, A. Martinez-Esparza, P. Diaz-Arocas, J. de Pablo, J. L. Paul, G. Marx, J. P. Glatz, K. Lemmens, K. Ollila, H. Christensen

Institut für Nukleare Entsorgungstechnik

Februar 2000

Forschungszentrum Karlsruhe
Technik und Umwelt

Wissenschaftliche Berichte

FZKA 6420

Long-Term Safety of Radioactive Waste Disposal:

Source Term for Performance Assessment of Spent Fuel as a Waste Form

Final report

B. Grambow[1], A. Loida, A. Martinez-Esparza[2], P. Diaz-Arocas[3], J. de Pablo[4], J.L. Paul[5], G. Marx[6], J.P. Glatz[7], K.Lemmens[8], K. Ollila[9], H. Christensen[10]

Institut für Nukleare Entsorgungstechnik

[1]Ecole de Mines de Nantes (F)
[2]Empresa Nacional de Residuos Radioactivos S.A. (ENRESA), Madrid (E)
[3]CIEMAT-ITN, Madrid (E)
[4]Universidad Politecnica de Cataluna (UPC), Barcelona (E)
[5]Commissariat à l' Energie Atomique (CEA-Marcoule) (F)
[6]Freie Universität Berlin, FB Chemie (D)
[7]JRC Institute for Transuranium Elements, Karlsruhe (D)
[8]Studiezentrum voor Kernenergie (SCK-CEN) (B)
[9]Technical Research Centre of Finland (VTT) (SF)
[10]Studsvik Material AB (S)

Forschungszentrum Karlsruhe GmbH, Karlsruhe

2000

This work was performed in the years 1994-1998 under the contract

FI4W - CT95-0004

Nuclear Fission Safety

with the Commission of the European Communities (Brussels)

Forschungszentrum Karlsruhe GmbH
Postfach 3640, 76021 Karlsruhe

Mitglied der Hermann von Helmholtz-Gemeinschaft
Deutscher Forschungszentren (HGF)

ISSN 0947-8620

ABSTRACT

The solid waste form „spent fuel" constitutes both the dominant radionuclide source as well as a first radionuclide retention barrier of planned future high level nuclear waste isolation systems in deep geological formations. A source term shall quantify the release/retention of individual radionuclides from the spent fuel waste package in the case of groundwater access for as much as millions of years as a function of disposal time and disposal conditions.

MOX fuel shows significantly higher release rates for Pu and other radionuclides than UOX-fuel. The general reaction mechanism of the spent UOX fuel matrix dissolution was found similar in various geological formations. Differences in UOX spent fuel corrosion rates were explained by the effect of groundwater constituents on solubility, surface complex formation and electrochemical corrosion potentials. key parameters were radiation field, redox conditions and carbonate concentrations. Salinity and humic acid concentrations were less significant. In the presence of repository rock and iron (container material) spent fuel matrix dissolution rates are similar as in their absence, but the environmental materials retained up to 99% of the total released radioactivity. Partial pressures of hydrogen (generated by container corrosion) of 2.7 bar were observed to reduce spent fuel corrosion rates by a factor of 500. Coprecipitation was found to be an important retention mechanism for actinides.

Model development (electrochemical, geoohemical, solid solution, reaction path, surface complexation and radiolysis) and modelling results of various aspects (rates, solution concentrations, reaction products, corrosion potentials, pH etc.) of the spent fuel dissolution process were confirmed experimentally.

For spent fuel corrosion rates are expected to remain lower than 10^{-6}/yr. Due to uncertainties in the prediction of the temporal evolution of radiolysis effects on surface oxidation potentials, it is not yet possible to describe the transition from radiolytically dominated anaerobic to reducing environments in a realistic manner. It is recommended to treat grain boundary inventories as part of the instant release term in a source term.

KURZFASSUNG

Quellterm für die Abfallform Abgebrannter Kernbrennstoff

Die feste Abfallform „Abgebrannter Kernbrennstoff" stellt sowohl die dominierende Quelle von Radionukliden, als auch eine erste Rückhaltebarriere für freigesetzte Radionuklide aus einem geplanten zukünftigen Endlager für hochradioaktive Abfälle in tiefen geologischen Formationen dar. Der Quellterm soll für den Fall eines Zutritts von Grundwasser über viele Millionen Jahre die Freisetzung/Rückhaltung von einzelnen Radionukliden aus dem verpackten abgebrannten Brennstoff quantifizieren in Abhängigkeit von der Lagerzeit und den Lagerbedingungen.

Bei MOX Brennstoff werden deutlich höhere Raten für die Freisetzung von Pu und anderen Radionukliden gefunden gegenüber UOX Brennstoff. Der generelle Reaktionsmechanismus der UO_2 Matrix bei UOX Brennstoff ist ähnlich auch bei unterschiedlichen geochemischen Bedingungen. Unterschiede bei den UOX Korrosionsraten werden erklärt durch den Einfluss von Grundwasserbestandteilen auf die Löslichkeit, Oberflächenkomplexierung und elektrochemischen Korrosionspotentialen. Vorherrschende Parameter sind das Strahlenfeld, die Redoxbedingungen und die Karbonatkonzentration. Dagegen sind die Salinität und Konzentration von Huminsäure von geringerer Bedeutung. In Gegenwart von Wirtsgestein und korrodierendem Behältermaterial sind die Korrosionsraten ähnlich wie bei deren Abwesenheit, aber durch diese Nahfeldmaterialien werden ca. 99% der freigesetzten Radionuklide zurückgehalten. Eine Reduzierung der UO_2-Matrix Korrosionsrate um ca. Faktor 500 wurde beobachtet bei einem H_2-Überdruck von 2,75 bar, der sich auf Grund der Korrosion von korrodierendem Behältermaterial eingestellt hatte. Es hat sich gezeigt, dass Mitfällung einen sehr wichtigen Rückhaltungsmechanismus für Aktiniden darstellt.

Die Modellentwicklung (elektrochemisch, geochemisch, feste Lösungen, Reaktionswege, Oberflächenkomplexierung, Radiolyse) und Ergebnisse von Modellierungen unterschiedlicher Aspekte (Raten, Lösungskonzentrationen, Reaktionsprodukte, Korrosionspotentiale, pH, etc.) von Prozessen, die bei der Brennstoffauflösung ablaufen wurden experimentell bestätigt.

Für abgebrannten Brennstoff werden Korrosionsraten erwartet, die unter 10^{-6}/a liegen. Entsprechend der Unsicherheiten bei der Vorhersage der zeitabhängigen Entwicklung von Radiolyseeffekten auf die Oberflächenoxidationspotentiale ist es noch nicht möglich den Übergang von radiolytisch dominierten anaeroben zu reduzierenden Bedingungen in einer realistischen Weise zu beschreiben. Es wird empfohlen, Inventare der Korngrenzen als einen Teil der instantanen Freisetzung in einem Quellterm zu betrachten.

LONG - TERM SAFETY OF RADIOACTIVE WASTE DISPOSAL

According to nuclear waste management regulations, high-level radioactive waste products such as HLW-glass and /or spent fuel shall be disposed in deep geological formations. The release of hazardous quantities of radionuclides from the repository into the biosphere shall be excluded for all future. For this purpose several in part independent barriers ("multi-barrier concept") shall limit the transport of ground water to and from the waste and shall also reduce the mobility of radionuclides by retention within stable waste matrices, by remineralization and sorption processes. The innermost barrier is an engineered system consisting of the waste form "high-level waste glass" or "spent nuclear fuel", the packaging material (e.g., steel container) and the backfilling material (e.g., salt chippings, clay, apatite). In addition, geoengineered barriers (e.g.,filling material, dams) and the geological barrier (host rock, overburden) contribute to safety by delaying the transport of the radionuclides (e.g., by sorption). Without comprehensive knowledge of the performance of each of the various barriers under disposal conditions long-term safety of the repository cannot be guaranteed.

Performance of the engineered barrier system

Experimental programs are currently under way at our research center (FZK-INE), aiming at performance assessment of glass and spent fuel as barriers for radionuclide immobilization. The dissolution or corrosion behavior of the waste forms and the containers is studied in order to evaluate the potential mobilization of radionuclides, the subsequent reimmobilization within newly formed mineral phases (secondary reaction products) or by sorption on surfaces of host rock or engineered materials. The waste form corrosion behavior is studied in conjunction with basic studies on the chemistry (solubility, complexation, coprecipitation...) of important radionuclides (in particular the actinides) in repository relevant aqueous solutions (deep groundwaters, brines). For assessing of the performance of the engineered barrier system, dissolution, remineralisation and migration phenomena must be analysed in the context of an integrated geochemical model. Results obtained in this research project were and will be published in a number of FZKA-reports (previously KfK-reports) related to the subject of "long-term safety of radioactive waste disposal".

The corrosion behavior of real high radioactive waste products and container materials is studied under repository relevant conditions. Waste products currently under investigation are

- high-level waste borosilicate glass R7T7, similar in composition to the COGEMA produced HAW-glass for the German base load customers,
- high burnup UO_2 fuel (burnup > 50 MWd/kg U) from the Biblis and Gösgen (Switzerland) nuclear power plants.

Principal container materials studied include

- thick fine grained carbon steels (corrosion allowance concept)
- thin Ti0.2Pd alloys (corrosion resistant concept)

The behaviour of the waste forms in contact with solutions is evaluated on the basis of the type and amount of radionuclides released to solution and gas phase and the structural change of the solid phases (e.g., decomposition of the microstructures, formation of secondary phases). Corrosion mechanisms, rate laws and processes governing release of individual radionuclides (sorption, coprecipitation, solubility, etc.) are to be determined. Container corrosion is evaluated on the basis of corrosion rates, mechanism and corrosion products. The effect of simoultaneously corroding container materials and of waste forms is investigated inserting container materials in the glass and spent fuel corrosion experiments.

Our work serves the purpose of developing models by means of which the contribution of the engineered barrier system to repository long-term safety can be assessed. The significance of individual experimental observations can only be evaluated in the general context. The relevance of laboratory findings for the natural system must be assessed as well as the validity of the models developed.

PARTICIPANTS

B. Grambow*, A. Loida, H. Geckeis, Th. Fanghänel	Forschungszentrum Karlsruhe FZK, INE (Coordinator) –Germany * since 9/1998 Ecole des Mines de Nantes
A. Martinez-Esparza, J.A. Esteban, J.A. Gago	Empresa Nacional de Residuos Radiactivos S.A. (ENRESA) –
P. Díaz Arocas, J. Quiñones, J.Serrano, J. Cobos, J.L: Rodríguez Almazán	CIEMAT-
J. De Pablo, I. Casas, J. Giménez, F. El Aamrani and M. Rovira	UPC
K. Le Lous, J.L. Paul	Commissiariat à l' Energie Atomique, Direction du Cycle du Combustible Service de Confinement des Déchets (CEA/DCC/SCD), France
G. Marx, F. Feldmaier, J. Engelhardt, A. Kupfer	Freie Universität Berlin FUB, FB Chemie; Germany
J.P. Glatz, M. Coquerelle, P. Bottomley, M. Wegen	JRC, Institute for Transuranium Elements (ITU), Karlsruhe, Germany
Christelle Cahoir, K. Lemmens, P. Van Iseghem	Studiecentrum voor Kernenergie, Waste & Disposal, (SCK·CEN); Belgium
K. Ollila	Technical Research Center of Finland, Chemical Technology (VTT); Finland
H. Christensen, S-O. Pettersson	Studsvik Material AB; Sweden

ACKNOWLEDGEMENT

In addition to the European Commission, financial support by Svensk Kärnbränslehantering AB (SKB) for Studsvik, by POSIVA for VTT and by ONDRAF for SCK·CEN are gratefully acknowledged.

The authors would like to thank the European Commission for making possible this mulit-partner project and for the guidance of the project provided by T. McMenamin.

For hot cell manipulations and a multitude of radionuclide analyses, the authors would like to thank N. Müller, F. Geyer, and A. Görtzen at INE-FZK.

The authors would like to express their thank for performing analyses to A. Quejido by ICP-MS at CIEMAT, M. Rodriguez J.L. Gascon and J.A. Suarez by Pu and U-233 analyses and for their help on. Laboratory to M.J. Tomas, A. Fariñas, M. Altelarrea and A. Calleja and to J. Esteban for his comments

The authors would like to thank Ms. R. Zilliacus and Ms. M. Lipponen for performing the ICP-MS analyses for VTT. The contribution of K. Helosuo is also gratefully acknowledged.

The authors gratefully acknowledge E. Vercauter, B. Gielen and L. Van Ravestyn for the technical assistance at SCK.CEN, and Ann Dierckx for the scientific assistance.

Page

TABLE OF CONTENTS

EXECUTIVE SUMMARY

Nine European research organizations were working together under this contract in a cooperative effort to develop a *Source Term for Performance Assessment of Spent Fuel as a Waste Form.* This topic is included in the specific R & D conducted as part of a more ambitious programme on the *Safety of Nuclear Fission* directed by the European Commission.

Dissolution behaviour of spent UO_2 or MOX fuel, unirradiated UO_2 or SIMFUEL has been studied experimentally and by modelling techniques in a large suite of groundwater compositions, typical for European repositories in salt, granite and clay formations. The experimental data and models are integrated in a consistent description of the electrochemistry, geochemistry and radiation chemistry involved in spent fuel dissolution.

In order to evaluate the performance of spent fuel as part of the multibarrier containment system in a future deep geologic repository, the radionuclide release properties in groundwater must be predicted over very long time periods. Radionuclide release is not an inherent materials property of the fuel but depends, besides fuel specific parameters mainly on time but as well on the geochemical and hydraulic environment of the disposal location. For quantification of the time dependency of radionuclide release it is important to account for the heterogeneous distribution of radionuclides in the fuel rod, i.e. the fuel matrix, grain boundaries, the cladding, the fuel sheath gap and the surfaces of the fractured matrix. This radionuclide distribution depends on fuel type (MOX or UO_2 fuel), irradiation history, linear power and burn-up. Major focus of the present project was the behaviour of the fuel matrix, however certain insight in grain boundary release and in the behaviour of the Zircaloy cladding was also acquired.

The general reaction scheme of the fuel matrix dissolution mechanism was found to be similar for the various geological formations. As a consequence, our generic study of fuel performance in various formations yielded important insight, relevant to all sites. For example, differences in the corrosion rates in various groundwaters from different geological settings could be explained by the effect of groundwater constituents on solubility constraints, surface complex formation and the establishment of electrochemical corrosion potentials. Key groundwater parameters were redox conditions and carbonate concentrations. Salinity and humic acid concentrations were less significant.

Electrochemical dissolution mechanism are operative in all groundwaters under oxic and anoxic conditions, in certain cases even at negative Eh, whereas solubility controlled dissolution prevails under reducing conditions. Under oxidizing, and possibly also under anoxic conditions in the strong radiation fields of fresh spent fuel, the dissolution mechanism comprises an oxidation of the fuel surface and the dissolution of this oxidised layer. An oxidative dissolution threshold (Eh) was defined thermodynamically as the equilibrium potential for the reaction $UO_2^{2+} + 2e^- = UO_2(s)$, or kinetically by equal rates of electrochemical and solubility limited dissolution.

Electrochemical calibration curves were obtained to establish a quantitative relation between corrosion potential and corrosion rate both for carbonate waters and carbonate free waters. The same calibration curves apply to granite bentonite groundwater, Boom Clay water and high-concentrated NaCl solutions, indicating similar corrosion mechanism. Corrosion potentials for MOX-fuels are lower than those of UOX-fuels

In order to simulate the expected near field redox conditions in the laboratory, three ranges of redox domains were differentiated: Oxic, anoxic and reducing. Anoxic conditions were not sufficient to simulate natural low Eh conditions. This simulation required the addition of reducing species such as S^{2-}.Reducing conditions were also maintained by addition of

metallic Fe, thus simulating the effect of container materials.

Studies on SIMFUEL, UO_2 and spent fuel are complementary in the assessment of the performance of irradiated fuel in geological formations. Radiolytic effect are minimized in the two first cases and overestimated in the last one for repository relevant times. More work is necessary to simulate spent fuel with radiation representing decay times of 1000-10000 yr. Dissolution mechanism and dissolved inventory fractions of the spent fuel matrix, of UO_2 and of SIMFUEL are similar under similar geochemical conditions. MOX fuel shows significantly higher release rates for Pu and other radionuclides. Exceptions are U-release rates, which are similar for all fuels.

There are also significant differences between UO_2 and spent fuel. Corrosion rates of spent fuel were found independent of pH and pCO_2 in the studied range whereas, under similar conditions, dependency of corrosion rates on carbonate was found for unirradiated UO_2. The insensitivity of spent fuel to these geochemical parameters is explained by rate control by radiolytic oxidants. A radiolytic mass balance was established with radionuclide release closely matching the consumption of radiogenic oxygen.

To assess the performance of spent fuel it is important to know the maximum uranium concentrations in repository relevant groundwaters upon contact with spent fuel. Steady state U-concentrations in contact with either UO_2, SIMFUEL and spent fuel are under oxic conditions in the range of 10^{-5} M., close to the theoretical solubilities of schoepite or another uranyl oxide hydrate e.g. becquerelite (possibly Na-polyuranate). Under reducing conditions, depending on carbonate concentrations, in the range between 10^{-6} and 10^{-9} M. UO_2-solubility is enhanced under reducing conditions due to CO_3^{2-}–UO_2^{+2} complex formation, stabilizing U(VI) in solution. Under reducing conditions, in the presence of reducing species (S^{2-}, Fe^{II}) the solubility both from over and under saturated conditions was at, 10^{-9} M, at the level of the theoretical solubility of the well-crystallized UO_2. This result reduces the uncertainty in the magnitude of U-solubility under reducing conditions, with literature values in the range between 10^{-5} and 10^{-10} M. Higher U concentrations between 10^{-6} and 10^{-7} M were observed in carbonate rich groundwaters such as Boom Clay water with 800 ppm HCO_3 or granite bentonite water under high partial pressures of CO_2 of 0.01 bar. In the absence of reducing species, the solubility was one order of magnitude higher. This higher solubility was a result of U(VI) in solution.

In experiments approaching U-solubility by precipitation from anoxic oversaturated solutions, the solubilities were in agreement with the results of UO_2 dissolution experiments with reducing S(-II) species, suggesting thermodynamic equilibrium. The analyses of the solid phases gave weakly crystalline $UO_2-U_3O_7$ as a result with fresh, saline and highly saline composition.

Uranium concentrations decreased strongly when metallic iron (simulating container corrosion) and to a lesser extent when iron corrosion products (magnetite) were added to oxic or anoxic (UO_2 or SIMFUEL)/groundwater systems. The effect can be modeled assuming pseudo first-order kinetics. Rate constants were lower in carbonate rich waters, due to carbonate complexation stabilizing U(VI) in solution.

Redox sensitive elements such as the actinide ions, Tc or Mo, showed a strong dependency of release/retention properties on the redox conditions. Strongest retention in the presence of iron was observed for Pu, Am, Cm and Np concentrations well below 10^{-9} M. In contrast, Sr leaching behaviour in co-dissolution experiments with Fe did not show any changes with the redox potential of the media.

Radionuclide retention in secondary phases has been observed in some cases even for Cs and Sr. These phases were observed to redissolve if the geochemical environment is changed to favourable conditions. Observed secondary reaction products include uranyl silicate and Na-polyuranate. In presence of metallic iron UO_2 and/or U_4O_9 was observed as secondary reaction product.

Coprecipitation is an important retention mechanism for actinides. Solution concentrations of Am, Pu and Np were similar in spent fuel dissolution experiments and in coprecipitation tests. In these tests spent fuel or SIMFUEL was dissolved entirely in strong acid and precipitation was initiated by subsequent adjustment of pH to the same geochemical conditions of the dissolution tests. It can be concluded that results from coprecipitation tests can be used to empirically assess maximum radionuclide concentrations for given geochemical environments. More work is necessary, to assess coprecipitation behaviour under reducing conditions.

The trivalent actinide concentrations in solution achieved in coprecipitation experiments were in most cases lower than solubility of pure hydroxide solid phase. In contrast, Pu-concentrations are not controlled by coprecipitation. From spent fuel and U-Pu coprecipitation tests, Pu solubility appears to be controlled by precipitation of a pure "$Pu(OH)_4(s)$" phase. Geochemical solid solution modelling explains retention of pentavalent actinides by uranyl oxide hydrates, Na-polyuranates, trivalent actinides by REE-hydroxide solid solution. Also (Ba, Sr)CO_3 or (Ba,Na,Am)MoO_4 solid solutions are predicted to form.

Results from integral tests (corrosion of spent fuel or SIMFUEL in the presence of crushed granite or clay and iron in preconditioned clay or granite groundwater) show similar fuel matrix dissolution rates as in tests with the absence of near field materials. However, the retainement of the environmental materials depended on the radionuclides, from 66 to 99% of the total radioactivity released from the spent fuel. Analysis of the filtered leachates also showed that some species including Pu and Cm are sorbed on colloids suspended in the aqueous phase. The aqueous phase concentrations were on the order of 10^{-8} M for U, 10^{-12} M for Pu and 10^{-13} to 10^{-14} M for Cm; these very low concentrations are attributable to sorption of these species on the granite and clay

The results confirm that tests performed in the absence of near field materials will yield conservative upper limits for release. However, for a realistic assessment, more efforts should be directed in future projects towards quantifying the various aspects of the integral reaction behaviour.

Partial pressures of hydrogen of 2.7 bar were observed to reduce spent fuel corrosion rates by a factor of 500. Long-term dissolution rates are close to the detection limit.

Model development and modelling results of various aspects (rates, solution concentrations, reaction products, corrosion potentials, pH etc.) of the spent fuel (and UO_2 and SIMFUEL) dissolution process were confirmed successfully by experimental data.

Electrochemical and geochemical models were coupled ("electro-geochemical model") to explain and predict corrosion rates, corrosion and redox potentials, as well as fractional reaction orders with respect to HCO_3, O_2 and pH. UO_2 dissolution rates were predicted in Eh/pH diagrams.

A kinetic-geochemical reaction model has been proposed and validated for predicting the dissolution behaviour of spent fuel matrix (UO_2) under several conditions. Alternatively to the electrochemical model, fractional reaction orders were described by formation of surface complexes.

Geochemical solid solution modelling was used to explain the retention of pentavalent actinides by uranyl oxide hydrates, trivalent actinides by REE-hydroxide solid solutions and possibly molybdate solid solutions. Also (Ba, Sr) CO_3 solid solutions are predicted to form.

Radiolysis models have shown a strong potential for explaining corrosion rates of spent fuel which are much higher than the respective rates for unirradiated UO_2. However, there are a lot of assumptions in rate constants of radiolytic species with UO_2, and more work will be necessary to validate the existing models.

Reaction path models were used to simulate the simultaneous interactions of spent fuel, iron and gas phases with the groundwater, considering initial dissolution, formation of secondary

reaction products, evolution of solution composition and pH as well as oxidant generation by radiolysis. The model explains the dependence of solution pH on redox conditions by the formation of secondary phases. The results emphasize the importance to quantify the relative rates of spent fuel and iron corrosion.

For a more realistic modelling of the spent fuel alteration a quantification and modelling of all retention mechanism of would be necessary, and not only of the dissolution process, taking into account the geochemical composition of waters and other spent fuel and waste form parts.

Finally, one may conclude that the results allow quantification of kinetically based conservative source terms for performance assessment of spent fuel in various repository location, either for anoxic or reducing environments. Present data indicate that grain boundary release may become fast and it is recommended to treat grain boundary inventories as part of the instant release term in a source term. In the presence of iron or other reducing species, anticipated for most repository designs, corrosion rates are expected to remain lower than 10^{-6}/yr. Though U-solubility under reducing conditions has clearly been determined, this information cannot yet be used to formulate a solubility based source term for reducing conditions. The reason is that solid phase transformation under reducing conditions has not yet been quantified. Due to uncertainties in the prediction of the temporal evolution of radiolysis effects on surface oxidation potentials, it is not yet possible to describe the transition from radiolytically dominated anaerobic to reducing environments in a realistic manner.

INTRODUCTION

The project aimed at source term quantification for spent fuel performance assessment in granite, clay and salt formations. Processes which may control radionuclide release from the spent fuel are: (1) kinetics of corrosion of the fuel matrix and of segregated phases (2) formation of secondary alteration products ((co-)precipitation processes limiting solubility), (3) sorption on surfaces of near field materials and (4) colloid formation. Environmental factors controlling radionuclide release include radiation field, temperature, S/V, pH, pCO_2, redox conditions and the presence of backfill materials or of corrosion products of container materials (iron etc.). The uncertainties in mechanistic interpretations and in the quantification of release controlling processes would be reduced by combining various experimental techniques and by interpretation of results consistently using modelling techniques. The work programme was directed simultaneously towards the basic understanding of the mechanism and quantification of rates of fuel matrix dissolution in the three geological environments (salt, clay, granite) both under oxidizing and reducing conditions, understanding and quantification of solubility, sorption and coprecipitation equilibria for individual radionuclides, understanding the effect of near field materials on reaction rates and radionuclide release and by development of models which describe the multitude of experimental results in a consistent manner and which allow source term formulation.

Four materials (UO_2, SIMFUEL, Spent UO_2-fuel (burn-up to 50 MWd/kgU) and Spent MOX-fuel) were studied under a variety of conditions. Given the limitations related to the handling of irradiated fuel, spent fuel dissolution experiments combined with more detailed studies using non-irradiated chemical analogues are very useful. Irradiated fuel is characterized by intense radioactivity, which increases with the burnup, and which causes the radiolysis of the aqueous leachant leading to the formation of chemical species like O_2, H_2O_2, which can enhance fuel dissolution [91CHR; 92SUN/SHO; 95ERI/EKL]. Moreover, as a result of irradiation, UO_2 fuel incorporates as much as 6 wt% of various actinides, fission and activation product elements some of which segregate as individual phases, but most of them forming solid solutions, whose overall chemistry is still dominated mainly by the chemistry of UO_2. As for pure UO_2 the corrosion behaviour of the spent fuel matrix is strongly dependent on parameters like oxygen/uranium ratio, but additional parameters like burnup and linear power rating play a significant role. The changes in chemical composition and, partially, also the microstructure changes occurring in UO_2 during irradiation are simulated in part by SIMFUEL [89LUC/VER; 91LUC/VER; 91MAT/LUC]. However, some physical changes that occur during irradiation, namely grain growth, crack and porosity formation due to coalescence of bubbles containing gaseous fission products are not reproduced by SIMFUEL.

A large amount of data is available in the literature concerning the dissolution behaviour of spent UO_2 fuel and its chemical analogues in aqueous solutions under different conditions [82JOH/SHO; 86FOR/WER; 90GRA/FOR; 92BRU/CAS; 92GRA/THO; 92OLL; 96RON/MAT; 95GLA/TOS; 96RON/MAT; 96PAB/CAS; 96RON/SER]. However, there are still uncertainties that are necessary to solve in order to feed properly data for performance assessment studies.

Five types of experiments are performed: dissolution tests, co-dissolution tests, precipitation tests and co-precipitation tests and electrochemical tests.

WORK PACKAGES

WP	Work package/ Activities: Description of Work	Laboratory
I	Basic understanding of long-term spent fuel dissolution process	
I.1	Spent UO_2 and MOX fuel static dissolution test at high surface area to solution volume ratios (S/V).	FZK
I.2	Surface area measurement of fuel powder.	ITU
I.3	Dissolution of Spent MOX and UO2 fuel rod segments with preset defects.	ITU
I.4	Static dissolution of UO_2 and SIMFUEL.	ENRESA-UPC ENRESA-CIEMAT SCK.CEN, VTT
I.5	Dynamic dissolution tests of UO_2.	ENRESA
I.6	Electrochemical investigations on UO2 and SIMFUEL electrodes	FUB
I.7	Electrochemical investigations of spent UO2 and MOX fuel electrodes	ITU
II	Radionuclide retention during spent fuel dissolution	
II.1	Precipitation tests of dissolved spent UO_2 fuel or SIMFUEL	ENRESA, FZK, VTT
II.2	Coprecipitation with of dissolved U with Pu.	ENRESA
II.3	Determination of oxidation states during spent fuel dissolution.	FZK
III	Effect of near field materials	
III.1	Co-dissolution of spent fuel, UO_2 and SIMFUEL with metallic iron	FZK, ENRESA, VTT
III.2	Co-dissolution tests of UO_2 with iron (III) corrosion products	ENRESA
III.3	Integral co-dissolution tests of spent fuel and SIMFUEL	CEA

	with rocks and/or backfill materials	
IV	Modelling	
IV.1	Geochemical reaction path models and actinide chemistry	FZK, VTT, ENRESA-UPC ENRESA-CIEMAT
IV.2	Modelling of solid solution formation	FZK ENRESA
IV.3	Modelling of radiolysis product formation	STUDSVIK(+FZK)
IV.4	Source term quantification	FZK, CEA
V	Project management/coordination	FZK

STATE OF THE ART

SPENT FUEL SOURCE TERMS

A high-level waste form, like spent fuel, may serve three different containment roles in the multibarrier system of an underground repository: (1) it could be the only effective barrier, (2) it could be an effective but not necessary primary important barrier or (3) it could be an inefficient barrier, mainly used for handling. The role of spent fuel in overall repository safety assessments is often masked by the geological barrier, the geo-engineered barriers (bentonite backfill etc.) or the container barrier [e.g.92SKB]. However, recent models, suggest only a few percent of spent fuel alteration despite many millions of years of contact with groundwaters. A direct prediction of long-term behaviour of spent fuel from laboratory experience and laboratory based models is not possible. The spent fuel performance and its role in the multibarrier system must be assessed by a systems approach, passing from mechanistic interpretation of surface reactions via integral geochemical near field modelling and conservative simplifications to source term quantification. The objective of the present project is to clarify the scientific basis various spent fuel degradation mechanisms in relation to source term development

Spent LWR MOX and UOX fuels are heterogeneous substances with highest radionuclide inventories in the fuel matrix. The release of the actinide elements including the matrix elements uranium and plutonium will be limited by the low solubility product of the actinide-bearing solids and the flow rate of the water through the waste package [90WIL1, 90WIL2]. On the other hand, the release of highly soluble radionuclides like cesium and iodine may depend both on the heterogeneous distribution of these radionuclides within the fuel as a consequence of migration to the grain boundaries (together with other fission products) and to the pellet periphery (together with fission gases) and on the durability of the fuel matrix in a potential repository. The dissolution of soluble radionuclides from spent fuel can be divided into components that come from three different areas [91GRA/STR]:

- The fuel/cladding gap, including the spaces between fuel pellets and the open porosity and cracks within the pellets.
- The grain boundaries of the fuel pellets.
- The UO_2 matrix.

The **cladding** is considered to contain only activation products, and small quantities of fission products, resulting from recoil phenomena. The release from fracture surfaces and the fuel sheath gap (**gap release**) comprises a significant fraction of overall radioactivity release from the fuel and is considered in the instant release fraction (IRF). IRF values depend mainly on burn-up and linear power rating [92STR].Fission products, which are insoluble in the fuel matrix segregate in part to the grain boundaries. This includes fission gas bubbles and metal particles, and sometimes perovskite phases. To estimate the **alteration of the fuel matrix**, slow reducing (UO_2(fuel) $\rightarrow$ U^{IV}(aq)) and fast oxidative dissolution (UO_2(fuel) $\rightarrow$ U^{VI}(aq)) must be distinguished. Oxidative dissolution is often accompanied by surface oxidation with O/U ratio at the surface of UO_{2+x} as high as 2.33 (U_3O_7, the stoichiometric limit of the fluorite structure). The surface oxidation state is influenced by the geochemical environment and by radiolysis.

For an oxidizing repository, oxidative dissolution is the main spent fuel degradation mechanism. However, most repositories are planned in reducing geological formations. Here oxidative dissolution may prevail temporarily, resulting form an oxidizing operation period and from radiolysis. A large uncertainty in estimating future spent fuel performance arises from modelling the long-term evolution of the redox state at the fuel surface, particularly the effect of radiolysis. Experiments performed in the 3rd Framework programme of the EC show that

spent fuel corrosion can be about two orders of magnitudes faster than dissolution of unirradiated UO_2 [97GRA/LOI]. However, under strong overpressures of O_2 [95GRA/WIL], as well as in carbonate solutions [97GRA/LOI], the reaction rates become similar. Radioactivity is not the only explanation for this difference. Other explanations include effective surface area, defect structure, fission product accumulation at grain boundaries etc.

Cladding release: Cladding release probably covers the release from structural materials. Uncertainties are large for C14 and Cl36 inventories. The rates estimated by performance assessment for complete activation product release from the fuel cladding are in the range of 50 years (salt) to 1000/10000 years (granite). The differences between salt and granite may reflect different reactivities in the two geochemical media. Some work in the project is directed to clarify this difference.

Gap release: Gap inventories can be determined reliably from short-term laboratory leach tests. Typical gap values used in performance assessment are 5% of Cs135 and 5-10% of I129 and 1 to 5% of C14 and similar amounts of Cs and I are associated to grain boundaries. Other important IRF inventories are those of Tc99, Pd107, Cl36, Se79 and Sn126.

Grain boundary release is difficult to quantify and is considered often together with the gap-term in the instant release fraction (IRF). There is considerable uncertainty in the radionuclide inventories associated to the grain boundaries. It is generally assumed that the release from the fuel matrix is congruent. If not considered in the IRF, the assumed dissolution rate for grain boundaries considered in PA varies between 500 and 10000 years. The different life times are not related to differences in various geological disposal concepts, but to different assumptions used.

Uncertainties in the effective surface area of spent fuel: The surface area measured by the BET gas adsorption technique of spent fuel was higher than the geometric surface area, due to pathways along grain boundaries to a depth of about 6-8 grain layers [95GRA/WIL, 95FOR]. It remains unclear, whether all gas containing grain boundaries are water accessible. The surface area of the fuel may increases with time: Grain pull out during leaching was observed experimentally as well as complete disintegration to individual grains under accelerating acid conditions [95LOI], or in undersaturated (water) testing [97FIN],similar to fuel powderization upon oxidation to U_3O_8. A minimal surface area of ca. 7 cm^2/g is the geometric area, including surface roughness factors of 3 and fracture surfaces created during reactor operation. The maximum surface area could well be a factor of 200 higher after complete fuel disintegration. Based on the experimental observation of fuel disintegration in a few years, even the assumed 500 years of grain boundary alteration cannot be justified. At least under oxidizing conditions, current knowledge requires the inclusion of grain boundary inventories into the IRF-values.

What is the state of validation of fuel matrix dissolution models? UO_2 is a highly corrosion and radiation resistant semiconductor with a crystal structure similar to that of the mineral Uraninite, occurring as principal uranium bearing phase in many natural uranium ore deposits, including the well known 2 Ma old Oklo site in Gabon, studied in a parallel EU-project. The times estimated by performance assessment for complete degradation of the fuel matrix vary between 625 years [93BRE/BUH] and many million years. 625 years is for salt, the higher life times for other geological formations. The difference does not reflect different fuel behaviour in different disposal locations but different assumptions used.

The redox mass balance at the oxide/solution interface mainly governs spent fuel dissolution. Oxidative dissolution models for the fuel matrix can in part be validated using experimental data either of spent fuel or of unirradiated UO_2. Under oxidizing conditions, two cases can be distinguished: unlimited supply of oxygen in unsaturated (water) horizons and limited supply by dissolved oxygen in slow flowing water. In the first case, reaction rates under oxidizing conditions may be used, in the second case, maximum release would be governed by the flux of dissolved oxygen through the waste package (solubility of oxygen in water times

groundwater flow rate). In any case, complete disintegration of the fuel to individual grains can hardly be ruled out.

Models for reducing conditions are more difficult to validate, (1) because much less data are available and (2) because they must predict the transition from oxidizing to reducing mechanism and they usually predict spent fuel corrosion rates orders of magnitude lower than empirically measured. Most models used are based on radiolytic self-oxidation [96JOH] either by α or γ radiation. However, there is no clear empirical relation between fuel matrix dissolution rates and α- or γ-activity (or dose rate DR). The only empirical data stem from electrochemical work with electrodes made from pure UO_2 . Results can be described by a power law $r=k \cdot DR^b$ with the exponent b being 2.7 in case of α and 1-1-4 in case of γ radiation. It remains to be shown that these relations are applicable to spent fuel. Using these relations, laboratory rates of spent fuel dissolution experiments would have to be interpreted as being controlled by γ and not α radiolysis. The statistical ensemble for these observations is rather small and more work is necessary. The extrapolation of short-term rate data to the long-term is always an uncertain step, in particular when using electrochemical data. A significant part of the work programme of the present project was directed towards a better understanding of electrochemistry of irradiated fuel dissolution.

The assumed relation between α-activity and extrapolated rates is very sensitive to surface area. The proportionality factor would directly increase with increasing fuel surface area. As the spent fuel surface area increases with time, due to disintegration of the fuel pellets into individual grains the corrosion rate may even increase with time.

Facing these uncertainties in the self-oxidation model, some simplifications are made and conservatism is introduced for source terms in performance assessment. Measured redox controlled spent fuel dissolution rates would be applicable to natural environments if the radiation level is the same, because the rates are rather insensitive to groundwater composition and environmental parameters (other than redox) such as pH, pCO_2, pressure and temperature. Since radiation level and dose ratio $\alpha/\beta/\gamma$ are different under disposal conditions than in the laboratory the measured rates cannot be used directly in performance assessment. A comparison between the calculated dose rates [94HAU] for laboratory experiments with a full sized disposal cask (Pollux) is given in FIGURE 1.

Though the total dose rates expected under disposal conditions are much higher (FIGURE 1) than in the experiment (both for α and for β,γ) it should be kept in mind, that

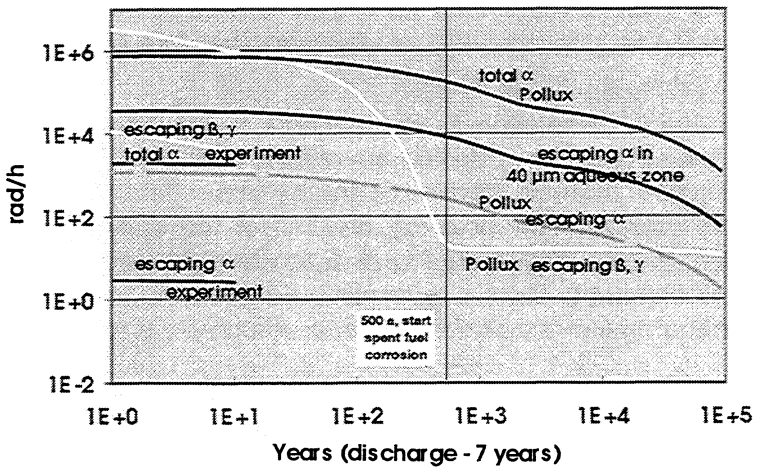

FIGURE 1: Time dependence of dose rates from spent fuel in experiments (1g in 100 ml soln) and for a water filled Pollux container with 4 tons of fuel. Comparison of dose rates considering the total alpha events with dose rates from alpha events with in an escape depth of 10 µm from beneath the fuel surface. Comparison to hypothetical irratiation of total water volume with irradiation of a volume given by the 40 µm maximum pathway of apha particles in water

only a small fraction of α-particles can escape the fuel (19% from 10 µm escape depth) and in the aqueous phase they can only penetrate to a depth of about 30-50 µm. Consequently the α dose rate within this 30-50 µm water layer is the same, both in the experiment and under disposal conditions. The experimental, ß,γ dose rate corresponds to a β,γ dose rate expected after 200 years under disposal conditions.

Models are developed [e.g. 91SHO/SUN, 95ERI/EKL] which intend to describe both the laboratory data and the expected behaviour under disposal conditions consistently. One has to use a relation between dose rates and spent fuel corrosion rates together with a choice between α/β/γ radiation. In one case of spent fuel performance assessment γ and not α radiation is assumed [96JOH]. Two relations are considered: (i) proportionality between α dose rate (DR) (or more simple: α activity) and corrosion rate: $r(t)=k \cdot DR_\alpha(t)$ with the proportionality constant k adjusted by experimental data from reducing or oxidizing conditions, (ii) the electrochemically determined relation between dose rate and corrosion rate $r=k \cdot DR^b$. In case (i) the choice of α radiation instead of β or γ radiation is conservative due to slower decay with time, whereas in case (ii) γ radiation is conservative, due to higher rates. Though the relation (i) is more pessimistic than (ii) because the experimentally determined relation would result in a much faster decrease of corrosion rates with decreasing α-dose rate and time, for both options, there is a lack of fundamental understanding of the underlying mechanism. It seems difficult to validate these empirical relationships to predict fuel dissolution rates, orders of magnitude lower than experimentally measured. Moreover, the cases (i) and (ii) are not conservative, considering the possibility of increasing the fuel surface area by degradation of the fuel matrix into individual grains during long-term exposure to aqueous solutions. In contrast, the formation of alteration products of UO_2 at the surface may retard back-diffusion of oxidizing radiolysis species and reaction rates may become much lower. Indeed, a square root of time decrease in reaction rates was observed [89GRA].

Recently, attempts are made to take full credit from recombination effects in spent fuel performance assessment, using models with 39 rate constants for the radiolysis of water and rate constants between the oxidants H_2O_2 and O_2 with the UO_2 surface [97SKB]. It has been shown that oxygen is consumed in the system without leading to equivalent release of U^{VI} from the fuel [95ERI/EKL]. The rate of oxygen consumption should give a maximum value for oxidative fuel degradation.

Under conditions of overall reducing groundwaters, the decay of radiation sources will finally lead to a decrease in reaction rates. However, a simple extrapolation of the radioactive decay effect to very low rates is definitely neither conservative nor realistic. The rate cannot approach zero. What is the *threshold rate*, at which another rate limiting reaction takes over? Various boundary conditions may be considered.

(1) The rate of fuel matrix dissolution cannot become lower than the limit governed by the solubility of the UO_2-matrix under reducing conditions multiplied by the mass transfer rate (advective flow, diffusion through bentonite) in the near field. The lower the reference solubility of UO_2 the later the threshold for the limit of the self-oxidation model would be approached. It is well known, that solubility of tetravalent Uranium depends on carbonate complexation and attachment to natural colloids. A realistic range is between 10^{-6} and 10^{-9} M. In some assessments of spent fuel performance, a difference is made between the solubility of UO_2(fuel) with $2*10^{-7}$ mol/l and UO_2(pure) with 10^{-9}mol/l [95SKB]. A large part of the present project was directed towards a better understanding of UO_2-solubility in different reference groundwater.

(2) The solubility of UO_2 can only limit the release, if UO_2 is thermodynamically stable. This is only the case if there is no other solid phase with a lower solubility. Already the supposed solubility difference between "UO_2(fuel)" and "UO_2(pure)" could provide a thermodynamic driving force of phase transformation (the solubility difference corresponds to an affinity

$A^{product}$ of 13.14 kJ/mol at 25°C) if UO_2(pure) would precipitate as secondary phase. Moreover, in silica containing groundwaters, coffinite ($USiO_4$) is more stable than UO_2. Natural analogue data indicate release of trace elements (lanthanides) upon coffinitization of UO_2 [92JAN/EWI]. Under these circumstances the release rate of radionuclides may be governed by the rate of coffinitization of UO_2. This rate in turn will depend on the supply of silica from the ground water and/or on the growth rate constants of coffinite crystals. The latter will depend strongly on temperature. Similarly as discussed for coffinitization, there may also be sorption, coprecipitation or precipitation of Uranium (IV) on the canister or canister corrosion products. UO_2 precipitation on metallic iron from U^{VI} containing solutions [98GIM/MOL], sorption and coprecipitation [96GRA/SMA] of both U^{VI} and U^{IV} on corrosion products (magnetite) were observed experimentally. The thermodynamic driving force imposed on spent fuel dissolution has not yet been quantified.

(3) Motivated by the attempt to avoid quantifying a solubility limited release model under reducing conditions, an empirical threshold rate (a kinetic approach) rather than a thermodynamic assessment can be used [98GIM/MOL]. An upper limit of this threshold corrosion rate based on dissolution rates with unirradiated UO_2 of $2 \cdot 10^{-7}$ $mol_U/(m^2a)$ is used, based on electrochemical data on pure UO_2. This corresponds to a typical fuel dissolution rate of a non-disintegrated fuel pellet (specific surface area ca. 2 cm^2/g, surface roughness factor 2.5) of 10^{-7}/a. This is much lower than any dissolution rate measured for real spent fuel under reducing conditions. It is questionable whether such low rates extrapolated from electrochemical data of unirradiated material are applicable to irradiated material.

DISSOLUTION OF UNIRRADIATED UO_2 AS ANALOGUE FOR SPENT FUEL

The dissolution behaviour of unirradiated uranium (IV) dioxide (UO_2) has been thoroughly studied as a chemical analogue of the spent fuel matrix. These studies have been focused on two different aspects: a) Identification of uranium secondary phases in dissolution experiments, which can control the uranium concentration in solution and consequently the radionuclide release both under reducing [98CAS/PAB, 98OLL] and oxidizing [92WRO/BAT, 97OLL, 97GRA, 98TRO/CAC, 98DIA/GRA, 94CAS/GIM] conditions. b) Determination of dissolution rates as a function of water chemistry parameters and redox conditions by measuring uranium concentration in solution [99SER/GLA, 92GRA/LEI] as well as by measuring corrosion potentials [89SHO/SUN, 98MAR/FEL].

Generally, a batch test methodology is used to identify uranium secondary phase formation and solubility constraints. These results of solution analyses are normally complemented with the study of the solid by means of X-Ray Diffraction, Scanning Electron Microscope and Energy Dispersive X-Ray Spectroscopy among other analytical techniques One of the critical parameters in these experiments is the S/V ratio. At low S/V, in dissolution experiments Ollila [97OLL] has reported an increase of the uranium concentration even after 4 years which means no solubility control. However, at high S/V several uranium secondary phases have been reported depending on the water chemistry used in the experiment [92WRO/BAT,98TRO/CAC].

For the determination of dissolution rates, the continuous dynamic tests (flow-through reactor) has shown an advantage over batch systems. This experimental device reduces the probability of secondary phase precipitation. By changing the conditions of the inflow leaching solutions (i.e. pH, oxidant concentrations, complexing agent concentrations, temperature, etc.), rates as a function of these parameters can be obtained. These reactors have been extensively used with both unirradiated UO_2 and spent fuel

[95GRA/WIL,97PAB/CAS].

Solubility

Secondary solid phase formation and solubility constraints by either primary (UO_2) or secondary phases are very dependent on the redox conditions of the experiments.

Anoxic and reducing conditions

Experiments under reducing conditions have been performed by using different reducing species such as hydrogen with Pd catalyst, iron, magnetite and sulfide. Results obtained for different authors [98CAS/PAB, 98OLL, 98QUI/GAR, 97GRA/LOI, 86FOR/WER, 98AAM/CAS] are shown in FIGURE 2.

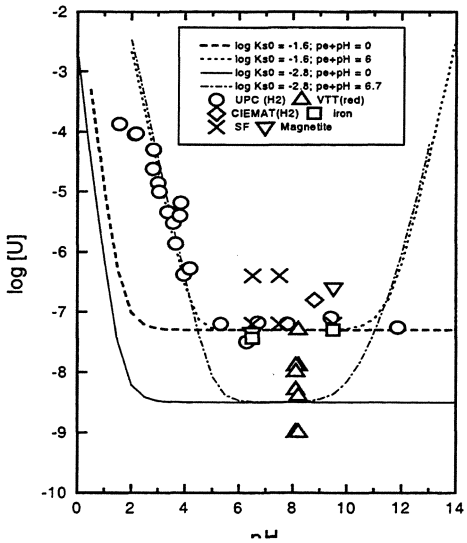

FIGURE 2 : Uranium concentration *vs.* pH under reducing conditions.

In earlier dissolution experiments with UO_2 pellets in synthetic groundwaters (Allard groundwater [81ALL/LAR], bentonite groundwater [86SNE under anoxic (N_2) atmosphere [95OLL], the measured concentrations of uranium at steady state seemed to be in equilibrium with U_4O_9 ($UO_{2.25}$), which was clearly higher than the solubilities of well-crystallized UO_2. No reducing species were added to the solutions in those experiments. The oxidation state of uranium in the aqueous phase was determined at the end of the experiments, after the contact time of 500 days. According to the analyses, uranium was mainly at the U(VI) state. Obviously, the trace oxygen content in the atmosphere of the box is enough to cause slightly oxidizing conditions for uranium in the absence of reducing agents. This is in agreement with the solution concentrations being at the level of $UO_{2.25}$ (U_4O_9) solubilities, which is a surface oxidation product of UO_2. The reported data in literature for UO_2 solubility under anoxic conditions vary over orders of magnitude [98OLL/AHO]. In practice, there are difficulties in maintaining the reducing conditions in the experiments, problems with sorption, with removal of fine particles from solution.

Based on the thermodynamic database for uranium published by the NEA [92GRE/FUG] and Bruno and Puigdomenech [89BRU/PUI], the solubility of uranium dioxide is represented in FIGURE 2 (full line). However, experimental uranium concentrations measured under

reducing conditions do not agree with such thermodynamical model. Recently, Casas et al [98CAS/PAB] have proposed a new interpretation of uranium dioxide solubility considering the co-existence of a solid phase of uranium (IV), probably a low-crystalline phase with a solubility constant higher than the one corresponding to the high-crystalline phase compiled by the NEA, together with aqueous uranium (IV) and (VI) complexes. Therefore, in this model both the pH and the redox potential should be considered. As it is observed in FIGURE 2, the model (dashed lines) based in both pH and pe experimentally measured fits much better experimental results.

This model is obtained by considering the water-oxygen equilibrium reaction:

$$O_2(g) + 4\ H^+ + 4\ e = 2\ H_2O \qquad (1)$$

From the equilibrium constant of this reaction, the following equation can be written:

$$\log P_{O2} = 4\ (pH+pe) - 83.12 \qquad (2)$$

with this equation, the UO_2 solubility constant and the stability constants for U(IV) and U(VI) complexes, the solubility was calculated. The best agreement was obtained at pH+pe value range from 6 to 7 (FIGURE 2) which corresponds to log P_{O2} as low as $\approx$ -59 and $\approx$ - 55.

Oxidizing conditions

A great experimental effort has been undertaken in order to identify uranium secondary phases in UO_2 dissolution experiments. However, the identification is not easy and potential solubility controlling phases are assessed by calculating their saturation index for experimentally measured steady state uranium concentration by using geochemical codes. Ollila [97OLL] studied the solubility behaviour of UO_2 pellets. under oxic, air-saturated conditions in deionized water, in $NaHCO_3$ solutions and in synthetic granite (Allard) groundwater for up to 6 years. Different controlling factors for U steady-state concentrations were observed depending on the water composition. In deionized water at $pO_2 = 0.2$ atm, the U concentration in solution attained a steady state value of $3\text{-}5 \cdot 10^{-6}$ mol dm^{-3}, equal to the solubility of schoepite.

In dissolution experiments with unirradiated UO_2 pellets in synthetic granite groundwater (Allard groundwater) [81ALL/LAR] under air-saturated conditions, a constant value for the solution concentration of uranium was reached after a 500-days'-period at a concentration of $1 - 2 \cdot 10^{-5}$ mol/l [95OLL], which is in good agreement with the results of the spent fuel dissolution experiments [92FOR/WER]. The measured data in Allard groundwater is difficult to correlate with the solubility calculated assuming chemical equilibrium. It has previously been observed in evaluating solubility-limiting (steady-state) factors, that assuming a redox potential controlled by the U_3O_7/U_3O_8 equilibrium, a good agreement could be obtained between calculated and measured data [89GRA, 92FOR/WILL, 95OLL].. A low S/V ratio (1.8 m^{-1}, geometric) was used in those experiments. In the dissolution experiments with UO_2 powder using a higher S/V, schoepite and a uranyl silicate (possibly sodium boltwoodite) were identified as secondary phases in air-saturated Allard groundwater [93OLL/LEI]. The surface of UO_2 powder was oxidised in air prior to the initiation of these experiments, which may have had an effect on the dissolution mechanisms. In synthetic bentonite groundwater, which simulates the effects of bentonite on fresh granite groundwater [86SNE], a steady state was at the level of the solubilities of uranyl silicates ($1 \cdot 10^{-6}$ mol/l) at low S/V. No secondary phase of U was identified. In deionized water, the corresponding steady-state value was $3 - 5 \cdot 10^{-6}$ mol/l, which is close to the calculated solubility of schoepite [95OLL].

The effect of the S/V ratio on the final steady state uranium concentration has also been studied by Diaz-Arocas et al. [97DIA/GAR], but no identification of secondary phase formation was reported. The same authors [95DIA/QUI] have identified studtite in UO_2 leaching experiments at high hydrogen peroxide concentration.

Short duration (less than one year) UO_2 leaching tests under oxidizing conditions, in which schoepite was considered to explain the experimental data, have also been reported by Torrero et al. [94TOR/CAS] in 1 M NaCl medium and Trocellier et al. [98TRO/CAC, 95TRO/GAL] in a synthetic granite water at 96°C; schoepite crystals were identified in both cases.

Wronkiewicz et al. [92WRO/BAT, 97WRO/BUC] have studied uranium release and secondary phase formation contacting UO_2 pellets with an intermittent flow of dripping groundwater (EJ-13) under atmospheric conditions at 90°C. After the first 13 or 20 weeks of testing, notable increases in U release occurred and secondary uranyl alteration minerals began to form. This change reflects the onset of oxidative dissolution of the UO_2 surface and the formation of dehydrated schoepite. After 1.5 to 2.0 years of reaction, the rapid pulsed-release of U subsided, and release rates declined to an extended time interval of moderate uranium release. Most of the uranium that was released from the samples eventually precipitated back as alteration phases onto surfaces of the test components. The sample reaction trends observed in the experiments display a sequence of phase formation characterized by the following paragenetic trend: UO_2 → dehydrated schoepite → compreignacite + becquerelite → soddyite → boltwoodite + uranophane + palygorskite clay. These sequence replicates processes that occur in natural geologic systems, therefore this similarity suggests that the UO_2 in the experiments has reacted by the same mechanism as uraninite in the natural deposits.

Studies of long-term behaviour of spent nuclear fuel were performed by Finn et al. [97FIN/HOH,98FIN/FIN]. The examination of the ATM-103 fuel after 3.7 years of reaction, provided insight into the possible reaction pathways that contribute to matrix dissolution: through-grain dissolution with formation of alteration products and slower grain-boundary dissolution. The major alteration product identified was, Na-boltwoodite $Na[(UO_2)(SiO_3OH)]\cdot H_2O$, which was formed from sodium and silicon in the water leachant. Additional minor phases were detected, including uranophane, $Ca[(UO_2)_2(SiO_3OH)_2]\cdot 5H_2O$. The phase formation observed in these experiments, agrees with that identified in the case of intermittent flow dripping groundwater tests using unirradiated UO_2, previously reported.

Dissolution rates

A classical kinetic approach to study the parameters, which affect the dissolution rate, is given by the following expression:

$$r = k_0 e^{-(E_a/RT)} a_H^m \prod_i a_i^{n_i} \cdot f(\Delta G) \qquad (3)$$

where k_0 is the rate constant, E_a is the apparent activation energy, R is the gas constant, T is the temperature, a_h is the proton activity, m is the fractional reaction order with respect to the proton activity, A_i are the activities of species i (oxidants, carbonate species etc.) which affect the rate, n_i are the respective fractional reaction orders and ΔG is the Gibbs energy of the reaction. When experiments are performed far from the equilibrium, the term $f(\Delta G)$ is the unity.

In general, dissolution rates have been determined varying one parameter and maintaining constant the others. UO_2 dissolution rates have been determined as a function of oxidant concentration, pH, carbonate concentration and temperature.

Effect of oxidant concentration

The presence of oxidants in the near field can be correlated to the radiolysis of water. In this sense, the dependence of the matrix dissolution rate on the oxidant concentration is very important. However, the results found in the literature are controversial since different oxidant concentration dependencies have been reported, varying from 0 to 1.

When the dissolution rate is determined at the beginning of the experiment, the dependence of the oxidant concentration corresponds to a fractional reaction order of 1. In salt brines, a linear relationship was found for three different oxidants: O_2, H_2O_2 and ClO^- [96GIM/BAR]. The same dependence was obtained in electrochemical experiments [92SHO/SUN]. A comparison of both results is shown in FIGURE 3.

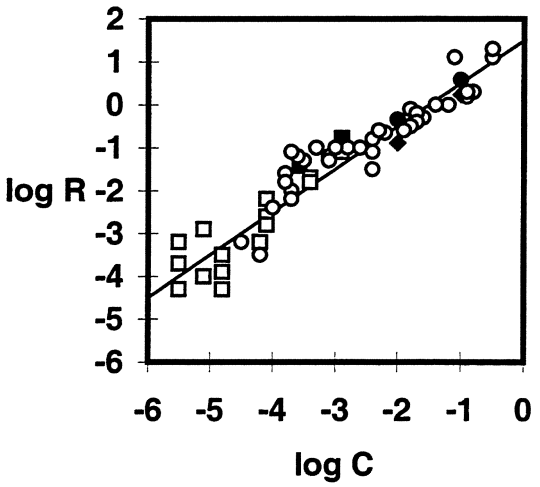

FIGURE 3 : Dissolution rates [mg/m^{2}d] vs. Oxidant concentration [mol/l]. ■ O_2 ;□ O_2 and○ H_2O_2 ◆ H_2O_2 and ● ClO^-

In contrast, the long-term dissolution rate determined in batch experiments as well as the dissolution rates determined by using flow-through reactors has given different dependencies. In salt brines, Gimenez et al. [97GIM/PAB] reported a value of 0.4. Gray and Wilson [95GRA/WIL] obtained with unirradiated UO_2 a dependency of 0.39-0.50 while with spent fuel at 25ºC this dependency was 0.05. With uraninite, the same discrepancies were obtained, Posey et al. [87POS/AXT] determined a dependency of 0.5 and Grandstaff of 1 [76GRA].

Effect of pH

Recently, Torrero et al. [97TOR/BAR] studied in detail dissolution rates as a function of both pH and oxygen partial pressure. Results are shown in FIGURE 4. Data treatment showed that both proton and oxygen partial pressure dependencies are fractional. For pH between 3 and 6.7 a value of 0.37 was obtained while at higher pH no dependency was observed. For oxygen partial pressure, similar results were obtained at acid pH, the dependency was 0.31 while at basic pH, and this dependency can be considered negligible. Torrero et al. [97TOR/BAR] determined a fractional order respect to proton concentration. Thomas obtained similar results and Till [84THO/TIL], a calculation with their data has given a value of 0.30 between pH 2 and 5.

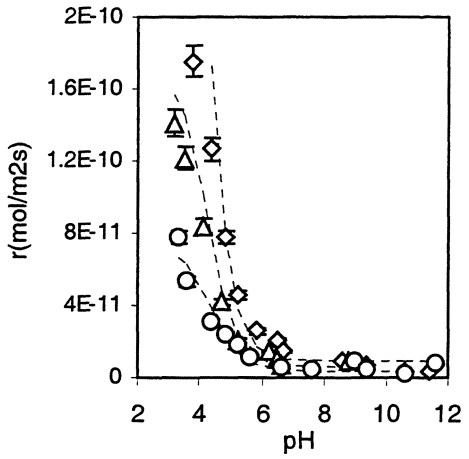

FIGURE 4: Dissolution rates vs. pH. O_2 pressure: o 5%; Δ 21%; ◊ 100%

Electrochemical results at two different pH [89SHO/SUN, 91SUN/SHO] give also a fractional dependency equal to 0.24. Results with spent fuel [89GRA] showed also a fractional dependency equal to 0.52. The fractional rate order with respect to proton concentration is interpreted by surface complexation prior to the detachment of the dissolved ions [90STU/WOL]. The trend observed in the experiments points to an acid-promoted surface controlled mechanism, where the lower the pH the higher would be the concentration of surface protonated complexes leading to higher dissolution rates.

Effect of Carbonate

Carbonate is present in all granite groundwaters to a major or minor extent. Therefore, several authors [92GRA/LEI, 95GRA/WIL, 97PAB/CAS, 87POS/AXT, 76GRA] have studied the effect of carbonate on the dissolution rate. Although some discrepancies have been found in the literature related to the reaction order, most of the experiments performed at 25 ºC indicate a fractional dependency. In FIGURE 5, dissolution rates are plotted as a function of carbonate concentration for both unirradiated UO_2 and spent fuel. A similar trend is observed for both solids.

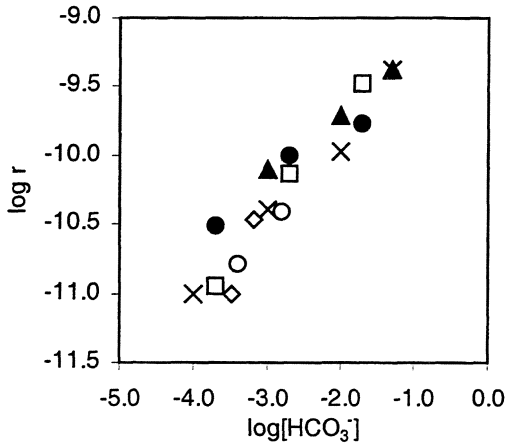

FIGURE 5: Dissolution rates vs. bicarbonate concentration

From this plot a reaction order equal to 0.60 was determined. This value can be interpreted by a surface complexation mechanism in both spent fuel and unirradiated UO_2 due to the carbonate. This result will be evaluated in the modelling section. However, a similar interpretation to the one described with the proton can be applied to the effect of carbonate. When the carbonate concentration is high, carbonate surface complexes are also high and the dissolution rate increases.

Effect of Temperature

The effect of temperature on the oxidative dissolution process of UO_2 has not been extensively studied. The apparent activation energy values range between 20 - 60 kJ mol^{-1} [92GRA/LEI, 76GRA, 79HIS, 57ARO/ROO]. This wide range of activation energy does not allow to identify which will be the process controlling the dissolution of uranium dioxide. Indeed, apparent energies lower than 40 kJ·mol^{-1} indicate diffusion controlled processes, while a value in the range 40 - 85 kJ·mol^{-1} seems to be indicative of a surface controlled mechanism [84LAS].

Recently, de Pablo et al. [97PAB/CAS] have performed dissolution experiments as a function of carbonate concentration and temperature (10 – 60 ºC). The apparent activation energy calculated was 49.5 ± 16 kJ mol^{-1}, which is much higher than the value determined with spent fuel [92GRA/LEI]. On the other hand, leaching experiments performed with spent fuel have shown no differences on radionuclide release at different temperatures (25 and 150 ºC). No definitive conclusions can be obtained about the effect of the temperature on dissolution rates.

GROUNDWATERS

COMPOSITION AND PREPARATION OF SYNTHETIC GROUNDWATER

In the project, except in one case (clay) no real but synthetic groundwaters were used. The selected water compositions represent the three types of sites for geological disposal (salt, granite and clay). In case of granite, also a water composition, modified by bentonite interaction was studied. Five types of synthetic granite groundwaters were used in the experiments (TABLE 1). Appendix 4, TABLE 1 and Appendix 5, TABLES 3 and 4 give more details on the compositions.

The saline granite groundwater represents the groundwater found at a depth of 600 m in granite bedrock. The composition was based on groundwater studies within the site investigations for spent fuel disposal in the Olkiluoto area. The saline Na-Ca-Cl water has a low alkalinity. The ionic strength is 0.5 M. The composition of the synthetic water was planned separately for air-saturated and anoxic (N_2 atmosphere) conditions with the help of EQ3/6 modelling and stability tests [97VUO/OLL].

The Allard groundwater is the reference groundwater for fresh groundwater conditions at great depths in granite bedrock. The composition was modified due to the stability problems of the original Allard groundwater both under air-saturated conditions and in N_2 atmosphere [98VUO/SNE]. The Ca, Mg, Si and carbonate contents were lowered in order to prevent the precipitation of calcite and silicate phases, and the loss of carbonate from solution.

The near-field groundwater simulates the effects of bentonite on saline groundwater (TDS= 67 g/l). It is very saline Na-Ca-Cl water with a low alkalinity. The ionic strength is 1.6 M. The composition was based on measured laboratory data on bentonite/saline groundwater interaction [98MUU/VUO].

A summary and comparison of the selected groundwater compositions is given in TABLE 1. In the following, some preparation methods are briefly described.

95% saturated sodium chloride solution

For this solution 34.1 g of dry sodium chloride were dissolved in 100 ml deionized water.

Granite-bentonite water

The granite/bentonite groundwater by ENRESA/Ciemat [96MAR/MEL] simulates the effects of bentonite on Spanish granite groundwater. This saline synthetic groundwater has a high NO_3^- content (110 mg/l) compared with all the other groundwaters and high chloride concentrations with respect to granite waters (TABLE 1).This synthetic groundwater describes a water composition, obtained from the interaction of a granite groundwater with bentonite from Almeria (Spain). Chemicals used for this purpose were calcium chloride hexahydrate, magnesium chloride hexahydrate, potassium bromide, potassium chloride, potassium nitrate, sodium chloride, sodium hydrogen carbonate, sodium metasilicate pentahydrate, sodium nitrate, sodium sulfate decahydrate and hydrochloric acid. The amount of magnesium chloride hexahydrate was controlled by argentometric titration and the synthetic groundwater was checked for pH and Eh.

Leaching solutions in integral tests

The two leachants used by CEA in integral tests represent the deep clay or granite geological repository sites under consideration in France: one simulates a clayey groundwater, the other a granite groundwater. After synthesis, both groundwater samples were

stored at room temperature in the leaching cell feed tanks; however, their compositions represent equilibrium temperatures for clay and granite materials (16°C and 90°C, respectively). The leaching experiments were performed at 90°C. The composition of the synthetic groundwater compositions were verified after preparation and at the end of the leaching experiments.

Clay Groundwater

An interstitial water from the Boom clay site has been used with a chemical composition at 16°C as indicated in TABLE 1, closely resembling the other clay waters from the Boom clay site, studied by the group of SCK.CEN (TABLE 1). The pH of an interstitial water sample exposed to ambient air for a few hours rises from 8.2 (measured *in situ* at 17.6 bars, $P_{CO_2} \approx 3.5 \times 10^{-3}$ atm and 16°C) to 9.5. [98LEM/CAN, 85HEN/MON]. Boom clay is highly reducing *in situ*, with interstitial water potential of about –250 mV_{SHE} at 17.6 bars and 16°C. However, it is also highly sensitive to oxygen pollution by contact with air. The redox potential of the synthetic boom clay groundwater used in WP I.4.3 is controlled by the reducing action of humic acids [98LEM/CAN] at –140 mV_{SHE}. However, to avoid complications no humic acids were added in the integral test. The redox potential in contact with air was thus +400 mV_{SHE}. The bicarbonate concentration was be estimated by charge balance constraints, i.e. by the sum of the equivalents of the major ionic solution species [89MIC].

Granite Equilibrium Groundwater

The reference chemical composition of the granite groundwater was determined by thermodynamic calculations using the PHREEQE code and validated by analysis of samples taken at different temperatures from several outfalls in the Pyrenees. The calculations provided the simultaneous saturation equilibrium values of the water at 90°C with respect to quartz, calcite, laumontite, albite, kaolinite, microcline and chlorite, as well as the CO_2 fugacity, the pH and the alkalinity. The redox potential of the granite groundwater synthesized in the laboratory air was +250 mV_{SHE}.

MAINTAINING REDUCING CONDITIONS

An important parameter to be considered in spent fuel dissolution is the Eh of the aqueous phase. In deep geological repository conditions, after the site is sealed and the near field engineered barrier has been restored, the spent fuel will be in a reducing environment. Since the spent fuel dissolution mechanism is highly dependent on the redox conditions, the experiments must suitably reproduce such reducing conditions. Reducing conditions can only be achieved in an anoxic environment. Earlier UO_2 dissolution studies in synthetic groundwater (Allard) in N_2 atmosphere in the absence of reducing species have shown that dissolved uranium was mainly (> 90 %) at the U(VI) state [96OLL]. Obviously, the trace oxygen content in the atmosphere of the box is enough to cause slightly oxidizing conditions for uranium. The different partners of the project implemented different procedures as described below.

VTT

The earlier tests in Allard and saline groundwater [97VUO] have shown that lower Eh values can be achieved by the addition of reducing species, Fe^{2+}, S^{2-}, typically present in natural groundwaters, or metallic Fe to synthetic deaerated groundwater. The Eh values in the presence of these redox species ranged from -300 ... -200 mV (1 ppm Fe^{2+} , 1-5 ppm S^{2-}). The Eh value for deaerated synthetic groundwater in the absence of redox species fluctuates. Values from -20 ... +175 mV have been measured for synthetic groundwater after short periods (< 1 month) in the glove box. During longer periods in the box a trend towards

lower Eh was observed.

The stability of the water chemistry (pH, Eh, S^{2-}, Fe^{2+}) in the experiments, as well as in parallel groundwater samples without UO_2 pellets, was followed during long dissolution periods (up to 300 days). FIGURE 6 gives the measured Eh and pH values as a function of time in a parallel sample of saline groundwater with 3 ppm S^{2-} during a follow-up period of

TABLE 2. The stability of water chemistry in the UO_2 dissolution experiments under anoxic conditions.

Redox species addition	Saline S(-II), Fe(+II) [ppm]	Saline Eh [mV] pH	Allard (modif.) S(-II), Fe(+II) [ppm]	Allard (modif.) Eh [mV] pH
1 ppm S(-II) (+0.01 ppm Fe(+II):saline)	0.46 ± 0.04	-216 ± 5 8.69 ± 0.07	0.59 ± 0.02	-235 ± 16 9.08 ± 0.06
3 ppm S(-II)	1.99 ± 0.14	-265 ± 17 9.22 ± 0.06	2.01 ± 0.11	-275 ± 8 9.35 ± 0.06
5 ppm S(-II)	3.69 ± 0.11	-281 ± 16 9.56 ± 0.07	3.39 ± 0.12	-297 ± 10 9.45 ± 0.04
1 ppm Fe(+II)	0.87	-138 ± 68 8.05 ± 0.08	0.16 ± 0.04	-318 ± 114 8.79 ± 0.08

600 days. A platinum electrode (Yokogawa) was used as the redox electrode in combination with an Ag/AgCl reference electrode (Yokogawa). The reference electrode is filled with a gelled electrolyte solution. The sulfide content was decreased rapidly after the addition to synthetic groundwater, probably by reacting with trace oxygen left in the solution after deaeration with N_2, but remains rather stable afterwards, see TABLE 2, which gives the average values and deviations of all the S(-II) determinations carried out during the dissolution experiments in different aqueous phases. The determination was made using a standard spectrophotometric method (SFS 3038). The stability of redox conditions in synthetic groundwaters with S(-II) was shown also by the Eh and pH measurements. The scatter in the measured Eh was small, whereas in synthetic groundwaters with Fe(+II) as reducing species, there is more scatter in the measured Eh values. The determination of the ferrous iron was made by a ferrozine method [79DIM].

FZK

Anoxic or reducing conditions was assured by performing the tests in closely tight Ar filled autoclaves or quarz glass vessels. The autoclaves as well as the glass vessels were equipped with two ball valves allowing solution sampling through one valve, while streaming Ar through the other. The tightness of the reaction vessels was determined by gas analyses during the test and at test termination. N_2 contamination of the gas phase was interpreted as resulting of air intrusion. Typically less than 10 ppm of N_2 were found in the gas phase, even at reaction times as high as 1000 d.

SCK·CEN

Experiments were performed in glove boxes filled with inert gas. The oxygen content was in most cases lower than 5 ppm, but oxygen intrusion was encountered. To avoid this, a second test series was performed in the presence of reducing species (sulfide).

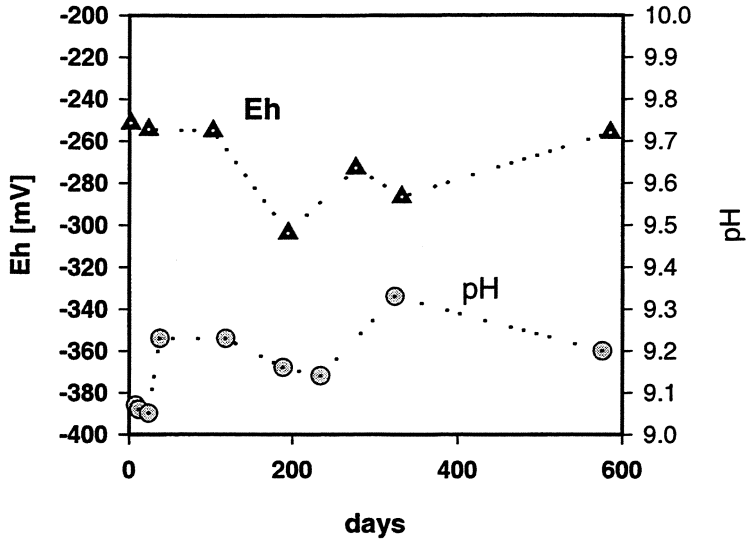

FIGURE 6: The measured Eh and pH values in a parallel sample of saline groundwater with 3 ppm S(-II) during a follow-up period of 600 days under anaerobic conditions.

ENRESA/CIEMAT

Experiments performed under anoxic conditions were carried out in a glove box (FIGURE 7) with an N_2 overpressure of approximately 150 kPa. Oxic experiments were carried under air atmosphere.

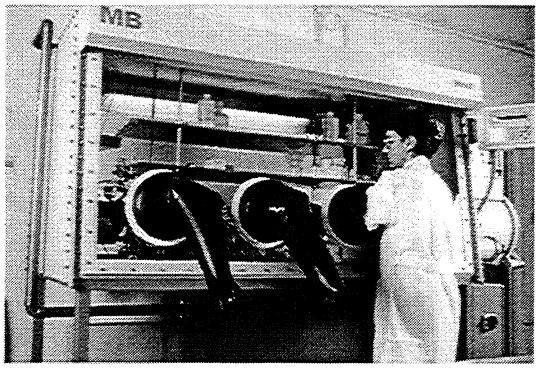

FIGURE 7 Glove box used for experiments performed under anoxic atmosphere.

Reducing conditions in integral tests by CEA

The experimental procedure for imposing and controlling reducing conditions in the system is based on eliminating the oxygen present not only in the leaching solution synthesized in air in the laboratory but also in the environmental materials and in the leaching pot. Before the leaching solution was supplied to the test vessel, it underwent the following operations:

The solution was bubbled for about two hours with a hydrogenated gas mixture (argon containing 3% H_2 and 300 ppm CO_2) in the feed tank, and maintained under a blanket of the

same gas mixture throughout the experiment. Under applicable safety regulations, the maximum permissible hydrogen molar fraction in a restricted zone was 3%. The CO_2 content of the gas should prevent decarbonated leachant. The leachant was percolated over a palladium catalyst to eliminate any residual oxygen. The percolation medium consisted of divided palladium dispersed in a polymerized divinylbenzene resin. The advantage of this technique was its room-temperature catalytic performance.

Before adding water, the leaching pot containing the environmental materials was swept by the same gas mixture. The materials contain adsorbed oxygen that must be eliminated as much as possible to conserve the benefits of the deoxygenated leachant. The time required for the gas to obtain an oxygen concentration below 5 ppm in the pot was determined using a Jacomex® oxygen trace analyzer inserted in the outflow line from the Simfuel leaching pots. The 35 mm Hg negative pressure inside the shielded cell precluded the use of this probe; the pots containing spent fuel were therefore swept with the gas mixture for the same time as in the Simfuel experiments.

Iron was added to the environmental materials by placing a mild carbon steel (E24-2) plate measuring about 9 × 1.9 × 0.3 cm with a total surface area of about 40 cm^2 in the midst of the materials in the pot. Oxidation of the iron reduced any remaining oxygen fixed on the environmental materials after the gas treatment.

TABLE 1: Composition (mg/l) of simulated groundwaters used in the project

	Salt	Granite							Clay				
	NaCl-water	equilib. granite water EGW	Saline granite SGW (air) [1]	Saline granite SGWN[1](N_2) log pCO_2=-7	Fresh granite AGW[2] (air)	Modif Allard AGWM (air)[1]	Modif. Allard GW (N_2)[1] log pCO_2=-4	Granite bentonite GBW (air)[3]/	Real interstitial GW RIC[4]	Synthetic GW SCW[5]	SCW+ humic acid SCWHA[6]	SCWHA without carbonat SCWHA/C[7]	Boom Clay water
Specification	FZK[8]	CEA[9]	VTT	VTT[10]	VTT	VTT	VTT	CIEMAT	SCK	SCK	SCK	SCK	CEA
Na^+	1.3E5	95	4800	4800	52	52	52	3750	387	345	547-611	239-256	368
Ca^+		2.4	4000	4000	18	10	5.1	135	3.9	3.1	2.6-3.1	0.9-1.1	5.6
Mg^{2+}			56	55	4.3	2.8	0.7	600	2.9	2.7	2.4-2.7	2.7-2.9	2.4
Sr^{2+}			35	35	-	-	-	-					
K^+		2.0	21	21	3.9	3.9	3.9	20	31	18	18-24	21	11
HCO_3^-		28	10	-	123	91	65	27	808-915	793-829	808-865	26-34	915
SiO_2		66	2.5	-	8	2.9	1.7	8.3	3.1	2.9-3.2	1.6-3.4	1.9-4.5	
Br^-			105	105	-	-	-	15					
F^-		5.7	1.2	1.2	-	-	-	-	5	0.9		0.8	3.6
I^-			0.9	0.9	-	-	-	-					
SO_4^{2-}			4.2	4.2	9.6	9.6	9.6	1500	7	22	22-26	22-24	11
B^{3+}		0.1	0.9	0.9	-	-	-	-	6				
Cl^-	2E5	103	14600	14600	58	47	52	6550	45-110	51-56	335-428	334-382	37
TOC[11]									77-98	<5	100	100	
NO_3^-								110	0.9	1.2	1.5	1.2	
pH_{meas}	7.0	7.6-8.1	7.0- 7.1	8.0- 8.1	8.4	8.3- 8.4	8.7- 8.8	7.5	8.4	8.4-	8.4	8.4	8.7-9.3
pH_{theor}		8.7-9.3	7.4	8.3	8.2	8.4	8.8	7.3	pH fixed by titration				

[1] [97VUR/OLL. Vuorinen U. and Ollila K., Stability of synthetic Allard groundwater, Posiva memo KH-M-101/97 (in Finnish).
[2] [81ALL/LAR]
[3] [96MAR/MEL]
[4] RIC (Real Boom Claywater) is sampled in situ in the Underground Research Laboratory of SCK·CEN, and transferred to the laboratory in containers that are purged with inert gas
[5] Procedure for preparation of SCW:To degassed HPLC (High Performance Liquid Chromatography) water, add 40 mg/l NaCl, 22 mg/l $MgCl_2.6H_2O$, 30 mg/l Na_2SO_4, 25 mg/l KCl, and 1170 mg/l $NaHCO_3$. To this solution, an excess of $CaCO_3$ is added. The suspension is stirred for 24 hours at room temperature, in order to obtain an equilibrated solution.
[6] Preparation of SCWHA similar to the preparation of SCW, but a concentrated soln. of humic acids is added as well. The added humic acids are purified acids, extracted from RIC.
[7] The SCWHA\C is similar to SCW, but HPLC water is not $CaCO_3$ equilibrated and no $NaHCO_3$ is added. A conc. solution of humic acids is added (as for SCWHA).
[8] CO_2 and O_2 content reduced by bubbling Ar.
[9] Composition calculated for equilibrium of deep granite water with granite and fracture filling minerals
[10] The anoxic conditions of deep groundwaters are simulated in an anaerobic glove box filled with nitrogen (adsorbers for O_2 and CO_2 : Cu catalyst and molecular sieve, respectively). The oxygen concentration in the atmosphere of the box normally stays below 1 ppm (0.1...0.5 ppm). The carbon dioxide content is ≈ 0.1 ppm
[11] TOC=total organic carbon (=humic acid in mg C/l)

SOLID PHASE CHARACTERIZATION

The corrosion properties of four materials were studied and compared in the project : UOX and MOX spent fuel, unirradiated UO_2 and SIMFUEL.

SPENT FUEL

FZK:

TABLE 3: List of data from spent fuel rod SBS 1108, segment N 0203.

Discharge date	May, 27th, 1989
Burnup	50 400 MWd/tU
Irradiation time in the reactor	1226 days (1986-1989)
Average linear power (segm.N 0203)	260 W/cm
Maximum linear power (segm.N 0203)	315 W/cm
Specific activity (1-2-92)	$7.4*10^{10}$ Bq/g
Initial density	10.41 g/cm^3
Initial ^{235}U enrichment	3.8 wt.%
U_{tot}	1171.0 g
Pu_{tot}	14.0 g
Initial gap (fuel/cladding)	0.17 mm
Cladding	Zircaloy 4

A high burnup LWR-UO_2-spent fuel rod segment (N 0203) from the PWR power plant Gösgen, Switzerland was obtained from SIEMENS/KWU. The following data of the fuel rod were provided by SIEMENS/KWU The fuel powder used by FZK originated from the previous EU-project. Spent fuel powder was prepared by anoxic crushing and milling of a total amount of ca. 18,5 g cm-sized spent fuel (LWR-UO_2 from PWR Gösgen/CH; 50 MWd/kg U) fragments obtained from decladded pellets. Prior to starting the leaching test, the dust fraction generated during milling was removed by washing with DI-water in an ultrasonic bath. The dried powder was separated and stored in "gas-tight" capsules under N_2 until its use in the various experiments. For geometric specific surface area see the compilation in Table 10. Because of uncertainties the effective specific surface area as well as S/V ratio may deviate about 100% from the geometric values.

ITU

The UO_2 fuels used in the experiments of ITU were taken from the 1-551 pin and the MOX fuels from the F-6565 pin; both irradiated in the BR3 reactor. The UO_2 pin was enriched with a 8.25 w/o of U-235 and was fabricated by the "Franco-Belge de Fabrication de Combustible" (FBFC) in Dessel and the MOX pin had an enrichment of 6.9 % in fissile plutonium and was fabricated by "Belgonucleaire" in Dessel, according to the Micronized-Master blend process (MIMAS). The characteristics of the fuel pellets are shown in TABLES 4 and 5 shows the isotopic composition of the fuel pellets. The fuel samples used in these experiments are shown in TABLE 6 together with the burn-up of the fuel.

TABLE 4: Characteristics of the fuel pellets.

		UO_2 fuel	MOX fuel
Fuel Pellet	Mean diameter (mm)	8.04	8.22-8.24
	Height (mm)	12.22-12.41	11-12.5
	Weight (g)	6.323-6.419	-
	Mean Density (g/cm^3)	10.34-10.35	-
	(% TD)	94.3-94.6	94-95
Fuel	B Equivalent (ppm B)	0.6	0.74
	Stoichiometry (O/M)	1.997	1.991
	Mean Grain Size (μm)	11	5

TABLE 5: Isotopic composition of the pellets.

Isotope	UO_2 fuel	MOX fuel
U-234	0.063	0.003
U-235	8.253	0.309
U-236	0.052	0.007
U-238	91.632	99.681
Pu-238	-	1.663
Pu-239	-	58.228
Pu-240	-	24.848
Pu-241	-	9.716
Pu-242	-	5.545

TABLE 6: Samples used in the experiments.

Fuel	Sample	burn-up (GWd/tU)
UO_2	1-551-1-6	30
	1-551-2-8	50
	1-551-2-5	50
MOX	F-6565-1-4	12
	F-6565-2-6	20
	F6565-2-7	25

TABLE 7 Cladding characteristics.

	UO_2 fuel	MOX fuel
Alloy	Zry-4	Zry-4
Outer Diameter (mm)	9.50	9.6
Internal Diameter (mm)	8.24	8.4
Wall Thickness	0.58	0.56

TABLE 8: Gap size evaluation of fuel samples.

fuel	burn-up (GWd/tU)	gap-min (μm)	gap-max (μm)	Gap-mean (μm)
UO_2	30	15	55	26 ± 12
UO_2	52	4	37	14 ± 9
MOX	12	18	78	41 ± 14
MOX	23	9	71	37 ± 20
MOX	19	28	114	59 ± 26
MOX	24	25	80	51 ± 17

A first approximation for the composition of the fuels for the different burn-ups was made using the ORIGEN code; the results obtained in these calculations are shown in Appendix 6, TABLES 7-10.

One UO_2 (1-551-1-6) and one MOX (F-6565-2-8) cross section samples were observed with a JEOL 35 CX Scanning Electron Microscope. Both samples were polished first to metallographic quality and further coated with a conductive gold layer of a few hundreds of nm thick.

SIMFUEL

SIMFUEL is a chemical analogue of irradiated fuel developed and manufactured by AECL Research Laboratory. It is a complex material based in a UO_2 matrix in that is included some elements simulating fission products [91LUC/VER]. SIMFUEL used in the work of ENRESA-CIEMAT had a composition that simulates SF burned to 50 MWd/kg U, whereas SIMFUEL of CEA simulated a burnup of 6 at% (ca. 60MWd/kgU). The table shows the composition of the two types of SIMFUEL used.

TABLE 9 SIMFUEL compositions ENR=ENRESA-CIEMAT, nominal values for 50MWd/kgU simulates, CEA= measured values for 60MWd/kgU simulates

Element	% w		Element	%w	
	ENR	CEA		ENR	CEA
Sr	0.27	1.09	Pd	0.29	0.11
Y	0.06	0.32	Ba	0.37	0.26
Zr	0.57	0.54	La	0.31	0.30
Mo	0.52	0.46	Ce	0.88	1.88
Ru	0.38	0.07	Nd	1.00	0.61
Rh	0.63	0.60	U	94.78	

SAMPLE PREPARATION

Most experiments were performed at high surface area to solution volume ratio (S/V) using powdered spent fuel (CEA, FZK), powdered UO2 (SCK.CEN, VTT, ENRESA-UPC) and powdered SIMFUEL (CEA, ENRESA-CIEMAT). Pellet sized samples were used for UO_2 (VTT) and spent fuel (FZK, continuation of tests from 3rd EU-Framework programme and ITU, pellets in rodlet). Spent fuel and SIMFUEL powders for integral tests at CEA were produced with similar surface area.

For preparing the powdered UO_2 and SIMFUEL samples pellets chosen for leaching experiments were grounded and sieved to obtain a suite of preselected particle sizes. The selected particle size fraction was washed with water in order to eliminate fine particles produced during powder preparation. These fine particles would contribute to a large surface area that may lead to overestimation dissolution rates.

Spent fuel powders (CEA) were prepared under oxidizing conditions. A procedure was developed for crushing and screening the fuel samples with the main criterion of feasibility in a shielded cell environment. The resulting particles were sieved with the aide of 12 mm diameter stainless steel balls on a set of screens (250 µm and 50 µm) on a vibrator modified for remote operation. Applying this procedure to the 60 $GWd \cdot t_{HM}^{-1}$ fuel yielded a fraction (50–250 µm) representing about 42% of the total, for a useful mass of 11 g (i.e. approximately 0.22 TBq) sufficient for our experimental purposes. The powder fraction was washed

by rinsing with Milli-Q double-distilled water for 140 days to remove any fines and to eliminate the labile activity thus facilitating analyses of the alteration of the fuel matrix.

SURFACE AREA DETERMINATION

The water accessible specific area is an essential parameter for calculating the leach rate of spent fuel, SIMFUEL and UO_2, and for comparing the results of leaching experiments. Spent fuel dissolution data are in most cases reported in terms of Fractions of radionuclide Inventories of fuel samples, release during the experiments into the Aqueous Phase (FIAP). This unit is convenient and it is significant for describing the release of labile radioactivity from the fuel (gap and grain boundary contributions) but this unit masks that fuel matrix dissolution is essentially related to the accessible surface area. Direct comparisons using the very large amount of experimental data available in the literature of irradiated UO_2 and MOX and non-irradiated UO_2 and SIMFUEL is often very difficult, not only because of the existing irradiation differences between SIMFUEL or non-irradiated UO_2 and spent fuel but also the effective surface area is quite different. Spent fuel pellets have a larger specific surface area than non-irradiated pellets due to the formation of thermal gradient cracks and pores due to the volatile fission products. Forsyth [95FOR] compiled specific surface area values from irradiated and unirradiated fuels concluding that for irradiated fuel the average specific surface area is around 6 times higher than for unirradiated fuel. In the case of MOX, microstructure differences may also affect the accessible surface area. Higher fractional release of uranium from irradiated material in tests under oxic conditions was found explainable in terms of different surface areas [98SER/RON].

Hence, normalization to surface area seems to be necessary when comparing different materials behaviour. The various partners of the project employed different methods of surface area determinations : Brunauer, Emmet and Teller BET measurements, geometric estimations from particle size distributions and shape factors and by mercury porosimetry ("geometric surface area). The BET measurement overestimated the specific surface area, since pores inaccessible to water are accessible to the gas and the geometric surface area underestimates the surface area.

ENRESA-CIEMAT characterized their SIMFUEL powders prior to the experiment also by the BET method but also by laser diffraction for measuring the particle size distribution. The specific surface area obtained was 0.043 m^2/g.

The specific area of the CEA-SIMFUEL powder was measured by BET with Kr gas in the CEA's Uranium Fuel Laboratory (DRN/DEC/SPU/LCU) at Cadarache. Values of 0.018 $\pm$ 0.002 $m^2 \cdot g^{-1}$ were obtained. A geometric surface area was calculated, using the area of an average sphere of 150 µm in diameter and a shape factor of 3 for SIMFUEL and 5 for spent fuel (the higher shape factor for spent fuel provides for its heterogeneity, its degree of cracking and its high porosity after reactor irradiation). The calculated geometric specific surface area values were 0.012 $m^2 \cdot g^{-1}$ for SIMFUEL and 0.02 $m^2 \cdot g^{-1}$ for spent fuel. The effective specific surface area of the SIMFUEL powder sample was thus between 0.012 and 0.018 $m^2 \cdot g^{-1}$. The SIMFUEL powder alteration calculations were therefore performed assuming a specific surface area S of 0.016 $m^2 \cdot g^{-1}$. The 3:5 ratio area ratio between the SIMFUEL and spent fuel was conserved by using a value of 0.027 $m^2 \cdot g^{-1}$ for the latter.

Liquid mercury porosimetry: An attempt to measure effective surface area of non irradiated UO_2 samples (original work package I.2).

Liquid mercury porosimetry is a well-known technique used to measure open porosity, pore size distribution and the density of solid, metal and non-metal, materials. For powder samples the technique is used to measure the particles size distribution.

In the framework of the present work this technique was applied to calculate, the effective pore surface of non-irradiated UO_2 pellet samples from the total pore volume. These values will enable the wetted surface areas to be measured and thus the measured leaching data to be converted to effective corrosion rates.

At ITU the Hg pycnometer (Carlo Erba 400) is used to measure the total pore volume and pore size distribution up to a pressure of 4000 Bar of non-irradiated alpha contaminated materials.

The cumulative volume in mm^3/g of a sample of a non-irradiated UO_2 pellet (6 mm in diameter, 1.35 mm high, geometric density 9.5 g/cm^3) is shown in Figure 8 with a histogram of cumulative mercury volume (mm^3/g). It shows that the majority, approximately 70%, of the measured pores are in the range of a few nanometers. Assuming a cylindrical pore shape an effective pore surface of 2.38 m^2/g was calculated from the specific pore volume measured.

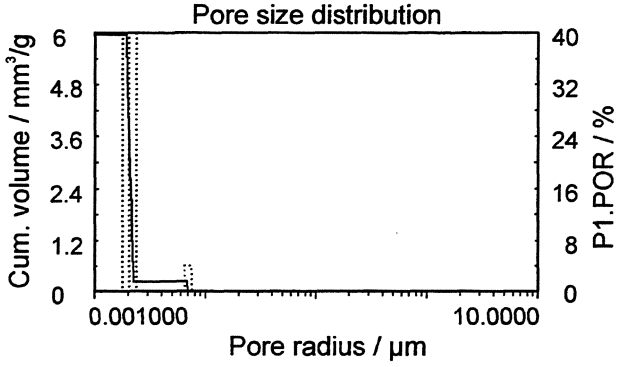

FIGURE 8: Liquid mercury porosimetry histogram. Pore radius versus cumulative volume for a UO_2 sintered and non-irradiated sample.

The large order of magnitude of the effective pore and micro crack surface clearly demonstrate the importance of correct pore surface calculations and the minor effect of the external specimen surface on the leaching behaviour of UO_2. This value is much higher than typically assumed for UO_2 and this high value was attributed to the much lower than theoretical density of the sample. For the case of spent fuel samples the performance of similar effective surface area measurements failed mainly due to experimental complications: delicate manipulations for the specimen preparation and measurement were impossible in the hot cell, and would have required cost intensive modifications.

A comparison of the results of our surface area measurements with those of the literature is given in TABLES 10 and 11. BET and geometric estimates were consistent with the literature values for similar sample types. In contrast, Hg-porosimetry of unirradiated UO_2 gave much higher values. If correct, much lower surface area normalized corrosion rates would result. However, since the Hg-porosimetry value results from a single individual sample, and no data for irradiated material are available, we use BET or geometric estimates and refrain from using the Hg-porosimetry data for calculating surface area normalized reaction rates.

TABLE 10. Specific surface area of SIMFUEL and UO_2 samples and comparison with literature data

References	Shapes of fuel samples	Measurements method	Surface ($m^2.g^{-1}$)	Notes
Our work/CEA	powders 50-250 µm	geometry	0,012	S.R.F. : 3
		BET	0,018	
/ENRESA	SIMFUEL Powder 50/100 µm	BET	0.043	
/SCK-CEN	UO_2 Powder 50-100 µm	BET	0.044	
/VTT	UO2 pellet	geometric	0.00033	
/VTT	$UO_{2.1}$ powder, 0.7 µm	BET	5.4	
/ITU	pellet	Hg-porosimetry	2.38	
96RON/MAT	pellet	BET	0,00015	
95BRU/CAS	pellet	BET	0,000192	
	powders 100-300 µm	BET	0,0113	
96GAR/SER	powders 50-100 µm	BET	0,1	Not washed
	powders 100-315 µm	BET	0,026	Included fines
92BRU/CAS	pellet	geometry	0,000058	
92OII	pellet	BET	0,015	

TABLE 11. Specific surface area of spent fuel samples and comparison with literature data

References	Burnup (GWj/t_U)	Shapes of fuel samples	Measurement method	Surfaces ($m^2.g^{-1}$)	Notes
Our work/CEA	60	powders 50-250 µm	Analog SIMFUEL	0,027	
/FZK	50	Powder 2.5-4.5 µm	geometry	0.3	SRF. 2.5
94FIN/BAT, 94FIN/GON, 95FIN/BUC, 96FIN/HOH1, 96FIN/HOH2	30 & 43	fragments	geometry	0,00021	
92GRA/STR, 92GRA/LEI	33	powders 0,5-5 mm	geometry	0,0006	S.R.F.: 3
		powders 15-25 µm	geometry, PSD	0,086	S.R.F.: 3
96GRA/LOI, 96LOI/GRA, 94LOI/GRA	50,4	pellet	geometry	0,0002	
		fragments	geometry	0,0007	
95FOR	42 & 43	fragments (2 to 4 mm)	BET	0,007 - 0,012	
94GRA/THO	31	powders 7-20 µm	geometry, PSD	0,098	S.R.F.: 3
		powders 700-1700 µm	geometry, PSD	0,0017	S.R.F.: 3
	50	powders 7-20 µm	BET	0,277	
		powders 700-1700 µm	geometry, PSD	0,0019	S.R.F.: 3
95GLA/TOS	31 & 5	fragments	geometry	0,0002	

PSD : Particle-Size Distribution; S.R.F.: Surface Roughness Factor

ENVIRONMENTAL MATERIALS

The selected environmental materials were analyzed to determine their contents of impurities, corresponding to elements found in the fuel, whose releases into solution might interfere with the release of elements from spent fuel. The solutions obtained by solubilizing the environmental materials either by acid rinses or by alkaline melting were analyzed by ICP-AES and ICP-MS.

Iron and its corrosion products

At VTT metallic iron was added as iron chips (Baker Chemicals, reducing power as Fe 100.3 %). At ENRESA and FZK, metallic iron Fe(s) (Merck) 99.5%, was used with particle size 10 μm. Magnetite Fe_3O_4(s) (Aldrich) 98% used by ENRESA had a particle size < 5 μm.

Clay

In integrated experiments, CEA used smectite 4a (also known as FoCa 7) clay. This material contains appreciable quantities of Sr, Y, La, Ce, Nd, Ba, Cs and I, which constitute a source of interference in determining the release rates of the same elements from the fuel source terms. The Mo, Ru, Rh, Pd, U and Sb concentrations in smectite 4a are below the detection limit (10 ppm), but may also interfere with fuel release measurements. Results are given in the following TABLE 12

TABLE 12. Chemical composition of smectite 4a

Main elements (%)		Impurities elements found also in Simfuel (ppm)		Other elements (ppm)	
Si	20,300	Sr	100	Li	55
Al	11,500	Y	30	B	< 10
Mg	0,410	Zr	110	Cr	350
Na	0,130	Mo	< 10	Sb	< 10
Fe	5,500	Ru	< 10	Cs	100
Ti	0,640	Rh	< 10	Pb	60
K	0,190	Pd	< 10	Co	20
Ca	1,900	La	45	Ni	70
Mn	0,052	Ce	80	Rb	10
P	0,080	Nd	40	W	400
		U	< 10	F	65
		Ba	290	I	30

Granite

For the integrated tests, we selected French granite from the Fanay-Augères massif (TABLE 13). As with smectite 4a, Fanay-Augères granite contains appreciable amounts of Sr, Y, Zr, La, Ce, Nd, U, Ba and Cs, as well as traces of Mo, Ru, Rh, Pd and Sb, with the same risk of interference for identification of release locations.

Sand

Clay alone would be much too impermeable to obtain water percolation times compatible with our experimental time frame. We therefore used a mixture of sand and clay. A satisfactory tradeoff between a sufficient quantity of clay and the resulting impermeability was obtained using a mixture of 90 wt% *Sika F25* sand (TABLE 14) and 10 wt% clay.

TABLE 13. Chemical composition of Fanay-Augères granite

Main elements (%)		Impurities elements found also in Simfuel (ppm)		Other elements (ppm)	
Si	31,90	Sr	50	Li	140
Al	7,50	Y	15	B	< 10
Mg	0,20	Zr	80	Cr	300
Na	2,48	Mo	< 10	Sb	< 10
Fe	0,98	Ru	< 10	Cs	100
Ti	0,12	Rh	< 10	Pb	60
K	4,20	Pd	< 10	Co	< 10
Ca	0,50	La	20	Ni	30
Mn	0,03	Ce	50	Rb	440
P	0,18	Nd	20	W	280
		U	20	F	6
		Ba	180	I	28

TABLE 14. Chemical composition of Sika F25 sand

Main elements (%)		Impurities elements found also in Simfuel (ppm)		Other elements (ppm)	
Si	45,500	Sr	< 10	Li	< 10
Al	0,300	Y	< 10	B	< 10
Mg	0,040	Zr	40	Cr	600
Na	0,060	Mo	20	Sb	< 10
Fe	0,800	Ru	< 10	Cs	< 10
Ti	0,020	Rh	< 10	Pb	40
K	0,110	Pd	< 10	Co	< 10
Ca	0,200	La	< 10	Ni	100
Mn	0,005	Ce	350	Rb	< 10
P	0,030	Nd	< 10	W	400
		U	< 10	F	6
		Ba	50	I	28

DETAILS AND ACHIEVEMENTS OF THE PROJECT WORK PACKAGES (WP)

WP I: BASIC UNDERSTANDING OF THE MECHANISM OF FUEL MATRIX DISSOLUTION

More than 95% of the radiotoxicity of spent nuclear UOX or MOX fuel is concentrated in the UO_2 or $(Pu,U)O_2$ matrices. Consequently, the dissolution behaviour of this matrix must be understood to allow reliable performance assessment for disposal sites in granite, clay or salt formations. Natural analogue studies as well as laboratory testing have distinguished two principal dissolution modes: (1) under oxidative conditions UO_2 is thermodynamically unstable and is dissolved comparatively fast by formation of aqueous U(VI) species and formation of secondary U(VI) solid phases and (2) under reducing conditions UO_2 will dissolve by non oxidative formation of aqueous U(IV) species and/or secondary solid U(IV) phases. If secondary U(IV) containing phases cannot be formed, UO_2 may become thermodynamically stable, once solubility limits are reached. Additionally, an intermediate case (3) may be operative under anoxic conditions, with UO_2 dissolution by formation of U(VI) species (e.g. uranyl(VI) carbonate complexes) until UO_2 becomes thermodynamically stable.

The dissolution mechanism of the UO_2-matrix is studied under conditions relevant to various European repository designs, combining empirical and theoretical approaches and comparing the behaviour of real spent UOX and MOX fuel with SIMUEL and pure UO_2. Both (geo)chemical and electrochemical aspects of the dissolution mechanism are considered for oxic, anoxic and reducing conditions.

Under reducing conditions expected to prevail in all European repositories, the mechanism (2) or (3) should prevail. For example, the spent fuel from Finnish nuclear power plants is planned to be disposed of in a repository to be constructed at a depth of about 500 m in crystalline granite bedrock, with reducing conditions prevailing in deep granite groundwater, German spent fuel is planned to be disposed in 800 m depth in a domed salt, and potential intrusion of Fe(II) containing reducing salt brines must be considered. Similarly, in the Boom clay formation in Belgium, reducing conditions are expected. The composition of groundwater, which will come into contact with spent fuel, depends on the geological formation and the interactions with bentonite. The presence of Si and Ca in groundwater has been observed to affect the dissolution rate of unirradiated UO_2. Gray and Wilson [95GRA/WIL] showed that the addition of Si and Ca to a bicarbonate solution could reduce the dissolution rate up to 100 times.

WP I.I DISSOLUTION OF SPENT FUEL AT HIGH SURFACE TO SOLUTION VOLUME RATIO

Dissolution experiments were performed with powdered spent fuel samples (grain size < 3 µm) at high ratios of sample surface to solution volume (S/V) to simulate the long-term corrosion at lower S/V ratios. The high surface area leads to a much faster increase of solution concentrations of radionuclides as could be achieved with fuel pellet samples. The small grain size allows for complete washout of radionuclide inventories from the grain boundaries, thus allowing improved assessment of the fuel matrix behaviour. Though powder preparation occurred under N_2, high corrosion rates in the range $1*10^{-4}$/d and $2*10^{-4}$/d have indicated that some powder oxidation might have occurred during storage in gas tight capsules over some years. Nevertheless, in relative terms, significant insight into fuel dissolution properties could be obtained.

Two types of experiments were performed at INE-FZK with the same powder: Tests as a function of pH and pCO_2 in NaCl-solution (samples P56(I), P56(II), P56(III)) and for comparison tests in granite water and granite bentonite water (P4).

Effect of pH and pCO_2 at high S/V

To assess the influence of pH and pCO_2, on the dissolution behaviour of spent fuel in saline solution, static spent fuel corrosion experiments were performed using powdered spent fuel samples in 95% saturated NaCl-solution. Quartz glass reaction vessels were used (FIGURE I.1-1), equipped with fittings, allowing to insert electrodes (pH, Eh), adding of acid or base (pH-control), sampling of solutions, sampling of gases and inserting the desired gas atmosphere.

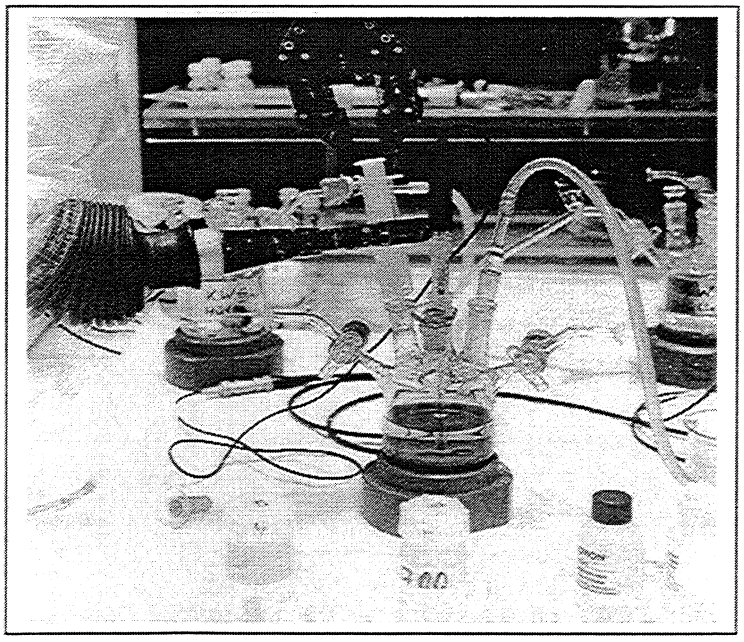

FIGURE I.1 –1: Glass reaction vessel used for spent fuel powder dissolution tests under various Ar/CO_2 gas atmospheres at controlled pH values.

In FIGURE I.1 –1 the procedure of solution sampling is shown. The carbonate content of the solution was fixed by the CO_2 content of the gas phase, and the pH was varied stepwise. One of the tests was performed under Ar (100%) atmosphere, another one under Ar 99 / (1%) CO_2 atmosphere and a third one under Ar 99,97 / (0,03%) CO_2 atmosphere.

During the first two months two solution samples were taken from each test without adjustment of pH. Thereafter, the pH-values of the experiments were adjusted to 7, 9, 11, then back to pH 7 (addition of 0,1n NaOH, or 0,1n HCl). To avoid CO_2 contamination NaOH and HCl solutions were flushed with argon for at least 2 hours. Sampling of solution was performed at least three weeks, after the desired pH-value was adjusted. All solution samples were filtered by a microfilter membrane (0.45 µm) and aliquots were additionally ultrafiltered (18 Å) by means of centrifugation. Filtered aliquots were acidified with 1m HNO_3 to stabilize the radionuclides in solution prior to analyses. The sampling interval of the dissolution tests are summarized in TABLE I.1 –1.

TABLE I.1 –1: Time (days) of solution sampling since start of the static experiment

Atmosphere	Sample	Wash	Time (days) since start of the static test					
		days	no pH control		pH adjusted to			
					7	9	11	7
Ar	P56(I)	85	14	62	83	173	236	277
Ar /0,03% CO_2	P56(III)	162	19	74	102	158	223	329
Ar /1 % CO_2	P56(II)	89	15	59	80	169	230	274

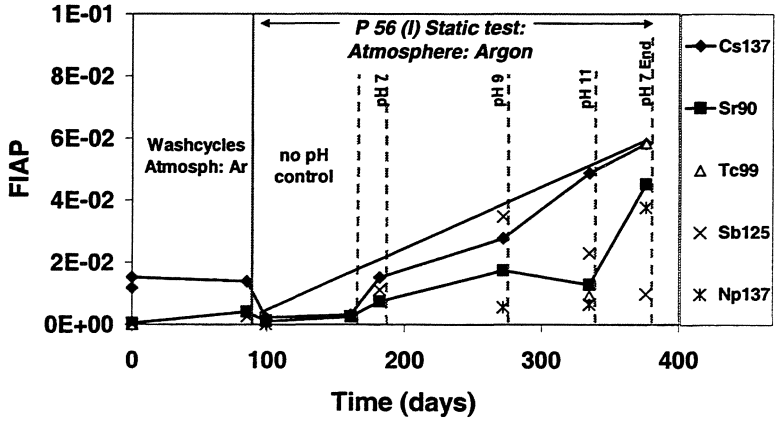

FIGURE I.1-2: Released fractions of matrix bound radionuclides Cs137, Sr90, Np137, Tc99 as a function of time during dissolution of spent fuel powder P56(I) in 5m NaCl solution under Ar-Atmosphere

Matrix dissolution rates and release of radionuclides

The dissolution behaviour of the fuel matrix is usually deduced from the released quantity of radioelements which are encountered with preference in the UO_2 matrix and which, after dissolution, do not become incorporated into secondary phases. Based on the previous experience in the past EU-project on spent fuel corrosion, the release of Sr may tentatively be used as indicator for fuel matrix degradation. However, caution is necessary, since previous experiments were performed in the absence of CO_2. Presence of CO_2 may lead to the precipitation of carbonate phases, which could incorporate relevant quantities of Sr. Also the release of Cs may be considered as indication for fuel matrix dissolution of fine grained fuel powder since all grain boundaries are exposed to the solution and washing over at least 85 days (TABLE I.1-1) will have dissolved all gap and grain boundary bound Cs. The extent of dissolution of Sr and Cs from spent fuel powder in the experiment performed under CO_2 free Ar-atmosphere is plotted in terms of FIAP-values (Fraction of the inventory in the aqueous phase) as a function of time in FIGURE I.1 –2. Fractional release data of Sr- and Cs during three wash cycles (Cycle 1: 10 minutes, Cycle 2: 10 minutes, and Cycle 3: 85 days) are included. Additionally, FIAP values of other matrix bound radionuclides such as Np137, Sb125 and Tc99 are shown. The times of solutions sampling with non-adjusted and adjusted pH-values are indicated. Decrease of FIAP values after washing is due to replacement of the solution by fresh leachant. FIAP values of Sr and Cs achieved in the subsequent static test increase with time. At the end of the static test of 277 days of duration, the fractional release of Sr (Cs) was found to be $4{,}53*10^{-2}$ ($5{,}84*10^{-2}$). Within experimental uncertainty, the release rate of Cs was constant and seems not be influenced markedly by the variation of pH between pH 7 and 11. At most pH values the fractional release of Sr was similar to that of Cs, with the exception of pH 11. This similarity indicates that release data of both elements can be used as indicator for matrix dissolution between pH 7 and 9, however, at pH 11 only Cs release remains controlled by matrix dissolution. Lower Sr-release is probably associated to retention on the fuel surface, on the reaction vessel or in secondary reaction products. Indeed, a subsequent decrease in pH to a value of 7 has lead to an accelerated remobilization of this retained fraction of Sr, with instantaneous Sr release rates even higher than those of Cs, resulting in final FIAP values of Sr at test termination similar to those of Cs.

Based on these observations one obtains a matrix dissolution rate for this experiment in the range between $1{,}6*10^{-4}$/d (based on FIAP values of Sr at pH<11) and $2{,}1*10^{-4}$/d (based on FIAP values of Cs,Tc,Sb). This is at least one order of magnitude higher than observed in dissolution tests with spent fuel powders under similar test conditions (NaCl-solution under Ar-atmosphere) in the previous EU-program. This difference is probably due to an oxidation of the powder during storage over some years before it was used in the test. The kinetics of matrix dissolution was almost the same, if CO_2 was present in the system with amounts of 0,03% or 1% in the gas phase. In FIGURE I.1 – 3 the FIAP values of matrix bound radionuclides Cs137, Sr90, Tc99, Sb125 and Np137 obtained in the test using Ar / 1% CO_2 atmosphere are plotted as a function of time. Data from the test with Ar / 0.03% CO_2 atmosphere are similar and are given in the appendix. The matrix indicator nuclides Cs137 and Sr90 were released in solution to the same extent (at test termination FIAP Cs137: $5{,}83*10^{-2}$; FIAP Sr90: $4{,}52*10^{-2}$) and in a similar fashion as in the test with CO_2 free Ar-atmosphere. Within experimental uncertainty the rates of matrix dissolution were also found the same ($1{,}7*10^{-4}$/d, based on FIAP values of Sr and $2{,}1*10^{-4}$/d, based on FIAP values of Cs and Sb). Again the pH values did not influence the kinetics of matrix dissolution, again Sr retention was observed at pH 11 and again redissolution of retained Sr was observed once the pH was lowered again. The release of plutonium and americium into solution was found to be enhanced in the presence of CO_2 if the pH was below 7 (up to one order of magnitude) during the first 83 (or 80) days of the test. If the pH was shifted up to 11 and back to 7 during the remaining time, no clear dependency of the americium and plutonium concentrations from the CO_2 content of the atmosphere was obvious. This is shown in FIGURE I.1– 4,

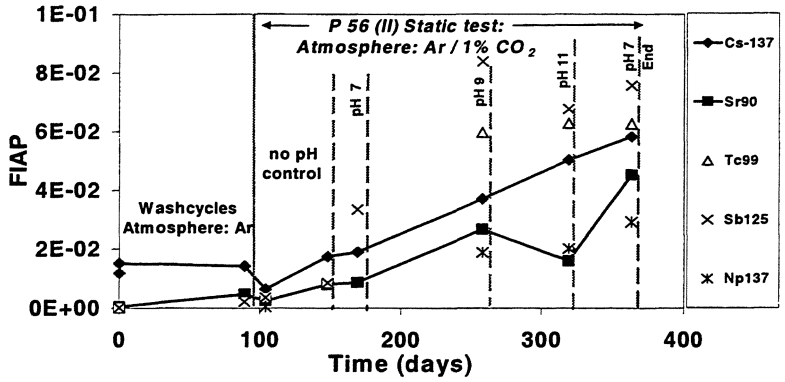

FIGURE I.1-3: Released fractions of matrix bound radionuclides Cs137, Sr90, Np137, Tc99 as a function of time during dissolution of spent fuel powder P56(II) in 5m NaCl solution under Ar/ 1% CO_2-Atmosphere

where the released fractions of plutonium and americium are plotted together with the matrix indicator nuclides Sr90 and Cs137 as a function of time.

Concentrations of Cs, Sr, Am, Pu and Np in solution obtained during the static test are plotted as a function of pH in FIGURE I.1 –5. For comparison solution concentrations of the same radioelements from a corrosion test with spent fuel powder P1 (previous EU-program), when the pH was 6,6 after 40 days and from coprecipitation tests, performed in 5m NaCl-solution and completely dissolved spent fuel (this report ; WP II.2) at pH values of 8 and 8,6 are indicated.

During the first stage of the test, after 14 days, when the pH was 6,02 and after 62 days at pH 6,4 (no pH adjustment) the concentrations were scattering for plutonium and neptunium around $5{,}9*10^{-9}$ Mol/l, and for americium at $3{,}5*10^{-9}$ Mol/l, not very far away from concentrations encountered in spent fuel corrosion tests with powder P 1.

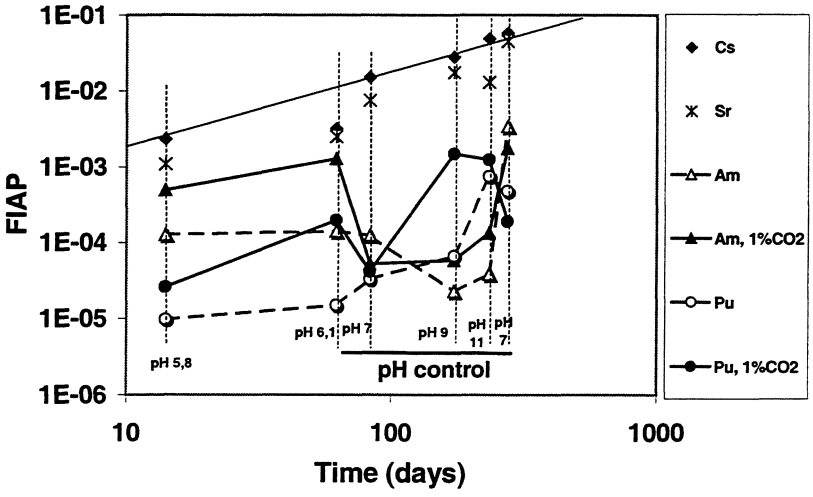

FIGURE I.1-4: Effect of CO_2 on the release of Pu, Am, as a function of time during dissolution of spent fuel powder in 5m NaCl solution

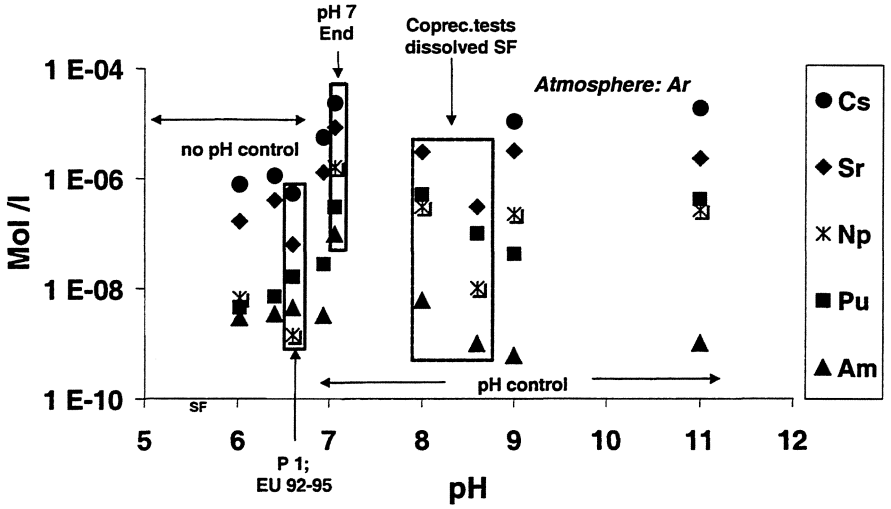

FIGURE I.1-5: Concentrations of radioelements as a function of pH during dissolution of spent fuel powder P56(I) in 5m NaCl solution under Ar-Atmosphere

However, concentrations of matrix indicators Sr and Cs were found to be distinctly lower in corrosion test with powder P 1 (up to one order of magnitude), which might reflect less oxidation of this powder, because this material was inserted immediately in the corrosion test, after the powder preparation was completed.

When the pH was adjusted to 7, 9 and 11 the Sr (Cs) concentration was increasing at first to $1{,}3*10^{-6}$ Mol/l ($5{,}5*10^{-6}$ Mol/l) and remained in this order of magnitude. Concentration of americium decreased from $3*10^{-9}$ to $1*10^{-9}$ Mol/l, whereas concentration of plutonium was at first around $3*10^{-8}$ Mol/l and was increasing surprisingly to $4{,}1*10^{-7}$ Mol/l at pH 11. A fairly good agreement can be observed when comparing concentrations of plutonium and americium at pH 9 obtained during this test with Pu and Am concentrations from coprecipitation tests at pH 8,6 (WP II.2 – this report). Readjustment of the pH back to 7 resulted in distinct higher concentrations of the investigated radionuclides as found when the pH 7 was adjusted for the first time. No clear dependency between the dissolution of the fuel powder and the associated release of radionuclides on the pH was obvious.

The effect of the presence of CO_2 on solution concentrations of Cs, Sr, Am, Pu and Np as a function of pH is shown in FIGURE I.1 – 6 (Ar/0,03% CO_2) and FIGURE I.1 – 7 (Ar/ 1 % CO_2). As expected, during the *first phase* of both tests *(no pH adjustment)*, the pH values were between 5 and 6, distinctly lower than found under CO_2 free Ar-atmosphere (pH between 6 and 6,5). Concentrations of Pu, Am and Np (as far as data are available) were found to be significantly higher (up to one order of magnitude) than under pure Ar atmosphere, but the maximum concentrations were encountered if the amount of CO_2 in the atmosphere was 0,03%. Cs- and Sr concentrations in solution were only slightly increased in comparison to CO_2-free atmosphere. During the *second phase* (the pH was adjusted to 7,9,11 and back to 7) concentrations of Pu (Am) were found to be in the range between $2{,}5*10^{-8}$ ($5*10^{-10}$) and $8*10^{-7}$($8*10^{-8}$) Mol/l, with no clear dependency neither on CO_2 nor on pH.

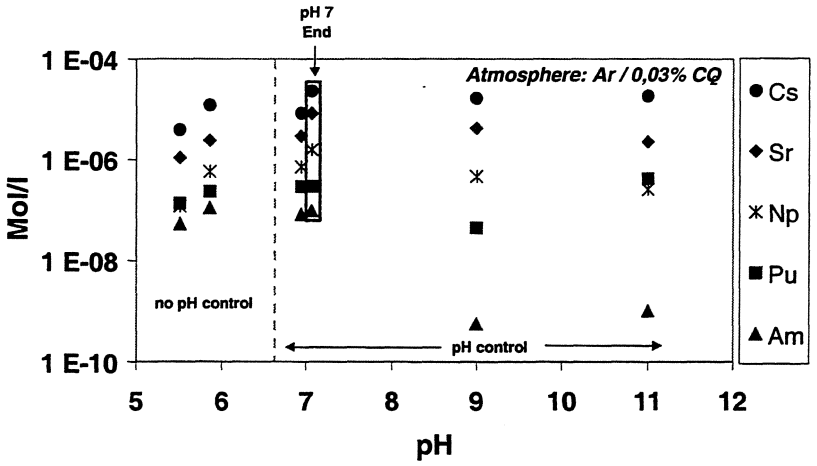

FIGURE I.1-6: Concentrations of radioelements as a function of pH during dissolution of spent fuel powder P56(II) in 5m NaCl solution under Ar / 0,03% CO_2 -Atmosphere

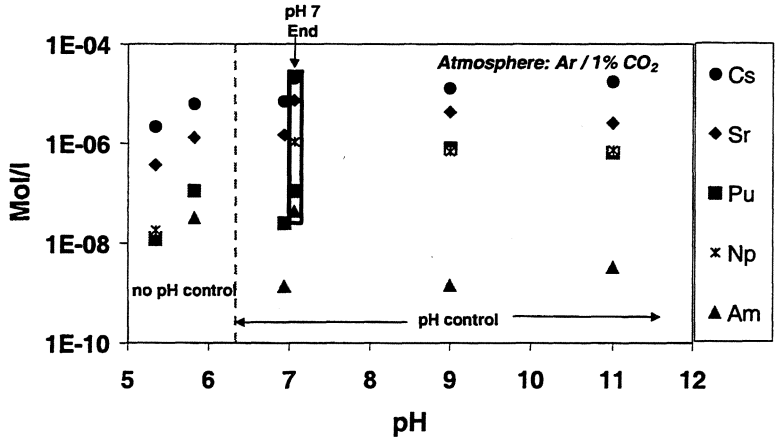

FIGURE I.1-7: Concentrations of radioelements as a function of pH during dissolution of spent fuel powder P56(III) in 5m NaCl solution under Ar / 1 % CO_2 -Atmosphere

A possible explanation might be that the dissolution of powdered spent fuel and the associated release of radionuclides is governed more by effects of radiolysis, production/consumption of radiolysis products rather than by the effect of pH and pCO_2.

WP I.1.2: Comparison of fuel matrix dissolution in salt solution and granite water

In order to allow a direct comparison and to identify potential differences for spent fuel performance in salt and granite environments similar experiments were performed in granite water as in the previous EU-project [12] with NaCl solutions. Important issues addressed are (1) grain boundary inventories of various radionuclides of the fuel used, (2) corrosion rates of the fuel matrix, (3) release of radionuclides from the fuel matrix, (4) generation of colloids during spent fuel dissolution.

The corrosion experiments were performed as in the previous EU-project in gas tight Ti/0.02Pd lined autoclaves equipped with two ball valves for sampling of gases and solutions, and not in quartz vessels as described under I.1.1 for studying the pH and CO_2 dependency. Powdered spent fuel (sample P4: 2,8 g) prepared by the same way and with the same characteristics as described in section I.1.1 was inserted together with 200 ml synthetic equilibrium granite ground water (EGW). Additionally, cladding material (0.7 g), and a metal chip (1.6 g Ti/0.02Pd for analyzing sorption on liner material) were added. This allows investigations of sorbed or precipitated solid particles after the end of the test. The atmosphere in the autoclave was 99,97% Ar and 0,03% CO_2. The experiment was started by a wash cycle of 55 days to remove gap inventories and possibly oxidised surfaces. Afterwards the solution was replaced by a new batch. Sampling of solutions was performed 49, 201 and 545 days since start of the static test. Afterwards the remaining solution was replaced by 200-ml synthetic granite – bentonite ground water (GBW) (see TABLE 1, GROUNDWATERS). Solutions were sampled after 72 and 205 days since replacement of the solutions, respectively 617 and 750 days since start of the static test with granite water. Moreover, during this phase of the test samples of radiolytic and fission gases were taken directly before sampling of solution.

The pH value of the EGW solution was 9,8 after preparation, and shifted to 8.00, 7.96 and 7.21 after 49, 201 and 545 days since start of the static test. Measured values of Eh were 178 mV (initial), 214 mV, 128 mV, and 171 mV by the same order. The GBW solution was characterized by pH values of 7.61 as prepared, and 7.42, 7.38 after 72 days of leaching, respectively 205 days after the replacement (end of the test). Measured Eh values were 238 mV initially, and 70 mV at the end of the test.

Using an evacuated (10^{-6} bar) gas collection cylinder (V=50 cm^3), the atmosphere inside of the reaction vessels was sampled. The gas collection vessel was connected to the autoclaves by stainless steel tubing. Prior to opening the valves of the autoclave and the gas collection vessel, the tubing was evacuated for about 5 minutes by a pump (ca. 1 mbar). Gas composition was analyzed quantitatively by a quadrupole mass spectrometer (GAM 445, Balzers, Lichtenstein). Calibration was performed, using a gas mixture of known amounts of H_2, N_2, O_2, Kr and Xe in Ar.

In order to protect the experiment against air intrusion, the autoclaves were inserted into gas-tight canisters, which were filled with Ar/0,03% CO_2 before sealing. Solution samples were all filtered through a microfilter (45 µm) and in part through an ultrafiltration membrane (18 Å) by means of centrifugation. Filtered aliquots were acidified with 1m HNO_3 to stabilize the radionuclides in solution. Further preparation of the solutions and radiochemical analyses was performed as described in detail in the final report of the previous EU-programme [97GRA/LOI].

At the end of the test the corroded spent fuel powder was dried and a few particles were isolated and fixed on a double-side coated carbon tape, which was fixed on a brass disc. The dose rate was around 10 µSv, which was low enough to perform investigations by means of SEM, outside of the shielded boxes.

Dissolution behaviour of the matrix and release of radionuclides

The fractions of inventories of Cs, Sr, Tc, Np, Am, Eu, Pu and U found in solution during the contact with EGW granite water and GBW granite bentonite water are shown in FIGURE I.1 – 8 as a function of time. During the test in granite water it seems that the matrix dissolves congruently, expressed by FIAP values around $1*10^{-3}$ for most of the matrix bound radionuclides (FIAP between $3,4*10^{-4}$ [U] and $2,4*10^{-3}$ [Pu];exception Cs: FIAP $1,5*10^{-2}$ and Tc: FIAP $5,8*10^{-2}$;). The fastest release of Sr, Np, Tc and Cs in solution occurred during the first 50 days of the static test. Afterwards only small fractions of these radionuclides were released additionally. In particular the last interval of 344 days is characterized by constant FIAP values.

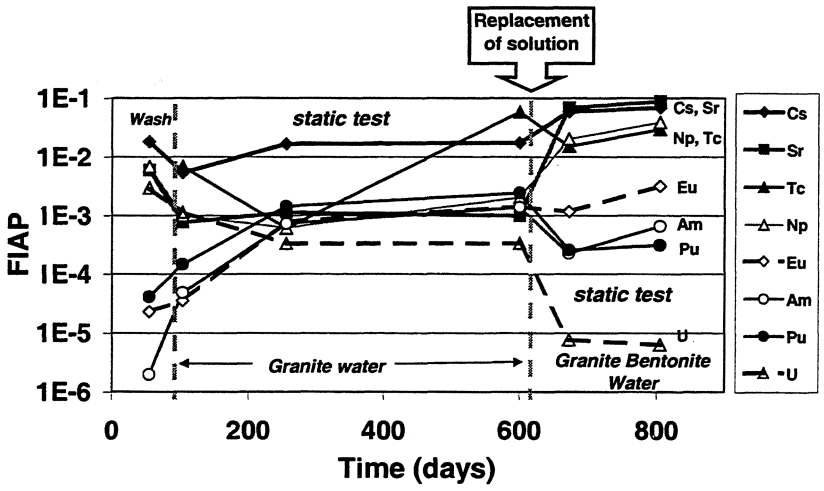

FIGURE I.1 – 8: Fractions of the inventory of radioelements in solution during corrosion of spent fuel powder in granite and granite bentonite water.

After 545 days since start of the static test the water was replaced by granite-bentonite – water (GBW, ENREAS/CIEMAT specification). The main characteristics of GBW-water are a much higher salinity, and sulfate content, whereas CEA-granite water contains much more Si. HCO_3 contents and pH are similar. Sampling of solutions and of gases was performed 72 and 133 days after the replacement. The fractional release rates of Sr90, Cs137 and Np237 increased dramatically. The fraction of Sr90 in solution increased by a factor of 100. Final solution concentrations were at$1*10^{-5}$ m (pH 7,3). Similar fractional release of Cs137, Tc99, Np137 and Sr90 at test termination indicates release control by congruent fuel matrix dissolution without significant grain boundary contributions. Released fractions of Eu, Am, Pu and U were found to be between 1 and 4 orders of magnitude lower than Cs and Sr.

Analysis of fission (Kr,Xe) and radiolytic gases (H_2, O_2) has shown that also Xe and Kr releases during corrosion in granite bentonite (GBW) water are controlled by matrix dissolution. When comparing to O_2 generation, there was a deficit in O_2 contents of the gas phase. This deficit was equal to the extent of fuel matrix dissolution. Consequently, this O_2 deficit is consumed by oxidative fuel dissolution. There is good agreement between oxygen consumption rate and release rates of fission gases. This is illustrated in FIGURE I.1 – 9 where the fractional release rates of Sr, Cs, Tc and Np into solution are compared with the rates of fission gas release and of oxygen consumption.

The fast rise in release rates after changing EGW to GBW-water allow a better understanding of the behaviour of Cs and Sr in EGW water. In this medium and for the conditions of this test, Sr is no indicator for the fuel matrix dissolution, but is retained in solid phases or is sorbed on surfaces (fuel, liner). Redissolution of this phase or desorption in GBW-water explains the extremely high Sr-release rate. Redissolution is not substantiated

by high U-concentrations in GBW-water (with 10^{-6} –10^{-7} m U-concentrations are lower than in CEA-granite water) but by the fact that fractional Sr-release rates of the 72 days leachate are much higher than those of Cs and of Oxygen consumption and that all release values are equal at test termination.

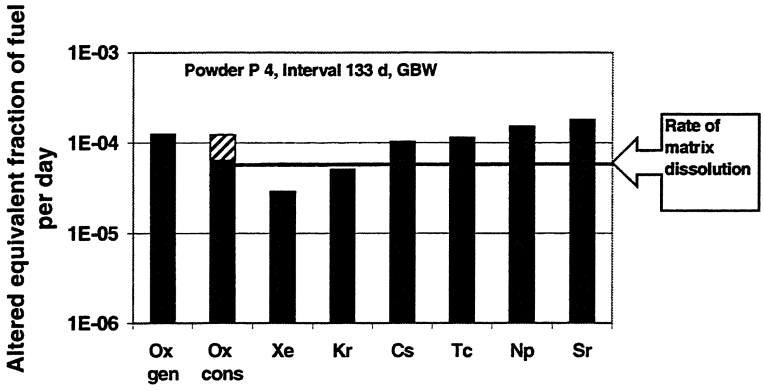

FIGURE I.1 – 9: Comparison of fractional release rates of radionuclides, fission gases and oxygen co water.

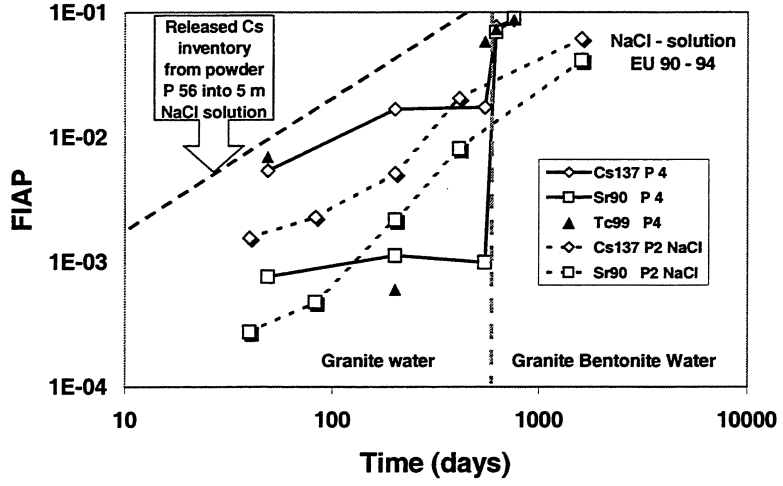

FIGURE I.1 – 10: Comparison of spent fuel powder corrosion data in salt and two granite media. Diagonal for NaCl-media (this project) indicates test P56 with probably oxidised powder

As indicated by Tc data located after 600 days on the diagonal, matrix dissolution continues with constant rates even in EGW-water. Hence, decrease in Cs-release rates during long-term exposure to EGW-water indicates that also Cs becomes incorporated into a solid phase. All alkali earth sulfate (e.g. $CaSO_4$) and carbonate phases (e.g. calcite) are undersaturated in both waters (pH 7 – 7,5). May be Sr (and Cs) become incorporated into uranyl silicate phases. Redissolution would thus be a consequence of U(VI) phase transformations caused by the lower silica content of GBW water. A conclusion is that the dissolution rates of the fuel are equal in both types of granite water, but lower Sr and Cs-concentrations are due to sorption or secondary phase formation. Dissolution rates are similar to the initial rates in EGW-granite water and similar to those in NaCl-solution at various pH and pCO_2. This is illustrated in FIGURE I.1 – 10 where the released fractions of Sr90, Cs137 and Tc99 are shown as a function of time, obtained with powder P4 in granite water, in granite-bentonite water, with powder P 56 in NaCl-solution (see WP I.1.1) and with powder P 2 in NaCl-solution (previous EU project, [97GRA/LOI]). Higher Sr and Cs release rates in the test with powder P56 in NaCl solution in comparison to results from test with powder P 2 may be explained with probably oxidation during > 4 years of storage before start of the test (Spent fuel powder P 2 was immediately inserted into the corrosion experiment).

We can conclude that the dissolution rates of the fuel matrix are (1) equal in both types of granite water, but lower Cs concentrations are due to secondary phase formations and (2) that they are not very different than found in NaCl-solutions.

Concentration of radioelements in solution and formation of colloids

During the first phase of the corrosion test (granite water, EGW) solution concentrations were found to be up to $1,5*10^{-6}$ mol/l (Plutonium), $5,4*10^{-5}$ mol/l (Uranium), 2,5 - $3,6*10^{-8}$ mol/l (Europium, Americium), which is roughly one or two orders of magnitude higher than found in tests in NaCl-solution at the same pH. Due to rapid dissolution of the fuel matrix, high solution concentrations, low ionic strength of the leachant colloids are present to a large extent. The importance of the presence/absence of colloids in the system is substantiated that they represent the possibly mobile fraction in the corrosion solution. The extent of colloid generation has been determined by ultrafiltrating solution aliquots. The difference of both fractions may be attributed to colloid formation. However, also radionuclide sorption on filter membranes may cause some differences in the solution concentrations of radionuclides between the original and the filtrate solution. Consequently, differences between FIAP and FIS (fraction in solution) values give only upper values for colloid formation. In contrast to NaCl-media where almost no formation of colloids have been detected (previous EU-program, [97GRA/LOI]), colloids are present to a large extent in the experiments with granite water. Differences of two orders of magnitude or more between FIAP- and FIS value were determined for Am, Cm, Pu, Eu and Ce. Np and U reveal a minor, but still significant difference of both fractions. The extent of colloid formation increased with time. After 545 days since start of the static test about 96 % of the U and 99% of Pu, Am, and Eu in solution was colloidal. Almost no colloid formation was observed with Ru, Cs, Sr and Tc. The evaluation of Am-, Pu- and U colloid formation can be assessed from FIGURE I.1 – 11 where the concentrations of Am, Pu and U in solution in the micro(0,45µm) and the ultra-filtrated (18 Å) aliquots are plotted as a function of time.

After the replacement of the solution by higher ionic strength granite-bentonite groundwater the solution concentrations of these elements were generally lower, and their concentration in the micro- and the ultrafiltrated aliquots were in the same order of magnitude, which means that under the changed conditions the amount of colloids was decreased drastically. This behaviour is expected, because high ionic strength lead to decreased stability of colloidal suspensions.

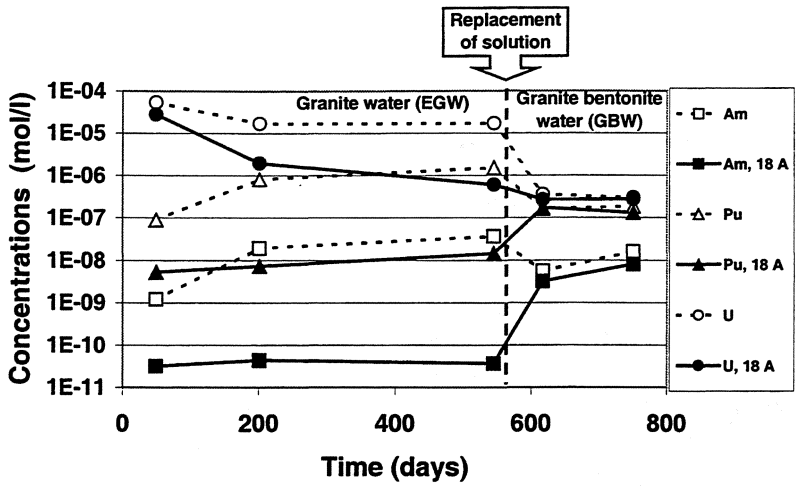

FIGURE I.1 – 11: Concentrations of Am, Pu and U in 0,45 µm and 18 A filtered aliquots during static spent fuel powder corrosion in granite and granite bentonite ground water.

Characterization of solid phases

At the end of the test after totally 805 days of corrosion in EGW granite water, respectively GBW granite-bentonite water (including the wash cycle) some particles of the corroded spent fuel powder were investigated by means of scanning electron microscopy (SEM). In FIGURE I.1 – 12 SEM micrographs from particles separated from corroded spent fuel powder P 4 are shown. The micrograph on the left gives an impression of the size of the individual particles which was found to be varying from 3-4 µm to less than 1 µm. In the image on the right the spent fuel particles are shown, and additionally a newly formed secondary phase is present. On the marked position "J" Uranium, Silicon and Oxygen was found qualitatively by means of EDX analyses, which could indicate the formation of a U-silicate.

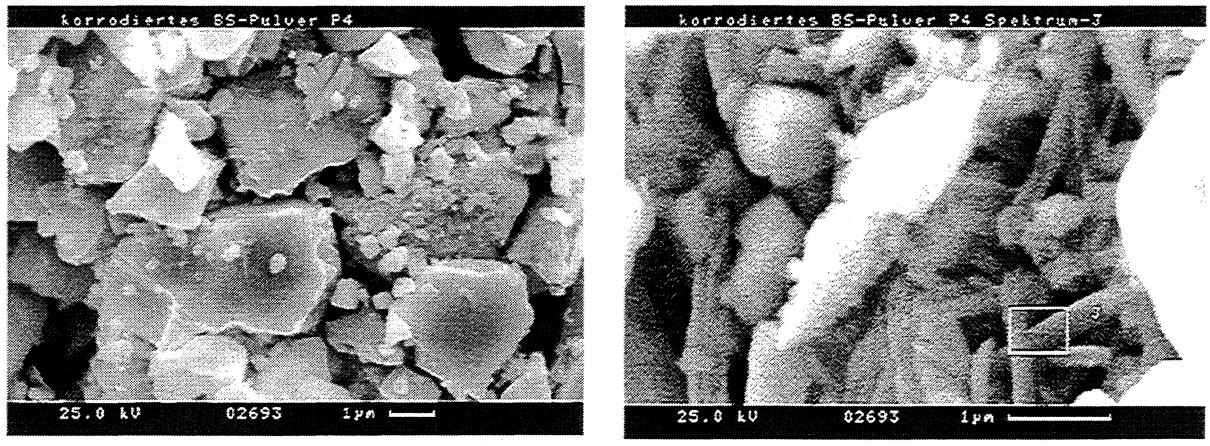

FIGURE I.1 – 12: Spent fuel particles from powder P4 after corrosion over 805 days first in EGW granite water and then in GBW granite bentonite water under Ar / 0,03 %CO_2 atmosphere at 25°C. At position "J" U, Si and O were found by EDX analyses.

WP I.2 SPENT FUEL SURFACE AREA DETERMINATION

Results are discussed in section "SOLID PHASE CHARACTERIZATION" above

WP I.3 LEACH TESTS ON DEFECTIVE RODLETS OF IRRADIATED FUELS

In case of water access to the waste radionuclides may become released from spent fuel by dissolution and transport by groundwater flow [95GRA/WIL]. The cladding will be the last barrier before the water comes into contact with the fuel, namely with the outer RIM of the pellet. In safety analyses, the cladding is seldom considered as a protective barrier, mechanical failure is assumed and fuel leaching is assumed to start as soon as the water has entered the waste container. However, even if the fuel rod is defect, it is still not dissolved immediately and may indeed last for thousands of years. If groundwater penetrates inside of the fuel rod through a defect, S/V ratios of porous UO_2 are high. The relative importance of α-radiolysis is increased due to an increased inventory of α-emitters as a consequence of increased epithermal neutron capture in the outer pellet zone. To study these effects, different spent fuel rodlets (including MOX and UO_2 fuels with varying burn-up) with preset defects on the cladding were leached in the present study (for fuel description see TABLES 4 to 8 in SOLID PHASE CHARACTERIZATION).

One UO_2 fuel rod with a burn-up of 50 GWd/tU (sample 1-551-2-5) was provided with two series of defects (in each case, 3 holes of 1 mm diameter), one series at the top and in contact with vapor and the other at the bottom of the rodlet and in contact with the leaching solution. In all the other samples, the defects were placed in the center of the rodlet and the autoclave was filled completely with the leaching solution.

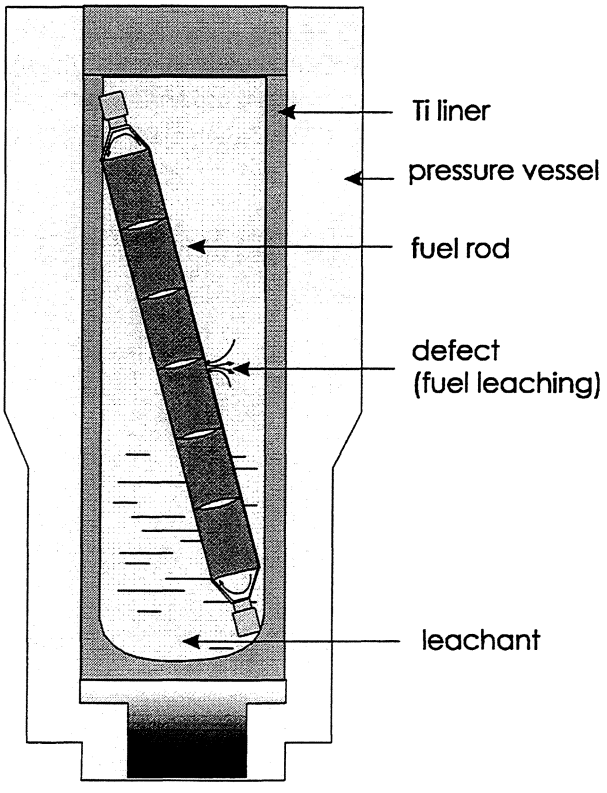

FIGURE I.3.1: Schematic representation of the experimental set-up (leaching of fuel rod, 1 defect immersed).

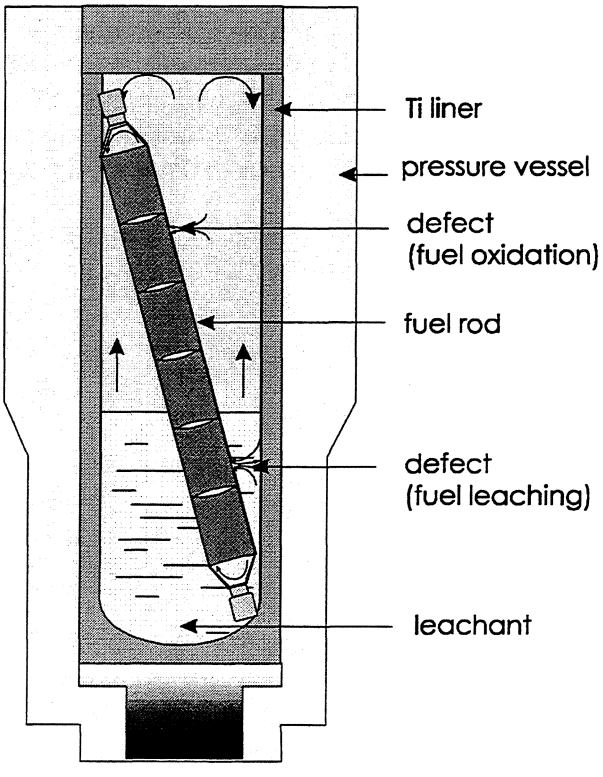

FIGURE I.3.2: Schematic representation of the experimental set-up (leaching of fuel rod, 2 defects, 1 immersed, and 1 in vapor phase).

The leaching was carried out in autoclaves with Ti-liners using deionized water at 100°C under anoxic or reducing conditions. Large metal surfaces, i.e. titanium (autoclave liners), Zircaloy (cladding) and stainless steel (end-caps) could be efficient scavengers of oxidising species. In FIGURES I.3.1 and I.3.2 schematic representations of the experimental set-up are shown. A picture of the rodlet can be seen in FIGURE I.3.3.

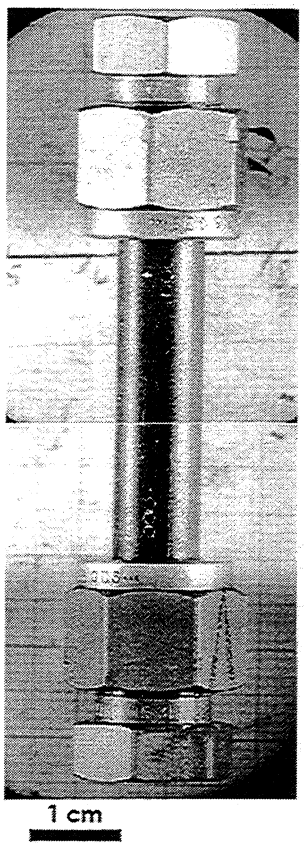

FIGURE. I.3.3: Photograph of the spent fuel rodlet with 2 pre-set defects

The released amounts of radionuclides were measured by ICP-MS using a Perking Elmer Elan 250, with sensitivity between 1 and 10 ng/ml. The analysis of the samples by this technique was carried out after the addition of two internal standards (1 µg/ml of indium and 1 µg/ml ppm of thorium). The pH of the samples was measured by means of a Combined pH Electrode (Metrohm).

Radionuclide release

The results obtained for the different elements are shown in the appendix . FIGURE I.3.4 show the evolution of the concentration of uranium, plutonium, cesium, iodine and strontium in solution with time for MOX (25 GWd/tU) and UO_2 (50 GWd/tU) fuels. The behaviour is very similar in both fuels, with an initial fast dissolution followed by a much slower long-term dissolution. Iodine shows a slightly different behaviour, i.e. after a fast initial dissolution there is a second increase of the iodine concentration in solution (up to 50 days) before the slow dissolution rate is observed.

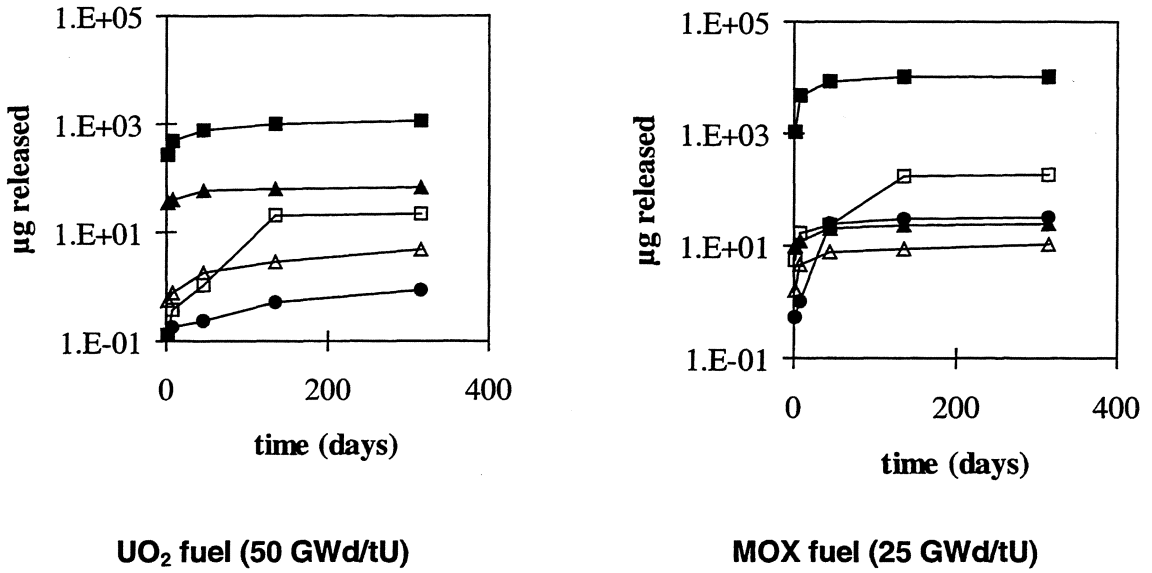

UO_2 fuel (50 GWd/tU) **MOX fuel (25 GWd/tU)**

FIGURE I.3.4: Release of the different radionuclides studied (in µg) for both types of fuels. ■ cesium, ▲uranium, iodine, Δ strontium and ● plutonium

Except for uranium, the release is higher in the case of MOX fuels, one order of magnitude for fission products and almost two for plutonium, despite a burn-up which is only half that of UO_2. FIGURE I.3.5 shows a comparison of uranium release data of different fuels.

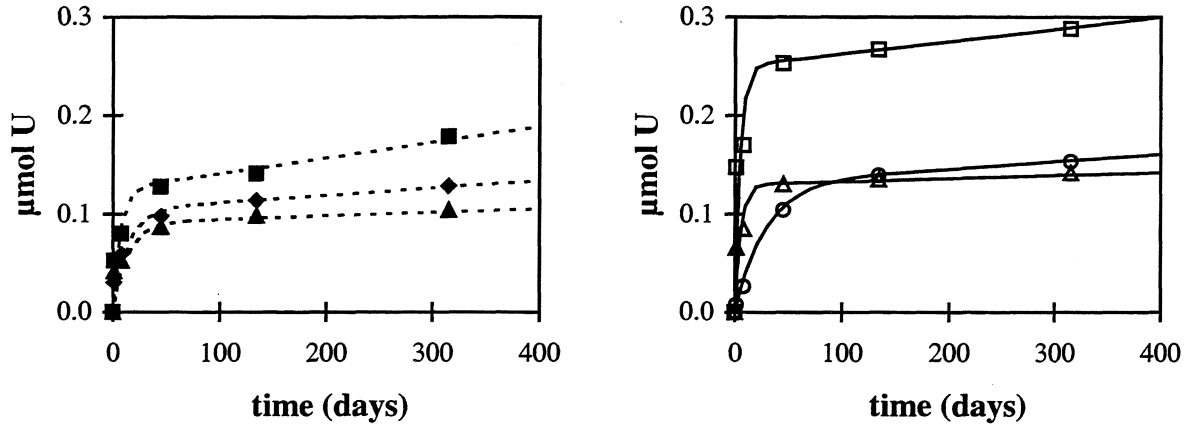

MOX fuels UO_2 fuels

FIGURE I.3.5: Comparison of experimental data for uranium release from the different fuels. ◆ MOX fuel (12 GWd/tU), ■ MOX fuel (20 GWd/tU), ▲ MOX fuel (25 GWd/tU), Δ UO_2 fuel (30 GWd/tU), □ UO_2 fuel (50 GWd/tU) and O UO_2 fuel (50 GWd/tU with two series of defects).

Respective data for plutonium, cesium and strontium are shown in FIGURE I.3.6.

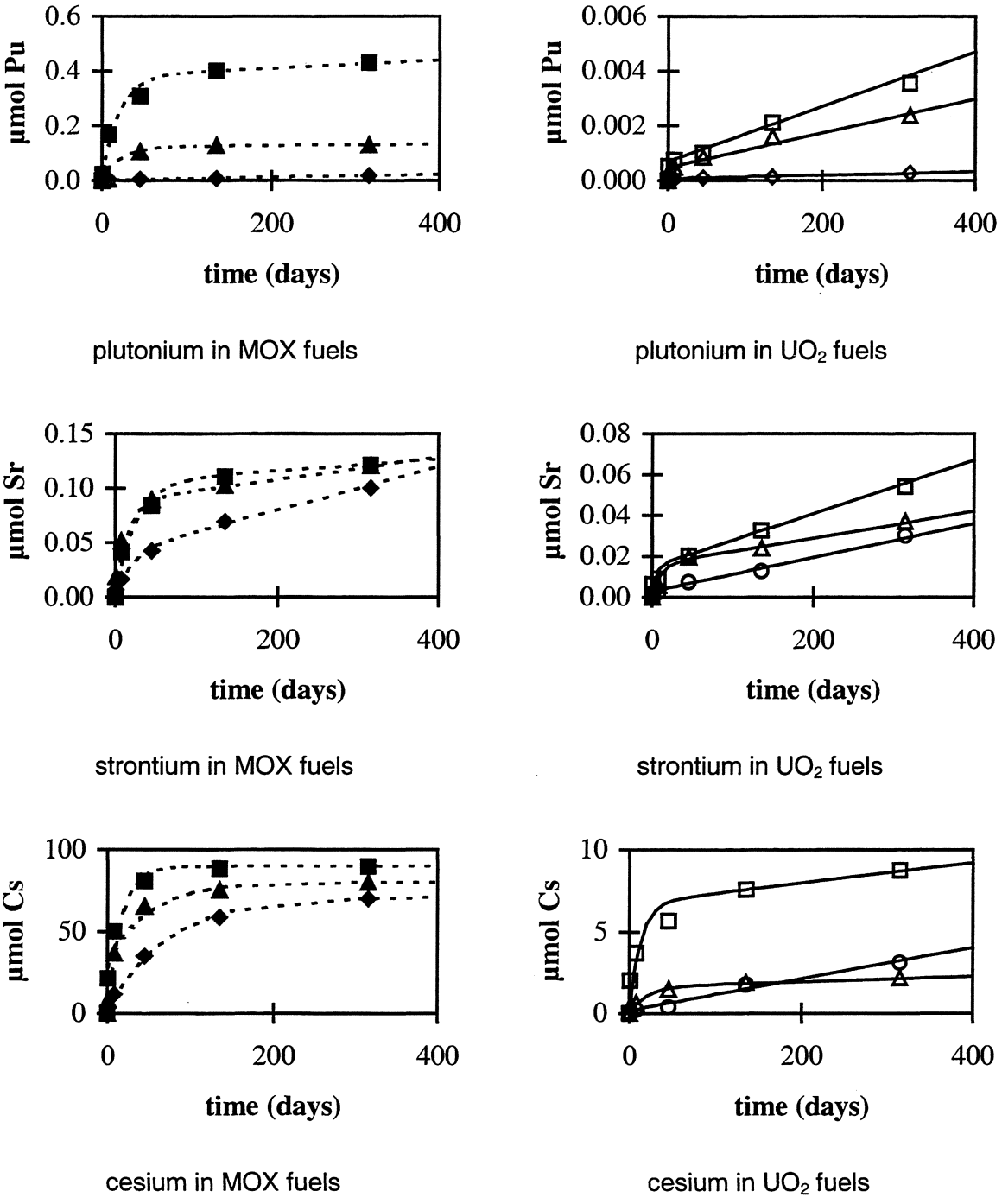

FIGURE I.3.6: Comparison of experimental data for plutonium, strontium and cesium. ◆ MOX fuel (12 GWd/tU), ■ MOX fuel (20 GWd/tU), ▲ MOX fuel (25 GWd/tU), Δ UO_2 fuel (30 GWd/tU), UO_2 fuel (50 GWd/tU) and O UO_2 fuel (50 GWd/tU with two series of defects).

Fraction of Inventory in the Aqueous Phase (FIAP)

FIAP values were calculated taking into account the specific elemental mass inventory of the fuels obtained by means of the ORIGEN code [96COQ/BOT]. The values obtained for uranium are shown in FIGURE I.3.7.

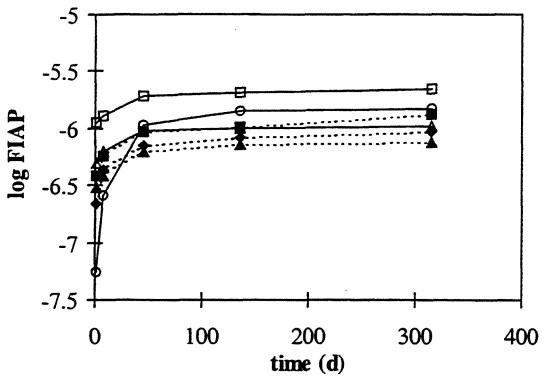

FIGURE. I.3.7: FIAP values for uranium.◆ MOX fuel (12 GWd/tU), ■ MOX fuel (20 GWd/tU), ▲MOX fuel (25 GWd/tU), ΔUO_2 fuel (30 GWd/tU), UO_2 fuel (50 GWd/tU) and O UO_2 fuel (50 GWd/tU with two series of defects)

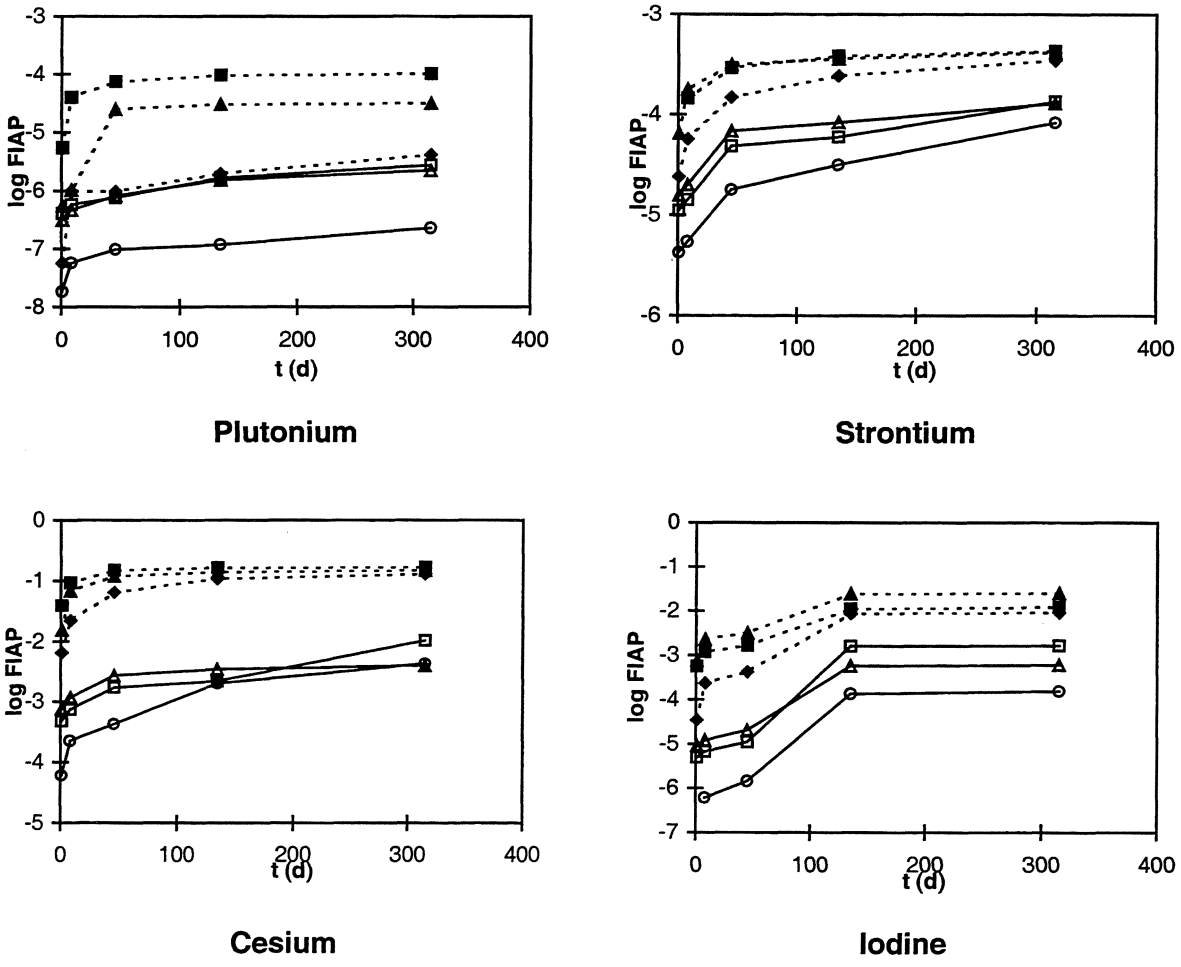

FIGURE I.3.8: FIAP values for Pu, Sr, Cs and I. ◆ MOX fuel (12 GWd/tU), ■ MOX fuel (20 GWd/tU), ▲MOX fuel (25 GWd/tU), ΔUO_2 fuel (30 GWd/tU), UO_2 fuel (50 GWd/tU) and O UO_2 fuel (50 GWd/tU with two series of defects).

The FIAP values after 315 days are similar for all the fuels and almost independent on the burn-up and type of fuel. The slightly higher FIAP value for the high burn-up UO_2 is due to a higher initial dissolution of oxidised UO_2 and could be related to a higher inventory of α-emitters in the RIM zone produced by epithermal neutron capture. The increased radiation dose could have led to an increased oxidation of the surface. FIAP values for plutonium, strontium, cesium and iodine are shown in FIGURE I.3.8. As it can be seen, for all the radionuclides the FIAP values are always about two orders of magnitude higher for MOX than for UO_2 fuels.

These values are in good agreement with literature data in similar experiments on UO_2 fuel rods by Wilson and Oversby [85WIL/OVE] and on CANDU UO_2 by Stroes-Gascoyne et al. [89STR/JOH] For the differences observed between UO_2 and MOX several explanations are possible:

- a lower burn-up of MOX and consequently a larger gap between fuel and cladding, i.e. a larger surface in contact with water
- the special structure of MOX with agglomerates containing 20 % of plutonium (fissile material) incorporated in natural UO_2 upon irradiation. This structure leads to:
    - a concentration of fission events in the agglomerates (>200 GWd/tU) and release of volatile fission products (cesium, iodine).
    - Strong neutrons capture by depleted uranium in the outer periphery leading to an increased inventory of fission products and plutonium.

Comparison with results obtained by Serrano et al. [98SER/GLA] on particles from the center of fuel pellet shows a significantly higher release of cesium, strontium and plutonium for both MOX and UO_2 fuels in our experiments. This difference can again be attributed to the higher inventory of these elements in the RIM zone [96WAL/GOL, 96SPI/VEN].

Especially the high plutonium release could also be due to galvanic effect, which could increase the dissolution of the two-phase material.

Long-term oxidative dissolution

The long-term oxidative fuel dissolution rates, normalized to the surface area, were calculated both from uranium data and from strontium data as potential indicator element for fuel matrix dissolution. For this normalization the specific surface area measured by the BET method for pellets of unirradiated uranium dioxide [96GIM/BAR], of $1.9\ 10^{-4}\ m^2 \cdot g^{-1}$ was used. It can be considered that this is a conservative value, assuming that spent fuel has a higher surface area at the fuel-pellet interface due to the formation of cracks and fissures in the pellet with a contribution from the highly porous micrograin structure.

The values obtained which represent the long-term oxidative dissolution are presented in TABLE I.3-1. Fractional release rates (FIAP/d) are given in TABLE I.3-2.

TABLE 1.3-1: Dissolution rates (in mg (fuel)m^{-2} d^{-1}).

	MOX 12	MOX 20	MOX 25	UO2 30	UO2 50
Uranium	$2.61\ 10^{-3}$	$5.56\ 10^{-3}$	$1.22\ 10^{-3}$	$1.04\ 10^{-3}$	$4.17\ 10^{-3}$
Strontium	0.90	0.25	0.47	0.11	0.15

TABLE 1.3-2: Fractional long-term fuel dissolution rates (FIAP d^{-1}).

	MOX 12	MOX 20	MOX 25	UO2 30	UO2 50
Uranium	$5.4\ 10^{-9}$	$14{\cdot}10^{-9}$	$1.9{\cdot}10^{-9}$	$2.2{\cdot}10^{-9}$	$7.3{\cdot}10^{-9}$
Strontium	$15{\cdot}10^{-7}$	$5{\cdot}10^{-7}$	$9{\cdot}10^{-7}$	$2.2{\cdot}10^{-7}$	$2.5{\cdot}10^{-7}$
Cesium	$11\ 10^{-5}$	$1.2{\cdot}10^{-5}$	$4.0{\cdot}10^{-5}$	$0.2{\cdot}10^{-5}$	$1{\cdot}10^{-5}$
Iodine	$3.2\ 10^{-6}$	$4.8{\cdot}10^{-6}$	$6.9{\cdot}10^{-6}$	$0.2{\cdot}10^{-6}$	$0.2{\cdot}10^{-6}$
Plutonium	$6.6\ 10^{-9}$	$22{\cdot}10^{-9}$	$3{\cdot}10^{-9}$	$3.5{\cdot}10^{-9}$	$5.2{\cdot}10^{-9}$

As expected, the long term fuel dissolution rates are quite similar for both types of fuel.

In order to assess the barrier function of the cladding on fuel dissolution, results of the present project with high burnup UOX fuel (sample UO250) are compared in FIGURE I.3-9 with respective dissolution results of decladded high burnup spent fuel in deionized water (samples K1 and K2), as observed in the previous EC-project [97GRA/LOI] . Burnups of the two fuels were similar with about 50 MWd/kg_{HM}. Tests were also similar (static, deionized water, 25°C). In the test with decladded fuel, the instant release fraction was washed off prior to starting the static test. In FIGURE I.3-9 the cumulative release fractions (fraction of inventory in wash solutions + fractions of inventory in static test) are compared with results obtained only in the static test.

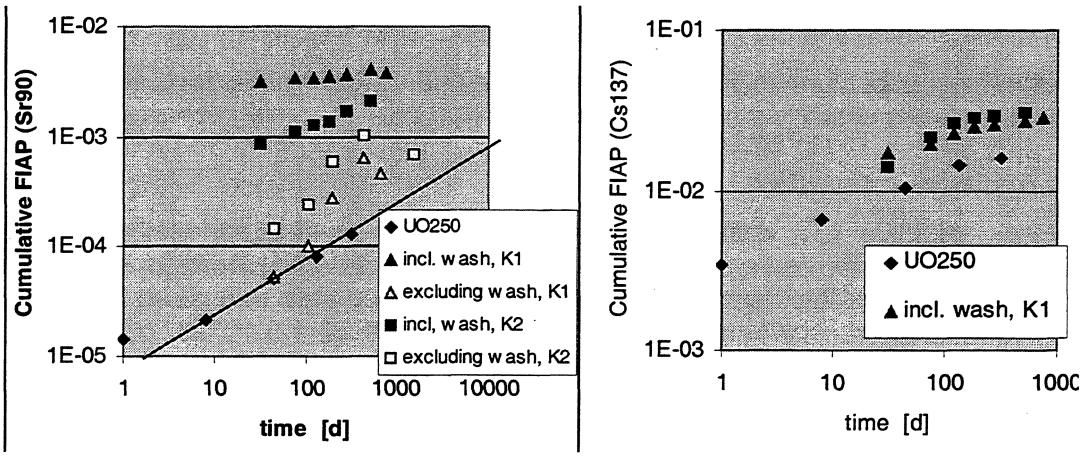

FIGURE I.3-9. Comparison of cumulative release fractions of Cs137 and Sr90 from decladded and non-decladded (preset defects) high burnup spent UOX fuel (ca. 50 MWd/kg_{HM}) in deionized water.

The results show a significant higher cummulative release of Sr90 from decladded fuel when compared with non-decladded fuels with preset defects. The results only resemble each other if the washed off fraction is not taken into consideration. In contrast to Sr, results for Cs are verly similar in both experiments. The similarity in Cs-results indicates that a cladding with deffects is not expected to be an efficient diffusion barrier for retarding instant release of Cs135 or I129.

Conclusions

The present study on defect UO_2 and MOX fuel rods simulating water intrusion into the fuel pin in case of cladding failure shows that the dissolution process can be described by a two-step process with a fast initial dissolution possibly associated to an oxidised layer on the pellet surface, followed by oxidative matrix dissolution.

The FIAP values representing the fast initial dissolution show that the uranium release is almost the same for UO_2 and MOX fuels. Higher release rates and cumulative release values for Cs, I, Pu and Sr in MOX fuels compared to UO_2 fuels are due to the special two-phase structure of MOX fuel leading to an increased inventory at the pellet periphery, i.e. the surface in contact with the leachant. Especially high FIAP values were found for cesium and iodine. This is considered to be due to a migration of these radionuclides to the grain boundaries in the RIM zone of the pellet upon irradiation.

The long-term dissolution rates of UOX and MOX fuels seems to approach each other, both indicated by uranium release rates and apparent matrix corrosion rates (based on Sr-data). U-data seems to indicate an increase of release rates with burnup, however, this was not confirmed by the fractional dissolution rates of Sr.

Detailed examination of the leached samples by EPMA, optical and electron microscopy should help to better understand ongoing processes during the dissolution process including the definition of the surface in contact with water or the formation of secondary phases during the leaching process.

WP I.4 DISSOLUTION OF UNIRRADIATED UO_2 AND SIMFUEL

For mechanistic understanding and comparison dissolution experiments with unirradiated UO_2 pellets and powders were performed both in granite and clay groundwaters. Experiments were performed under oxic, anoxic and reducing conditions.

Under reducing conditions normally prevailing in deep granite groundwater, UO_2 (or U_4O_9), the main component of the spent fuel, is the stable uranium solid and has a very low solubility or dissolution rate. Under disposal conditions the stability of spent fuel depends on the near-field chemical conditions, the effects of radiolysis (α), canister materials (steel, copper) and their corrosion products, backfill materials (bentonite) and the composition of the groundwater. The dissolution rate of UO_2 is strongly affected by the redox conditions, especially by the availability and the nature of oxidants from α-radiolysis. The composition of groundwater, which will come into contact with spent fuel, depends on the geological formation and, if present , on the interactions with bentonite. The presence of Si and Ca in groundwater has been observed to affect the dissolution rate of unirradiated UO_2. [95GRA/WILL] showed that the addition of Si and Ca to a bicarbonate solution could reduce the dissolution rate up to 100 times.

WP I.4.1 Dissolution rates and solubility of unirradiated UO_2 fuel in synthetic Granite and Granite Bentonite groundwater

Under normally prevailing reducing conditions in deep granite groundwater, UO_2 (or U_4O_9), the main matrix component of the spent fuel, has a very low solubility or dissolution rate. Under disposal conditions the stability of spent fuel depends on the chemical near-field conditions, the effects of radiolysis, canister materials (steel, copper) and their corrosion products, backfill materials (bentonite) and the composition of the groundwater. The dissolution rate of UO_2 is strongly affected by the redox conditions, especially by the availability and the nature of oxidants from α-radiolysis. The composition of granite groundwater, which will come into contact with spent fuel, depends on the geological formation and, if present, on the interactions with bentonite. The presence of Si and Ca in groundwater has been observed to affect the dissolution rate of unirradiated UO_2. [95GRA/WILL] showed that the addition of Si and Ca to a bicarbonate solution could reduce the dissolution rate up to 100 times.

This chapter presents the results obtained from static dissolution/solubility experiments of unirradiated UO_2 pellets and UO_2 powder in various synthetic groundwaters (compositions: Appendix 1, Table 1). The main objective of the dissolution experiments was to determine maximum solution concentrations of uranium and on secondary alteration products that possibly control the uranium concentration in solution. Additionally, under oxidizing conditions, dissolution rates were determined. The solubility under anoxic conditions was also approached from oversaturation by precipitation experiments (WP IV.2).

Redox conditions included oxidizing (air-saturated), anaerobic (N_2, $O_2 < 1$ ppm) and reducing (N_2, low Eh) environment. The low Eh conditions were maintained by the addition of reducing species, S(-II), Fe(+II) or metallic Fe, to synthetic groundwater prior to the start of the experiments.

Procedure of UO_2 dissolution tests at VTT

The method of the dissolution experiments was, both under oxic and anoxic conditions, a static batch dissolution procedure. UO_2 pellets or a UO_2 powder was immersed in equilibrated synthetic groundwater in polyethylene bottles. The ratio of UO_2 surface area to

water volume (S/V) is 0.66...19.8 m^{-1} (geometric surface area) in the experiments with pellets, and 1000 m^{-1} (specific surface area by BET) in the experiments with powder. Small aliquots (0.5...2 ml) were periodically taken for analysis of dissolved uranium. These aliquots were replaced with fresh water, which had a similar composition, in order to keep the water volume the same. The amounts of uranium in unfiltered, microfiltered (membranes of 0.45 μm, selected samplings) and ultrafiltered (nominal cut-off value of 50 000 M, selected samplings) samples were measured as a function of time.

The synthetic groundwaters were allowed to equilibrate after preparation for at least one week. The pH was readjusted if necessary. The redox species were added to the equilibrated groundwaters from stock solutions ($Na_2S \cdot 9H_2O$ or $FeCl_2 \cdot 4H_2O$ in deionized water) in the glove box. The synthetic groundwaters with S(-II) or Fe(+II) were allowed to stabilize for a couple of weeks after the addition of reducing species. The experimental conditions of the dissolution experiments with UO_2 pellets and UO_2 powder performed in oxic and anoxic conditions are listed in Appendix 4, TABLES 2-4, respectively.

Prior to the start of the dissolution experiments, oxidised surface layers were removed by predissolution of the pellets. The selected groundwater was changed every two days for 2 weeks. The amount of uranium released into the water phase per day was measured. The dissolution rate of U decreased during this predissolution period by 1-1.5 orders of magnitude (see FIGURE I.4.1 of anaerobic saline groundwater). The rates were calculated per specific surface area, which was based on the BET determination made by Universitat Politecnica de Catalunya (UPC) [97PAB].

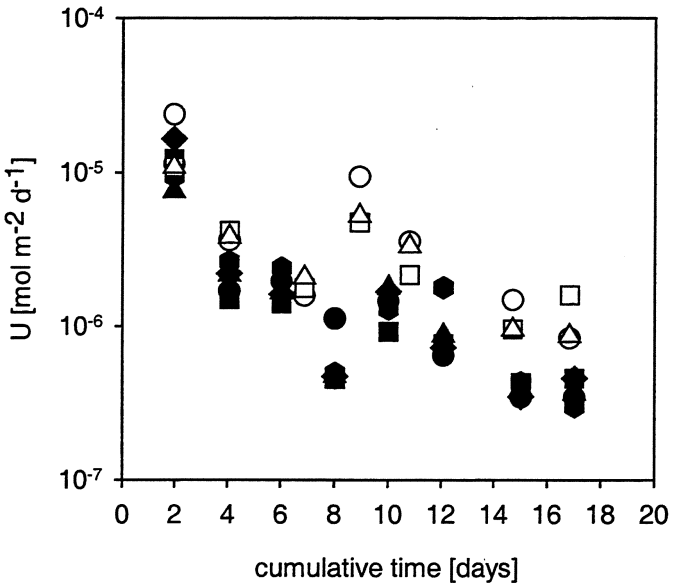

FIGURE I.4-1. Dissolution rates of uranium from UO_2 pellets during the predissolution period in saline groundwater under anaerobic conditions (N_2) (filled symbols: S/V= 6.6 m^{-1}, open symbols: S/V= 19.8 m^{-1}).

Solution concentrations of U under oxidizing conditions

Under oxidizing conditions, UO_2 is not thermodynamically stable. The oxidation of UO_2 leads to the formation of progressively higher oxidation states of surface layer with a composition of UO_{2+x}, where $0 \leq x \leq 1$. The UO_2/UO_{2+x} matrix is unlikely to achieve a solubility limit. The system will evolve to form thermodynamically stable secondary phases controlling U(VI) concentrations in solution. The composition of these alteration products depends on the composition of groundwater. Several parallel dissolution tests with UO_2 powder (S/V= 1000 m^{-1}) and UO_2 pellets (S/V= 0.66, 1.98 and 19.8 m^{-1}) were initiated under oxic conditions in order to study the solid phases at the different stages of dissolution. UO_2 powder was allowed to be in contact with synthetic groundwater for different time periods. The solid phases were analyzed at the end of the periods. In one experiment in each of the groundwaters, the evolution of the uranium concentration was followed vs. contact time. The contact time in these experiments was 350 days. The duration of the experiments with UO_2 pellets was 700 days.

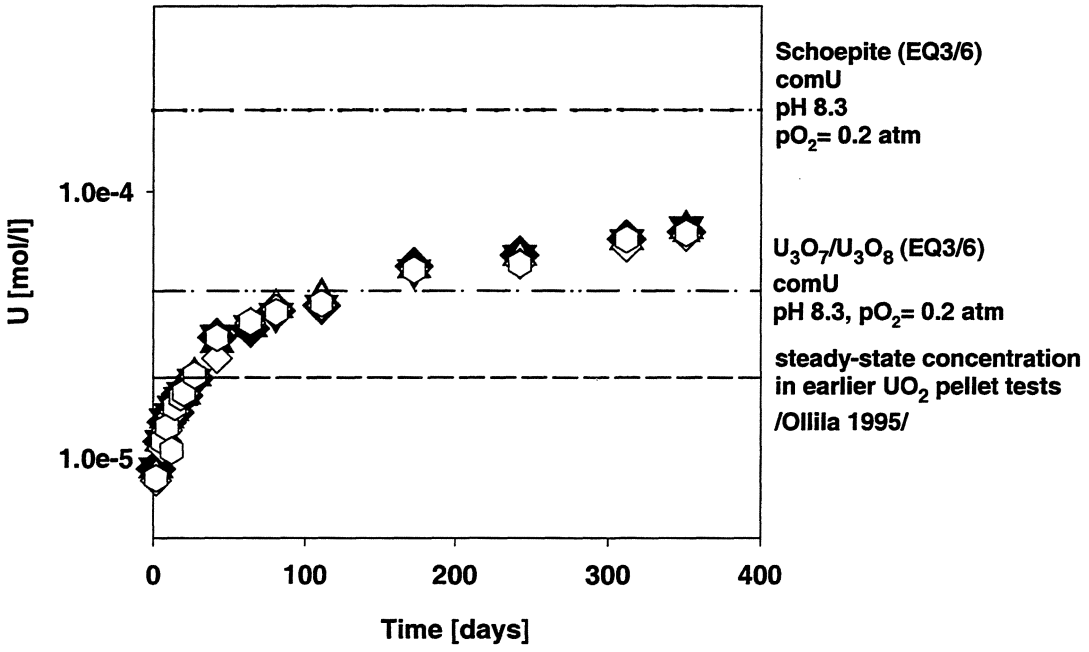

FIGURE I.4.2. Uranium concentration vs. contact time in air-saturated Allard groundwaters during dissolution of UO_2 powder, S/V= 1000 m^{-1} (filled symbols: Allard groundwater *[81ALL/LAR]*, open symbols: modified Allard groundwater [98VUO/SNE], see Appendix 4., Table 1). The dashed lines show the theoretical uranium solubilities in equilibrium with the marked phases (comU= Data.0.com.R2 [92WOL]).

FIGURE I.4-2 gives the measured uranium concentrations vs. contact time in Allard groundwaters under air-saturated conditions. The modification of the composition of the original Allard groundwater *[81ALL/LAR]*, does not have any effect on dissolution by the end of the experimental time. The main reason for the modification was the oversaturation with respect to calcite [98VUO/SNE]. Hence the Ca^{++} and HCO_3^- contents were lowered (see Appendix 4, Table 1). The filtration (with membranes of 12 000 molecular weight cutoff) did not have influence on the measured U contents. The pH remained stable during the experiments.

At the early stages of dissolution, the uranium concentration increases linearly. The dissolution rate calculated per specific surface area is $(1.2 \pm 1.1) \cdot 10^{-6}$ mol m^{-2} d^{-1}. After

~ 20 days the U-release rate slows down, but the uranium concentration continues to increase with a constant rate of $(2.1 \pm 1.0) \cdot 10^{-7}$ mol m^{-2} d^{-1}until the end of the experimental time.

The reference lines in FIGURE I.4-2 present the theoretical solubilities of some uranium solid phases, which were calculated with the EQ3/6 code (Version 7.2b) using the Data0.com.R2 thermodynamic database by Lawrence Livermore National Laboratory [92WOL]. This composite data file includes the compilation of thermodynamic data for uranium minerals, aqueous species and gases evaluated by the Nuclear Energy Agency [92GRE/FUG]. The formation of uranyl oxide hydrates, e.g. schoepite or becquerelite, is predictable at the early stages of dissolution. Schoepite is thermodynamically stable in water with low activities of dissolved Ca and silica [95BRU/CAS, 92FIN/EWI]. The thermodynamic data for becquerelite have not been included in the Data0.com.R2. The uranium concentration rests below the theoretical solubility of schoepite. The steady state in the earlier experiments in Allard groundwater [95OLL] at considerably lower S/V (1.8 m^{-1}, geometric) was close to the uranium solubility at the redox potential of the U_3O_7/U_3O_8 phase boundary see FIGURE I.4-2. A very slowly increasing trend was observed in those experiments until the end of the experimental time (2000 days). The present results show that longer duration and possibly higher S/V tests are needed to determine maximum solution concentrations $>8 \cdot 10^{-5}$ mol/l.

In saline and granite/bentonite GBW groundwaters, the U concentration attained a steady state after 80-100 days, upper FIGURE I.4-3. The main differences of these groundwaters compared with Allard groundwater were the lower HCO_3^- content, lower pH and higher ionic strength (see Appendix 4, TABLE 1). The steady state in saline groundwater is somewhat higher than the theoretical solubility of schoepite. The formation of another uranyl oxide hydrate, becquerelite, $Ca(UO_2)_6O_4(OH)_6 \cdot 8\ H_2O$, is favourable with this composition due to the high Ca^{2+} content. Further geochemical calculations of these solubilities are provided in WPIV using a database valid for high ionic strengths (Pitzer coefficients)with becquerelite or Na-polyuranate as solubility controlling phases. The solubility of becquerelite is at the same level as the solubility of schoepite. Similar solubility is obtained for ($Na_2U_2O_7$). In Spanish granite/bentonite groundwater, the steady state was attained at U concentration close to schoepite/becquerelite solubility, lower FIGURE I.4-3. In the highly saline Na-Ca-Cl near-field groundwater (I= 1.6 M), there is a decreasing trend towards the end of the experimental time, FIGURE I.4-4 The U concentration is close to the solubility of schoepite (or becquerelite).

In addition to the experiment with UO_2 powder (S/V= 1000 m^{-1}), three series of dissolution experiments with UO_2 pellets using different S/V ratio (0.66, 1.98 and 19.8 m^{-1}, based on geometric surface area) were performed in synthetic saline groundwater under air-saturated conditions. FIGURE I.4-5 summarizes the results of all these experiments. In the experiments with UO_2 pellets and hence lower S/V, long experimental times are needed to reach steady states. In contrast, Uranium concentration has leveled out only in the experiment with UO_2 powder (FIGURE I.4-3). At the highest S/V (19.8 m^{-1}) with pellets, the uranium concentration increases rapidly in the beginning, the dissolution rate being $(7.4 \pm 5.3) \cdot 10^{-7}$ mol m^{-2} d^{-1} ($\leq$ 60 days), which is followed by a slower increase. The decrease of U release may result from the formation of alteration products. The dissolution rate after 60 days is $(1.3 \pm 0.7) \cdot 10^{-7}$ mol m^{-2} d^{-1}. The rates were calculated based on the specific surface area (0.00019 m^2/g /de Pablo 1997/). At lower S/Vs, 1.98 and 0.66 m^{-1}, the U release remains high until the end of the experimental time, being $(1.0 \pm 0.4) \cdot 10^{-6}$ and $(1.2 \pm 0.4) \cdot 10^{-6}$ mol m^{-2} d^{-1}, respectively. The U release rate per surface area unit in the experiment with UO_2 powder is $(3.4 \pm 0.5) \cdot 10^{-7}$ mol m^{-2} d^{-1}, which is at the same level as the slower rate with UO_2 pellets at the highest S/V.

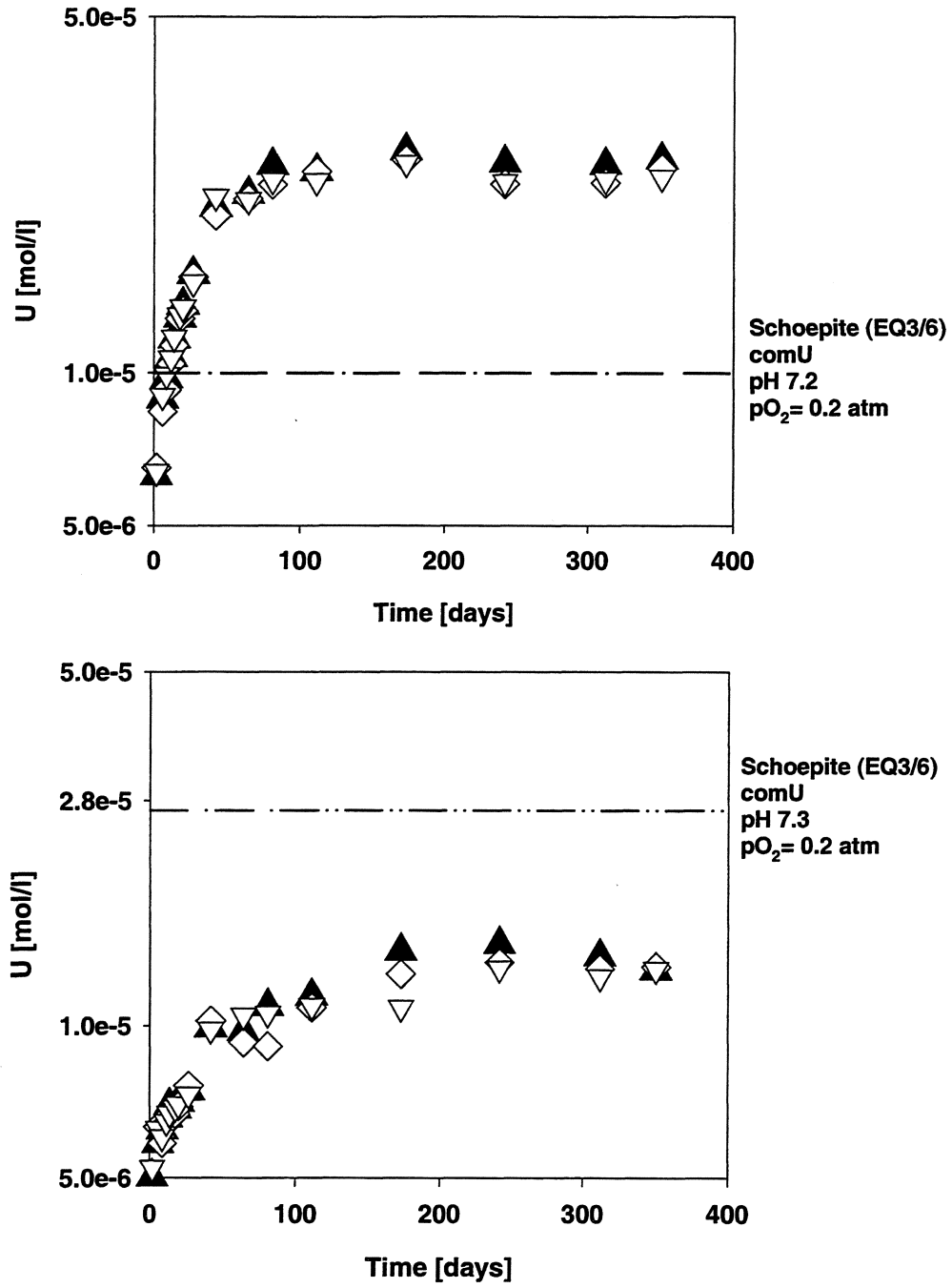

FIGURE I.4-3. Uranium concentration vs. contact time in air-saturated saline (upper figure), and Granite/bentonite (GBW) groundwater (lower figure) during dissolution of UO_2 powder, S/V= 1000 m^{-1} (filled symbols: unfiltered samples, open symbols: filtered samples, 12 000 M). The dashed lines show the theoretical solubilities of schoepite (comU= Data0.com.R2 [92WOL]).

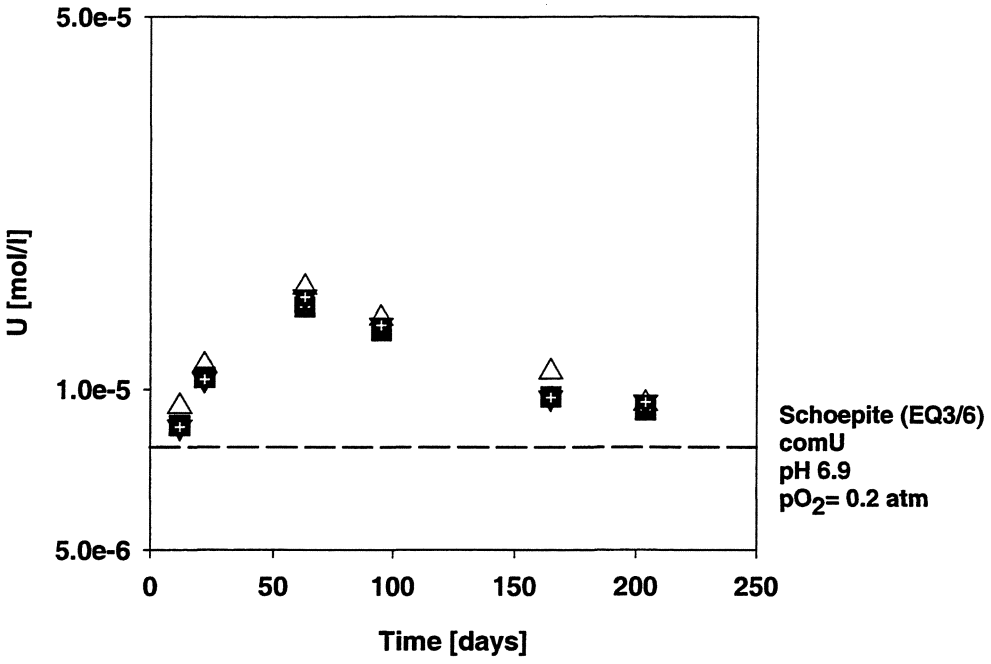

FIGURE I.4-4. Uranium concentration vs. contact time in air-saturated near-field groundwater during dissolution of UO_2 powder, S/V= 1000 m^{-1} (filled symbols: unfiltered samples, open symbols: filtered samples, 12 000 M). The dashed line shows the theoretical solubility of schoepite (comU= Data0.com.R2 [92WOL]).

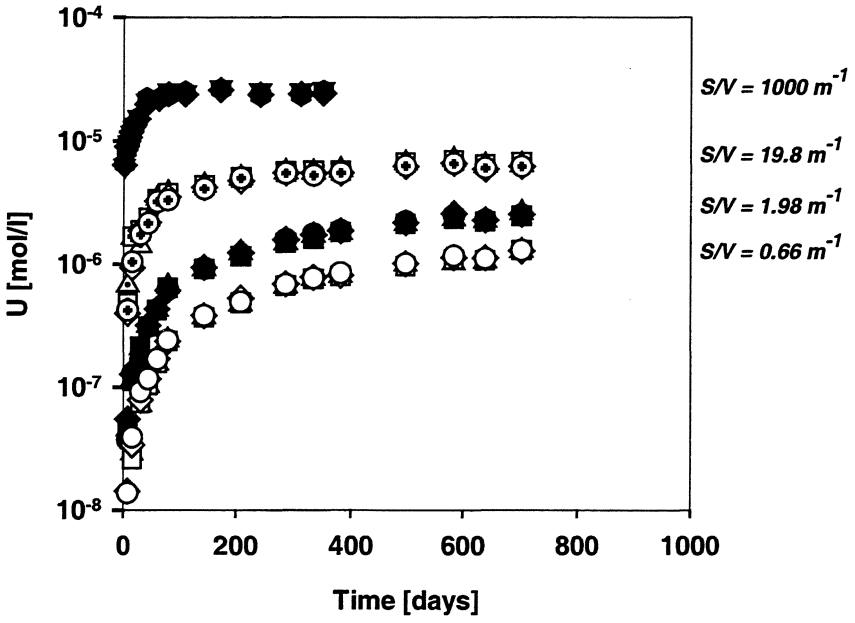

FIGURE I.4-5. Uranium concentration vs. contact time in air-saturated saline groundwater in the experiments with different S/V. The measured data at each S/V is for two parallel experiments.

An attempt was made to experimentally identify possible secondary alteration products during dissolution of UO_2 powder. The separation of UO_2 powder from aqueous solutions was made by filtration using ultrafiltration membranes (Amicon XM 300). The powder on filter membrane was analyzed with X-ray powder diffractometry. The analyses were made after the contact times of 200, 300 days and 1 year in Allard, modified Allard, saline and Spanish granite/bentonite (GBW) groundwaters, and after the contact times of 160 and 225 days in near-field groundwater. After 200 and 300 days, no secondary phases were found in any of the synthetic groundwaters. The X-ray diffraction patterns showed only the major UO_2 peaks, see Appendix 4, which shows the diffraction patterns obtained from UO_2 powder samples after the contact time of 200 days. After the contact time of 1 year in Allard, modified Allard, saline and Spanish groundwaters, the diffraction patterns showed weak peaks of a higher uranium oxide, $U_3O_8 - UO_3$, Appendix 4. No schoepite or other uranyl oxide hydrates were found. In near-field groundwater, the contact time was shorter. No secondary phases were found by the end of the experimental time.

TABLE I.4-1 gives a comparison of steady-state uranium concentrations and dissolution rates for various groundwater compositions under air-saturated conditions. The dissolution rates have been calculated per specific surface area.

TABLE I.4-1. **Measured steady-state solution concentrations and dissolution rates of U in the dissolution experiments with UO_2 in various groundwaters under oxic conditions.**

Material/ groundwater composition	Ionic strength	pH	$[HCO_3^-]$ mmol/l	U-steady state concentration [mol/l]	U dissolution rate mol m^{-2} d^{-1}	Second ary phases
UO_2 powder, Allard, fresh	0.004	8.4	2.00	increasing >$8\cdot10^{-5}$	$(1.2 \pm 1.1) \cdot 10^{-6}$ 1) $(2.1 \pm 1.1) \cdot 10^{-7}$ 2)	U_3O_8 or UO_3
UO_2 powder, mod. Allard, fresh	0.004	8.4	1.50	increasing >$8\cdot10^{-5}$	$(1.2 \pm 1.1) \cdot 10^{-6}$ 1) $(2.1 \pm 1.0) \cdot 10^{-7}$ 2)	"
UO_2 powder, saline	0.5	7.0	0.16	$(2.5 \pm 0.1)\cdot10^{-5}$	$(3.4 \pm 0.5) \cdot 10^{-7}$	
UO_2 pellets, saline	"	"	"	increasing	$(1.1 \pm 0.4) \cdot 10^{-6}$ 3) $(1.3 \pm 0.7) \cdot 10^{-7}$ 4)	"
UO_2 powder, GBW	0.25	7.5	0.44	$(1.3 \pm 0.1) \cdot 10^{-5}$	$(1.6 \pm 0.4) \cdot 10^{-7}$	"
UO_2 powder, saline near-field	1.6	6.8	0.14	$(1.2 \pm 0.2)\cdot10^{-5}$	$(1.4 \pm 0.4) \cdot 10^{-7}$	none

1) initial dissolution rate, < 20 days, 2) dissolution rate ≥ 20 days
3) initial dissolution rate, S/V= 19.8 m^{-1}: ≤ 60 days, S/V= 1.98 and 0.66 m^{-1}: 700 days
4) dissolution rate, S/V= 19.8 m^{-1}: ≥ 60 days

In summary, the main objective of the dissolution experiments with UO_2 powder and UO_2 pellets under oxidizing air-saturated conditions was to obtain information on

maximum solution concentrations of uranium with different groundwater compositions and on secondary alteration products that control the concentration . The salinity of groundwater had a minor effect on the measured steady-state concentrations. The higher alkalinity of the fresh (Allard) composition increases the uranium concentration in the aqueous phase. The steady-state concentrations in saline, Spanish granite/bentonite (GBW) and highly saline near-field groundwaters, $(1.2...2.5) \cdot 10^{-5}$ M, were at the level of the theoretical solubilities of schoepite or another uranyl oxide hydrate e.g. becquerelite (possibly Na-polyuranate). Unfortunately, the contact time in the experiments with UO_2 powder was obviously not long enough to experimentally show the presence of these secondary phases in the groundwaters. Only some kind of oxidised U-phase ($U_3O_8 - UO_3$) was identified in the analyses of the solid phases after the contact time of one year. Longer contact times are needed to identify secondary phases predicted by reaction path modelling (EQ3/6).

Solubility of UO_2 under anoxic conditions

Due to consumption of remaining oxidants by container corrosion or by the action of bacteria, the geochemical conditions in European repositories are expected to become reducing, shortly after closing the repositories. The main oxidant source is radiolysis. After the decay of radioactivity inventories, anoxic conditions are expected to prevail. These conditions are characterized by the absence of air (anaerobic conditions) and by the presence of reducing groundwater species (reducing conditions). In order to determine maximum solution concentrations under both anaerobic and reducing conditions, static dissolution tests were performed in a glove box filled with N_2 ($O_2 < 1$ ppm) Reducing conditions, were assured by the addition of reducing species to the aqueous phase: S(-II), Fe(+II), or by addition of metallic Fe. The detailed conditions are given in Appendix 4, TABLE s 3 and 4. All the anoxic experiments were carried out with UO_2 pellets. A low and higher ratio of surface area to water volume were used, S/V= 0.66 and 19.8 m^{-1}, respectively. The surface of pellets was pretreated with predissolution periods prior to the start of the batch dissolution experiments.

Under reducing conditions, i.e. in the redox regime where U(IV) is the predominant oxidation state, UO_2 is thermodynamically stable. The dissolution reaction,

$$UO_2 + (n\text{-}2)\ H_2O \rightarrow U(OH)_n^{(4-n)+} + (n\text{-}4)\ H^+$$

attains equilibrium in the absence of oxidants. U^{4+} is hydrolyzed or complexed in solution. The concentration of uranium in solution is limited by the solubility of the dissolving solid, which is very low in the absence of oxidants ($\leq 10^{-9}$ mol/l). UO_2 limits the solubility in low-Eh environments. Coffinite ($USiO_4$) may become stable relative to UO_2 in groundwaters with a high silica content [98LAN]. With increasing Eh, however surface oxidation and dissolution is enhanced, particularly when carbonate is present. The uranium concentration in solution remains still low if oxidizing species are absent. The complex formation with carbonate affects the relative stability of the oxidation states. The relative amounts of the U(VI)-carbonate complexes and the U(IV)-hydroxide complexes depend on carbonate content, pH and Eh [91SKI].

Anaerobic (N_2) conditions

The measured solution concentrations of uranium as a function of contact time in synthetic groundwaters with saline and fresh (modified Allard) compositions under anaerobic conditions are given in FIGURE s I.4-6 and I.4-7 at S/V= 0.66 and 19.8 m^{-1}, respectively. The main differences between the compositions are the higher ionic

strength of the saline one (0.5 M) and the presence of carbonate (1.07 mM) in the fresh one (Appendix 4, TABLE 1). At lower S/V, 0.66 m^{-1}, the concentration of uranium increases slowly in both groundwaters, FIGURE I.4-6. There was no difference between unfiltered and filtered (0.45 μm) samples. In the case of saline composition, there were practical difficulties to use ICP-MS due to blocking of tubes. For that reason the follow-up of U concentration in the experiments in saline groundwater was finished after the experimental time of 300 days. The concentrations of uranium were reanalyzed using a method with uranium separation from saline solution (see Analytical methods, Appendix 4) after 700 days. The comparison with theoretical solubility calculations with the EQ3/6 code was made in order to evaluate the solubility-limiting uranium oxide. The results show that the solution concentrations are higher than the solubility of the unoxidised, well-crystallized UO_2 predicts. There is a difficulty in giving the redox parameter input in the modelling calculations. Based on the O_2 level in the N_2 gas of the anaerobic box (0.3 ... 0.5 ppm [97VUO]), a very high Eh is resulted, see TABLE I.4.2.

TABLE I.4-2. Redox conditions and U speciation under anaerobic conditions.

	Saline	Fresh (modified Allard)
pH/Eh measured in the absence of UO_2 pellets	8.0 ...8.1/- 0.020 ... + 0.175 V	8.8/-0.050 ...+0.120 V
pH/Eh measured in the presence of UO_2 pellets	8.3/-0.1 V (S/V= 0.66 m^{-1}) 8.0/-0.15 V (S/V= 19.8 m^{-1})	9.0/-0.110 V
pH/Eh calculated: log O_2 fugacity= -7	8.3/0.6 V	9.0/0.6 V
pH/Eh, U speciation calculated: UO_2/U_4O_9	8.3/-0.035 V $UO_2(OH)_2(aq)$ (64 %) $UO_2(OH)_3^-$ (22 %) $U(OH)_4$ (aq) (14 %)	9.0/-0.083 V $UO_2(CO_3)_3^{4-}$ (63 %) $UO_2(CO_3)_2^{2-}$ (25 %) $UO_2(OH)_2(aq)$ (6 %) $UO_2(OH)_3^-$ (5 %)
pH/Eh, U speciation calculated: UO_2/U_3O_7	8.3/-0.020 V U speciation as above	9.0/-0.060 V U speciation as above
U oxidation state measured	0-15 % U(IV) 85-100 % U(VI)	100 % U(VI)

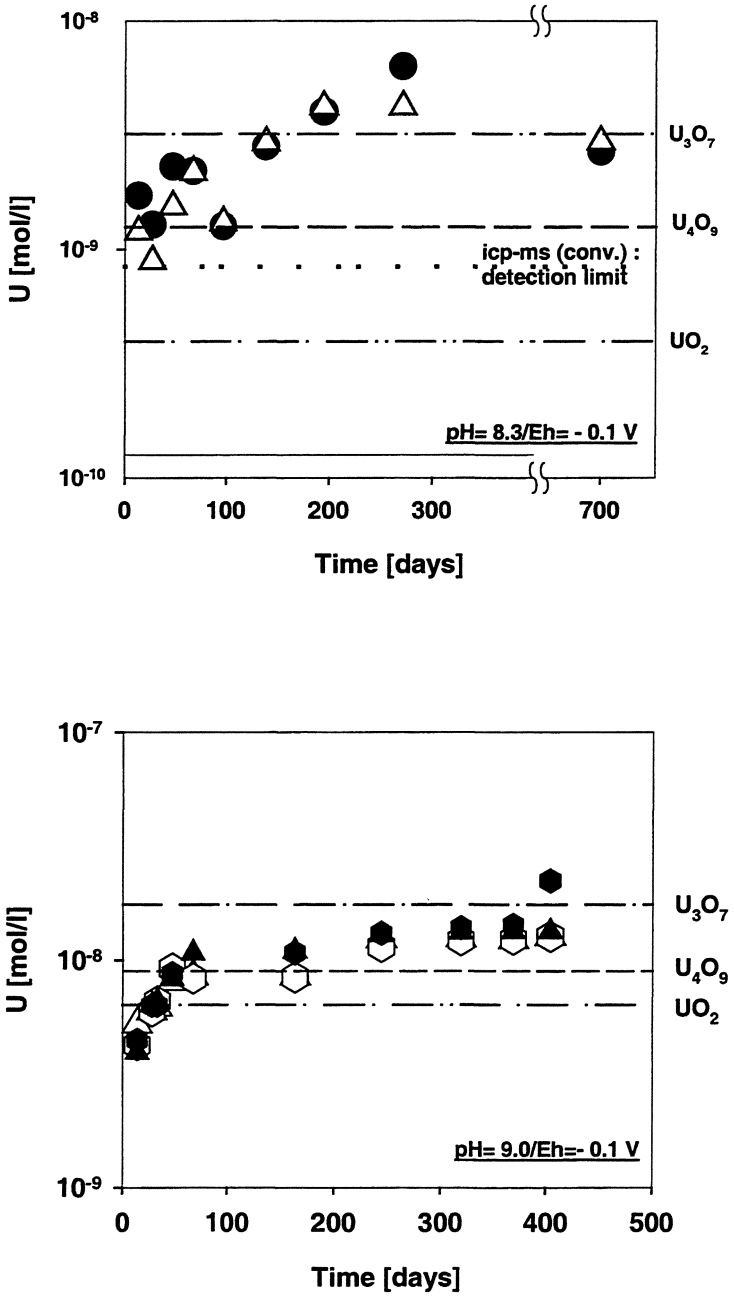

FIGURE I.4-6. Uranium concentration vs. contact time in anaerobic (N_2) saline (upper figure) and modified Allard (lower figure) groundwaters during dissolution of UO_2 pellets, S/V= 0.66 m^{-1}. The measured data are for two parallel experiments in each of the figures. The dashed lines show the theoretical solubilities of uranium oxides in equilibrium (EQ3/6, composite database) at measured pH and Eh values.

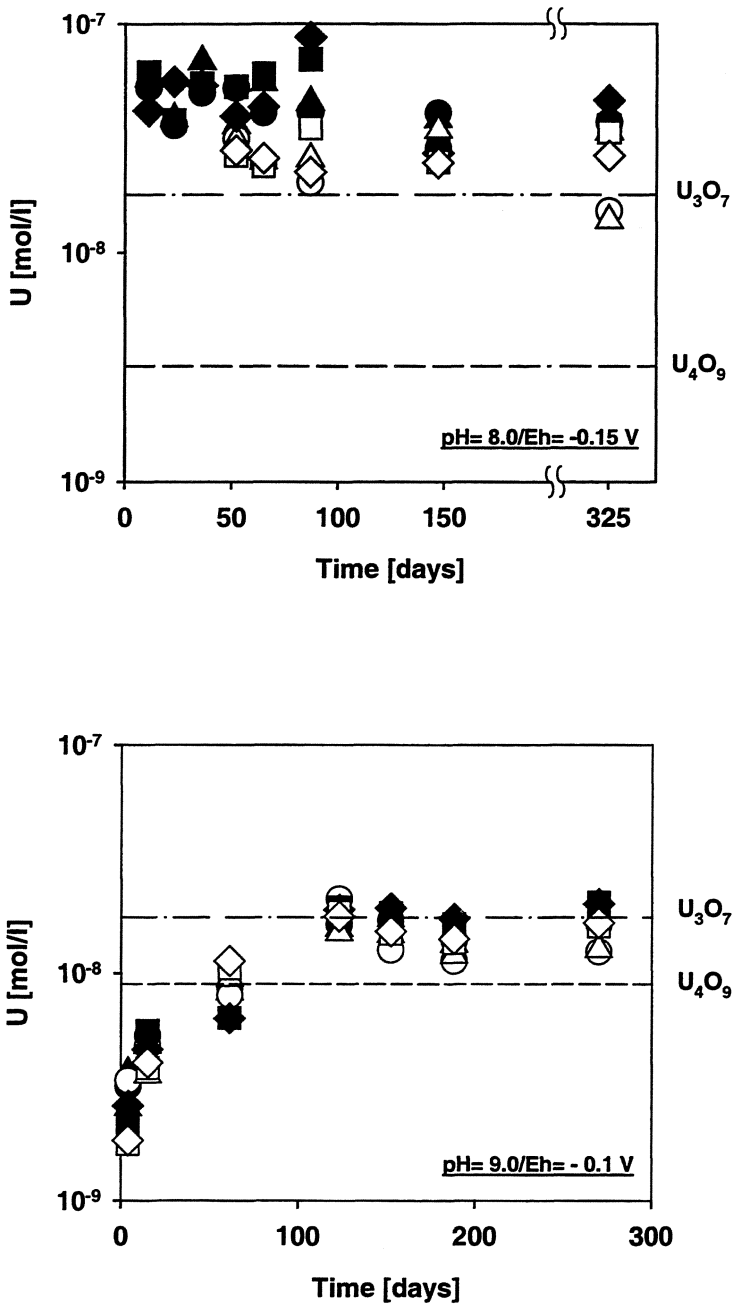

FIGURE I.4-7. Uranium concentration vs. contact time in anaerobic (N_2) saline (upper figure) and modified Allard (lower figure) groundwaters during dissolution of UO_2 pellets, S/V= 19.8 m^{-1}. The measured data are for two parallel experiments (filled symbols: unfiltered samples, open symbols: filtered, 0.45 µm, samples) in each of the figures. The dashed lines show the theoretical solubilities of uranium oxides in equilibrium (EQ3/6, composite database) at measured pH and Eh values.

The measured redox values in the absence of UO_2 pellets are varying, whereas in the presence of UO_2 pellets they are relatively stable, being -0.1 ... -0.15 V. The values suggest that the UO_2 surface/U in solution has effect on the measured Eh. Under these conditions the formation of oxidised surface layer, U_4O_9 or U_3O_7, cannot be excluded. The effect of these oxide layers on the Eh can be simulated in the EQ3/6 assuming that the equilibrium between different U oxides, UO_2/U_4O_9 or UO_2/U_3O_7, fixes the oxygen fugacity. The equilibrium with U_4O_9 or U_3O_7 is the constraint assigned to $O_2(g)$. The Eh values calculated in this way for UO_2/U_4O_9 and UO_2/U_3O_7 are presented in TABLE I.4-2. They are much lower than the value given by the O_2 fugacity. The calculated UO_2/U_4O_9 redox potential in Allard groundwater is at the same level with the measured one. In saline groundwater, the measured value is lower. The speciation of U under these redox conditions is dominated by the U(VI) state. This is in agreement with the U oxidation state measurements, which showed that uranium was mainly at the U(VI) state, see TABLE I.4-2.

The theoretical solubilities presented in FIGURE s I.4-6 and I.4-7 were calculated using the measured Eh in the presence of UO_2 pellets as the redox parameter input. The solution concentrations measured in the anaerobic Allard groundwater during dissolution of UO_2 pellets are in good agreement in the experiments with different S/Vs, and in good agreement with the earlier measurements (S/V= 0.45 m^{-1}) in the original Allard groundwater as well [95OL]. The uranium concentration at steady state is close to the calculated solubilities of U_3O_7 or U_4O_9. On the contrary, there is a difference between the measured data at different S/Vs in saline groundwater. This may be related to the analytical problems due to salinity. The measured concentrations at S/V= 19.8 m^{-1} are higher, but there is a decreasing trend towards the end of the experimental time and some difference between unfiltered and filtered samples is observed at the end. Another explanation could be insufficient removal of surface layer during predissolution periods causing high release in the beginning of the experiment and precipitation afterwards. The predissolution periods were carried out under similar conditions using saline groundwater as leachant and S/V= 19.8 m^{-1} (see FIGURE I.4-1). The solution concentration at the end of the experiments with the higher S/V is at the same level in both groundwaters.

After the conclusion of the higher S/V experiments (FIGURE I.4-7) the aqueous phases in both experiments were ultrafiltered (Amicon, Diaflo XM 50) and the material retained on membrane filter was analyzed with X-ray diffractometry. The diffraction pattern of the solid material filtrated from saline groundwater is given in Appendix 4. It shows the presence of UO_2 (or U_4O_9) in the aqueous phase, which may have formed as a secondary phase. This suggests the occurrence of precipitation phenomena, possibly caused by the dissolution of more soluble pre-oxidised surface layer and subsequent precipitation, or different dissolution mechanisms. No solid material was filtrated from Allard groundwater.

Reducing (low Eh) conditions

The measured solution concentrations of uranium as a function of contact time in synthetic groundwaters with saline and fresh (modified Allard) compositions under reducing conditions are given in FIGURES I.4.8 and I.4-9 at S/V= 0.66 and 19.8 m^{-1}, respectively.

The batch experiments at low S/V were performed in the presence of varying amounts of redox species. The measured Eh values were between –200 and –300 mV. The pH was allowed to change due to the redox species additions (Appendix 4, TABLE 4). The filtration (0.45 μm) did not have effect on the measured uranium contents. In the

experiments of saline groundwater the concentrations were close to the detection limit of the ICP-MS. The solution concentrations were followed vs. contact time for 300 days, after which the experimental vessels were left in the anaerobic box. The solution concentrations were reanalyzed using the method with uranium separation after 700 days. The results were in good agreement with the earlier ICP-MS analyses.

The control of the Eh by the addition of reducing species lowers the amounts of uranium in the aqueous phase at low S/V, FIGURE I.4-8. A steady state was attained in both groundwaters after a few days. The effect in the solubility is greater in Allard groundwater. The uranium concentration was decreased by one order of magnitude. The measured concentrations are very similar with fresh and saline composition. Comparison of the measured data with the calculated solubilities shows that the solution concentrations are at the level of the theoretical solubility of the well-crystallized solid, UO_2, in both groundwaters.

In the experiments with the higher S/V (19.8 m^{-1}), somewhat different results were obtained, FIGURE I.4-9. The results are for two parallel batch experiments in both groundwaters. In saline groundwater, there was a clear difference between the measured amounts of uranium in the unfiltered and filtered (0.45 µm) samples. The total U concentration in the aqueous phase seems to stay at the same level as under anaerobic conditions (FIGURE I.4-7). The U concentrations in the filtered samples were low. They are at the same level as in the experiments with the lower S/V (FIGURE I.4-8). The difference between unfiltered and filtered samples suggests the presence of some kind of colloidal material in the aqueous phase. This result was not expected, because colloid stability was expected to be lower in saline solutions. In Allard groundwater, the filtration had only a small effect on the measured contents, but the U concentration is again higher than in the low-S/V experiments. There is a decreasing trend at the later stages of the experiment.

After the conclusion of the experiments with S/V= 19.8 m^{-1} (FIGURE I.4-9) the aqueous phases were ultrafiltered (Amicon, Diaflo XM 50) and the material retained on membrane filter was analyzed with X-ray diffractometry. The diffraction pattern obtained from the solid material, which was filtrated from saline groundwater, is given in Appendix 4. Likewise under anaerobic conditions, UO_2 (or U_4O_9) was identified. The amount of this material seemed to be greater under reducing conditions. As suggested earlier, the possible effect of the incomplete removal of pre-oxidised surface layer cannot be excluded. No solid phase was found in Allard groundwater.

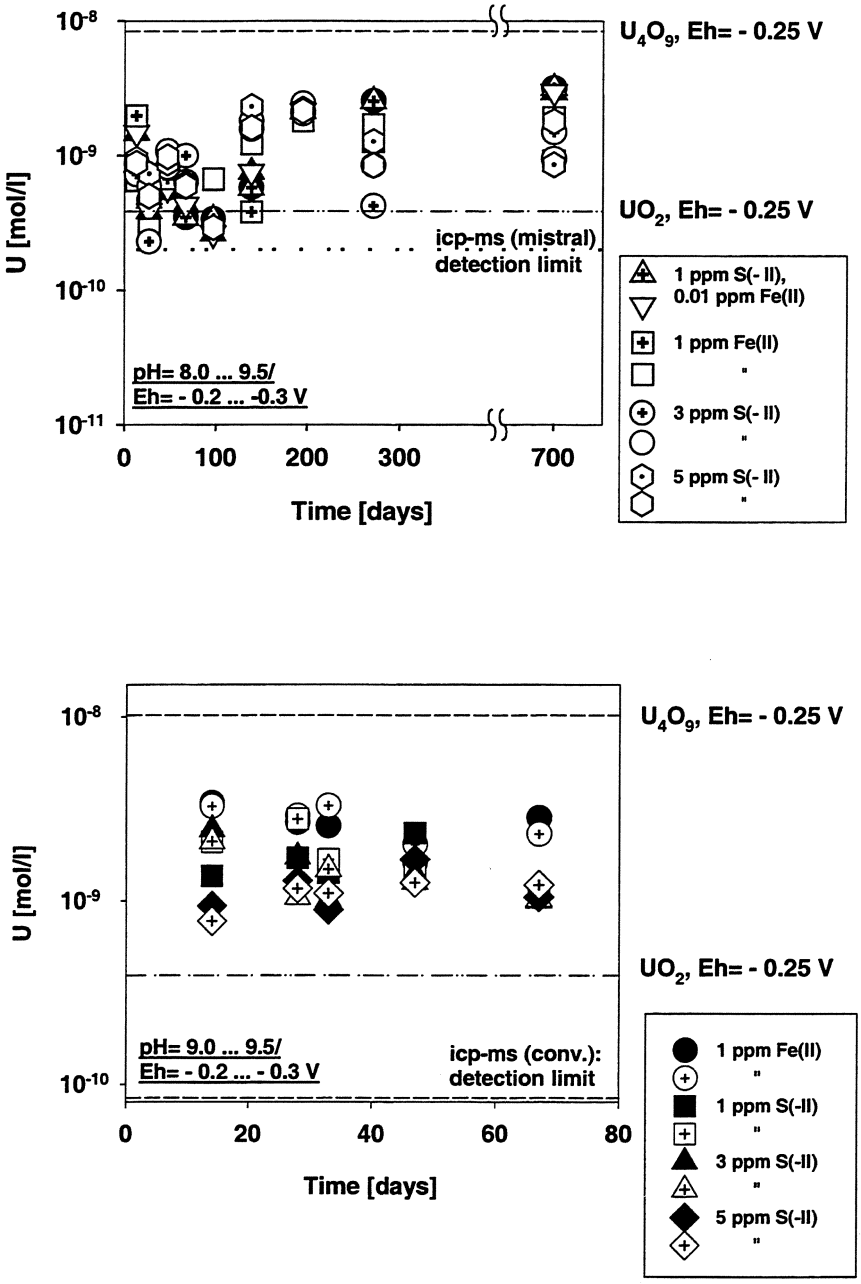

FIGURE I.4-8. Uranium concentration vs. contact time in saline (upper figure) and modified Allard (lower figure) groundwaters under reducing conditions during dissolution of UO_2 pellets, S/V= 0.66 m^{-1}. The measured data are for four batch experiments (including parallel experiments in each) in the presence of varying amounts of reducing species. The Eh and pH values are given in detail in Appendix 4, TABLE 4. The dashed lines show the theoretical solubilities of uranium oxides in equilibrium (EQ3/6, composite database) at average measured Eh values.

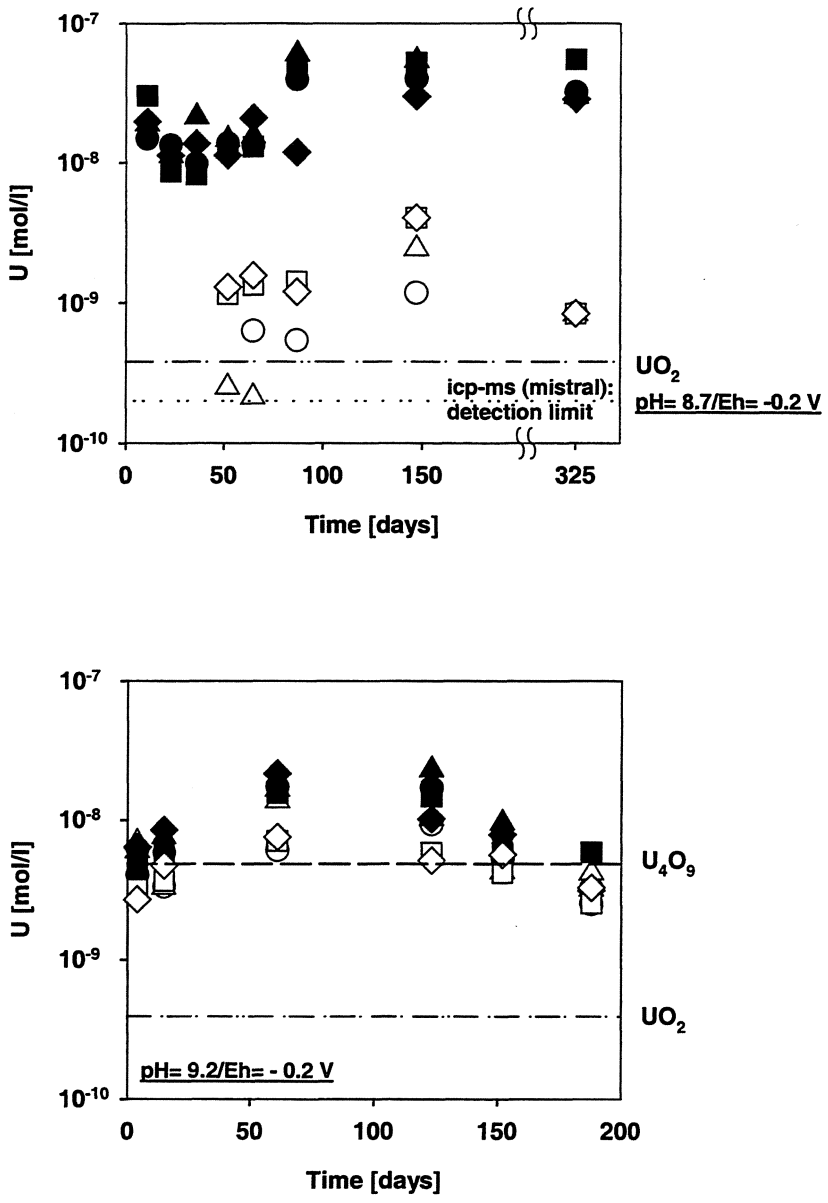

FIGURE I.4-9. Uranium concentration vs. contact time in saline (upper figure) and modified Allard (lower figure) groundwaters under reducing conditions during dissolution of UO_2 pellets, S/V= 19.8 m^{-1}. The measured data is for two parallel experiments (filled symbols: unfiltered samples, open symbols: filtered, 0.45 μm, samples) in each of the figures. The dashed lines show the theoretical solubilities of uranium oxides in equilibrium (EQ3/6, composite database) at measured pH and Eh values.

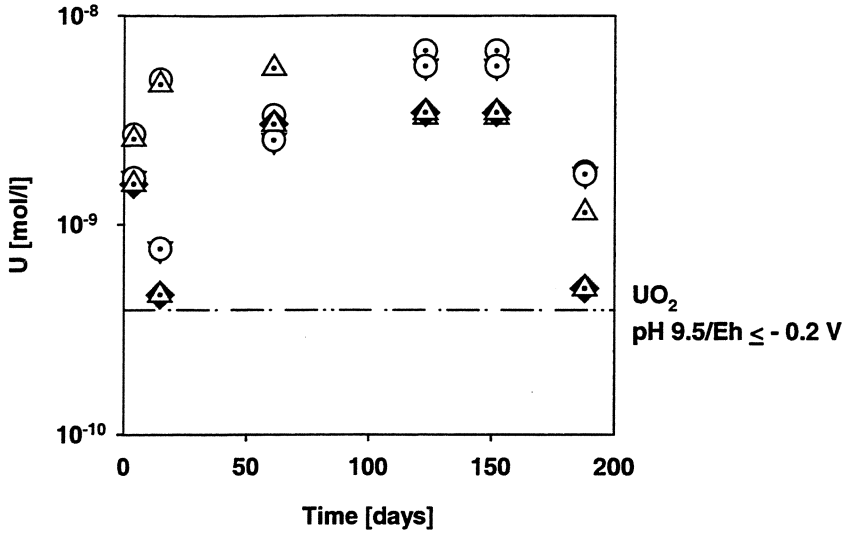

FIGURE I.4-10. Uranium concentration vs. contact time in modified Allard groundwater during dissolution of UO_2 pellets (S/V= 19.8 m^{-1}) in the presence of metallic Fe. The measured data (unfiltered samples) is for two parallel experiments (I: black symbols, II: open symbols). The dashed line shows the theoretical solubility of UO_2 at measured pH in reducing conditions (EQ3/6, composite database).

Finally, the measured solution concentrations of uranium as a function of contact time in the presence of metallic Fe are given in FIGURE I.4--10 for the parallel batch experiments in Allard groundwater. The data, which is for the unfiltered samples, show some scatter. The measurement data was similar for the experiments in saline groundwater, the U concentrations ranging from 10^{-9} ... 10^{-8} mol/l [97OLL]. The U contents in the filtered (0.45 µm) samples were below the detection limit of the ICP-MS in both groundwaters ($\leq 10^{-10}$ M). The aqueous phases were ultrafiltered (Amicon, Diaflo XM 50) after the conclusion of the experiments. The solid material retained on membrane filter was analyzed with X-ray diffractometry. The identification of a possible secondary phase of uranium was made difficult by the small amount of particulate material collected from the solutions. A very weak peak suggesting the presence of UO_2 and some iron compounds (possibly Fe-oxy-hydroxide) were observed. Additional experiments to study the effect of metallic Fe on dissolution mechanisms of UO_2 are needed.

The following TABLE I.4-3 summarizes the results of the solubility experiments of UO_2 pellets in synthetic groundwaters under anaerobic and reducing conditions. The solubilities are given as average values of the steady-state concentrations and their deviations. The results of the analyses of the oxidation states of uranium are included in TABLE I.4-3. Some results of earlier solubility measurements are given for comparison.

TABLE I.4-3. Measured uranium solubilities (mol/l) in the dissolution experiments of unirradiated UO_2 pellets in synthetic groundwaters under anoxic conditions.

Aqueous media	Redox conditions, pH/Eh measured	U oxidation state	Uranium solubility mol/l	Reference
Saline groundwater, I= 0.5 M no carbonate	anaerobic (N_2) pH 8.0...8.3 Eh –0.15...-0.1 V	0-15 % U(IV) 85-100 % U(VI)	$(3.5 \pm 1.4) \cdot 10^{-8}$	this study
Fresh granite groundwater (modif. Allard) [98VUO/SNE] I= 0.004 M $[HCO_3^-]$ 1.07 mM	anaerobic (N_2) pH 9.0 Eh –0.1 V	100 % U(VI)	$(1.5 \pm 0.3) \cdot 10^{-8}$	"
Fresh granitic groundwater [81ALL/LAR] I= 0.004 M $[HCO_3^-]$ 1.7 – 2.0 mM [95OLL]	anaerobic (N_2) pH 9.0	10 % U(IV) 90 % U(VI)	$(1.9 \pm 0.2) \cdot 10^{-8}$	[95OLL, 96OLL]
Bentonite groundwater /Snellman 1988/ I= 0.014 M $[HCO_3^-]$ 8.6 – 9 mM [95OLL]	anaerobic (N_2) pH 8.9	100 % U(VI)	$(2.7 \pm 0.5) \cdot 10^{-8}$	"
Saline groundwater, I= 0.5 M no carbonate	reducing S(-II), Fe(+II) pH 8.0...9.5 Eh –0.2...-0.3 V	63-80 % U(IV) 20-37 % U(VI)	$(9.6 \pm 5.6) \cdot 10^{-10}$	this study
Fresh granite groundwater (modif. Allard) [98VUO/SNE] I= 0.004 M $[HCO_3^-]$ 1.07 mM	reducing S(-II), Fe(+II) pH 9.0...9.5 Eh –0.2...-0.3 V	30-40 % U(IV) 60-70 % U(VI)	$(1.7 \pm 0.6) \cdot 10^{-9}$	"
Saline groundwater, I= 0.5 M no carbonate	reducing metallic Fe pH 8.8-9.3	40 % U(IV) 60 % U(VI)	no filtration: $(1.1 \pm 1.0) \cdot 10^{-8}$ filtration: ≤ d.l.	"
Fresh granite groundwater (modif. Allard) [98VUO/SNE] I= 0.004 M $[HCO_3^-]$ 1.07 mM	reducing metallic Fe pH 9.5	50 % U(IV) 50 % U(VI)	no filtration: $(3.2 \pm 1.5) \cdot 10^{-9}$ filtration: ≤ d.l.	"

WP I.4.2 Precipitation experiments

In order to check whether maximum solution concentrations of U were obtained in the dissolution tests (WP I.4.1), precipitation tests were performed at VTT. Using initial supersaturated solutions with U-concentrations well above the solubility of known U-controlling phases, the evolution of U-concentrations was followed as a function of time. Results of this test are also expected to show whether equilibrium was achieved.

Procedure of precipitation experiments

All solutions for precipitation experiments were handled in N_2 atmosphere in the glove box. U(IV) stock solution (~ 0.56 M) was prepared by dissolving $U(IV)Cl_4$ (anhydrous, Strem Chemicals) in 1 M HCl. Earlier tests have shown that U(IV) is stable in 1 M HCl under anaerobic conditions (O_2 < 1 ppm) for several months [96OLL].

Just before the initiation of the experiments the U(IV) stock solution was diluted with deaerated deionized water. An aliquot of this solution, U(IV) in 0.1 M HCl, was added to synthetic groundwater. The final uranium concentration was approximately 0.56 mM. The pH was immediately adjusted with NaOH. Upon pH adjustment dark-green precipitates were observed in modified Allard and saline groundwaters. In near-field groundwater, the color of precipitate was different, light green.

The precipitates were allowed to equilibrate for periods of different length (7 ... 50 days). At the end of the equilibration periods, the supernatant solution was sampled by syringe, filtered (membranes of 0.45 μm or 50 000 molecular weight cutoff) and analyzed for uranium (ICP-MS). In the case of Allard groundwater the U concentration was followed during aging of the solid phase after precipitation. The solid phases were analyzed by X-ray diffractometry at the end of selected periods by Geological Survey of Finland. Contact with air during diffraction measurements could not be avoided. TABLE 6 in Appendix 4 gives the conditions of the precipitation tests. The measured Eh values were influenced by the presence of U precipitates. This is discussed more in the connection of the results.

Solution concentrations and solid phases in anoxic precipitation tests

In the precipitation experiments the solubility equilibrium of uranium was approached from oversaturation in order to confirm the results obtained in the dissolution experiments with UO_2 pellets. The precipitations were performed with fresh (modified Allard), saline and near-field compositions (Appendix 4, TABLE 1). Critical in these experiments is the length of the equilibration periods. The crystallization of the precipitates is known to progress gradually [90RAI /FEL, 95YAJ/KAW]. The results presented in this report are all for the equilibration periods of relatively short duration.

FIGURES I.4-11 and I.4-12 show the aqueous uranium concentrations measured as a function of time in modified Allard groundwater during the aging of the precipitates. Likewise in the dissolution experiments with UO_2 pellets, the precipitation was carried out in the absence (anaerobic) and in the presence of reducing species, S(-II) or metallic Fe. The presence of U precipitates had a clear effect on the measured Eh in the precipitation experiments. Eh was low also in the absence of S(-II). The measured Eh values were given in TABLE I.4-2 and are presented also in the connection of the results. This suggests that the surface of UO_2 is a controlling factor for the Eh in the precipitation experiments. The presence of metallic Fe reduced the measured Eh. The low Eh is in agreement with the measured aqueous concentrations of uranium. In Allard groundwater, the solubilities are low in all cases, FIGURES I.4-10 and I.4-11. The solubilities are lower by a half order of magnitude, than measured in the pellet experiments with redox control (TABLE I.4-3). They are in good agreement with the theoretical solubility of well-crystalline UO_2. The X-ray diffraction patterns obtained from the solid phases after the aging

time of 7-43 days showed the peaks of weakly crystalline UO_2 - U_3O_7 (Appendix 4). There is a possibility that U_3O_7 has formed as oxidation product during diffraction measurements. The solid samples were transferred from the anaerobic box to X-ray diffractometer without contact with air, but during the measurements the contact could not be avoided.

TABLES I.4-4 and I.4-5 give the solubilities of uranium measured in saline and near-field groundwaters. The solubilities are the results of 2-3 parallel equilibration periods (≤ 45 days). Due to the salinity, a method for uranium separation was used for all the samples before the ICP-MS measurements in order to lower the detection limit. As in Allard groundwater, the Eh and the solubilities of uranium were low also in the absence of reducing species. The solubility in saline groundwater with the S(-II), TABLE I.4-4, is in good agreement with the solubility measured in the pellet experiments (TABLE I.4-3). The increase in salinity does not seem to have effect in the solubility. In the presence of metallic Fe, a higher solubility by one order of magnitude was measured. As in Allard groundwater, the analyses of solid phases gave weakly crystalline UO_2 – U_3O_7 as a result in all cases, Appendix 4. In addition, the peaks of impure U(IV) oxide, including a cation, possibly Sr- or $CaUO_3$, were observed. This phase seemed to be more crystalline than UO_2 – U_3O_7.

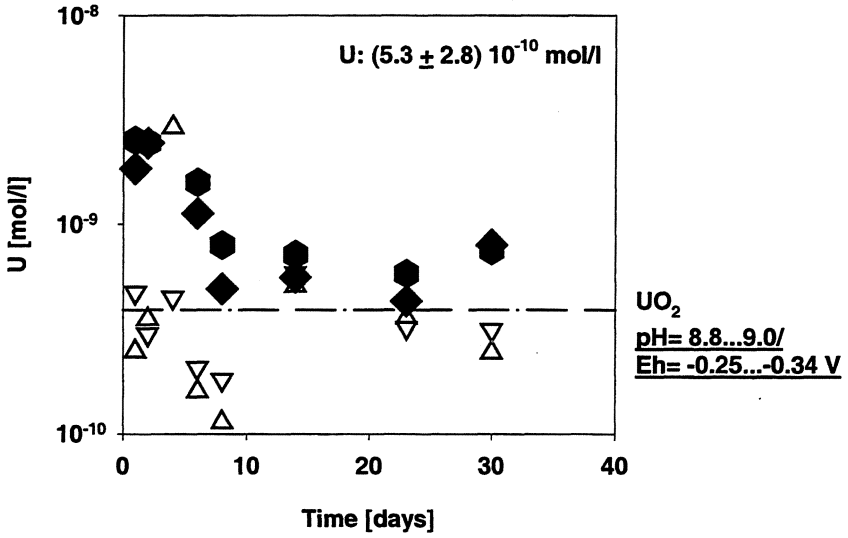

FIGURE I.4-11. U-Concentrations in the oversaturation experiments in modified Allard groundwater under anoxic conditions (open symbols: without S(-II) addition, filled symbols: with 3 ppm S(-II)). The dashed line shows the theoretical solubility of UO_2 (EQ3, composite database) at measured Eh values.

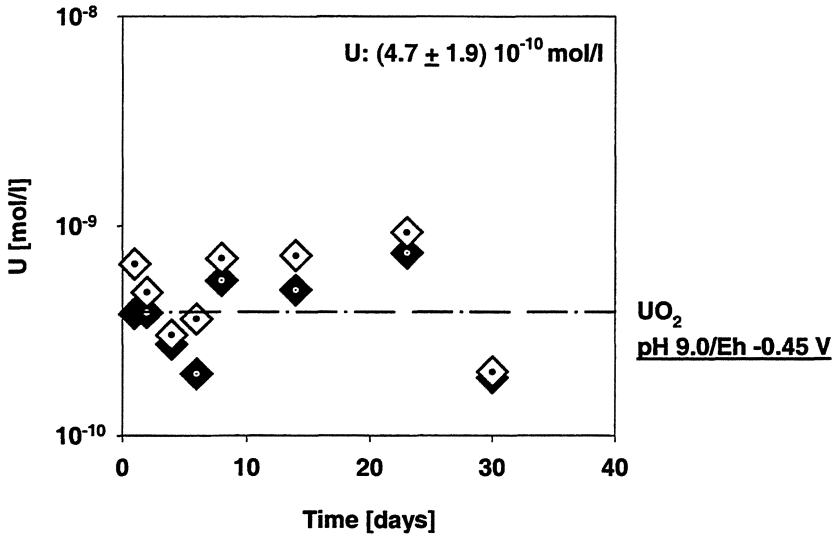

FIGURE I.4-12. Concentrations of uranium vs. time in the oversaturation experiments in modified Allard groundwater under anoxic conditions in the presence of metallic Fe. The dashed line shows the theoretical solubility of UO_2 (EQ3, composite database) at measured Eh value.

TABLE I.4-4. Concentrations of uranium and solid phases in the oversaturation experiments in saline groundwater under anoxic conditions.

Saline groundwater/ Equilibration period	pH	Eh [V]	Solubility [mol/l]	Solid phase (X-ray diffraction)
no S(-II) addition 15-40 days	8.3	-0.30	$(6.5 \pm 2.8) \cdot 10^{-10}$	15, 30 days: weakly crystalline: $UO_2 - U_3O_7$ 40 days: U(IV)oxide including a cation (Sr, Ca), possibly Sr- or $CaUO_3$
3 ppm S(-II) 25-45 days	9.2	-0.31	$(9.6 \pm 8.6) \cdot 10^{-10}$	weakly crystalline $UO_2 - U_3O_7$
met. Fe 28-43 days	8.4...8.8	-0.47	$(1.8 \pm 1.6) \cdot 10^{-9}$	weakly crystalline $UO_2 - U_3O_7$ U(IV)oxide including a cation (Sr, Ca), possibly Sr- or $CaUO_3$

TABLE I.4-5. Concentrations of uranium and solid phases in the oversaturation experiments in near-field groundwater under anoxic conditions.

Near-field groundwater/ Equilibration period	pH	Eh [V]	Solubility [mol/l]	Solid phase (X-ray diffraction)
no S(-II) addition 7-44 days	7.5	-0.31	$(1.2 \pm 0.6) \cdot 10^{-9}$	weakly crystalline $UO_2 - U_3O_7$ Sr- or $CaUO_3$ (as above)
3 ppm S(-II) 25-43 days	7.5	-0.31	$(8.3 \pm 6.6) \cdot 10^{-10}$	weakly crystalline $UO_2 - U_3O_7$
met. Fe 27-43 days	7.6...8.0	-0.48	$(8.9 \pm 1.0) \cdot 10^{-9}$	weakly crystalline $UO_2 - U_3O_7$

Under anoxic conditions (WP I.4.1), the control of the Eh (-0.2...-0.3 V) had effect on the solubility of UO_2 pellets in synthetic groundwater. The solubility at low Eh, 10^{-9} M, was at the level of the theoretical solubility of the well-crystallized solid, UO_2. In synthetic groundwater without the Eh control, the solubility was one order of magnitude higher, being at the level of the theoretical solubility of U_4O_9 or U_3O_7. The presence of the U(IV) species at low Eh in the aqueous phase (30-80 %) was shown by the analyses of the oxidation state distribution. Under anaerobic conditions, without the Eh control, the dominant oxidation state was the U(VI). The composition of groundwater had a minor effect.

In the anoxic oversaturation experiments, the measured solubilities were generally in good agreement with the results of the pellet experiments in synthetic groundwater with reducing S(-II) species. A trend to lower solubility was observed with fresh (Allard) composition. The solubilities were low also under anaerobic conditions without S(-II). The presence of U precipitates had a clear effect on the measured Eh values, which were low also in the absence of the S(-II). This suggests that the surface of U precipitate may control the Eh in the precipitation experiments. The analyses of the solid phases gave weakly crystalline $UO_2 - U_3O_7$ as a result with fresh, saline and highly saline composition. There is a possibility that U_3O_7 has formed as oxidation product during the X-ray diffraction measurements. In saline groundwaters, an impure U(IV) oxide, including possibly Sr or Ca, seemed to precipitate with the $UO_2 - U_3O_7$. The duration of the oversaturation experiments was relatively short, $\leq$ 45 days.

WP I.4.3. STATIC DISSOLUTION OF UO_2 IN INTERSTITIAL BOOM CLAY WATER

To assess the performance of the possible final disposal of spent fuel in the Belgian Boom Clay layer, it is important to know the maximum uranium concentrations in the interstitial Boom Clay water upon contact with spent fuel. The objectives of the experimental programme are (1) to measure the uranium solubility in real Boom Clay Water, with unirradiated UO_2 as the solid phase and (2) to assess the impact of dissolved organic matter and carbonate concentration on this solubility. The measured uranium solubility may be representative for the dissolution in reducing conditions of spent fuel with an alpha activity that has decayed to the level where the fuel

dissolution kinetics is chemically controlled. The tests are supported by calculations with geochemical codes, to suggest possible solubility controlling solid phases.

Experiment

Depleted UO_2 powder with a particle diameter between 50 and 100 µm was immersed in Teflon® containers with real and synthetic clay waters for various test duration, at a target SA/V (= UO_2 surface area/leachant volume) of 1000 m^{-1}. The specific surface area of the UO_2 powder was estimated to be 0.044 m^2/g, based on BET measurements. Four types of clay water were used: real Boom Clay water ("RIC", sampled in the underground laboratory), synthetic Boom Clay water without humic acids ("SCW"), synthetic Boom Clay water with humic acids ("SCWHA") and synthetic Boom Clay water with humic acids, and with low carbonate content ("SCWHA\C"). To prepare the SCWHA and SCWHA\C, humic acids, extracted from real clay water, were used. This extract is a concentrate of dissolved organic matter ("DOM"), consisting mainly of humic acids. The media differ mainly in their Na, Cl, sulfate, carbonate and organic content. Typical compositions of the blank test media are presented in TABLE I.4-6. Only the main elements are presented.

Two duplicate test series have been performed:

For the **first test series**, the test temperature was 25°C. All tests were performed in a glove box with argon atmosphere. No reducing species were added. The carbonate containing media suffered from CO_2 degassing, leading to a strong and continuous pH increase. Attempts to stabilize the pH by HCl addition were ineffective.

For the **second test series**, the test temperature was 20°C. The tests at low carbonate contents were performed in an argon glove box; the other tests were performed in a glove box with in Ar/0.4% CO_2. Small solution volumes of 10 mg/l sulfide in degassed high performance liquid chromatography water were added at regular time intervals, to keep the redox potential lower than -150 mV_{SHE}. The pH in the carbonate rich media was stabilized by the high CO_2 content of the box.

The redox measurements for both test series were performed with a combined Ag/AgCl redox electrode; the pH measurements were performed with a combined glass electrode. At regular points of time, samples of a few ml were taken from the leachates, and the test containers were replenished to the original volume. The uranium, carbonate and organic matter in the leachates were measured after ultrafiltration over 30 000 molecular weight cut-off filter membranes. The uranium concentrations were measured by Inductively Coupled Plasma - Mass Spectrometry (ICP-MS). The carbonate and organic matter concentrations were measured with a Total Organic Carbon - Total Inorganic Carbon analyzer.

Before the solubility tests were started, the oxidised layer of the UO_2 powder was removed in the so-called "predissolution". About 4 g of the UO_2 powder was weighed, and transferred in a Teflon® container of 200-ml volume. 40 ml of the test medium was added. The containers were kept at 25 or 20°C in the argon or argon/CO_2 purged glove boxes. Every few days, the leachate was replaced by fresh medium. The uranium concentrations in the leachates were measured by ICP-MS. When the corrosion rate was constant, the oxidised layer was considered to be more or less removed, and the solubility tests were started. We did not control the completeness of the predissolution by surface analysis.

TABLE I.4-6: Composition range of the blank test media (main elements)

	Na mg/l	Cl mg/l	SO_4 mg/l	HCO_3^- mg/l	DOM mg/l	U mole/l
RIC	380 / 420	25 / 110	0 / 7	800 / 900	131 / 167	$2x10^{-9}$ / $7x10^{-9}$
SCW	344 / 345	51 / 56	22 / 26	"	<10	$5x10^{-10}$ / $1x10^{-8}$
SCWHA	547 / 611	335 to 428	"	"	160 / 177	$1x10^{-9}$ / $7x10^{-9}$
SCWHA\C	239 / 256	"	"	30[1] / 4[2]	"	$2x10^{-9}$ / $4x10^{-8}$

[1] first test series; [2] second test series

Results from the first test series

In the predissolution stage, which lasted almost 3 months, the leachant was refreshed 14 times. For the first test series, the media for the predissolution were the same as those for the solubility tests. The dissolution rate was found to decrease drastically in this period, as demonstrated by the results shown in TABLE I.4-7. This indicates the removal of U(VI) from the UO_2 surface. In spite of this, we are not sure that the oxidised layer was completely removed, especially in SCWHA\C, where the dissolution rate was relatively high at the end of the predissolution stage.

TABLE I.4-7: Dissolution rate in the predissolution of the first test series, based on the uranium concentration in the test containers (ultrafiltered over 30000 MWCO membranes); na = not available

	UO_2 dissolution rate (µmole U /l/day or µmole U /m²/day)			
replacement	RIC	SCW	SCWHA	SCWHA\C
1	33	41	36	1.9
2	2.3	3.8	3.4	1.8
3	0.78	1.7	1.3	1.1
5	0.15	0.77	0.39	0.95
9	0.042	0.14	0.055	na
11	na	na	na	0.14
14	0.055/0.061	0.080/0.12	0.052/0.023	0.16/0.17

After 14 solution replacements, the containers were filled with 180 ml of leachant to start the actual solubility tests; the medium replacement was then restricted to the replacement of the volume needed for analysis. The measured uranium concentrations are presented in FIGURE I.4-13. Figure I.4-13a shows the concentrations measured in the first 58 days, when the atmosphere in the (argon) glove box was anoxic. Figure I.4-13b shows the concentrations measured until 240 days. After about 80 days, the glove box was severely contaminated with oxygen, with clear consequences for the uranium concentration. After about 120 days, the containers with the carbonate rich media were transferred to a glove box with an argon/0.4% CO_2 atmosphere.

Because of the small number of sampling intervals in the anoxic stage (until 80 days), we cannot demonstrate that saturation values have been reached in this period. The results suggest nevertheless that we are heading towards saturation concentrations. In SCWHA\C, U concentrations decreased between 31 and 58 days; and in SCW, SCWHA and RIC, the corrosion

rate between 10 and 45 days was an order of magnitude smaller than the corrosion rate between 0 and 3 days, so here also we appear to be heading towards saturation. After 45 to 60 days, all uranium concentrations are between 10^{-7} and 10^{-6} mole/l. We take these concentrations as approximate values for the equilibrium concentrations, giving the results presented in TABLE I.4-9.

The near-saturation concentrations increase in the order RIC < SCWHA < SCW < SCWHA\C (this order is confirmed also after 2 or 3 and 10 days). The high concentrations in SCW and SCWHA\C are not expected. Possible explanations for the high uranium concentration in SCWHA\C are (1) high HA complexation constants at alkaline pH values, compensating for the lower carbonate content, and (2) incomplete predissolution.

The existence of high HA complexation constants at alkaline pH values would be in contradiction with results from a study with U(VI) and similar Boom Clay humic acids, where uranium appeared to have little affinity for the humic acids [97VER]. This explanation is therefore unlikely. As an alternative explanation, we must consider the possibility of an incomplete dissolution of the oxidised layer in the predissolution stage. The high uranium concentrations in solution may be due to the dissolution of the remnants of this oxidised layer (the most likely U(VI) solids are more soluble than the U(IV) species).

The high concentration in SCW, compared to SCWHA and RIC, is probably caused by the higher pH and E_h in SCW (the organic material acts as a redox buffer against oxygen contamination and as a pH buffer against CO_2 escape). Because of the pH and E_h variation, we cannot distinguish the net effect of the absence of humic acids. The E_h effect is, however, much smaller than expected. This can be explained by the hypothesis that the potential at the UO_2 surface rather than the potential of the bulk solution is the controlling factor [89GRA]. This potential may be lower because of the presence of reduced uranium (UO_2, $UO_{2.25}$).

The pH and E_h values of TABLE I.4-8 were used as input in HARPHRQ calculations, using the NEA thermodynamic database, release 9, to determine the theoretical solubilities of potentially solubility limiting solid phases and the corresponding dominant species in solution. The selected phases were schoepite in SCW, and UO_2(am),UO_2(c) and U_4O_9 in the other media. We found no good agreement with the tested solid phases, except in RIC, where a relatively good fit was obtained with uraninite (1.7×10^{-7} M). The main cause for the bad agreement was probably the poor reliability of the redox measurements, because of the absence of strong redox couples. In all cases, $UO_2(CO_3)_3^{4-}$ or $UO_2(CO_3)_2^{2-}$ were the dominant species in solution, even in the medium

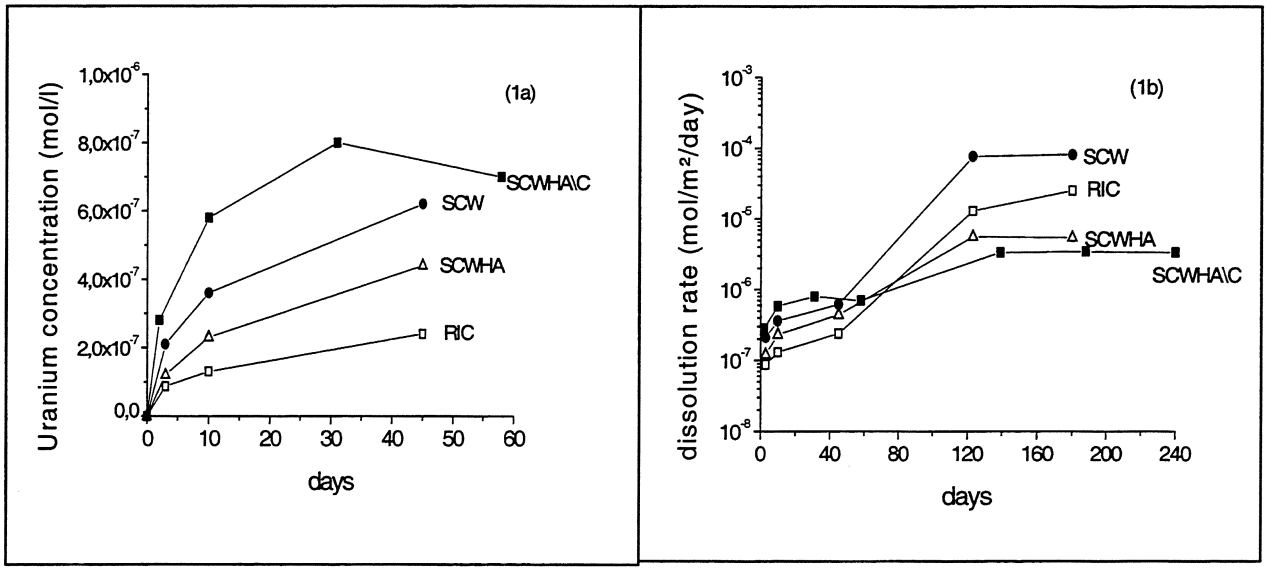

FIGURE I.4-13: Mean uranium concentrations of the first series of solubility tests in the first 58 days (1a) and until 240 days (1b). (RIC = real Boom Clay water; SCW= Synthetic Clay Water; SCWHA= Synthetic Clay Water with humic acids; SCWHA\C = Synthetic Clay Water with humic acids and low carbonate content.

with lower carbonate content.

After 180 and 240 days, the uranium concentrations were between $3.4x10^{-6}$ to $8.2x10^{-5}$ mole/l (see also Figure I.4-13) in the order SCWHA\C < SCWHA < RIC < SCW, and the pH was 8.1 to 8.2 (table I.4-9). For the tests with the carbonate rich media, the low pH is due to the fact that after the oxygen contamination, these containers were transferred to an argon/CO_2 glove box. It is likely that in the relatively oxidising conditions after 80 days and more, U(IV) has been oxidised to U(VI) and that the U(VI) species are stabilised in solution by carbonate. In these conditions, the humic acids seem to have a negative effect on the uranium concentrations (the U concentrations are lower in SCWHA and RIC than in SCW). The humic acids seem to disturb the influence of carbonate.

TABLE I.4-8: Uranium concentrations, pH and E_h in the first series of solubility tests after 45 to 58 days (U concentrations after ultrafiltration over $3x10^4$ MWCO filter membranes)

	near-saturation U concentration (mole/l)	mean U concentration (mole/l)	pH	E_h mV_{SHE}
RIC	$\geq 2.4x10^{-7}$	2.4×10^{-7}	9.0	-140
SCWHA	$\geq (4.1x10^{-7} / 4.8x10^{-7})$	4.4×10^{-7}	8.9 / 9.1	-112 / -119
SCW	$\geq (5.9x10^{-7} / 6.3x10^{-7})$	6.2×10^{-7}	9.7 / 9.8	+182 / +189
SCWHA\C	$\geq (6.3x10^{-7} / 7.8x10^{-7})$	7.0×10^{-7}	8.6 / 8.6	-74 / -82

Table I.4-9 : Uranium concentration in the first set of solubility tests after 180 and 240 days.

Medium	leaching duration	[U] mol/l	pH
SCW	180	8,2E-05	8.1
RIC	180	2,5E-05	8.1
SCWHA	180	5,4E-06	8.2
SCWHA\C	240	3,4E-06	8.2

Results from the second test series

In the predissolution of the second test series, the leachant was refreshed 50 times in 207 days for the carbonate rich media and 22 times in 126 days for the low carbonate medium. The predissolution for all the tests with carbonate rich media was performed with SCW (900 mg/l carbonate), because this medium appeared most effective in the first test series; using only one type of predissolution medium, we also make sure that we have a comparable UO_2 surface for all carbonate rich media at the end of the predissolution. The predissolution for the low carbonate

tests was performed with a similar medium as SCW, but with only 10 mg/l carbonate. As for the first test series, the dissolution rate decreases drastically in this period, as demonstrated by FIGURE I.4-14. The dissolution rate is smaller in the low carbonate medium; this may be a mixed effect of the lower oxygen content in this box (≤ 1 ppm in the argon box, contrary to 3 ppm in the Ar/CO_2 box) and the lower carbonate content. By the end of the predissolution stage, when most U(VI) is dissolved, the uranium concentrations are very sensible to fluctuations of the oxygen concentration in the glove box (the oxygen pressure variation is presented in Apendix 7) . Therefore, it is difficult to decide whether the uranium dissolution rate was stable at the end of the predissolution; the dissolution rate was then floating around $3x10^{-8}$ mole $U/m^2/day$ in the carbonate rich media. For the low carbonate medium, the dissolution rate was about $4x10^{-9}$ mole $U/m^2/day$ after 126 days of predissolution. The final dissolution rate and the complete results of predissolution are respectively presented in TABLE I.4-10 and in Appendix 7.

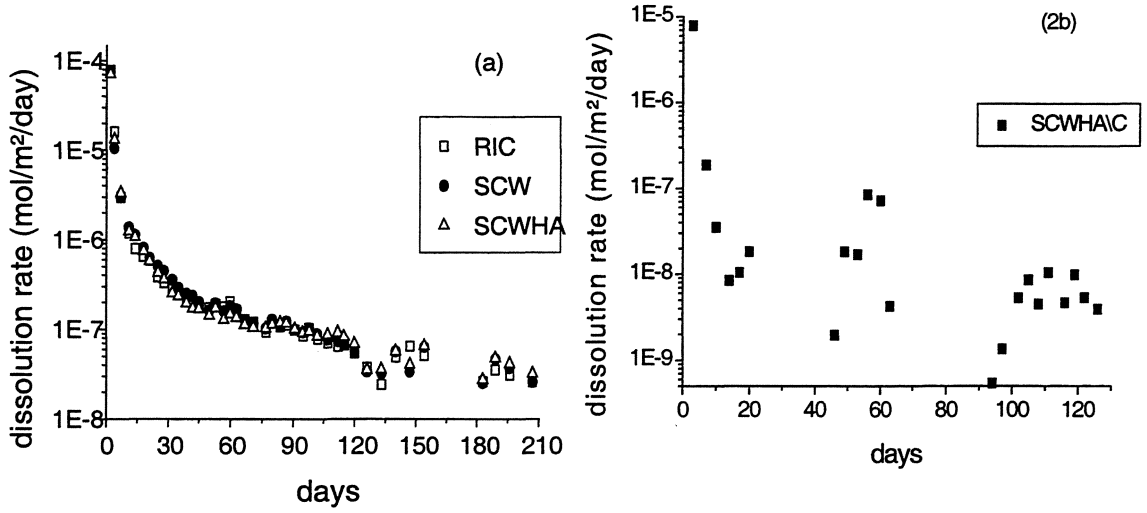

FIGURE I.4-14: UO_2 dissolution rate during the predissolution of the second test series in the carbonate rich media (a) and in the low carbonate medium (b).

TABLE I.4-10 : Dissolution rate in the predissolution of the second test series, based on the uranium concentration in the test containers.

UO_2 dissolution rate (µmole U /l/day or µmole U /m²/day)				
replacement	RIC	SCW	SCWHA	SCWHA\C
50	0.0258	0.0258	0.0318	
22				0.00389

Data for the second series of solubility tests are available for the carbonate-rich media until 277 days and for the carbonate-poor media until 215 days. The test containers were filled with 180 ml of the respective media (RIC, SCW, SCWHA and SCWHA\C). A sample of the leachate was taken every three or four days during the first 15 days of experiment and after this period every 15 days. The corresponding mean uranium concentrations are shown in FIGURE I.4-15.

The pH was in general between 8.2 and 8.6. The addition of sulphide species stabilised the redox potential of the clay waters at values lower than -150 mV, the presumed threshold for oxidative dissolution in carbonate rich-media. During the experiments, fresh sulphide solution was added after 25 and 84 days to the carbonate rich media, but only after 117 days for the carbonate poor medium. The carbonate poor medium required less adjustment, because of the smaller quantity of oxygen in the latter glove box (normally $\leq$ 1 ppm, no peaks > 20 ppm), and - hence - the slower oxidation of sulphide species. The different behaviour confirms the importance of the oxygen concentration in the glove box atmosphere.

The uranium concentrations initially increase to values, similar to those observed in anoxic conditions, but afterwards, they decrease to values that are 1 to 2 orders of magnitude lower, between $6x10^{-9}$ and $6x10^{-8}$ M.

This decrease occurs only for the carbonate-rich media. It occurs sooner for the tests in the real clay water (after 13 to 25 days) than for the tests in synthetic clay waters (after about 100 days). Minimum uranium concentrations are reached after 40 to 70 days in RIC, after about 200 days in SCW, and after about 250 days in SCWHA. The minimum uranium concentrations show some variation, which is probably due to small oxygen contaminations. In RIC and SCW, they are often close to $1x10^{-8}$ M, whereas in SCWHA, they are not smaller than 3 to 4 x 10^{-8} M .

The decrease of the uranium concentrations is probably caused by the reduction of U(VI) to U(IV). The fact that the final concentrations are very similar in RIC, SCW and SCWHA, suggests that complexation of uranium by humic acids is not important for the total uranium concentration in these conditions. The humic acids retard the reduction of U(VI) to U(IV) in the synthetic clay waters, but this was not observed in the real clay water.

We assume that the faster reduction in RIC is due to the presence of iron traces ([Fe] = $1x10^{-6}$ mol/l). When we add sulfide species, the redox potential in RIC is controlled by the couple Fe/Pyrite whereas the redox couple is probably SO_4^{2-}/S^{2-} in the synthetic medium. At the beginning of leaching test (< 15 days), the uranium profile for RIC presents the same variation as SCW and SCWHA because the establishment of equilibrium with Pyrite is slow. When the equilibrium is reached, the uranium concentration decreases.

For the RIC medium, the measured redox potential control was verified by the results of

geochemical simulations (PHREEQC version 1.6). Three phases have been tested as solubility controlling phases : uraninite, $UO_2(a)$ and $(U(OH)_4)_a$. The better results is obtained for $(U(OH)_4)_a$ with an equilibrium concentration equal to $1.2x10^{-8}$ mol/l. The calculated E_h value was, however, around -308 mV. This value disagrees with our experimental measurement, so we cannot draw a consistent conclusion.

For the medium with low carbonate content, the results are similar to the first test series. The uranium concentration was higher than in the test with high carbonate concentration. After 30 days and until 215 days, it stabilized around [U] $=1.5x10^{-6}$ mol/l. When carbonate is absent, or present in small quantities, the presence of humic acids in solution seems to contribute to the complexation of the uranium (VI) in spite of its presumed little affinity for humic acids. The results illustrate the possible competition between humic acids and carbonate taken in evidence in carbonate media. However, though the dissolution rate was very low after 126 days of predissolution (10^{-9} mol U/m²/d), the oxidised layer was probably not totally removed, because of the low carbonate content in the solution during the predissolution stage. Because of this, we cannot give any conclusion about the relative complexation properties of humic acids and carbonates. Because of the apparent steady-state observed for the uranium concentration in solution, the leaching tests have been stopped after 249 days.

In all cases, solution concentrations of U tend to approach a constant value. Solution saturation is almost obtained after 74 days (carbonate rich media) and 31 days (low carbonate medium).

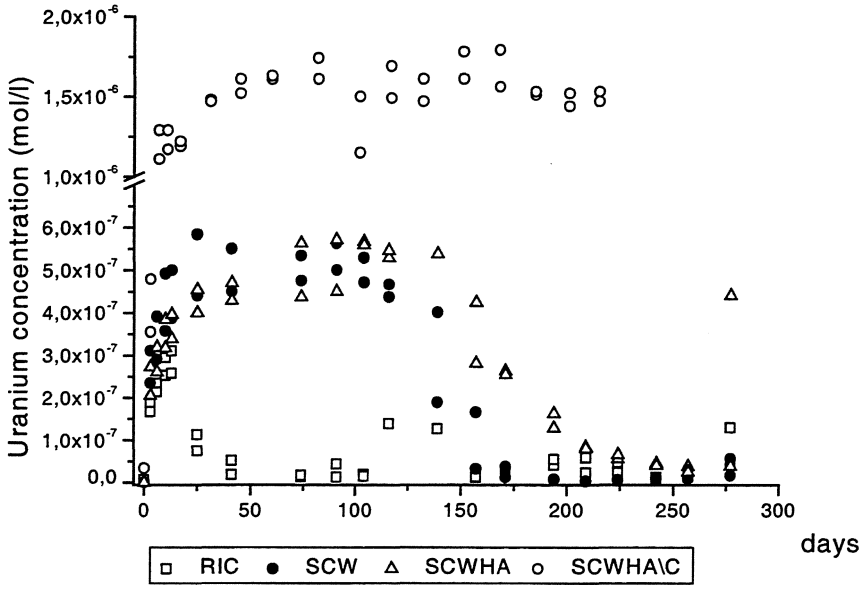

FIGURE I.4-15: Uranium concentrations in the carbonate rich media and in the medium with low carbonate content as a function of time for the second test series

Comparison of results of UO_2 dissolution in boom clay with data from granite water (WP1.4.1 and with literature data)

The "near saturation" concentrations, found in boom clay water prior to oxygen intrusion in the first test series, are about 10 times larger than the concentrations measured in anoxic conditions in 600 mg/l carbonate solutions ($4x10^{-8}$ M uranium), and simulated granite groundwaters (Allard groundwater: 123 mg/l carbonate, with 2 to 2.5 10^{-8} M uranium; bentonite water: 600 mg/l carbonate, with 2 to $2.5x10^{-8}$ M uranium) under anaerobic conditions (N_2, O_2<1ppm) [96OLL/OLI]. In tests with SIMFUEL in Allard water under similar conditions, concentrations between 10^{-8} and 10^{-7} M were found. We see two possible causes for the difference with our results: (1) The glove box used in [96OLL/OLI] had an oxygen content <1 ppm; (0.1ppm at best), the oxygen content in the argon glove box for tests with Boom Clay waters showed some fluctuations during the test period, and values were always higher. (2) In the tests by Ollila, an intact fuel pellet was used. In our tests, UO_2 powder is used. Bruno mentions in [89BRU/PUI] that the solubility product of solid UO_2 depends on the particle size.

The final U concentrations are in boom clay water about 10 times larger than the concentrations measured at a SA/V of 19.8 m^{-1} under anoxic conditions (E_h from -20 to +130 mV) on UO_2 pellets in synthetic saline groundwater [96OLL]. This difference may be caused by the difference in carbonate content (there was no carbonate in the saline groundwater), the UO_2 particle size (pellet versus powder), the oxygen content (so E_h), or the salinity affecting the activity coefficients of the dissolved species.

The uranium concentrations are slightly higher than in a saline brine, at 1000 m^{-1}, in anoxic conditions ($E_h \approx$ -300 mV), where concentrations of about $2x10^{-7}$ M were found after 30 days [97CAS/PAB]. In these experiments, UO_2 powder was used of the same size fraction as in our tests (50-100 µm). The small difference with our results may be caused by the difference in carbonate content.

The high concentrations found after oxygen intrusion after 180 and 240 days in the first test series ($3.4x10^{-6}$ to $8.2x10^{-5}$ mole/l) are comparable with the concentrations found in granite water for oxidising conditions under similar experimental conditions (see FIGURES I.4-2 to I.4-5).

The uranium concentrations in the second test series are higher than those found by Ollila et al. in saline and granite groundwater, namely about 10^{-9} M (TABLE I.4-3), though in both cases, sulfide was added. This may be due to the higher oxygen concentration in the SCK argon/CO_2 glove box (about 3 ppm). Sulfide may have been lost (oxidized) from solution at the early stages of the experiments by reacting with trace oxygen, leading to higher Eh values (~ -150 mV) as the experiments proceeded. At the higher carbonate concentrations this may cause the stabilization of U(VI) carbonate complexes, and hence an increase in solubility.

The uranium concentrations in reducing conditions are close to the concentration measured in fresh real Boom Clay water ($7x10^{-9}$ M). The redox potential and the pH were always higher than expected in the Boom Clay host rock, so the measured uranium concentrations are conservative values. Moreover, no clay has been added in the tests performed so far. If the dissolved uranium species sorb onto the clay, this may cause a further decrease of the equilibrium concentrations. Existing data suggest however, that the clay impact is small. Indeed, in the presence of clay, U concentrations of the order of magnitude 10^{-8} mole/l were found [97LEL], which is similar to the concentrations found in reducing Boom Clay water.

Conclusions on UO_2 solubility in clay

Within 2 months or less in anoxic conditions, the uranium concentrations appear to approach a steady state. The observed "near steady-state" concentrations are all between 2.4 and $7.8x10^{-7}$ M. They tend to be higher than the concentrations found in literature for similar E_h and/or pH conditions; the difference is an order of magnitude at most, and can probably be explained by small differences in experimental conditions (carbonate concentration and oxygen concentration in the glove box). However, the influence of the carbonate concentration and humic acids on the uranium concentration was apparently small under oxidizing and reducing conditions, but uncontrolled pH and Eh variations hamper the interpretation. In contrast, under oxidizing conditions carbonate rich waters showed highest steady state concentrations of dissolved uranium.

No relation was found between experimental solubilities and values calculated for some candidate solubility controlling solids, except for the tests in RIC, where a relatively good agreement was found with uraninite as the solubility controlling solid phase.

In the synthetic clay media, the addition of sulfide species to the carbonate rich media caused a lowering of the redox potential, but the uranium concentration was about $5x10^{-7}$ M which is similar than in the absence of sulfide. This high concentration may be due to the presence of traces of oxygen. In the real clay water, the uranium concentration decreased in the presence of sulfide species after more than 15 days, possibly because the presence of traces of iron in solution resulted in a lower redox potential (control by Fe/Pyrite). After 74 days, the uranium concentration was about 10^{-8} M.

The redox potential and the pH in the anoxic stage were always higher than observed in the pore waters of Boom Clay host rock. Moreover, no clay has been added, and adsorption was avoided. The measured uranium concentrations are conservative values in the tests performed so far. The effect of Boom Clay should be studied in a future program.

Comparison of steady state solution concentrations of U in various groundwaters under oxic, anoxic and reducing conditions

A comparison of final U-concentrations achieved under oxic, anoxic and reducing conditions are given in TABLE I.4-11. Uranium concentration values in GBW were about two orders of magnitude lower in experiments performed in anoxic atmosphere than in experiments under oxidizing. In salt media under oxidizing conditions uranium concentration values in solution ($4 \cdot 10^{-6}$ mol/l) are only one order of magnitude higher than in the experiments performed under anoxic atmosphere, because, probably due to carbonate complexation, solution concentrations under oxic conditions were higher in carbonate containing granite bentonite solutions than in carbonate free salt media.

Comparison with anoxic UO_2 dissolution data from granite (VTT-data) and salt media suggests that, after 45 days of leaching, saturation should be reached at SA/V = 1000 m^{-1}. In leaching tests of VTT with UO_2 in anoxic saline groundwater at a SA/V of 19.8 m^{-1}, the U concentrations reached a constant concentration after a few days. Since the tests of SCK.CEN are performed at much higher SA/V, these tests should approximate equilibrium much faster than the tests at 19.8 m^{-1}. The uranium concentrations in clay water are slightly higher than about $2 \cdot 10^{-7}$ M in anoxic saline solution, at 1000 m^{-1} ($E_h \approx$ -300 mV). UO_2 powder was used of the same fraction as for clay water (50-100 µm). The main difference between SCK·CEN tests in clay water and the tests in granite or salt water is the much higher carbonate concentration in clay waters (even in SCWHA\C). This may explain why constant U concentrations were not reached in Boom Clay water after 10 days and why steady state solution concentrations were higher in clay water. Indeed, the dominant solution complex of dissolved uranium was calculated (SCK·CEN) to be $UO_2(CO_3)_3^{4-}$. (see also WP IV.1: modelling).

The data from WPI.4 show that differences in experimental U-solubilities under anoxic and reducing conditions are directly related to the U(VI) content in solution. This can be seen in FIGURE I.4-16, using U(VI) concentrations from TABLE I.4-3 experimentally measured by VTT.

TABLE I.4-11: Comparison of steady state U-concentrations (molality, ultrafiltered) for various groundwater compositions and redox states – Tests at 25°C and surface to volume ratio of 1000 m^{-1} (*=19 m^{-1}, **=0.66 m^{-1}) CIEMAT=SIMFUEL, UPC/VTT/SCK·CEN=UO_2, FZK=spent fuel, CEA=spent fuel and SIMFUEL). Reducing conditions are assured either by presence of iron of by addition of reducing agents. log pCO2 $-3.5,$$-2.0

			oxic		anaerobic		reducing	
			U [m]	trend	U [m]	trend	U [m]	trend
Salt	NaCl	CIEMAT	$5\cdot10^{-6}$	incr.	10^{-7} $ $8\cdot10^{-7}$ $$	decr. const.	$4\cdot10^{-8}$ $ $1\cdot10^{-7}$ $$	const. const.
		UPC			$2\cdot10^{-7}$	const		
		FZK			$2\cdot10^{-6}$		$2\cdot10^{-8}$	const
Granite	GBW	CIEMAT	$3\cdot10^{-5}$	const	$5\cdot10^{-7}$ $ $8\cdot10^{-5}$ $$	decr. incr.	$2\cdot10^{-8}$ $ $2\cdot10^{-7}$ $$	const. decr.
		UPC			$4\cdot10^{-7}$	const.		
		VTT	$1\cdot10^{-5}$	const				
	EGW	FZK			$6\cdot10^{-7}$	decr.	$7\cdot10^{-8}$	const
		CEA					$1\cdot10^{-8}$	const
	AGW	VTT	$7\cdot10^{-5}$	incr.	$2\cdot10^{-8}$ [95OLL]	Const.		
	AGWM	VTT	$7\cdot10^{-5}$	incr.	10^{-8} (*,**)	Const.	$2\cdot10^{-9}$ (**)	const
	SGW	VTT	$2.5\cdot10^{-5}$	const.	10^{-9} (*) with colloids:10^{-8} $5\cdot10^{-9}$ (**)	const incr.	10^{-9} (**)	const
Clay	RIC	SCK			$2\cdot10^{-7}$	Incr.	10^{-8}	const
		CEA					10^{-8}	const
	SCW	SCK			$6\cdot10^{-7}$	incr.	10^{-8}	const
	SCWHA	SCK			$4\cdot10^{-7}$	Incr.	$3\cdot10^{-8}$	Decr.
	SCWHA/C	SCK			$7\cdot10^{-7}$	const	$1.5\cdot10^{-6}$	const

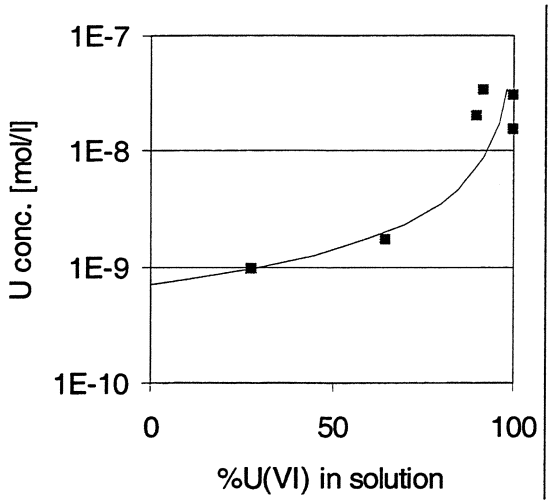

FIGURE I.4-16, dependency of UO2 solubility under reducing conditions on the experimentally measured U(VI) content in solution.

WP I.5 DYNAMIC TESTS

Dynamic tests (UO_2 dissolution tests in flowing groundwater) are considered to yield more reliable initial reaction rate values than static tests, because the effect of saturation of the solution or precipitation of secondary reaction products can be avoided if the water flow rate is sufficient high. The dissolution rate obtained in such an experiment with UO_2 in NaCl solution in presence of 0.01 M Na-hypochlorite (a simulated radiolysis product) was 0.33 $mg \cdot m^{-2} \cdot d^{-1}$, this value is one order of magnitude lower than the value reported in [96GIM/BAR], where the dissolution rate was determined when the UO_2 surface was previously cleaned. XPS observation of the UO_2 surface indicated a percentage of U(VI) close to 33%, which could passivate the surface.

TABLE I.5.1 Detail of the experiments performed in UO_2 leaching tests.

Experiment	Conditions	UO_2 (g)	Medium	pH
UODS	UO_2 + ClO^- 0.01 M	0.3	NaCl 5 m	11.0± 0.1
UODGW25	UO_2; 25ºC	0.3	GBW	8.3± 0.1
UODGW60	UO_2; 60ºC	0.3	GBW	8.3± 0.1

The dissolution rate in GBW-water (experiment UODGW25) was 0.33 $mg \cdot m^{-2} \cdot d^{-1}$ at 25°C this value has been plotted in Fig.IV.1-7 ("Modelling") as a function of the carbonate content in the GBW. The good correlation of this value with those obtained in bicarbonate medium points out that one of the most important parameters for the UO_2 dissolution is the bicarbonate concentration. The dissolution rate determined in experiment in GBW water at 60°C (UODGW60) was 0.45 $mg \cdot m^{-2} \cdot d^{-1}$; this value is lower than expected due to effect of temperature [97PAB/CAS], the reason is probably calcite precipitation onto the UO_2 surface since XPS observations indicated a high increase of calcium on the UO_2 surface.

WP I.6/I.7 ELECTROCHEMICAL INVESTIGATIONS OF UNIRRADIATED UO_2, SPENT UO_2 AND MOX FUEL ELECTRODES

The dissolution properties of the UO_2 matrix in the presence of oxidants can only be understood if the electrochemical nature of this reaction is taken into account. UO_2 is a semiconductor. From this point of view the dissolution of UO_2 is the anodic reaction, characterised by the corrosion current i_{corr}. The cathodic counter reaction is the reaction of oxidants.

Extensive electrochemical measurements are described in the literature on unirradiated UO_2 and on SIMFUEL to determine the mechanisms of dissolution or precipitation and quantification of the rate determining step [88BRU/CAS, 75NIC/NEE, 94SHO/HOC, 91SHO/SUN]. Shoesmith et. al. [85BAI/JOH, 92SUN/SHO, 97SUN/SHO] carried out examinations of unirradiated UO_2 electrodes in water, and of the effects of α- and γ-sources on the non-irradiated UO_2 electrode. Since then this group has prepared used CANDU fuel electrodes [96SHO/SUN and has confirmed its previous findings. It is important to test whether the findings of these studies are applicable to expected European repository conditions and to different fuel types. In the project various electrochemical techniques are applied at ITU and at FUB to understand and quantify the electrochemical processes and to provide complementary data to the non-electrochemical approaches of other project partners.

Electrochemical impedance spectroscopy (EIS)

AC impedance measurements were performed by ITU. This technique provides a wealth of kinetic and mechanistic information for the study of corrosion, semiconductors, batteries, electroplating phenomena, and electro-organic synthesis. Some introductory articles of corrosion rate determinations with EIS are given by several authors [70SLU/REH, 81MAN, 82MAN/KEN, 81LOR/MAN, 72EPP/KED, 85JÜT/LOR].

Because the ac impedance measurements does not involve a wide range potential scan, experiments can be carried out in low conductivity solutions and also on high resistivity electrodes like UO_2 and spent fuel where dc methods are subject to serious potential-control errors (IR drop).

In impedance spectroscopy the ac equivalent of a dc resistance of a system is measured using a sinusoidal potential excitation with the magnitude E_0 over a frequency range from 10^{-3} up to 10^6 Hz. If the potential E(t) as a function of time t is given by

$$E(t) = E_0 \cdot \sin(\omega \cdot t); \qquad \omega = 2 \cdot \pi \cdot f \tag{I.6-1}$$

then a linear system will have the current response I(t)

$$I(t) = I_0 \cdot \sin(\omega \cdot t + \Phi) \tag{I.6-2}$$

where I_0 is the current amplitude and Φ is the phase shift. For pure ohms behaviour is $\Phi = 0$. Analogous to Ohm's law the impedance Z of the system is defined by

$$Z = \frac{E(t)}{I(t)} \tag{I.6-3}$$

The simplest way to describe the impedance Z of an electrode/electrolyte interface is to use an equivalent circuit with a resistance R_{pol} in parallel with a capacitance C_{dl}. R_{pol} represents the polarization resistance, R_{sol} the resistance between the electrode surface and the tip of the reference electrode and C_{dl} is the double layer capacitance

$$Z(\omega) = R_{pol} \cdot \frac{1}{(1 + j \cdot \omega \cdot R_{pol} \cdot C_{dl})} + R_{sol} \tag{I.6-4}$$

Impedance of irradiated UO_2 fuel

The irradiated fuel electrode can be interpreted as a fuel-coated metal electrode. If there are no defects in the coating, the electrochemical behaviour of the electrode is only determined by the fuel sample. This commonly found for non-irradiated UO_2 fuel specimens. For such specimens equivalent circuits were proposed [96ENG/FEL, 96BOT/WEG] consisting of two circuits in series, the first describing resistivity and dielectric behaviour (RC) of the electrode bulk with a resistance R_{bulk} in parallel with a capacitance C_{bulk}. The second circuit is related to the electrode/electrolyte interface and consists of the polarization resistance in parallel to the double layer capacitance followed by a series connection of the electrolyte resistance (in practice the uncompensated ohms resistance R_Ω) (FIGURE I.6.1). The formation of adsorption and/or passive layers on the surface is considered with another RC circuit in series or an resistance of the layer in series and a capacitance in parallel connection to both this resistance and faradic circuit. A calculated impedance spectrum for this model is given in FIGURE I.6.3. The parameters (R_{bulk} = 40 kΩ, C_{bulk} = 5 pF) for the first circuit were calculated from the resistivity and dielectric constant for natural UO_2 [96BOT/WEG]. At open circuit potential a very low corrosion rate is expected, therefore a high polarization resistance of 10 MΩ is used.

Spent fuel has not the uniform structure of non-irradiated UO_2. The fuel has a different porosity distribution and also there are many cracks in the fuel. Here electrolyte solution can penetrate into the fuel and may find a pathway to the metal holder. This would mean that the highly resistive fuel sample is short-circuited and the electrochemical behaviour of the working electrode is determined by the fuel and by the metal. Relevant electrochemical data on irradiated fuel can only be obtained if theses effects are quantified. A model describing such behaviour is shown in FIGURE I.6.2. The whole fuel electrode circuit is short-circuited by a network representing a simple metal dissolution. The polarization resistance of the metal $R_{Me,pol}$ is in parallel to the associated double layer capacitance $C_{Me,dl}$ at the bottom of the pathway. R_{por} represents the resistance of the pathway. A theoretical calculation is given in FilGURE I.6.4. It is assumed that the corrosion rate of the metal is also very low and that the attacked area of metal surface is small, that means that $R_{Me,pol}$ will be high (7 MΩ) and $C_{Me,dl}$ (0.1 μF) will be smaller than C_{dl}. The pathway resistance was assumed to be 10 kΩ.

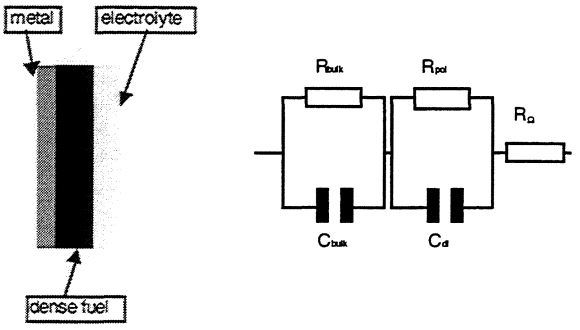

FIGURE. I.6.1: Equivalent circuit of a fuel electrode without conductive pathways between metal support and electrolyte solution. The capacitance and resistance of the fuel bulk is represented by C_{bulk} and R_{bulk}., the polarization resistance R_{pol} electrode/electrolyte interface and the double layer capacitance. R_Ω represents the uncompensated ohms resistance consisting of electrolyte resistance R_{sol}, resistance of the metal support and measuring leads R_{lead}.

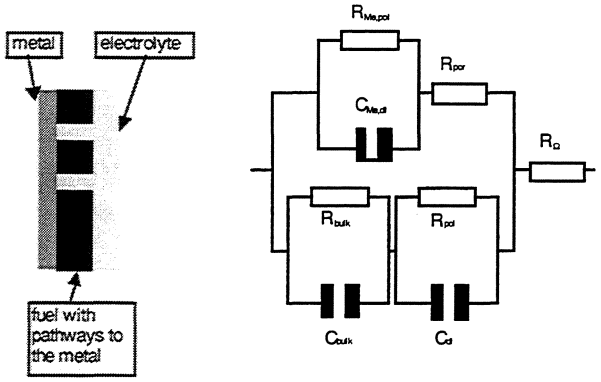

FIGURE. I.6.2: Equivalent circuit of a fuel electrode with conductive pathways like unsealed **cracks and/or pores between metal support and electrolyte solution. At the metal/electrolyte interface at the bottom of the pathway an additional polarization resistance $R_{Me,pol}$ and a double layer capacitance $C_{Me,dl}$ correlated with metal corrosion is expected. R_{por} represents resistance of the pathway.**

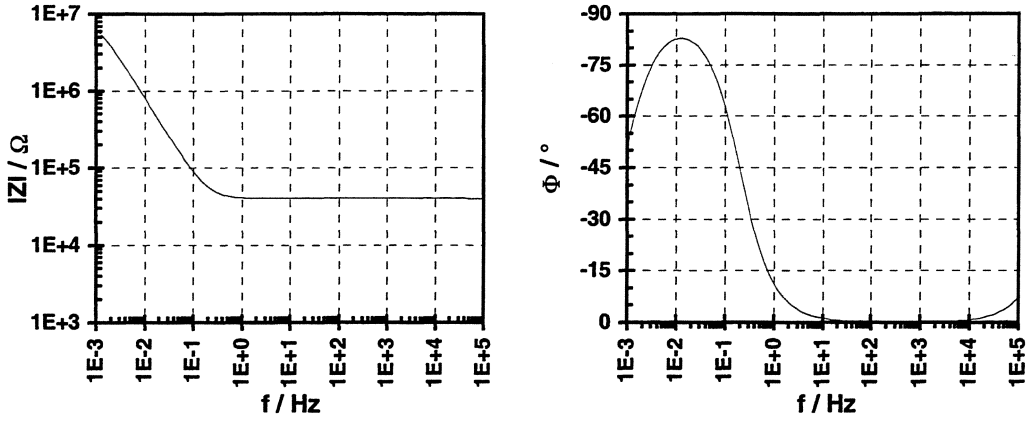

FIGURE. I.6.3: Calculated impedance spectrum for an equivalent circuit of a fuel electrode without any conductive pathways (R_{bulk} = 40 kΩ, C_{bulk} = 5 pF, R_{pol} = 10 MΩ, C_D = 20 µF, R_Ω = 100 Ω).

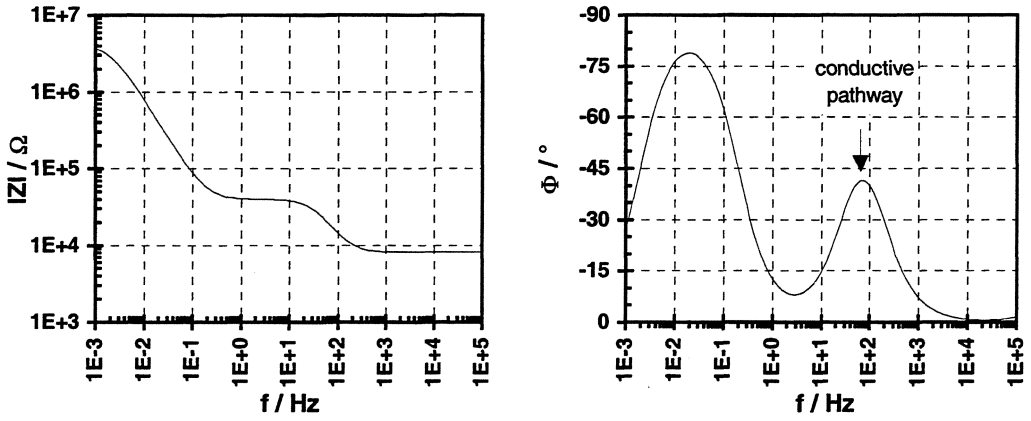

FIGURE. I.6-4: Calculated impedance spectrum of an equivalent circuit of a fuel electrode with conductive pathways (R_{bulk} = 40 kΩ, C_{bulk} = 5 pF, R_{pol} = 10 MΩ, C_D = 20 µF, R_Ω = 100 Ω, $R_{Me,pol}$ = 7 MΩ, $C_{Me,dl}$ = 0.1 µF, R_{por} = 10 kΩ).

In comparison with the dense model (FIGURE I.6-3) it can be see that the magnitude of the impedance is decreased at the low frequency limit and a further step occurs at medium frequencies. This step is accompanied with a further phase angle minimum in the same frequency range. The appearance of such a minimum in a measured spectrum may be a hint for conductive pathways and mixed electrode behaviour.

Current-Potential distribution

The basis for electrochemical determination of corrosion rates is the relation between measured current density and potential E_{pol} or polarization $E_P = E_{pol} - E_{corr}$ (E_{corr}: free corrosion potential). At the free corrosion potential (no application of an external potential like under normal corrosion conditions) the sum of all partial currents equals zero. In case of electrodes with a high resistivity like UO_2 and spent fuel also the potential drop across the bulk resistance, R_{bulk}, must be taken into account: $E_{pol} = E_{app} - I \cdot R_{bulk}$ with $I = i \cdot A_{el}$ (E_{app}: applied potential). For a homogeneous electrode (see also impedance model FIGURE I.6-1) the equation

$$i = i_{corr} \cdot \left[e^{\left(\frac{\ln 10}{b_a} \cdot E_P \right)} - e^{-\left(\frac{\ln 10}{b_c} \cdot E_P \right)} \right] \qquad \text{(I.6-5)}$$

is valid. The corrosion current i_{corr} can be obtained by extrapolation of anodic, b_a, and cathodic, b_c, Tafel lines (log i = f (E_p)) to the corrosion potential or by measurement of the differential polarization resistance $R^*_{pol} = R_{pol} \cdot A_{el}$ (A_{el} = corroding surface area of the electrode) that is defined as

$$\frac{1}{R^*_{pol}} = \left(\frac{di}{dE_P} \right)_{E_{corr}} . \tag{I.6-6}$$

Differentiation of Eq I.6-5 gives:

$$\frac{di}{dE_P} = i_{corr} \cdot \ln 10 \cdot \left[\frac{1}{b_a} \cdot e^{\left(\frac{\ln 10}{b_a} E_P \right)} + \frac{1}{b_c} \cdot e^{-\left(\frac{\ln 10}{b_c} E_P \right)} \right]. \tag{I.6-7}$$

At the corrosion potential $E_{pol} = E_{corr}$ ($E_P = 0$) this reduces to the well known Stern Geary relations [57STE/GEA, 73MAN]

$$i_{corr} = \frac{B}{R^*_{pol}} \quad \text{with} \quad B = \frac{b_a \cdot b_c}{\ln 10 \cdot (b_a + b_c)} \tag{I.6-8}$$

For higher anodic potentials Ep > 60 mV it is possible to derive the relationship between the measured current density and the differential polarization resistance from Eq I.6-5 and Eq. I.6-7 by eliminating the exponential term

$$\frac{di}{dE_P} = \frac{\ln 10}{b_a} \cdot i . \tag{I.6-9}$$

If E_P < - 60 mV the relation

$$\frac{di}{dE_P} = \frac{-\ln 10}{b_c} \cdot i \tag{I.6-9a}$$

is valid. In potentiostatic experiments it is possible to determine the Tafel slopes b_a and b_c and also the composite Tafel parameter B by measuring the current densities and impedance spectra at various applied potentials.

Simplified corrosion model of a defective specimen

In case of a specimen with conductive pathways to the metal holder Eq I.6-5 is not valid, because of the additional electrochemical reaction at the metal surface. This is a severe limitation for using irradiated fuel electrodes. In order to overcome this problem, a model was proposed to quantify the additional electrochemical reaction. Assuming no interactions at pore walls, no diffusion and mass transport effects and an ideal current and potential behaviour (e.g. no side reactions, each electrode is homogeneous) the following model is used (FIGURE I.6.5).

The current $I_{fuel} = i_{fuel} \cdot A_{fuel}$ (A_{fuel}: fuel surface (FIGURE I.6.5)) related to the fuel oxidation at the fuel surface (surface/solution interface) is given by Eq I.6-5 and the polarization $E_{P,fuel}$ is in this case given as

$$E_{P,fuel} = E_{app} - E_{corr} - I_{fuel} \cdot R_{bulk} . \tag{I.6-10}$$

An equation analogous to Eq I.6-5 can be formulated with I_{Me}, $E_{p,Me}$, $b_{a,Me}$, $b_{c,Me}$ and $I_{corr,Me}$ for the metal holder corrosion with $I_{corr,Me} = i_{corr,Me} \cdot A_{Me}$. were $i_{corr,Me}$ represent the corrosion current density of the metal and A_{Me} is the total defect area. The total defect area A_{Me} can be estimated from impedance measurements due to the relation

$$A_{Me} = \frac{\rho_{sol} \cdot d_{el}}{R_{por}} \qquad \text{(I.6-11)}$$

ρ_{sol} is the resistivity of the solution in the defect, which is estimated from impedance measurements (~1 Ωm). d_{el} is the electrode thickness that is assumed to be the defect length and R_{por} represents the measured resistance of the pathway.

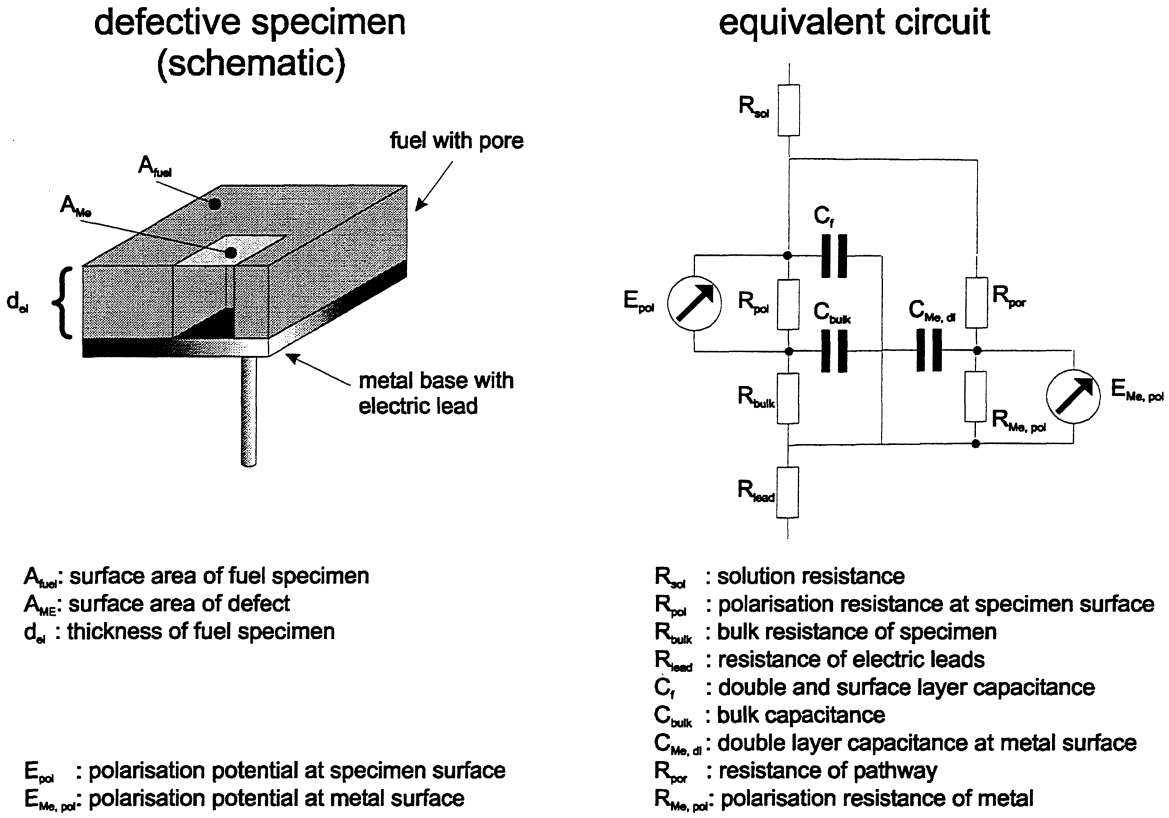

FIGURE.I.6.5: Simplified corrosion model of a spent fuel electrode that has conductive pathways from the electrode surface to the metal base. It is assumed that all defect pore areas can be added to give the total surface area of the defect, A_{Me}, with a length equal to the electrode thickness, d_{el}. In the related equivalent circuit also the potentials E_{pol} and $E_{Me,pol}$ are given, which are determining the electrochemical reactions occurring at the fuel surface and the metal surface.

The parameters needed for the model are summarised in TABLE I.6.1. An example of a calculated current-potential behaviour of an electrode with a conductive pathway is shown in FIGURES I.6.6 and I.6.7. As easily can be seen from FIGURE I.6.7 in case of a galvanic coupling a determination of the anodic Tafel slope $b_{a, fuel}$ from the measured current I_{tot} has to be done very carefully to avoid errors.

TABLE I.6.1: Input parameters used for the calculation of current-potential distributions at leaking electrodes using the simplified contact corrosion model.

electrode parameters	fuel parameters	metal parameters
total surface area (geometric) A_{el}: 0.1 – 1 cm^2	free corrosion potential E_{corr}: 100 - 500 mV_{SHE}	free corrosion potential $E_{corr,Me}$: -300 - 400 mV_{SHE}
thickness d_{el}: 1 - 4 mm	corrosion current density i_{corr}: 10^{-9} A/cm^2	corrosion current density $i_{corr,Me}$: 1.6 10^{-8} A/cm^2
bulk resistance R_{bulk}: 1 – 100 kΩ	anodic Tafel slope $b_{a,fuel}$: 80 mV	anodic Tafel slope $b_{a,Me}$: 120 mV
pore resistance R_{pore}: >100 kΩ	cathodic Tafel slope $b_{c,fuel}$: 250 mV	cathodic Tafel slope $b_{c,Me}$: 60 mV
resistivity of solution: ρ_{sol}: 0.8 Ω·m (estimate from measured solution resistance R_{sol})		

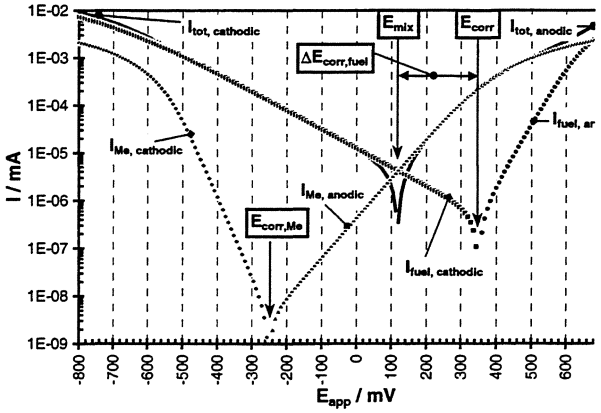

FIGURE. I.6.6: Theoretically calculated ideal current-potential behaviour for a defective fuel electrode (A_{el} = 0.5 cm^2, d_{el} = 3 mm, R_{bulk} = 15 kΩ, R_{por} = 100 kΩ, E_{corr} = 350 mV, $E_{corr,Me}$ = -250 mV, further parameters see TABLE). The diagram shows the current-potential curve $I_{tot} = f(E_{app})$ obtained directly from the experiment and the partial currents of fuel and metal corrosion. In this case no IR-drop correction is applied.

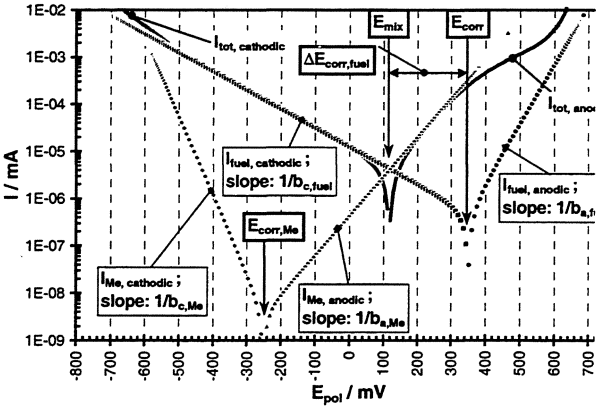

FIGURE. I.6.7: The diagram shows the I_{tot}-curve (see also FIGURE I.6.6) including the I_{tot}·R_{bulk}-drop correction that gives in case of non-defective homogeneous electrodes the correct Tafel slopes $b_{a,fuel}$ and $b_{c,fuel}$. For comparison also the ideal current-potential curves of fuel and metal corrosion are shown. The defect area A_{Me} is here 0.047% of the total area A_{el} and the mixed potential E_{mix} is 117 mV lower than the free corrosion potential E_{corr} of the fuel.

The model allows the interpretation of electrochemical data of defected fuel electrodes and it also allows to optimize the electrode fabrication process. The defect size has to be minimized in electrode preparation as far as possible. Therefore a new impregnation device was developed. A further factor is to reduce the deviation of the open circuit potential from the free corrosion potential by choosing in future a material such as gold that is inert to corrosion in solution instead of brass, copper or steel, which were successfully used for electrical contacts of non-irradiated UO_2 and low burn-up fuels [81SUN/SHO, 92SUN/SHO, 92HEP/WEG, 96SHO/SUN].

Spent fuels used for electrochemical experiments

For the investigation of electrode potentials of spent fuel it was decided to use a German commercial UO_2 fuel with 3 different burn-ups (B2 - B4) in the range from 30 to 50 GWd/t (see Tab. I.6.2). And also one MOX fuel with a burn-up of 21.1 GWd/t was chosen.

TABLE I.6.2: Spent fuels used for electrochemical investigations.

designation of fuel	fuel type	Burn-up GWd/t	calculated composition
B2	UO_2	31.5	Appendix 6, Tab. 7
B3	UO_2	45.2	Appendix 6, Tab. 8
B4	UO_2	53.1	Appendix 6, Tab. 9
MOX	MOX	21.1	Appendix 6, Tab. 10

UO_2 fuel

The irradiated UO_2 shows several restructured zones (FIGURES I.6.8-11). In going from the pellet periphery towards the fuel center these are:

An outer rim of 60-240 µm where UO_2 presumably reacted with fission product Cs and appears to have a second phase present: which may be cesium uranate. This zone exists at and above 45 GWd/t average burn-up for the cross section (B3, B4) (FIGURE I.6.8). During sample preparation for the electrochemical measurements this outer zone may be damaged.

A densification zone with a low measured porosity of 2.4 %. If the reaction zone UO_2/Cs is not present (B2), this zone stretches up to the outer rim of the pellet (FIGURE I.6.9).

The subsequent 3rd zone is characterised by the appearance of intergranular porosity with increasing temperature. In the same temperature range grain growth starts; a maximum value of 11 µm was measured for the grain diameter compared to average diameter of approximately 7 µm for the non-irradiated fuel (FIGURE I.6.10).

A central zone with inter- and intragranular porosity (FIGURE I.6.11). Here grain boundary porosity (ca. 1 µm diameter) is visible on the grain facets.

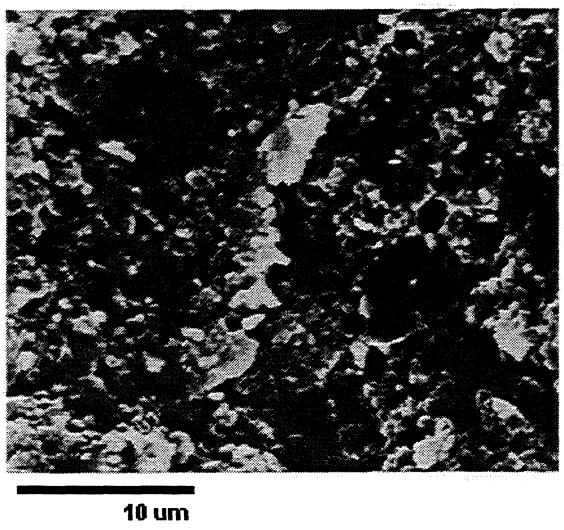

FIGURE. I.6.8: SEM micrograph of zone I

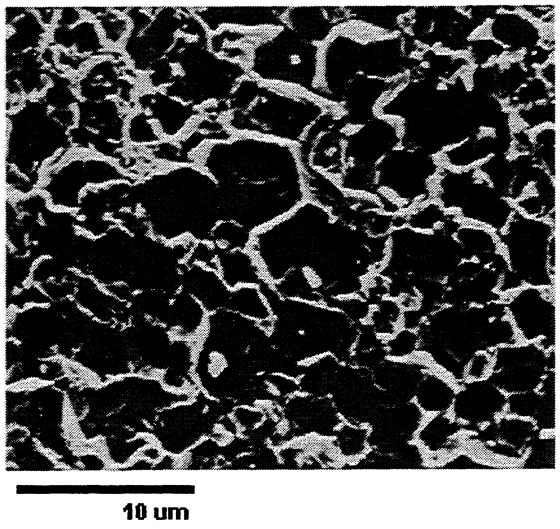

FIGURE. I.6.9: SEM micrograph of zone II.

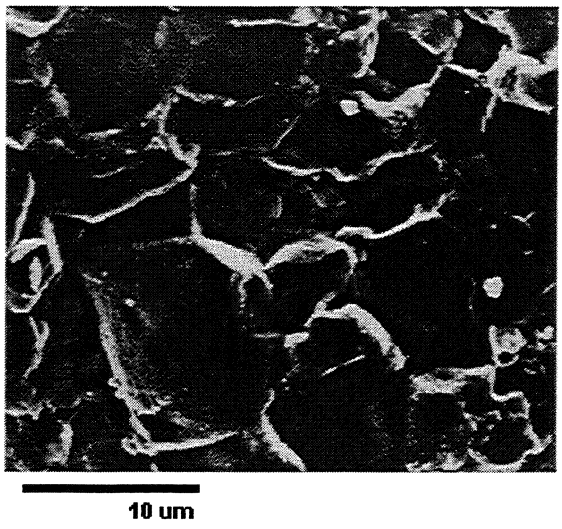

FIGURE. I.6.10: SEM micrograph of zone III.

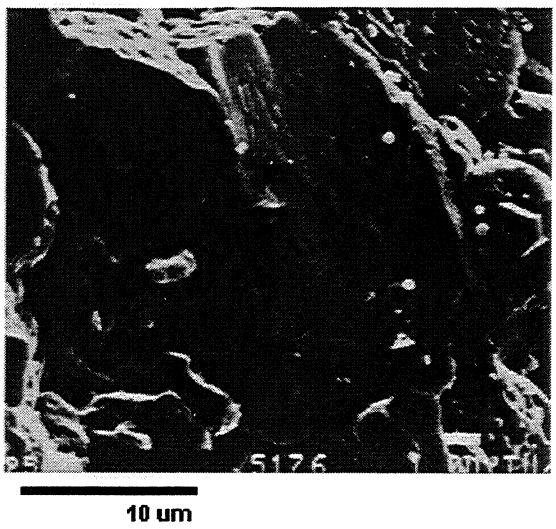

FIGURE. I.6.11: SEM micrograph of zone IV.

MOX fuel

This fuel has a approximately Pu content of 7.5%. Pu-rich particles contain 25% PuO_2. The mean grain size is 5 µm and its density is 94.5% of theoretical density. The fuels calculated composition is given in Appendix 6, TABLE 10.

The micrographs shown in FIGURES I.6.12 and I.6.13 illustrate the structural differences between irradiated UO_2 and MOX fuel. The UO_2 fuel has a relatively homogeneous structure while the MOX fuel has a heterogeneous structure of a UO_2 matrix with embedded Pu-rich agglomerates.

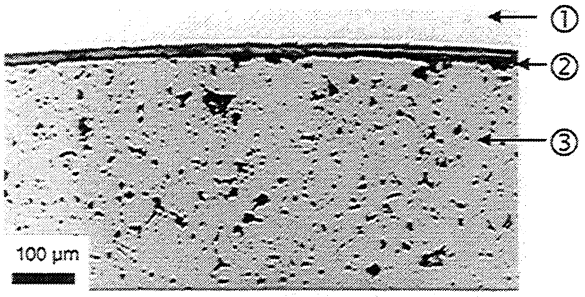

FIGURE. I.6.12: Micrograph of UO_2 fuel with a burn-up of 53 GWd/t (1: cladding, 2: gap, 3: fuel)

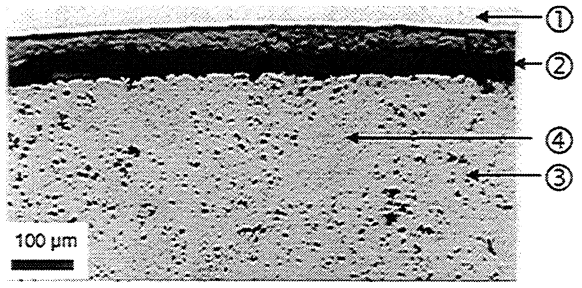

FIGURE. I.6.13: Micrograph of MOX fuel with a burn-up of 24 GWd/t (1: cladding, 2: gap, 3: UO_2 matrix of fuel, 4: Pu-rich agglomerates)

Non-irradiated UO_2

For some electrochemical experiments also unirradiated UO_2 was used. This fuel was delivered from NUKEM with a mean grain size of 4 – 5 µm and a density of 10.18 g/cm^3. The sintered pellets have a diameter of 8 mm and a length of 10 mm.

Preparation of samples for electrochemical experiments

For the preparation of the working electrode a 2 – 3 mm thick slice is cut from the fuel rod or pellet and is then decladded. In the case of high burn-up fuel the material is often very brittle and it easily breaks into smaller pieces. One of these pieces is fixed on the brass stub of the electrode head with conductive glue (FIGURE I.6.14). After hardening, the stub with the sample is screwed into the body of the electrode head. The cavity is then filled with epoxy resin (EPOFIX, Struers) for embedding. After hardening the sample is polished down to 1 µm (FIGURE I.6.15). The mean geometric surface area of the spent fuel samples is around 0.1 cm^2.

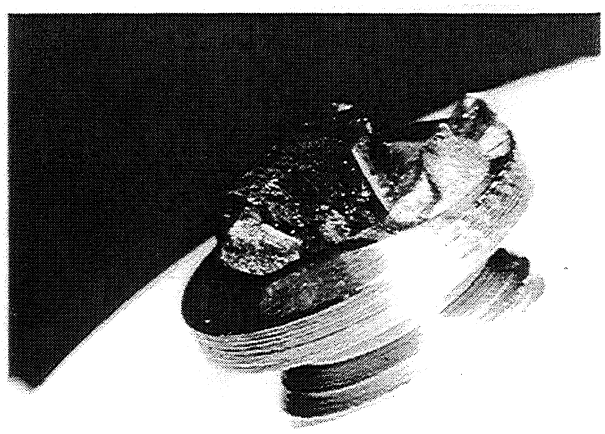

FIGURE. I.6.14: Piece of spent fuel (B4) mounted on brass stub of electrode head (diameter of brass stub: 10 mm).

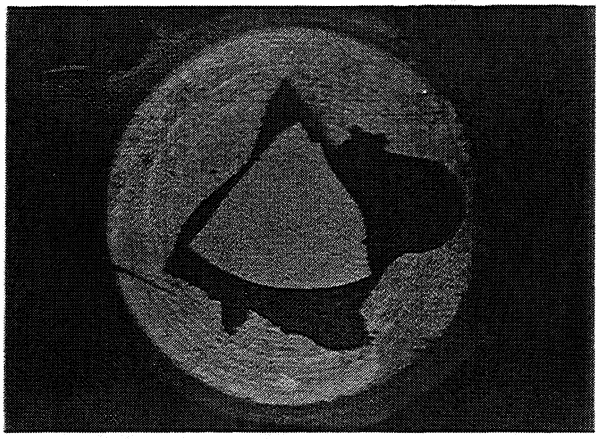

FIGURE. I.6.15: Piece of spent fuel (B4) mounted on brass stub of electrode head (diameter of brass stub: 10 mm) and embedded and polished.

After electrochemical experiments using SEM (FIGURE I.6.16) it was found that a sample is divided by a crack in two separate parts. The right side shows a grain boundary attack while the left side remains as polished. This means that the left side was electrically isolated from the main part. To avoid such problems in subsequent tests the surface preparation was modified. The sample pieces were now pre-embedded in a Perspex tube to get a good electrical insulation. Then the sample is polished on the back to get a plane surface for good electrical contact to the brass stub.

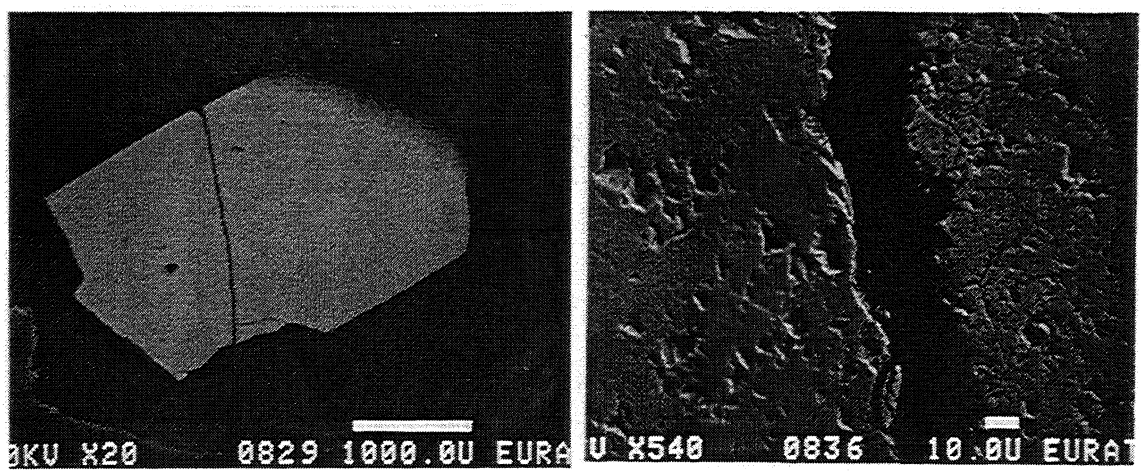

Fig. I.6.16: SEM micrographs of a spent fuel sample divided into two separate parts by a crack. Left side remains as polished and right side shows grain boundary attack.

Vacuum-pressure impregnation chamber

Nevertheless potential breakdowns were observed in long-term corrosion tests performed on spent fuel electrodes that indicates conductive pathways through the samples (open cracks and/or pores). To get a much better filling of those critical structures with resin the fuel sample must be impregnated under vacuum. Then the impregnation chamber is set under overpressure to press resin into cracks and pores. Therefore a new impregnation chamber was designed and tested. A schematic diagram is shown in FIGURE I.6.17.

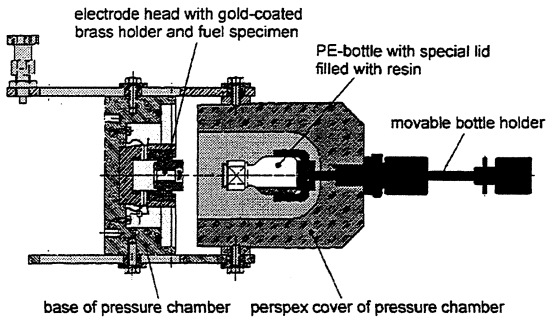

Fig.I.6.17: Schematic diagram of the impregnation chamber.

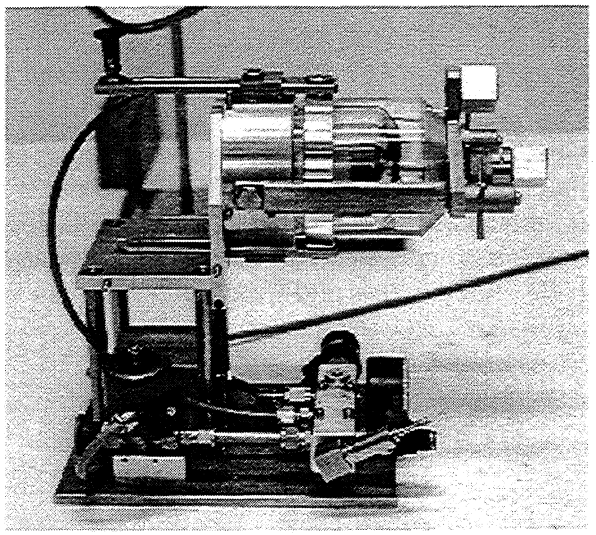

Fig. I.6.18: Impregnation chamber ready for evacuation.

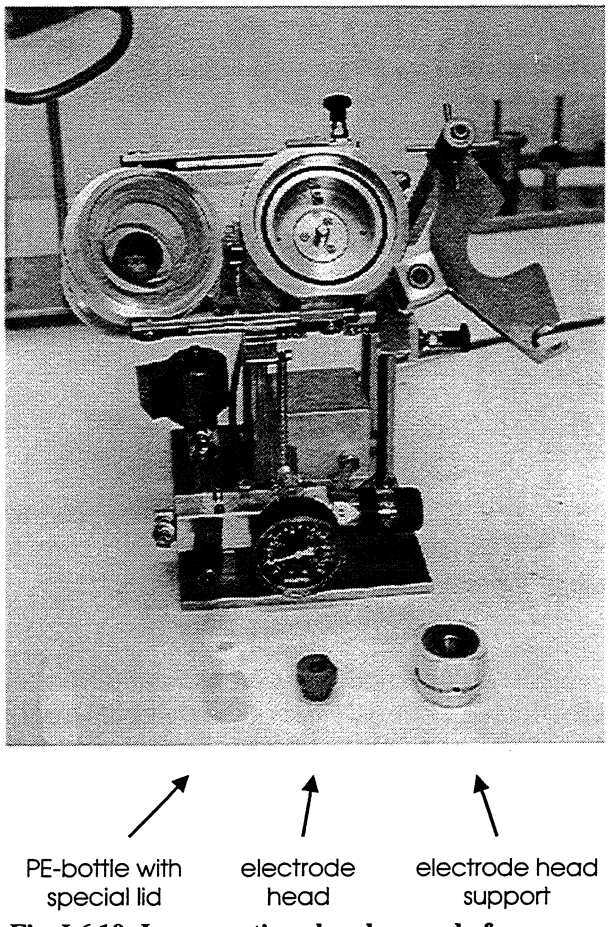

Fig. I.6.19: Impregnation chamber ready for use

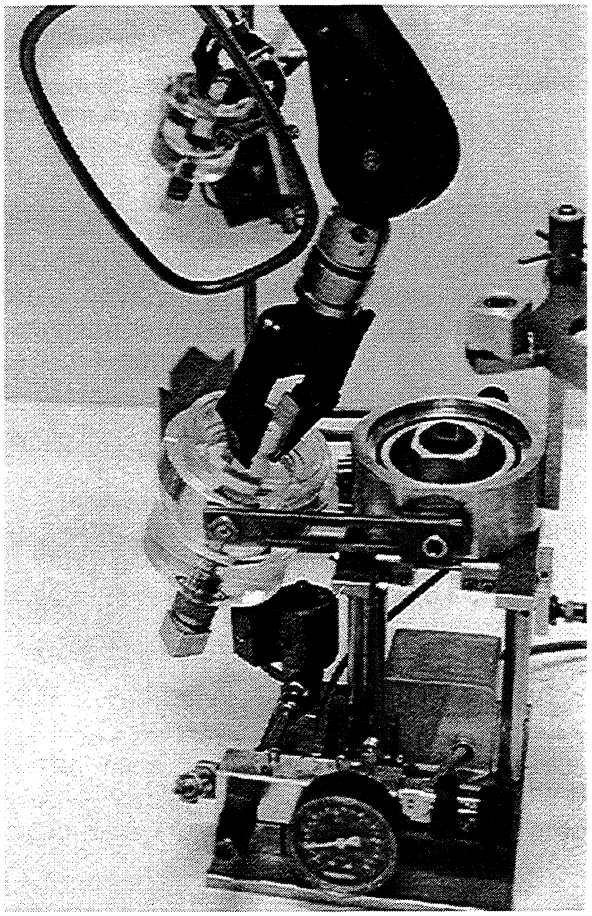

Fig. I.6.20: Placing PE-bottle into position

The new cell is designed specially for remote handling in the hot cells (FIGURE I.6.20). FIGURE I.6.18 shows the chamber, closed. FIGURE I.6.19 shows the chamber open with its component parts. After evacuation the chamber is pivoted in an upright position and the resin will flow from the bottle into the electrode head for embedding the fuel sample. Afterwards the chamber is pressurized up to 3 bar to obtain a good filling of void spaces of the specimen.

Experimental set-up for electrochemical experiments

The cell consists of a commercial 100-ml reaction vessel (inner diameter 62-mm) with a special cover to hold the electrodes in place. The electrolyte volume is 60 ml. As reference electrode a commercial double junction Ag/AgCl gel electrode is used with a high temperature stability up to 60°C (FIGURE I.6.21). For temperature control a remote-controlled magnetic stirrer thermostat (Variomag, Thermomodul 40ST) was purchased from H+P Labortechnik and was modified in our workshop for hot cell handling.

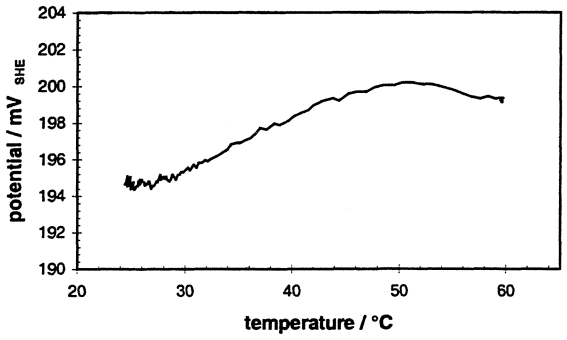

FIGURE I.6.21: Temperature stability of a double junction Ag/AgCl gel electrode measured in simulated ground water vs. a saturated calomel electrode at 22°C.

Reference electrode calibration

The potential of the reference electrode was checked against the reference electrode of a freshly calibrated redox combination electrode (saturated calomel electrode (Ingold) or Ag/AgCl electrode before and after each corrosion potential experiment. The potential shift of the reference electrode during 1000 h was within a range of some 10 mV.

Experimental procedures

Impedance spectrometry

Impedance measurements were carried out with the IM6 system distributed by Zahner Elektrik. The impedance was measured over the frequency range from 10^5 Hz down to $5 \cdot 10^{-3}$ Hz with a sine wave amplitude of 20 $mV_{p.p.}$.

Small amplitude cyclic voltammetry (SACV)

To obtain impedance data in the low frequency region an Autostat 251 potentiostat (Sycopel) was used for SACV measurements under potentiostatic control. Triangular potential scans with an amplitude of 20 $mV_{p.p.}$ were used at very low scan rates. Potential scans down to 0.3 µV/s representing a frequency of $6 \cdot 10^{-6}$ Hz are possible with this equipment. The obtained hysteresis curves were fitted using the set of equations given by D. D. Macdonald [78MAC1, 78MAC2].

Open circuit potential measurements on UO_2 and spent fuel

Before transfer into the hot cell the electrolyte was deoxygenated below 0.1 ppm of dissolved oxygen, by bubbling nitrogen and the initial pH was measured. In the hot cell the solution was poured in the electrochemical cell, which was kept under N_2/5% O_2 (~2 ppm in solution) atmosphere during the experiments .(T= 22°C to 28°C). The samples were introduced in the electrolyte and precathodised at -1.8 V_{SHE} for 5 minutes to reduce any oxidised surface. Then the electrolyte was renewed and the potential run started using an Ag/AgCl double junction reference electrode. During the experimental period the potential recording was stopped in order to execute additional investigations. Impedance measurements and SACV measurements were carried out under potentiostatic control at the open circuit potential

measured previously to obtain impedance data in the low frequency region.

Potentiostatic polarization

Potentiostatic polarization experiments were performed on non-irradiated UO_2 samples in 95% saturated NaCl solution and in simulated granite bentonite groundwater at ~25°C and 60°C. The electrodes were polarized at a fixed potential for 10 min. up to 1 h before the current was measured. Best results were obtained with 1 h polarization time t_{pol}. Then immediately the impedance was measured at the same potential for the IR-drop correction and the R_{pol}. The impedance spectra were fitted using the equivalent circuit for a non-defective electrode (FIGURE I.6.1) with a loss capacitance of some 1 nF in parallel. After finishing this measurement the procedure was repeated at a new potential.

Results and discussion of electrochemical experiments performed at ITU

The whole set of results is given in Appendix 6. No significant difference in the results were found between the potential scan directions in the anodic range indicating that the electrode was near equilibrium condition in the high anodic range.

In the potential range between +300 mV_{SHE} and +500 mV_{SHE} a weaker slope is visible. Here we have indications for a "pseudo-equilibrium" caused by very slow reaction rates. The reciprocal polarization resistance measured at the corrosion potential after 1 week exposure time does not fit with the values from the following stepping experiment. It is much closer to the extrapolated anodic Tafel line. Which means that the measured currents in this potential region will drop with time, a behaviour which was also found by other authors [98SUN/STR].

We assume that this process will occur until the anodic Tafel line, which describes the anodic dissolution process, is reached. This implies that the free corrosion potential estimated by extrapolation of the anodic and cathodic Tafel lines is the free corrosion potential for the "equilibrium state" or in other words the state in which the free corrosion potential is only determined by the anodic dissolution and the corresponding cathodic reaction. Other anodic reactions like surface oxidation are then negligible. Under these assumptions the extrapolated corrosion potentials can be considered as upper limit potentials. In TABLE I.6.3 the obtained results are summarized. In most cases the extrapolated free corrosion potentials are as expected higher than those directly measured. Only one experiment shows a lower extrapolated E_{corr} value. In this case the polarization time t_{pol} was too short to reach quasi-stationary conditions.

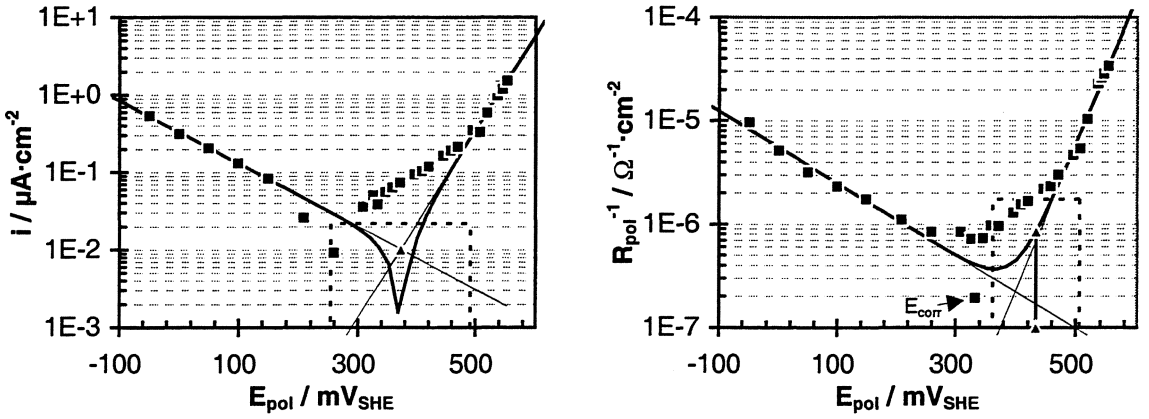

FIGURE. I.6.22: Potentiostatic polarization curves obtained from unirradiated UO_2 in simulated groundwater (T = 60°C, $p(O_2)$ < 1 mbar, initial pH 7.7).

TABLE. I.6.3: Electrochemical parameters obtained from potentiostatic polarization experiments (b_a: anodic Tafel slope; B: composite Tafel parameter; t_{pol}: polarization time at each potential before measuring current and impedance; EIS: obtained from impedance data; extrap.: obtained from extrapolation; meas.: directly measured; E_{corr}: free corrosion potential).

conditions					potentiostatic polarisation					
electrolyte	$C(O_2)$ ppm	initial pH	T. °C	$^{meas}E_{corr}$. mV_{SHE}	$^{extrap}E_{corr}$. mV_{SHE}	b_a. mV	$^{EIS}b_a$. mV	B. mV	^{EIS}B. mV	t_{pol}. min
95% sat. NaCl	7.4	7.1	22	168	440	76 ± 26	53 ± 40	25 ± 7	20 ± 14	10
synthetic groundwater	0.05	8.4	23	296	-63	82 ± 18	80 ± 8	23 ± 23	27 ± 34	10
synthetic groundwater	0.05	7.5	60	328	335	73 ± 60	56 ± 31	21 ± 10	26 ± 17	20
synthetic groundwater	0.05	7.7	60	346	372	83 ± 35	70 ± 15	27 ± 9	25 ± 4	60

The anodic Tafel slopes b_a (Eq. I.6-5) obtained from current-potential measurements and from impedance data are in good agreement. The values range between 53 and 83 mV.

Sunder and Shoesmith claim values of 40-60 mV for carbonate free solutions and values of ~90 mV for carbonate containing electrolytes [88SHO/SUN, 91SHO/SUN]. Combining electrochemical methods with solution analysis a slope of 80 mV was found (FIGURE I.6-32).

The composite Tafel parameters B (Eq I.6-8)) range between 20 mV and 27 mV. No significant difference between the data sets belonging to electrochemical and impedance measurements exists.

Open circuit potentials of unirradiated UO_2

The results obtained from unirradiated UO_2 specimen are summarized in TABLE I.6.5. In deoxygenated synthetic groundwater UO_2 an open circuit potential of ~300 mV_{SHE} was found. As can be seen in Appendix 6, FIGURE 5 the potential time curve show only little scatter in the first 10 hours. Then it became much more scattered between 10 to 40 hours. After this period the potential is increasing and much more stable. This behaviour may be attributed to little conductive pathways that are then closed by oxidation products of UO_2. This potential increase implies an increasing dissolution rate. Using the calibration curve (FIGURE I.6-32) derived from potential measurements and solution analysis the corrosion rates were calculated. They increase from 1.6 mg/m^{2}d at 23°C up to 11 mg/m^{2}d for the highest potential at 50°C. The corrosion rate can also be calculated from impedance measurements using the Stern-Geary relation (Eq I.6-8). Assuming a mean composite Tafel parameter of B= 25 mV dissolution rates between 1.3 and 17.5 mg/m^{2}d were obtained. The values found with two different methods are thus in good agreement.

In 95 % sat. NaCl solution the open circuit potentials was between 200 mV_{SHE} and 300 mV_{SHE} at pH 6 – 6.8. In the more acidic solution (pH 3.8) at higher oxygen content potentials higher than 500 mV_{SHE} can be reached. One of the most important parameters is the oxygen content of the solution. As shown in Appendix 6, FIGURE 7 the free corrosion potential reaches 299 mV_{SHE} with an oxygen content of 2 ppm in solution. After deoxygenation with N_2 the potential drops 80 mV to 220 mV_{SHE} (see also Appendix 6 FIGURE 8): potential drop from 500 mV_{SHE} to 350 mV_{SHE} at pH 3.8). The recorded redox potential E_h also drops from 550 mV_{SHE} down to 430 mV_{SHE}. It is interesting to look here at the potential difference $\Delta E_{h,corr} = E_h - E_{corr}$. $\Delta E_{h,corr}$ is with 180 mV to 250 mV in the range of

200 mV. This potential difference is predicted theoretically (see below) for UO_2.

After 100 h the temperature was increased to 50°C (Appendix 6, FIGURE 7) leading tot a sudden potential break down caused by a defect of the electrode due to thermal expansion. Similar break down of a lesser extent are observable also at other electrodes (Appendix 6, FIGURES 6 and 8) after 25 h and 100 h. Unfortunately no electrode has reached its equilibrium state before the break down occurred. But an estimate can be made assuming a potential out above. In case of pH 6 (Appendix 6, FIGURE 6) the estimated corrosion potential is in the range of 330 to 400 mV_{SHE}. Furthermore is the potential drop after 25 h with -180 mV in the same range as expected from the simplified corrosion model (TABLE I.6.6) when an open circuit potential of UO_2 of 350 mV_{SHE} is assumed.

Determination of dissolution rates from electrochemical data

The conversion from corrosion current densities to dissolution rates can be done via Faraday's law assuming an overall oxidation from U(IV) to U(VI). The electrochemical equivalent is for UO_2 $1.399 \cdot 10^{-3}$ g/As and for U $1.234 \cdot 10^{-3}$ g/As. The factor with the highest uncertainty is the surface area. All surface related data given are normalized to the geometric surface area and no roughness and porosity is taken into consideration. To compare electrochemical dissolution rates with those obtained from leaching experiments the real wetted surface of the fuel must be known.

Open circuit potentials of used fuel

First results

The first results obtained from long term corrosion tests are shown in FIGURES I.6.23 and I.6.24 and in TABLE I.6.4. The potential increases initially linearily on logarithmic scale from -750 mV_{SHE} to -600 mV_{SHE} of a clean non-oxidised surface to more anodic values. This can be attributed to a surface layer formation by a dissolution-precipitation mechanism [87GAD/ABD, 92HEP/WEG]. In the case of fuel B4 (TABLE I.6.23) thereafter a distortion of the potential occured, caused by other experiments using a high frequency furnace. After 10 to 12 days a maximum potential of +50 to +70 mV_{SHE} is reached. Then the potential drops to -100 mV_{SHE} and after 600 h a slight increase is seen. In contrast the potential measured with UOX fuel B2 (FIGURE I.6.24) only reaches -100 mV_{SHE} after 1 h running time. The general potential development is very scattered with large potential breakdowns in cathodic direction during the first 300 h.

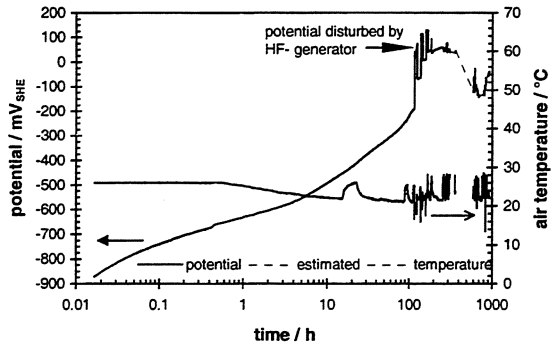

FIGURE. I.6.23: Open circuit potentials of UO_2 fuel B4 in 95% sat. NaCl solution (initial pH = 7.3, $C(O_2) < 2$ ppm).

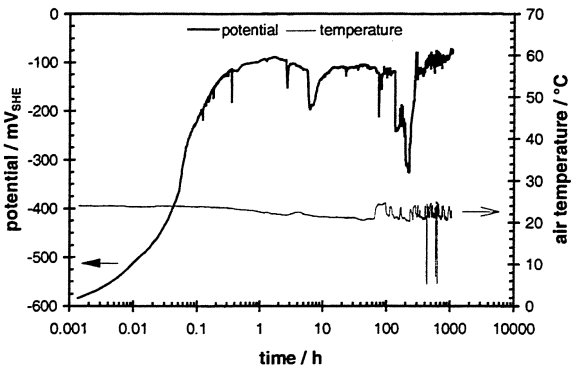

FIGURE. I.6.24: Open circuit potentials of UO_2 fuel B2 in 95% sat. NaCl solution (initial pH = 7.3, $C(O_2) < 2$ ppm).

TABLE. I.6.4: Open circuit potentials firstly measured in 95% sat. NaCl solution (mean values)(Defective samples!).

fuel		conditions				free corrosion potential			
type	burn up GWd/tU	electrolyte	$C(O_2)$ ppm	initial pH	T. °C	$^{min}E_{corr.}$ mV_{SHE}	$^{max}E_{corr.}$ mV_{SHE}	$^{mean}E_{corr.}$ mV_{SHE}	$t_{exp.}$ h
UO_2 (B2)	31.5	95% sat. NaCl	<2	7.2	22-28	-134	-71	-96	1072
UO_2 (B4)	53.1	95% sat. NaCl	<2	7.2	22-28	-145	-28	-105	928

In comparison with literature data the measured open circuit potentials are very low. For UO_2 in salt brines at pH 7 values between +130 mV_{SHE} and +210 mV_{SHE} are reported [92HEP/WEG]. Under the influence of α-radiation in sodium perchlorate solution (pH 9.5) UO_2 shows an open circuit potential of +100 mV_{SCE} (+244 mV_{SHE}) [97SUN/SHO]. For used nuclear fuels in sodium perchlorate solution (pH 9.5) values in the range -201 to +340 mV_{SCE} (+43 to +584 mV_{SHE}) were found [96SHO/SUN]. The observed shift of the open circuit potential in to lower potentials can result from (1) an increase of the anodic partial current, (2) an decrease of the cathodic partial current, e. g. due to passivation effects and/or surface layer formation, or (3) the establishment of mixed potentials with additional electrochemical reaction with a more cathodic equilibrium potential. Optical micrographs taken from sample B2 after the experiment show only slightly attacked grain boundaries, but nearly complete coverage by a crystalline NaCl film, which may have an inhibiting effect. On the other hand, the formation of a mixed potential between UO_2 fuel and brass holder is a possible explanation for lower open circuit potentials, if conductive pathways between brass and solution exist. This was proved by impedance spectroscopy.

Impedance measurements

Impedance measurements were performed firstly at the beginning of each long-term experiment during pre-cathodisation to check the electrode's behaviour. As an example the spectrum taken from UO_2 fuel B2 is shown in FIGURE I.6.25. The spectrum is typical for a dense electrode. The high bulk resistance of 80 kΩ indicates, that only a small amount of the solution can have penetrated into the fuel's pores and cracks.During the test several impedance spectra were taken with time. For fuel B2 this series is shown in FIGURE. I.6.26

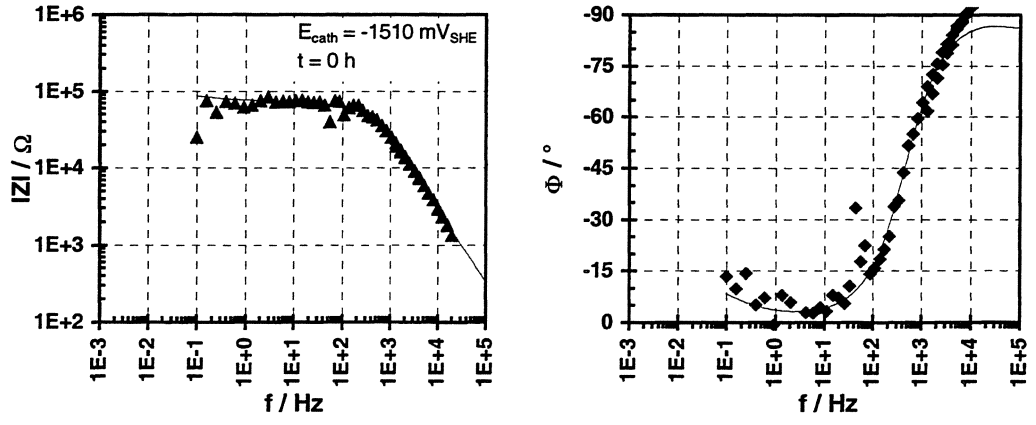

FIGURE I.6.25: EIS spectrum measured during pre-cathodisation of fuel B2 in 95% sat. NaCl solution.

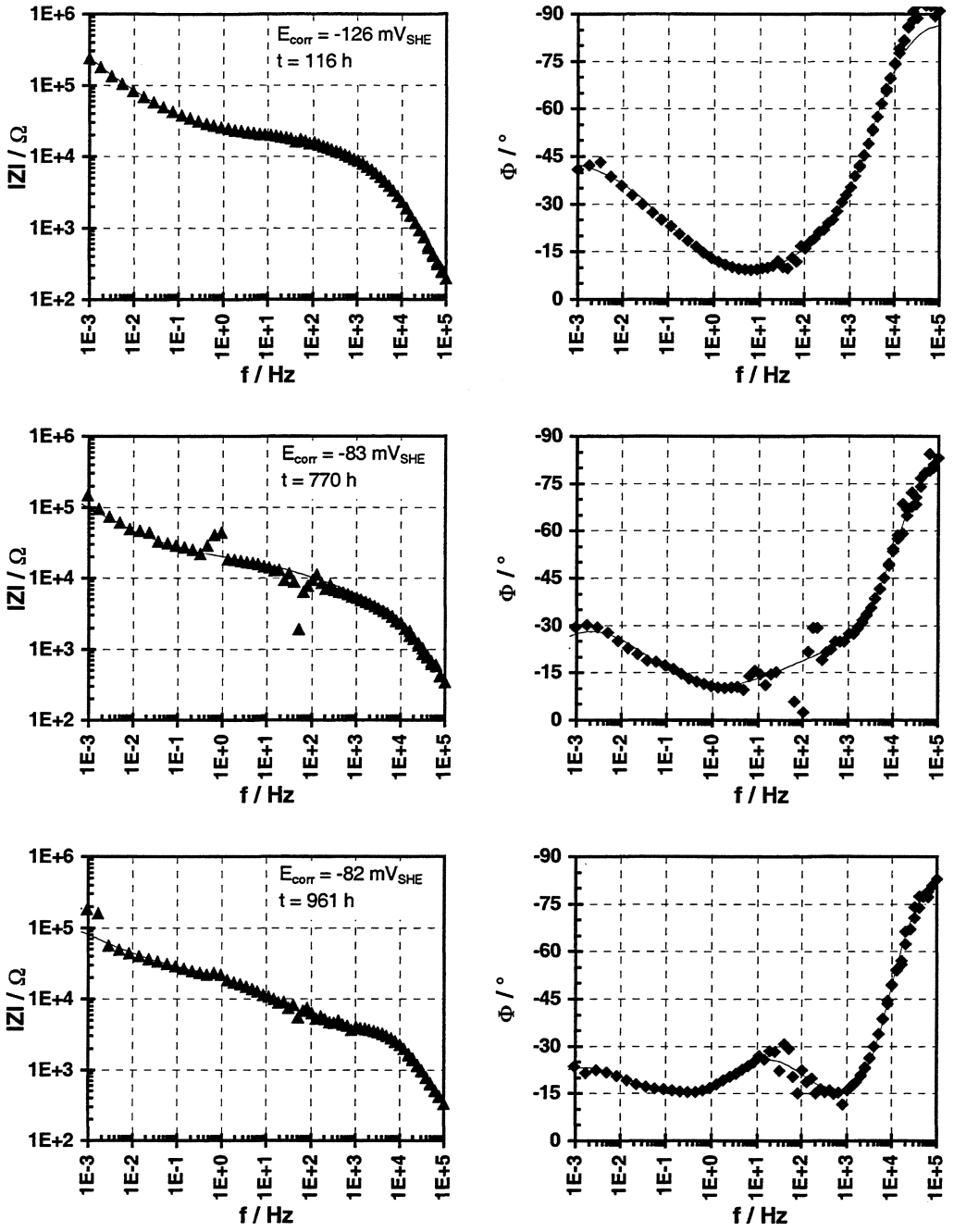

FIGURE. I.6.26: EIS spectra series (part I) showing the evolution of conductive pathways measured during an open circuit potential experiment performed on fuel B2 in 95% sat. NaCl solution (continuous line: fitted data using equivalent circuit shown in FIGURE. I.6.2).

Firstly the bulk resistance, mainly influencing the spectra in the range from 1 to 100 Hz, has decreased to 20 kΩ due to penetration of the solution in the bulk material. Furthermore a decrease of the impedance at the low frequency limit with time is observable as is expected for the formation of a conductive pathway to the underlying brass. Also in the phase angle plot the development of a further minimum at 100 Hz with time is seen, which is also attributed to conductive pathways. The existence of conductive pathways was also proved for specimen B4. Impedance spectra taken during this experiment show also indications for conductive pathways FIGURE I.6.27.

An optical examination of sample B4 after 1000 h immersion in NaCl solution shows attacked

and non-attacked regions on the surface. The protected areas always have pits at their centers (FIGURE I.6.28). These pits may be mouth's of conductive pathways to the underlying brass, which protects the fuel cathodically.

It follows that the corrosion potential of UO_2 fuel can be shifted to a potential region in which the dissolution of UO_2 is solubility controlled [97SUN/SHO, 92SHO/SUN] if the fuel is in contact with less noble metal.

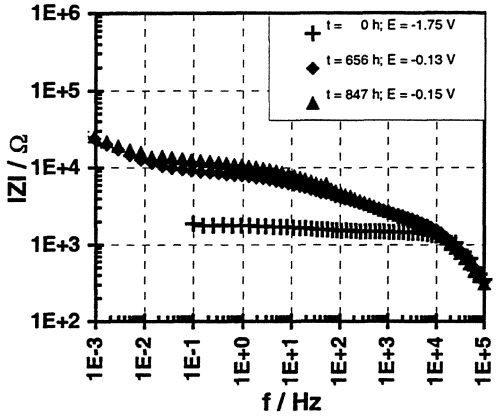

FIGURE. I.6.27: EIS spectra measured during an open circuit potential experiment performed on fuel B4 in 95% sat. NaCl solution

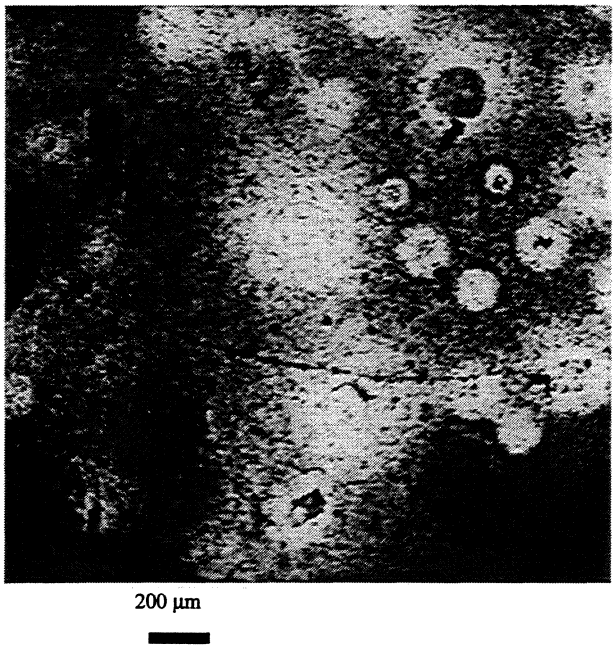

FIGURE. I.6.28: Optical microscopy of irradiated fuel (B4) after 1000 h at open circuit potential in 95% saturated NaCl solution. Overall view showing reflective and dark zones of protected and attacked surfaces. In the center of each reflective zone is a pit (mouth of a conductive pathway?) that cathodically protects the surrounding area.

Open circuit potentials of spent UO_2 fuel

Due to the problems occurred during the first tests the next set of specimen were prepared very carefully. Only thick pieces (d_{el} > 3 mm) of fuel were mounted and embedded in resin. After polishing all locations, where cracks may appear (border fuel/resin; resin PE-holder) got a second resin sealing.

The results obtained from these experiments are summarized in TABLE I.6.5.

In addition to the previous performed experiments also the initial open circuit potential E_{init} was measured before the specimens were cathodically polarized for surface cleaning.

The initial potentials are in the range of 291 mV_{SHE} to 384 mV_{SHE}. The highest potential was found for the UO_2-fuel with the highest burn-up of 53.1 GWd/t. No significant difference was detected between granite groundwater and 95% saturated NaCl solution. The initial potentials are also in good agreement with the open circuit potentials obtained from unirradiated UO_2.

Furthermore the maximal and the mean free corrosion potential, $^{max}E_{corr}$ and $^{mean}E_{corr}$, are given in TABLE I.6.12. The latter was calculated if possible at the end of an experiment over at least 5 h. In case of sudden potential break down the data until this point were used for the calculation (also at least 5 h). The potentials obtained are approximately 100 - 180 mV lower than the initial potentials. The most likely reason for this behaviour is a penetration of electrolyte into the fuel specimen with time, which leads to an increasing defect area with time. Therefore two contrasting processes occur: Firstly a potential increase due to the free corrosion potential of the fuel and secondly a potential decrease due to an increasing galvanic coupling. In this case the open circuit potential-time curve must have an extreme. All potential-time curves measured (Appendix 6, FIGURES 9-13 show a potential maximum after 30 to 60 h. In case of fuel B4 with the highest burn-up this maximum or potential break down was reached faster in 0.5 to 8 h.

It seems that due to fuel restructuring more cracks and microcracks are available to form conductive pathways to the metal backing. Defect specimens were also detected with impedance spectroscopy (grayish rows in TABLE I.6.5). These problems does not occur at this extend during the experiments done on CANDU fuel (maximal burn-up 11 GWd/t) at AECL [96SHO/SUN]. But nevertheless for one experiment the authors also assume a galvanic coupling to the base metal.

The most reliable data are the initially measured potentials followed by the $^{max}E_{corr}$ values.

However, corrosion rates were calculated from the potentials using the calibration curve obtained from combined potential measurements and solution analysis (FIGURE I.6-32). The initial corrosion rates are in the range of 1.4 to 20 mg/(m^2·d) and for the $^{max}E_{corr}$ data the rates are between 0.04 to 0.6 mg/(m^2·d).

Open circuit potentials of spent MOX fuel

MOX-fuel shows in 95% sat. NaCl solution a very low maximal corrosion potential of -225 mV_{SHE} (TABLE I.6.5 and Appendix 6, FIGURE 14). The potential curve is very smooth and impedance spectra taken during the experiment show no indication for conductive pathways, but an additional phase angle minimum in the low frequency region may indicate an additional layer or reaction.

Open circuit potential measurements performed on pure PuO_2 electrodes [98WEG] show also free corrosion potentials between –190 mV_{SHE} and –300 mV_{SHE}.

Taking into account the MOX fuel structure (FIGURE I.6.13) the electrode is not homogeneous but heterogeneous. Areas of Pu-rich agglomerates are surrounded by the normal UO_2 phase. Therefore a galvanic coupling between the different phases seems to be possible. As a result a mixed potential between the free corrosion potentials of the pure phases, Pu-rich agglomerate and UO_2, will be obtained. This also influences the dissolution rates. The corrosion rate of the nobler partner (UO_2) will be decreased while the other (Pu-rich agglomerate) will dissolve faster. In case of different active surface areas of the two materials the material with the larger surface will be less affected than that with the smaller one. Such an effect was observed during the leaching tests on spent fuel rodlets with pre-set defects. However, to prove this hypothesis more and detailed investigations are necessary.

TABLE. I.6.5: Overview of the free corrosion potentials measured on spent fuel and unirradiated UO_2.

fuel		conditions				free corrosion potential			corrosion rate			
							after electrochemical reduction		extrapolation of anodic Tafel line to E_{corr}			derived from impedance data
type	burn up GWd/tU	electrolyte	$C(O_2)$ ppm	initial pH	T °C	$E_{init.}$ mV_{SHE}	$^{max}E_{corr.}$ mV_{SHE}	$^{mean}E_{corr.}$ mV_{SHE}	initial $^{ext}v_{UO2-i}$ $mg \cdot m^{-2} \cdot d^{-1}$	max $^{ext}v_{UO2-i}$ $mg \cdot m^{-2} \cdot d^{-1}$	mean $^{ext}v_{UO2-i}$ $mg \cdot m^{-2} \cdot d^{-1}$	$^{EIS}v_{UO2-i}$ $mg \cdot m^{-2} \cdot d^{-1}$
UO_2 (B2) /	31.5	synthetic groundwater	< 2	8	22 - 28	321	168	158	3.3	0.04	0.03	
			< 2	7.6	22 - 25	379	204	162	17	0.11	0.03	(22) *
UO_2 (B3)	45.2	synthetic groundwater	< 2	8	22 - 28	291	260	209	1.4	0.56	0.13	(4) *
UO_2 (B4) /	53.1	synthetic groundwater	< 2	7.6	22 - 25	384	239		20	0.31		
UO_2 (B4) /	53.1	95% sat. NaCl	< 2	7.2	22 - 28	341	190	180	5.8	0.08		
MOX	21.1	95% sat. NaCl	< 2	7.2	22 - 28		-225	-272				
UO_2		synthetic groundwater	0.05	8.4	23			296			1.6	1.3
UO_2		synthetic groundwater	0.05	7.7	60		364	346		11.2	6.7	5.8
			0.05	7.5	60			328			4.0	17.5
UO_2		95% sat. NaCl		6.8	22		226	200 ↑		0.21	0.1	
			2	6	25		299	297 ↗		1.7	1.6	
			0.2	6	25			254			0.5	
UO_2		95% sat. NaCl	3.4	3.8	25		543	527 ↗		1940	1220	
			0.2	3.8	25			373			14	

/: samples with conductive pathways to underlying metal holder

( ) *: surface area estimated $A_{fuel} = 0.15\ cm^2$

Estimation of free corrosion potential errors

To estimate the maximal error of the corrosion potentials measured using brass backings for spent fuel electrodes a simplified corrosion model was developed. This model was used to calculate E_{corr} when different measured free corrosion potential E_{corr} of brass, gold coated brass and gold were used as input parameters. Also the influence of the conductive glue and the electrolyte was tested.

The input parameters and results are given in TABLE I.6.6 for an assumed free corrosion potential of the fuel of 350 mV_{SHE}. In case of pure brass (MS58) the potential error can reach -193 mV_{SHE} in 95% sat. NaCl solution and –70 mV_{SHE} in synthetic groundwater. Using gold or gold coated brass specimen the errors can be reduced to approximately 60 mV in 95% sat. NaCl solution and to approximately 20 mV in synthetic groundwater.

Therefore in future experiments gold-coated metal will be used as backing material for spent fuel electrodes and to get a better impregnation a vacuum/pressure procedure will be used.

TABLE I.6.6: Estimation of the maximum errors of free corrosion potential measurements on spent fuel performed with different metal contacts in chloride containing media. All calculations were done using the simplified corrosion model.

electrolyte	specimen	initial	end	max	mean(>5h)	estimated
		Ecorr mV_{SHE}	Ecorr mV_{SHE}	Ecorr mV_{SHE}	Ecorr mV_{SHE}	ΔEcorr ($350mV_{SHE}$) mV
simulated groundwater	pure gold	305	300	320	315	<1
	gold coated MS58	411	471	471	462	7
	gold coated MS58 (partially covered with conductive glue)	210	214	258	214	-2
	gold coated MS58 (complete covered with conductive glue)	176	103			-19
	pure brass (MS58)	-5	-5			-70
95% sat. NaCl solution	gold coated MS58	463	582	582	543	35
	gold coated MS58 (partially covered with conductive glue)	65	-11	65	5	-50
	pure MS58 (complete covered with conductive glue)	125	7			-63
	pure MS58	-345	-200	-160	-190	-193

Parameter used for the estimation of ΔEcorr($350mV_{SHE}$):

Electrode:		Fuel:		Metal:	
area:	A_{el} = 0.5 cm^2	corrosion potential:	$E_{corr,fuel}$ = 350 mV_{SHE}	corrosion potential:	mean E_{corr}
thickness:	d_{el} = 3 mm	corrosion current density:	$i_{corr,fuel}$ = 1 nA/cm^2	gold:	$i_{corr,Au}$ = 10 nA/cm^2
resistance of fuel:	R_{bulk} = 15 kΩ			brass:	$i_{corr,MS58}$=16 nA/cm^2
resistivity of fuel:	ρ_{fuel} = 250 Ω·m	Tafel slopes:	$b_{a,fuel}$ = 80 mV	Tafel slopes:	$b_{a,me}$ = 120 mV
resistance of pore:	R_{por} = 100 kΩ		$b_{c,fuel}$ = 250 mV		$b_{c,me}$ = 60 mV
resistivity of electrolyte:	ρ_{sol} = 0.8 Ω·m			relative defect size:	A_{el}/A_{me} = 0.047%

Potentiostatic simulation of the effect of oxidants

The effect of oxidants on corrosion rates was evaluated at FUB. The potential at the interface of the semiconductors UO_2 SIMFUEL or spent fuel and an aqueous redox solution depends on the concentration of oxidants in solution, because the Fermi level of UO_2 is shifted, by the Fermi level of the redox system of the contact solution. The electrode potential can be adjusted by shifting the Fermi level of UO_2 by potentiostatic polarization (FIGURE I.6-29).

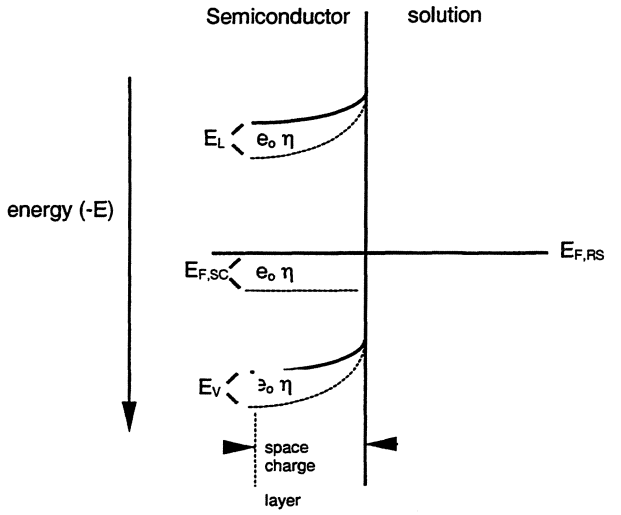

FIGURE .I.6-29: Shift of Fermi-level $E_{F,SC}$ and conductivity and valence bands in contact with an electrolytic system in absence (solid lines) and presence of applied anodic overvoltage (dashed line)

Potentiostatic simulation of the effects of oxidants is used to obtain reliable data in systems with rapidly varying oxidant concentrations. For example the dissolution rate of UO_2 is enhanced in presence of Fe(III) – or MnO_4^- ions for example by the reaction

$$UO_2 + 2/3\ MnO_4^- + 16/3\ H^+ \longrightarrow UO_2^{2+} + 2/3\ Mn^{2+} \qquad 8/3\ H_2O \qquad (I.6\text{-}11)$$

At the beginning (t_1) the MnO_4^- concentration and therefore the cathodic current density is higher than at a later time (t_2). By this way the corrosion potential (U_1, U_2) as well as the corrosion rates decreases with decreasing cathodic current density (FIGURE I.6-30).

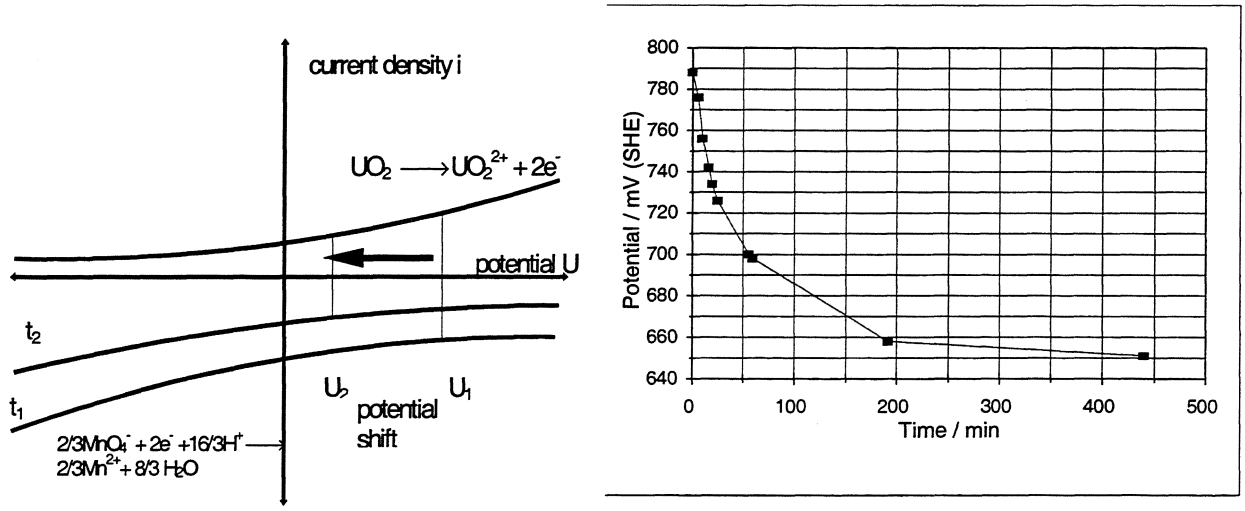

FIGURE I.6-30: Effect of the decrease in concentration of oxidizing species on corrosion potentials in closed system: left: Schematic view: Partial current densities in presence of MnO_4-. U_1 and U_2 are the corrosion potentials at t_1 and t_2 respectively. right: Experimental data: Change of corrosion potential of a UO_2 -electrode after addition of 0.01 M $KMnO_4$ at 25°C, pH = 1, with time

Corrosion rates at applied polarization voltage

Corrosion rates were obtained from the radiochemical (LSC) or photometrical (arsenazo III) solution analyses of dissolved uranium. For electrochemically simulating the effects of oxidants the measurements were carried out at specific polarization voltages. In FIGURE I.6-31 the corrosion rates in a redox system as a function of the corrosion potential are compared with corrosion rates under applied potentials.

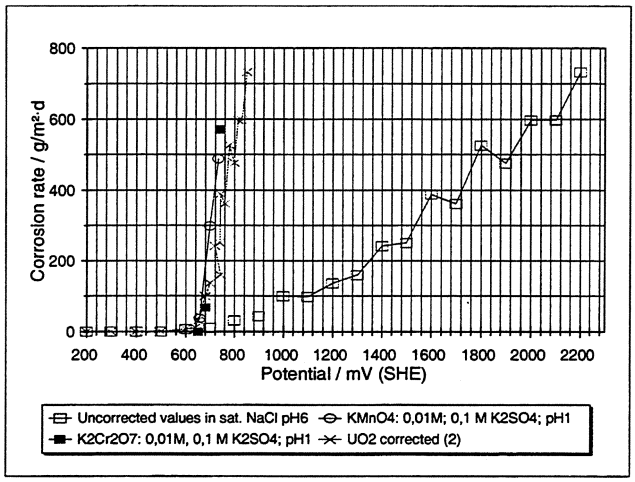

FIGURE I.6-31: Comparison between corrosion rates depending on potentials, obtained from adding a redox system and also from potentiostatic polarization

To achieve a given corrosion rate, the necessary applied potentials are much higher than the corrosion potentials. This difference is due to a potential drop at the space charge region of the semiconductor $E_{surf} = E_{meas} - E_{drop}$. The potential-drop corrections are performed by impedance measurements according to $R_{tot} = R_{bulk} + R_{pol}$ with R_{bulk} being the resistance of the UO_2 - pellet, R_{pol} is the polarization resistance an E_{drop} is the potential drop given by

$$E_{drop} = i_{meas} \cdot R_{el} \qquad \text{with} \quad R_{el} = f(E) \qquad \text{(I.6-12)}$$

By comparing the corrected corrosion rates (FIGURE I.6-31) originating from specific redox media with those from applied potentials the precision of the method is to be seen.

Calibration of potential vs. corrosion rates

A calibration curve (FIGURE I.6-32) was obtained by measuring the corrosion potentials in bentonite pore water, sat. chlorine and bromine solutions with the addition of various oxidizing species. Additional data were obtained by potentiostatic measurements, corrected by impedance procedures.

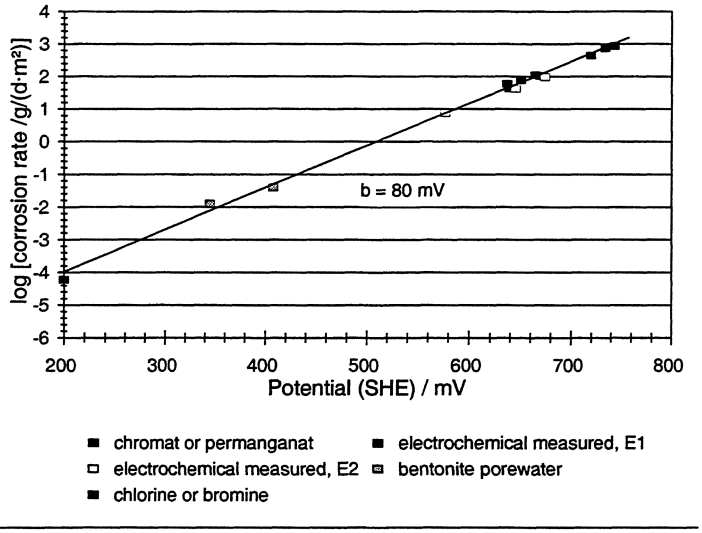

FIGURE I.6-32: calibration curve for determining the corrosion rates from potentials at UO_2 at 25°C.The specific systems used:0.01M $K_2Cr_2O_7$ pH1 in sat. NaCl, 0.01M $KMnO_4$ pH1 in sat. NaCl, sat. bromine in sat. NaCl, 1 atm chlorine in sat. NaCl. The electrochemical measurements (E1 and E2, two different electrodes),carried out in sat. NaCl

The fact that a single calibration curve is valid for sat. NaCl solution and for bentonite pore water, demonstrates that besides temperature only the composition of the UO_2 surface and the electrical surface potential dominates the corrosion rates. Using calibration curves corrosion rates can be predicted from the corrosion potential of UO_2 electrodes, From equation I.6-8 it can be seen, that there is a linear relationship between the logarithm of the polarization resistance and the polarization voltage, the slope of which delivers b_a as 80 mV j_{corr} can be obtained from the intersection of the straight line with the ordinate. So corrosion current densities (corrosion rates) at corrosion potentials are to be calculated from impedance measurements alone.

The thickness of the relevant layer

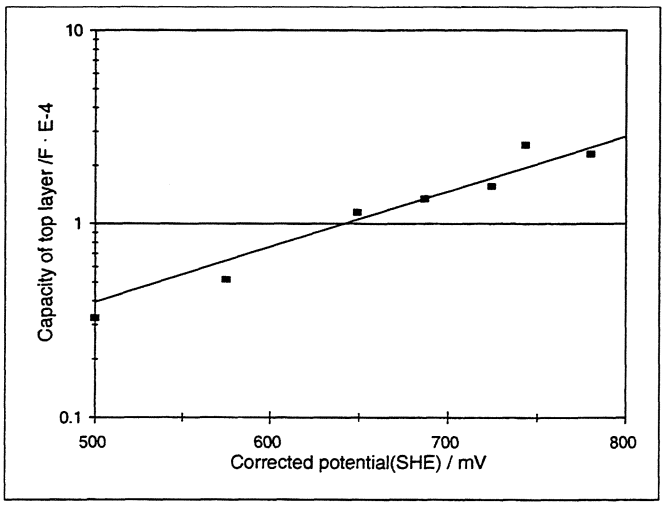

FIGURE I.6-33 : Capacity vs. corrected potential in sat. NaCl solution at 25°C

Furthermore by applying the well known capacitor formula ($C = \varepsilon\varepsilon_0 \frac{A}{d}$) to the C-values resulting from impedance measurements (s. FIGURE I.6-33) the thickness d of the relevant layer is found to be approximately 0.13 nm [with $C=10^{-4}$ F; $\varepsilon = 25$; $\varepsilon_0 = 8.85\ 10^{-12}$ Fm^{-1} and A = 0.6cm^2] the crucial point being the value of the dielectric number ($\varepsilon = 25$). This corresponds to the thickness of a monolayer. One may conclude that there is not an extended space charge region in the fuel.

Influence of the radiolysis product H_2O_2 on UO_2 corrosion

In order to measure the corrosion of UO_2 influenced by H_2O_2 accurately the primary difficulty is the necessity to keep the H_2O_2 concentration constant. The H_2O_2 concentration is decreased by consumption in redox reactions, by nitrogen bubbling or by decomposition of H_2O_2

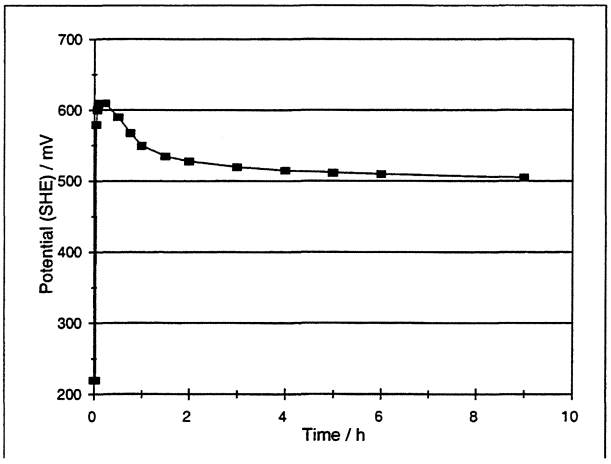

FIGURE I.6-34: Corrosion potential of UO_2 0.1M H_2O_2 95% sat. NaCl solution

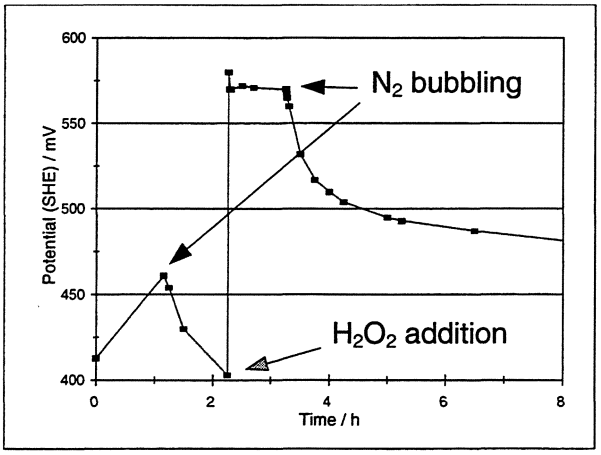

FIGURE I.6-35: potential of platinum electrode 0.1M H_2O_2 with bubbling of nitrogen

Under practical conditions of a waste repository on the other hand the H_2O_2 concentration is kept constant due to radiolysis of water. Therefore, all the corrosion rates of UO_2 were determined by electrochemical measurements alone (determination of potentials) on condition that a relevant calibration curve (potential vs. corrosion rate) obtained from radiochemical measurements was available. By this procedure the obstacles mentioned above could be circumvented.

The potential measurements on UO_2 had to be carried out in presence of 0.1M H_2O_2 (conditions: 95% sat. NaCl solution, 25°C, nitrogen saturation, FIGURE I.6-35). Before adding H_2O_2 nitrogen bubbling was stopped. At the beginning the potential increased to 620 mV (SHE). According to the calibration curve in FIGURE I.6-32 this potential corresponds to a corrosion rate of 27 g/d·m^2 . Due to the decreasing H_2O_2 concentration, the potential dropped to 510 mV (SHE) after 10 h. The corresponding corrosion rate is 1.2 g/d·m^2. In case of permanent nitrogen bubbling the corrosion rate is smaller because of the total expulsion of H_2O_2 from the solution [97GRA/LOI].

Influence of Carbonate on corrosion of UO_2

FIGURE I.6-36 shows the shift of corrosion rates of UO_2 to higher values caused by addition of carbonate. The shifting depends on the amount of carbonate added.

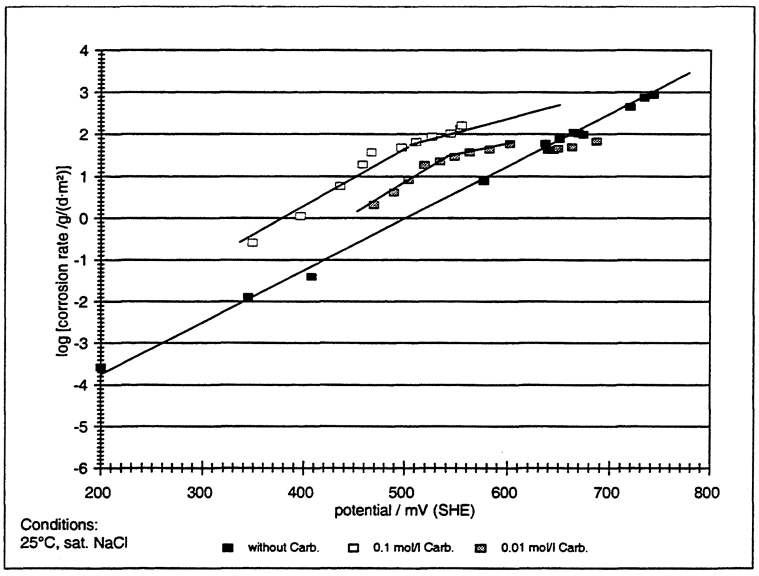

FIGURE I.6-36: Comparison of calibration curves for UO_2 corrosion rates vs. potential in presence and absence of carbonate

The shift of corrosion rates in presence of carbonate is due to the difference in the Standard Free Activation Enthalpies. Using the generally accepted symbols (see Appendix 8) for the well-known Butler-Volmer equation it follows:

$$j_a = +zFk_a\Gamma_{red}e^{\frac{\alpha zF\Delta\varphi}{RT}} \qquad \text{(I.6-13)}$$

with $k_a = k_a^0 e^{\frac{-\Delta G_a^{0\#}}{RT}}$ it follows: $j_a = +zFk_a^0 e^{\frac{-\Delta G_a^{0\#}}{RT}}\Gamma_{red}e^{\frac{\alpha zF\Delta\varphi}{RT}}$ (I.6-14)

Inserting $\Delta\varphi + \Delta\varphi_B = E$ and after logarithmation it can be written:

$$\ln j_a = \ln(zFk_a^0\Gamma_{red}) - \frac{\Delta G_a^{0\#}}{RT} + \frac{\alpha zF\Delta\varphi_B}{RT} + \frac{\alpha zFE}{RT} \qquad \text{(I.6-15)}$$

According to equation (Eq I.6-15) the slopes of the curves in FIGURES I.6-36 are equal. If in case of hydrogen standard electrode $\Delta\varphi_B = 0$, it follows

$$\ln j_{a1} - \ln j_{a2} = \ln\left(\frac{j_{a1}}{j_{a2}}\right)_E = \frac{\Delta G_{a2}^{0\#}}{RT} - \frac{\Delta G_{a1}^{0\#}}{RT} \qquad \text{(I.6-16)}$$

resulting in:

$$RT\ln\left(\frac{j_{a1}}{j_{a2}}\right)_E = \Delta G_{a2}^{0\#} - \Delta G_{a1}^{0\#} \qquad \text{(I.6-17)}$$

(for instance, in case of UO_2- Electrodes in sat. NaCl solution without and with 0,01M Carbonate the difference is -4kJ/mol, with 0,1 M Carbonate it is -10 kJ/mol). The crucial point of this calculation is the fact, that Γ_{red} was considered to be independent of temperature. The Standard Free Activation Enthalpy can be calculated from corrosion experiments on UO_2 at different temperatures:

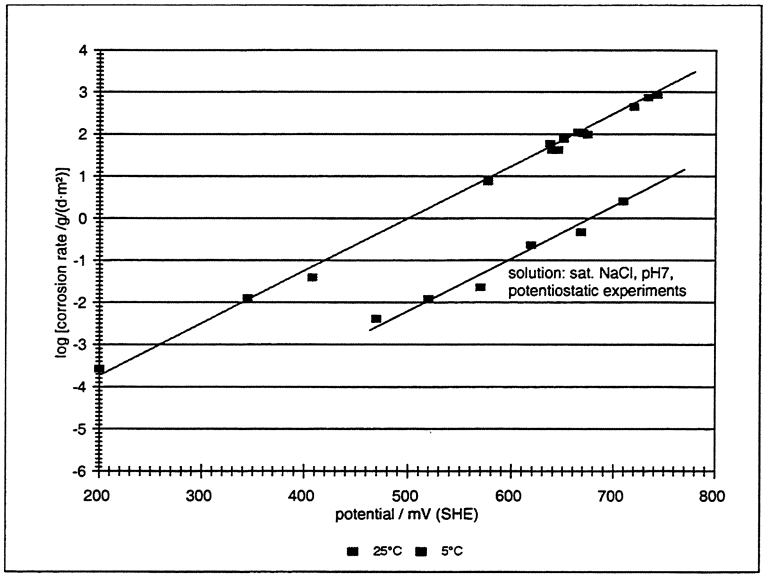

FIGURE I.6-37: Calibration curves for corrosion on UO_2 in sat. NaCl solution at 25 and 90°C

For temperature T_n it is:

$$\ln j_a^{Tn} = \ln(zFk_a^0\Gamma_{red}) - \frac{\Delta G_a^{0\#}}{RT_n} + \frac{\alpha zF(\Delta\varphi_B)_{Tn}}{RT_n} + \frac{\alpha zFE}{RT_n} \qquad \text{(I.6-18)}$$

For a temperature difference (T1, T2) it follows with $(\Delta\varphi_B)_{T_1} \neq (\Delta\varphi_B)_{T_2}$, and $(\Delta\varphi_B)_{T2}$ corrected to $(\Delta\varphi_B)_{T1} = 0$ it follows:

$$\ln\frac{j_a^{T_1}}{j_a^{T_2}} = \frac{\Delta G_a^{0\#}}{R}\left(\frac{T_1 - T_2}{T_1T_2}\right) + E\left(m_{T_1} - m_{T_2}\right) \qquad \text{(I.6-19)}$$

with $m_{T_i} = \frac{\alpha zF}{RT_i} = \frac{1}{b_{a_i}}$, resulting in:

$$\Delta G_a^{0\#} = \left(\ln \frac{j_a^{T_1}}{j_a^{T_2}} + E\left(m_{T_2} - m_{T_1}\right) \right) \frac{RT_1T_2}{T_1 - T_2} \qquad \text{(I.6-20)}$$

From the experiments performed it can by calculated:

Carbonate free solution: $\Delta G_a^{0\#}$ = 158 kJ/mol

with 0.01 M carbonate: = 154 kJ/mol

with 0.1 M carbonate: = 148 kJ/mol

Relation between corrosion potential and Eh

The geochemical environment of nuclear waste disposal is generally characterized by the Eh-value as a master variable, relevant for Pourbaix-diagrams, used for speciation of redox sensitive radionuclides. But very often the Eh-value is also considered under the aspect of influencing corrosion, UO_2 corrosion for instance, when spent fuel is present as radwaste. The Eh-value is defined as the cell voltage of a distinct cell, the left side of which is the Standard Hydrogen Electrode (SHE).

Therefore the Eh-value describes the electrode potential at equilibrium. But at equilibrium there isn't any corrosion any more. Since the electrode potential at equilibrium E_{gl} is the sum of voltage potential, diffusion-and contact potential it is :

$$E_h = E_{gl} = E_{gl} - E_{(SHE)} = \Delta\varphi + \varepsilon_{diff} + \varepsilon_{cont} \cong \Delta\varphi \qquad \text{(I.6-21)}$$

For a redox-system

$$S_{ox} + ne^- \Leftrightarrow S_{red} \qquad \text{(I.6-22)}$$

$\Delta\varphi$ can be calculated from Nernst equation neglecting ε_{Diff} and ε_{cont} and using the generally known symbols for an indifferent Pt-electrode

$$E_h \cong \Delta\varphi = \Delta\varphi^0 + \frac{RT \ln K}{nF} + \frac{RT}{nF} \ln \frac{\tilde{a}(S_{ox})}{\tilde{a}(S_{red})} \qquad \text{(I.6-23)}$$

For a redox system, which depends on pH, as for instance

$$S_{ox} + ne^- + mH^+ \Leftrightarrow S_{red} \qquad \text{(I.6-24)}$$

it is: $$E_h = \Delta\varphi^0(S_{ox} / S_{red}) + \frac{RT}{nF} \ln \frac{\tilde{a}(S_{ox})}{\tilde{a}(S_{red})} + \frac{RT}{F} \cdot \frac{m}{n} \ln \tilde{a}(H^+) \qquad \text{(I.6-25)}$$

The Eh-value for the UO_2^{2+} / U^4 -electrolyte system (Pt-electrode) is:

$$E_h(U^{4+} / UO_2^{2+}) = \Delta\varphi^0(U^{4+} / UO_2^{2+}) + \frac{RT}{2F} \ln K + \frac{RT}{2F} \ln \frac{\tilde{a}(UO_2^{2+})}{\tilde{a}(U^{4+})} - \frac{2 \cdot 2.303 \cdot RT}{F} pH$$

(I. 6.26)

If $\tilde{a}(U^{4+})$ is constant due to presence of UO_2 solid and also $\tilde{a}(UO_2^{2+})$ due to saturation then $E_h(U^{4+} / UO_2^{2+})$ will be strictly linear to pH, on condition that $d_p = d_T = 0$.

The UO_2 - Electrode

For $(UO_2)_s \Longleftrightarrow UO_2^{2+} + 2\,e^-$ it is:

$$Eh\,(UO_2 / UO_2^{2+}) = E^0\,(UO_2 / UO_2^{2+}) + \frac{RT}{2F} \ln \tilde{a}\,(UO_2^{2+}) \qquad \text{(I.6-27)}$$

Therefore, for a UO_2 electrode dipping into the same solution it is:

$$Eh\,(UO_2 / UO_2^{2+}) \neq Eh\,(U^{4+}/UO_2^{2+}/Pt) = Eh\,(e^{I}/e^{II}/Pt) \qquad \text{(I.6-28)}$$

In this case the UO_2 electrode shall be considered as a metallic electrode.

The corrosion potential

For corrosion the corrosion potential is of highest importance. The corrosion potential is defined as the distinct potential, at which the anodic current density, that means the corrosion current density, equals the amount of the relevant cathodic current density

$$j_a = |j_k| \qquad \text{(I.6-29)}$$

Taking *Butler-Volmer's* equation into consideration

$$\ln j_a = \ln j_a^0 + \frac{\alpha_a z_a F}{RT}\left(E - E_{gl}^a\right) \qquad \text{(I.6-30)}$$

$$\ln|j_k| = \ln\left|j_k^0\right| - \frac{\alpha_k |z_k| F}{RT}\left(E - E_{gl}^a\right) \qquad \text{(I.6-31)}$$

it can easily be verified that the following equation is valid:

$$E_{corr} = \frac{\left(\ln\left|j_k^0\right| - \ln j_a^0\right)RT}{F\left(\alpha_a z_a + \alpha_k |z_k|\right)} + \frac{\alpha_a z_a}{\alpha_a z_a + \alpha_k |z_k|} E_{gl}^a + \frac{\alpha_k |z_k|}{\alpha_a z_a + \alpha_k |z_k|} E_{gl}^k \qquad \text{(I.6-32)}$$

Equation (I.6-32) demonstrates, that the rest potential or corrosion potential E_{corr} is linear to the redox potential of the redox system at equilibrium. The curve of various rest potentials vs. the relevant redox potentials at equilibrium is a straight line, but the crucial point is the fact, that $\ln | j_k^0 |$ has to be assumed to be constant in this case. This assumption cannot be accepted because $\ln | j_k^0|$ differs for the various redox systems at equilibrium. But due to the mathematical form in which $\ln | j_k^0|$ exists the first term of equation can be considered to be approximately constant.

For a given specific redox system E_{gl}^K must be constant, in order to get a constant E_{corr} . This condition demands that the concentration of the oxidant must be high enough in order not to be changed by the running redox process. Due to this fact the superiority of electrochemical procedures is verified again, which can simulate E_{corr} by applying a potential $\tilde{E}$, guaranteeing its constant value.

From the relevant calibration curve i_{corr} can be obtained for each E_{corr}, which is to be got from E_{gl}^K due to equation (I.6-32). Therefore i_{corr} is to be directly gained from E_{gl}^K. If E_{gl}^K is linearly related to pH, then i_{corr} can be obtained even from pH-values. But it should be always kept in mind, that for all these procedures suitable calibration curves must be available, being specific for the systems under investigation. The most important conditions to be looked at are the fact that E_{gl}^a has to be the same value for the specific system, otherwise the relevant calibration curve is changed.

WP I.8 (NEW) INVESTIGATIONS INTO CORROSION ON ZIRCONIUM AND ON ZIRCALOY-4

Since all the investigations into corrosion of SIMFUEL planned within the frame of this project could not be carried out due to the bad quality of the SIMFUEL pellets delivered, which always brittled, studies on corrosion of zircaloy-4 in brines were performed instead. Zircaloy-4 is the cladding of spent fuel elements, generally used, and its corrosion behaviour towards brines should be tested due to the fact that this material is the only remaining one, which could delay spent fuel corrosion after the break down of the Pollux container.

Experimental details

The corrosion rates were measured either by weighing the mass loss or by radio-analytical methods, which manufactured zirconium electrodes were irradiated for by thermal neutrons for 200h (ϕ =8.0 ·10^{13} s^{-1}·cm^{-2}) and mounted into a Teflon holder. Afterwards the electrodes were dipped into the relevant solutions. The corrosion rates were determined by continuous measurements of γ -radiation in the solutions (^{95}Zr obtained from irradiated ^{94}Zr emits two γ -lines, s. FIGURE I.8-1.)

The γ-line of ^{95}Zr (0.724 MeV) was used and according to the counts obtained from different calibration solutions the relevant mass losses were determined.

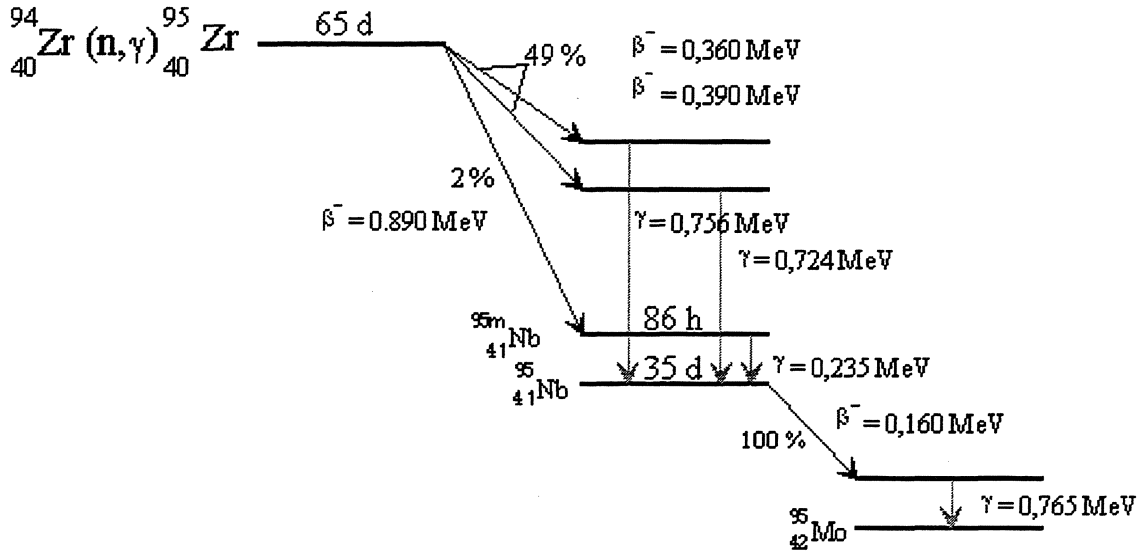

FIGURE I.8-1.: Block diagram of 95Zr decay

Electrochemical procedure

Measurements at rest potentials and applied potentials were carried out. The rest potential towards a Ag/AgCl reference electrode were measured continuously in brines for 160 h at least. The electrodes were pretreated by etching them in a mixture of HF / HNO_3 / H_2O (1:4:5). This treatment influences the electrochemical behaviour of the electrodes.

Investigations without activating the electrodes by neutrons were performed to detect any corrosive attack on the surface of the electrode by applying optical microscopy.

Attempting to measure the corrosion rate by weighing the mass loss no relevant mass losses could be obtained at all (below 5 µm/a). These results are in accordance with those from neutron activation energy.

Discussion of the results

FIGURE I.8-2 show the corrosion rates of titanium, zirconium, Ti99.8Pd alloy and Zircaloy-4 in saturated NaCl solution at different temperatures. All the measurements were carried out at rest potentials. Under these conditions the values of corrosion rates are in the range from 0.1 to 0.4 µm/a.

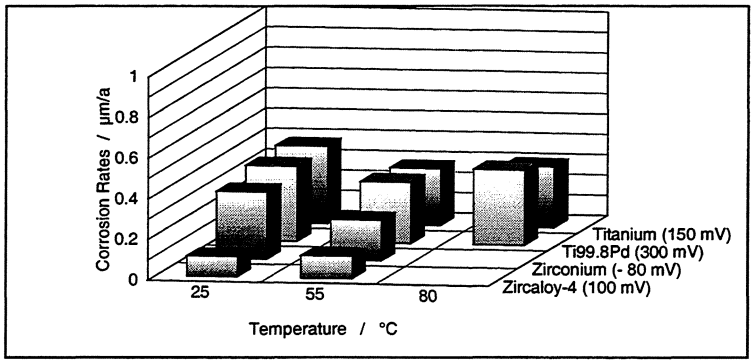

FIGURE I.8-2: Corrosion rates of Zirconium and Titanium at corrosion potential

The corrosion rates of Titanium, Ti99.8Pd, Zirconium and Zircaloy-4 will be within a small range, if the measurements are carried at corrosion potentials (see above). However the relevant results obtained from potentiostatic experiments differ to a greater extent (FIGURE I.8-3).

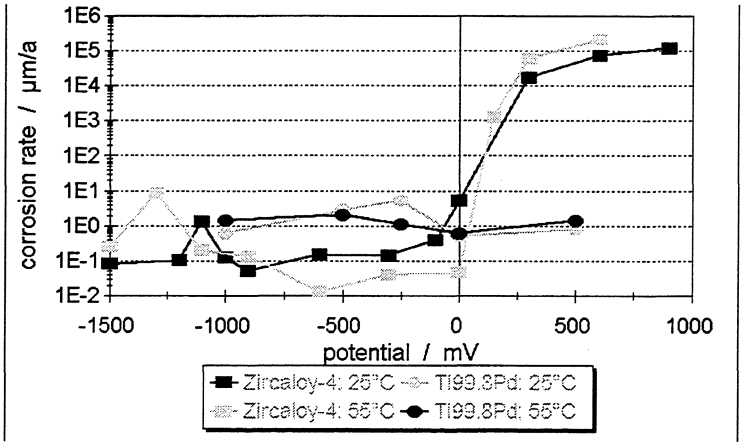

FIGURE I.8-3: Corrosion on Ti99.8Pd and Zircaloy-4

The corrosion rates of Zircaloy-4 increase drastically in the area of higher potentials in contrast to Ti99.8Pd, the corrosion rates of which are lower than 2µm/a. The following FIGURES (I.6-4a-f) show the formation of the oxide layer and its thickness on zircaloy-4 electrodes in saturated NaCl solution with time and potential at various temperatures (25°C, 55°C, 80°C).

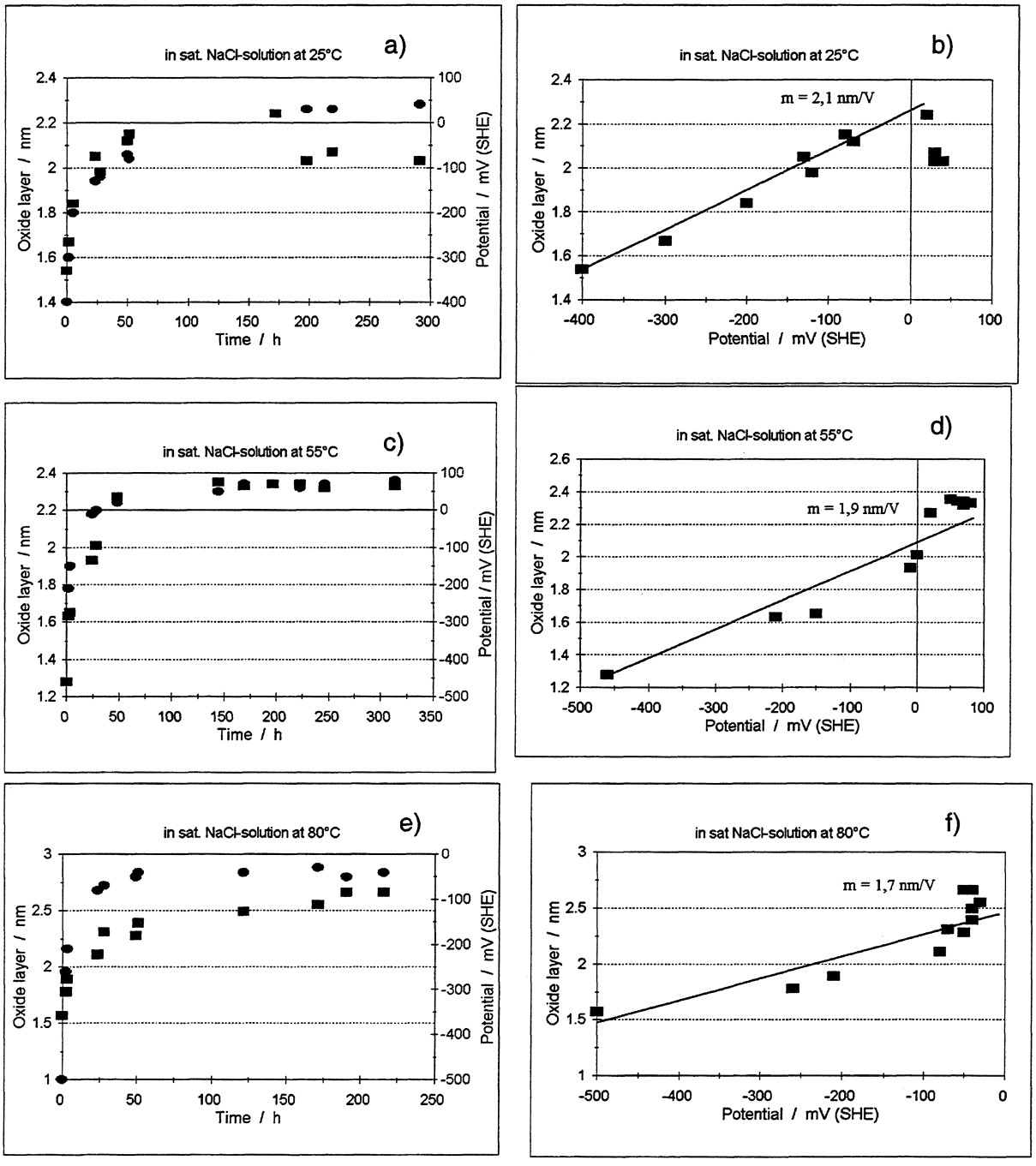

FIGURE I.8-4 a-f: Formation of oxide layer and its thickness on zircaloy-4 electrode in saturated NaCl solution

It can be seen that at all temperatures the relevant oxide layer is built up after approximately 50 h, its increase per volt varying from 1.7 nm over 1.9 nm to 2.1 nm for 80°C, 55°C, and 25°C respectively.

WP II. RADIONUCLIDE RETENTION DURING SPENT FUEL DISSOLUTION

WP II.1.1: SPENT FUEL AND SIMFUEL (CO-)PRECIPITATION TESTS

In order to determine upper concentration limits for radionuclides under disposal conditions, coprecipitation tests were performed with spent fuel ((FZK,ENRESA) and SIMFUEL (ENRESA-CIEMAT) in various groundwaters.

Experimental set-up

A few mg of a high burnup spent fuel sample or of SIMFUEL were dissolved entirely in aqua regia (for sample composition see "solid phase characterisation"). An aliquot of this solution was added under Argon (or Nitrogen in case of SIMFUEL) via a syringe into a borosilicate glass reaction vessel containing the groundwater. The reaction vessel was equipped with two valves. Air intrusion during liquid transfer and later sampling was avoided by passing the syringe through one valve while letting the inert gas stream in through the other. The resulting solution had a pH of about 1. The pH was adjusted by the addition of NaOH to relevant pH ranges between 5 and 12. The pH adjustment resulted in the precipitation of a yellow solid phase. Solution samples were taken in regular time intervals filtered by 0.22 µm filters but without ultrafiltration. At test termination the final solution sample was ultrafiltered.

In order to analyze the precipitation process in detail, certain experiments were performed in an excess of Uranium (ratio of U to other radionuclides higher than in real spent fuel). If coprecipitation prevails, the higher U-concentrations should lead to lower radionuclide concentrations in solution.

Results for spent fuel

Experimental concentrations of Sr, Am, Cm, Eu, Np, Pu and U during coprecipitation process in the pH range 5 – 12.0 are reported for 5 m NaCl solution. Results are included in FIGURES. II.1-1-4, comparing both solution concentrations of radionuclides resulting from spent fuel dissolution experiments with "powders" and "pellets" (data from this project and from previous EU project [97GRA/LOI]). Results form coprecipitation tests performed in the presence of an excess of uranium are denoted "U+SF", ultrafiltered samples are denoted by "UF".

For all radionuclides except Sr (not shown) a significant decrease of concentrations was observed. Sr concentrations remained nearly constant. Apparent equilibrium concentrations were achieved within less than 10 days and remained constant until test termination.

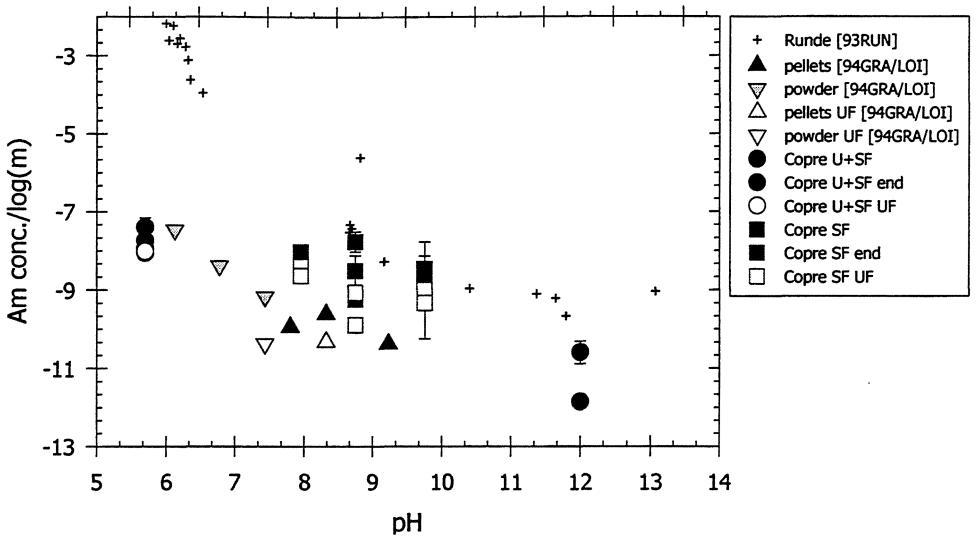

FIGURE II.1.1 Am conc. from leaching and coprecipitation SF test in saline solutions.

Similar trends in the pH dependence of the apparent equilibrium concentrations were observed for Am, Cm and for Eu. Trivalent actinides (Am, Cm) and rare earth elements (Eu, Nd, La, Ce) have also been found to behave alike during spent fuel dissolution [94GRA/LOI, 95LOI/GRA], due to their similar chemical properties. Data from the previous SF dissolution tests [97GRA/LOI] and from the present coprecipitation tests resemble each other in the trend with pH. The FIGURE II.1.1 shows that apparent equilibrium concentrations of Am decrease with pH.

The apparent equilibrium concentrations of coprecipitation tests were in most cases lower than the solubilities of pure $Am(OH)_3$, $Cm(OH)_3$ or $Eu(OH)_3$ for this system as has been reported for SF dissolution tests. For comparison, experimental data for the pure phase solubility of $Am(OH)_3$ [93RUN] are included. However, in SF experiments Am data were close to solubility values of $Am(OH)_3$ between pH 8 and 10. The comparison of pure phase solubility data with the results of our experiments should be taken cautiously, since literature solubility data normally vary by orders of magnitude, depending on degree of crystallinity and in some cases also on the thermodynamic methods of deriving solubility products of measured solution data.

Np concentrations obtained are plotted FIGURE II.1.2 together with data obtained in the leaching experiments of SF. Comparison is made with the solubility of NpO_2OH(aged) measured by Runde [93RUN] and with the calculated solubility of this phase using the solubility products and conditional hydrolysis constants taken from the literature [95NEC/FAN]. Measured concentrations are similar for spent fuel dissolution and precipitation tests, indicating achievement of equilibrium states. In the absence of the results from precipitation tests, it was not clear, whether solution concentrations of Np would raise with time. The results of the precipitation tests show that this is not the case. Higher concentrations are unstable and lead to precipitation. This shows that precipitation tests are an effective tool for the determination of upper concentration limits for radionuclides. On the other hand it is not yet clear which phase controls this upper concentration limit. Solubility of pure NpO_2OH(aged) is orders of magnitude higher than this value.

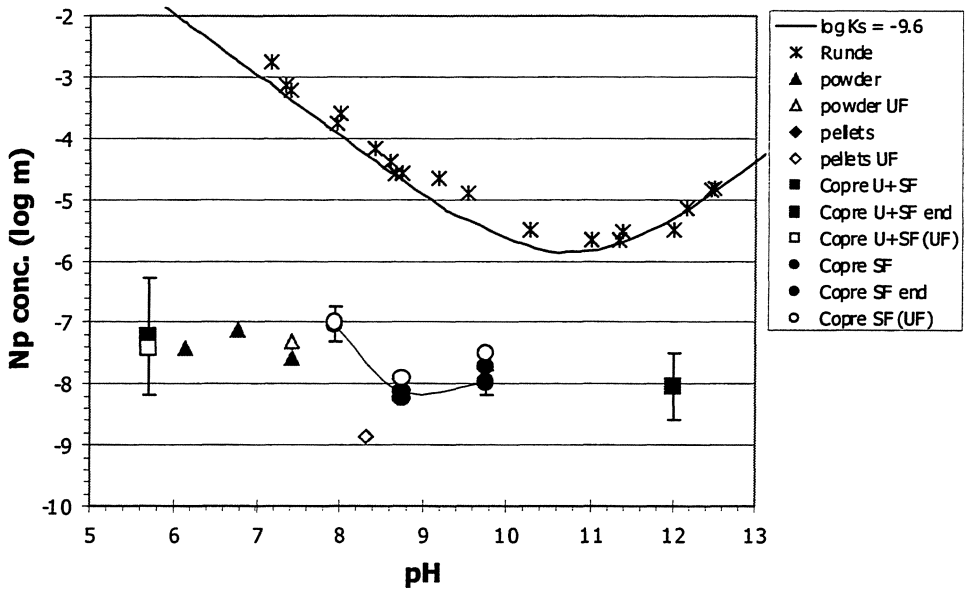

FIGURE II.1.2 Np conc. from leaching and coprecipitation tests in saline solution

Comparison of Pu concentration values with those SF leaching test vs. pH is shown in FIGURE II.1.3. No attempt has been made to determinate the valence state of dissolved Pu under these conditions and, therefore, solubility constraints are not well defined. By comparing our Eh/pH measurements with the Eh/pH stability diagram for various aqueous Pu-species [92CAP/VIT] we may assume that $Pu(OH)_4^0$ would be the dominant solution species.

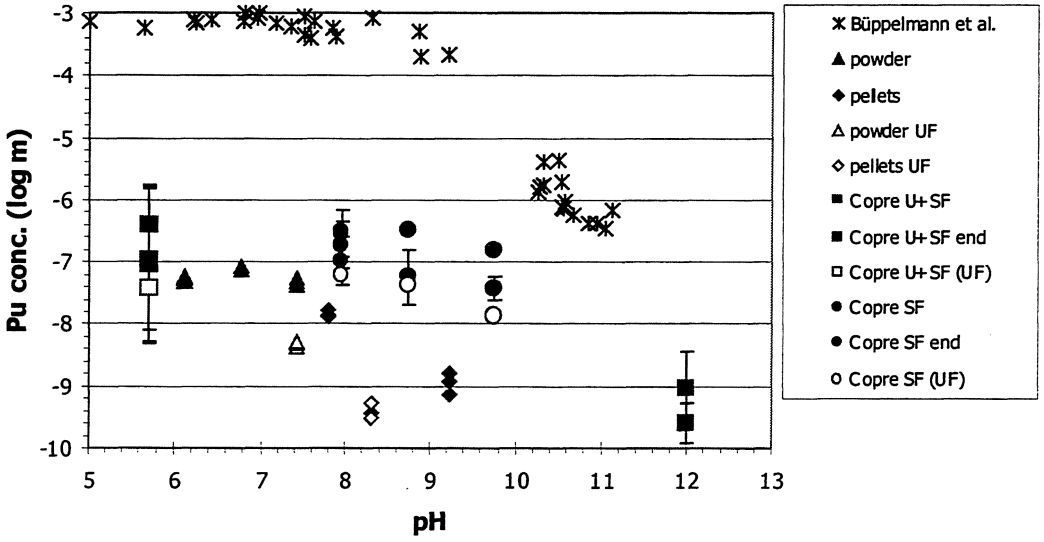

FIGURE II.1.3 Pu conc. from SF, SIMFUEL experiments in saline solutions

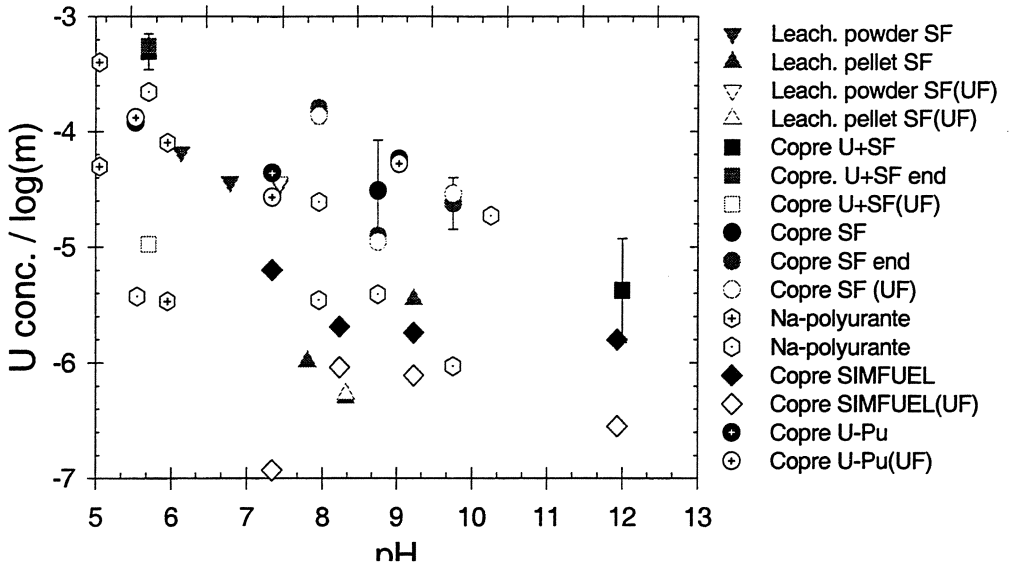

FIGURE II.1.4 U concentration from SF, SIMFUEL, UO_2, U-Pu experiments in saline solutions.

However, this is only valid if the α-radiation field is low and ClO^- complexation can be ignored. Not only the redox state of solution species is uncertain also the solid phases may contain either Pu(IV) or Pu(VI).

Equilibrium concentrations of U(VI) obtained in SF precipitation tests are similar to those found in the inactive experiments performed under similar condition (FIGURE II.1.4) [95QUI/GRA, 96QUI/GRA, 98DIA/GRA]. The U(VI) concentrations determined in SF dissolution tests were in most cases lower than in precipitation test [94GRA/LOI, 95LOI/GRA]. Within a relatively large scatter in the data, a similarity between the apparent equilibrium concentrations of both in leaching test of SF, and the two types of coprecipitation experiments the U concentrations in equilibrium with Na-polyuranate were observed. This indicates that Na-polyuranates are the solubility controlling phases under the present experimental conditions.

Results from SIMFUEL

Coprecipitation experiments of SIMFUEL were performed in GBW and saline solutions. Experime,ntal conditions are given in Appendix 3. GBW used has the composition that could have a granite groundwater supersaturated in bentonite [96MAR/MEL]. The tests were performed under oxidising conditions. The initial supersaturated solution had the same mole fraction (related to U) as in SIMFUEL.

Results of U steady state concentration obtained in GBW are given in FIGURE II.1.5. During the tritation process a yellow solid phase was precipitated in all the experiments. This phase formed explained the decrease of U concentration in solution. XRD analyses showed a Na-polyuranate type phase as the main solid formed. As can be observed, for pHs higher than 8 the U steady state concentration is around 10^{-4} mol/kg H_2O. The trials were performed, under atmospheric conditions and due to carbonate complex formation, an increase in U steady state concentration in the pH range of 7 to 9 is detected.

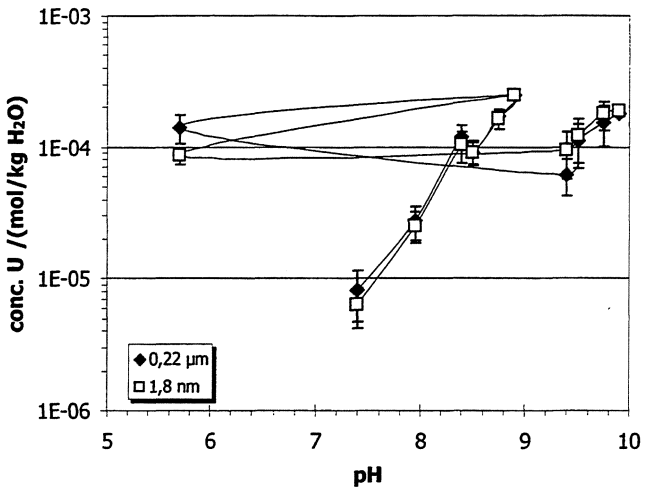

FIGURE II.1.5 Steady state U concentration in GBW.

Results from Sr and Ba steady state concentrations in GBW are given in FIGURE II.1.6. Initial average concentration for each element is plotted as dotted lines. As can be observed, there is a low influence of colloid formation in steady state concentration for both elements. For pH > 7 a decrease respect to the initial concentration are measured. In case of Ba in all tests the steady state concentrations undergo a high reduction, i.e. for pH > 8 the reduction is higher than two orders of magnitude.

In SIMFUEL coprecipitation experiments performed in saline media the U concentration values at pseudo-equilibrium conditions are included in FIGURE II.1.4 for the samples filtered by 0.22 µm and for the samples filtered by membranes of nominal pore size of 1.8nm (ultrafiltration).

Precipitation ratios of the minor elements of SIMFUEL in solution are shown in TABLE II.1.1. Precipitation ratios are calculated as the ratio between initial and final concentration values. The average of the last five concentration values is provided. Those signed by «*» represent concentrations lower than detection limits.

TABLE II.1.1. Precipitation ratios of the minor elements of SIMFUEL. Experiments performed in 5m NaCl solutions. *: the precipitation ratio was calculated, when possible, by considering the last concentration value obtained.

pH	Precipitation ratio										
	Ba	Ce	La	Mo	Nd	Pd	Rh	Ru	Sr	Y	Zr
7.4	1.87	3.24	2.50	20.53	2.41	14.23	21.98	3.88	1.45	2.87	97.03
±0.1	2.12	6.03	4.51	57.9*	7.98	22..9	132.9	7.76	1.03	8.1*	79.1*
8.3	69.73	225.9*	132.6*	*	668.9	13.6	14.89	62.7*	2.55	*	188.3
±0.2	13.8	118*	150*	1.5	841	9.7*	142*	27*	1.95	53*	309*
	3.8	131	321*	5.49	737*	73.5*	145*	69*	1.61	*	291
9.3	5.86	*	*	10.5	*	31..9	*	*	1.28	10.6*	*
±0.1	3,55	*	*	4.36	*	39.9*	*	*	0.55	*	276.4*
	2.95	211*	29*	2.75	48*	10.6	*	21*	1.3	23.7*	*
12	6.8	9.5	8.2	9.8	10.1	35.4	4.6	74.3	1.89	4.5	375.9
±0.1	16.2	39	1.59	78	4.79	368	60.9	135.4	2.1	27.7*	87.5

By considering the chemical analysis of solid phases it was assumed that if the precipitation ratio was lower than 2, then the minor element considered was not coprecipitated. Therefore, Sr does not precipitate, in the experimental conditions considered, for the pH value tested.

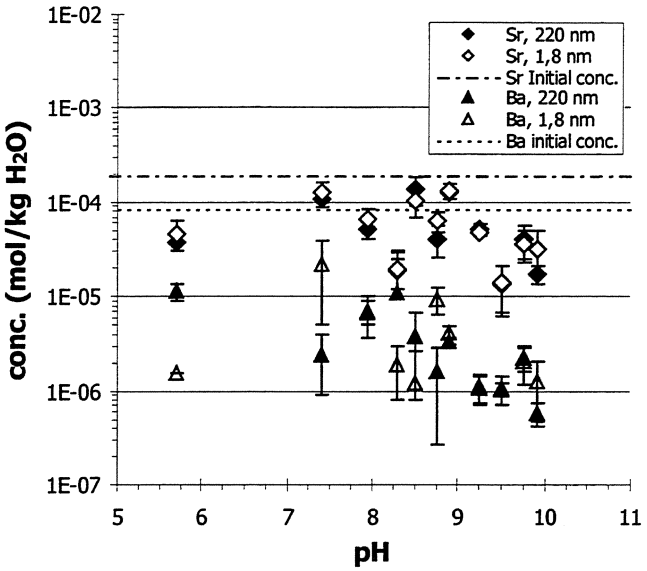

FIGURE II.1-6 Steady state concentration of Sr and Ba in GBW

The behaviour of minor elements as function of pH in the coprecipitation tests may be described as follows: 1) La, Ce, Nd: Massive precipitation in the pH range of 8 < pH < 12. At pH = 7.4 and at pH = 12 these elements were partially retained in the solid. 2) Zr, Rh, Y and Pd were retained in the solid phase for all pH values tested. Solubility of these elements could be controlled by formation of an individual phase [96DIA/GAR]. 3) Ru precipitates at all pH values tested, Precipitation ratio increased in the pH range 7.4<pH<8.3. At pH ≥ 8.3 precipitation ratio remained constant. 4) Ba is partially precipitated. Precipitation ratios showed small variation with pH. Ba solubility may be controlled by formation of $BaMoO_4$(s). 5) Mo at pH 7.4 and 12 stayed on the solid phase. Concentration in solution showed a different behaviour respecting the minor elements described before. For 7.4 < pH < 12 Mo was found in solution and in solid phase with different precipitation ratios. Mo behaviour is not well understood due to the lack of thermodynamical data of U(VI)-molybdate phases [96DIA/GAR].

X ray diffraction of the solids showed that the main phase precipitated was a schoepite type with Na/U ratio of about 0.3, as was obtained in previous U precipitation experiments performed in the system Na-Cl-U-H_2O [98DIA/GRA].

WP II.2 COPRECIPITATION WITH DISSOLVED U AND PU

As for SIMFUEL and spent fuel, a similar precipitation experiment was started with solutions containing only Uranium and Plutonium.

Uranium and Pu concentration in solution versus pH are shown in FIGURE II.I.4 and FIGURE II.2.1 for the experiments performed in 5 m NaCl solutions free of carbonates.

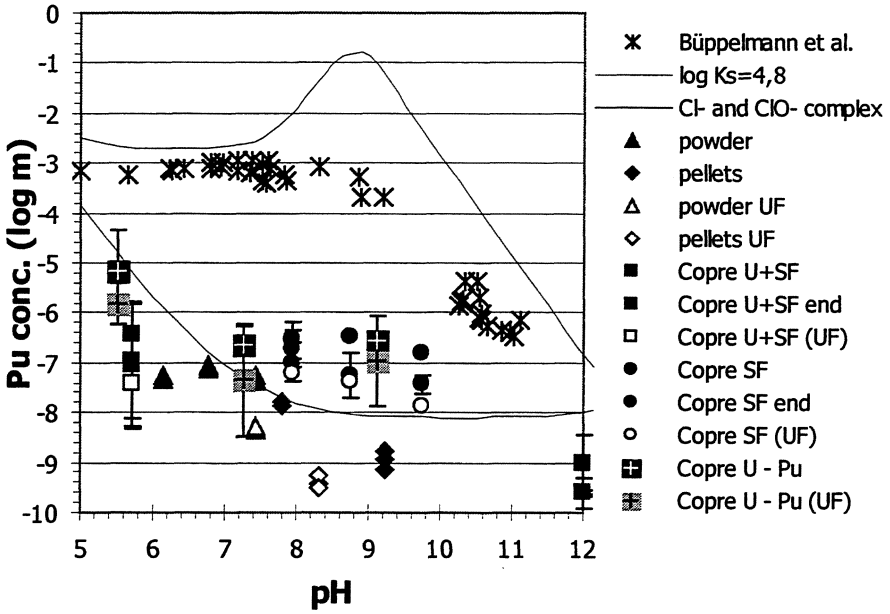

FIGURE II.2.1 Pu concentration from leaching and coprecipitation of SF and U/Pu tests in saline solutions.

Evolution of plutonium and uranium concentration with time was also studied. FIGURE II.2.2 shows the uranium and Pu concentration versus time for one of the pH values tested. Concentration in solution remained almost constant after the first week of precipitation process for all pH tested. After precipitation process Pu concentration remains about two orders of magnitude lower than uranium concentration. A comparison with data from SF coprecipitation experiments showed a good agreement (FIGURE II.2.1). It seems that Pu concentration is controlled by $Pu(OH)_4(s)$ formation. Nevertheless, Pu thermodynamical database should be carefully reviewed for better understanding of the system.

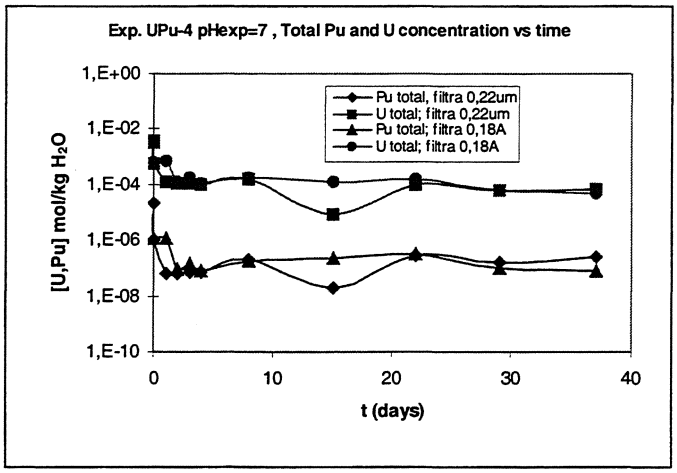

FIGURE II.2.2 Evolution of U and Pu conc. in 5 m NaCl.

Conclusions from precipitation and coprecipitation tests WPII.1 and WPII.2

The results of WPII1 and WPII.2 show that coprecipitation tests are very useful to determine upper concentration limits in a given aqueous environment. Starting with high initial concentrations of radionuclides, precipitation and coprecipitation show, that these concentrations are not stable, neither for actinides nor for long-lived fission products such as Pd107 etc. This is important considering the fact, that high radionuclide solubilities are still used in many repository safety analyses. Additionally, geochemical predictions of radionuclide solubilities are often very uncertain due to uncertainties in the nature of the solid phase assumed to control solubility, in its crystallinity (particle size) and in the effect on non-stoichiometry.

The relevance of coprecipitation tests is demonstrated by the fact that solution concentrations in this type of tests are often similar to results from dissolution tests with spent fuel performed under similar conditions. One of the drawback of the present work is that the solubility-controlling phase is not known. More work is necessary to identify the crystallographic sites for radionuclide incorporation in various host phases.

WP II.3 DETERMINATION OF OXIDATION STATES OF PU DURING SPENT FUEL DISSOLUTION

The mobility of Pu strongly depends on its oxidation state. Pu(V) is rather mobile, Pu(IV) not. An attempt was made by FZK to determine the oxidation state of Pu during corrosion of spent fuel (powder, pellet, pellet + Fe) in 95% saturated NaCl-solution at 25°C after a total static corrosion time of at least 1588 days according to the proposal of Neu et al.[94NEU/HOF]. Aliquots of 250 µl of corrosion solutions were added to various organic solution cocktails to extract the different Pu-species from the aqueous to the organic phase. After mixing and centrifugation the organic phase was separated. Pu-activities were measured (α-spectroscopy or liquid scintillation) either by aliquots from the organic phase or after reextraction of Pu into the aqueous phase.

Since Pu-concentrations in corrosion solutions were rather low ($3{,}8*10^{-7}$ mol/l [spent fuel powder], $5*10^{-10}$ mol/l [spent fuel pellet], $4*10^{-11}$ mol/l [spent fuel pellet +Fe]), evaluation of results did not reveal a clear tendency of assignment of Pu oxidation states. In no case was the distribution of Pu species in solution reproducible.

WP III EFFECT OF NEAR FIELD MATERIALS

WP III.1 CO-DISSOLUTION WITH METALLIC IRON

To assess the influence of the corroding container on the fuel matrix dissolution and the associated release/retention of radionuclides, corrosion experiments in the presence of iron/iron corrosion products were carried out in bentonite water and saline solutions with spent fuel, by FZK, with unirradiated UO_2 by VTT and with SIMFUEL by ENRESA/CIEMAT.

Long-term test in NaCl solutions with spent UO_2 fuel pellets and iron

Long-term experiments from previous EU-project [97GRA/LOI] with high burn-up spent fuel (pellets K 9 and K 4; each 7,5 g; 50 MWd/kgHM) in 95% saturated NaCl-solution in the absence/presence of 8,5 g metallic iron powder, respectively iron corrosion products were terminated after 1624 (1619) days. During this time five times samples of solution were taken. The interval between the end of the experiment and the fourth sampling was 1183 (1181) days. Additionally, radiolytic and fission gases generated during the last interval were analyzed. FIGURE III.1 – 1 shows the release of Cs137, Sr90, Eu144, Am241, Ru106, Ce144, Pu239/40 and U238 in terms of FIAP values as a function of time for both test conditions.

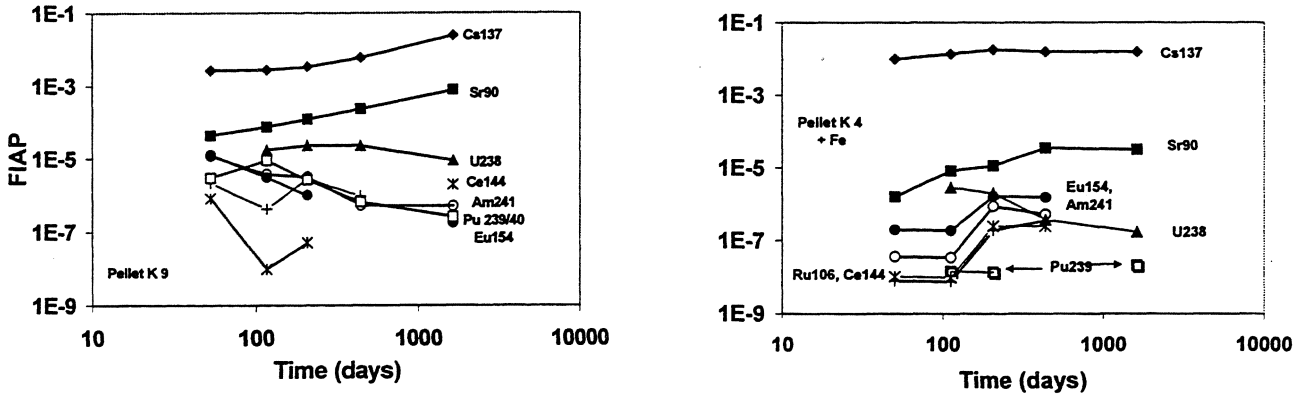

Figure III.1 –1: Effect of iron on the dissolution of spent fuel pellets in 5m NaCl-solution under anaerobic conditions: Sample K9, 1623 days (left), K4, 1619 days in the presence of 8,5 g Fe powder (right).

During the whole test about $7*10^{-2}$ % (K 4 + Fe $3*10^{-3}$ %) of the matrix was dissolved, indicated by FIAP values of Sr90 around $7*10^{-4}$ (K4+Fe $3*10^{-5}$). In the absence of Fe (K9) the matrix dissolved with a constant rate of ca $5*10^{-7}$/d. FIAP values of all other radionuclides (except Cs) were between 1 and 3 orders of magnitude lower than Sr. In the presence of Fe release of Cs137 was higher, whereas FIAP values for all other radionuclides were found to be in the range between 10^{-6} and 10^{-8}, which indicates strong retention effects, too. During the interval of 1181 days between the fourth sampling and the end of the experiment the progress of matrix dissolution seems to stop, as can be seen from FIAP values of Sr90 (corrosion rate < $1,6*10^{-9}$ /d based on Sr90) and Cs137 which are remaining constant;

Pu239/40 remains also constant, U238 shows a slight decrease, Am241, Eu154, Ru106 and Ce 144 are no more detectable in solution. In TABLE III.1-1 data (FIAP, reaction rates, concentrations of radioelements,...) from both tests are summarized.

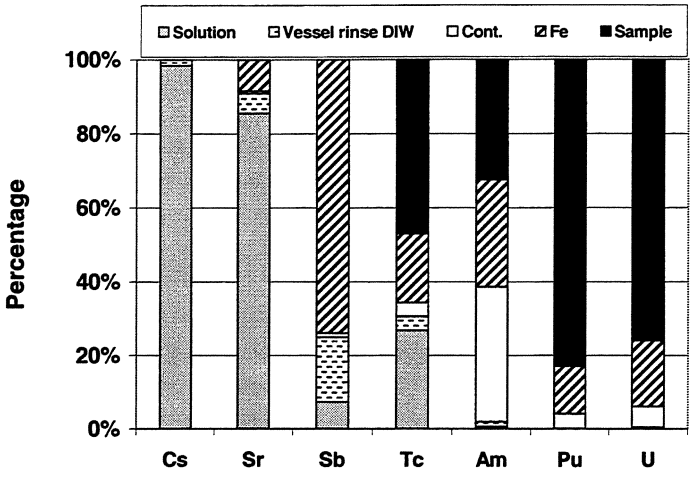

Figure III.1 –2: Dissolution of pellet K 4 for 1619 days in 5 m NaCl-solution under anaerobic conditions in the presence of 8,5 g Fe powder

TABLE III.1-1: Results from long-term corrosion tests with spent fuel pellets (each 7,5 g; 50 MWd/kgHM) in absence (K9) and presence of corroding container material (K4 + Fe) in 5m NaCl-solution.

	Pellet K 9	Pellet K4 + Fe
Duration of static test	1697 days	1692 days
Reaction rate (FIAP Sr)	4,6 E-7/d	< 1 E-9/d
Dissolved amount of fuel	0,077 %	0,003 %
H2 pressure during 1088 d	0,2 bar	2,75 bar
Pu conc. (end)	5,1 E-10 Mol/l	4,1 E-11 Mol/l
U conc. (end)	1,5 E- 6 Mol/l	2,8 E- 8 Mol/l
Am conc. (end)	4,3 E-11 Mol/l	< 2,1 E-11 Mol/l
Tc conc. (end)	6,4 E - 7 Mol/l	5,4 E -9 Mol/l
pH (end), Eh meas. (end)	10,3; 271 mV	9,45; -137mV

The distribution of radionuclides between solid (iron corrosion products, fuel sample, container wall) and liquid phases was studied and results are shown in FIGURE III.1 – 2. The results are similar as those reported for the parallel sample for 1000 days less reaction time in the last EU-project. Only Cs and Sr were mainly found in solution, Sb was mainly

sorbed on iron or its corrosion products. The actinide elements are retained to a significant extent on the sample. An important new result is the very low reaction rate. This may have been caused by the high pressure of H_2 of 2.7 bar, build up during the test allowing for effective competition with oxidative radiolysis effects.

Spent fuel powder in granite bentonite water

The effect of the presence of iron and its corrosion products on the dissolution behaviour of spent fuel in granite water was studied using powdered spent fuel samples (notation P3, 2,6 g LWR-UO2 from PWR Gösgen/CH; 50 MWd/kg U). The samples were washed in granite water (EGW) for 54 days to remove fines and to dissolve labile radionuclides. Thereafter the sample was exposed in autoclaves first again to equilibrium granite (EGW) water for 542 days and then to granite-bentonite (GBW) water for another 209 days. Iron powder (2,6 g), cladding material (0,7 g), and a metal chip (1,6 g Ti/Pd: same material as the liner) were added into the autoclave after washing. The gas phase in the autoclave (ca. 200 ml) was Ar/CO_2 (99,97% / 0,03%). Sampling of solution and of gases (fission and radiolytic gases) was performed in regular time intervals.

The initial pH of 9.8 shifted to 8.8, and 10.0 after 50, and 196 days and remained constant in EGW water but decreased after solution exchange with GBW-water to a value of 9.1. The initial measured Eh shifted from -50 – 400 mV_{SHE} at the moment of solution exchange and decreased thereafter to -460 mV_{SHE}. FIGURE III.1-3 shows the released fractions of radioelements in solution as a function of corrosion time. Released fractions of actinides and Tc were about 2 orders of magnitude (U) to more than 3 orders of magnitude lower for Pu, Am, Eu, Np, Sb than in the test in the absence of iron (compare with FIGURE I.1-8). This results from sorption and (co)precipitation phenomena. After 542 days corrosion in EGW water, significant colloidal contribution to total dissolved radionuclides were only found for Uranium (analyzed by sequential filtration/ultrafiltration). In the absence of iron, significant colloid generation was observed in EGW-water. The concentrations of other actinides were

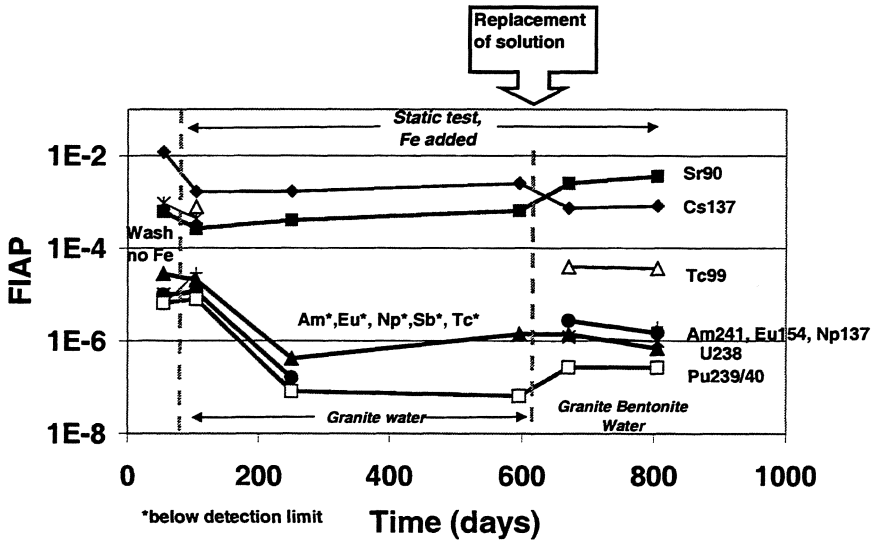

Fig. III.1-3: Corrosion of spent fuel powder in synthetic granite water and granite (bentonite) water in the presence of Fe: Released fractions (non-cumulative) of radioelements as a function of corrosion time (FZK)

close to or lower than detection limit. With values of $4 \cdot 10^{-11}$ m for Pu and $7 \cdot 10^{-8}$ m for U, final concentrations in 0.45 µm filtered solutions were similar to values obtained by CEA in the integral test (see below).

The subsequent replacement of granite water by granite-bentonite (GBW) water resulted in an increase of the dissolved fractions of Pu239/40, Sr90, Np237, Am241, Eu154, and Tc99 in comparison to the first phase of the test where EGW water was used. Constant or decreasing release fractions was found for U238. Nevertheless, despite this increase in solution concentration, retention of Pu239/40, Np237, Am241, Eu154, and Tc99 is still strong in the presence of iron in granite bentonite water (GBW).

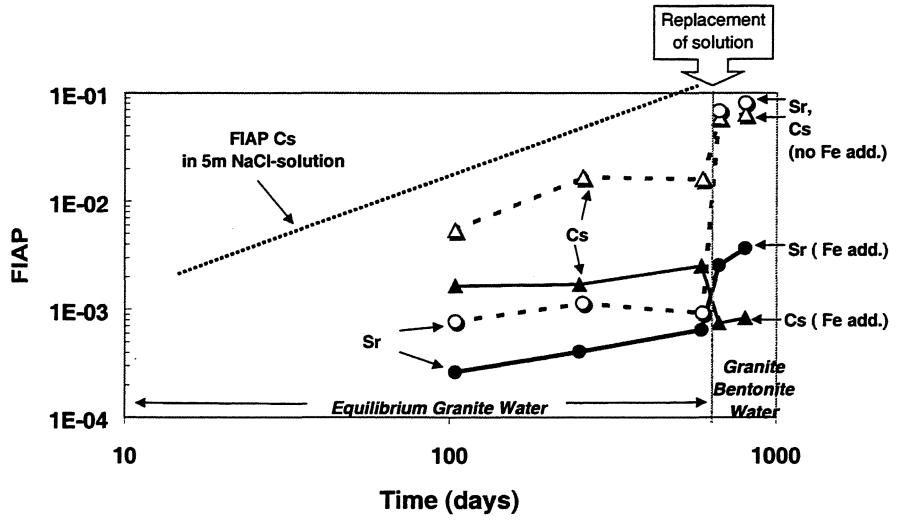

Fig. III.1-4 : Comparison of cumulative Sr and Cs release data from tests with (sample P3) and without iron (P4) present (compare Fig. I.1-8 with Fig. III1-3)

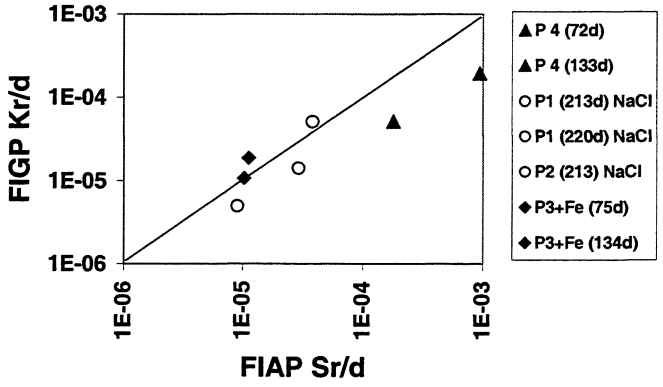

Figure III.1-5: Comparison of Kr-release rates vs. Sr release rates during corrosion of spent fuel powders in GBW (P3,P4) and P1,P2 (NaCl)

A comparison of test results with and without iron present is given in FIGURE II.1-4 both for Cs and for Sr. Cs was found to be a good indicator for matrix dissolution both in EGW and in GBW water in the absence of iron (see discussion of FIGURE I.1-8 in WP I.1). Similarly in the presence of Fe one might expect the same behaviour. In contrast, Sr was found retained in secondary phases in EGW water, which were redissolved in granite bentonite water.

At the end of the first test phase in EGW-water, the released fractions of Sr90 ($FIAP_{Sr}$ ca $6*10^{-4}$) were about a factor of 1,5 lower when compared to Fe-free similar tests. The extent of the increase of FIAP(Sr90) after the replacement of the solution is less pronounced than in the test with powder P4 in absence of Fe, but the similarity of Sr behaviour with and without Fe indicates that again, during corrosion in granite (EGW) water, Sr is involved in newly formed secondary phases, which were dissolved afterwards. This is confirmed by comparing the released fractions of Kr into the gas phase per day (FIGP/d) with the release rates of Sr in terms of FIAP/d (FIGURE III.1 – 5). Representative data points of P3+Fe and for comparison of samples P1 and P2 (NaCl-solution; previous EU-programme [97GRA/LOI]) are close to the diagonal where Sr– and Kr-release rates are matching.

Additionally, Kr- and Sr release rates measured during the test with powder P4 (no Fe) in granite bentonite (GBW) water are displayed. It seems that Kr release rates are much lower than Sr release rates in the absence of Fe than in the presence of Fe, which could be interpreted by the redissolution of a larger quantity of a Kr free Sr containing precipitated phase, formed during the first phase of the test performed in granite (EGW) water. Using both final Cs and Sr data in GBW water as indicator for matrix dissolution it can be concluded from FIGURE III1-4 that congruent release has been achieved. A comparison of final release rates of Cs in tests with and without iron present shows that the matrix dissolution rate has been slowed down in the presence of iron by at least a factor of 20.

One of the reasons for slowing down reaction rates in the presence of iron may be the generation of hydrogen as discussed above for NaCl solutions. The amounts of hydrogen per mass unit of heavy metal (g HM) produced during corrosion tests in the presence of iron using spent fuel powder P3 in granite bentonite (GBW) water as well as pellets K3 and K4 in 95% saturated NaCl-solution are plotted as a function of the sampling interval in FIGURE III.1-6. The corresponding amounts of oxygen per g heavy metal (HM) which were found simultaneously are displayed, too. The highest amount of H_2 about $8*10^{-3}$ Mol/g_{HM} was found in the course of corrosion of spent fuel pellet K 4 during the last sampling period of 1088 days, which corresponds to a H_2 pressure of 2,75 bar. The amount of oxygen was about 10^{-7} Mol/g_{HM}, which is near the detection limit and indicate the "total" consumption of the oxygen mainly by the corrosion of iron. Higher amounts of H_2 were found during corrosion of powder P3 (2,6 g of fuel; 2,6g Fe) than during experiments with pellets K3 or K4 (7,5g fuel; 8,5g Fe) which is an indication for an enhanced H_2 production when using powders.

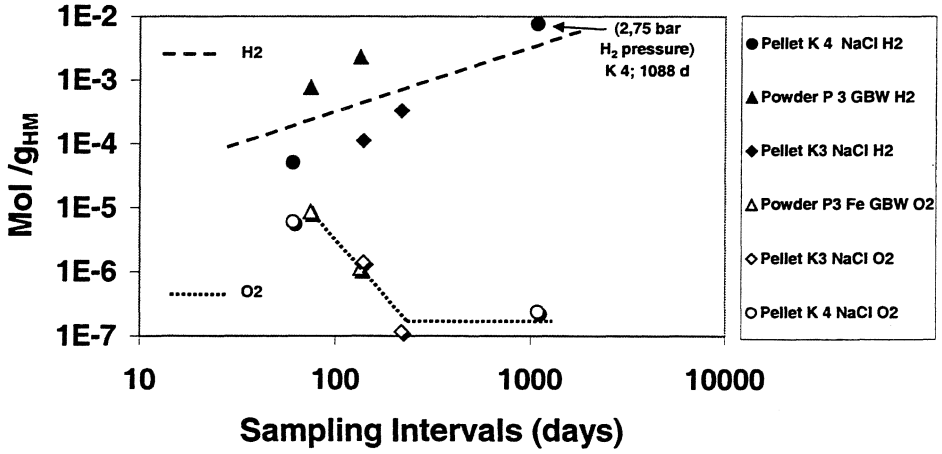

Figure III.1-6: Amounts of hydrogen and oxygen occurring during corrosion of spent fuel in the presence of Fe.

Characterization of solid phases

In the course of 805 days of corrosion in granite and granite/bentonite water, a "cementation" between the powders of spent fuel and iron and the Ti/Pd liner was observed. Sampling of the reacted powder mixture was possible only by using tools such as spatula. A complete discharge was impossible. An agglomeration of a mixture of corroded powders of fuel and Fe which is surrounded by a bright reaction zone up to 50 µm in width on the surface of a Ti/Pd chip is shown in Figure III.1 – 7. Few particles of the various solid compounds were isolated for SEM studies outside the shielded cells (maximum dose rate was 10 µSv/h).

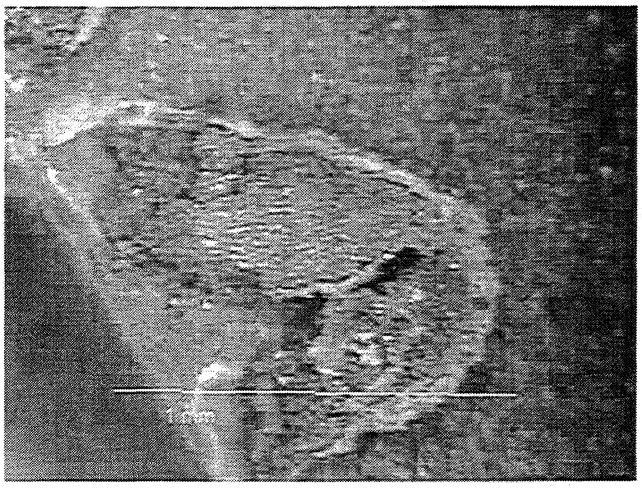

Figure III.1 –7: Agglomeration of corroded powder of spent fuel and iron (P3+Fe) surrounded by a reaction zone inherent on a Ti/Pd chip.

Figure III.1 –8 shows SEM micrographs of particles of the corroded powder mixture of spent fuel and iron. The image on the right (back-scattered electron image) allows to identify the spent fuel particles (brightest particles). Less bright particles may represent elements less heavy than U as iron or its corrosion products or other secondary phases. A part of the iron is still present in the metallic state, as found by EDX analyses (sphere in the upper part of the image). Needle like crystals, where Fe and O were found may represent Goethite (FeOOH).

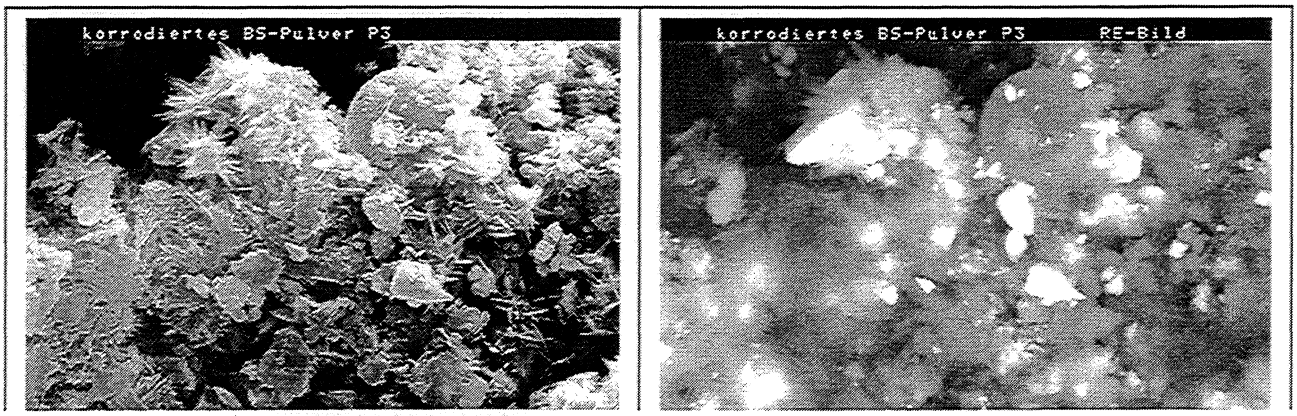

Figure III.1-8: SEM micrographs of corroded powder mixture of spent fuel and Fe (sample P3) obtained after 805 days of corrosion in granite (EGW) and granite –bentonite water (GBW); secondary electron image (left), backscattered electron image (right).

In Figure III.1 – 9 a newly formed Fe-Mg-O phase (dark area in the center) is shown besides spent fuel particles and corrosion products of iron is shown. (Secondary electron image on

the left, back scattered electron image on the right). SEM micrographs of a part from the reaction rim are shown in Figure III.1-10. The leaf like crystal agglomerates consists of Fe, Si, O and Cl.

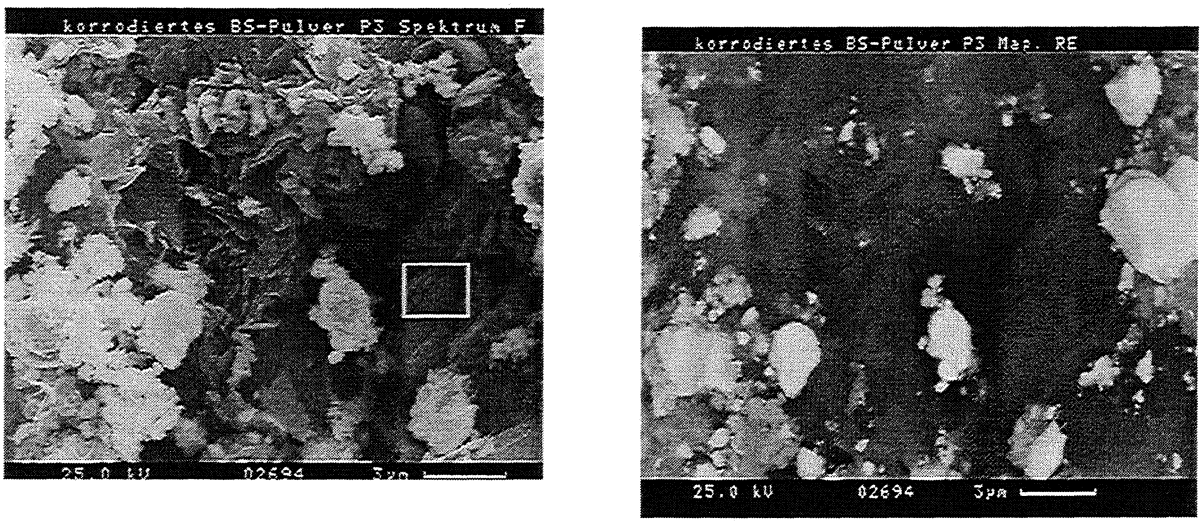

Figure III.1-9: Newly formed Mg-Fe-O-Phase (dark crystals, white rectangle point of EDX analyses), spent fuel particles, corrosion products. Secondary electron image on the left; back scattered electron image on the right (bright particles: heavy elements [spent fuel particles], grey or dark particles [Fe, Mg,... containing phases]

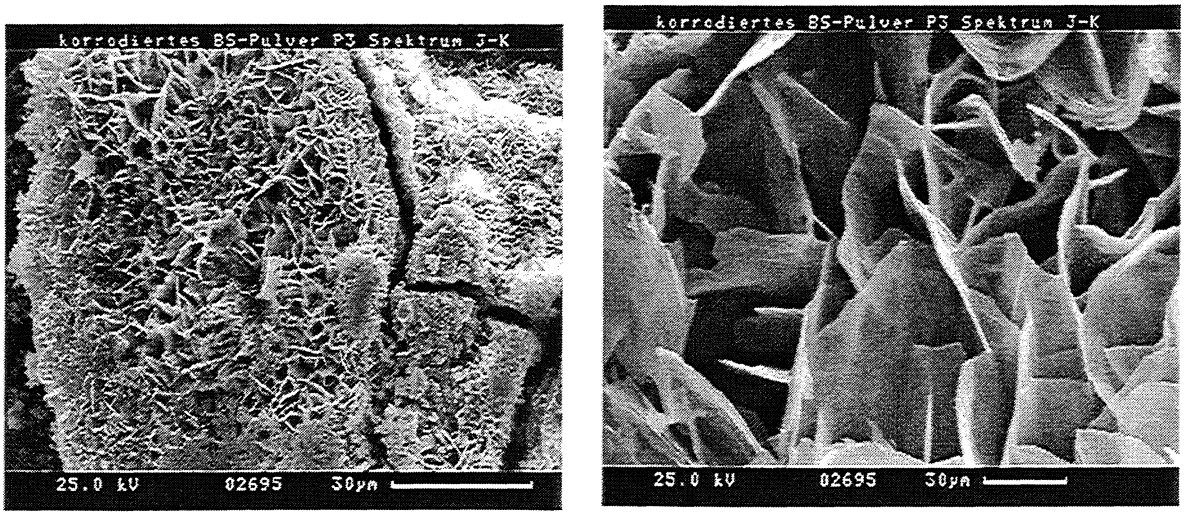

Figure III.1-10: SEM micrograph of reaction zone formed during 805 days corrosion of powdered spent fuel and Fe containing Fe, Si, O, and Cl in granite (EGW) and ganite bentonite water (GBW).

The following phases were identified by SEM/EDX so far

Uranium containing phases:

Besides particles of spent fuel (UO_{2+x}), secondary phases were identified with U, Si, O, and with U,Na,Cl,O

Fe containing phases:

Metallic Fe-particles were found (spheres ca 3µm) as inserted when starting the experiment, as well as oxidised Fe, probably Goethite (FeOOH),. This phase is encountered frequently very close to the fuel particles. It is likely that this FeIII phase is formed by action of radiolytic oxidants. Most part of the reaction rim consists of leave like crystals, containing Fe, Si, O and Cl.

Mg containing phases:

Phases containing Mg are found in the reaction rim as well as inside the fuel powder agglomerates; they consist of Mg(Fe)O and Mg, Na and O. In this phase, Fe is probably in the oxidation state II, hence, this phase is likely to be formed also in the absence of radiolytic oxidants;

Effect of Fe on the solubility of UO_2

Corrosion experiments of unirradiated UO_2 in anoxic Allard water (N_2) in the presence of metallic Fe, were performed at VTT. The measured uranium concentrations (non-filtered) in the aqueous phase show some scatter, see FIGURE III.1-11. In the filtered (0.45 µm) samples the concentrations were lower, below the detection limit of ICP-MS in every sampling. This is significantly lower than the solubility of uranium in the presence of iron in tests with real spent fuel. The increase in solution concentrations with spent fuel is probably caused by the presence of traces of oxidants, which are not consumed by reaction with iron.

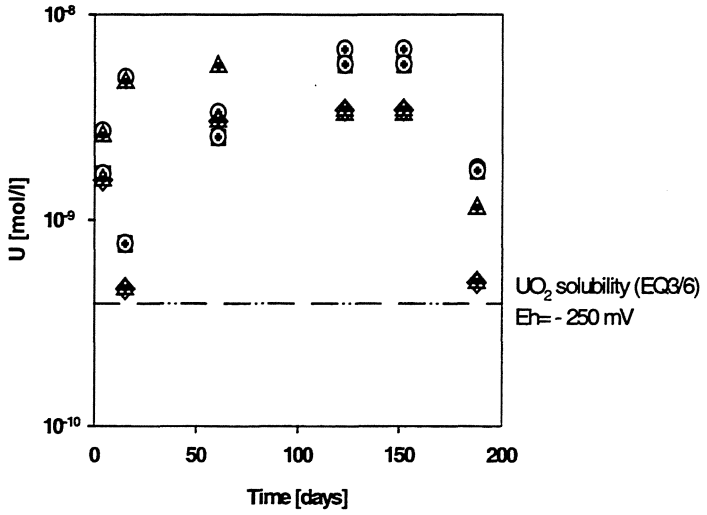

FIGURE III.1-11 Measured uranium concentration (Non-filtered) in anaerobic Allard groundwater (N_2) in the presence of metallic Fe. Solution concentrations in 0.45 µm filtrates were below the detection limit

Precipitation kinetics of uranium in the presence of UO_2 and iron

The kinetics of the decrease in solution concentration of uranium in the presence of UO2 and iron was studied by ENRESA-UPC. Experimental conditions are given in TABLE III.1-2. In FIGURE s III.1-12 and II.1-13, the effect of iron on the uranium concentration in both GBW (experiment UOFGW) and salt brine (experiment UOFUS) are shown. The uranium concentration decreases to reach a final value of $4 \pm 2 \cdot 10^{-8}$ mol·kg^{-1} in the case of brine and $3 \pm 1 \cdot 10^{-8}$ mol·kg^{-1} in the case of GBW. The reproducibility of the data indicates that this value is probably controlled by the solubility of the UO_2(s).

TABLE III.1-2 Experimental conditions for dynamic UO_2 leaching tests in presence of iron.

Experiment	Conditions	UO_2 (g)	Fe (g)	$[U(VI)]_0$ (mol l^{-1})	Medium	pH
UOFUS	UO_2 in N_2 + Fe + U(VI)	3.5	3.5	$2.2\ 10^{-6}$	150 ml NaCl 5 m	8.3 ± 0.1
UFS	U(VI) in N_2 + Fe		1	$1.8\ 10^{-6}$	150 ml NaCl 5 m	8.0 ± 0.1
UOFGW	UO_2 in air + Fe	3.5	0.5		150 ml of GBW	8.2 ± 0.1

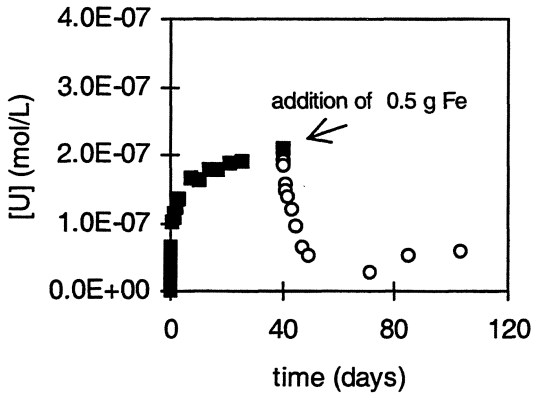

FIGURE III.1-12 Uranium concentration vs. time in the UOFGW experiment

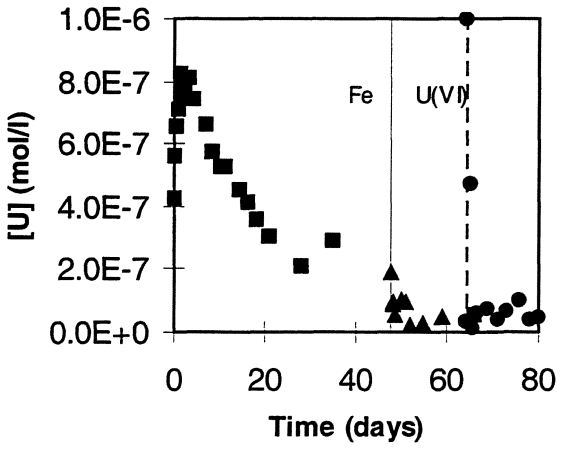

FIGURE III.1-13 Uranium concentration vs. time in the UOFUS experiment

In the UOFUS experiment, once the uranium concentration reached a steady state a new input of U(VI) was added. In FIGURE III.1-13, it can be observed that the same final uranium concentration is obtained. This behaviour was studied in more detail in the experiment UFS, where the iron was added to an U(VI) solution. Though results are not shown here, once again the final uranium concentration was similar to the values obtained in UOFUS and UOFGW experiments. At the end of UFS experiment, Scanning Electron Microscope photographs of the sample showed the presence of UO_2 particles, indicating the precipitation of UO_2 in this experiment [98GIM/MOL].

According to the literature [91BRU/CAS, 97GIM/PAB], the uranium concentration decrease has been modeled assuming that follows a pseudo first-order kinetics. The integration of the corresponding equation results in the following one:

$$[U] = [U]_f + ([U]_0 - [U]_f)e^{-kt} \qquad \text{(III.1-1)}$$

where $[U]_0$ and $[U]_f$ are the initial and final uranium concentrations in solution in $mol \cdot kg^{-1}$, respectively, and k is the rate constant.

This model has been fitted to the results obtained in the different experiments. The best fitting has been obtained with the parameters shown in TABLE III.1-3.

From these results, it can be seen that the final average uranium concentration in the presence of metallic iron in both leaching solution is $4 \pm 2 \cdot 10^{-8}$ $mol \cdot kg^{-1}$, almost one order of magnitude lower than the final uranium concentration under anoxic conditions and in absence of iron.

TABLE III.1-3 Parameters of the fitting of the model to the experiments

Experiment	$[U]_f$ (mol kg^{-1})	k (d^{-1})	$t_{1/2}$(h)
UOFUS before adding the U(VI) solution	$3.6 \pm 0.7\ 10^{-8}$	5±1	3.33
UOFUS after adding the U(VI) solution	$5.6 \pm 0.9\ 10^{-8}$	164±14	0.10
UFS	$2 \pm 1\ 10^{-8}$	28±2	0.59
UOFGW	$4.6 \pm 1\ 10^{-8}$	0.21±0.02	79.22

Considering the values of the rate constant obtained in the experiments with a high U(VI)-concentration, 164 and 28 d^{-1} in the presence and in absence of UO_2(s), respectively, the presence of UO_2(s) seems to increase the rate of reduction-precipitation process. One possible explanation of this difference is that, according to Stumm et al. [83STU/FUR], precipitation is faster if the solid is formed in contact with some other phase, especially if there is some similarity in the atomic structure of the two phases.

The low rate constant obtained in GBW can be attributed to the presence of bicarbonate in this water, since carbonate can form very strong U(VI)-carbonate complexes which would make slower the reduction and precipitation of the U(VI) in solution.

Effect of Fe and f_{CO2} on the corrosion of SIMFUEL (ENRESA-CIEMAT)

Experimental Conditions

Batch leaching experiments were performed in both 5 m NaCl and granite bentonite water (GBW). The surface to solution volume ratio used in all tests was 1000 m^{-1}. The composition of the GBW used in these experiments is showed in TABLE 1. Uranium concentrations of the leachants were analyzed by laser fluorescence. Minor elements concentrations from SIMFUEL were determined by ICP-MS. Surface of the Solid/Volume of the leachant ratio (S/V) used in whole tests was 1000 m^{-1}.

Influence of iron

In order to simulate the influence of container's corrosion on spent fuel degradation, several SIMFUEL corrosion experiments were performed in presence of metallic iron both with and without CO_2. The experimental procedure is shown in FIGURE III.1-14. Initially, SIMFUEL was placed in contact with the aqueous solution. After one month of leaching in duplicate tests three different follow-up experiments were performed:

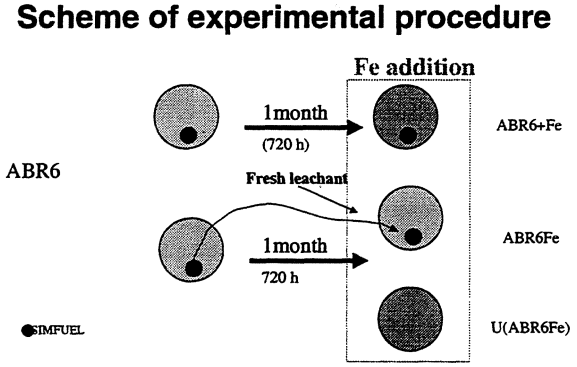

FIGURE III.1-14 Example for test procedure (Anoxic conditions and GBW (ABR6))

ABRR6 + Fe. Metallic iron with a particle size of 10 μm was added to the SIMFUEL/groundwater system.

ABR6Fe. The leachant was replaced by a fresh solution and metallic Fe is added to this SIMFUEL/groundwater system.

U(ABR6Fe). The leachant was removed from SIMFUEL and was put in contact with Fe powder to study potential sorption/precipitation of dissolved SIMFUEL compounds on Fe. Prior to Fe addition, element concentrations in the leachant were characterised.

TABLE III.1-4 Code for experimental conditions used for test designation

Atmosphere	Leachant	Code
Anoxic, log f_{CO2}=-3.5	GBW	ABR6
f_{CO2}=0	5m NaCl	ASR6
Oxic, log f_{CO2}=-3.5	GBW	OBR6
	5m NaCl	OSR6
Anoxic, log f_{CO2}=-2	GBW	CB
	5m NaCl	CS

The rest of experiments were carried following the same experimental procedure. TABLE shows the code used to designate leachant and atmosphere in each test. Test performed in GWB under anoxic/reducing conditions were performed in an N_2/log f_{CO2} = -3.5 atmosphere in order to prevent degassing of dissolved inorganic carbon during the experimental time.

TABLES III.1-5 to III.1-10 describe the experimental conditions of the influence of iron and CO_2 on SIMFUEL leaching behaviours.

TABLE III.1-5 SIMFUEL leaching experiments in GBW under anoxic and reducing conditions (log f_{CO2}=-3.5).

Tests	Initial [U] (M)	Solid	SIMFUEL (g)	Fe (g)	Leachant (ml)
ABR6	-	SIMFUEL			
ABR6+Fe	-	SIMFUEL+Fe	3.45	-	150
ABR6Fe	-	SIMFUEL+Fe	3.45	3.45	150
U(ABR6Fe)	$8 \cdot 10^{-8}$	Fe	3.45	3.45	150

TABLE III.1-6 SIMFUEL leaching experiments in GBW under oxidising conditions (log f_{CO2}= -3.5).

Tests	Initial [U] (M)	Solid	SIMFUEL (g)	Fe (g)	Leachant (ml)
OBR6	-	SIMFUEL			
OBR6+Fe	-	SIMFUEL+Fe	3.45	-	150
OBR6Fe	-	SIMFUEL+Fe	3.44	3.45	150
U(OBR6Fe)	$1 \cdot 10^{-5}$	Fe	3.45	3.46	150

TABLE III.1-7 SIMFUEL leaching experiments in 5m NaCl under reducing conditions (f_{CO2}=0).

Tests	Initial [U] (M)	Solid	SIMFUEL (g)	Fe (g)	Leachant (ml)
ASR6	-	SIMFUEL	3.44	-	150
ASR6+Fe	-	SIMFUEL+Fe	3.45	3.45	150
ASR6Fe	-	SIMFUEL+Fe	3.45	3.45	150
U(AS6Fe)	$3 \cdot 10^{-6}$	Fe			150

TABLE III.1-8 SIMFUEL leaching experiments in 5m NaCl under oxidising conditions (log f_{CO2}=-3.5).

Tests	Initial [U] (M)	Solid	SIMFUEL (g)	Fe (g)	Leachant (ml)
OSR6	-	SIMFUEL	3.44	-	150
OSR6+Fe	-	SIMFUEL+Fe	3.45	3.45	150
OSR6Fe	-	SIMFUEL+Fe	3.45	3.45	150
O(AS6Fe)	$3 \cdot 10^{-8}$	Fe			150

TABLE III.1-9 SIMFUEL leaching experiments in GBW under reducing conditions (log f_{CO2}=-2).

Tests	Initial [U] (M)	Solid	SIMFUEL (g)	Fe(g)	Leachant (ml)
CB	-	SIMFUEL	3.45	-	150
CB+Fe	-	SIMFUEL+Fe	3.45	3.45	150
CBFe		SIMFUEL+Fe	3.45	3.45	150
U(CBFe)	$1 \cdot 10^{-5}$	Fe	-	3.45	150

TABLE III.1-10 SIMFUEL leaching experiments in 5 m NaCl under reducing conditions (log f_{CO2}=-2).

Tests	Initial [U] (M)	Solid	SIMFUEL (g)	Fe (g)	Leachant (ml)
CS	-	SIMFUEL	3.44	-	150
CS+Fe	-	SIMFUEL+Fe	3.45	3.45	150
CSFe		SIMFUEL+Fe	3.45	3.45	150
U(CSFe)	$1 \cdot 10^{-6}$	Fe	-	3.45	150

Results

FIGURE III.1-13 shows the results of experiments carried out under oxidising and reducing conditions in GBW water at log f_{CO2}=-3.5.

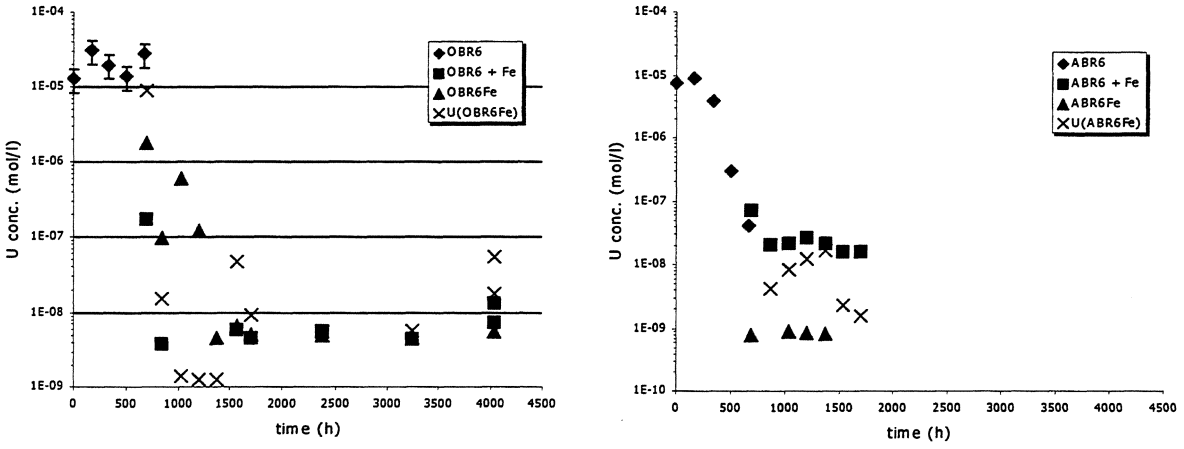

oxidising reducing

FIGURE III.1-15 [U] evolution under oxidising and reducing conditions respectively in GBW (log f_{CO2}=-3.5). Fe is present in the system after 720 h leaching time.

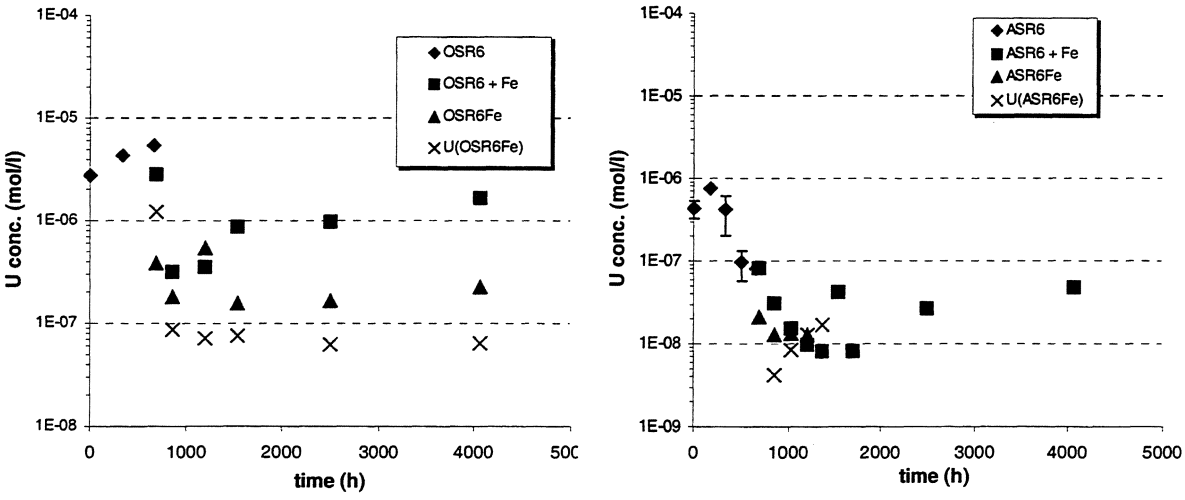

oxidising reducing

FIGURE III.1-16 Uranium concentration against time under oxidising and reducing conditions respectively in 5m NaCl. Fe is present in the system after 720h leaching time

The Fe addition produced a sharp decrease of uranium concentration in solution. This effect is much more remarkable in the case of the experiments under oxic conditions due to the low potential reached after metallic iron is added. Uranium concentrations, without iron, under oxic conditions were approximately $1 \cdot 10^{-5}$ M and under anoxic conditions $8 \cdot 10^{-8}$ M. Uranium concentration fell down to 10^{-8} - 10^{-9} M, under both redox conditions, once Fe was added.

Similar behaviour was found in NaCl solution, FIGURE III.1-16. Prior to Fe addition in the first month of leaching, [U] in solution was $5 \cdot 10^{-6}$ M in the case of oxidising tests and $1 \cdot 10^{-7}$ M for reducing conditions. When Fe is present, concentrations around $1 \cdot 10^{-7}$ M were achieved for oxidising and $5 \cdot 10^{-8}$ M for reducing conditions.

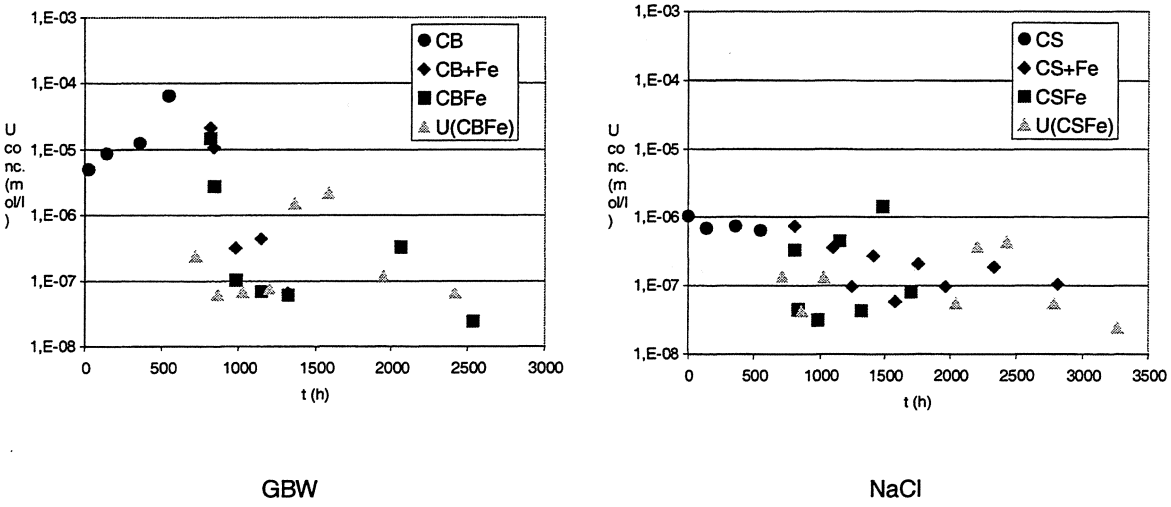

GBW NaCl

FIGURE III.1-17 [U] against time under N_2/CO_2 (p f_{CO2}=2) atmosphere for both, GBW and NaCl leachants. Fe is present in the system after 720 h leaching time.

FIGURE III.1-17 shows the results obtained under N_2/CO_2 atmosphere (p f_{CO2} = 2) for both, GBW and NaCl leachants. As can be observed leaching behaviour is similar than above-mentioned. The presence of iron in the system leads to a decrease of uranium concentration in solution. However, the U concentrations remained higher than under N_2 (NaCl) or N_2/log f_{CO2}=-3.5 (GBW) atmospheres. In GBW-water in presence of Fe, U concentrations were in the range of $1 \cdot 10^{-8}$ M under N_2/log f_{CO2}=-3.5 atmosphere and abut a factor 10 higher under N_2/CO_2 (FIGURE III.1-17). FIGURE III.1-18 compares the average concentration values of each experimental conditions. The values are grouped by experimental procedure (FIGURE III.1-14). "s+l" means solid + leachant, "s+l+Fe" means SIMFUEL plus leachant plus iron; "s+Fe+l(fresh)" are the data obtained when SIMFUEL plus iron and fresh leachant were tested; the last one "l+Fe", means the conditions when leached solution was put in contact with iron without SIMFUEL.

In the absence of Fe as well as at the highest CO_2 pressure, higher concentration values were obtained in GBW than in NaCl solution.

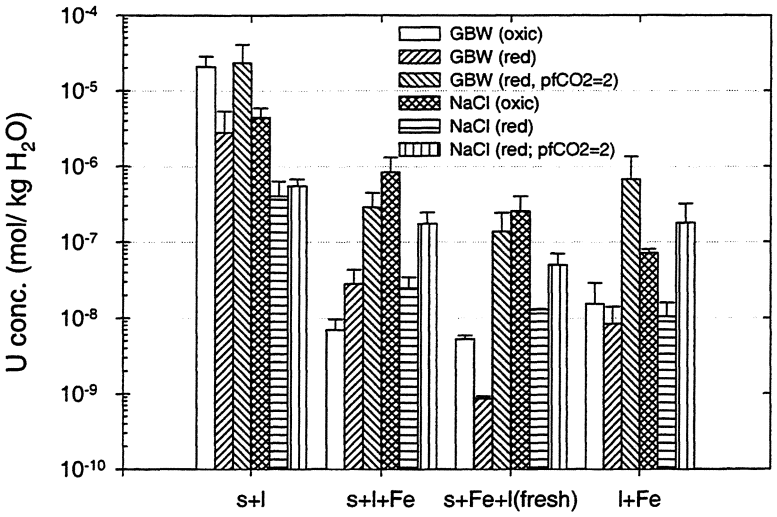

FIGURE III.1-18: Comparison of U concentrations in solution of various tests with and without iron being present

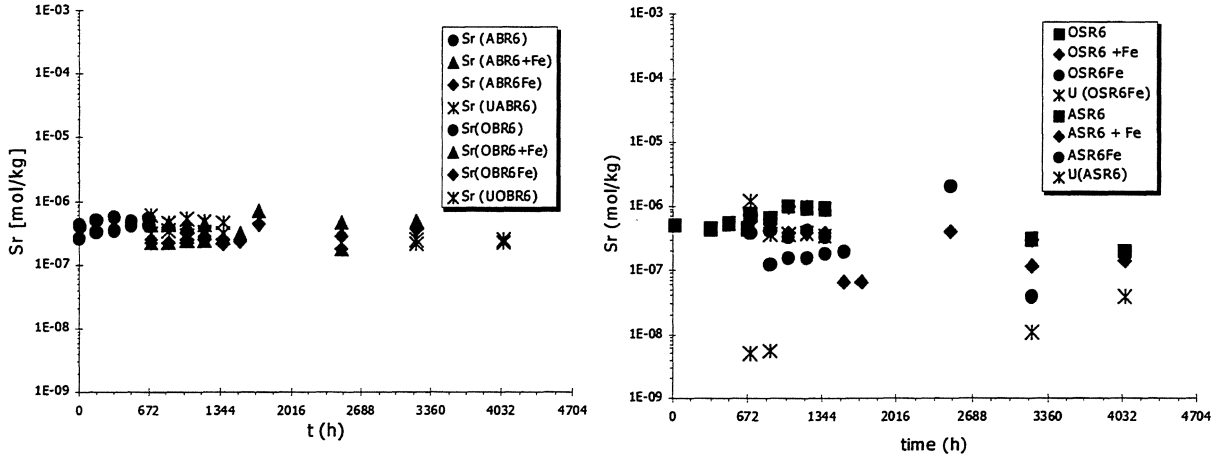

FIGURE III.1-19 [Sr] vs. time in GBW and in 5 m NaCl for both oxidising and reducing low carbonate conditions. Fe is present in the system after 720 h leaching time

Minor Elements behaviour during SIMFUEL dissolution in the presence of iron

One of the advantages of SIMFUEL against UO_2 as chemical analogues for spent fuel is the possibility of obtaining valuable information about behaviour of fission products leaching.

FIGURE III.1-19 gives the Sr concentrations values in dissolution from experiments performed in GBW and 5 m NaCl aqueous solutions. Observed Sr concentration remained stable during the entire test, independent of the addition of Fe. That means that Sr leaching behaviour seems not affected for any changes in the redox potential of the media.

On the other hand, for the redox sensitive element Mo, FIGURE III.1-20, higher concentrations were measured under oxic than under reducing conditions. Moreover, after Fe addition Mo concentration decreased from $2 \cdot 10^{-6}$ M to $1 \cdot 10^{-8}$ M for the tests in GBW. In

NaCl experiments the decrease in Mo was less pronounced.

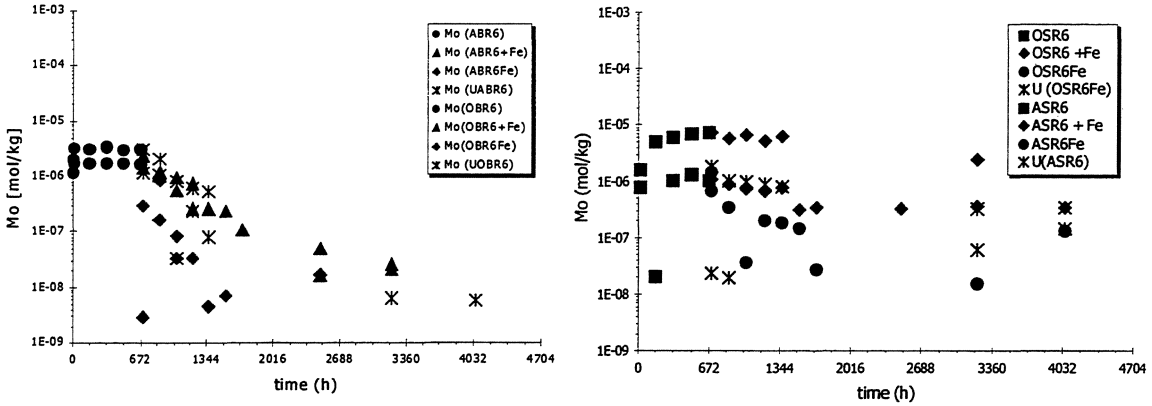

GBW ClNa

FIGURE III.1-20 [Mo] against time in GBW and in 5 m NaCl for both oxidising and reducing low carbonate conditions. Fe is present in the system after 720 h leaching time.

TABLE III.1-11 compiles the fraction of inventory in aqueous solution (FIAP) obtained in the experiments above described. These FIAP values have been calculated according the initial composition presented in TABLE . A comparison of SIMFUEL FIAPs values with spent fuel data (TABLE III.1-12) demonstrates the good agreement each other and the convenience of using SIMFUEL to provide important insight for the knowledge of spent fuel dissolution behaviour.

TABLE III.1-11 FIAP values obtained in GBW water and in NaCl solution.

	GBW		NaCl	
	Oxic	Red	Oxic	Red
Sr	10^{-3}-10^{-4}	10^{-3}-10^{-4}	10^{-3}-10^{-4}	10^{-3}-10^{-4}
Mo	10^{-2}-10^{-3}	10^{-3}	10^{-3}	10^{-4}
Ba	10^{-3}	10^{-3}	10^{-4}	10^{-3}

TABLE III.1-12 FIAP values from SF for Mo, Cs and Sr (GCW: granite-clay, *GW*: granite water).

	GCW [97PAU]	GW [88WER]	GW [90GRA/FOR]	GW [86FOR/WER]	GW [95GLA/TOS]	GW [97SER/RON]
Mo	10^{-3}	10^{-3} - 10^{-4}	-	-	-	10^{-3}
Cs	10^{-4}	-	-	10^{-4}	10^{-2}	-
Sr	10^{-5}	10^{-3} - 10^{-4}	10^{-4}	10^{-3}	10^{-3}	10^{-3}-10^{-4}

Conclusions on Spent fuel, SIMFUEL and UO_2 experiments in presence of iron

Uranium concentration in solution depends strongly of redox potential, being the concentration obtained under oxic conditions in the range of 10^{-5} M and as low as 10^{-9} M for reducing conditions.

Presence of iron in the system brings on a sharp decrease in the concentrations of iron and other actinides in solution. As shown by SIMFUEL data, this effect is more remarkable in the case of the experiments performed under oxic conditions since the changing of the redox potential is more significant.

High content of carbonates in dissolution minimizes the decreasing effect of Fe in the U concentration. This fact is attributed to the stabilization of U concentrations by carbonate complexation.

Strongest effects of iron on solution concentrations of radionuclides were observed for redox sensitive elements. Presence of container material has a great influence on the dissolution of Pu, U, Am, Tc and Mo. On the contrary, Sr concentration was not affected by presence of iron. Sr can be used as indicator for matrix corrosion in GBW water but not in EGW water.

In presence of iron, spent fuel corrosion rates in granite bentonite water were decreased by about a factor of 20 when compared to a similar experiment in the absence of iron. Decrease of corrosion rates is associated to an increase in the partial pressure of hydrogen. In long-term experiments (>4 yr.) in NaCl solution partial pressures of 2.9 bar were achieved. Fractional corrosion rates were as low as 10^{-9}/d. This is 500 times lower than under anoxic conditions in the absence of iron.

The good agreement observed between FIAPs from spent fuel and SIMFUEL confirms the use of SIMFUEL as an adequate chemical analogue of spent fuel.

WP III.2 CO-DISSOLUTION WITH FE (III) CORROSION PRODUCTS

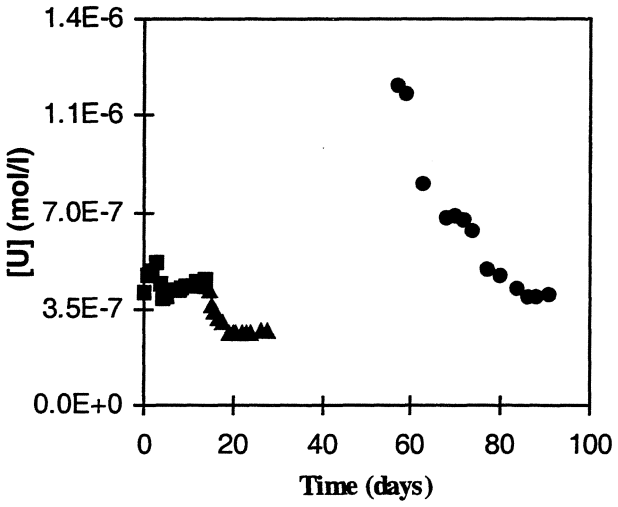

FIGURE III.2-1 Uranium concentration vs. time in time UOFOUGW experiment

One of the potential corrosion product of metallic iron containers under reducing conditions is magnetite, Fe_3O_4. The effect of magnetite on the corrosion of UO_2 and the associated Uranium concentrations in solutions were studied by ENRESA/UPC. Particular emphasis was on the precipitation kinetics. Experimental conditions age given in TABLE III.1-2. In FIGURES III.2-1 and III.2-2, the effect of magnetite on the uranium concentration in both GBW (experiment UOFOUGW) and salt brine (experiment UOFOUS) are shown. In 5 m NaCl the final uranium concentration ($\approx 4 \cdot 10^{-8}$ mol·l^{-1}) was independent on initial uranium concentration while in GBW two final steady state uranium concentrations are obtained. The final uranium concentrations are summarized in TABLE III.2-2.

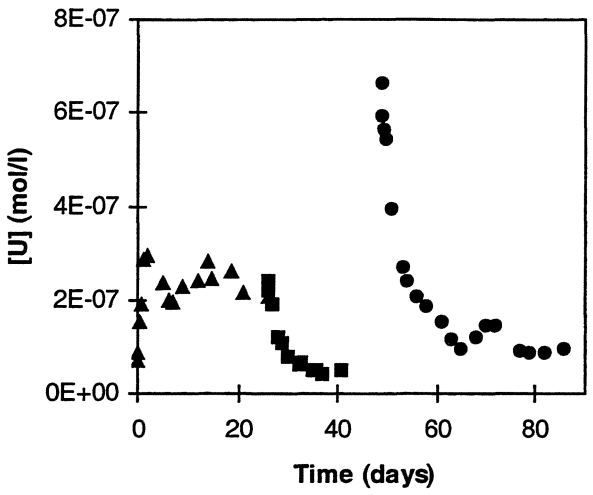

FIGURE III.2-2 Uranium concentration vs. in experiment UOFOUS

Concentrations measured in 5 m NaCl solution are similar to those obtained in the presence of iron (FIGURE III.1-12 and III.1-13). On the other hand, it is clear that the chemical composition of GBW affects the behaviour of uranium in solution. This can be explained by the presence of carbonate in this groundwater; the formation of U(VI) complexes could, as it has been pointed out in the experiments with iron, decrease the reduction rate of U(VI) or the sorption onto magnetite. At the present, it is clear that magnetite decreases the uranium concentration, but the process responsible for this behaviour is still unknown.

TABLE III.2.1 Detail of the experiments performed in UO_2 leaching tests.

Experiment	Conditions	UO_2 (g)	Fe_3O_4 (g)	$[U(VI)]_0$ (mol l^{-1})	Medium	pH
UOFOUS	UO_2 in N_2 + Fe_3O_4 + U(VI)	1	1	$8.0\ 10^{-7}$	150 ml 5 m NaCl	8.2 ± 0.1
UFOS	U(VI) + Fe_3O_4		1	$8.0\ 10^{-7}$	155 ml 5 m NaCl	
UOFOUGW	UO_2 in N_2 + Fe_3O_4 + U(VI)	1	1	$1.4\ 10^{-6}$	180 ml of GBW	8.3 ± 0.1
UFOGW	U(VI) in N_2 + Fe_3O_4		1	$9.2\ 10^{-7}$	150 ml of GBW	8.3± 0.1

TABLE III.2-2 Final uranium concentrations and k values in magnetite experiments

Experiment	log [U]	k (d^{-1})	$t_{1/2}$(h)
UOFOUS before adding U(VI) solution	-7.34±0.07	0.38±0.04	43.78
UOFOUS after adding U(VI) solution	-6.96±0.15	0.31±0.03	53.66
UFOS	-6.95±0.15	0.37±0.05	44.96
UOFOUGW before adding U(VI) solution	-6.58±0.07	-	-
UOFOUGW after adding U(VI) solution	-6.47±0.20	0.08±0.01	207.94
UFOGW	-6.70±0.15	0.04±0.008	415.89

The same mathematical treatment described above for the effect of iron (Eq III.1-1) has been applied to the results obtained in the presence of magnetite. In TABLE III.2-2 the rate constants are summarized.

The k values obtained in the presence of magnetite are lower than the ones obtained with iron, indicating a lower reduction capacity of the magnetite. Similar to the results obtained with iron, in salt medium k values is higher than in GBW. This finding confirms that water composition and consequently uranium speciation can be important in the reduction process.

WP III.3 INTEGRAL TESTS

The presence of near field materials such as metallic canister materials and their corrosion products, clay backfill materials (bentonite) or the host rock minerals will strongly alter the fuel dissolution behaviour. The aim of the present study is to assess the synergistic effect of certain key materials (iron, iron corrosion products, bentonite and granite) on spent fuel dissolution.

A hot-cell system was designed to investigate the leaching of spent fuel with a burnup of 60 $GWd \cdot t_U^{-1}$ (with a specific activity of about 0.5 $Ci \cdot g^{-1}$) in the presence of geological materials (clay or granite) under reducing conditions (–310 and –160 mV_{SHE}, respectively) that are very difficult to obtain. The specifications of the experimental setup were defined to take account of scientific requirements (temperature and pressure corresponding to those of a geological repository site, redox potential of actual groundwater, fuel particles of controlled surface area) and safety requirements associated with any implementation of radioactive materials (containment of fuel powder samples, containment of part of the leaching pot solution feed system).

The experimental setup included two major subsystems: the first comprised a leaching solution storage tank, a hydropneumatic pump, a flow meter and a catalyzing column, all supplying the second subsystem consisting of two temperature- and pressure-regulated leaching pots. An identical system was used for the non-radioactive SIMFUEL leaching experiments.

The systems were highly reliable and allowed three-month leaching studies to be conducted according to protocols initially tested on the non-radioactive setup. The SIMFUEL leach tests were monitored for comparative purposes. A schematic representation of the leach experiments is given in FIGURE III.3.1

Experimental procedure

Two types of fuel (UO_2 with a burnup of 60 $GWd \cdot t_U^{-1}$ and a SIMFUEL, for compositions see Appendix 5, TABLE s 13-15) were leached in four different media: granite with granite water (G/GW), granite with clayey water (G/CW), clay with granite water (C/GW) and clay with clayey water (C/CW). Reducing conditions were maintained throughout the tests, as described in section "GROUNDWATERS". Water compositions are given in TABLE 1. compared with other groundwaters and in Appendix 5, TABLE s 1-4. Eight integral experiments were initiated: four with spent fuel and four with SIMFUEL. The leaching pots contained the following simulated media:

clay/sand and granite water

granite and granite water

clay/sand and clayey water

granite and clayey water.

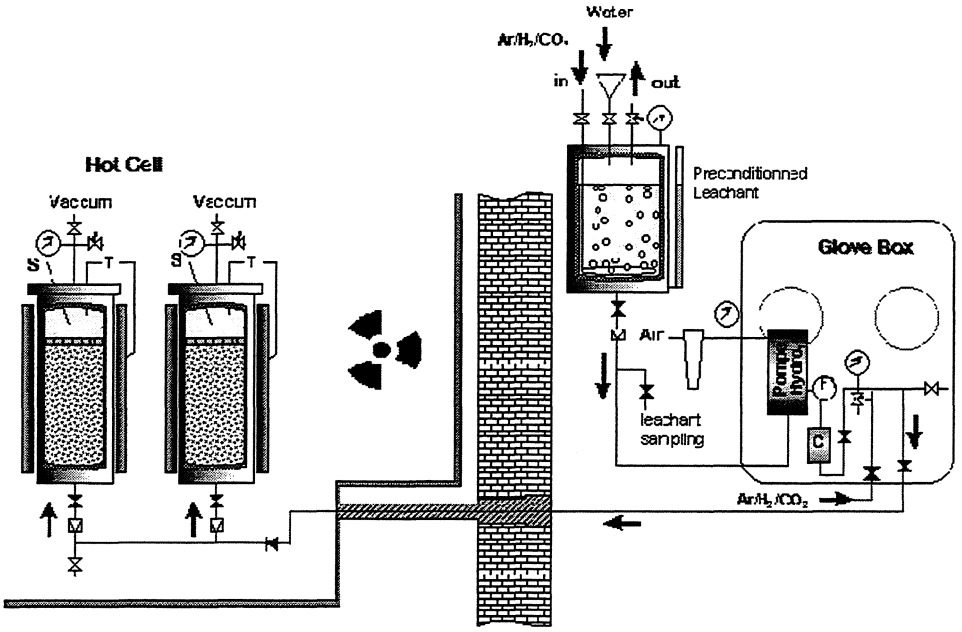

FIGURE II.3.1 : Schematic representation of integral leach tests, including preconditioning devices and redox control for groundwater outside and leaching apparatus inside the hot-cells.

The environmental materials were weighed (260 g of granite or 240 g of a mixture of sand and 10 wt% clay) and placed at the bottom of a leaching pot. A sample holder containing 1 ± 0.01 g of spent fuel or 1.5 ± 0.01 g of SIMFUEL was positioned over the environmental materials. The pot was closed and swept from bottom to top for at least five hours by a hydrogenated argon gas mixture (Ar + 3% H_2 + 300 ppm CO_2) to ensure the residual oxygen concentration was less than 5 ppm.

A quantity of synthesized groundwater was added to a feed tank where it was deoxygenated by bubbling for at least two hours with the same hydrogenated argon mixture. The leaching solution was then gradually allowed to flow into the leaching pot from bottom to top until it flowed out from the overflow valve on the cover; the valve was then closed. The leaching pot was heated to 90°C. After temperature stabilization, the pot was pressurized with the pump to 40 bars.

Sampling Procedure

At weekly intervals, 5 ml to 10 ml leachate samples were taken from the outlet at the top of the pot, and the same volume of fresh leachant was added via the bottom of the pot. These solutions are referred to as the "weekly samples". The solutions were filtered through a membrane filter of 0.45 µm pore diameter, to eliminate clay and sand particles in suspension. The membrane filters were rinsed with 8 ml of 1M nitric acid; the resulting solutions will be referred to as the "filter rinsing solutions".

Each experiment lasted 13 weeks. At test termination the "final supernatant" was withdrawn and filtered. A sufficient quantity of the final supernatant was available to allow ultrafiltration of a solution aliquot; the molecular weight cutoff was 10 000 Daltons, corresponding to a pore size of about 22 nm. The material filtered on this ultrafiltration membranes (particle dimension between 22 and 450 nm) was considered as colloids. The sample holder was rinsed with 215 ml of Milli-Q double-distilled water, the solution is denoted as "sample-holder rinse".

The environmental materials and the interstitial leachate (approx. 80 ml) were rinsed in

215 ml of 1M nitric acid for 24 hours; the resulting solution is designated the "material rinse". The analyses did not discriminate between the activity sorbed on the environmental materials, the activity sorbed on the iron plate and the activity present in the interstitial leachate. In the case of experiments with clay/sand, the mixture was stirred to place the materials in suspension, then filtered across a 100 µm strainer (the 100 µm mesh exceeds the size of the clay particles, and represents a tradeoff between clay/sand separation efficiency and the time necessary for performing this operation in a shielded cell environment). The dose rate of the resulting clay suspension on contact with the flask was 35 mrad·h^{-1}, the maximum permissible value transferable from the hot cell to a fume chamber. The clay mixture was then subjected to alkaline melting with lithium tetraborate according to the procedure described in Appendix 5. The resulting solution was denoted as "alkaline melt". After removal of all materials, the leaching pot was filled with 250 ml of 1M nitric acid. A sample of this "pot rinsing solution" was taken after 24 hours.

From each integral experiment a large quantity of liquid samples were generated as indicated in FIGURE III.3.2. Sample analyses procedures are described in Appendix 5, TABLE s 6 and 7 and Appendix 5, ANNEX 1.

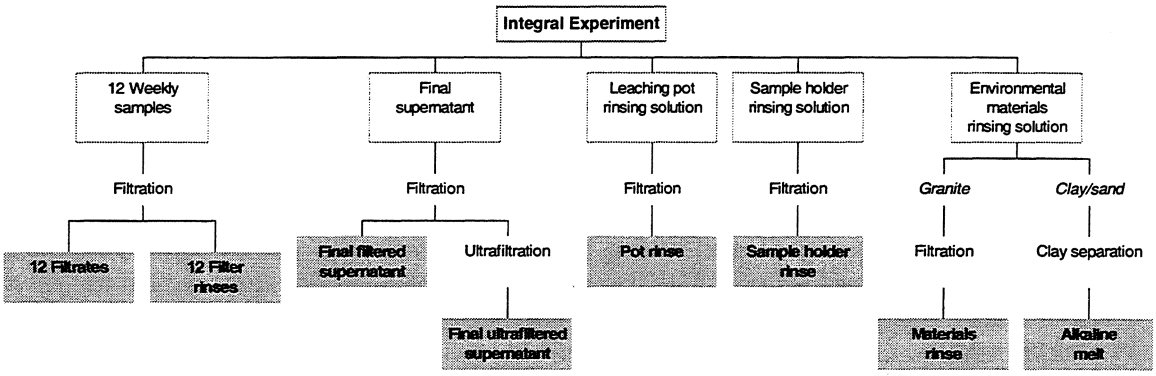

FIGURE III.3.2: Scheme of sample origins, resulting from integral tests

Calculation procedures

The experimental results are described in terms of

$a^n_{preleach}$, a^n_{sample}, a^n_{filter}, $a_{materials}$, a_{melt}, a_{pot}, $a_{sample\text{-}holder}$ designate the specific activity (Bq·ml^{-1}) in solution or the concentration (µg·l^{-1}) of a given radionuclide as measured in preleaching solution *n*, in weekly sample *n*, in filter rinse *n*, in the materials rinse, the alkaline melt, the pot rinse or the sample-holder rinse, respectively.

$V^n_{preleach}$ and v^{n-1}_{sample} designate the deionized water volume used for the n^{th} preleaching of the spent fuel, and the water volume remaining from the preceding rinse (ml).

V and $V_{interstitial}$ designate the free supernatant leachate volume above the fuel and the interstitial leachate volume in the materials (ml). V = 50 ml, $V_{interstitial}$ = 80 ml,

v^n_{sample} designates the *n*th supernatant sample volume (ml).

v_{melt} designates the total solution volume (ml) resulting from alkaline melting of the clay, v_{melt} = 1 l.

v_{filter}, $v_{materials}$, v_{pot} and $v_{sample\text{-}holder}$ designate the volume (ml) of 1M nitric acid or deionized water used to rinse the filters, the environmental materials, the leaching pot and the sample holder. v_{filter} = 8 ml, $v_{materials}$ = 215 ml, v_{pot} = 250 ml, $v_{sample\text{-}holder}$ = 215 ml (Milli-Q

water),

A designates the specific activity in the spent fuel ($Bq \cdot g_U^{-1}$) or the mass ($g \cdot g_U^{-1}$) of a given radionuclide per gram of uranium at the beginning of the test.

M and m designate the total preleached fuel mass $M = 11 \pm 0.1$ g and the fuel sample mass leached during an integral experiment (g). $m = 1.0 \pm 0.01$ g (spent fuel), $m = 1.5 \pm 0.01$ g (SIMFUEL),

M_{clay} and m_{clay} designate the total clay mass used for an experiment and the clay mass submitted to alkaline melting (g). $M_{clay} = 24 \pm 0.1$ g.

f_U is the UO_2-to-U conversion factor ($f_U = 0.8815\ g_U \cdot g_{UO_2}^{-1}$).

The specific surface area S of the spent fuel and SIMFUEL is discussed in chapter "SOLID PHASE CHARACTERIZATION"..

The Gravelines 3+2 spent fuel (60 GWd/t_U) radionuclides and mass inventories used for the exploitation of preleaching data and integral leaching experiments are reported in Appendix 5, table 1 and table 2 respectively. The SIMFUEL mass inventory is reported in Appendix 5, TABLE 3 .

In view of the difficulty of estimating the specific surface area of spent fuel, experimental leaching results are generally expressed in terms of the released fuel inventory fraction. The same convention was applied here to the SIMFUEL results.

Disregarding the activity sorbed on the flask, the activity released from the spent fuel during preleaching is found only in solution. For a given radionuclide, the inventory fraction released into the aqueous phase (FIAP) between rinse n-1 and rinse n is expressed as follows:

$$FIAP_n = \frac{a^n_{preleach} V^n_{preleach} - a^{n-1}_{preleach} v^{n-1}_{preleach}}{A \cdot M \cdot f_U} \qquad \text{(III.3-1)}$$

The cumulative fuel inventory fraction released into the aqueous phase ($FIAP_C$) during the nth rinse is thus:

$$FIAP_{C_n} = \frac{a^n_{preleach} V^n_{preleach} + \sum_{i=1}^{i=n-1} a^i_{preleach} (V^i_{preleach} - v^i_{preleach})}{A \cdot M \cdot f_U} \qquad \text{(III.3-2)}$$

For the integral experiments, we defined the following fractions for each radionuclide:

The *Fuel Inventory fraction released into the Aqueous phase* (*FIA*) corresponds to the released activity (or mass) in dissolved or colloidal form in the supernatant, calculated from the "weekly samples" and "final supernatant" solutions. For a given radionuclide, the cumulative inventory fraction released into the aqueous phase (FIA_C) for the nth sample is thus:

$$FIA_{C_n} = \frac{a^n_{sample} V + \sum_{i=1}^{i=n-1} a^i_{sample} v^i_{sample}}{A \cdot m \cdot f_U} \qquad \text{(III.3-3)}$$

In calculating the inventory fractions released into the aqueous phase, we assumed that the leachate contact volume was the supernatant volume (V). The actual quantity of leachate in

contact with the fuel was between the supernatant volume (V) and the total leachate volume including the supernatant and interstitial leachate.

The *released Fuel Inventory fraction fixed on the environmental Materials* (*FIM*) may be calculated from the "materials rinse", "alkaline melt" (for clay tests) and "filter rinse" solution samples. The "materials rinse" sample also includes the inventory fraction released into the interstitial leachate and the released fraction sorbed on the iron plates. For a given radionuclide, the released inventory fraction fixed on the environmental materials is calculated as follows:

$$FIM = \frac{\left[\sum_{n=1}^{n=12} a_{filter}^{n} v_{filter}\right] + \left[a_{materials}\left(v_{materials} + V_{interstitial}\right)\right] + \left[a_{melt} \cdot v_{melt} \frac{M_{clay}}{m_{clay}}\right]}{A \cdot m \cdot f_U} \quad \text{(III.3-4)}$$

The *released Fuel Inventory fraction Sorbed on the leaching pot and sample holder* (*FIS*) may be calculated from the "pot rinse" and "sample-holder rinse" solution samples. For a given radionuclide, the released inventory fraction sorbed on the leaching pot and on the sample holder is calculated as follows:

$$FIS = \frac{a_{pot} \cdot v_{pot} + a_{sample-holder} \cdot v_{sample-holder}}{A \cdot m \cdot f_U} \quad \text{(III.3-5)}$$

The *Total released Fuel Inventory fraction* (*FIT*) is the sum of the cumulative released inventory fraction in the aqueous phase throughout the duration of the experiment with the fraction fixed on the environmental materials and the fraction sorbed on the stainless steel components, and is calculated from the preceding values using

$$FIT = FIA_C + FIM + FIS \quad \text{(III.3-6)}$$

The mean release rate for a given radionuclide was calculated by linear regression from the cumulative inventory fraction released into the aqueous phase over the total time period. The resulting slope was normalized with respect to the specific surface area (see page 36) of the fuel. This mean release rate is in fact a mean *apparent* radionuclide or element release rate since it integrates only the inventory fraction present in the aqueous phase and does not allow for sorption and/or (co)precipitation phenomena on the stainless steel walls, the environmental materials or on the surface of the fuel itself.

The matrix alteration rate was determined from the cumulative fraction of an alteration tracer released into the aqueous phase, i.e. of a radionuclide (or element) in solid solution in the matrix and soluble in the aqueous phase; strontium is an example of such a tracer. The mean release rate of strontium (or one of its isotopes) into the aqueous solution is thus an indicator of matrix alteration. However, for the same reasons as above, this is again an *apparent* rate. Although every attempt has been made to determine a rate as close as possible to the actual matrix alteration rate from the activity or element balances, it is impossible in the scope of this experimental programme to quantify the fraction sorbed or (re/co)precipitated on the surface of the fuel sample.

Preleaching results of Spent Fuel

The release of labile activity of ^{134}Cs, ^{137}Cs and ^{90}Sr, from gap and to a certain extent also from grain boundaries in the experiments was reduced by preleaching the fuel. The analysis results of preleach solution are indicated in Appendix 5, TABLE 7. After 91 days of preleaching, the cumulative released inventory fractions in the aqueous phase reached 0.66% and 0.83%, respectively, for ^{134}Cs and ^{137}Cs; approximately 64% of this release occurred during the first day of leaching. These values were one to two orders of magnitude

higher than for the other elements. We concluded that the preleaching phase eliminated the labile activity together with some of the activity segregated at the grain boundaries. After 91 days, the cumulative released inventory fraction in the aqueous phase was about 0.13% for strontium, five to six times lower than for cesium. The cumulative released inventory fraction in the aqueous phase was about 0.054% for uranium after the same time. The cumulative inventory fractions released into solution over 140 days of preleaching were 0.66% for ^{134}Cs, 0.83% for ^{137}Cs, 0.13% for ^{90}Sr, 0.24% for Tc, 0.17% for ^{125}Sb and 0.11% for Mo and less than 0.1% for ^{244}Cm, $^{239+240}Pu$, $^{238}Pu+^{241}Am$, Zr, U and Nd.

Results from Spent Fuel Integral Leaching Experiments

This section describes the measurement and analysis results for all the solution samples in the spent fuel integral leaching experiments. These results include the weekly sample pH, the evolution of the major cations between the synthetic leaching solution and the final supernatant, the form (colloidal or dissolved) of the species in the final supernatant, the radionuclide leaching kinetics throughout the experiment, and the overall released material balance.

pH

The pH of granite water ranged from 7.02 to 8.12 for the clay/sand medium, and from 7.39 to 8.09 for the granite medium (TABLE III.3.1). The pH variations for the clayey water ranged from 7.62 to 8.54 with the clay/sand medium and from 7.71 to 8.85 for the granite medium.

The pH diminished in all the media during the initial sampling period (similar behaviour was not observed during the SIMFUEL leaching experiments: During the last ten weeks, the pH measured at 25°C in the weekly samples and in the final supernatant was virtually constant near the initial leachant pH: oscillating within ± 0.3 around a value of 8.4 or 8.6 for the clayey water tests, and around 8.0 for the granite water tests. The rise in the pH thus occurred in the first three weeks.

TABLE III.3.1 . **Gravelines 3+2 spent fuel integral leaching experiments: pH in weekly samples**

Sampling n°	1	3	5	7	9	11	Final Supernatant
Clay/Granite Groundwater	7,02	7,96	7,87	7,96	7,87	8,00	8,12
Granite/Granite Groundwater	7,39	8,09	8,06	7,82	7,96	7,99	7,86
Clay/Clayey Groundwater	7,62	8,41	8,44	8,41	8,54	8,51	8,34
Granite/Clayey Groundwater	7,71	8,85	8,55	No sampling	8,65	8,53	8,61

Major Cations in Final Supernatant

The major cations present in the synthetic groundwaters were determined in the final supernatants. The analysis results are indicated in TABLE III.3.2 together with their initial concentrations. The principal modification of the granite water was calcium enrichment, notably on contact with the clay/sand mixture (a twenty-fold increase). It was also enriched in potassium and, to a lesser extent, in magnesium, silica and aluminum, but was sodium-depleted. The clayey water was also calcium-enriched (about ten-fold), but only on contact with the clay/sand mixture. It was also enriched in silica and aluminum, and slightly depleted in sodium and magnesium.

TABLE III.3.2. **Gravelines 3+2 spent fuel integral leaching experiments : Major cation concentrations ($mol \cdot l^{-1}$) in leachates (precision: Ca, Na 3%; Si, K, Mg 5%; Al 10%) (nd=not determined)**

	Granite Groudwater			Clayey Groundwater		
	As synthesized	Final Leachate Clay/Sand	Final Leachate Granite	As synthesized	Final Leachate Clay/Sand	Final Leachate Granite
K	$5{,}9\times10^{-5}$	$1{,}9\times10^{-4}$	$2{,}2\times10^{-4}$	$2{,}8\times10^{-4}$	$2{,}1\times10^{-4}$	$2{,}9\times10^{-4}$
Ca	$6{,}6\times10^{-5}$	$1{,}2\times10^{-3}$	$2{,}1\times10^{-4}$	$9{,}9\times10^{-5}$	$7{,}0\times10^{-4}$	$9{,}2\times10^{-5}$
Na	$3{,}8\times10^{-3}$	$2{,}4\times10^{-3}$	$2{,}3\times10^{-3}$	$1{,}6\times10^{-2}$	$6{,}0\times10^{-3}$	$6{,}9\times10^{-3}$
Al	$1{,}4\times10^{-5}$	$2{,}3\times10^{-5}$	$1{,}4\times10^{-5}$	nd	$1{,}3\times10^{-5}$	$3{,}2\times10^{-5}$
Si	$1{,}1\times10^{-3}$	$1{,}2\times10^{-3}$	$1{,}3\times10^{-3}$	nd	$1{,}4\times10^{-3}$	$1{,}2\times10^{-3}$
Mg	nd	$4{,}9\times10^{-5}$	$4{,}9\times10^{-6}$	$1{,}0\times10^{-4}$	$5{,}3\times10^{-5}$	$9{,}9\times10^{-6}$

Colloidal Species

Filtered and ultrafiltered aliquot samples of the final supernatants were analyzed and the results were used to calculate the distribution of various radionuclides and elements in colloid and dissolved form (TABLE III.3.3).

Regardless of the type of leachant and environmental materials, Sr, Sb, Cs, U and Mo were found mainly in dissolved form in the supernatant. Curium was found primarily in colloid form when granite was present; its form in the clay/sand experiments was undetermined. Considering the large (30–50%) errors on the measured $^{239+240}Pu$ and $^{238}Pu+^{241}Am$ activity, it is only possible to conclude that these nuclides were present in both forms in solution

Radionuclide release

The weekly sample and final supernatant analysis results are indicated for each experiment in Appendix 5, TABLES 8, 9 and 18 for cumulative release fractions, elemental concentrations and activities respectively. Each experiment lasted 91 days. However, the final supernatant sample was taken on the 91st day at 25°C in contact with air, i.e. under oxidizing conditions, unlike the other weekly samples (90°C under reducing conditions). The final supernatant sample was therefore disregarded when assessing the evolution of the radionuclides in solution. Moreover, the activity of all the radionuclides and elements in the 84-day sample (except for ^{238}U) was interpolated from the final sample; the radionuclide release from the spent fuel into the aqueous phase was therefore studied over the first 77 days. The Gravelines 3+2 spent fuel-leaching experiments lasted from December 1996 to March 1997. The results were therefore interpreted based on the fuel inventory as of 1 January 1997 (Appendix 5, TABLE 14).

In FIGURE III.3.3, for each experiment, the cumulative inventory fractions released into the aqueous phase (FIA_C) for ^{90}Sr, ^{134}Cs, ^{137}Cs, $^{239+240}Pu$, $^{238}Pu+^{241}Am$, ^{244}Cm, ^{238}U and for Mo, and plotted logarithmically versus the cumulative contact time.

The cumulative inventory fractions released into the aqueous phase for a given radionuclide or element were on the same order of magnitude for all the test media, and may be classified in decreasing order as follows:

Mo	$\sim 10^{-3}$
^{134}Cs and ^{137}Cs	$\sim 10^{-4}$
^{90}Sr	$\sim 10^{-5}$
^{238}U	$\sim 10^{-6}$
^{244}Cm, $^{238}Pu+^{241}Am$ and $^{239+240}Pu$	$\sim 10^{-8}$

TABLE III.3.3. **Gravelines 3+2 spent fuel integral leaching experiments : Distribution (%) of species in solution, in colloid (2 nm < ∅ < 0,45 µm) or dissolved form**

	Clay/Granite Groundwater		Granite/Granite Groundwater		Clay/Clayey Groundwater		Granite/Clayey Groundwater	
	Dissolved form	colloid	Dissolved form	colloid	Dissolved form	colloid	Dissolved form	colloid
^{90}Sr	87	13	100*	0*	100*	0*	97	3
Minimum	*65*	*35*	*75*	*25*	*90*	*10*	*72*	*28*
Maximum	*100**	*0**	*100**	*0**	*100**	*0**	*100**	*0**
^{125}Sb	< DL	< DL	100*	0*	< DL	< DL	< DL	< DL
Minimum			*91*	*9*				
Maximum			*100**	*0**				
^{134}Cs	100*	0*	100*	0*	100*	0*	100*	0*
Minimum	*89*	*11*	*91*	*9*	*92*	*8*	*92*	*8*
Maximum	*100**	*0**	*100**	*0**	*100**	*0**	*100**	*0**
^{137}Cs	100*	0*	100*	0*	100*	0*	100*	0*
Minimum	*88*	*12*	*88*	*12*	*66*	*12*	*88*	*12*
Maximum	*100**	*0**	*100**	*0**	*100**	*0**	*100**	*0**
$^{239+240}Pu$	< DL	< DL	75	25	50	50	12	88
Minimum			*25*	*75*	*17*	*83*	*4*	*96*
Maximum			*100**	*0**	*100*	*0*	*36*	*64*
$^{238}Pu+^{241}Am$	65	35	34	66	100*	0*	57	43
Minimum	*35*	*65*	*18*	*82*	*72*	*28*	*31*	*69*
Maximum	*100**	*0**	*64*	*36*	*100**	*0**	*100*	*0*
^{244}Cm	< DL	< DL	8	92	< DL	< DL	8	92
Minimum			*4*	*96*			*4*	*96*
Maximum			*14*	*86*			*14*	*86*
Mo	< DL	< DL	100	0	100	0	100*	0*
Minimum			*82*	*18*	*82*	*18*	*85*	*15*
Maximum			*100**	*0**	*100**	*0**	*100**	*0**
^{238}U	100*	0*	97	3	94	6	98	2
Minimum	*84*	*16*	*79*	*21*	*77*	*23*	*80*	*20*
Maximum	*100**	*0**	*100**	*0**	*100*	*0*	*100*	*0*

DL : detection limit

In the following, these fractions are compared together with the respective concentrations in solution for each radionuclide and each medium for the cumulative contact time.

The element concentrations were calculated from the radionuclide analysis results using the radionuclide/element mass ratios in the spent fuel. The contribution of ^{239}Pu and ^{240}Pu to the measured activity was calculated from their specific activity ratio in the Gravelines spent fuel inventory as of 1/01/97 (Appendix 5, TABLE 14). Although they varied slightly with the nature of the synthetic leaching solution or the environmental materials, the weekly sample concentrations for each element evolved on the same order of magnitude. With a few exceptions according to the test media, the actinide and strontium concentrations in solution decreased sharply during the first 3 or 4 weeks. Again with a few exceptions according to the test media, the actinide concentrations in solution increased significantly in the final supernatant. As previously noted, this solution was sampled at a different temperature and redox potential than the weekly samples.

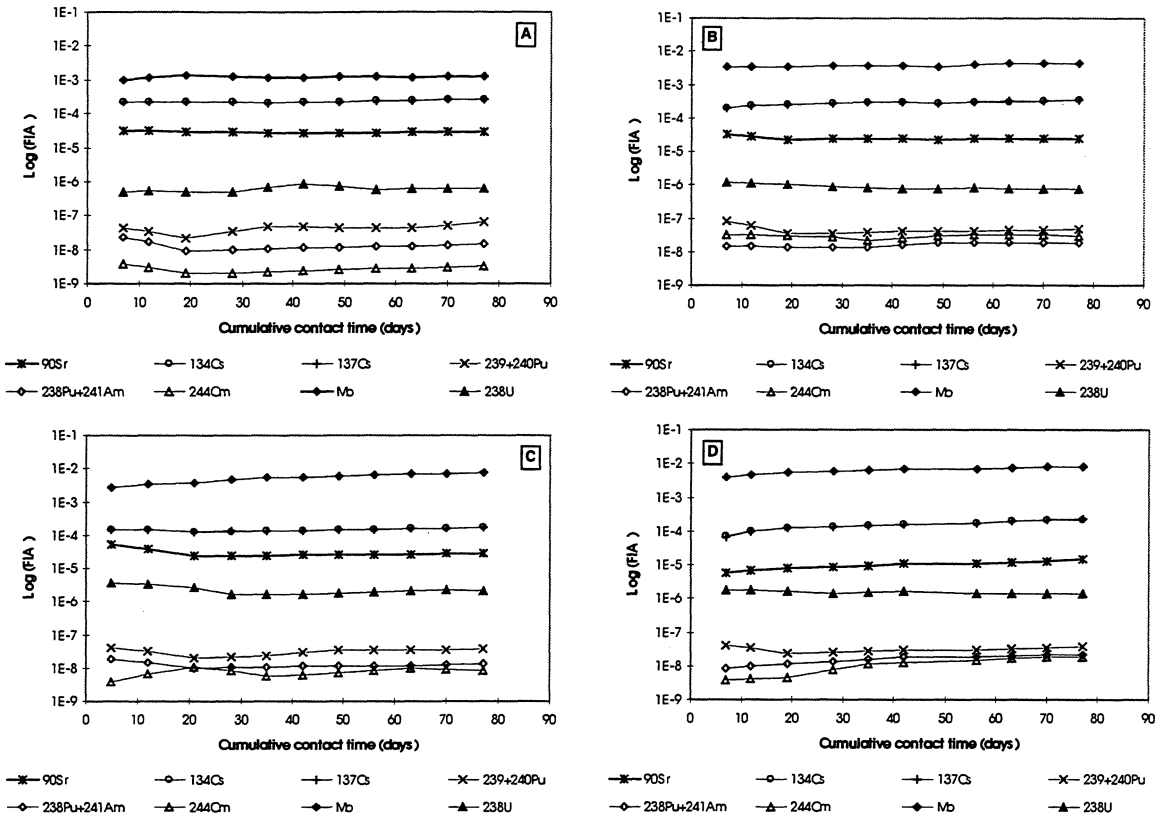

FIGURE III.3.3. **Gravelines 3+2 spent fuel leaching experiment: FIAc of radionuclides and elements Clay/Granite water medium ; (B) Granite/ Granitic water medium. (C) Clay/Clayey water medium; (D) Granite/Clayey water medium.**

With few exception, the FIA_C for elements such as strontium, cesium, uranium, plutonium and americium diminished in the first three weeks of leaching, especially in the clay/granite water, granite/granite water and clay/clayey water media.

The mean release rates were calculated by linear regression based on a spent fuel specific surface area of 0.027 $m^2 \cdot g^{-1}$. The cumulative radionuclide or element inventory fraction released into the aqueous solution sometimes evolved very different during the first few weeks compared with the subsequent experimental period; in these cases the first values are not taken into account. It is important to note that the resulting calculated rates are apparent release rates, since they are based on the aqueous phase, and not on the total release from the fuel. In these integral experiments the total release can only be determined at the end of the experiment. The linear correlation coefficient for each rate is indicated in parentheses.

Strontium 90

The long-term release of Sr in three of the four experiments was similar. In the clay/granite water and the granite/granite water medium a slight, and in the clay/clayey water medium a significant, drop in initial concentrations is observed. In the granite/clayey water medium the Sr release to the aqueous phase was lowest. The strontium concentrations were constant in the granite/clayey water medium and diminished considerably between the first and third weeks in the other media. The final concentrations were all close to 10^{-9} $mol \cdot l^{-1}$.

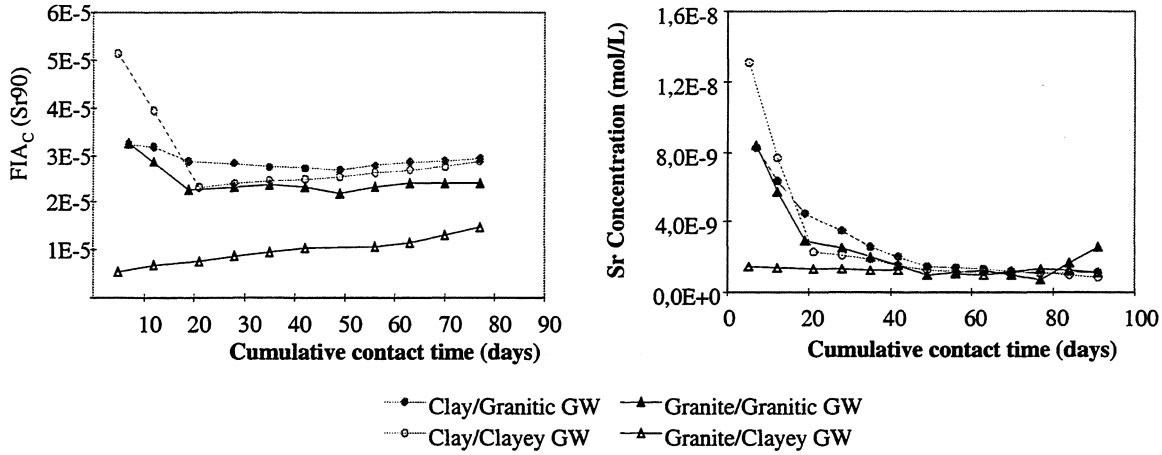

FIGURE III.3.4. **Gravelines 3+2 spent fuel leaching experiment: ^{90}Sr FIAc versus cumulative leaching time, environmental materials and groundwater composition**

Except in the granite/clayey water medium, only the final eight weeks were taken into account for calculating apparent release rates:

clay/granite water 0.37 $\mu g \cdot m^{-2} d^{-1}$ ($r^2 = 0.07$)

granite/granite water 0.74 $\mu g \cdot m^{-2} d^{-1}$ ($r^2 = 0.31$)

clay/clayey water 3.33 $\mu g \cdot m^{-2} d^{-1}$ ($r^2 = 0.98$)

granite/clayey water 3.70 $\mu g \cdot m^{-2} d^{-1}$ ($r^2 = 0.96$)

However, in the two media containing granite water, the overall trend changed again beginning with the 7th week. Considering only the period from the 7th to the 11th weeks, we obtain rates comparable to those obtained in clayey water:

clay/granite water 3.70 $\mu g \cdot m^{-2} d^{-1}$ ($r^2 = 0.96$)

granite/granite water 2.96 $\mu g \cdot m^{-2} d^{-1}$ ($r^2 = 0.75$)

Caesium 134/137

As the cumulative fractions released into the aqueous phase were approximately equal at all times for both caesium isotopes, we considered the isotope with the smallest uncertainty margin: ^{134}Cs. The Cs concentration decreased with time and was generally lower in presence of clay than in presence of granite.

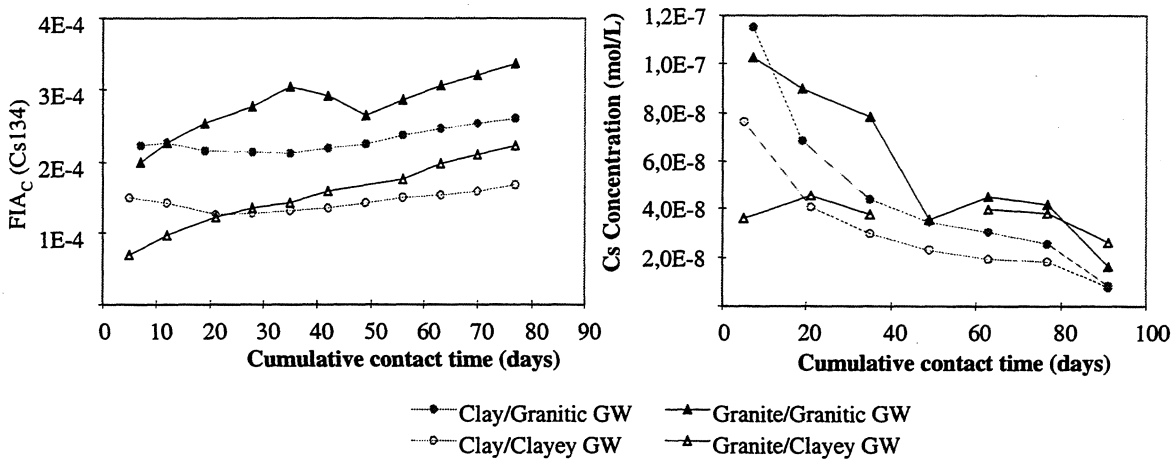

FIGURE III.3.5. **Gravelines 3+2 spent fuel-leaching experiment: ^{134}Cs FIAc and solution concentrations of Cs versus cumulative leaching time, environmental materials and groundwater composition**

For calculating apparent release rates, all the experimental points were taken into account for the granite water media, but only the last eight values for the clayey water media. The apparent cesium release rates into the aqueous phase were:

clay/granite water	33.3 $\mu g \cdot m^{-2} d^{-1}$	($r^2 = 0.90$)
granite/granite water	74.1 $\mu g \cdot m^{-2} d^{-1}$	($r^2 = 0.79$)
clay/clayey water	25.9 $\mu g \cdot m^{-2} d^{-1}$	($r^2 = 0.98$)
granite/clayey water	74.1 $\mu g \cdot m^{-2} d^{-1}$	($r^2 = 0.98$)

The mean apparent caesium release rates were one to two orders of magnitude higher than for strontium, and were twice as high in granite media as in clayey media.

Molybdenum

The cumulative molybdenum fraction released into the aqueous phase increased steadily in all the test media, lowest for clay/granite water and granite/granite water and higher for clay/clayey water and granite/clayey water. The molybdenum concentration generally diminished in the successive weekly samples. The following mean apparent release rates were calculated over 11 weeks of leaching:

clay/granite water	40 $\mu g \cdot m^{-2} d^{-1}$	($r^2 = 0.17$)
granite/granite water	370 $\mu g \cdot m^{-2} d^{-1}$	($r^2 = 0.85$)
clay/clayey water	2220 $\mu g \cdot m^{-2} d^{-1}$	($r^2 = 0.97$)
granite/clayey water	1850 $\mu g \cdot m^{-2} d^{-1}$	($r^2 = 0.96$)

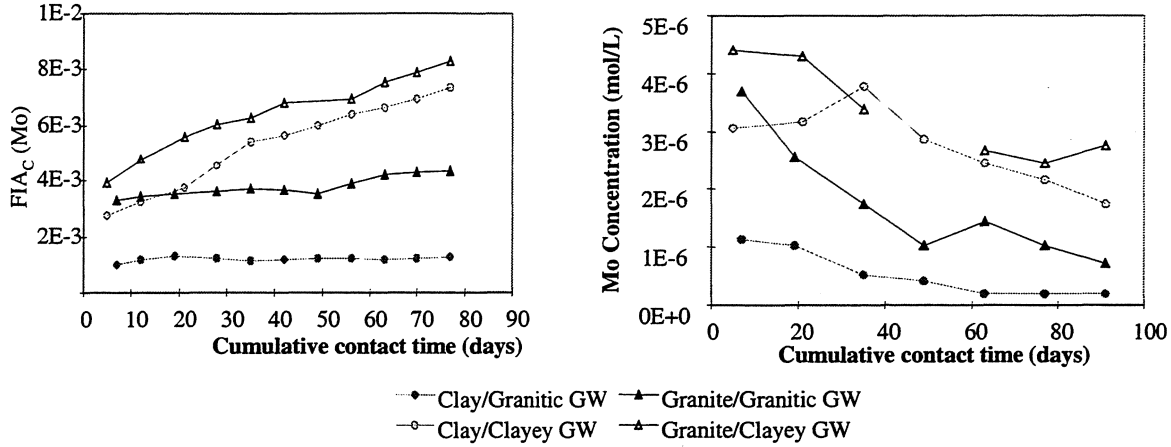

FIGURE III.3.6. **Gravelines 3+2 spent fuel-leaching experiment: Mo FIAc and solution conc. of Mo versus cumulative leaching time, environmental materials and groundwater composition**

In view of the very poor correlation for the clay/granite water experiment, the apparent leach rate is subject to caution. For a given groundwater medium, the rates were apparently on the same order of magnitude irrespective of the nature of the environmental materials, and were one to two orders of magnitude higher in clayey media than in granite media.

Uranium 238

Except in the clay/granite water medium, the cumulative uranium fraction released into the aqueous phase decreased during the first three weeks of leaching, stabilizing at about 6-8 x 10^{-7} in the granite water and 1.4-2.1x 10^{-6} in clay water media. Dissolved fractions of U are significantly lower than those of Cs, Sr and Mo.

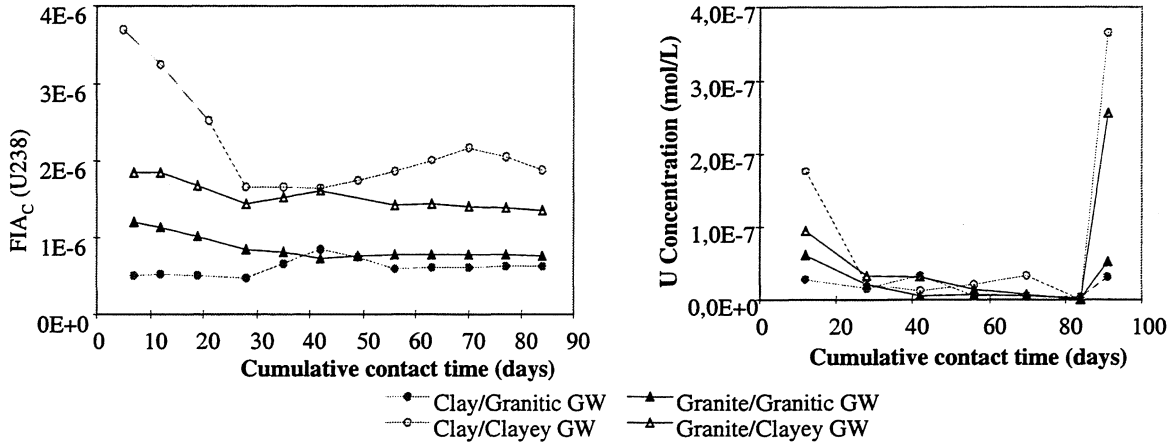

FIGURE III.3.7. **Gravelines 3+2 spent fuel-leaching experiment: ^{238}U FIA_c and solution concentrations of U versus cumulative leaching time, environmental materials and groundwater composition.**

In all the test media the uranium concentrations in the weekly samples first dropped sharply during the first four weeks, then decreased more slowly. The uranium concentrations rose significantly in the final supernatant, probably due to oxygen access. The mean uranium

concentrations in the aqueous phase between the fourth and twelfth weeks were:

clay/granite water 1.2×10^{-8} mol·l^{-1} (i.e. 3 µg·l^{-1})
granite/granite water 7.8×10^{-9} mol·l^{-1} (i.e. 2 µg·l^{-1})
clay/clayey water 1.8×10^{-8} mol·l^{-1} (i.e. 4 µg·l^{-1})
granite/clayey water 1.7×10^{-8} mol·l^{-1} (i.e. 4 µg·l^{-1})

The concentrations were generally lower in the granite media than in the clayey media.

Plutonium 239+240

The measurement errors on the $^{239+240}$Pu activity were on the order of 50%. In all the test media, the released fraction diminished between the first and third weeks, particularly in the granite/granite water medium. Fractions of Pu in solution are about 10 to 100 times lower than those of U. The mean plutonium concentrations between the 3rd and 11th weeks were:

clay/granite water 1.5×10^{-11} mol·l^{-1}
granite/granite water $< 7.6 \times 10^{-12}$ mol·l^{-1}
clay/clayey water 8.9×10^{-12} mol·l^{-1}
granite/clayey water 7.6×10^{-12} mol·l^{-1}

The concentrations were slightly higher in the clay media than in the granite media.

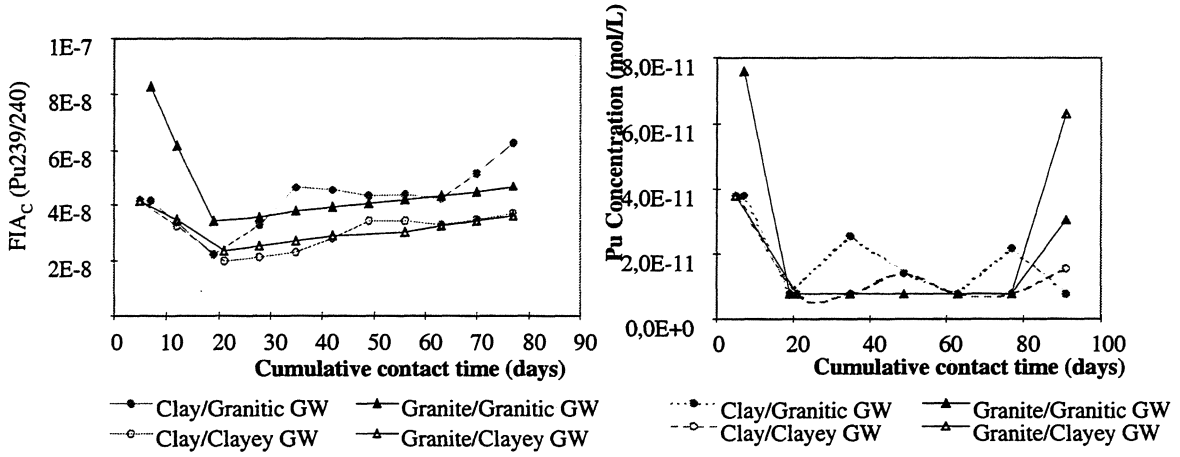

FIGURE III.3.8. **Gravelines 3+2 spent fuel experiment: $^{239+240}$Pu FIA$_c$ and solution concentrations of Pu versus cumulative leaching time, environmental materials and groundwater composition**

Curium 244

As for Pu, the uncertainty in activity measurements makes it difficult to comment on the fluctuations of the curium release. For the clay/granite water experiment the dissolved Cm activity were below the determination limit . Only upper limits are given in the FIGURE III.3.9. The mean curium concentrations between the 5th and 11th week were as follows:

clay/granite water $< 7.3 \times 10^{-15}$ mol·l^{-1}

granite/granite water 6.4×10^{-14} mol·l^{-1}

clay/clayey water 9.0×10^{-15} mol·l^{-1}

granite/clayey water 7.4×10^{-14} mol·l^{-1}

The concentrations were slightly higher in the clay media than in the granite media.

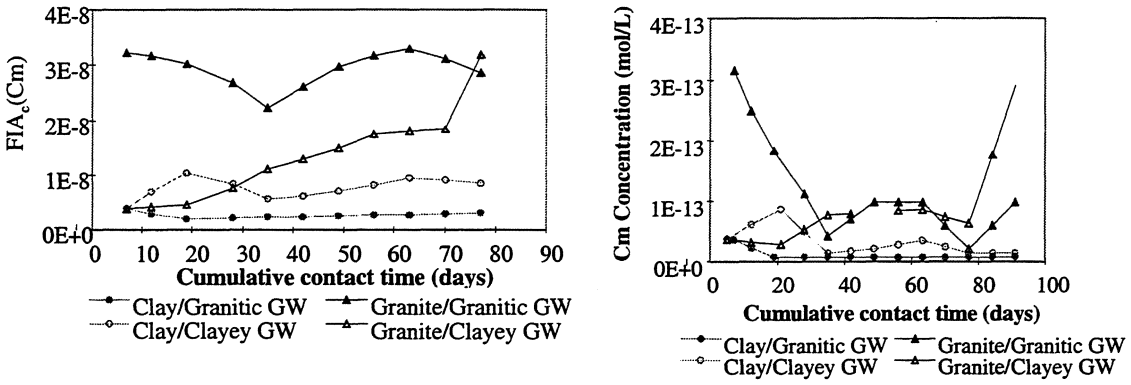

Figure III.3.9. **Gravelines 3+2 spent fuel leaching experiment: ^{244}Cm FIA$_c$ and solution concentrations of Cm versus cumulative leaching time, environmental materials and groundwater composition**

Released Material Mass Balance

The *FIM* is used to designate the radionuclide or element inventory fraction released and sorbed on the environmental materials. However, the *FIM* also includes the inventory fraction present in the interstitial leachate and the fraction sorbed on the iron plates added to the environmental materials.

The released activity balances were determined from the solution analysis results for the "filter rinse", (Appendix 5, TABLE 19) the "material rinse", the "alkaline melt" when applicable, the "pot rinse" and the "sample-holder rinse" (Appendix 5, TABLE 20).

In the filter rinse solutions, the activity values (or concentrations) of many radionuclides (^{60}Co, ^{106}Ru, ^{125}Sb, ^{144}Ce, ^{241}Am, ^{99}Tc, ^{237}Np, ^{238}U, ^{240}Pu) and elements (Mo, Tc, Zr, Nd and U) were almost always below the determination limits. Uranium–238 was determined in 4 of the 5 granite/clayey water solutions (short contact times) and in 3 of the 6 clay/clayey water solutions (extended contact times).

In the material rinse, alkaline melt and sample-holder rinse solutions, the activity values (or concentrations) of many radionuclides (^{60}Co, ^{106}Ru, ^{125}Sb, ^{144}Ce, ^{241}Am, ^{99}Tc, ^{237}Np, ^{240}Pu) and elements (Mo, Tc, Zr, Nd and U) were almost always below the determination limits; with the exception of Mo, U, Zr and Nd, the same was true for the pot rinse solutions. Neodymium could not be determined in the clay/sand mixture rinsing solutions; antimony was determined in a few pot and sample-holder rinsing solutions, and molybdenum was determined in 3 of the 4 sample-holder rinsing solutions. The measured activity in the pot rinse was higher in the clay/granite water than in the other media. The ^{90}Sr, ^{134}Cs and ^{137}Cs activity in particular was ten times higher; the ^{106}Ru and ^{125}Sb activity were above the determination limits; the measured activity values for $^{239+240}$Pu, ^{238}Pu+^{241}Am and ^{244}Cm were 10 times higher.

Significant concentrations (2300–6100 µg·l^{-1}) of ^{88}Sr were found in the material rinse

solutions; the concentrations in the clay/sand mixtures were 2 to 3 times higher. The ^{238}U concentrations ranged from 2500 to 9500 $\mu g \cdot l^{-1}$ in the same environmental material rinse solutions, and were 3 to 4 times higher in the presence of granite. Relatively high concentrations were also observed in the pot rinsing solutions. In view of the many analytical results for molybdenum at the detection limit, the molybdenum release balance was not determined.

In calculating the cumulative fuel inventory fraction released into the aqueous phase (*FIA*) we took the total duration of each experiment (13 weeks) into account. The various fractions (*FIA*, *FIM*, *FIS* and *FIT*) calculated for each experiment is reported in TABLE III.3.4 and is indicated in relative units in FIGURE III.3.10

The released inventory fractions and sorbed on the environmental materials and on the stainless steel walls were generally higher in the clay/granite water medium – particularly for $^{239+240}Pu$. For the transuranic nuclides, the released inventory fractions and sorbed on the environmental materials were larger in clay media ($> 5 \times 10^{-4}$) than in granite media ($< 10^{-4}$).

For all the radionuclides, the total released inventory fractions were higher in clay/granite water. The total released ^{90}Sr inventory fractions were 4.77×10^{-4} and 4.95×10^{-4} in the granite media, but twice as high (8.72×10^{-4} and 1.39×10^{-3}) in the media containing clay. The total released ^{134}Cs and ^{137}Cs inventory fractions were the same (on the order of 1×10^{-3}) in three of the test media, but on the order of 3×10^{-3} in the clay/granite water medium.

The total released transuranic nuclide inventory fractions were generally an order of magnitude lower in the media containing granite, and were lower in granite water (2.5×10^{-5} for $^{239+240}Pu$, 3.81×10^{-5} for $^{238}Pu+^{241}Am$, and 6.36×10^{-5} for ^{244}Cm) than in clayey water (7.84×10^{-5} for $^{239+240}Pu$, 8.21×10^{-5} for $^{238}Pu+^{241}Am$, and 7.55×10^{-5} for ^{244}Cm). In the clay tests, the released fractions were higher in granite water (7.83×10^{-3} for $^{239+240}Pu$, 9.15×10^{-4} for $^{238}Pu+^{241}Am$, and 5.77×10^{-4} for ^{244}Cm) than in clayey water (2.97×10^{-4} for $^{239+240}Pu$, 1.25×10^{-4} for $^{238}Pu+^{241}Am$, and 2.94×10^{-4} for ^{244}Cm).

The total released uranium inventory fractions were comparable in the granite tests (2.54×10^{-3} and 2.82×10^{-3}, compared with 4.53×10^{-3} in the clay/granite water test and 6.8×10^{-4} in the clay/clayey water test. Except in the clay/clayey water medium, the fractions were higher than for ^{90}Sr.

The total released activity distribution among the aqueous phase, the environmental materials and the stainless steel walls is indicated in FIGURE III.3.10 . In all the test media, the released inventory fraction sorbed on the environmental materials always accounted for the bulk of the total released activity (66% to 99% depending on the radionuclides).

In all the test media, over 90% of the ^{90}Sr were sorbed on the environmental materials. The strontium inventory fraction released into the aqueous phase was two to three times greater than the fraction sorbed on the stainless steel walls except in the clay/granite water medium, where the opposite was true.

In the media containing clay, the caesium inventory fraction sorbed on the environmental materials represented 80–86% of the total released inventory fraction, compared with 66–74% for the media containing granite. From 2 to 3% of the caesium was sorbed on the stainless steel and the remainder (16–30%) was found in the aqueous phase – except in the clay/granite water medium where the caesium not sorbed on the environmental materials was almost equally distributed between the fraction sorbed on the stainless steel and the fraction in the aqueous phase.

TABLE III.3.4. **Gravelines 3+2 spent fuel integral leaching experiments: Overall radionuclide release from spent fuel**

Clay/Granite Groundwater					
		FIA	**FIM**	**FIS**	**FIT**
^{90}Sr		3,29E-5	1,28E-3	8,24E-5	1,39E-3
	Absolute error	*1,76E-6*	*1,63E-4*	*1,31E-5*	*1,64E-4*
	Relative error (%)	*11*	*19*	*22*	*18*
^{134}Cs		2,45E-4	2,41E-3	1,74E-4	2,83E-3
	Absolute error	*5,48E-6*	*1,24E-4*	*1,16E-5*	*1,24E-4*
	Relative error (%)	*13*	*16*	*18*	*15*
^{137}Cs		2,47E-4	2,70E-3	1,88E-4	3,14E-3
	Absolute error	*6,27E-6*	*1,60E-4*	*1,43E-5*	*1,61E-4*
	Relative error (%)	*7*	*10*	*12*	*9*
$^{239+240}Pu$		5,69E-8	7,29E-3	9,67E-5	7,38E-3
	Absolute error	*9,01E-9*	*3,70E-3*	*4,93E-5*	*3,70E-3*
	Relative error (%)	*22*	*57*	*57*	*56*
$^{238}Pu+^{241}Am$		1,68E-8	8,60E-4	5,52E-5	9,15E-4
	Absolute error	*2,21E-9*	*2,31E-4*	*1,71E-5*	*2,32E-4*
	Relative error (%)	*19*	*33*	*37*	*31*
^{244}Cm		1,83E-8	5,28E-4	4,90E-5	5,77E-4
	Absolute error	*1,24E-9*	*1,51E-4*	*1,52E-5*	*1,52E-4*
	Relative error (%)	*28*	*50*	*52*	*47*
^{238}U		1,05E-6	4,39E-3	1,41E-4	4,53E-3
	Absolute error	*5,60E-8*	*2,21E-4*	*8,48E-6*	*2,21E-4*
	Relative error (%)	*6*	*6*	*7*	*6*

Granite/Granite Groundwater					
		FIA	**FIM**	**FIS**	**FIT**
^{90}Sr		3,36E-5	4,31E-4	1,27E-5	4,77E-4
	Absolute error	*2,16E-6*	*6,89E-5*	*1,64E-6*	*6,90E-5*
	Relative error (%)	*12*	*22*	*19*	*20*
^{134}Cs		3,24E-4	7,11E-4	3,11E-5	1,07E-3
	Absolute error	*6,81E-6*	*4,98E-5*	*1,58E-6*	*5,03E-5*
	Relative error (%)	*13*	*18*	*16*	*16*
^{137}Cs		3,32E-4	7,63E-4	3,29E-5	1,13E-3
	Absolute error	*7,97E-6*	*6,11E-5*	*1,91E-6*	*6,16E-5*
	Relative error (%)	*6*	*12*	*10*	*9*
$^{239+240}Pu$		7,93E-8	2,14E-5	3,49E-6	2,50E-5
	Absolute error	*1,98E-8*	*1,09E-5*	*1,76E-6*	*1,10E-5*
	Relative error (%)	*31*	*57*	*56*	*50*
$^{238}Pu+^{241}Am$		2,68E-8	3,12E-5	6,83E-6	3,81E-5
	Absolute error	*3,36E-9*	*9,69E-6*	*1,97E-6*	*9,88E-6*
	Relative error (%)	*19*	*37*	*35*	*32*
^{244}Cm		3,86E-8	5,28E-5	1,08E-5	6,36E-5
	Absolute error	*4,44E-9*	*1,64E-5*	*2,92E-6*	*1,66E-5*
	Relative error (%)	*32*	*52*	*48*	*47*
^{238}U		1,50E-6	2,39E-3	1,49E-4	2,54E-3
	Absolute error	*9,17E-8*	*1,43E-4*	*8,57E-6*	*1,43E-4*
	Relative error (%)	*7*	*7*	*7*	*7*

TABLE III.3.4 (continuation). **Gravelines 3+2 spent fuel integral leaching experiments: Overall radionuclide release from spent fuel**

Clay/Clayey Groundwater					
		FIA	**FIM**	**FIS**	**FIT**
^{90}Sr		2,95E-5	8,35E-4	6,81E-6	8,72E-4
	Absolute error	*1,86E-6*	*1,17E-4*	*7,99E-7*	*1,17E-4*
	Relative error (%)	*12*	*20*	*18*	*19*
^{134}Cs		1,60E-4	7,33E-4	2,15E-5	9,15E-4
	Absolute error	*3,40E-6*	*4,25E-5*	*1,11E-6*	*4,27E-5*
	Relative error (%)	*13*	*17*	*16*	*16*
^{137}Cs		1,64E-4	8,15E-4	2,24E-5	1,00E-3
	Absolute error	*3,96E-6*	*5,27E-5*	*1,32E-6*	*5,29E-5*
	Relative error (%)	*6*	*10*	*10*	*9*
$^{239+240}Pu$		5,00E-8	2,95E-4	1,79E-6	2,97E-4
	Absolute error	*1,02E-8*	*1,36E-4*	*8,81E-7*	*1,36E-4*
	Relative error (%)	*26*	*52*	*55*	*52*
$^{238}Pu+^{241}Am$		1,43E-8	1,23E-4	2,00E-6	1,25E-4
	Absolute error	1,56E-9	2,76E-5	6,05E-7	2,76E-5
	Relative error (%)	17	28	36	28
^{244}Cm		9,34E-9	2,92E-4	1,93E-6	2,94E-4
	Absolute error	*9,17E-10*	*8,67E-5*	*5,77E-7*	*8,67E-5*
	Relative error (%)	*31*	*51*	*51*	*50*
^{238}U		7,22E-6	6,16E-4	5,69E-5	6,80E-4
	Absolute error	*6,00E-7*	*4,04E-5*	*2,95E-6*	*4,05E-5*
	Relative error (%)	*9*	*8*	*6*	*7*

Granite/Clayey Groundwater					
		FIA	**FIM**	**FIS**	**FIT**
^{90}Sr		1,64E-5	4,69E-4	9,37E-6	4,95E-4
	Absolute error	*9,21E-7*	*7,51E-5*	*1,20E-6*	*7,51E-5*
	Relative error (%)	*12*	*22*	*19*	*21*
^{134}Cs		2,37E-4	7,40E-4	3,09E-5	1,01E-3
	Absolute error	*5,33E-6*	*5,18E-5*	*1,66E-6*	*5,21E-5*
	Relative error (%)	*13*	*18*	*16*	*16*
^{137}Cs		2,45E-4	7,92E-4	3,28E-5	1,07E-3
	Absolute error	*6,41E-6*	*6,33E-5*	*2,02E-6*	*6,37E-5*
	Relative error (%)	*7*	*12*	*10*	*10*
$^{239+240}Pu$		1,09E-7	7,72E-5	1,10E-6	7,84E-5
	Absolute error	*3,62E-8*	*3,94E-5*	*4,98E-7*	*3,94E-5*
	Relative error (%)	*39*	*57*	*51*	*56*
$^{238}Pu+^{241}Am$		5,01E-8	7,99E-5	2,17E-6	8,21E-5
	Absolute error	*9,04E-9*	*2,48E-5*	*6,47E-7*	*2,48E-5*
	Relative error (%)	*24*	*37*	*36*	*36*
^{244}Cm		4,81E-8	7,09E-5	4,60E-6	7,55E-5
	Absolute error	*9,44E-9*	*2,20E-5*	*1,42E-6*	*2,20E-5*
	Relative error (%)	*41*	*52*	*52*	*50*
^{238}U		5,09E-6	2,56E-3	2,55E-4	2,82E-3
	Absolute error	*4,17E-7*	*1,54E-4*	*1,52E-5*	*1,55E-4*
	Relative error (%)	*9*	*7*	*7*	*6*

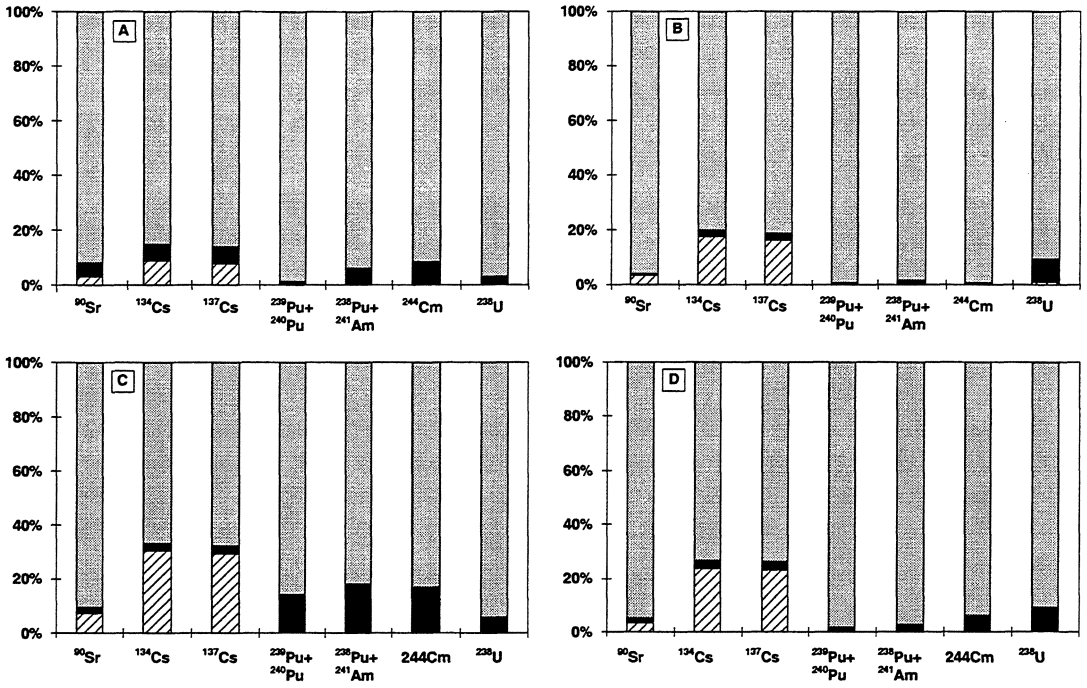

FIGURE III.3.10. **Interaction between spent fuel and environmental materials. A: C/GW medium. B: C/CW medium. C: G/GW medium. D: G/CW medium. Key: *Hatched bars*: Aqueous phase inventory fraction; *Dark bars*: Sorbed inventory fraction; *Light bars*: Inventory fraction fixed on environmental materials**

.

In all the test media, the transuranic nuclide inventory fractions released into the aqueous phase were negligible (less than 0.3% of the released plutonium) compared with the other two fractions. Over 91% of the released transuranic nuclides were sorbed on the environmental materials except in the granite/granite water medium, where 14–18% were sorbed on the stainless steel walls.

Uranium was distributed in a similar manner: no more than 1% of the uranium was found in the aqueous phase. Unlike the transuranic nuclides, however, the uranium distribution was no different in the granite/granite water medium. The *FIM* accounted for over 90% of the uranium released in the clayey water media, and over 94% in the granite water media.

Interpretation and Discussion

pH

As the pH decrease in all four media was not observed in the SIMFUEL leach tests, for which all the other parameters were identical, we attribute this phenomenon to the spent fuel itself and propose several hypotheses to account for the drop in the pH.

The phenomenon may be attributed to different preleach conditions or to radiolysis of the water by the spent fuel, which did not affect the SIMFUEL. Many surface reactions occur on the fuel when radiolysis products are present in solution, including oxidizing dissolution, recombination of radicals, decomposition of H_2O_2, reduction of the oxidised UO_2 layers, oxidation or reduction of ionic species and reactions liable to modify the solution pH. The subsequent rise of the pH could then be due to a buffering effect of the natural medium.

Alteration of Environmental Materials

The leaching solutions were not at equilibrium with the environmental materials. As a result, the materials were leached and cation exchange, precipitation and dissolution phenomena

modified the solution composition. Sodium-rich(Na^+) water enhanced the release of calcium (Ca^{2+}) from the clay. Ion exchanges also occurred with the radionuclides released from the fuel and found as cations in solution. For example, as discussed below, the clay fixed strontium (Sr^{2+}) released from the fuel, no doubt through cation exchange with the calcium (Ca^{2+}).

Alteration of the environmental materials not only modified the leachate composition, but also affected the release of species that could interfere with those analyzed to characterize the spent fuel leaching results. Examples include ^{88}Sr, ^{238}U and Mo.

The ICP-MS analysis spectra revealed that most of the strontium in solution was not radiogenic. Fuel leaching is a chemical process independent of the isotopic abundance. Thus, if the strontium in solution arose primarily from spent fuel leaching, its isotopic distribution should have been the same as in the spent fuel, i.e. approximately 55.57% ^{90}Sr, 44.37% ^{88}Sr and 0.06% ^{86}Sr, according to the spent fuel mass inventory. In fact, however, the ICP-MS spectra indicated the following distribution: 0.56% ^{84}Sr, 9.86% ^{86}Sr, 7% ^{87}Sr and 82.5% ^{88}Sr, which is representative of the natural strontium abundance [95FOR].

The ^{88}Sr in solution thus originated in the spent fuel and the environmental materials, in which it was found as an impurity, while the ^{90}Sr came only from the spent fuel. Therefore, based on the ^{88}Sr determination by ICP-MS and the β counts of ^{90}Sr, and on the isotopic distribution of strontium in the spent fuel compared with its natural abundance, we were able to calculate the relative proportions of strontium released from the environmental materials and from the spent fuel by assuming that the isotopic distribution in the environmental materials corresponded to its natural abundance. The percentage of the total strontium concentration in solution arising from the *spent fuel* was thus:

clay/granite water:	0.05%
granite/granite water:	0.137%
clay/clayey water:	0.079%
granite/clayey water:	0.029%.

The radionuclides ^{134}Cs, ^{137}Cs, ^{238}Pu, ^{239}Pu and ^{240}Pu, ^{241}Am and ^{244}Cm were not present in the environmental materials; their presence in solution was therefore exclusively due to leaching from the spent fuel. Conversely, the natural abundance of ^{238}U is 99.27%; the total released fractions of the ^{238}U inventory were thus generally higher than for ^{90}Sr except in the clay/clayey water medium, where the value for ^{238}U (6.8×10^{-4}) was lower than for ^{90}Sr (8.7×10^{-4}). In addition to the analytical uncertainties, dissolved uranium may have reprecipitated on the fuel surface during the leaching experiment, and may not have been entirely recovered during the sample-holder rinsing operation.

Molybdenum Release

The cumulative molybdenum inventory fractions released into the aqueous phase were very high (about 10^{-3}) – an order of magnitude higher than for cesium (~ 10^{-4}) and two orders of magnitude higher than for strontium (~ 10^{-5}).

Significant molybdenum release has already been reported in the literature [95GLA/TOS, 91FOR]. Granite was also present in the leaching experiments conducted by Glatz *et al* [95GLA/TOS]. Forsyth [91FOR] suggests that the molybdenum present in metallic form in Mo-Ru-Rh-Pd-Tc inclusions is preferentially oxidised, and selective leaching of molybdenum thus occurs. Moreover, molybdenum was analyzed by ICP-AES, so its origin in the spent fuel or the environmental materials could not be determined and it is not currently possible to discriminate this fraction from the spent fuel fraction.

Explanations for initial fast release: Dissolution of Oxidised Layer?

The unexpected decrease of release fractions during the first three or four weeks may be attributable to a rapid dissolution of an oxidised surface layer on the spent fuel particles. The spent fuel powder was prepared in air before use (Chapter "SOLID PHASE CHARACTERIZATION"), certainly forming a U_3O_7-U_3O_8 layer on the surface. Rapid dissolution of this layer on contact with the leaching solution resulted in an initially high rate of radionuclide and element release. As the subsequent rate of release was slower, the cumulative inventory fractions released into the aqueous solution diminished.

However, this phenomenon does not explain why a similar drop was not observed in the granite/clayey water medium (except for ^{238}U and $^{239+240}Pu$). It is unlikely that the fuel powder sample used for this leaching experiment was less oxidised than the other three. An alternative explanation may be the establishment of redox conditions at different rates in the leaching pots. This phase may have been shorter for the granite/clayey water test than for the other three; in this case, the oxidised layer would have been leached gradually, rather than immediately.

Radionuclide Sorption on Environmental Materials

Radionuclide retention on solid phases such as the environmental materials is generally characterized by a distribution coefficient *CKD* describing the equilibrium partition of an element between a solid and a liquid phase: i.e. the ratio between the quantity of the element sorbed per unit mass of solid sorbent ($mol \cdot g^{-1}$) and the equilibrium concentration of the same element in the aqueous phase ($mol \cdot ml^{-1}$). The distribution coefficient includes the effects of phenomena such electrostatic sorption/desorption and/or chemical exchanges at specific sites on the solid phase, (co)precipitation of compounds on the solid phase or in the aqueous phase, radionuclide inclusions in minerals and radionuclide sorption on colloids or microparticles produced by the solid phases under high solution pH conditions [92LEG]. For a given element and solid phase, *CKD* depends on the pH, the temperature, the redox potential and the species in solution.

In these experiments, the distribution coefficient of each radionuclide may be expressed as a function of the inventory fractions released into the aqueous phase and sorbed on the environmental materials according to .

$$Kd = \frac{FIM}{M_{materials}} \cdot \frac{\left(V + V_{interstitial}\right)}{FIA} \qquad \text{(III.3-7)}$$

where $M_{materials}$ designates the mass of sorbent environmental materials (i.e. 24 g for the clay tests and 260 g for the granite tests); the total volume of the aqueous phase in the leaching pot (130 ml) is taken into account. *FIM* represents not only the released inventory fraction sorbed on the environmental materials, but also the fraction sorbed on the iron plates and the fraction found in the interstitial leachate.

The calculated coefficients are given in TABLE III.3.5. Except for uranium, the radionuclide distribution coefficients were higher in the clay than in the granite experiments. The nature of the groundwater had little effect: the C_{KD} values were imposed by the material. Our observations seem to contradict those reported by Tait *et al.* [89TAI/STR], who observed strontium on granite to a greater extent than cesium. This may be due to methodological differences: the environmental materials were not the same and the experimental conditions were significantly different.

TABLE III.3.5. **Gravelines 3+2 spent fuel integral leaching experiments: Radionuclide distribution coefficients C_{KD} (ml·g^{-1}) calculated from integral experiments**

	Clay/Granite Groundwater	Granite/Granite Groundwater	Clay/Clayey Groundwater	Granite/Clayey Groundwater
^{90}Sr	210	6	153	14
^{134}Cs	53	1	25	2
^{137}Cs	59	1	27	2
$^{239+240}Pu$	693 407	135	31 958	355
$^{238}Pu+^{241}Am$	276 839	584	46 395	797
^{244}Cm	156 256	684	169 552	737
^{238}U	22 640	795	462	252

TABLE III.3.6. **Gravelines 3+2 spent fuel integral leaching experiments: Distribution coefficients published in the literature**

	[92LEG/BLA] [a]	Crystalline rock/Groundwater System [94STE/PÖT]			Bentonite/Groundwater System [94STE/PÖT]		
		NAGRA	SKB	TVO	NAGRA	SKB	TVO
Sr	45±1	–	–	–	1	100	–
Cs	3000 ± 900	50	50	50	1	200	200
Pu	474 ± 8	500	1000	500	500	1000	300
Am	15000 ± 2000	500	1000	40	500	1000	300
Cm	–	500	1000	–	500	–	–
U	32±1	100	3000	100	500	100	50

[a] Natural mineral phases taken to 12-12,2 m depth with the following mineralogical composition : different phases than quartz 8%, Illite, Glauconite 5%, Smectite 5%; water reconstituted and in equilibrium with these mineral phases, pH 8,0.

For a given radionuclide, the different orders of magnitude observed between the two media containing the same environmental material were probably due to the analytical uncertainty, and to differences in water composition as well.

The values obtained for uranium are not significant for two essential reasons: ^{238}U released into the aqueous phase by the environmental materials during the leaching experiments was included in the *FIA* fraction, additional ^{238}U released during acid rinsing of the environmental materials was included in the *FIM* fraction.

TABLE III.3.6 compares the distribution coefficients published in the literature [92LEG, 94STE/PÖT]. Some of these have been used for repository site performance assessment studies: they are conservative figures, i.e. not exceeding the experimentally determined values. The distribution coefficients obtained in this experiment are thus consistent with published results. Although for the actinides in clay media, we found coefficients higher than those indicated in TABLE III.3.6 , values on the order of 10^5 or 10^6 have been reported [98LY].

Radionuclide sorption on the environmental materials provides another explanation for the drop in the cumulative inventory fractions released into the aqueous phase for ^{90}Sr, ^{134}Cs (and ^{137}Cs), ^{238}U, $^{239+240}Pu$ and $^{238}Pu+^{241}Am$ during the first few weeks of leaching. In spent fuel-leaching experiments with clay and granite, Tait *et al.* [89TAI/STR] observed that the clay very effectively retained cesium and strontium during the first few days; the sorbed fraction then diminished as the concentration of these elements increased in solution.

No drop was observed in the cumulative molybdenum inventory fraction released into the aqueous phase. This result is consistent with the sorption behaviour of molybdenum, which

is found in solution in anion form, perhaps as molybdate MoO_4^{2-} and is thus not retained in large quantities by the negatively charged surfaces of the environmental materials.

In addition, sorption on the environmental materials may also account for the decrease in the cumulative ^{238}U and $^{239+240}Pu$ inventory fractions released into the aqueous phase in the granite/clay water medium, contrary to the behaviour observed for the other radionuclides (^{90}Sr, ^{134}Cs, ^{137}Cs). The distribution coefficients estimated for this medium indicate that ^{238}U ($CKD = 252$) and $^{239+240}Pu$ ($CKD = 355$) were retained in greater amounts by the granite than ^{90}Sr ($CKD = 14$) or ^{134}Cs and ^{137}Cs ($CKD = 2$).

We are unable to account for the behaviour of ^{244}Cm although its distribution coefficient ($CKD = 737$) were on the same order of magnitude as for the other transuranic nuclides, the cumulative inventory fraction released into the aqueous phase did not diminish during the initial weeks of leaching. This may be due to the different valences of these radionuclides: americium and curium are always trivalent, while uranium and plutonium were probably tetravalent during leaching experiments under reducing conditions, and hexavalent after the leaching pot was opened. Sr^{2+} and Cs^{+} ions were fixed on the clay minerals by cation exchange with Ca^{2+} and possibly K^{+} ions.

Decrease of solution concentration by dilution phenomena?

The weekly leachate samples, replaced by an equivalent volume of fresh leaching solution, created a pseudo flow resulting in dilution of the test medium. The material entering solution by leaching of the fuel (and/or the environmental materials in the case of ^{238}U and Mo) could thus be eliminated from the aqueous phase not only by sorption or (co)precipitation – inherent in the system itself – but also as a result of the sampling procedure.

In calculating the inventory fractions released into the aqueous phase, this phenomenon was taken into account in the $\sum_{i=1}^{i=n-1} a^i_{sample} v^i_{sample}$ term (Eq III.3-3), which represents the sum of the activity (or mass) of the radionuclides or elements removed from the system in the samples. The effects of this dilution on the evolution of the concentrations is difficult to be analyzed :

The evolution of the actinide concentrations in the leachate shows that they remained virtually constant after the third or fourth week of leaching under the test conditions. This suggests that the concentrations in solution were unaffected by dilution. The actinide concentrations are limited by (co)precipitation of phases with low solubility limits and/or by sorption on environmental materials. These processes result in a readjustment of solution concentrations after dilution. The investigation of the effect of dilution on the solution concentration of Sr, Cs and Mo yield the following results:

The decrease in the solution concentrations of Cs in presence of granite was slower than expected from dilution, indeed, caesium was only slightly retained by the granite (CKD = 1 to 2). The same was true for Mo in the clayey water media and for strontium in the granite/clayey water medium

The decrease in the solution concentrations of Cs was faster in presence of clay than expected by pure dilution, at least during the first six or seven weeks of leaching. This is consistent with the $Kd_{Cs} = 30–60$. The same was true for Sr in both clay experiments and in the granite/granite water experiment indicating that sorption phenomena predominated during the first few weeks of leaching Kd_{Sr}(Clay)= 150–200.

Actinide Concentrations

The actinide concentrations in the aqueous phase of these integral experiments were limited by (co)precipitation of oxides, hydroxides and/or carbonated compounds, and/or by sorption

on the environmental materials. The mean steady-state uranium, plutonium and curium concentrations are given in TABLE III.3.7.

TABLE III.3.7. **Gravelines 3+2 spent fuel integral leaching experiments: Aqueous phase actinide concentrations ($mol \cdot l^{-1}$) in the four test media**

	Clay/Granite Groundwater	Granite/Granite Groundwater	Clay/Clayey Groundwater	Granite/Clayey Groundwater
U	$1,2\times10^{-8}$	$7,8\times10^{-9}$	$1,8\times10^{-8}$	$1,7\times10^{-8}$
Pu	$1,5\times10^{-11}$	$< 7,6\times10^{-12}$	$8,9\times10^{-12}$	$7,6\times10^{-12}$
Cm	$< 7,3\times10^{-15}$	$6,4\times10^{-14}$	$9,0\times10^{-15}$	$7,4\times10^{-14}$

For comparison, Grambow *et al.* [96GRA/LOI] reported the following actinide concentrations in solution after leaching spent PWR fuel (burnup: 50.4 $GWd \cdot t_U^{-1}$) in brine under argon :

uranium: 10^{-8} (determination limit) to 10^{-4} $mol.l^{-1}$

plutonium: 10^{-11} (determination limit) to 10^{-7} $mol.l^{-1}$

curium: 10^{-13} (determination limit) to 10^{-9} $mol.l^{-1}$

The lower concentrations limits where found in presence of metallic iron (see also WP III.1, results of sample K4). The concentrations obtained in our integral experiments were on the same order of magnitude as these lower limit for uranium, and little below the lower limit for Pu and Cm.

The expected solubility of radionuclide compounds in a geological repository at pH 7.5 with a redox potential of about -100 mV_{SHE} and a CO_2 partial pressure between 10^{-2} and 10^{-1} atm were reported by Guillaumont [94GUI] as follows:

uranium: 10^{-11} to 10^{-5} $mol.l^{-1}$

plutonium: 10^{-8} to 10^{-4} $mol.l^{-1}$

americium: 10^{-8} to 10^{-3} $mol.l^{-1}$

The aqueous species considered were hydroxide and carbonate complexes. Given the similar behaviour of americium and curium as trivalent actinides, we compared our curium concentrations with the solubility data reported for americium. While our uranium concentrations were within the indicated range, the plutonium and curium concentrations were much lower.

This point is of particular importance. Disregarding possible radiolysis phenomena, spent fuel alteration under the reducing conditions imposed by our experiments can be modeled by chemical phenomena based on the solubility of uranium compounds. With additional uranium released by the environmental materials, the solubility limit for the uranium compound(s) could be reached more quickly than through alteration of the spent fuel alone, possibly slowing down the alteration rate. Moreover, radionuclides – and notably the transuranic nuclides – are retained by the environmental materials, leading to very low concentrations in the aqueous phase.

Congruence of Radionuclide and Elements

Assuming strontium is a suitable fuel matrix alteration tracer, the release of a radionuclide or element (X) is congruent with the spent fuel matrix if the *total* cumulative released inventory fraction is equal to that of strontium, i.e. if the ratio ($FIT_X / FIT_{^{90}Sr}$) is equal to 1.

In these integral experiments the calculated released inventory fractions sorbed on the

environmental materials and on the stainless steel walls are less than or equal to the actual values: because the rinsing operations for the leaching pot, sample holder and environmental materials were not 100% effective, notably for the actinides.

If the transuranic radionuclides were released congruently from the spent fuel matrix, the $FIT_{Transuranic}/FIT_{^{90}Sr}$ ratios should be less than or equal to 1 for $^{239+240}Pu$, $^{238}Pu+^{241}Am$ and ^{244}Cm. This should also logically be the case for ^{238}U; however, as noted above, the relative ^{238}U fractions were altered by the additional release of this isotope from the environmental materials. The $FIT_{^{238}U}/FIT_{^{90}Sr}$ ratios can thus be expected to exceed 1.

Caesium is released from spent fuel by several mechanisms: release of labile activity, of the activity segregated at grain boundaries, and congruent release with the fuel matrix. The activity segregated at grain boundaries accounts for the fact that the cumulative inventory fractions released into the aqueous phase are about an order of magnitude higher for cesium than for strontium. The preleaching eliminated the labile activity and part of the grain boundary activity. Our spent fuel particles in the 50–250 µm size fraction included many unexposed grain boundaries: the segregated activity at the grain boundaries is released gradually over several years. Hence the expected values exceed 1 for the $FIT_{^{134}Cs}/FIT_{^{90}Sr}$ and $FIT_{^{137}Cs}/FIT_{^{90}Sr}$ ratios.

The ratios calculated from the total released inventory fractions (TABLE III.3.4) are shown in TABLE III.3.8. Despite the analytical errors and the many operations performed, the calculated ratios were within the expected ranges in most cases. Three discrepancies were noted:

TABLE III.3.8. **Gravelines 3+2 spent fuel integral leaching experiments: Values of FIT_X / $FIT_{^{90}Sr}$ ratios**

X	Clay/Granite Groundwater	Granite/Granite Groundwater	Clay/Clayey Groundwater	Granite/Clayey Groundwater
^{90}Sr	1,00	1,00	1,00	1,00
^{134}Cs	2,03	2,23	1,05	2,03
^{137}Cs	2,25	2,37	1,15	2,16
$^{239+240}Pu$	5,31	0,05	0,34	0,16
$^{238}Pu+^{241}Am$	0,66	0,08	0,14	0,17
^{244}Cm	0,41	0,13	0,34	0,15
^{238}U	3,26	5,32	0,78	5,70

The $FIT_{Transuranic}/FIT_{^{90}Sr}$ ratios were well below 1, except for $^{239+240}Pu$ in the clay/granite water medium (5.31). As expected, the device and environmental materials rinsing operations did not desorb all the transuranic nuclides and the obtained values were underestimated. Moreover, the analytical uncertainties were appreciable (30–50% on the activity measurements). The aberrant value of 5.31 is certainly an artifact, and corresponds to unusually high released $^{239+240}Pu$ inventory fractions sorbed on the environmental materials and on the stainless steel walls.

As expected from U release from environmental materials, the $FIT_{^{238}U}/FIT_{^{90}Sr}$ ratios were higher than 1, except in the clay/clayey water medium (0.78). In addition to the analytical uncertainty, a large quantity of uranium may have precipitated on the fuel surface and was not dissolved during the sample-holder rinsing step.

The third discrepancy concerned the inconsistently low (1.05 and 1.15) total caesium inventory fraction released into the clay/clayey water medium. If the labile activity release is assumed equal in all the media and if caesium is released congruently from the fuel matrix,

then the ratio of the total released activity fractions for caesium and ^{90}Sr should be similar in all the test media. It is unlikely that a smaller amount of labile activity was released from this fuel powder specimen, since the preleaching step was performed on the entire powder sample, which was then divided into leaching specimens of equal mass and placed in the sample-holders.

Comparative Mean Leaching Rates

In order to estimate the actual spent fuel leach rate, we considered the total ^{90}Sr inventory fraction released in each experiments and obtained the following *mean leach rates*:

clay/granite water: 0.57 ± 0.07 mg·m^{-2}d^{-1}

granite/granite water: 0.19 ± 0.03 mg·m^{-2}d^{-1}

clay/clayey water: 0.35 ± 0.05 mg·m^{-2}d^{-1}

granite/clayey water: 0.20 ± 0.03 mg·m^{-2}d^{-1}.

These mean rates overestimate the 91-day spent fuel matrix leach rates since they include the rapid initial release due to dissolution of the oxidised layer on the fuel surface. This factor cannot be disregarded in experiments of short duration such as these. These rates are all on the same order of magnitude, and were lower in the granite media. They were significantly higher than the corresponding *apparent* rates (by a factor of 100–150 in the clay media, and 50–60 in the granite media); these factors are consistent with the higher strontium distribution coefficients for clay than for granite.

TABLE III.3.9 indicates spent fuel leach rates published in the literature, together with the experimental conditions under which these values were obtained. The table also includes the rates measured during these integral leaching experiments, although they are not directly comparable: the rates calculated from the cumulative inventory fractions released into the aqueous phase are *apparent* leaching rates, covering not only leaching of the spent fuel but also sorption and (co)precipitation phenomena related to the presence of the environmental materials.

The mean rates can be compared with the published values. The rates obtained in this experiment were on the same order of magnitude as those reported by Grambow *et al.* [96GRA/LOI] for fuel pellets (50.4 GWd·t$_U^{-1}$) in argon atmosphere in the presence of iron, and by Gray *et al.* [92GRA/STR] for 15–25 µm powder samples (33 GWd·t$_U^{-1}$) at low oxygen partial pressures (0.003 atm, i.e. 3000 ppm), but higher than the results obtained by Grambow *et al.* [96GRA/LOI] for 3 µm fuel grains (50.4 GWd·t$_U^{-1}$) in argon atmosphere.

TABLE III.3.9. **Spent fuel leach rates published**

Burnup (GWj/t_U)	Particle Size	Leaching Mode	Time (days)	T (°C)	Leachant	pH	P_{O2} (atm)	Carbonates (mol.L^{-1})	Other	Leaching rate ($mg.m^{-2}.d^{-1}$)		Reference
31,5	fragment	flow (Soxhlet)	100	100	Bidistilled water		Air		with granite	0,04		[95GLA/TOS]
50,4	pellet	static	~750	25	NaCl 5M	9,2	Ar			1		[96GRA/LOI]
50,4	pellet	static	~750	25	NaCl 5M	7,8	Ar			1		
50,4	pellet	static	~750	25	Deionized water	7,3	Ar			3 à 4		[94LOI/GRA]
50,4	pellet	static	~750	25	Deionized water	7,3	Ar			3 à 4		
50,4	grains ~3µm	static	~750	25	NaCl 5M	6,3	Ar			0,05		
50,4	grains ~3µm	static	~750	25	NaCl 5M	6,6	Ar			0,05		
50,4	pellet	static	~750	25	NaCl 5M	9,6	Ar		Fe powder	0,2		
50,4	pellet	static	~750	25	NaCl 5M	9,6	Ar		Fe powder	0,1		
50,4	fragment	static	~750	25	NaCl 5M	7,2	Ar			2		
33	15 to 25 µm	flow		50	2×10^{-3} $Na_2CO_3/NaHCO_3$	9,0	0,200	2×10^{-3}		6,3		[92GRA/LEI]
33	15 to 25 µm	flow		50	2×10^{-3} $Na_2CO_3/NaHCO_3$	9,0	0,200	2×10^{-3}		7,1		
33	15 to 25 µm	flow		50	2×10^{-3} $Na_2CO_3/NaHCO_3$	9,0	0,200	2×10^{-3}		5,1		[94STE/GRA]
33	15 to 25 µm	flow		22	2×10^{-3} $Na_2CO_3/NaHCO_3$	8,0	0,200	2×10^{-2}		3,5		
33	15 to 25 µm	flow		74	2×10^{-3} $Na_2CO_3/NaHCO_3$	10,0	0,200	2×10^{-2}		14,2		
33	15 to 25 µm	flow		74	2×10^{-3} $Na_2CO_3/NaHCO_3$	8,0	0,200	2×10^{-4}		8,6		
33	15 to 25 µm	flow		21	2×10^{-3} $Na_2CO_3/NaHCO_3$	10,0	0,200	2×10^{-4}		0,6		
33	15 to 25 µm	flow		22	2×10^{-3} $Na_2CO_3/NaHCO_3$	9,0	0,200	2×10^{-2}		2,8		
33	15 to 25 µm	flow		22	2×10^{-3} $Na_2CO_3/NaHCO_3$	10,0	0,200	2×10^{-3}		2,0		
33	15 to 25 µm	flow		27	2×10^{-3} $Na_2CO_3/NaHCO_3$	8,0	0,020	2×10^{-4}		1,8		
33	15 to 25 µm	flow		78	2×10^{-3} $Na_2CO_3/NaHCO_3$	10,0	0,020	2×10^{-4}		1,5		
33	15 to 25 µm	flow		25	2×10^{-3} $Na_2CO_3/NaHCO_3$	10,0	0,020	2×10^{-2}		2,1		
33	15 to 25 µm	flow		77	2×10^{-3} $Na_2CO_3/NaHCO_3$	8,0	0,020	2×10^{-2}		2,9		
33	15 to 25 µm	flow		23	2×10^{-3} $Na_2CO_3/NaHCO_3$	8,0	0,003	2×10^{-2}		2,8		
33	15 to 25 µm	flow		74	2×10^{-3} $Na_2CO_3/NaHCO_3$	10,0	0,003	2×10^{-2}		0,7		
33	15 to 25 µm	flow		78	2×10^{-3} $Na_2CO_3/NaHCO_3$	8,0	0,003	2×10^{-4}		2,0		
33	15 to 25 µm	flow		19	2×10^{-3} $Na_2CO_3/NaHCO_3$	10,0	0,003	2×10^{-4}		0,5		
33	15 to 25 µm	flow		50	2×10^{-3} $Na_2CO_3/NaHCO_3$	10,0	0,003	2×10^{-2}		1,0		
33	15 to 25 µm	flow		21	2×10^{-3} $Na_2CO_3/NaHCO_3$	9,0	0,003	2×10^{-3}		1,9		
33	15 to 25 µm	flow		75	2×10^{-3} $Na_2CO_3/NaHCO_3$	10,0	0,020	2×10^{-2}		4,8		
33					mean					3,1		
30	fragments	drip test	581	90	EJ13 well	8,4	Air	$3,3\times10^{-4}$		0,7		[95FIN/BUC]
43	fragments	drip test	581	90	EJ13 well	8,4	Air	$3,3\times10^{-4}$		1,5		
										apparent	*overall**	Our work
60	50 to 250 µm	quasi static	77	90	Granite groundwater	7,8	$Ar/H_2/CO_2$	$5,2\times10^{-4}$	Clay/sand + Fe	0,004	0,57	
60	50 to 250 µm	quasi static	77	90	Granite groundwater	7,8	$Ar/H_2/CO_2$	$5,2\times10^{-4}$	Granite + Fe	0,003	0,19	*mean*
60	50 to 250 µm	quasi static	77	90	Clayey groundwater	8,8	$Ar/H_2/CO_2$	$1,4\times10^{-2}$	Clay/sand + Fe	0,003	0,35	*rates*
60	50 to 250 µm	quasi static	77	90	Clayey groundwater	8,8	$Ar/H_2/CO_2$	$1,4\times10^{-2}$	Granite + Fe	0,004	0,20	

**Rates calculated from ^{90}Sr fraction of inventory released in the aqueous phase for each experiment*

Results and discussion of SIMFUEL integral leaching tests

Evolution of chemical environment

Redox Potential

The measured potentials were below –310 mV_{SHE} in the clay media, and below –160 mV_{SHE} in the granite media. Both of these values are upper limits, as the solution may have been slightly oxidised on contact with air when the pot was opened before the measurement.

In the clay experiments, the redox potential measured for the synthetic groundwater was consistent with actual groundwater potentials, while in the granite experiments the measured values were slightly higher than the actual groundwater potentials (the lower limits of the redox potential are –250 mV_{SHE} for clayey groundwater and –300 mV_{SHE} for granite groundwater). Nevertheless, the measured potentials may be considered satisfactory and representative of the reducing conditions of a geological repository site.

pH

The results are detailed in TABLE III.3.11. The pH of the synthetic groundwater samples was stable within 0.1 pH unit. The measured pH of the granite groundwater was 7.9 for the clay experiment and 7.8 for the granite experiment (slightly higher than the initial pH of 7.6 at the moment the sample was prepared). The corresponding values for the clayey synthetic groundwater were 8.2 with clay and 8.4 with granite, compared with the initial value of 7.8). Contrary to the spent fuel leaching experiments, no drop in the pH was observed.

TABLE III.3.11. **SIMFUEL integral leaching experiments : pH measurements in weekly samples**

Sampling n°	1	3	5	7	9	11	Final Supernatant
Clay/Granite Groundwater	7,8	7,8	7,9	8,0	8,0	8,0	7,8
Granite/Granite Groundwater	7,8	7,8	7,8	7,8	7,7	7,8	8,3
Clay/Clay Groundwater	8,1	8,1	8,1	8,2	8,2	8,2	8,0
Granite/Clay Groundwater	8,4	8,3	8,4	8,4	8,4	8,6	8,4

Major Cations in Final Supernatant

The major cations present in the groundwaters in the final supernatants are indicated in TABLE III.3.12 with their initial concentrations.

TABLE III.3.12. **Simfuel integral leaching experiments :**
Major cation concentrations ($mol \cdot l^{-1}$) in leachates (precision: K, Al 5%; Mg, Ca, Na, Si 3%)

	Granite Groundwater			Clayey Groundwater		
	As synthesized	Final Leachate Clay/Sand	Final Leachate Granite	As synthesized	Final Leachate Clay/Sand	Final Leachate Granite
K	$5,7\times10^{-5}$	$2,0\times10^{-4}$	$1,8\times10^{-4}$	$3,1\times10^{-4}$	$1,2\times10^{-4}$	$1,9\times10^{-4}$
Ca	$6,9\times10^{-5}$	$1,9\times10^{-3}$	$2,8\times10^{-4}$	$9,8\times10^{-5}$	$1,5\times10^{-4}$	$1,2\times10^{-4}$
Na	$4,2\times10^{-3}$	$5,4\times10^{-3}$	$4,9\times10^{-3}$	$1,7\times10^{-2}$	$1,1\times10^{-2}$	$1,3\times10^{-2}$
Al	$1,1\times10^{-5}$	$3,4\times10^{-5}$	$8,2\times10^{-6}$	nd	$3,3\times10^{-6}$	$1,4\times10^{-5}$
Si	$1,1\times10^{-3}$	$1,3\times10^{-3}$	$1,7\times10^{-3}$	nd	$1,5\times10^{-3}$	$1,6\times10^{-3}$
Mg	nd	$1,5\times10^{-4}$	$4,1\times10^{-6}$	$1,0\times10^{-4}$	$5,8\times10^{-5}$	$1,9\times10^{-5}$

nd : not determined

The leaching solution was modified during the SIMFUEL leaching experiments. Significant potassium and calcium enrichment of the granite water was observed; in particular, the calcium concentration rose from 6.9×10^{-5} to 1.9×10^{-3} mol·l^{-1} in contact with the clay/sand mixture. The sodium and silica concentrations increased slightly. The cation composition modifications were less significant in clay water: the calcium concentration increased while the potassium, sodium and magnesium concentrations diminished slightly.

Colloidal Species

The distribution of elements in colloid and dissolved form was calculated from the analysis results for filtered and ultrafiltered aliquot samples of the final supernatant solutions (Appendix 5, TABLE 10). Regardless of the test medium, most of the Sr, Mo, Ba and U were present as colloids (84–88% of the strontium, 61–88% of the molybdenum, 69–97% of the barium and 81–89% of the uranium), contrary to the spent fuel experiments in which virtually all the Sr, Mo and U was found in dissolved form.

Leaching Kinetics

The ICP-MS analysis results are indicated in Appendix 5, TABLE 22 . Only Sr, Mo and Ba were determined in all the samples. The Y, Zr, Ru, Rh, Pd, La, Ce and Nd concentrations were always below the determination limit (2 µg·l^{-1}). Uranium was found in scattered samples at concentrations ranging from 5.2 to 46 µg·l^{-1}. As in the spent fuel leaching experiments, the final supernatant analysis was not taken into account in the kinetic study, since this sample was taken under different temperature and redox conditions. The study thus covered the first 84 days of leaching.

Cumulative Inventory Fraction Released into Aqueous Phase

The cumulative SIMFUEL inventory fractions released into the aqueous phase are indicated in Appendix 5, TABLE 11. The observed fractions were generally very high, on the order of 10^{-3} to 10^{-1}, and increased in a regular manner throughout the duration of the experiments (FIGURE III.3.13).

In all the test media, contrary to the spent fuel leaching experiments, the cumulative molybdenum inventory fraction released into the aqueous phase was lower than for strontium. The contradiction is only apparent, however: these results include ^{88}Sr, which is known to be released in large proportions by the environmental materials.

The FIA_c for each element is indicated as a function of the cumulative contact time in each of the test media.

Molybdenum

The cumulative released molybdenum fraction appeared to be higher in the granite tests (rising from 6.1×10^{-3} to 1.1×10^{-2} in the granite/granite water medium and from 1.3×10^{-2} to 2.3×10^{-2} in the granite/clayey water medium) than in the clay tests (1.4×10^{-3} to 2.4×10^{-3} in clay/granite water and 2.9×10^{-3} to 3.2×10^{-3} in clay/clayey water). These fractions were generally higher than those observed during the spent fuel leaching experiments (1.1×10^{-3} to 8.3×10^{-3}). The molybdenum analyzed in the aqueous phase came from the environmental materials as well as from the SIMFUEL. The proportion of molybdenum from the environmental materials cannot be estimated until the results of the control tests (environmental materials without fuel) are analyzed.

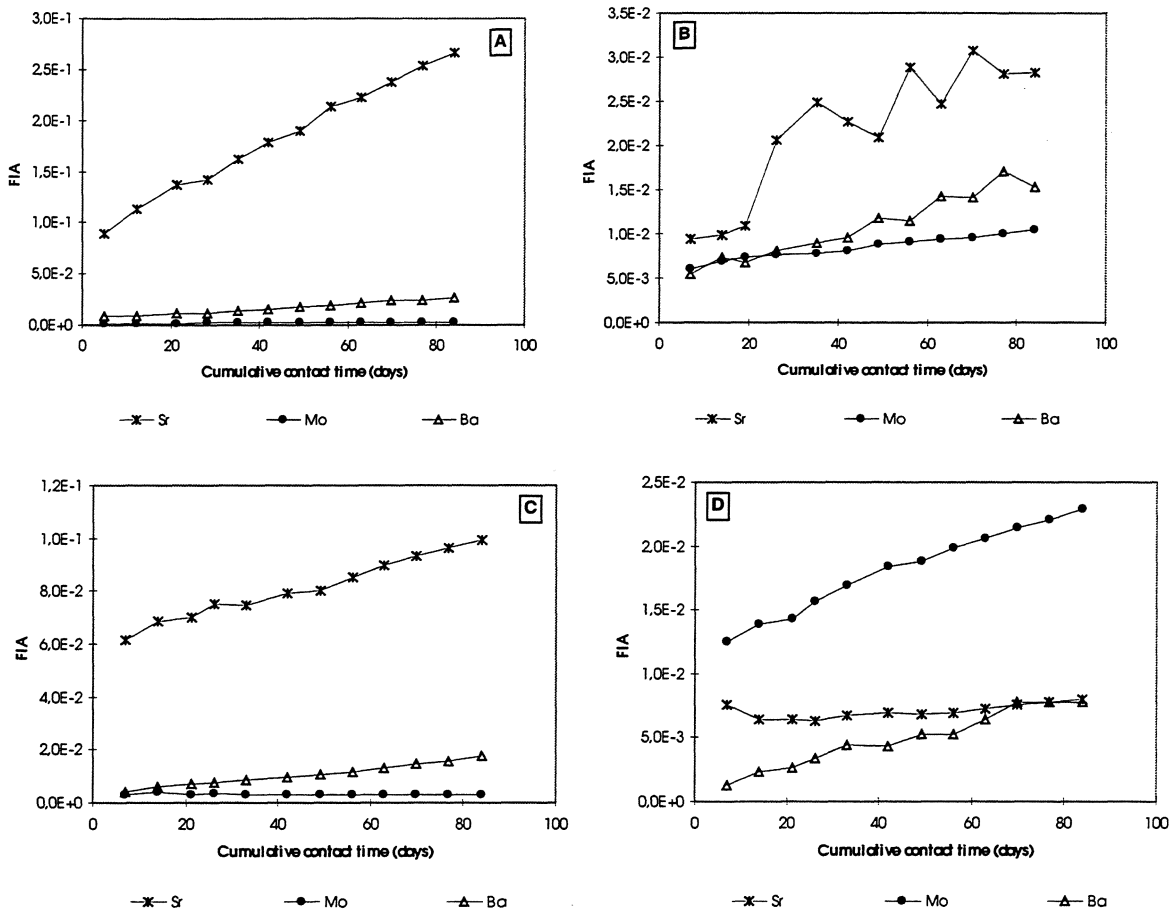

FIGURE III.3.13. **Simfuel leaching experiments: FIAc of elements (A) Clay/Granite water medium ; (B) Granite/ Granite water medium. (C) Clay/Clayey water medium; (D) Granite/Clayey water medium.**

Barium

The cumulative barium fraction released into the aqueous phase was on the same order of magnitude in all the test media, ranging from 8.2×10^{-3} to 2.7×10^{-2} in the clay/granite water medium, from 4.2×10^{-3} to 1.7×10^{-2} in the clay/clayey water medium, from 5.4×10^{-3} to 1.5×10^{-2} in the granite/granite water medium and from 1.3×10^{-3} to 7.8×10^{-3} in the granite/clayey water medium. As for molybdenum, some of the barium in solution was released from the environmental materials and not from the SIMFUEL.

Released Material Balance

Pending the results of the blank tests, no conclusions can be drawn concerning the SIMFUEL leaching behaviour in the test media. Nevertheless, the solution analysis results are presented below. The "filter rinse" solution analysis results are detailed in Appendix, TABLE 23, and the analysis results of the "material rinse", the "alkaline melt" when applicable, the "pot rinse" and the "sample-holder rinse" in Appendix 5, TABLE 24.

Strontium, molybdenum and barium were always determined in the filter rinse solutions, whereas the Ru, Rh and Pd concentrations were always below the determination limit; Y and Zr were rarely determined in the granite water medium. The La, Ce and Nd concentrations

could be determined in about half the granite water solutions, but never in the clayey water media.

The materials rinse solutions were indicative of the elements released by the environmental materials. For example, 3 to 4 times more strontium and 5 to 8.5 times more barium were released from the clay than from the granite, while 5 to 11 times more yttrium and 10 to 50 times more uranium were released from granite than from clay. The granite also released larger amounts of lanthanum, cerium and neodymium than the clay; the same was true for molybdenum, the concentration of which was below the determination limits (25 and 50 $\mu g \cdot l^{-1}$) in the media containing clay.

The pot rinse solutions also reflected the alteration of the environmental materials. The solutions from the clay experiments contained larger quantities of strontium and barium, but smaller quantities of yttrium, zirconium, uranium and molybdenum than the solutions from the granite experiments.

The sample-holders for the clayey water tests were rinsed by error with 1M nitric acid rather than with Milli-Q double-distilled water, and the results thus cannot be taken into account. In view of the low concentrations in the sample-holder rinse solutions, they may be disregarded in determining the overall material release balance. In the granite water tests, the granite was again observed to release more molybdenum and uranium, and less strontium and barium than the clay.

Solid state analyses of leached SIMFUEL samples

SIMFUEL particles leached in the clay/granite water and granite/granite water media were sampled for SEM observation after the sample-holders were rinsed in Milli-Q double-distilled water. No precipitates were observed on the fuel surface: either none were formed, or any existing precipitates were dissolved after the pot was opened to air (restoring oxidizing conditions) and the sample was rinsed for 24 hours in double-distilled water.

Interpretation and Discussion

Pending analysis of the blank tests (SIMFUEL alone or environmental materials alone leached separately in synthetic groundwater) it is impossible to discriminate between the elements released from the SIMFUEL and those released from the environmental materials.

Redox Potential

The redox potentials measured at the end of the SIMFUEL leaching experiments were representative of the reducing conditions expected in a geological repository. As the hot-cell procedures implemented for the spent fuel leaching experiments were identical, it may be assumed that similar redox potentials were reached in those experiments. This assumption is corroborated by the uranium concentrations (on the order of 10^{-8} $mol \cdot l^{-1}$) measured during these experiments.

The uranium concentrations in the weekly SIMFUEL leaching solution samples were generally below the ICP-MS determination limit (4 $\mu g \cdot l^{-1}$ in this case). Nevertheless, uranium was determined in the final supernatant solutions at concentrations of 32 and 58 $\mu g \cdot l^{-1}$ in the clay tests, and 2728 and 152 $\mu g \cdot l^{-1}$ in the granite tests. We infer that uranium(IV) was oxidised to uranium(VI) in the final supernatants, causing it to enter solution; each 50 ml final supernatant sample was obtained in successive 5 ml fractions with a micropipette after measuring the redox potential, favouring rapid oxidation of the solution.

Colloids

The SIMFUEL supernatant solutions were analyzed more than two weeks after sampling, compared with less than a week for the spent fuel experiments. Colloids may have developed during this period, particularly since the leachates contained iron, which oxidises to Fe(III) and can precipitate in hydroxide form, favouring the formation of colloids.

Alteration of Environmental Materials

Alteration of the environmental materials was revealed by the high orders of magnitude (10^{-2} to 10^{-3}) of the cumulative inventory fractions of Sr, Mo and Ba released into the aqueous phase, and by the changes in the major cations in the groundwater.

Contrary to the results observed for the radionuclides in the spent fuel experiments, the cumulative element inventory fractions released into the aqueous phase did not diminish during the first few weeks. We monitored the release of radioactive (i.e. *labeled*) species in the spent fuel tests, making it possible to discriminate between the strontium released by the spent fuel (^{90}Sr) and by the environmental materials (^{88}Sr). A similar distinction could not be made for the SIMFUEL tests: only the overall release of elements from the SIMFUEL, the environmental materials and sorption of (co)precipitation phenomena could be observed; most of the strontium was released into solution from the environmental materials.

Conclusions on Spent Fuel and SIMFUEL Leaching under integral test conditions

We investigated the influence of four combinations of simulated groundwater and environmental materials at 90°C under a pressure of 40 bars: a clay/sand mixture with granite water, granite and granite water, a clay/sand mixture with clayey water, and granite and clayey water. Leachate samples were taken at weekly intervals, and the final overall distribution in the closed, multiphase systems was analyzed.

We assessed the leaching behaviour of several radionuclides (^{88}Sr, ^{90}Sr, ^{134}Cs, ^{137}Cs, $^{239+240}Pu$, ^{240}Pu, ^{238}Pu+^{241}Am, ^{244}Cm and ^{238}U) and of molybdenum to provide data on the corresponding elements. Some elements were found both in the spent fuel and in the geological materials. Strontium was of particular interest in that it is considered as a fuel alteration tracer.

In addition to the technical difficulties, a number of experimental difficulties were also encountered. Although the labile activity and a fraction of the activity segregated at the fuel grain boundaries (0.83% of the calculated initial ^{137}Cs activity) was eliminated prior to leaching, the activity of certain radionuclides predominated over that of the others, and thus complicating the radiochemical analyses. Moreover, low or very low quantities were leached from the fuel, and the elements were sorbed differently by the environmental materials. In addition, the quantities of the stable elements in the SIMFUEL – and even of uranium – were sometimes at the detection limits of the ICP-MS system.

The overall results of our 91-day leach tests with 60 GWd·tU-1 spent fuel show that the radionuclides were predominantly found in the environmental materials rather than in the aqueous phase: depending on the species and the nature of the environmental materials, they retained between 66% and 99% of the activity released from the spent fuel. Some species in solution (e.g. curium and plutonium) were also sorbed on colloidal particles.

Concerning the dissolved species, we observed that the groundwater composition was not a major factor, and that the cumulative actinide inventory fractions released into the aqueous phase stabilized after about one month, following which the concentrations in the aqueous phase were about 10^{-8} mol·l^{-1} for uranium, 10^{-12} mol·l^{-1} for plutonium and 10^{-13} to 10^{-14} mol·l-1 for curium. These low values were attributable to sorption on granite or clay. The behaviour of these species thus depends on fuel leaching, on multiple interactions, on the equilibrium with unidentified crystalline or amorphous phases and with the environmental materials.

The material balance for the ^{90}Sr released from the fuel during the experiments were twice as high with clay as with granite. Additional studies of longer duration will be necessary before it may be asserted that the presence of smectite 4a clay is detrimental to the durability of spent fuel. Strontium was retained in larger amounts by clay than by granite, while the ^{90}Sr concentrations in the aqueous phase were comparable for all the test media.

The mean spent fuel alteration rates determined from the total ^{90}Sr inventory fractions release in the test media were consistent with other published findings:

clay/granite water medium:	0.57 ± 0.07 mg·m^{-2}d^{-1}
granite/granite water medium:	0.19 ± 0.03 mg·m^{-2}d^{-1}
clay/clayey water medium:	0.35 ± 0.05 mg·m^{-2}d^{-1}
granite/clayey water medium:	0.20 ± 0.03 mg·m^{-2}d^{-1}

When the blank tests have been completed and analyzed, we will be able to quantify the proportions of elements and radionuclides released by the environmental materials alone, without the fuel, and to determine the quantity of material released by spent fuel in the absence of environmental materials. We will then be able to interpret the SIMFUEL leaching experiments and, perhaps, to identify a possible radiolysis effects on fuel leaching behaviour. We will also be able to assess the possible effect of the environmental materials on the quantity of material released from the fuel, at least over the duration of our experiments. The results were not available for the final report.

WP IV: MODELLING

The final goal of the experiments in the project is to develop sufficient quantitative understanding of the spent fuel dissolution process to develop models for allowing meaningful long-term prediction by source terms. Due to the complicated nature of the overall reaction mechanism, a series of submodels was developed. To account for the electrochemical nature of the dissolution process, three electrochemical models were developed by various laboratories. Modelling by ITU was focussed on quantification of experimental errors caused by defected electrode samples (see WP I.6/7). At FUB a model is developed (WP I.6/7) to rationalize the effect of carbonate and on the calibration curves (corrosion rate versus electrochemical potential). Progress has been made in combining electrochemical and geochemical data and models to provide a mechanistic basis for source term development and to identify rate regimes and oxidative dissolution thresholds in the frame of Eh/pH-diagrams. Geochemical reaction path models describe the evolution of solid and liquid phases, ideal solid solution models account for the incorporation of radionuclides in solid reaction products. A problem of these models is that they apply equally well to unirradiated UO_2 and to spent fuel without accounting explicitly for the differences. Developing radiolysis models shall close this gap.

WP IV.1 REACTION PATH MODELLING OF SPENT FUEL BEHAVIOUR AND ACTINIDE CHEMISTRY

Geochemical modelling of the reaction path of spent fuel in saline solutions was carried out at FZK both for oxidizing and reducing conditions. The evolution of solution composition and the quantity of newly formed secondary reaction products were calculated both as a function of the amount of spent fuel dissolved and as a function of time. The calculations were performed with the geochemical code EQ3/6, using the Pitzer equations for activity coefficient calculations at high ionic strength.

Under oxic closed system conditions (calculation results: FIGURE IV.1), for the simulated stepwise addition of UO_2 into an air saturated NaCl solution. Na-polyuranate was calculated to be the first phase to form. Indeed, Na-polyuranate was observed in coprecipitation tests. This resulted in a decrease of solution pH to values of about 5 and to U concentrations of about 10^{-5} m, as observed experimentally. Due to the redox buffer capacity of UO_2, further simulated addition of UO_2 to the solution resulted in a the consumption of oxygen and a decrease of Eh, in the redissolution of the Na-polyuranate and the formation of different types of superstoichiometric uranium oxide phases.

UO_2 dissolution under reducing conditions was simulated (FIGURE IV.1.2) by repeating the calculations in a similar way as before, considering this time the co-dissolution of UO_2 with iron. As before, Na-polyuranate was predicted to be the first phase to form. However, dissolved oxygen from air is expected to be consumed fast by the oxidative corrosion of iron, leading to the formation of hematite. Once all oxygen is consumed, the Eh drops and both hematite and Na-polyuranate become thermodynamically unstable. They are predicted to redissolve, driven by the formation of uraninite and magnetite. In reality, the dissolution of hematite is very slow and it is unlikely that it will occur in experimental time. Also in the experiments Goethite and not hematite were observed. Though goethite is less stable than hematite, is formation is favoured kinetically. Such kinetic constraints would have to be considered into the modelling to allow for a closer match with experimental reality. In contrast, the observed increase in solution pH is indeed observed experimentally (Appendix 2, TABLE 19).

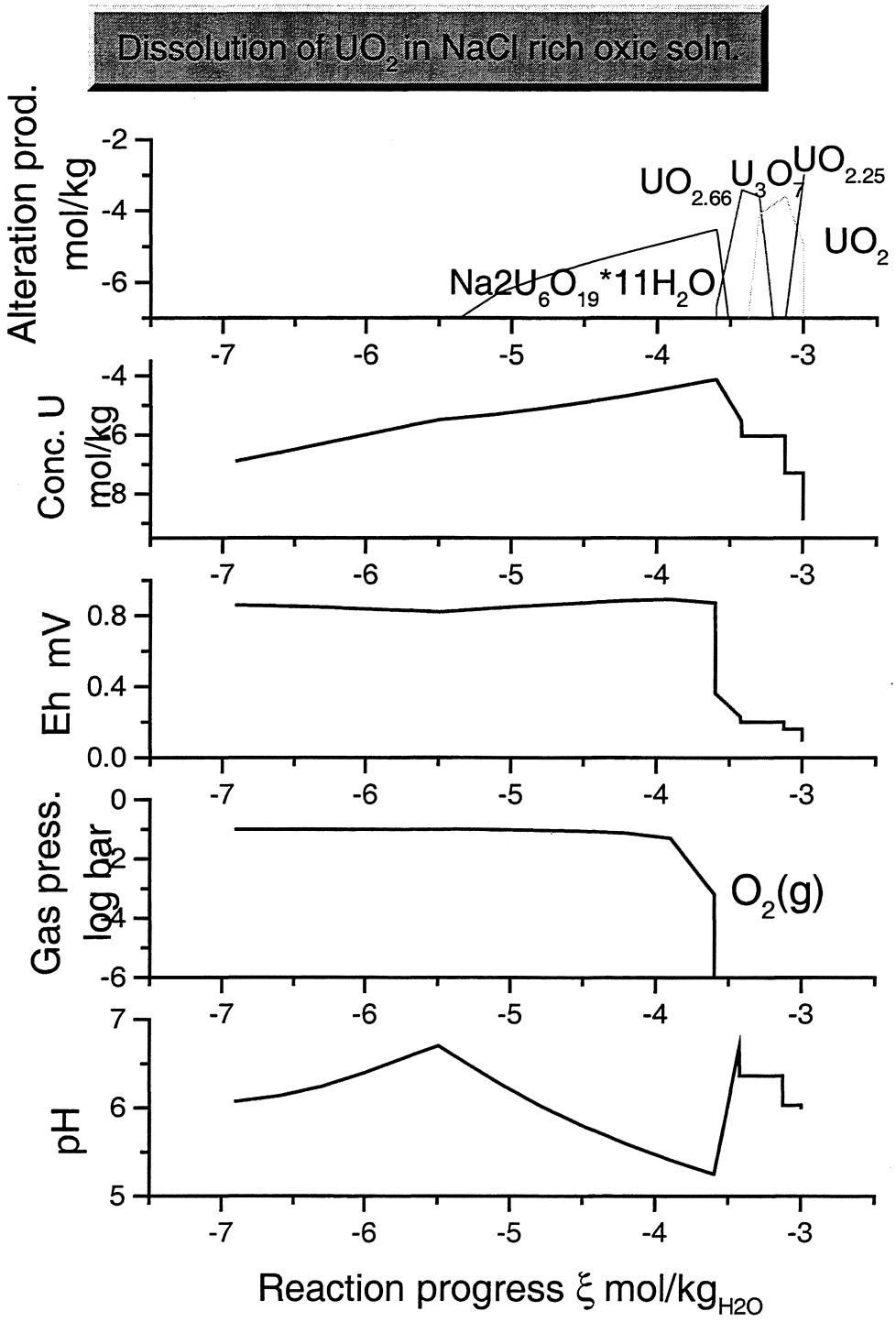

FIGURE IV.1.1: Geochemical simulation (code: EQ3/6) of the reaction path of UO_2 in 95% saturated NaCl solution in equilibrium with air at 25°C.

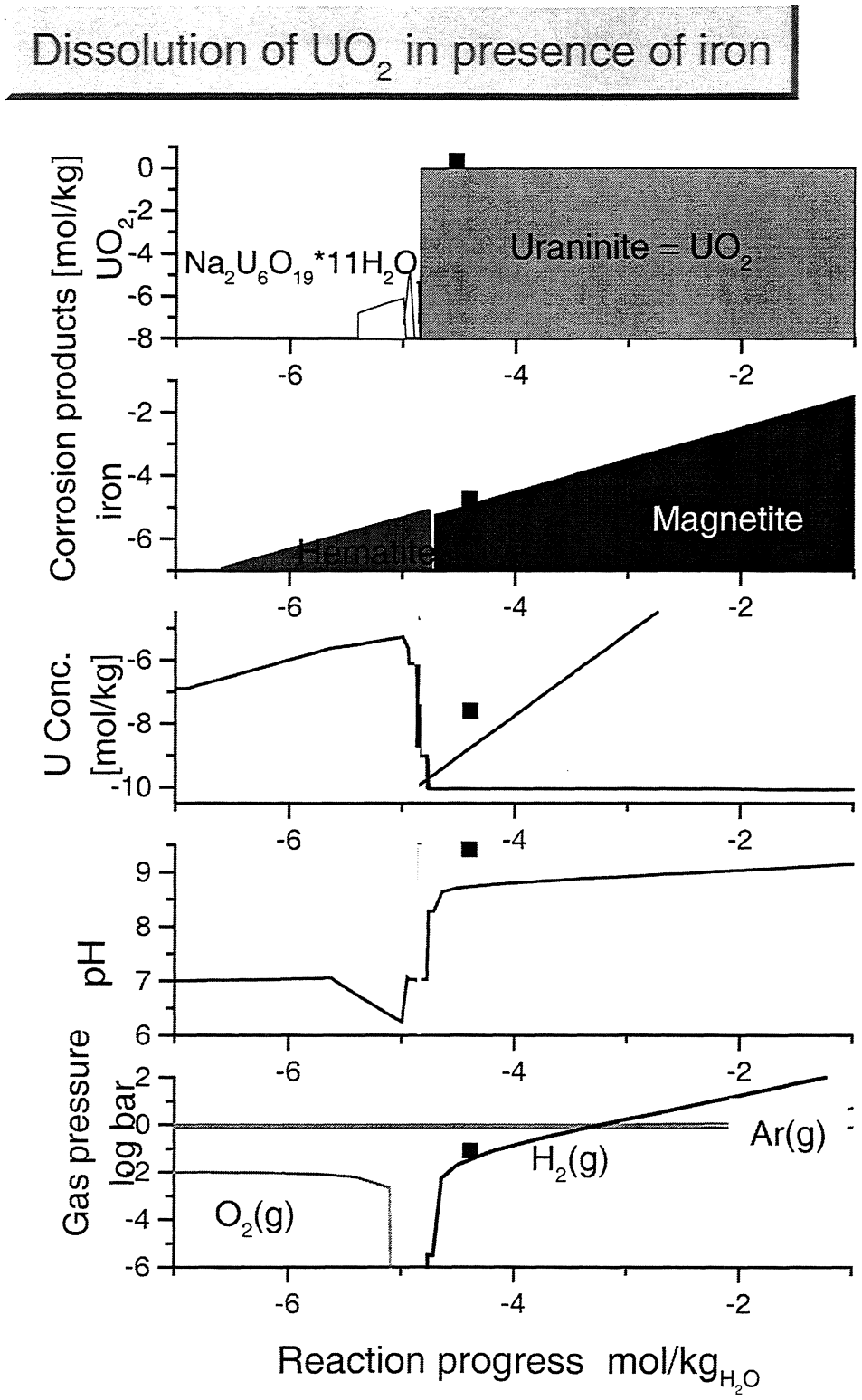

FIGURE IV.1.-2: Geochemical simulation of the reaction path of UO_2 in 95% saturated NaCl solution under anoxic closed system conditions (absence of radiolysis). Black dots: Experimental data, Appendix 2, TABLE 19)

The results of the above calculation provide a reasonable explanation for the variation of solution pH under oxidizing and reducing conditions in salt solutions: It is very important to know if it is just an experimental artifact that the pH under oxidizing conditions becomes as low as 5, because radionuclide solubilities become rather high under these conditions. The calculations show that this is not an artifact but that low pH results from Na consumption for polyuranate formation. This is not expected under reducing conditions, because no Na-containing U(IV) solid phases are expected to be formed. Also low pH values are not expected in oxic granite or clay waters. In these solutions much less alkali elements are available to become incorporated into U(VI) secondary phases.

Reaction path of UO_2 in granite water.

The reaction path for UO_2 dissolution in granite water is studied by FZK. Particular emphasis was on modelling the experimental data in saline granite water under oxic conditions, studied in WP I.4-1.

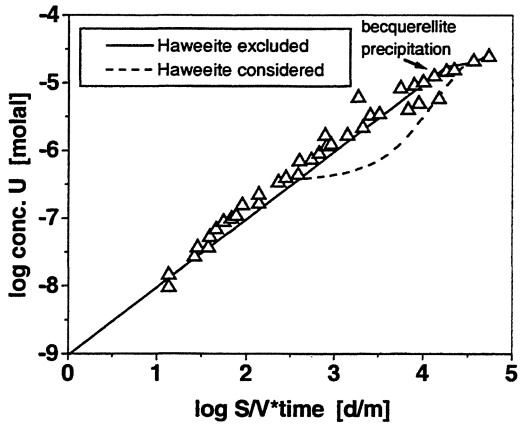

FIGURE IV.1-3: Time dependent reaction path of UO_2 dissolution in oxic saline granite waters (EQ3/6-calculation by FZK)

In order to compare experimental data with reaction path calculations, reaction progress values are translated to reaction time, using a rate constant of UO_2 dissolution in saline granite water. This rate constant has been determined from experimental data of VTT (0.3 mg/m^2d, same data as in FIGURE I.4-5). With respect to phase selection, two reaction path calculations are compared: (1) uranyl silicate formation (haweeite, soddyite) is ignored and (2) Haweeite is considered also. FIGURE IV.1-3 shows that only case (1) is compatible with the VTT-data. Discrepancies were even more pronounced when soddyite is also considered (results not shown). In all calculations, at very high reaction progress (long time) becquerellite and/or Na-polyuranate formation are predicted to occur. Though these predictions were not yet validated by solid phase identification techniques, two unambiguous conclusions can be drawn from these calculations: (A) The decrease in the rate of U accumulation in solution and the approach of steady state U concentrations is quantitatively compatible with a constant rate of UO_2 dissolution (dissolution/ precipitation mechanism). (B) If uranyl silicate formation (haweeite and/or soddyite) has occurred in the experiments this must be a non-equilibrium process (limitations in the precipitation rate).

Electro-geochemical model for spent fuel matrix dissolution mechanism

The electrochemical nature of spent fuel matrix dissolution under oxic and anoxic laboratory

conditions has clearly been confirmed by our project. It has been shown that a simple relationship between corrosion rate and corrosion potential holds, independent on groundwater composition ("calibration curves"). Thus, the effect of groundwater composition on fuel matrix dissolution rates is associated to an effect of the geochemical environment on the corrosion potentials. If we would know the corrosion potential of UO_2 or spent fuel in a given groundwater, we would be able to predict the corrosion rates. Since geochemical conditions in the repository near field depend strongly on waste package design, a generic approach is taken, allow prediction of corrosion potentials.

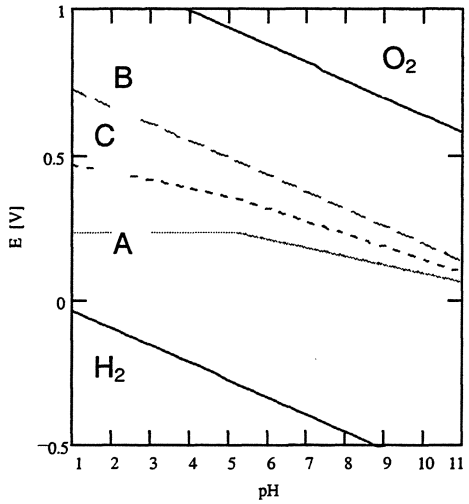

FIGURE IV.1-4: UO2 dissolution, log pO_2=-29, HCO_3=0, pH dependency of (A) equilib-rium ref. potential of anodic and (B) cathodic half reaction (=Eh) (C) corrosion potential

This is pursued at INE-FZK by explicitly coupling of electro- and geochemistry: The corrosion potential (no net current) at the surface of UO_2 is calculated by searching the potential at which anodic and cathodic partial currents equal. With the electrochemical data obtained (WP I.6/7), the two partial currents are calculated as a function of the potential difference to two reference potentials. The anodic dissolution reference potential is the equilibrium potential for $UO_2^{++} + 2e^- = UO_2$: $E_a = E_o + RT/2F \ln a_{UO2++}$, with a_{UO2++} calculated from total U(VI) concentration in solution, considering activity coefficients, hydrolysis and complex formation constants (curve A, FIGURE IV.1-4). As equilibrium potential for the cathodic reaction (oxidant reduction) the solution Eh is used. The interpretation of measured solution Eh is ambiguous, but Eh is a master variable in the assessment of redox properties of geochemical systems. The Eh is related to the oxygen partial pressure pO_2 by the equation

$$Eh = E_o + RT/ZF \ln (pO_2 * 10^{-4pH}/a_w^2) \qquad (IV.1.1)$$

Eh-values (in V) measured for air saturated waters can typically be described by a relation

$$Eh_{air} = (13\pm2 - pH)\cdot 0.0592 \text{ V}, \qquad (IV.1.2)$$

corresponding to a nominal equilibrium partial pressure of O_2 of 10^{-29}. In contrast, thermodynamic equilibrium with air would yield a relation

$$Eh_{thermod} = (20.77 - pH)\cdot 0.0592 \text{ V}. \qquad (IV.1.3)$$

For modelling air saturated waters the empirical relation (IV.1.2) is used (curve B). The calculated corrosion potential (curve C) is then situated between the two equilibrium curves B and C.

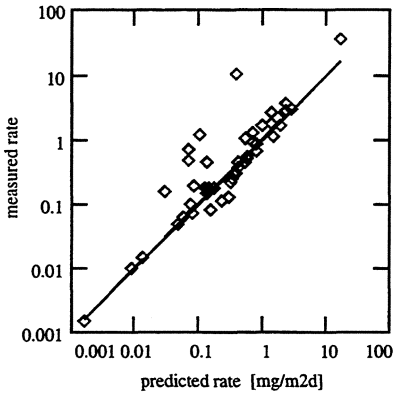

FIGURE IV.1-5: Comparison of predicted and measured corrosion rates of UO2 in various groundwaters (pH 1-10, HCO_3 0-0.1 m, oxic and anoxic)

The approach was tested and calibrated (Figure IV.1-5) using rate data for UO_2 corrosion, obtained in the present and the past EU-project for a variety of pH, Eh, and carbonate concentrations. As far as available, the experimental Eh was used. Missing Eh values were estimated. Eh_{air} was used (corresponding to log pO_2 = -29) for air saturated solutions or 21%O_2/N_2 solutions, log pO_2 = -30.4 for 5%O_2/N_2 and log pO_2 =-27.6 for solutions with 100% O_2. The average deviation of predicted and experimentally measured rates is about a factor of two.

The calculations are based on the experimental relation between corrosion potential and corrosion rate corresponding to a b_a value of 80 mV (see FIGURE I.6-32). For the cathodic reaction a b_k value of 240 mV/decade (Tafel slope) has been observed in section I.6. Better agreement with the experimental data can be obtained with lower values, expected for slightly oxidised fuel. A best-fit value of 167 mV was used for the calculations. Moreover, already a change of the anodic reference equilibrium potential for oxidised fuel would be different according to the reaction UO_2^{2+} +1.33 e^- +0.33 H2O= 1/3 U_3O_7 +0.66 H^+. Anodic exchange current densities were $5*10^{-12}$ A/cm^2, cathodic ones were $5{\cdot}10^{-11}$ A/cm^2. The approach also provides a quantitative interpretation of the dependency of calibration curves on carbonate concentrations (compare FIGURE IV.1-6 with FIGURE I.6-36) .

Fractional reaction orders nc for $r=r_o*[C_{tot}]^{nc}$ with respect to total dissolved carbonate vary with pH. At pH 4 there is no dependency of reaction rates on dissolved carbonate (nc=0), at pH 5 nc=0.177, at pH 7 it is 0.41, at pH 8 to 10 it is 0.53. Similarly, the reaction order np with respect to pH varies with pH. For pH<4 np=0.35, it is 0.18 at pH5, 0.12 form pH 6 to 7 and 0 at pH 8. Above pH 8 the reaction rate increases with a very small exponent 0f –0.06. Reaction orders with respect to oxygen partial pressures are only 0.09.

The electro-geochemical model provides a direct interface to full scale geochemical code calculations as these can be used to calculate both a_{UO2++} and Eh as a function of reaction progress and near field constraints. It allows to describe reaction rates of UO_2 directly in Eh/pH diagrams used in the geochemical assessment of geological nuclear waste disposal sites (see below WP IV.4).

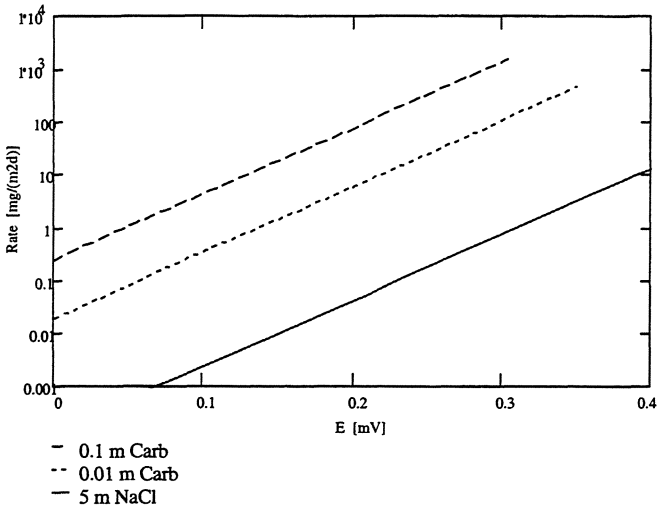

FIGURE IV.1-6: Predicted calibration curves in carbonate containing and carbonate free media

Surface complexation model

The reaction of UO_2 with different types of groundwaters was modeled by ENRESA/UPC considering the detachment of surface complexes as rate liming step. In hydrogen bicarbonate medium, the proposed mechanism includes three different steps [99PAB/CAS]:

Step 1: Oxidation of the surface of the solid

$$>UO_2 + O_2 \underset{k_{-1}}{\overset{k_1}{\rightleftharpoons}} >UO_3 \qquad \text{(IV.1-4)}$$

Step 2: Surface co-ordination of U(VI) by HCO_3^-

$$>UO_3 + HCO_3^- \xrightarrow{k_2} >UO_3 - HCO_3^- \qquad \text{(IV.1-5)}$$

Step 3: Detachment (dissolution) of the product species

$$>UO_3 - HCO_3^- \xrightarrow{k_3} \text{"U(VI)(aq)"} \qquad \text{(IV.1-6)}$$

The assumption of a fast detachment of the carbonate surface complex (step 3) agrees with the analysis by X-Ray Photoelectron Spectroscopy [95BRU/CAS]. From this mechanism, and after applying the stationary state approach to the reaction intermediate, $>UO_3\text{-}HCO_3^-$ the following rate equation is obtained:

$$r = \frac{k_1 k_2 \{>UO_2\}_{tot} [O_2][HCO_3^-]}{k_{-1} + k_2[HCO_3^-] + k_1[O_2]} \qquad \text{(IV.1-7)}$$

When the effect of pH is considered, following a similar procedure as in the previous case, the following rate equation is established [98TOR/CAS]:

$$r = \frac{k_1[O2][>UO2]_{tot}\left(k_3 + k_2[H^+]\right)}{k_{-1} + k_3 + k_2[H^+] + k_1[O2]} \qquad \text{(IV.1-8)}$$

In order to validate these models, experimental dissolution rates of UO_2(s) in bicarbonate media at different temperatures [97PAB/CAS, 99PAB/CAS] and as a function of pH [97TOR/CAS] have been adjusted to equations IV.1-7 and IV.1-8, respectively by fitting the kinetic parameters, which have been used for the modelling of experimental dissolution results published by different authors.

Studying uraninite dissolution under oxidising conditions, Grandstaff [76GRA] at low carbonate concentration determined the rate of uraninite dissolution to be directly proportional to the total hydrogen carbonate concentration. However, the same author found no dependence when working at higher carbonate concentrations. If the data obtained by Grandstaff at 23 ºC are compared with those obtained by the model in bicarbonate media, an important difference between the experimental values and the predicted ones is evidenced, which can be attributed to differences in the solid phases [89GRA]. Nevertheless, our model can predict the reaction order change with HCO3- concentration observed by Grandstaff.

Thomas and Till [84THO/TIL] also determined a linear dependence working at low carbonate/bicarbonate concentrations (<1 $mmol \cdot l^{-1}$) using unirradiated UO_2 and at 40 ºC, in agreement with the mechanism in bicarbonate media.

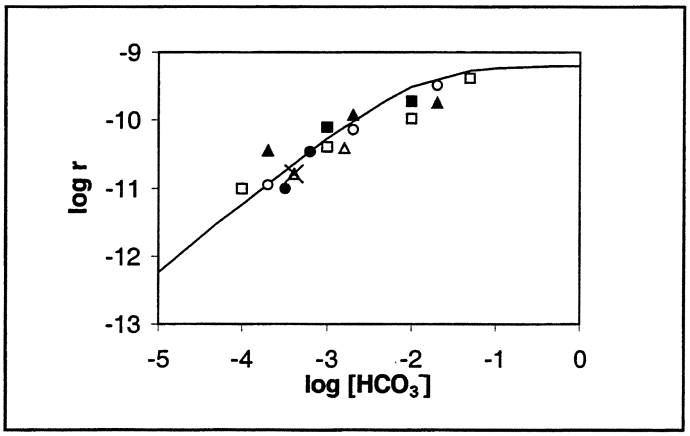

FIGURE IV.1-7 Comparison between the results obtained by different authors using both spent fuel and unirradiated UO_2 and the trend predicted by equation IV.1-7, represented by the solid line (■□ [97PAB/CAS], O, ▲ [95GRA/WIL], ●,Δ [89GRA], X this work: experiment UODGW25)

In FIGURE IV.1-7, the results obtained by several authors using both SF and unirradiated UO_2 under the same oxidising conditions, are summarized. In this case, the treatment of the whole data gives a fractional dependency of the dissolution rate on the HCO_3^- concentration which was found to be: 0.60 ± 0.06. The rates predicted by equation IV.1-7 are also plotted in FIGURE IV.1-7 and as can be seen good fit of the experimental data is achieved. Therefore, our model derived from unirradiated UO_2 results is able to predict dissolution rates for both SF and unirradiated UO_2, which react at about the same rate.

Thomas and Till [84THO/TIL] studied the rate of dissolution of unirradiated UO_2 pellets as a function of pH at 40 ºC, and they found that the rate increased with decreasing the pH and was minimal in the pH range 5-10. These values are in good agreement with the values simulated using equation IV.1-8.

In the case of the work compiled by Grambow [89GRA] using SF, the experimental results are higher than the estimated ones by equation IV.1-8, but the discrepancies observed are reasonable since SF rates are being considered.

Concerning the dissolution rates of uraninites [76GRA], experimental values are 2 orders of magnitude higher than the rates arising from equation IV.1-8

Dissolution rates from a detailed study of the corrosion mechanism of UO_2, using electrochemical techniques [89SHO/SUN, 91SUN/SHO], were compared with the values

calculated using equation IV.1-8 at the experimental conditions reported by the authors. The calculated values were in very good agreement with the experimental dissolution rates, although data are not reported here.

TABLE IV.1-1 Comparison between experimental and calculated dissolution rates

Reference	pH	$[O_2(aq)]$ (mol/l)	$e_{xperimental}$ (mol/m^{2}s)	$r_{calculated}$ (mol/m^{2}s)
[89GRA]	5.7	$2.67 \cdot 10^{-4}$	$2.9 \cdot 10^{-11}$	$1.4 \cdot 10^{-11}$
[89GRA]	5	$2.92 \cdot 10^{-4}$	$4.1 \cdot 10^{-9}$	$4.0 \cdot 10^{-11}$
[95ERI/ EKL]	7	10^{-5}	$5 \cdot 10^{-12}$	$9.7 \cdot 10^{-13}$

Other dissolution rates at different pH using both, unirradiated UO_2 and SF found in the literature are summarized and compared with the simulated data in TABLE IV.1-1. The difference between the predicted and measured values is of one order of magnitude or less except in the case of the data published by Grambow [89GRA].

As in the cases of proton and bicarbonate, the oxygen reaction orders found in the literature for uranium dissolution vary from fractional values ~0.5 up to 1. The two mechanisms presented in this work can explain this fact.

Thomas and Till [84THO/TIL] exposed UO_2 pellets to oxygen-containing leachants in distilled deionized water and in granite groundwater at 30 ºC. In the case of demonized water, a first order dependence of the dissolution rate on oxygen concentration was obtained. Unfortunately this trend can not be predicted by equation IV.1-7.

Nevertheless, the data modelling in granite groundwater, in which experimentally a fractional order is obtained (~0.6) provide satisfactory results.

In electrochemical experiments Shoesmith and Sunder [92SHO/SUN], found a first-order relationship for UO_2 dissolution rate as a function of dissolved oxygen concentration working at 0.1 M $NaClO_4$ and 25 ºC. The approach provided by equation IV.1-7 is presented in FIGURE IV.1-8.

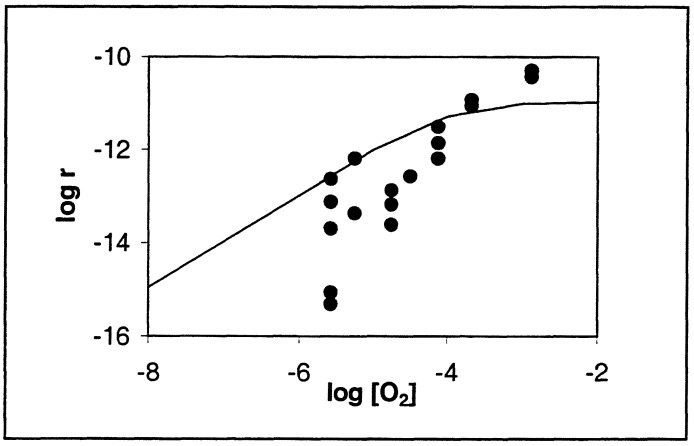

FIGURE IV.1-8 Comparison with the experimental data obtained by [92SHO/SUN] using UO_2 and electrochemical experiments, and the trend predicted by equation IV.1-8, represented by the solid line.

A first order with respect to oxygen concentration was determined [76GRA] with natural uraninite powders. The reaction order is in good agreement with the slope obtained by equation IV.1-8, but again the experimental dissolution rates are two orders of magnitude higher than the predicted ones, though the data is not shown here.

In the case of SF, some uncertainties in the oxygen concentration dependence were found [95GRAY/WIL]. At 25ºC the dissolution rate has not dependence on oxygen concentration, while at 75 ºC fractional dependencies were found (0.35 and 0.79, at $2 \cdot 10^{-2}$ and $2 \cdot 10^{-4}$ M HCO_3^-, respectively). Equation IV.1-7 can not explain this behaviour and more experimental work is needed in order to clarify these aspects.

Christensen [98CHR] developed a radiolysis model taking into account the gas production rates, and was able to explain SF dissolution experiments in 5 M NaCl and deionized water, although the predicted dissolution rates were overestimated one order of magnitude approximately. One attempt was made in order to simulate the same experiments using the mechanism presented here, but in this case the predicted values were several orders of magnitude lower compared with the experimental values. This disagreement can be attributed to the fact that radiolysis (see below, WP IV.3) is not considered in the models discussed here.

WP IV.2 MODELLING SOLID SOLUTION FORMATION

SF coprecipitation data in saline solutions were modeled [96QUI/GRA2]. The elements studied were Am, Cm, Eu, Np and Pu. From the data that now available on trivalent element behaviour one can conclude that solid solution formation of "(AN,REE)$(OH)_3$(s)" may occur under this experimental conditions (FIGURE IV.2-1).

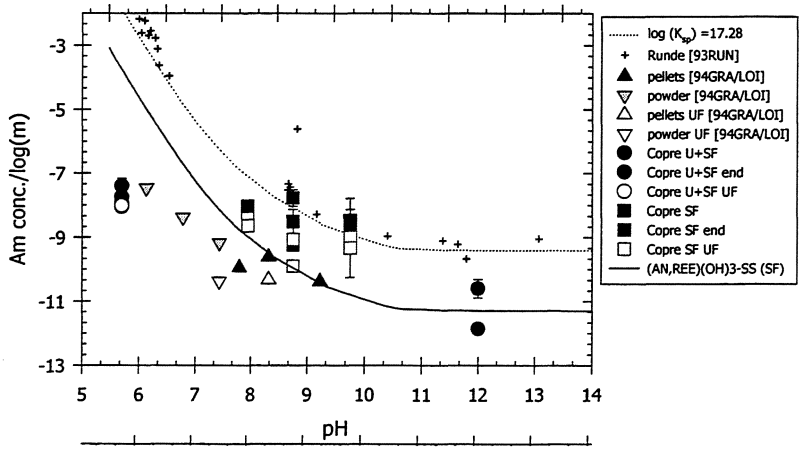

FIGURE IV.2-1 Solubility of Am in case of ideal solid solution formation (AN,REE)$(OH)_3$(s).

Using geochemical reaction path models, the interpretation of SIMFUEL coprecipitation phenomena in GBW under oxidising conditions has been performed. EQ3/6 [92WOL] and PHREEQC [97CHA/MAC]. The data files used for modelling were "data1.com" and "phreeqc.dat" for EQ3 and PHREEQC, respectively.

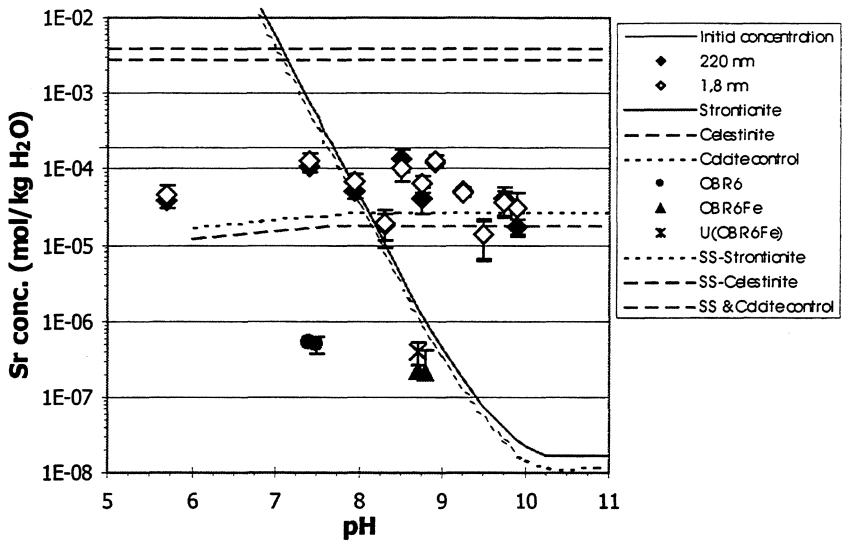

FIGURE IV.2-2 Sr concentration from experimental and calculated data.

A tentative approach for modelling Sr steady state concentration as a function of pH is given in FIGURE IV.2-2. In triangle points SIMFUEL leaching concentration values obtained are given. The lines represent the Sr solubility calculated as function of the control solid phase considered (celestite, strontianite or calcite). A comparison between experimental [98SER/QUI] and thermodynamic data [90PAR/THO] of Sr solubility considering a solid phase formation support the following chemical control model: For pH < 7 the solid phase that controls the Sr solubility is celestite; when 7 < pH < 8 the phase is strontianite, and for pH > 8 the calcite formation controls the Sr concentration in solution.

WP IV. 3 MODELLING OF RADIOLYSIS EFFECTS

Calculations of spent fuel corrosion and gas production have been carried out, simulating conditions of spent fuel leaching experiments carried out within a previous EU-project. In deionized water the calculated gas generation rates were $2 \cdot 10^{-8}$ and $1 \cdot 10^{-8}$ mol $\cdot$ (g U)$^{-1} \cdot$d^{-1} for hydrogen and oxygen, respectively, 6 – 10 times lower than the experimental values. The calculated fuel alteration rate was $2.2 \cdot 10^{-8}$ mol UO_2 (g U)$^{-1} \cdot$d^{-1} or 92 mg$\cdot$ m$^{-2} \cdot$d^{-1}, about 3 times higher than the experimental rate. Excess hydrogen decreased both fuel alteration and gas generation rates. Excess oxygen increased gas generation rates. The gas generation continued with the same rates for the whole calculation period (5 y). The calculated fuel alteration (=corrosion) rate was higher than the experimental values (about 10 times). The fuel oxidation is caused only by water radiolysis in a thin α-irradiated layer. The gas is produced almost entirely in the gamma-irradiated bulk water. Diffusion of gases from the thin α-irradiated layer is decisive for the magnitude of the UO_2 oxidation and dissolution. If diffusion is neglected hydrogen is built up in the thin water layer. This results in a considerably reduced corrosion rate of UO_2.

Used nuclear fuel is mainly UO_2, which has low solubility in water under reducing conditions. Although the groundwaters at the expected depth of a disposal vault in granite rock (500 to 1000 m) are generally reducing, redox conditions near the fuel surface may be altered by the radiolysis of water by the ionizing radiation associated with the fuel.

A previously developed radiolysis model for corrosion of UO_2.in deionized water (94CHR/SUN) was used to describe corrosion results from the last (F12W-CT90-0055) and

the present EU-project on spent fuel corrosion (96GRA/LOI, 95LOI/GRA) for experiments in deionized water and in 5 m NaCl solutions where, both fuel corrosion and gas production were measured

The MACKSIMA-CHEMIST computer programme (79CAR/HAN) was used. Also, the same reaction mechanism as used previously (94CHR/SUN, 86CHR/BJR)' was applied (see TABLE 1, Appendix 9). The mechanism shown is slightly modified to include diffusion as discussed below. In TABLE 2, Appendix 9, reactions in 5 m NaCl solutions are given. The applied G-values for both γ- and α-radiation are shown in TABLE 3, Appendix 9.

It was necessary to modify the model to be applicable also in concentrated NaCl solutions. By simulation of experiments by Giménez et al (96GIM/BAR) on the effect of ClO^- on oxidation of UO_2 in unirradiated, nitrogen saturated 5 m NaCl solutions a rate constant for the reaction of ClO^- with UO_2 and UO_3 H was obtained. The fitted value was $4 \cdot 10^{-3}$ $m^{-1} \cdot s^{-1}$. The model was further developed based on recent experiments by Kelm and Bohnert (98KEL/BOH1, 98KEL/BOH2) on α- and γ-radiolysis of 5 m NaCl solutions (in the absence of UO_2). The main modification was the introduction of the radical Cl_2^- as a primary species in α-irradiated solutions and the primary species $ClOH^-$ and Cl_3^- in α-irradiated solutions. These species are likely to be formed at high Cl^- concentration in the spur by fast reactions of OH radicals with Cl. Consequently, the primary yields of the other oxidizing species (OH and H_2O_2) are reduced. In the final calculations the primary yields proposed by Kelm and Bohnert (98KEL/BOH1, 98KEL/BOH2) were used, see TABLE 4, Appendix 9.

Spent fuel self oxidation and dissolution by radiolysis in deionized water

The model has been used to simulate results from a previous EU-contract (F12W-CT90-0055, 96GRA/LOI, 95LOI/GRA) . In these experiments both fuel corrosion and gas production were measured deionized water and in 5 m NaCl solutions. A summary of the original results is given in TABLE 5, Appendix 9. The system is divided into four phases, see FIGURE IV.3-1, requiring three separate calculations. Irradiation conditions are given in TABLE IV.3-1

Phase 1: a 30 μm thin surface layer on top of the pellet, irradiated by α-, β-, and γ-radiation. Volume 0.021 cm^3. SA 4.2 cm^2.

Phase 2: a 0.3 cm layer on top of phase 1, irradiated by β- and γ-radiation. Volume 1.28 cm^3. SA 4.2 cm^2.

Phase 3: The rest of the solution, irradiated by γ-radiation. Volume 200 cm^3.

Phase 4: Gas phase, unirradiated, volume 250 cm^3.

Fuel corrosion takes place only in phase 1, whereas gas production may take place in all three phases. Oxygen and hydrogen are then distributed between phase 3 and 4 according to their solubilities.

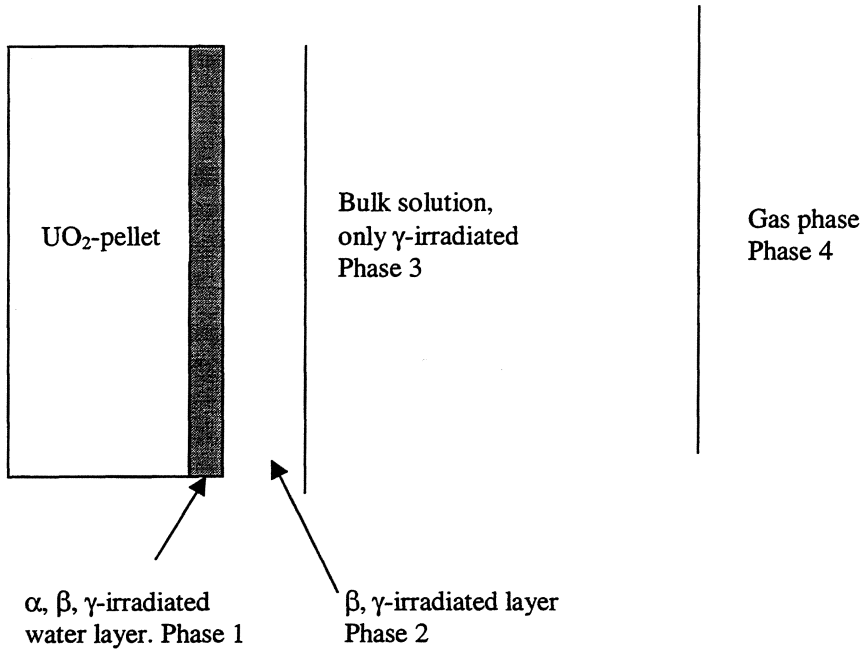

FIGURE IV.3-1: Phases considered in radiolysis model

Table IV.3-1 Irradiation conditions

Solution:	deionized water
pH:	initial 7, final 5.5-9.6, pH = 7.5 are used in calculations.
Temperature:	25°C.
Volumes:	200 ml solution; 250 ml gas; closed system.
UO_2-pellet:	7 g, d = 1 cm; V = 0.64 cm^3 (if ρ = 10.96), l = 0.82 cm. SA = 4.2 cm^2 (geometrical surface area).
Burn-up:	50 MWd/kg U (193 and 260 W/m), age about 2 y.

Dose rates, gy/h

	α	β	γ	Total
Phase 1	1400	8000	120	9520
Phase 2	0	2200	120	2320
Phase 3	0	0	80	80

These dose rates have been estimated, based on similar Swedish fuel (91ING/ELK). G-values: See TABLE 3, Appendix 9, separate values for phase 1 (14.7% α-radiation) and phase 2. The same G-values are applicable in phase 2 and phase 3.

Solubilities in H_2O, at 25ºC: H_2 $7.8 \cdot 10^{-4}$ mol/dm^3, O_2 $1.23 \cdot 10^{-3}$ mol·dm^{-3} (at 0.1 MPa).

Mechanism and rate constants: See TABLE 2, Appendix 9, UO_2 reactions with radiolytic species were only included in phase 1.

Diffusion of species between phases is accounted for by

Ficks law: $\frac{dn}{dt} = A \cdot D \cdot \frac{dc}{dx}$

Where A is the surface area and D the diffusion coefficient

$$\frac{dc}{dt} = \frac{1}{V} \cdot \frac{dn}{dt} = \frac{A \cdot D}{V} \cdot \frac{dc}{dx}$$

$V\ (Volume) = A \cdot l_i$; with l_i = thickness of inner phase

We assume steady state from phase 1 to phase 2 diffusion with a zero concentration boundary, hence $dx = l_o$ ($l$length of next phase) and $dc = c$.

$$\frac{dc}{dt} = \frac{A \cdot D}{V} \cdot \frac{dc}{dx} = \frac{A \cdot D \cdot C}{A \cdot l_i \cdot l_o} = \frac{D \cdot c}{l_i \cdot l_o}$$

TABLE IV.3-2 Parameter for diffusion of radiolytic species between adjacent phases

	l_i cm	l_o cm	H_2	O_2	H_2O_2
D, $cm^2 \cdot s^{-1}$			$6 \cdot 10^{-5}$	$2.5 \cdot 10^{-5}$	$1.9 \cdot 10^{-5}$
k (Phase 1 → Phase 2)	$5 \cdot 10^{-3}$	0.3	$4 \cdot 10^{-2}$	1.7·10-2	$1.3 \cdot 10^{-2}$
k (Phase 2 → Phase 3)	0.3	4.6	4.3·10-5	1.8·10-5	$1.4 \cdot 10^{-5}$

The mass transfer of gases from Phase 3 (bulk solution) to phase 4 (gas phase) is governed by the gas solubility, expressed in MAKSIMA chemist by the kinetic definition of solubility, i.e. by equal rates in forward and backward reaction.

	i	k_i s^{-1}
$H_2 \rightarrow H_2D$	(1)	100
$H_2D \rightarrow H_2$	(-1)	
$O_2 \rightarrow O_2D$	(2)	100
$O_2D \rightarrow O_2$	(-2)	

D denotes a species, which has diffused into another phase.

H2D is defined as H_2 (gas) $\cdot \frac{V_{gas}}{V_{liq}}$

k_1 and k_2 are set arbitrarily at 10^2 s^{-1} and . With these rate constants the back reaction rate constants k_{-1} and k_{-2} are fixed according to the Henry's law solubility equilibrium

$$k_1 \cdot H_2 = k_{-1} \cdot H_2D; \qquad k_1 \cdot \frac{H_2}{H_2D} = \frac{H_2}{H_2(gas)} \cdot \frac{V_{liq}}{V_{gas}}$$

V_{liq} = 200 ml, V_{gas} = 250 ml

For calculating $\frac{H_2}{H_2(gas)}$ we use for solubility (1 atm H_2) = $7.8 \cdot 10^{-4}$ mol·dm^{-3} (25°C)

The amount of H_2(gas) in a gas volume of 1 l is

$$H_2 \text{ (gas), 1 atm)} = \frac{1}{22{,}4} \cdot \frac{273}{298} = 4.09 \cdot 10^{-2} \text{ mol} \cdot \text{dm}^{-3}$$

$$k_{-1} = k_1 \cdot \frac{7.8 \cdot 10^{-4}}{4.09 \cdot 10^{-2}} \cdot \frac{200}{250} = 1.53\ s^{-1}$$

In a similar way, for the solubility of oxygen 25°C, 1 atm = $1.23 \cdot 10^{-3}$ mol · dm^{-3} we get

$$k_{-2} = 100 \cdot \frac{1.23 \cdot 10^{-3}}{4.09 \cdot 10^{-2}} \cdot \frac{200}{250} = 2.41\ s^{-1}$$

The species which diffuse from one phase to a second phase are added continuously to the second phase simmulated in MAKSIMA-CHEMIST by additional G-values:

Diffusion phase 1 → 2

$$G(D) = \frac{\text{number of molecules}}{100 \text{ eV}} = \frac{\Delta C \cdot 10^{-3} \cdot 6.02 \cdot 10^{23} \cdot 10^3 \cdot 10^2}{1.65 \cdot 10^{19} \cdot 100 \cdot 24 \cdot 3600} = \Delta C \cdot 0.422$$

ΔC is the increase in concentration (of diffusing species) in 100 d.

$$G(H_2) \text{ Phase 2} = G(H_2D) \cdot \frac{\text{Vol (Phase 1)}}{\text{Vol (Phase 2)}} =$$

$$\Delta C \cdot 0.422 \cdot \frac{2.13 \cdot 10^{-5}}{1.28 \cdot 10^{-3}} = \Delta C \cdot 7.03 \cdot 10^{-3}$$

Diffusion phase 2 → 3

$$G(D) = \frac{\Delta C \cdot 10^{-3} \cdot 6.02 \cdot 10^{23} \cdot 10^3 \cdot 10^2}{4.03 \cdot 10^{18} \cdot 100 \cdot 24 \cdot 3600} = \Delta C \cdot 1.728$$

$$G(H_2)\ \text{Phase 3} = G(H_2D) \cdot \frac{\text{Vol (Phase 2)}}{\text{Vol (Phase 3)}} = = \Delta C(D) \cdot 1.728 \cdot \frac{1.28 \cdot 10^{-3}}{0.2} = \Delta C(D) \cdot 1.106 \cdot 10^{-1}$$

Calculated diffusion controlled mass transfers are maximum values. Transient diffusion will yield lower flux from an inner to the outer phase. Also the accumulation of species in the outer phase is not considered explicitly. If the concentration in the outer phase became close to those in the inner phase diffusion rates will become lower. This was accounted for by adjusting the diffusion rate constants. Additional G-values due to diffusion are shown in TABLE 6, Appendix 9.

Calculation of corrosion rate, CR

$$CR = \Delta U(VI) \cdot 270 \cdot \frac{24}{h} \cdot V(H_2O) \cdot 10^6\ \mu g \cdot cm^{-2} \cdot d^{-1}$$

where $\Delta U(VI)$ is the increase in concentration of U(VI) species, mol/dm^3, h is irradiation time, in hour. V is volume of water (dm^3) per cm^2 UO_2.

If the range is assumed to be 30 μm as in previous α-radiolysis calculations then

$$CR = \Delta U(VI) \cdot 270 \cdot \frac{24}{h} \cdot 30\ 0.1 = \frac{\Delta U(VI)}{h} \cdot 1.944 \cdot 10^4\ \mu g \cdot cm^{-2} \cdot d^{-1}$$

With the results from calculation EU18 we obtain for example ΔUO_3D (200 d) $=\Delta U(VI)$ = 2.274 mol·dm^{-3}; h = 200 d = 4 800.

$$CR = 2.274 \cdot \frac{1{,}944 \cdot 10^4}{4800} = 9.2\ \mu g \cdot cm^{-2} \cdot d^{-1} = 92\ mg \cdot m^{-2} \cdot d^{-1}$$

The results of all calculations for deionized water are summarized in TABLE 7, Appendix 9. If the diffusion reactions of H_2, O_2, and H_2O_2 were removed in calculations of phase 1 (calculation No EU15), the final concentrations of hydrogen and UO_3D (UO_3 removed from the system) were both low, 2.3E-3 mol/dm^3, and the concentrations of O_2 and H_2O_2 were very low. This may be expected as high hydrogen concentrations lead to low radiolysis. (H_2 "protects" the water from radiolysis.) This effect is confirmed by our >1000 day corrosion experiments of spent fuel in the presence of iron (see.. where corrosion rates lower than $1.6 \cdot 10^{-9}$/d where achieved at final H_2 pressures of up to 2.7 bar. This demonstrates that the diffusion reactions are important if external pressures of H_2 are low. It was found necessary to reduce the original diffusion rate constants by a factor of 4 (EU 18). The results are shown in FIGURE IV.3-2.

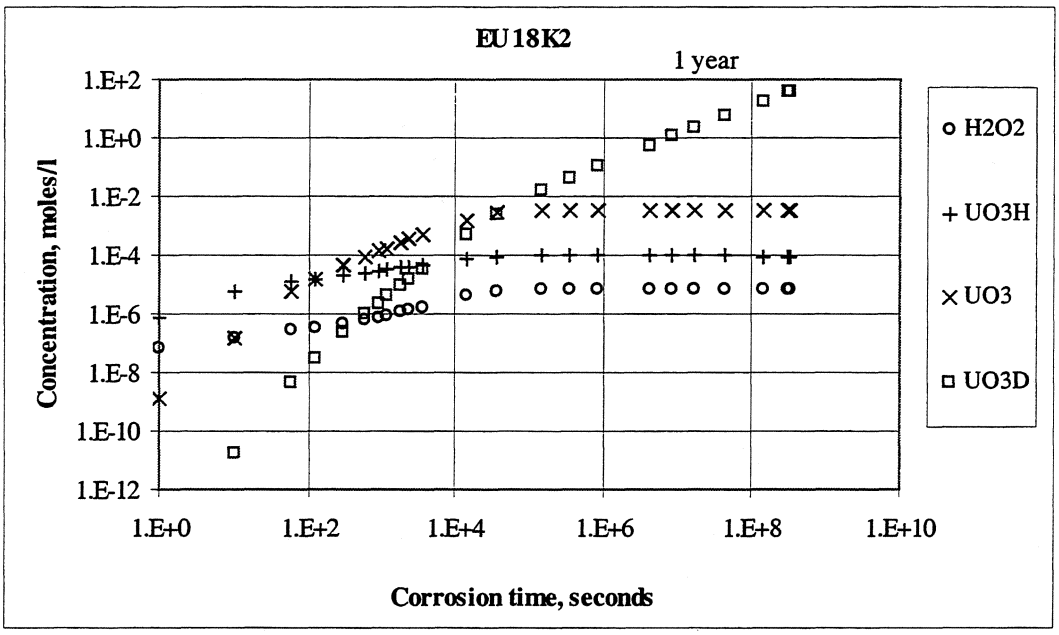

FIGURE IV.3-2 Radiolysis in phase 1 (surface layer with α,β,γ radiation). Deionized water. (Calculation EU18, Table 7, Appendix 9)

When this calculation was continued in phase 2 the results of EU19 were obtained. However, since the concentrations of O_2 and H_2O_2 were lower than found for phase 3 (EU20); diffusion of O_2 and H_2O_2 from phase 2 to phase 3 was not allowed in the a new phase 2 calculation (EU21). This calculation was then continued into phase 3, see EU22, TABLE 7, Appendix 9. It can be seen that stoichiometric amounts of H_2 and O_2 are transferred into the gas phase (H_2D and O_2D, respectively). The gas production rate of H_2 and O_2 were $1.2 \cdot 10^{-7}$ and $6 \cdot 10^{-8}$ mol/d, respectively. Radiolysis in phase 3 is very little affected by diffusion from phase 2, i e the gas is produced entirely in phase 3. (Apparently there is only a small reduction of gas yields in phase 3 due to a small diffusion of hydrogen from phase 2 to phase 3).

If it was assumed that the gas phase initially contained 0.1 atm of air due to a small air leakage ($2 \cdot 10^{-3}$ Mpa O_2), the mean gas production rates were $4.4 \cdot 10^{-7}$ and $2.1 \cdot 10^{-7}$ mol/d or $7 \cdot 10^{-8}$ and $3 \cdot 10^{-8}$ mol $\cdot$ g^{-1} d^{-1} for H_2 and O_2, respectively, see EU23, TABLE 7. The gas production was also increased if instead a small continuous leakage of air was assumed (about 1 cm^3/d).

In the experiments (96GRA/LOI) using a pellet (6.4 g U) in deionized water the gas production rates were $1.2 \cdot 10^{-7}$ and $9 \cdot 10^{-8}$ mol $(g\ U)^{-1} \cdot d^{-1}$ for hydrogen and oxygen, respectively. The alteration rate was $6.4 \cdot 10^{-9}$ mol UO_2 $g^{-1} \cdot d^{-1}$ (mean values, g refers to g U).

In the calculations the mean gas production rates were $1.2 \cdot 10^{-7}$ and $6 \cdot 10^{-8}$ mol/d for H_2 and O_2, respectively, corresponding to $2 \cdot 10^{-8}$ and $1 \cdot 10^{-8}$ $mol \cdot (gU)^{-1} \cdot d^{-1}$. Thus, the calculated production rates were lower than the experimental rates. Possible explanations for this discrepancy may be uncertainty in the dose rate, impurities in the aqueous solutions (pure water was assumed in the calculations), leakage of air, errors in the model.

The calculated corrosion rate was 92 $mg \cdot m^{-2} \cdot d^{-1}$ or $\frac{9.2 \cdot 10^{-6} \cdot 4.2}{270 \cdot 6.4} = 2.2 \cdot 10^{-8} \cdot mol \cdot g^{-1} \cdot d^{-1}$, about three times higher than the experimental

value ($6.4 \cdot 10^{-9}$ mol $(gU)^{-1}$ d^{-1}). Discrepancies may be associated to gas production rates and to simplifications in the calculations of diffusion controlled mass transfer (steady state).

In TABLE IV.3-3, a comparison between calculated and experimental results is shown.

TABLE IV.3-3 Comparison of experimental and calculated corrosion and gas production rates.

Solution	Corrosion rate			Gas production rates, mol·(gU)$^{-1}$·d^{-1}			
	calculated		experiment	calculated		experiment	
	μg·cm^{-2}·d^{-1}	mol·(gU)$^{-1}$·d^{-1}	mol·(gU)$^{-1}$·d^{-1}	H_2	O_2	H_2	O_2
5 M NaCl	9.6	$2.3 \cdot 10^{-8}$	$2.0 \cdot 10^{-9}$	$3 \cdot 10^{-6}$	$1.5 \cdot 10^{-6}$	$1.9 \cdot 10^{-7}$	$8.4 \cdot 10^{-8}$
Deionized water	9.2	$2.2 \cdot 10^{-8}$	$6.4 \cdot 10^{-9}$	$2 \cdot 10^{-8}$	$1 \cdot 10^{-8}$	$1.2 \cdot 19^{-7}$	$9 \cdot 10^{-8}$

Spent fuel oxidation and dissolution in 5 m NaCl solutions

The experimental details in the spent fuel corrosion experiments in NaCl solutions form the previous EU-project [96GRA/LOI, 95LOI/GRA] and their results are given in TABLE 5, Appendix 9. The results of the initial calculations, using the G values from deionized are shown in TABLE 8, Appendix 9. It can be seen that a slightly higher corrosion rate has been calculated for UO_2 in salt solutions compared with UO_2 in deionized solutions. This is in contradiction with the experimental results. Also, the calculated corrosion rate is about 10 times higher than the experimental value.

The introduction of the G values of Kelm and Bohnert [98KEL/BOH1, 98KEL/BOH2], see TABLE 9, EU125 resulted in a rather large increase in corrosion rate, from 96 to 14.3 μg·cm^{-2}·d^{-1}. In their experiments on α-radiolysis of concentrated NaCl solutions, Kelm and Bohnert (98KEL/BOH2) introduced a set of primary G values with $ClOH^-$ (from Cl^- + OH) and Cl^-_3 (from Cl^{2-} + Cl_2^-) as primary products, formed in the spur due to the high Cl^- concentration. Some further calculations were carried out to simulate the experiments by Giménez et al. (96GIM/BAR), where the corrosion of UO_2 from ClO^- in unirradiated solutions was studied. By further decreasing the rate constant for RE35 and 45 (reactions of HClO with UO_2 and UO_3H) a better agreement between calculated and experimental corrosion rates were obtained: 0.56 and 0.52 μg · cm^{-2} · d^{-1}, respectively. k_{38} and k_{45} were decreased to 4 E-3 from the previous value: 1 E-2. The resulting file is shown in TABLE 2, Appendix 9.

However, a change of these rate constants did not change the corrosion rate in the present calculations (spent fuel leaching), see TABLE 8, Appendix 9 (EU129) and FIGURE 4. A large decrease in the rate constants for reactions of Cl_2^- with UO_2 and UO_3H, RE37 and RE44, respectively, decreased the corrosion rate, see EU130-134. The real values of these rate constants are not known, initially they were taken to be the same as for similar reactions of the OH radical, which is a reasonable assumption. More experimental spent fuel leaching results are needed in order to have confidence in such a large change of the rate constants as used here in the final calculations (EU130-134).

The use of Kelm's G-values resulted in a large increase in the yield of $HClO_3$ and other chlorine-containing species. The hydrogen concentration increased only little, from 3.0 E-4 to 3.6E-4 mol·dm^{-3}.

Small adjustments of k_{69} and k_{72}, resulted in calculated yields close to the experimental yields of Kelm and Bohnert [98KEL/BOH1] TABLE IV.3-4,

TABLE IV.3-4 Comparison of experimental and calculated yields.

	H_2	O_2	$HClO_3$
Experimental G-values[9]	0.46	0.16	0.074
Calculated G-values EU123	0.60	0.18	0.082
Calculated G-values[12]	0.50	0.25	-0

In the previous calculation $G(HClO_3)$ was close to 0. Thus, as pointed out earlier (97CHR/PET), the calculated gas production is much higher than found in the spent fuel leaching experiments (95LOI/GRA). Also, the experimental gas yields of Kelm and Bohnert (98KEL/BOH1) are much higher than those found in the spent fuel leaching experiments (95LOI/GRA). In FIGURE 5 the results of radiolysis in phase 3 are shown.

Spent fuel corrosion at longer times (4 - 5 y)

Long-term corrosion experiments of spent fuel in salt brines and deionized water were started during the previous EU-programme and the 5th samplings were taken in the present project on Dec 12, 1996 and March 13, 1997 for leaching in deionized water and in 5 m NaCl-solutions, respectively. The uranium concentration in 156 ml deionized water after leaching for 1091 d (cumulative time 1604 d) was 0.0257 μg/ml. In 155 ml 5 m NaCl-solution the uranium concentration was 0.357 μg/ml after leaching for 1183 d (cumulative time 1697 d). This would correspond to corrosion rates of 2.10^{-12} mol (g U)$^{-1}$ d^{-1} and $2.71 \cdot 10^{-11}$ mol (g U)$^{-1}$ d^{-1} for deionized water and 5 m NaCl-solutions, respectively. The values are several order of magnitudes lower than the rates measured after 200 – 400 d. (6.3 E-9 and $2.0 \cdot 10^{-9}$ mol (g U)$^{-1}$ d^{-1}, respectively). Our previous calculations, carried out for shorter leaching times have been extended to 10 years of leaching. The results at various leaching times are shown in TABLE 9, Appendix 9.

It can be seen that in the calculations the corrosion rate does not change with time, see TABLE 9, Appendix 9 and FIGURES 2-5. One error source is the uncertainty in the dose rate: The calculations are based on calculated dose rates for similar Swedish fuel (γ-dose rate 80 Gy/h) whereas, the measured contact dose rate is about 400 times lower. Therefore, a reevaluation of the dose rates in the experiments would be very helpful in future modelling work. Such a reevaluation has been initiated in Germany. When the results appear a possible effect on the calculated corrosion results may be evaluated. In the previous calculations the corrosion has been assumed to be caused by radiolysis in the α-irradiated water layer (30 μm). However, the dose rate in this layer is so high that the diffusion length of the radicals will be lower than 30 μm. This is the case for OH-radicals and probably also for Cl_2^- radicals. As a result the calculated corrosion rate should be lower. If the UO_2 surface is partly covered with a porous Schoepite layer – with a lower dose rate – the "active" water layer will decrease and/or be irradiated with a lower dose rate. This will also result in a lower calculated corrosion rate. These effects should be implemented in the model in future studies.

The gas production in deionized water ceased after about 10^6 s, i.e. after about 10-20 d. Consequently a steady state was obtained, see FIGURE 3 in Appendix 9. In 5 m NaCl solutions the gas production continued with the same rate as at shorter times, see FIGURE 5.

One error source in the calculated gas production may be the fact that we assume idealized conditions. In the experiments with DI water impurities may be present. These will increase the yields, as found in the experiments. In 5 m NaCl solutions no steady state is obtained in accordance with experiments. Our calculated G values are close to the experimental G values found by Manfred Kelm by irradiation of 5 m NaCl solutions (in the absence of UO_2). But the calculated gas yield is higher than that found in the leaching experiments.

Conclusions on radiolysis modelling

In deionized water the calculated gas generation rates were $2 \cdot 10^{-8}$ mol $(gU)^{-1} \cdot d^{-1}$ for hydrogen and oxygen, respectively, 6-10 times lower than the experimental values. The calculated fuel alteration rate was $2.2 \cdot 10^{-8}$ mol $UO_2 \cdot (gU)^{-1} \cdot d^{-1}$, or 92 $mg \cdot m^{-2} \cdot d^{-1}$, about three times higher than the experimental rate. Excess hydrogen decreased both fuel alteration and gas generation rates. Excess oxygen increased gas generation rates.

In 5 m NaCl solutions the calculated gas generation rates were higher than the experimental values. The gas generation continued with the same rate for the whole calculation period (5 y) corresponding to G values of 0.60 and 0.18 for hydrogen and oxygen, respectively. The calculated fuel alteration (= corrosion) rate was 96 $mg \cdot m^{-2} \cdot d^{-1}$ before introduction of the primary G-values determined by Kelm and Bohnert. After introduction of these G-values the rate was 143 $mg \cdot m^{-2} \cdot d^{-1}$. Both values are higher than the experimental value (about 10 times).

The fuel oxidation is caused only by water radiolysis in the thin α-irradiated layer. The gas is produced almost entirely in the gamma-irradiated bulk water. Diffusion of gases from the thin α-irradiated layer is decisive for the magnitude of the UO_2 oxidation and dissolution. If diffusion is neglected hydrogen is built up in the thin water layer. This results in a considerably reduced corrosion rate of UO_2.

WP IV.4 SOURCE TERM DEVELOPMENT

It is convenient to relate the release of radionuclides to their inventory in the fuel The total inventory I_{SF} of a given nuclide at time t is given by

$$I_{SF}(t)=I_{UO2}(t)+I_{GB}(t)+I_{Z}(t)+I_{st}(t)+I_{G}(t)$$

where I denotes the inventory of a given nuclide, the indices SF, UO2, GB, G, Z and R denote the entire spent fuel element (SF), the UO2 matrix, the grain boundary inventory (GB), the Zircaloy (Z), G indicates the gap inventory and radionuclide fractions of fracture surfaces, and ST denotes radionuclide fractions in the structural parts of the fuel elements.

The total cumulative release Q of a nuclide i at time t is given by the following equation

$$Q_i = I_{BE,i} \cdot IRF_i + \int_{to}^{t} r_{+(UO2)} I_{UO2,i}(t)\,dt + \int_{to}^{t} r_{+(Z)} I_{Z,i}(t)\,dt + \int_{to}^{t} r_{+(St)} I_{St,i}(t)\,dt$$

where IRF denotes the instant release fraction (see below) and r+ denotes respective dissolution rates of fuel matrix, Zircaloy and structural parts.

Instant release fractions

The instant release particularly of I129 and Cs135 is known form current safety analyses of repositories to dominate the toxicity of radionuclide release for a spent fuel repository for thousands of years. The instant release fraction (IRF), is considered as labile radionuclide fraction to be released instantaneously upon water contact to the fuel. It is given by the equation

$$IRF=(I_Z \cdot f_Z + I_{GB} + I_G)/I_{SF}$$

where f_Z denotes the fraction of the radionuclide inventory of the cladding to be mobilized instantaneously. Instant is considered everything, which dissolves faster than the fuel matrix. This operative definition avoids individual quantification of I_Z, I_{GB} and I_G. An exception is Kr85, which might be released from the gap and fracture surfaces, even in the absence of water. According to this operative definition, even radionuclide inventories in metallic inclusions (Pd, Ru, Rh, Tc, and Mo) are considered as part of the IRF, if they are leached faster than the fuel matrix. On the other hand, fuel dissolution experiments in salt brines have shown release of Ru being controlled by the fuel matrix. Similar behaviour might be expected for Tc.

IRF values can be obtained directly from experiments with powdered fuel with a particle sized <3 µm.. FIGURE IV.4-1 shows the data for determining IRF values for Cs135 as an example. Experimental IRF values for other elements are included in table IV.4-1. The assumption is made that Cs137 data are representative for Cs135. Instant release fractions of Cs from experiments with powders and with pellets are compared. In all experiments the cladding was present. In the experiments with fuel powders, all grain boundary surfaces were accessible to water, allowing immediate release of the sum of gap and grain boundary inventories. The result is an IRF value of about 4%. Additionally to this instant release, there is a slower long-term release of Cs from the fuel powder. It can be shown by comparison to Sr-release (see FIGURE III.1-4 for example) and to fission gas release data, that this slow release results from fuel matrix dissolution. In the experiments with fuel powder, it takes much longer time until a release value of 4% of the Cs-inventory is obtained. The reason is that the grain boundary release is much slower with pellets than with powders. There is also a temperature dependency. At 150°C the value of 4% is achieved in about 100 days, whereas at 25°C 4 years were necessary. This result is surprising because it is known that in the dry state, fission gas bubbles may be entrapped at grain boundaries at very high pressures. Initially it was speculated that this result is specific the high power fuel (260 W/m) but the results were confirmed in the German spent fuel research project with another fuel with only 33 MWd/kgU and lower linear power rating. This means that in aqueous solutions, another grain boundary release mechanism is prevailing. The high rate of grain boundary wash out makes it useless to distinguish between gap and grain boundary release for IRF quantification. The observe IRF values of up to 4% are high (conservative) when compared to release data from the fuels studied in WP I.3 and WPIII.3. The reason for the higher values is probably the high linear power rating of the fuel used in the powder dissolution tests. Indeed, data from the Canadian research project with high temperature CANDU fuel show even higher IRF values.

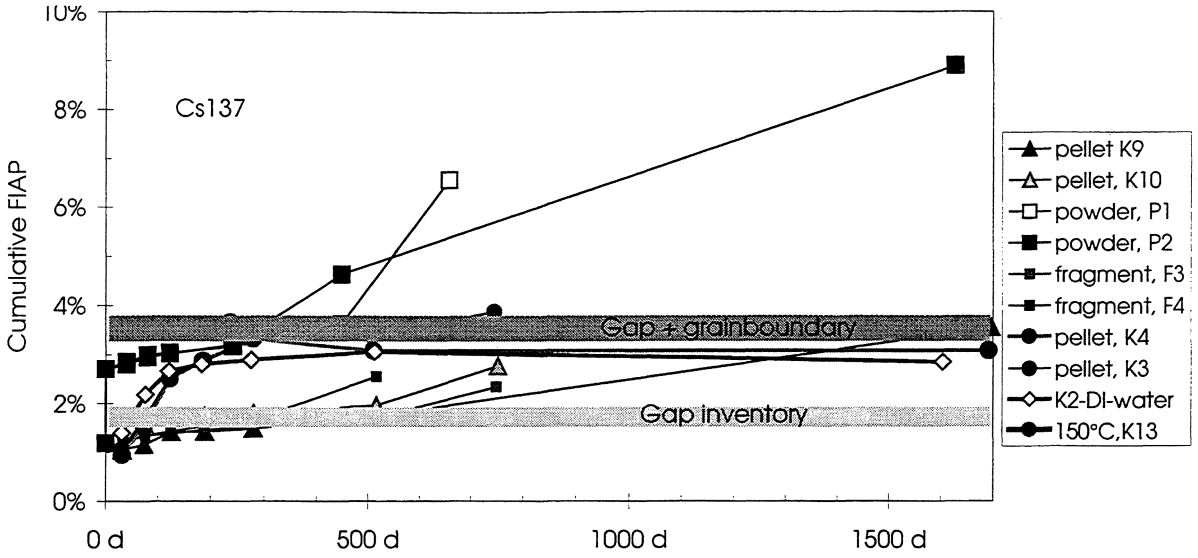

FIGURE IV.4-1: Cs release data from high burnup fuel powders and pellets to determine gap and grain boundary inventories

TABLE IV.4-1: IRF values based on initial powder dissolution test results in NaCl solution **(Gösgen** Reactor, **50 GWd/tHM, 260 W/m).**

Nuclide	IRF [%]	Nuclide	[IRF]
Cs134/137	3-4	Ce144	0.006
Sr90	0.07	Eu154/155	0.01
Tc99	0.003	U	0.02
Ru106	0.01	Sb125	0.1
Am241	0.006	Ag110m	0.3
Pu238/239	0.005		

Fuel matrix dissolution: interactions with environmental materials and reaction path

The elements released by the fuel were distributed among the aqueous phase, the environmental materials, possible precipitates and species sorbed on the leaching pot walls. At this point in the study it is impossible to model the accumulation of these elements in the aqueous phase because of the large number of parameters involved.

For a much simpler – or even simplistic – system, however, it can be shown that the concentration of element *M* in solution C_M depends at least on its complexation in solution, on the solubility product K_s of a precipitated phase *MX* and on its distribution coefficient *CKD* with a geological phase *MY*.

The concentration [*M*] of the aquo ion of *M* is related to C_M by the following relation:

$$[M] = \alpha C_M$$

where α includes the aquo ion complexation and hydrolysis constants. Moreover, omitting the charges to simplify the relation:

$$MX \leftrightarrow M + X \quad Ks$$

$$M + Y \leftrightarrow MY \quad Ke$$

$$Kd = \frac{V}{C_M} \cdot \frac{[MY]}{m_{MY}} = \frac{V}{\alpha[M]}$$

where V is the solution volume and m_{MY} is the mass of the geological phase MY.

If Q is the quantity of element M released by the fuel, and M_{MX} the quantity of precipitate MX, then:

$$Q = m_{MX} + V \cdot C_M + M_{MY}[MY]$$

hence:

$$[M] = F(\alpha, Q, M_{MX}, Ke, CKD, Ks)$$

FIGURE IV.4-2 is a schematic representation of the spent fuel alteration mechanisms, assuming that radiolysis of the water results in oxidizing conditions at the spent fuel leachate interface. The diagram shows the mechanisms controlling the radionuclide concentrations in solution, notably in the presence of environmental materials. In principle, all of these reactions could be modeled by geochemical reaction path calculations; However, many parameters, particularly those to surface complexation are unknown.

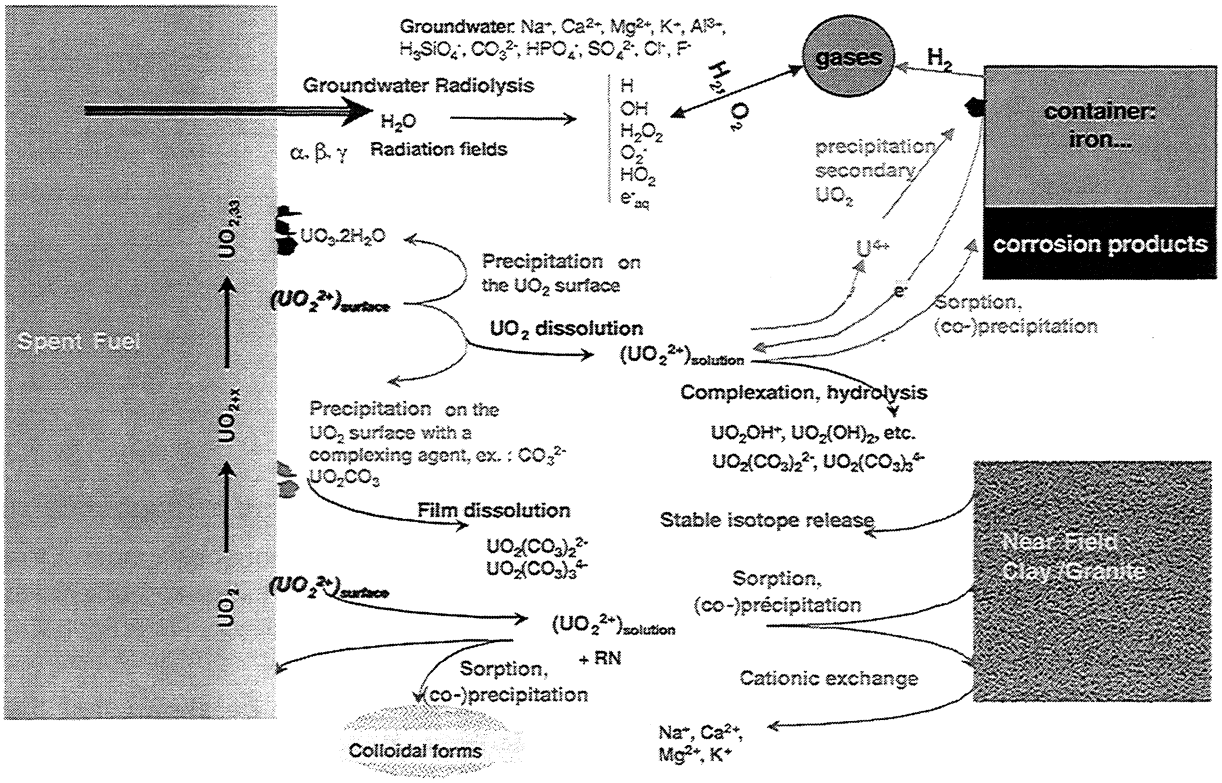

FIGURE IV.4-2. **Spent fuel alteration mechanisms and mechanisms controlling radionuclide concentration in solution in presence of environmental materials**

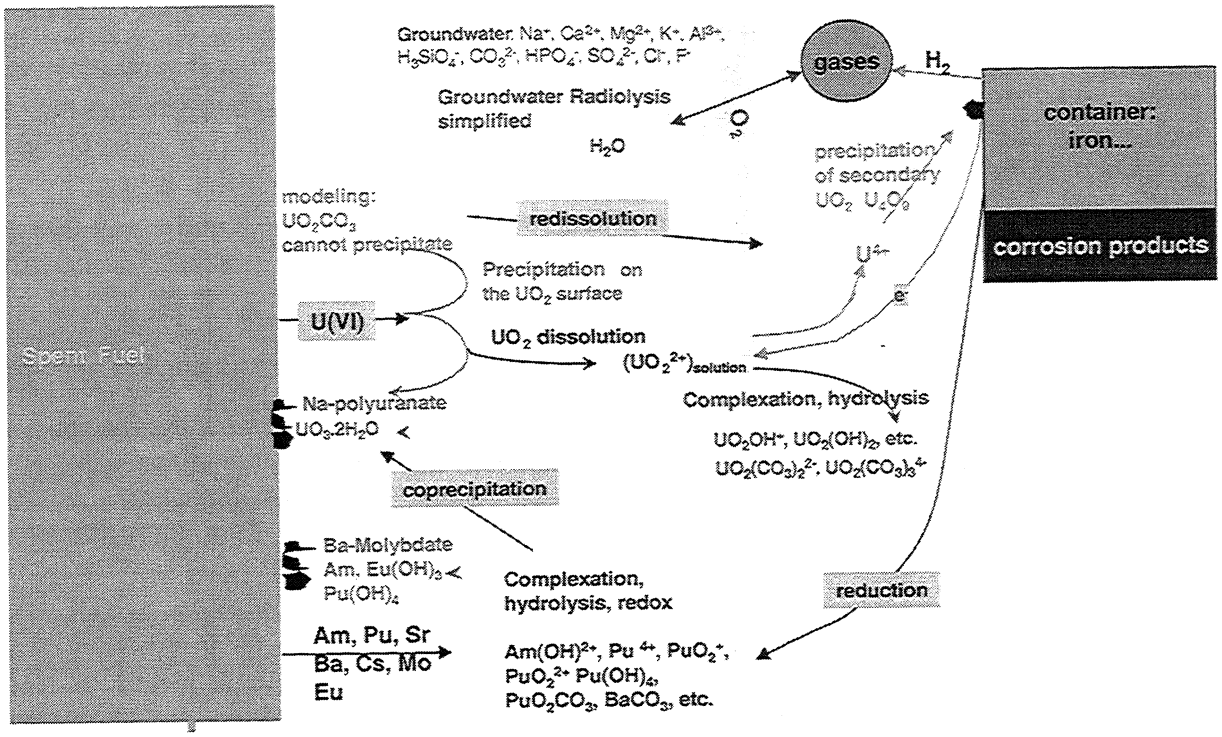

FIGURE IV.4-3. **Simplified Spent fuel alteration mechanisms for reaction path modelling**

A simplified version of FIGURE IV.4-2 is shown in FIGURE IV.4-3. This simplified reaction scheme is still quite complicated, but it can be modeled with current geochemical codes (EQ3/6). Thus, the next step in reaction path modelling was to include the release properties of actinides and fission products and to associate reaction path with time by using measured reaction rates under oxidizing conditions of 2 mg/(m^2d). The effect of radiolysis was considered by simulating the stepwise addition of oxygen as a reactant to the system. Also the co-dissolution of iron was considered, using a corrosion rate of 100 µm/a. The release of radionuclides with the dissolving fuel matrix was simulated by calculating the effect of a stepwise addition of a simplified mixture of UO_2 and selected radionuclides to an air saturated saline solution. Radionuclides considered simultaneously are Am, U, Pu, Sr, Cs and Eu. The used fuel inventories of Eu were higher than in real fuel, to represent the other inactive rare earth elements. Additional non-radioactive elements considered were Ba and Mo. Activity coefficients were calculated by using the Pitzer theory with the EQ3/6 geochemical code. References for the used thermodynamic data for aqueous actinide chemistry where as follows: interaction coefficient of Am from [98FAN/KÖN], interaction coefficients for Eu and trivalent Pu were considered to be similar than those of Am. Hydrolysis and complexation data for Am where taken from [97NEA]. Hydrolysis and complexation data and interaction coefficients for U and Pu were the same as those used in the previous EU project [97GRA/LOI]. Data for molybdate where taken from [91GRA/MÜL]. Interaction coefficients for Sr and Cs where taken from [89PIT]. Ideal solid solution formation was considered both for hydroxides/uranate (End members: schoepite, Na-polyuranate, $Sr(OH)_2$, $REE(OH)_3$, $Am(OH)_3$), and for molybdate (End members: $BaMoO_4$, $NaAm(MoO_4)_2$, $NaEu(MoO_4)_2$.). Two kinds of calculations were performed with different rates of radiolytic oxidant generation: the measured rate of oxygen generation under anaerobe conditions in the absence of iron (FIGURE IV.4-4), and an oxygen generation rate which is a factor of 100 reduced to represent fuel of about 200 yr. of radioactive decay prior to water access (FIGURE IV.4-5).

The results show that under conditions of immediate water contact radiolytic oxygen generation (gamma) would dominate over the reducing effect of canister corrosion, while for

200 yrs old fuel the reducing effect of iron corrosion dominates. This is somewhat surprising as in the experiments of this project (WPIII.1) iron corrosion was sufficient to consume the generated oxidants. The reason for this discrepancy is that in experiments the ratio of the surface area of iron powders to the fuel mass of about 10 cm^2/g(fuel) is much higher than in expected in reality, 0.02cm^2/g(fuel). If this ratio is high, oxygen consumption by iron corrosion may become faster than oxygen generation by gamma radiolysis.

Due to the different pH and Eh evolution, results for immediate water contact and 200 yr. data differ substantially. In the case of early water access, the pH is predicted to become very low, leading to high radionuclide solubilities. Main reaction products are molybdate and Na-polyuranates. In contrast, for late water access very low radionuclide concentrations are predicted. These data show the importance of the strongly non-linear coupling between spent fuel dissolution and actinide solubility, particularly in salt solutions. More specific experiments are necessary to validate the divers synergism predicted by modelling. In particular, the coupling of the rate of fuel dissolution with the rate of iron corrosion is predicted to play a strong role in overall spent fuel behaviour. The experiments of the present project provide valuable information in this regard, but they do not allow to quantify this effect for repository relevant conditions.

The solid solution model includes both Na-polyuranate and schoepite as end members. As shown by [98DIA/GRA] this allows to predict the variation of Na/U ratio in the secondary phases as the function of environmental conditions. Application of this model to NaCl solutions yields a mole fraction of 0.26 for schoepite and 0.74 for Na polyuranate. In contrast, in granite water very low Na/U ratios are predicted.

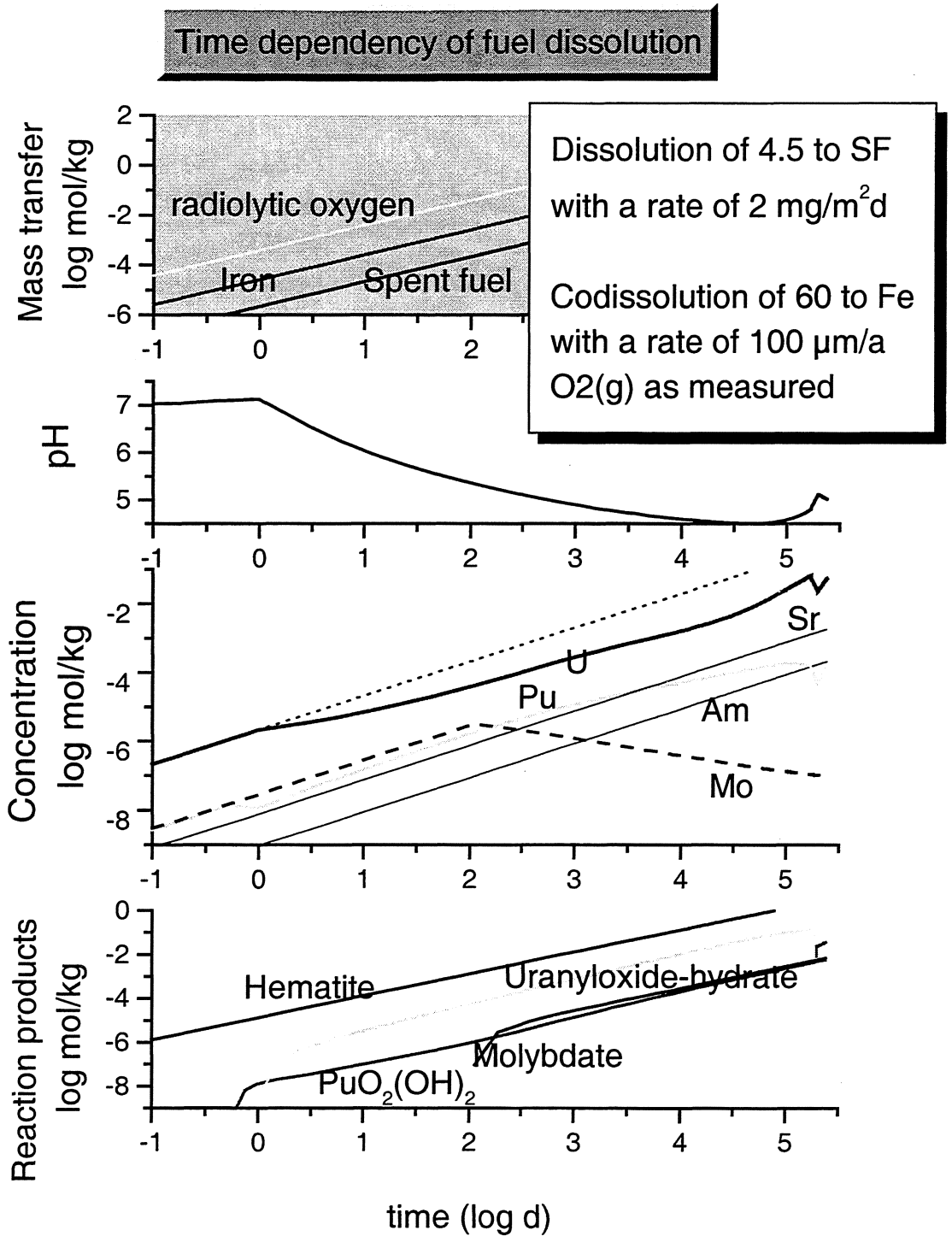

FIGURE IV.4-4: Time dependency for the reaction path of spent fuel in 95% saturated NaCl solutions, radiolytic oxygen is introduced in the reaction simulations by mass transfer rates similar as observed experimentally. No decrease in radiolytic oxygen generation due to decay is considered. Also it is assumed that spent fuel corrosion rates remain constant at high oxic rates. Experiments show that spent fuel corrosion rates generally decrease with time. As a consequence, the calculation yields strongly over-conservative radionuclide releases not yet applicable to the repository.

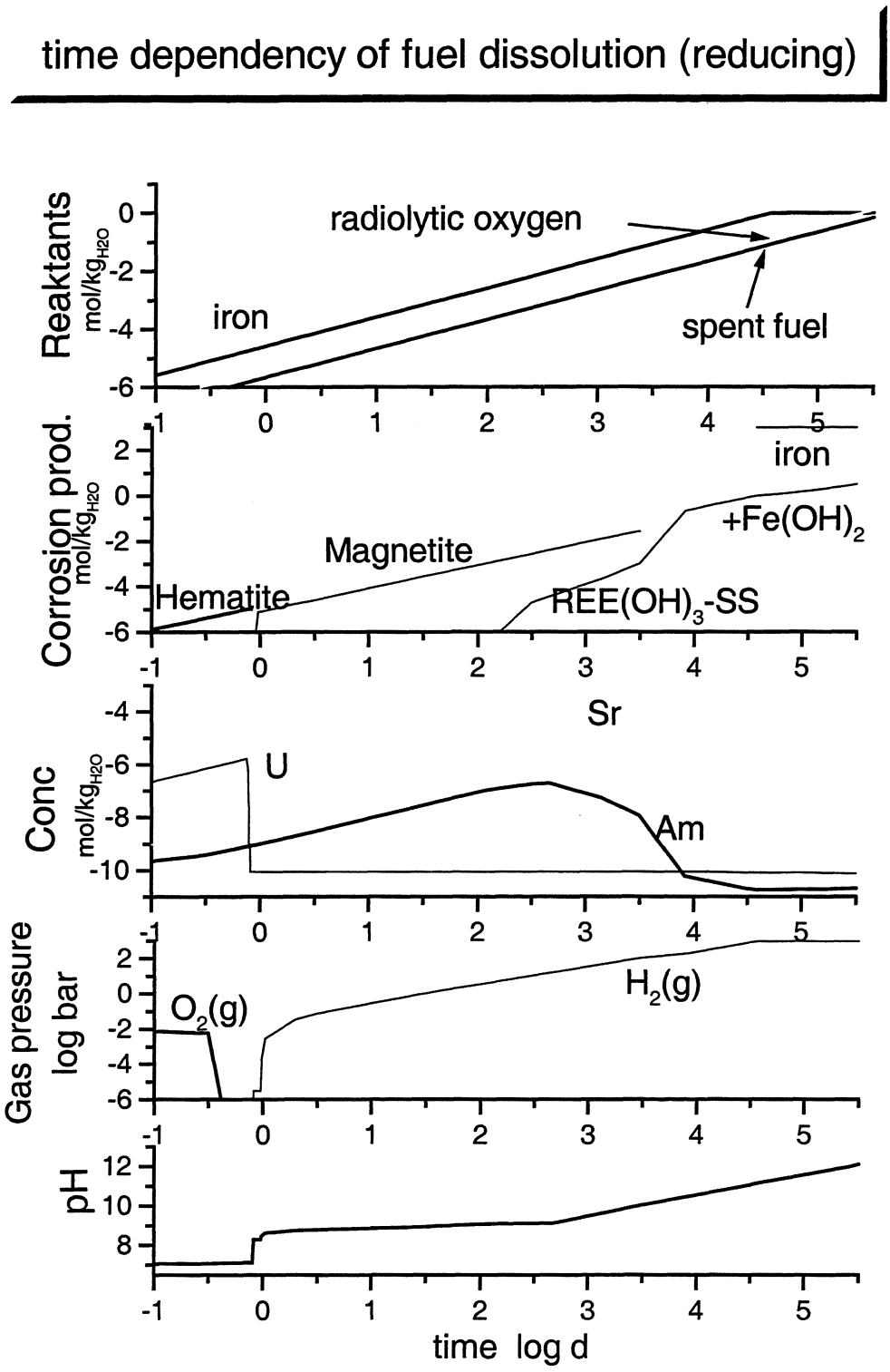

FIGURE IV.4-5: Time dependency of the reaction path for dissolution of spent fuel in 95% saturated NaCl solution at 25°C. Radiolytic oxygen generation is considered to be a factor of 100 lower than experimentally observed, to represent 200 yr. old fuel. The decay of the radiation field is not considered in the model. Also it is assumed that spent fuel corrosion rates remain constant at high oxic rates. Experiments show that spent fuel corrosion rates generally decrease with time. As a consequence, the calculation yields strongly over-conservative radionuclide releases not yet applicable to the repository.

Fuel matrix dissolution rates

The results of electro-geochemical modelling allow to define redox sensitive rate regimes in an Eh-pH- Pourbaix type diagram, to allow orientation for various geochemical settings in disposal location design. FIGURE IV.4-6 shows examples for (a) HCO3 free and (b) HCO3=0.01 m solutions.

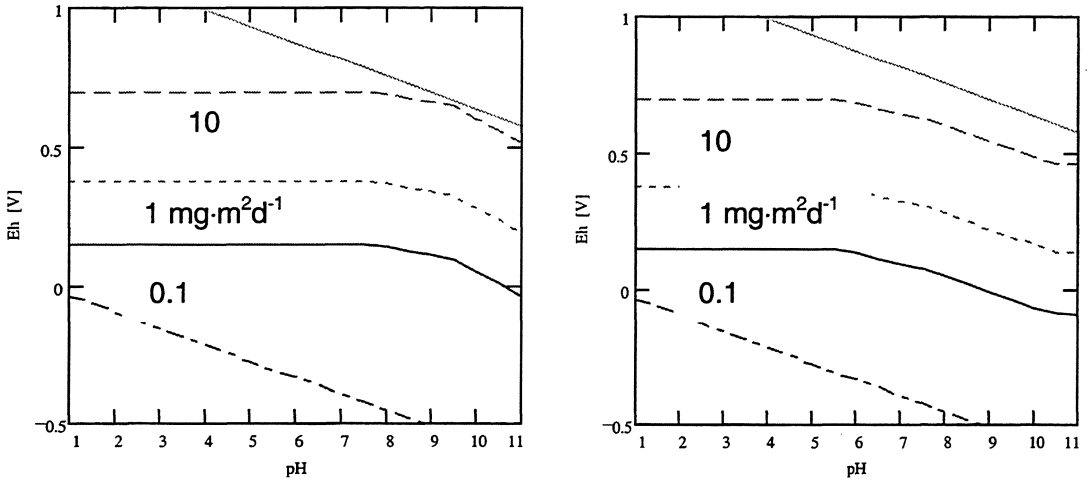

FIGURE IV.4-6: Isolines for equal corrosion rates of UO_2 in Eh-pH-space, (a) in the absence and (b) presence of 0.01 m carbonate

Using the electro-geochemical model described above, electrochemical governed dissolution rates for UO_2 can be compared directly with solubility controlled dissolution rates assumed to be the rate control under reducing conditions. Using a very conservative solubility for UO_2 under reducing conditions of 10^{-7}m, and assuming a hypothetical groundwater flow rate of 1 m^3/yr/canister, the times were calculated, necessary to dissolve 5 tons of spent fuel in a canister (life time). This lifetime is compared with the lifetime calculated for the oxidative (electrochemical) dissolution. For this purpose, surface area normalized reaction rates are converted to fractional dissolution rates using a specific surface area of 7cm^2/g (surface roughness factor of 3 included). Two ranges of solubility control were distinguished. For Eh values higher than the stability field boundary for U_3O_7 with respect of U(VI) containing phases such as schoepite, the fuel matrix is not stable and oxidative (electrochemical) dissolution prevails. In contrast, for more reducing conditions, the fuel matrix could become thermodynamically stable. Under these conditions, the electrochemical (oxidative) dissolution rate law rests valid, as long as U(VI) species remain to be the dominant solution species. Results from WP I.4 show that particularly in the presence of carbonate, U(VI) species rests important even under relatively strong reducing conditions. Under these conditions, solubility-controlled release and electrochemically controlled releases are sequential reaction, indicating that the slowest reaction step is rate controlling. If the release rate for solubility controlled release is faster than the release by electrochemical means, this means that solubility is never reached. The results are illustrated in FIGURE IV.4-7 both for solutions in the absence of carbonate and in the presence of high (0.01m) total dissolved carbonate contents. A conclusion from this diagram would be that for the expected reducing conditions of European repositories with Eh values lower than 200 mV the carbonate concentration should have no major influence of the long term fuel stability. The predicted long term stability of 10^8 years of lifetime under these conditions is not recommended yet to be used for

performance assessment studies, because it needs to be assured that there are no side reactions leading to faster corrosion rates. Examples for potential side reactions are the formation of secondary phases such as coffinite or the adsorption on iron or iron corrosion products stability which might lead to pump effects, causing the fuel to dissolve at the expense of sorption or coffinite formation. Results of the present study show that the adsorption on iron or the formation of secondary phases do not interfere with the strongly positive effect of reducing conditions on fuel long-term but slow reactions may be undetectable experimentally, though they might be important in the long-term.

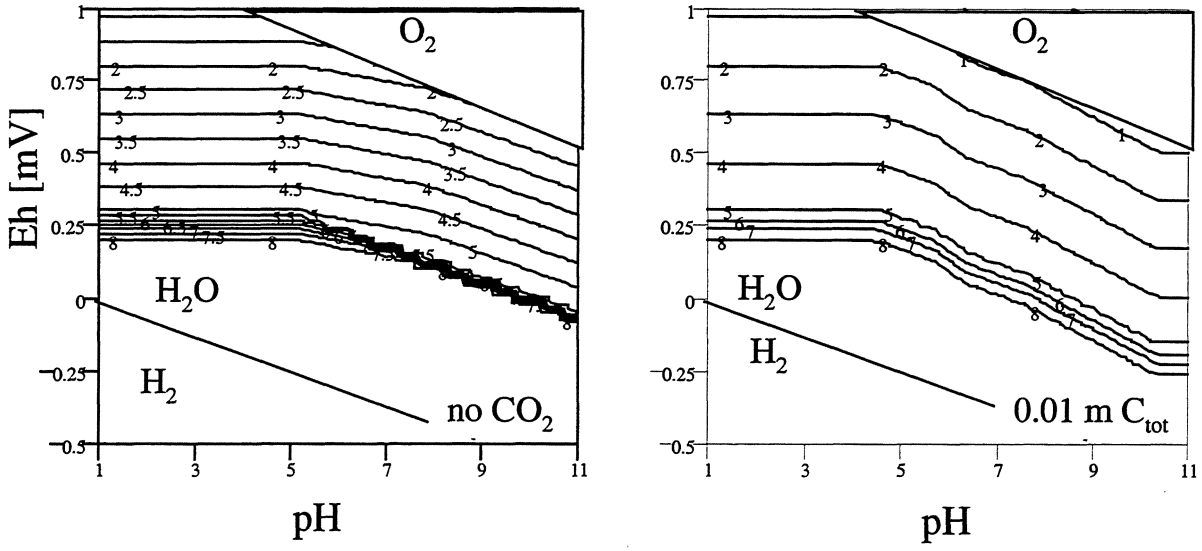

FIGURE IV.4-7: Estimated times (log yr.) necessary for the complete dissolution of a container with 5 tons of spent fuel in groundwater flowing with a hypothetical rate of 1 m^3/yr/canister. Transition from electrochemical (oxic) rate control to solubility control under reducing conditions. Comparison of results with and without carbonate

The results of this and the previous EU-project are going to be used by INE-FZK in Germany to formulate a site-specific source term for spent fuel performance in the Gorleben salt dome. Generic aspects of this source term are of relevance for the present EU-project:

High burn-up /high linear power fuel dissolution data are considered as conservative reference data for all types of LWR-UOX-fuel and WWER fuel.

Instant release data for high burnup fuel were reevaluated. The grain boundary inventories will be leached from full sized pellets in less than 4 years, even at 25°C. At 150°C few 100 days are necessary to wash out grain boundary inventories, and in powdered fuel, grain boundary inventories are leached instantaneously. Grain boundary inventories are leached faster in presence of metallic iron (container) than in its absence. This is probably caused by smaller quantities of solid reaction products formed under reducing conditions. Grain boundary release is faster than expected by diffusion control. The driving mechanism may be the formation of radiolysis gas bubbles in wetted grain boundaries.

Consequently, for long-term performance assessment, grain boundary inventories and gap inventories have to be considered together as an instant release fraction (IRF). IRF-values for Cs were 4% of the fuel inventory, for J129 3% is used. Instant release fractions for actinides were as low as 0.01%.

Two types of matrix dissolution rate regimes are formulated: dissolution rates under anoxic conditions were 10^{-4}/a whereas dissolution rates under reducing conditions are expected to be10^{-6}/a. Due to model uncertainty, no radiolysis model is yet formulated for the transition between anoxic and reducing conditions. Instead, transition between the two dissolution modes is based on container corrosion and parameters depending on site and packaging concepts. For example, with the concept of a Pollux container (65 t Fe), reducing conditions are expected to be maintained throughout the lifetime of the container.

The fuel cladding is expected to become corroded by a rate of 0.002/a (salt brines, see WP I.8) and radionuclide inventories are expected to be release by this rate. The cladding is expected to be defected instantaneously.

Empirical upper limits for radionuclide release may be formulated on the basis of coprecipitation experiments.

REFERENCES

[57ARO/ROO] Aronson S., Roof Jr. R.B. and Belle J. (1957) Kinetic study of the oxidation of uranium dioxide. J. Chem. Phys. 27, 137-144.

[57STE/GEA] M. Stern, A. L. Geary, J. Electrochem. Soc. **104** (1957) 56

[70EPE/KED] I. Epelboin, M. Keddam, J. Electrochem. Soc. **117** (1970) 1052

[70SLU/REH] M. Sluyters-Rehbach, J. H. Rehbach, Electroanal. Chem. **4** (1970) 1

[72EPP/KED] I. Eppelboin, M. Keddam, H. Takenouti, J. Appl. Electrochem. **2** (1972) 71

[73HAR/POM] J. E. Harrar, C. L. Pomernacki, Anal. Chem. **45** (1973) 57

[73MAN] F. Mansfeld, Corrosion-NACE **29** (1973) 397

[75NIC/NEE] M. J. Nicol, C. R. S. Needes, Radiochimica Acta **20** (1975) 585

[76GRA] Grandstaff D.E. (1976) A kinetic study of the dissolution of uraninite. Economic Geology 8, 1493-1506.

[78LAN] Langmuir D. /1978/, Uranium solution-mineral equilibria at low temperatures with applications to sedimentary ore deposits. Geochimica et Cosmochimica Acta 42, pp. 547-569.

[78MAC1] D. D. Macdonald, J. Electrochem. Soc. **125** (1978) 1443

[78MAC2] D. D. Macdonald, J. Electrochem. Soc. **125** (1978) 1977

[79CAR/HAN] M. B. Carver, D. V. Hanley. And K. R. Chaplin MAKSIMA-CHEMIST: A Programme for Mass Action Kinetics Simulation by Automatic Chemical Equation Manipulation and Integration Using Stiff Techniques. AECL-6413, Atomic Energy of Canada Ltd. (1979).

[79DIM/SET] Dimmock N. A., Settle C. and Webber H. M. /1979/, The use of ferrozine for the absorptiometric determination of iron in boiler-feed water, Laboratory note no RD/L/N41/79, Central Electricity Research Laboratories.

[79HIS] Hiskey J.B.(1979) Kinetics of uranium dioxide dissolution in ammonium carbonate. Trans. Inst. Nin. Metall. Sect. C, 88, C145-C152.

[81ALL/LAR] Allard B., Larson S. A., Albinsson Y., Tullborg E. L., Karlsson M., Andersson K. and Torstenfelt B. Minerals and precipitates in fractures and their effects on the retention of radionuclides in crystalline rocks. In: Near-Field Phenomena in Geologic Repositories for Radioactive Waste, Seattle, United States, USA: NEA Workshop Proc. pp. 93-101. ISBN 92-64-02236-8.

[81GÖH] H. Göhr, Ber. Bunsenges. Phys. Chem. **85** (1981) 274

[81LOR/MAN] W. J. Lorenz, F. Mansfeld, Corrosion Science **21** (1981) 647

[81MAN] F. Mansfeld, Corrosion **36** (1981) 301

[81SUN/SHO] S. Sunder, D. W. Shoesmith, M. G. Bailey, F. W. Stanchell, N. S. McIntyre, J. Electroanal. Chem. **130** (1981) 163

[82JOH/SHO] L.H. Johnson, D.W. Shoesmith, G.E. Lunansky, M.G. Bailey and P.R. Tremaine, Nucl. Technology 56 (1982) 238-253

[82MAN/KEN] F. Mansfeld, M. W. Kendig, S. Tsai, Corrosion **38** (1982) 570

[84LAS] Lasaga A.C (1984) Chemical kinetics of water-rock interactions. J. Geophys. Res. 89, 4009-4025.

[84THO/TIL] Thomas G.F and Till G. (1984) The dissolution of unirradiated UO2 fuel pellets under simulated disposal conditions. Nucl. Chem. Waste Manag. 5, 141-147.

[85BAI/JOH] M. G. Bailey, L. H. Johnson, D. W. Shoesmith, Corros. Sci. **25** (1985) 233

[85HEN/MON] P.N. Henrion, M. Monsecour, A. Fonteyne, M. Put and P. De Regge, Radioactive Waste Management and the Nuclear Fuel Cycle **6** (1985) 313-359.

[85JÜT/LOR] K. Jüttner, W. J. Lorenz, W. Paatsch, M. Kendig, F. Mansfeld, Werkstoffe und Korrosion **36** (1985) 120

[85MAN/KEN] F. Mansfeld, M. W. Kendig, W. J. Lorenz, J.Electrochem. Soc. **132** (1985) 240

[85WIL/OVE] C.T. Wilson and V.M. Oversby, "Radionuclide Release from PWR Fuels in a Reference Tuff Repository Groundwater" UCRL91464 (1985)

[86CHR/BJE] H. Christensen and E. Bjergbakke Application of Chemical for Groundwater Radiolysis. Nucl. Chem. Waste. Manage., 6, 265 (1986).

[86FOR/WER] Forsyth R.S., Werme L.O. and Bruno J. (1986) The corrosion of spent UO2 fuel in synthetic groundwater.. J. Nucl. Mat. 138, 1-15.

[86GÖH] H. Göhr, Z. phys. Chem. N. F. **148** (1986) 105

[87GAD/HEP] A. G. Gad-Allah, H. A. Abd El-Rahman, Corrosion-NACE **43** (1987) 698

[87POS/AXT] Posey-Dowty J., Axtmann E., Crerar D., Borcsik M., Ronk A. and Woods W. (1987) Dissolution rate of uraninite and uranium roll-front ores. Economic Geology 82, 184-194.

[87RAI] I. D. Raistrick, The Electrical Analogs of Physical and Chemical Processes, in: J. R. Macdonald (ed.), Impedance Spectroscopy, John Wiley & Sons (1987)

[88BRU/CAS] J. Bruno, I. Casa, I. Puigdomènech, Radiochimica Acta **44/45** (1988) 11

[88SHO/SUN] D. W. Shoesmith, S. Sunder, M. G. Bailey, G. J. Wallace, Can. J. Chem. **66** (1988) 259

[88SNE] Snellman M. /1988/, Chemical conditions in a repository - experimental and modelling studies. In Third Finnish-German Seminar on Nuclear Waste Management (ed. L. Lamberg), Espoo, Finland: VTT Synposium 87. pp. 146-168. ISBN 951-38-3175-2.

[88WER/FOR] L.O. Werme, R.S. Forsyth, Mat. Res. Soc. Symp. Proc. 112 (1988) 443-452.

[89BRU/PUI] J. Bruno and I. Puigdomenech, in Scientific Basis for Nuclear Waste Management XII, edited by W. Lutze and R.C. Ewing (Mater. Res. Soc. Proc. **127**, Pittsburgh, PA 1989), pp. 887-896.

[89BRU/PUI] Bruno J. and Puigdomènech I. (1989) Validation of the SKBU1 uranium thermodynamic database for its use in geochemical calculations with EQ3/6. Mat. Res. Soc. Symp. Proc. 127, 887-896.

[89GRA] Grambow B. /1989/, Spent fuel dissolution and oxidation. An evaluation of literature data. Stockholm, Sweden: Swedish Nuclear Fuel Waste Management Co. SKB Technical Report 89-13. 42 p. ISSN 0284-3757.

[89LEM/GAR] R.J Lemire and F Garisto The Solubility of U, Np, Pu, Th and Tc in Geological Disposal Vault for Used Nuclear Fuel. AECL-10009, Atomic Energy of Canada Limited, Whiteshell Laboratories (1989). 5

[89LUC/VER] P.G. Lucuta, B.J. Balmer, Hj Matzke and D.S. Hartwig, Preparation and

Characterization of SIMFUEL: Simulated CANDU High-Burnup Nuclear Fuel: Atomic Energy of Canada Report AECL-1017 (1989)

[89MIC] G. Michard, Équilibres chimiques dans les eaux naturelles, ed. Publisud (1989).

[89SHO/SUN] Shoesmith D.W., Sunder S., Bailey M.G. and Wallace G.J. (1989). The corrosion of nuclear fuel (UO2) in oxygenated solutions. Corros. Sci. 29, 1115-1128.

[89STR/JOH] S. Stroes-Gascoyne, L.H. Johnson, J.C. Tait and D.M. Sellinger, Mater. Res. Soc. Symp. Proc. **127** (1989) 301-307

[89TAI/STR] J.C. Tait, S. Stroes-Gascoyne, R.J. Porth, D. Wood and R.B. Heimann, Mat. Res. Soc. Symp. Proc. **127** (1989) 309-315.

[90GRA/FOR] B. Grambow, R.S. Forsyth, L.O. Werme, J. Bruno, Nucl. Technology 92 (1990) 204-213

[90GRA/LEI] W.J. Gray, H.R. Leider, S.A. Steward, J.Nuc. Mat. 190 (1992) 46-52.

[90MAC] D. D. Macdonald, Corrosion **46** (1990) 229

[90OLL] K. Ollila, J. Nucl. Mater. **190** (1992) 70-77.

[90PUI/CAS] I. Puigdomènech, I. Casas and J. Bruno, "Kinetics of UO_2(s) Dissolution under Reducing Conditions: Numerical Modelling", SKB Technical Report 90-25, SKB (1990)

[90RAI/FEL] Rai D., Felmy A.R. and Ryan J.L. /1990/, Uranium(IV) hydrolysis constants and solubility product of $UO_2 \cdot xH_2O$(am), Inorg. Chem., 29, pp. 260-264.

[90SKI] SKI Project-90 /1991/, Stockholm, Sweden: Swedish Nuclear Power Inspectorate. SKI Technical Report 91:23. Vol. 1. 239 p.

[90STU/WOL] Stumm W. and Wollast R. (1990) Coordination chemistry of weathering: Kinetics of the surface-controlled dissolution of oxides minerals. Reviews of Geophysics 28, 53-69

[90WIL1] C.N. Wilson, "Results from NNWSI Series 2 Bare Fuel Dissolution Tests", PNL-7170, Pacific Northwest Laboratory (1990)

[90WIL2] C.N. Wilson, "Results from NNWSI Series 3 Spent Fuel Dissolution Tests", PNL-7171, Pacific Northwest Laboratory (1990)

[91BRU/CAS] Bruno J., Casas I. and Puigdomènech I. (1991) The kinetics of dissolution of UO2 under reducing conditions and the influence of an oxidised surface layer (UO2+x): Application of a continuous flow-through reactor. Geochim. Cosmochim. Acta 55, 647-658.

[91CAS/SAN] I. Casas, A. Sandino, M.S. Caceci, J. Bruno and K. Ollila, Report YJT-91-18 (1991)

[91CHR] H. Christensen, Mat. Res. Soc. Symp. Proc. 212 (1991) 213-220

[91FOR] R.S. Forsyth, Mat. Res. Soc. Symp. Proc. **212** (1991) 177-188.

[91GRA/STR] W.J. Gray and D.M. Strachan, Mater. Res. Soc. Symp. Proc. **212** (1991) 205-212

[91GRA/WIL] Gray W. J. and Wilson C. N., Spent fuel dissolution studies, FY 1991 to 1994, Report PNL-10540, Pacific Northwest National Laboratory, 1995.

[91ING/ELK] T. Ingemansson and J. Elkert. Model for Calculation of Absorbed Alpha and Beta Radiation Dose to Water in Contact with Highly Burnt-Up Nuclear Fuel. M-91-23, Asea Brown Boveri (1991).

[91LUC/VER] P.G. Lucuta, R.A. Verrall, Hj. Matzke, and B.J. Palmer, J. Nucl. Mater. 178 (1991) 48-60

[91MAT/LUC] Hj. Matzke, P.G. Lucuta, R.A. Verrall, J. Nucl. Mater. 185 (1991) 292-296.

[91SHO/SUN] D.W. Shoesmith, Sunder, S.,Swedish Nuclear Fuel and Waste Management Co., Stockholm (Sweden), SKB-TR--91-63 (1991)

[91SUN/SHO] Sunder S., Shoesmith D.W., Lemire R.J., Bailey M.G. and Wallace G.J. (1991) The effect of pH on the corrosion of nuclear fuel (UO2) in oxygenated solutions. Corros. Sci. 32, 373-386.

[92BRU/CAS] J. Bruno, I. Casas, and A. Sandino, J. Nucl. Mater. **190** (1992) 61-69.

[92FIN/EWI] Finch R.J. and Ewing R.C. /1992/, The corrosion of uraninite under oxidizing conditions. J. Nucl. Mater. 190, pp. 133-156. ISSN 0022-3115.

[92FLE/JAM] J. Fleig, J. Jamnik, J. Maier, J. Electrochem. Soc. **143** (1996) 3636

[92FOR/WER] Forsyth R. S. and Werme L.O. /1992/, Spent fuel corrosion and dissolution. Journal Nuclear Materials 190, 3, pp. 3-19. ISSN 0022-3115.

[92GRA/LEI] Gray W.J., Leider H.R. and Steward S.A. (1992) Parametric study of LWR spent fuel dissolution kinetics. J. Nucl. Mat. 190, 46-52.

[92GRA/STR] W.J. Gray, D.M. Strachan and C.N. Wilson, Mat. Res. Soc. Symp. Proc. **257** (1992) 353-360.

[92GRA/THO] W.J. Gray, L.E. Thomas and R.E. Einzinger, Mat. Res. Soc. Symp. Proc. 294 (1993) 47-54

[92GRE/FUG] Grenthe I., Fuger J., Konings R.J.M., Lemire R.J., Muller A.B., Nguyen-Trung C. and Wanner H. (1992) Chemical Thermodynamics of Uranium (eds. H. Wanner and I. Forest). Elsevier Sci. Publishers B.V. Netherlands

[92HEP/WEG] P.-M. Heppner, D. Wegen, G. Marx, Radiochimica Acta **58/59** (1992) 21

[92JAN/EWI] J. Janeczek, R. C. Ewing, Mat. Res. Soc. Symp. Proc. **257**, 497-504 (1992)

[92LEG/BLA] Y. Legoux, G. Blain, R. Guillaumont, G. Ouzounian, L. Brillard and M. Hussonnois, Radiochimica Acta **58/59** (1992) 211-218.

[92OLL] K. Ollila, J. Nucl. Mater., 190 (1992) 70-77

[92SHO/SUN] Shoesmith D.W. and Sunder S., The prediction of nuclear fuel (UO2) dissolution rates under waste disposal conditions (1992). J. Nucl. Mat. 190, 20-35.

[92SKB] SKB 91, SKB technical report 92-20, Stockholm (1992)

[92STR] S. Stroes-Gascoyne, Journal of Nuclear Materials 190, 87-100 (1992)

[92SUN/SHO] S. Sunder, D. W. Shoesmith, H. Christensen, N. H. Miller, J. Nucl. Mat. **190** (1992) 78

[92WAT/MAD] S. W. Watson, B. W. Madsen, Corrosion **48** (1992) 727

[92WOL] Wolery T.J. /1992/, EQ3/6, A software package for geochemical modelling of aqueous systems (version 7.0). Lawrence Livermore National Laboratory, USA: UCRL-MA-110662, PT 1-4.

[92WRO/BAT] Wronkiewicz D.J., Bates J.K., Gerding T.J., Veleckis E. And Tani B.S. (1992) Uranium release and secondary phase formation during unsaturated testing of UO2 at 90ºC. J. Nucl. Mat. 190, 107-127

[93BRE/BUH] J. Brenner, D. Buhmann, R. Storck, GSF-Forschungszentrum für Umwelt und Gesundheit GmbH, Neuherberg, GSF-Bericht 13/93 (1993)

[93OLL/LIV] Ollila K. and Leino-Forsman H. /1993/, The dissolution of unirradiated UO_2 fuel pellets under simulated disposal conditions. Helsinki, Finland: Nuclear Waste Commission of Finnish Power companies. Report YJT-93-04. 29 p. ISSN-0359-548X.

[94CAS/GIM] Casas I., Giménez J., Martí V., Torrero M.E. and de Pablo J. (1994) Kinetic studies of unirradiated UO2 dissolution under oxidizing conditions in batch and flow experiments. Radiochim. Acta 66/67, 23-27.

[94CHR/SUN] H Christensen, S. Sunder and D. W: Shoesmith. Oxidation of Nuclear Fuel (UO2) by the Products of Water Radiolysis; Development of a Kinetic Model. J Alloys Compd., 213/214, 93 (1994).

[94FIN/BAT] P.A. Finn, J.K. Bates, J.C. Hoh, J.W. Emery, L.D. Hafenrichter, E.C. Buck and M. Gong, Mat. Res. Soc. Symp. Proc. **333** (1994) 399-407.

[94FIN/GON] P.A. Finn, M. Gong, J.K. Bates, J.W. Emery and J.C. Hoh, 1994 International High-Level Radioactive Waste Management Conference, Las Vegas, Nevada, May 22-26, 1994.

[94GRA/THO] W.J. Gray and L.E. Thomas, Mat. Res. Soc. Symp. Proc. **333** (1994) 391-398.

[94GUI] R. Guillaumont, Radiochimica Acta **66/67** (1994) 231-242.

[94HAU] W.Hauser, calculation with programm PRODOSS / Version Hp-Vectra, ha 1989-03, KfK/INE (1994)

[94LOI/GRA] A. Loïda, B. Grambow, P. Dressler, K. Friese and H. Geckeis, Mat. Res. Soc. Symp. Proc. **333** (1994) 417-424.

[94NEU/HOF] Neu, M.,Hoffmann, D., Roberts, K., Nitsche, H., Silva,R.; Radiochim.Acta, 66/67, 251-258,(1994)

[94SHO/HOC] D. W. Shoesmith, W. H. Hocking, S. Sunder, J. S. Betteridge, N. H. Miller, J. All. Comp. **213/214** (1994) 551

[94STE/GRA] S.A. Steward and W.J. Gray, High level Waste Management, V Annual International Conference, Las Vegas (1994) 2602-2608.

[94STE/PÖT] M.J. Stenhouse and J. Pöttinger, Radiochimica Acta **66/67** (1994) 267-275.

[94TOR/CAS] Torrero M.E., Casas I., de Pablo J., Sandino M.C.A and Grambow B. (1994) A comparison between and unirradiated UO2 (s) and schoepite solubilities in 1 M NaCl medium. Radiochim. Acta 66/67, 29-35

[95BRU/CAS] Bruno J., Casas I., Cera E., de Pablo J., Giménez, J. y Torrero M.E. (1995) Uranium (IV) dioxide and SIMFUEL as chemical analogues of nuclear spent fuel matrix dissolution. A comparison of dissolution results in a standard NaCl/NaHCO3 solution. Mat. Res. Soc. Symp. Proc. 353, 601-608.

[95COC/BOT] M. Coquerelle, D. Bottomley, D. H. Wegen, Study of UO_2 corrosion in carbonate and chloride solutions by electrochemical techniques, in: R. Schenkel, J. Richter, D. Pel, R. Wellum (ed.), EUR 16368 - Institute for Transuranium Elements - Annual report 1995, Luxembourg

[95DIA/QUI] Díaz-Arocas P., Quiñones J., Maffiote C., Serrano J., García J., Almazán J.R. and Esteban J.A. (1995) Effect of secondary phase formation in the leaching of UO2 under simulated radiolytic products. Mat. Res. Soc. Symp. Proc., 353, 641-652

[95ERI/EKL] T. E. Eriksen, U.-B. Eklund, L. Werme, J. Bruno, Journal of Nuclear Materials (1995) 227, 76-82

[95ERI/EKL] T.E. Eriksen, U. Eklund, L. Werme and J. Bruno, J. Nucl. Mater. 227 (1995) 76-82

[95FIN/BUC] P.A. Finn, E.C. Buck, J.C. Hoh and J.K. Bates, Global'95, Versailles, France, Sept. 11-14, 1995.

[95FOR] R.S. Forsyth, SKB technical Report 95-23 (1995).

[95GLA/THO] J.P. Glatz, E.H. Toscano, G. Pagliosa and A. Nicholl, J. Nucl. Mater. **223** (1995) 84-89.

[95GLA/TOS] J.P. Glatz, E.H. Toscano, G. Pagliosa and A. Nicholl, J. Nucl. Mater. 223 (1995) 84-89

[95GRA/WIL] W.J. Gray and C.N. Wilson, "Spent Fuel Dissolution Studies. FY 1991 to 1994", PNL-10540, Pacific Northwest Laboratory (1995)

[95HAN] Handbook of Chemistry and Physics, 75th Edition (1994-1995) CRC Press, Inc.

[95LOI/GRA] Loida, B. Grambow, H. Geckeis, and P. Dressler. Processes Controlling Radionuclide Release from Spent Fuel. Mater. Res. Soc. Symp. Proc., 353, 577 (1995).

[95OLL] Ollila K. /1995/, Solubility of unirradiated UO_2 fuel in aqueous solutions - comparison between experimental and calculated (EQ3/6) data. Helsinki, Finland: Nuclear Waste Commission of Finnish Power Companies. Report YJT-95-14. 27 p. ISSN-0359-548X.

[95SKB] SR 95, SKB technical report 96-05 (1995)

[95TRO/GAL] Trocellier P., Gallien J.P., Cachoir, C. and Toulhoat P. (1995) Study of the leaching behaviour of sintered UO2 in groundwater using nuclear microprobe techniques. Mat. Res. Soc. Symp. Proc. 353, 585-592

[95YAJ/KAW] Yajima T., Kawamura Y. and Ueta S. /1995/, Uranium(IV) solubility and hydrolysis constants under reduced conditions, in: Scientific Basis for Nuclear Waste Management XVIII, Part 2, (eds. T. Murakami and R:C. Ewing), Mat. Res. Soc. Symp. Proc., ISBN 1-55899-253-7, pp. 1137-1142.

[96BOT/WEG] P. D. W. Bottomley, D. H. Wegen, M. Coquerelle, J. Nucl. Mat. **238** (1996) 23

[96COC/BOT] M. Coquerelle, P.D.W. Bottomley, J.-P. Glatz and D. Wegen, "Electrode Potentials of Spent Fuel". EU-Programme "Nuclear Fission Safety" Annual Report 1996

[96ENG/FEL] J. Engelhardt, F. Feldmaier, M. Laske, G. Marx, J. Nucl. Mat. **238** (1996) 104

[96FIN/HOH1] P.A. Finn, J.C. Hoh, S.F. Wolf, S.A. Slater and J.K. Bates, Mat. Res. Soc. Symp. Proc. **412** (1996) 75-81.

[96FIN/HOH2] P.A. Finn, J.C. Hoh, S.F. Wolf, S.A. Slater and J.K. Bates, Radiochemica Acta **74** (1996) 65-71

[96GAR/SER] J. Garcia-Serrano, J.A. Serrano, P.P. Diaz-Arocas, J. Quinones and J.L.R. Almazan, Mat. Res. Soc. Symp. Proc. **412** (1996) 83-90.

[96GIM/BAR] J. Gimenez, E. Baraj, M. E. Torrero, J. Casas de Pablo Effect of H_2O_2, NaClO and Fe on the dissolution of unirradited UO_2, in NaCl 5 mol kg-1. Comparison with spent fuel dissolution experiments. J. Nucl. Mater. 238, 64-69 (1996).

[96GRA/LOI] B. Grambow, A. Loida, P. Dressler, H. Geckeis, J. Gago, I. Casas, J. De Pablo, J. Gimenez and M.E. Torrero, Long-Term Safety of Radioactive Waste Disposal: Chemical Reaction of Fabricated and High Burnup Spent

UO2 Fuel with Saline Brines.Final Report FZKA 5702 (Mars 1996).

[96GRA/SMA] B. Grambow, E. Smailos, H. Geckeis, R. Müller, H. Hentschel, Radiochimica Acta **74**, 149-154 (1996)

[96JOH] L. H. Johnson et al. , AECL Report-11494-2, Vol. 2 (1996)

[96LOI/GRA] A. Loïda, B. Grambow and H. Geckeis, J. Nucl. Mater. **238** (1996) 11-22

[96MAR/MEL] Martínez B., Melón A. and J. Valladares /1996/, Preparation of a synthetic bentonitic-granitic water. Madrid, Spain: Ciemat Geological Division. Ciemat specification, 10 p.

[96OLL/OLI] Ollila K., Olin M. and Lipponen M. /1996/, Solubility and oxidation state of uranium under anoxic conditions (N_2 atmosphere). Radiochimica Acta 74, pp. 9-13. ISBN 3-486-64251-0.

[96OLL] Ollila K. /1996/, Determination of U oxidation state in anoxic (N_2) aqueous solutions – method development and testing. Helsinki, Finland: Posiva Oy. Posiva Report 96-01, 33 p. ISBN 951-652-000-6.

[96PAB/CAS] J. de Pablo, I. Casas, J. Gimenez, V. Martí, M.E. Torrero, J. Nucl. Mater. 232 (1996) 138-145

[96RON/MAT] V.V. Rondinella and Hj. Matzke, J. Nucl. Mater. **238** (1996) 44-57.

[96RON/SER] V.V. Rondinella, J.A. Serrano, J.P. Glatz, Hj Matzke, Pres. at Spent Fuel '97, Avignon (1997).

[96SHO/SUN] D. W. Shoesmith, S. Sunder, M. G. Bailey, N. H. Miller, J. Nucl. Mat. **227** (1996) 287

[96SPI/VEN] J. Spino, K. Vennix and M. Coquerelle, J. Nucl. Mater. **231** (1996) 179-190

[96WAL/GOL] C.T. Walker, W. Goll and T. Matsumura, J. Nucl. Mater. **228** (1996) 8-17

[97CAS/PAB] I. Casas, J. De Pablo, J. Gimenez, M. Molera and M.E. Torrero, in Source term for Performance assessment of Spent Fuel as a waste form, Annual Report 1996 for EU-Programme "Nuclear fission Safety", Contract No. FI4W-CT95-0004, 1997

[97CHR/PET] H. Christensen and S-O Pettersson. Calculation of Spent Fuel Corrosion in 5 m NaCl solution. Studsvik Report STUDSVIK/M-97/121 (1997)

[97DIA/GAR] Diaz Arocas P., García Serrano J, Mendez F.J., Quiñones J., Rodriguez Almazan J.L., Serrano Agejas J. and Esteban Hernández J.A. (1997). Almacenamiento Definitivo de Residuos de Radiactividad Alta. Pub. Tec. ENRESA 04/97

[97FIN/HOH] Finn P.A., Hoh J.C., Wolf S.F., Surchik M.T., Buck E.C. and Bates J.K. (1997) Spent fuel reaction: The behaviour of ε-phase over 3.1 years. Mat. Res. Soc. Symp. Proc. 465, 527-534

[97GIM/PAB] Giménez J., de Pablo J., Torrero E. and Casas I. (1997) Conceptual and mathematical model for the UO2(s) dissolution in brines under different redox conditions. Radiochim. Acta 78, 21-15.

[97GRA/LOI] Grambow B., Loida A., Dressler P., Geckeis H., Müller N., Gago J., Casas I., de Pablo J., Giménez J. and Torrero M.E. (1997) Chemistry of the reaction of fabricated and high burnup UO2 fuel with saline brines. Final Report EUR 17111 FI2W-CT90-0055, European Commission.

[97GRA] Grambow et al. (1997) Source term for performance assessment of spent fuel as a waste form, Annual Report, European Union (contract FI4W-CT95-0004).

[97LEL] K. Le Lous, Etude de la lixiviation du combustible usé en présence de matériaux d'environnement, Thesis at Université de Paris Sud, 1997, p.145

[97OLL1] Dissolution of unirradiated UO_2 fuel in synthetic saline groundwater. Experimental methods and preliminary results. Helsinki, Finland: Posiva Oy. Posiva Report 97-09, 28 p. ISBN 951-652-034-0.

[97OLL2] Ollila K. (1997) Dissolution of unirradiated UO2 fuel under oxidizing conditions: A evaluation of solubility (steady state) limiting factors (EQ3/6). Mat. Res. Soc. Symp. Proc. 465, 549-556

[97OLL3] K. Ollila in Source term for Performance assessment of Spent Fuel as a waste form, Annual Report 1996 for EU-Programme "Nuclear fission Safety", Contract No. FI4W-CT95-0004, 1997

[97PAB/CAS] de Pablo J., Casas I., Giménez J., Molera M. and Torrero M.E. (1997) Effect of temperature and bicarbonate concentration on the kinetics of UO2(s) dissolution under oxidizing conditions. Mat. Res. Soc. Symp. Proc. 465, 535-542.

[97PAB/CAS] J. de Pablo, I. Casas, J. Gimenez, M. Molera, M.E. Torrero, Mat. Res. Soc. Symp. Proc.465.(1997) 535-542.

[97PAB] De Pablo J. /1997/, Personal communication.

[97PAU] J.L. Paul "Leaching of SIMULATED fuel and spent fuel in the present of environmental materials", NT/SCDN/Nº 98/29. Contract EU FI4wCT95004 (1997).

[97SAA/BEN] Saaltink M., Benet I. and Ayora C., (1997)RETRASO Fortran code for solving 2D REactive TRAnsport of SOlutes. User´s guide. UPC-CSIC, Barcelona.

[97SER/RON] J.A. Serrano, V.V. Rondinella, J.P. Glatz, E. Toscano, J. Quiñones, P.P. Diaz-Arocas, J. Garcia Serrano, Pres. at Migration '97, Senday, Japan (1997).

[97SKB] SKB-Annual Report 1996, SKB technical report 96-25, Stockholm (1997)

[97SUN/SHO] S. Sunder, D. W. Shoesmith, N. H. Miller, J. Nucl. Mat. **244** (1997) 66

[97TOR/BAR] Torrero M.E., Baraj E., de Pablo J., Giménez J. and Casas I. (1997) Kinetics of corrosion and dissolution of uranium dioxide as a function of pH. Int. J. Chem. Kinet. 29, 261-267.

[97VER] W. Verdickt, De Interactie van Europium en Uranium met Boomse Klei onder in situ omstandigheden, Thesis at Katholieke Universiteit Leuven, 1997, p. 77

[97VUR/OLL] Vuorinen U., Ollila K and Snellman M. (1997), Olkiluoto reference waters for brackish and saline groundwater. Helsinki, Finland: Posiva Oy. Posiva Working Report 97-25 (in Finnish). 65 p.

[97WRO/BUC] Wronkiewicz D.J., Buck E.C. and Bates J.K. (1997)Grain boundary corrosion and alteration phase formation during the oxidative dissolution of UO2 pellets. Mat. Res. Soc. Symp. Proc. 465, 519-526

[98AAM/CAS] El Aamrani F,. Casas I., Martin C., Rovira M. and de Pablo J. (1998) Effect of iron and canister corrosion products on the dissolution of UO2. Proceedings of Spent Fuel Workshop 1998. Las Vegas, Nevada

[98CAS/PAB] Casas I., de Pablo J., Giménez J., Torrero M.E., Bruno J., Cera E., Finch R.J. and Ewing R.C. (1998) The role of pe, pH and carbonate on the solubility of UO2 and uraninite under nominally reducing conditions. Geochim. Cosmochim. Acta 62, 2223-2231.

[98DIA/GRA] Diaz-Arocas P. and Grambow B. (1998) Solid-liquid phase equilibria of Uranium(VI) in NaCl solutions. Geochim. et Cosmochim. Acta 62, 245-263

[98FIN/FIN] Finn P.A., Finch R., Buck E.C. and Bates J.K. (1998) Corrosion mechanisms of spent fuel under oxidizing conditions. Mat. Res. Soc. Symp. Proc. 506, 123-131

[98GIM/MOL] J.Giménez, M. Molera, I.Casas, M.E. Torrero, J. de Pablo, "Kinetics of reduction and precipitation of U(VI) in the dissolution of UO2 under anoxic conditions in 5 m NaCl solutions. Influence of metallic iron., Mat. Res. Soc. Symp. Proc. 506, p. 105-122 (1998)

[98GRA] Grambow et al. /1998/, Source term for performance of assessment of spent fuel as a waste form. Annual Report 1997. 35 p.

[98HUS/GUI] Hussonnois M., Guillaumont R., Brillad L. and Fattahi M. /1989/, A method for determining the oxidation state of uranium at concentration as low as 10^{-10} M. In: Scientific Basis for Nuclear Waste Management XII (eds. W. Lutze and R.C. Ewing), Pittsburgh, Pennsylvania, USA: Mat. Res. Soc. Symp. Proc. Vol. 127. pp. 979-985. ISBN 0-931837-97-9.

[98KEL/BOH1] M. Kelm and E. Bohnert. Strahlenchemische Effecte im Endlager-nahbereich: y-Radiolyse in 6 molaler NaCl. Private communication 98-04-22.

[98KEL/BOH2] M. Kelm and E. Bohnert. α-Radiolyse von Konzentrierten NaCl-Lösungen. Private communication 98-04-22.

[98LEL/CON] Lelou K., Constantin S., Paul J.L., Sambugaro D., Vernaz E. Mat. Res. Soc. Symp. Proc. 506, 191-198 (1998)

[98LEM/CAN] Lemmens and P. de Cannières, (private communication).

[98LY] J. Ly (private communication) (1998).

[98MAR/FEL] Marx G., Feldmaier F., Engelhardt J. and Kupfer A. (this report)

[98MUU/VUO] Muurinen A., Vuorinen U., Lehikoinen J. and Aalto H. /1998/, Development of saline near-field reference water. Helsinki, Finland: Posiva Oy. Posiva Working Report 98-03, 18 p. (in Finnish).

[98OLL/AHO] Ollila K. and Ahonen L. /1998/, Solubilities of uranium for TILA-99. Helsinki, Finland: Posiva Oy. Posiva Report 98-13, 57 p. ISBN 951-652-051-0.

[98OLL1] Ollila K. (1998) Dissolution mechanisms of unirradiated UO2 fuel in synthetic groundwater. Proceedings of Spent Fuel Workshop 1998. Las Vegas, Nevada

[98OLL2] K. Ollila in Source term for Performance assessment of Spent Fuel as a waste form, Annual Report 1997 for EU-Programme "Nuclear fission Safety", Contract No. FI4W-CT95-0004, 1998

[98QUI/GAR] Quiñones J., García-Serrano J., Serrano J.A., Díaz-Arocas P. and Almazan J.L.R. (1998) SIMFUEL and UO2 solubility and leaching behaviour under anoxic conditions Mat. Res. Soc. Symp. Proc. 506, 247-252

[98SER/GLA] J.A. Serrano, J.-P. Glatz, E.H. Toscano, D. Papaioannou, J. Barrero and M. Coquerelle, J. Alloys Comp. **271-273** (1998) 573-576

[98SER/RON] J.A. Serrano, V.V. Rondinella*, J.P. Glatz*, E. H. Toscano*, J. Quiñones, P.P. Diaz-Arocas, J Garcia-Serrano, "Comparison of the leaching behaviour of irradiated fuel, SIMFUEL, and non-irradiated UO2 under oxic conditions", Radiochimica Acta 82 (1998)

[98SUN/STR] S. Sunder, L. K. Strandlund, D. W. Shoesmith, Electrochimica Acta **43** (1998)

2359

[98TRO/CAC] Trocellier P., Cachoir, C. and Guilbert S. (1998) A simple thermodynamical model to describe the control of the dissolution of uranium dioxide in granitic groundwater by secondary phase formation. J. Nucl. Mat. 256, 197-206

[98VUO/SNE] Vuorinen U. and Snellman M. (1998), Finnish reference waters for solubility, sorption and diffusion studies. Helsinki, Finland: Posiva Oy. Posiva Working Report 98- (to be published).

[98WEG] D. H. Wegen, ITU, unpublished results, 1998

[99ENG/MAR] J. Engelhardt, G. Marx, J. Nucl. Chem. **264** (1999) 161

[99SER/GLA] Serrano J., Glatz J.P., Toscano E.H., Quiñones J. and Diaz Arocas P.P. (1999) Comparison of the leaching behaviour of irradiated fuel, SIMFUEL, and non-irradiated UO_2 under oxic conditions. Radiochim. Acta (in press)

Final Report

APPENDIX

for contract
FI4W-CT95-0004
EU-R&D program 1994-1998

Nuclear Fission Safety

Title:

Source term for performance of assessment of spent fuel as a waste form

Decembre 1999

Appendix 1 : TABLE of contents in Appendix 2 to 9

APPENDIX 1 : TABLE OF CONTENTS IN APPENDIX 2 TO 9

APPENDIX 6: ORIGINAL TEST DATA OBTAINED BY ITU

Element concentration in solution measured by ICP-MS in the different samples (TABLEs 1-6).

Tab. 1: Composition of the samples obtained from the experiment with a MOX fuel with a burn-up of 12 GWd/tU. Concentrations are given in ng/mL of the element.
Tab. 2: Composition of the samples obtained from the experiment with a MOX fuel with a burn-up of 20 GWd/tU. Concentrations are given in ng/mL of the element.
Tab. 3: Composition of the samples obtained from the experiment with a MOX fuel with a burn-up of 25 GWd/tU. Concentrations are given in ng/mL of the element.
Tab. 4: Composition of the samples obtained from the experiment with a UO_2 fuel with a burn-up of 30 GWd/tU. Concentrations are given in ng/mL of the element.

Appendix 2: Original experimental data, obtained at INE-FZK

TABLE 1: Effect of pH and CO_2 : Activity of leach solutions from spent fuel powder corrosion tests (Bq/ml)

Sample: **P 56(I) : 1,7 g (=1,5 g HM)** Solution: 95% sat **NaCl** Starting volume: 131 ml **Atmosphere: Ar**

Temperature: 25 °C Final volume: 108 ml

				static test													
	Ultrason. cleaning of 18,9 g (16,7 g HM) pwdr in 200 ml DIW		**Wash** (85 d)	**no pH control** 1. Sampling 14 days*		**no pH control** 2. Sampling 62 days*		**pH = 7** 3. Sampling 83 days*		**pH = 9** 4. Sampling 173 days*		**pH = 11** 5. Sampling 236 days*		**pH = 7 (end)** 6. Sampling 277 days*	
Nuclide	0,45 µm -filtered			0.45 µm	1.8 nm	0.45 µm	1.8 nm	0.45 µm	1.8 nm	0.45 µm	1.8 nm	0.45 µm	1.8 nm	0.45 µm	1.8 nm'		
RU106	6,92E+3	6,29E+3	1,51E+3	6,09E+2	6,21E+2	9,06E+2	8,56E+2	2,02E+3	1,81E+3	2,59E+3	2,67E+3	4,66E+3	4,66E+3	3,66E+3	4,21E+3		
CS134	4,03E+6	5,11E+6	9,44E+4	2,35E+4	2,35E+4	3,15E+4	3,15E+4	1,58E+5	1,58E+5	2,83E+5	2,83E+5	4,72E+5	4,72E+5	5,24E+5	5,24E+5		
CS137	6,03E+6	7,66E+6	5,78E+5	1,46E+5	1,46E+5	2,11E+5	2,11E+5	1,06E+6	1,06E+6	2,00E+6	2,00E+6	3,49E+6	3,49E+6	4,35E+6	4,35E+6		
EU154	2,75E+2	2,85E+2	4,41E+1	1,27E+3	1,02E+3	1,43E+3	1,11E+3	1,38E+3	1,02E+3	1,76E+2	6,87E+1	3,16E+2	3,16E+2	1,86E+4	2,18E+4		
EU155	1,50E+2	1,35E+2	1,48E+1	4,43E+2	3,56E+2	4,94E+2	3,81E+2	4,33E+2	3,46E+2	5,89E+1	<2,93E+1	1,18E+2	1,18E+2	6,21E+3	7,47E+3		
SB125	9,25E+2	8,14E+2	1,03E+3	7,66E+2	8,02E+2	1,44E+3	1,49E+3	6,65E+3	6,54E+3	2,04E+4	2,00E+4	1,30E+4	1,30E+4	5,31E+3	6,23E+3		
SR90	8,88E+4	1,33E+5	1,17E+5	4,63E+4	4,76E+4	1,12E+5	1,25E+5	3,57E+5	4,02E+5	8,55E+5	8,88E+5	6,50E+5	6,50E+5	2,29E+6	2,41E+6		
CE144	1,11E+3	9,99E+2	4,34E+0	1,79E+2	1,71E+2	1,20E+2	1,06E+2	6,37E+1	4,69E+1	<9,98E+1	<9,35E+1	<3,45E+1	<3,45E+1	9,14E+2	1,11E+3		
TC99	<1,48E+0									1,96E+2	2,02E+2	9,26E+1	9,26E+1	5,53E+2	5,69E+2		
AG110M				8,00E+0	5,58E+0												
AM241	3,26E+1	2,59E+1	1,30E+1	1,55E+2	2,39E+2	1,84E+2	1,40E+2	1,72E+2	1,22E+2	<3,3E+1	<3,38E+1	3,42E+1	3,42E+1	5,42E+3	6,49E+3		
AM243	<3,70E-1	<3,70E-1															
NP237				4,04E-2	3,42E-2					1,33E+0	1,50E+0	1,58E+0	1,58E+0	9,46E+0	9,14E+0		
NP239	<3,70E-1	<3,70E-1															
CM244	2,07E+2	2,22E+2															
CM242	5,92E+0	5,55E+0															
PU238	1,33E+2	1,25E+2		3,23E+1	3,23E+1	4,53E+1	4,51E+1	1,27E+2	1,13E+2	2,77E+2	2,81E+2	2,56E+3	2,56E+3	1,98E+3	1,79E+3		
PU239/40	2,11E+1	2,00E+1		5,78E+0	5,70E+0	9,34E+0	8,64E+0	2,18E+1	2,02E+1	4,58E+1	4,91E+1	4,40E+2	4,40E+2	3,43E+2	3,04E+2		
PU241	3,89E+3	3,74E+3		5,06E+2	5,34E+2	8,36E+2	8,89E+2	2,30E+3	2,14E+3	5,94E+3	3,88E+3	4,40E+4	4,40E+4	3,88E+4	3,61E+4		
U (µg/ml)	*1,50E+1*									1,12E+2	1,13E+2	2,01E+2	2,01E+2	1,23E+1	7,49E+0		
pHmeas+0,5			6,51	pH 6,02		pH 6,4											
Eh(mV)**			-38	528 mV		402 mV		Eh meas.failed		408 mV		166 mV		674 mV			

**Ehmeas + 208 mV

* time since start of the static test

TABLE 2: Effect of pH and CO2: Released fractions of radionuclide inventories (FIAP) in leach solutions from spent fuel powder

Sample: **P 56(I) : 1,7 g (=1,5 g HM)** Solution: 95% sat **NaCl** Starting volume: 131 ml **Atmosphere: Ar**
Temperature: 25 °C Final volume: 108 ml

				static test												
	Ultrason. cleaning of 18,9 g (16,7 g HM) pwdr in 200 ml DIW		Wash (85 d)	no pH control				pH = 7		pH = 9		pH = 11		pH = 7 (end)	
				1. Sampling 14 days*		2. Sampling 62 days*		3. Sampling 83 days*		4. Sampling 173 days*		5. Sampling 236 days*		6. Sampling 277 days*	
Nuclide	0,45 µm -filtered			0.45 µm	1.8 nm	0.45 µm	1.8 nm	0.45 µm	1.8 nm	0.45 µm	1.8 nm	0.45 µm	1.8 nm	0.45 µm	1.8 nm'
RU106	3,03E-5	3,41E-5	1,45E-3	4,01E-4	4,09E-4	6,42E-4	6,06E-4	1,35E-3	1,21E-3	1,94E-3	2,00E-3	3,82E-3	3,74E-3	3,71E-3	4,27E-3
CS134	1,25E-2	1,76E-2	1,40E-2	2,34E-3	2,34E-3	3,16E-3	3,16E-3	1,50E-2	1,50E-2	2,79E-2	2,79E-2	4,82E-2	4,82E-2	5,84E-2	5,84E-2
CS137	1,19E-2	1,52E-2	1,40E-2	2,32E-3	2,32E-3	3,19E-3	3,19E-3	1,52E-2	1,52E-2	2,78E-2	2,78E-2	4,88E-2	4,88E-2	5,83E-2	5,83E-2
EU154	8,65E-6	9,20E-6	2,18E-5	4,13E-4	3,32E-4	4,48E-4	3,47E-4	4,09E-4	3,02E-4	5,12E-5	2,00E-5	1,41E-4	9,31E-5	5,37E-3	6,30E-3
EU155	9,16E-6	8,61E-6	1,85E-5	3,65E-4	2,94E-4	3,97E-4	3,06E-4	3,29E-4	2,63E-4	4,45E-5	<2,22E-5	1,15E-4	9,08E-5	4,81E-3	5,78E-3
SB125	7,53E-5	7,16E-5	2,76E-3	1,37E-3	1,43E-3	2,56E-3	2,64E-3	1,12E-2	1,10E-2	3,49E-2	3,42E-2	2,30E-2	2,29E-2	9,84E-3	1,15E-2
SR90	2,56E-4	3,87E-4	4,17E-3	1,08E-3	1,11E-3	2,50E-3	2,79E-3	7,53E-3	8,48E-3	1,75E-2	1,82E-2	1,29E-2	1,34E-2	4,53E-2	4,77E-2
CE144	5,50E-6	6,51E-6	1,13E-5	3,22E-4	3,08E-4	2,41E-4	2,13E-4	1,21E-4	8,92E-5	<2,22E-4	<2,08E-4	<9,05E-5	<8,35E-5	3,04E-3	3,69E-3
TC99	<2,59E-5									2,17E-2	2,24E-2	9,46E-3	3,80E-3	5,84E-2	6,85E-1
AG110M				2,49E-2	1,73E-2										
AM241	6,92E-6	5,15E-6	1,64E-5	1,28E-4	1,97E-4	1,41E-4	1,07E-4	1,25E-4	8,86E-5	<2,3E-5	<2,32E-5	3,83E-5	3,83E-5	3,40E-3	3,40E-3
AM243	<1,76E-6	<1,76E-6													
NP237				1,95E-4	1,65E-4					5,56E-3	6,27E-3	6,59E-3	6,64E-3	3,77E-2	3,64E-2
NP239	<1,76E-6	<1,76E-6													
CM244	5,60E-6	6,07E-6													
CM242	2,46E-6	3,74E-6													
PU238	4,81E-6	4,54E-6		8,81E-6	8,81E-6	1,17E-5	1,17E-5	3,12E-5	2,77E-5	6,57E-5	6,67E-5	6,97E-4	6,11E-4	4,50E-4	4,07E-4
PU239/40	4,87E-6	4,61E-6		9,74E-6	9,60E-6	1,49E-5	1,38E-5	3,30E-5	3,05E-5	6,69E-5	7,17E-5	7,49E-4	6,46E-4	4,78E-4	4,24E-4
PU241	5,86E-6	5,72E-6		6,88E-6	7,26E-6	1,09E-5	1,16E-5	2,83E-5	2,64E-5	7,14E-5	4,66E-5	5,79E-4	5,34E-4	4,56E-4	4,24E-4
U	1,92E-4									9,08E-3	9,16E-3	1,53E-2	1,64E-2	9,52E-4	5,79E-4
pHmeas+0,5			6,51	pH 6,02		pH 6,4									
Eh(mV)**			-38	528 mV		402 mV		Eh meas.failed		408 mV		166 mV		674 mV	

**Ehmeas + 208 mV

* time since start of the static test

TABLE 3: Effect of pH and CO2 : Concentrations of radionuclides in leach solutions from spent fuel powder (mol/L)

Sample: **P 56(I) : 1,7 g (=1,5 g HM)** Solution: 95% sat **NaCl** Starting volume: 131 ml **Atmosphere: Ar**
Temperature: 25 °C Final volume: 108 ml

				static test											
	Ultrason. cleaning of 18,9 g (16,7 g HM) pwdr in 200 ml DIW		**Wash** (85 d)	**no pH control** 1. Sampling 14 days*		**no pH control** 2. Sampling 62 days*		**pH = 7** 3. Sampling 83 days*		**pH = 9** 4. Sampling 173 days*		**pH = 11** 5. Sampling 236 days*		**pH = 7 (end)** 6. Sampling 277 days*	
Nuclide	0,45 µm -filtered			0.45 µm	1.8 nm	0.45 µm	1.8 nm	0.45 µm	1.8 nm	0.45 µm	1.8 nm	0.45 µm	1.8 nm	0.45 µm	1.8 nm[1]
RU106	1,3E-08	1,5E-08	3,71E-7	1,56E-7	1,59E-7	2,63E-7	2,49E-7	5,87E-7	5,26E-7	8,72E-7	8,99E-7	1,71E-6	1,67E-6	1,75E-6	2,01E-6
CS134	4,6E-06	6,5E-06	3,04E-6	7,73E-7	7,73E-7	1,10E-6	1,10E-6	5,53E-6	5,53E-6	1,06E-5	1,06E-5	1,83E-5	1,83E-5	2,34E-5	2,34E-5
CS137	4,4E-06	5,6E-06	3,03E-6	7,67E-7	7,67E-7	1,11E-6	1,11E-6	5,59E-6	5,59E-6	1,06E-5	1,06E-5	1,85E-5	1,85E-5	2,33E-5	2,33E-5
EU154	1,5E-10	1,6E-10	2,2E-10	6,40E-9	5,14E-9	7,31E-9	5,68E-9	7,06E-9	5,22E-9	9,2E-10	3,6E-10	2,51E-9	1,66E-9	1,01E-7	1,18E-7
EU155	1,6E-10	1,5E-10	1,9E-10	5,66E-9	4,55E-9	6,48E-9	5,00E-9	5,68E-9	4,54E-9	8,0E-10	<4,0E-10	2,04E-9	1,62E-9	9,01E-8	1,08E-7
SB125	1,7E-10	1,6E-10	3,69E-9	2,79E-9	2,92E-9	5,48E-9	5,67E-9	2,53E-8	2,49E-8	8,19E-8	8,03E-8	5,38E-8	5,34E-8	2,42E-8	2,84E-8
SR90	4,4E-08	6,6E-08	4,18E-7	1,66E-7	1,70E-7	4,03E-7	4,49E-7	1,28E-6	1,45E-6	3,09E-6	3,21E-6	2,27E-6	2,35E-6	8,38E-6	8,82E-6
CE144	1,8E-09	2,1E-09	2,11E-9	9,22E-8	8,81E-8	7,28E-8	6,43E-8	3,86E-8	2,84E-8	<7,32E-8	<6,85E-8	<2,97E-8	<2,74E-8	1,05E-6	1,28E-6
TC99	<3,80E-9									3,29E-6	3,39E-6	1,43E-6	5,74E-7	9,27E-6	1,09E-4
AG110M		3,3E-36		2,93E-7	2,04E-7										
AM241	1,8E-10	1,3E-10	2,5E-10	2,97E-9	4,58E-9	3,46E-9	2,64E-9	3,24E-9	2,30E-9	<6,1E-10	<6,2E-10	1,02E-9	1,02E-9	9,58E-8	9,58E-8
AM243	<4,6E-11	<4,6E-11													
NP237				6,74E-9	5,71E-9					2,22E-7	2,50E-7	2,62E-7	2,64E-7	1,58E-6	1,53E-6
NP239	<6,8E-11	<6,8E-11													
CM244	3,1E-11	3,4E-11													
CM242	1,4E-11	2,1E-11													
PU238	2,9E-09	2,7E-09		4,76E-9	4,76E-9	6,68E-9	6,65E-9	1,87E-8	1,67E-8	4,09E-8	4,15E-8	4,32E-7	3,79E-7	2,94E-7	2,66E-7
PU239/40	2,9E-09	2,8E-09		5,26E-9	5,19E-9	8,50E-9	7,86E-9	1,98E-8	1,84E-8	4,17E-8	4,47E-8	4,64E-7	4,00E-7	3,12E-7	2,77E-7
PU241	3,5E-09	3,5E-09		3,72E-9	3,92E-9	6,19E-9	6,59E-9	1,70E-8	1,59E-8	4,45E-8	2,90E-8	3,59E-7	3,31E-7	2,98E-7	2,77E-7
U	9,7E-06									4,71E-4	4,75E-4	7,90E-4	8,45E-4	5,17E-5	3,15E-5
pHmeas+0,5			6,51	pH 6,02		pH 6,4									
Eh(mV)**			-38	528 mV		402 mV		Eh meas.failed		408 mV		166 mV		674 mV	

**Ehmeas + 208 mV

* time since start of the static test

TABLE 4: Effect of pH and CO2: Incremental rates of radionuclides release from spent fuel powder (FIAP/d)

Sample: **P 56(I) : 1,7 g (=1,5 g HM)** Solution: 95% sat **NaCl** Starting volume: 131 ml **Atmosphere: Ar**

Temperature: 25 °C Final volume: 108 ml

			static test					
	Ultrason. cleaning of 18,9 g (16,7 g HM) pwdr in 200 ml DIW	**Wash** (85 d)	**no pH control** 1. Sampling 14 days*	**no pH control** 2. Sampling 62 days*	**pH = 7** 3. Sampling 83 days*	**pH = 9** 4. Sampling 173 days*	**pH = 11** 5. Sampling 236 days*	**pH = 7 (end)** 6. Sampling 277 days*
Nuclide	0,45 µm -filtered		0.45 µm 1.8 nm	0.45 µm 1.8 nm	0.45 µm 1.8 nm	0.45 µm 1.8 nm	0.45 µm 1.8 nm	0.45 µm 1.8 nm'
RU106		1,71E-5	2,86E-5	5,70E-6	3,65E-5	6,54E-6	2,98E-5	
CS134		1,65E-4	1,67E-4	2,11E-5	5,77E-4	1,43E-4	3,22E-4	2,49E-4
CS137		1,65E-4	1,66E-4	2,21E-5	5,83E-4	1,40E-4	3,34E-4	2,31E-4
EU154		2,56E-7	2,95E-5	1,42E-6			1,43E-6	1,28E-4
EU155		2,17E-7	2,61E-5	1,27E-6			1,11E-6	1,14E-4
SB125		3,25E-5	9,77E-5	2,70E-5	4,20E-4	2,64E-4		
SR90		4,91E-5	7,74E-5	3,13E-5	2,50E-4	1,11E-4		7,90E-4
CE144		1,33E-7	2,30E-5			1,12E-6		7,19E-5
TC99						2,41E-4		1,19E-3
AG110M			1,78E-3					
AM241		1,93E-7	9,11E-6	5,01E-7			2,49E-7	8,21E-5
AM243								
NP237			1,39E-5			6,17E-5	1,65E-5	7,59E-4
NP239								
CM244								
CM242								
PU238			6,29E-7	7,60E-8	9,72E-7	3,84E-7	1,00E-5	
PU239/40			6,96E-7	1,25E-7	9,20E-7	3,77E-7	1,08E-5	
PU241			4,92E-7	9,50E-8	8,75E-7	4,79E-7	8,06E-6	
U						1,01E-4	9,91E-5	
pHmeas+0,5		6,51	pH 6,02	pH 6,4				
Eh(mV)**		-38	528 mV	402 mV	Eh meas.failed	408 mV	166 mV	674 mV

**Ehmeas + 208 mV

* time since start of the static test

TABLE 5: Effect of pH and CO2 : Activity of leach solutions from spent fuel powder corrosion tests (Bq/ml)

Sample: **P 56(III) : 1,7 g (=1,5 g HM)** Solution: 95% sat **NaCl** Starting volume: 145 ml **Atmosphere:**
Temperature: 25 °C Final volume: 118 ml **Ar / 0,03%CO2**

				static test											
	Ultrason. cleaning of 18,9 g (16,7 g HM) pwdr in 200 ml DIW		**Wash** (162 d)	**no pH control** 1. Sampling 19 days*		**no pH control** 2. Sampling 74 days*		**pH = 7** 3. Sampling 102 days*		**pH = 9** 4. Sampling 158 days*		**pH = 11** 5. Sampling 223 days*		**pH = 7 (end)** 6. Sampling 329 days*	
Nuclide	0,45 µm -filtered			0.45 µm	1.8 nm	0.45 µm	1.8 nm	0.45 µm	1.8 nm	0.45 µm	1.8 nm	0.45 µm	1.8 nm	0.45 µm	1.8 nm'
RU106	6,92E+3	6,29E+3	2,85E+3	7,70E+2	8,83E+2	1,89E+3	2,05E+3	2,01E+3	1,58E+3	4,29E+2	1,14E+3	1,62E+3	1,62E+3	3,27E+3	2,87E+3
CS134	4,03E+6	5,11E+6	2,45E+5	9,81E+4	9,81E+4	2,76E+5	2,76E+5	1,89E+5	1,89E+5	3,67E+5	3,67E+5	4,09E+5	4,09E+5	6,71E+5	6,71E+5
CS137	6,03E+6	7,66E+6	1,74E+6	7,28E+5	7,28E+5	2,27E+6	2,27E+6	1,56E+6	1,56E+6	3,06E+6	3,06E+6	3,93E+6	3,93E+6	6,43E+6	6,43E+6
EU154	2,75E+2	2,85E+2	8,78E+3	1,40E+4	1,44E+4	3,27E+4	3,35E+4	2,93E+4	2,79E+4	3,14E+2	1,34E+2	3,11E+2	3,28E+2	1,54E+5	1,52E+5
EU155	1,50E+2	1,35E+2	3,08E+3	4,88E+3	5,04E+3	1,09E+4	1,12E+4	9,94E+3	9,39E+3	8,86E+1	2,98E+1	1,13E+2	8,88E+1	4,96E+4	4,85E+4
SB125	9,25E+2	8,14E+2	1,07E+3	1,30E+3	1,36E+3	1,77E+3	1,80E+3	2,13E+3	2,03E+3	6,34E+3	6,57E+3	8,97E+3	8,44E+3	1,14E+3	1,09E+3
SR90	8,88E+4	1,33E+5	6,25E+5	3,04E+5	3,24E+5	6,59E+5	6,29E+5	8,12E+5	8,46E+5	1,15E+6	1,21E+6	3,25E+5	2,98E+5	4,45E+6	4,41E+6
CE144	1,11E+3	9,99E+2	7,64E+2	1,09E+3	1,18E+3	1,88E+3	2,04E+3	8,49E+2	8,29E+2	<5,92E+1	<6,14E+1	3,13E+1	2,96E+1	8,55E+3	7,36E+3
TC99	<1,48E+0		<7,10E-1	1,37E+1	1,80E+1	1,81E+2	1,79E+2	2,83E+2	3,19E+2	4,38E+2	4,50E+2	7,37E+2	6,78E+2	1,20E+3	1,27E+3
AG110M															
AM241	3,26E+1	2,59E+1	1,45E+3	2,92E+3	3,01E+3	6,28E+3	6,44E+3	4,69E+3	4,68E+3	3,17E+1	2,22E+1	4,45E+1	3,88E+1	5,59E+4	5,45E+4
AM243	<3,70E-1	<3,70E-1													
NP237			8,71E-2	7,28E-1	7,52E-1	3,50E+0	2,89E+0	4,36E+0	4,79E+0	2,80E+0	2,88E+0	3,28E+0	2,98E+0	3,07E+1	2,90E+1
NP239	<3,70E-1	<3,70E-1													
CM244	2,07E+2	2,22E+2													
CM242	5,92E+0	5,55E+0													
PU238	1,33E+2	1,25E+2	3,16E+2	9,51E+2	9,31E+2	1,54E+3	1,52E+3	1,80E+3	1,71E+3	2,93E+2	2,04E+2	1,34E+3	1,34E+3	5,07E+3	4,26E+3
PU239/40	2,11E+1	2,00E+1	4,82E+1	1,63E+2	1,73E+2	2,67E+2	2,63E+2	3,52E+2	3,05E+2	5,03E+1	3,31E+1	2,34E+2	2,27E+2	8,61E+2	7,33E+2
PU241	3,89E+3	3,74E+3	6,30E+3	1,54E+4	1,52E+4	3,04E+4	2,97E+4	3,71E+4	3,37E+4	5,81E+3	3,68E+3	2,48E+4	2,47E+4	9,17E+4	7,77E+4
U (µg/ml)	*1,50E+1*		1,17E+1	2,81E+1	2,43E+1	1,04E+2	9,79E+1	4,23E+1	3,81E+0	1,18E+2	1,21E+2	2,96E+2	2,84E+2	4,10E+1	1,85E+1
pHmeas+0,5			5,45	pH 5,51		pH 5,36									
Eh(mV)**			198	514 mV		217 mV		658 mV		48 mV		528 mV		643 mV	

**Ehmeas + 208 mV

* time since start of the static test

TABLE 6: Effect of pH and CO_2 : Release fractions (FIAP) of radionuclide inventories in spent fuel powder leachates

-

Sample: **P 56(III) : 1,7 g (=1,5 g HM)** Solution: 95% sat **NaCl** Starting volume: 145 ml **Atmosphere:**
Temperature: 25 °C Final volume: 118 ml **Ar / 0,03%CO2**

				static test											
	Ultrason. cleaning of 18,9 g (16,7 g HM) pwdr in 200 ml DIW		**Wash** (162 d)	**no pH control** 1. Sampling 19 days*		**no pH control** 2. Sampling 74 days*		**pH = 7** 3. Sampling 102 days*		**pH = 9** 4. Sampling 158 days*		**pH = 11** 5. Sampling 223 days*		**pH = 7 (end)** 6. Sampling 329 days*	
Nuclide	0,45 µm -filtered			0.45 µm	1.8 nm	0.45 µm	1.8 nm	0.45 µm	1.8 nm	0.45 µm	1.8 nm	0.45 µm	1.8 nm	0.45 µm	1.8 nm'
RU106	3,03E-5	3,41E-5	3,73E-3	7,77E-4	8,91E-4	2,42E-3	2,62E-3	2,43E-3	1,91E-3	4,97E-4	1,32E-3	2,42E-3	2,42E-3	4,66E-3	4,09E-3
CS134	1,25E-2	1,76E-2	4,21E-2	1,26E-2	1,26E-2	3,88E-2	3,88E-2	2,51E-2	2,51E-2	4,68E-2	4,68E-2	5,88E-2	5,88E-2	9,19E-2	9,19E-2
CS137	1,19E-2	1,52E-2	4,22E-2	1,28E-2	1,28E-2	3,84E-2	3,84E-2	2,49E-2	2,49E-2	4,69E-2	4,69E-2	6,02E-2	6,02E-2	9,38E-2	9,38E-2
EU154	8,65E-6	9,20E-6	4,46E-3	5,19E-3	5,34E-3	1,19E-2	1,22E-2	1,01E-2	9,61E-3	1,04E-4	4,43E-5	1,05E-4	1,11E-4	4,95E-2	4,88E-2
EU155	9,16E-6	8,61E-6	4,06E-3	4,72E-3	4,88E-3	1,06E-2	1,09E-2	9,17E-3	8,67E-3	7,84E-5	2,64E-5	1,04E-4	8,21E-5	4,37E-2	4,28E-2
SB125	7,53E-5	7,16E-5	3,19E-3	2,88E-3	3,01E-3	4,14E-3	4,21E-3	4,70E-3	4,48E-3	1,34E-2	1,39E-2	2,07E-2	1,95E-2	2,51E-3	2,40E-3
SR90	2,56E-4	3,87E-4	2,23E-2	7,89E-3	8,41E-3	1,64E-2	1,57E-2	1,92E-2	2,00E-2	2,60E-2	2,74E-2	7,35E-3	6,74E-3	9,59E-2	9,50E-2
CE144	5,50E-6	6,51E-6	2,96E-3	3,32E-3	3,59E-3	7,89E-3	8,56E-3	3,36E-3	3,29E-3	<2,25E-4	<2,33E-4	1,66E-4	1,57E-4	4,32E-2	3,72E-2
TC99	<2,59E-5		<1,37E-4	1,92E-3	2,52E-3	2,41E-2	2,38E-2	3,56E-2	4,01E-2	5,29E-2	5,43E-2	8,80E-2	8,10E-2	1,37E-1	1,45E-1
AG110M															
AM241	6,92E-6	5,15E-6	1,74E-3	2,52E-3	2,60E-3	4,97E-3	5,10E-3	3,51E-3	3,50E-3	2,28E-5	1,59E-5	3,06E-5	2,67E-5	3,67E-2	3,58E-2
AM243	<1,76E-6	<1,76E-6													
NP237			6,35E-4	3,85E-3	3,97E-3	1,76E-2	1,45E-2	2,07E-2	2,28E-2	1,28E-2	1,31E-2	1,48E-2	1,34E-2	1,32E-1	1,25E-1
NP239	<1,76E-6	<1,76E-6													
CM244	5,60E-6	6,07E-6													
CM242	2,46E-6	3,74E-6													
PU238	4,81E-6	4,54E-6	1,31E-4	2,86E-4	2,80E-4	4,42E-4	4,36E-4	4,88E-4	4,63E-4	7,62E-5	5,30E-5	3,46E-4	3,46E-4	1,25E-3	1,05E-3
PU239/40	4,87E-6	4,61E-6	1,23E-4	3,01E-4	3,20E-4	4,69E-4	4,62E-4	5,85E-4	5,07E-4	8,02E-5	5,27E-5	3,69E-4	3,58E-4	1,29E-3	1,10E-3
PU241	5,86E-6	5,72E-6	1,32E-4	2,35E-4	2,32E-4	4,51E-4	4,40E-4	5,20E-4	4,72E-4	7,81E-5	4,94E-5	3,36E-4	3,35E-4	1,18E-3	1,00E-3
U	1,92E-4		1,65E-3	2,88E-3	2,49E-3	1,01E-2	9,55E-3	3,90E-3	3,51E-4	1,04E-2	1,07E-2	2,59E-2	2,49E-2	3,42E-3	1,54E-3
pHmeas+0,5			5,45	pH 5,51		pH 5,36									
Eh(mV)**			198	514 mV		217 mV		658 mV		48 mV		528 mV		643 mV	

**Ehmeas + 208 mV

* time since start of the static test

TABLE 7: Effect of pH and CO2: Concentrations of radionuclides in leach solutions from spent fuel powder (mol/L)

Sample: **P 56(III) : 1,7 g (=1,5 g HM)** Solution: 95% sat **NaCl** Starting volume: 145 ml **Atmosphere:**
Temperature: 25 °C Final volume: 118 ml **Ar / 0,03%CO2**

				static test													
	Ultrason. cleaning of 18,9 g (16,7 g HM) pwdr in 200 ml DIW		**Wash** (162 d)	**no pH control** 1. Sampling 19 days*		**no pH control** 2. Sampling 74 days*		**pH = 7** 3. Sampling 102 days*		**pH = 9** 4. Sampling 158 days*		**pH = 11** 5. Sampling 223 days*		**pH = 7 (end)** 6. Sampling 329 days*	
Nuclide	0,45 µm -filtered			0.45 µm	1.8 nm	0.45 µm	1.8 nm	0.45 µm	1.8 nm	0.45 µm	1.8 nm	0.45 µm	1.8 nm	0.45 µm	1.8 nm'		
RU106	1,3E-08	1,5E-08	9,60E-7	2,76E-7	3,17E-7	9,02E-7	9,78E-7	9,59E-7	7,54E-7	2,05E-7	5,44E-7	1,01E-6	1,01E-6	2,04E-6	1,79E-6		
CS134	4,6E-06	6,5E-06	9,22E-6	3,80E-6	3,80E-6	1,23E-5	1,23E-5	8,43E-6	8,43E-6	1,64E-5	1,64E-5	2,08E-5	2,08E-5	3,41E-5	3,41E-5		
CS137	4,4E-06	5,6E-06	9,22E-6	3,87E-6	3,87E-6	1,22E-5	1,22E-5	8,37E-6	8,37E-6	1,64E-5	1,64E-5	2,13E-5	2,13E-5	3,48E-5	3,48E-5		
EU154	1,5E-10	1,6E-10	4,57E-8	7,33E-8	7,54E-8	1,77E-7	1,81E-7	1,59E-7	1,51E-7	1,70E-9	7,25E-10	1,74E-9	1,83E-9	8,59E-7	8,48E-7		
EU155	1,6E-10	1,5E-10	4,16E-8	6,68E-8	6,90E-8	1,58E-7	1,63E-7	1,44E-7	1,36E-7	1,29E-9	4,32E-10	1,73E-9	1,36E-9	7,60E-7	7,43E-7		
SB125	1,7E-10	1,6E-10	4,30E-9	5,34E-9	5,59E-9	8,07E-9	8,21E-9	9,71E-9	9,26E-9	2,89E-8	3,00E-8	4,50E-8	4,24E-8	5,73E-9	5,47E-9		
SR90	4,4E-08	6,6E-08	2,26E-6	1,10E-6	1,17E-6	2,41E-6	2,30E-6	2,97E-6	3,09E-6	4,21E-6	4,43E-6	1,20E-6	1,10E-6	1,64E-5	1,63E-5		
CE144	1,8E-09	2,1E-09	5,60E-7	8,66E-7	9,37E-7	2,16E-6	2,35E-6	9,76E-7	9,53E-7	<6,81E-8	<7,06E-8	5,07E-8	4,80E-8	1,39E-5	1,19E-5		
TC99	<3,80E-9		<1,19E-8	2,30E-7	3,02E-7	3,04E-6	3,00E-6	4,75E-6	5,35E-6	7,35E-6	7,55E-6	1,24E-5	1,14E-5	2,01E-5	2,13E-5		
AG110M		3,3E-36															
AM241	1,8E-10	1,3E-10	2,68E-8	5,35E-8	5,51E-8	1,11E-7	1,14E-7	8,29E-8	8,27E-8	5,60E-10	3,92E-10	7,62E-10	6,64E-10	9,57E-7	9,33E-7		
AM243	<4,6E-11	<4,6E-11															
NP237			1,45E-8	1,22E-7	1,26E-7	5,84E-7	4,82E-7	7,28E-7	8,00E-7	4,67E-7	4,81E-7	5,48E-7	4,98E-7	5,13E-6	4,84E-6		
NP239	<6,8E-11	<6,8E-11															
CM244	3,1E-11	3,4E-11															
CM242	1,4E-11	2,1E-11															
PU238	2,9E-09	2,7E-09	4,67E-8	1,41E-7	1,38E-7	2,29E-7	2,26E-7	2,67E-7	2,54E-7	4,35E-8	3,03E-8	1,99E-7	1,99E-7	7,55E-7	6,34E-7		
PU239/40	2,9E-09	2,8E-09	4,39E-8	1,48E-7	1,57E-7	2,43E-7	2,39E-7	3,20E-7	2,78E-7	4,58E-8	3,01E-8	2,13E-7	2,07E-7	7,83E-7	6,67E-7		
PU241	3,5E-09	3,5E-09	4,72E-8	1,16E-7	1,14E-7	2,33E-7	2,28E-7	2,85E-7	2,59E-7	4,46E-8	2,82E-8	1,94E-7	1,93E-7	7,17E-7	6,07E-7		
U	9,7E-06		4,92E-5	1,18E-4	1,02E-4	4,37E-4	4,11E-4	1,78E-4	1,60E-5	4,96E-4	5,08E-4	1,24E-3	1,19E-3	1,72E-4	7,77E-5		
pHmeas+0,5			5,45	pH 5,51		pH 5,36											
Eh(mV)**			198	514 mV		217 mV		658 mV		48 mV		528 mV		643 mV			

**Ehmeas + 208 mV

* time since start of the static test

TABLE 8: Effect of pH and CO_2 : Incremental rates of radionuclides release from spent fuel powder (FIAP/d)

Sample: **P 56(III) : 1,7 g (=1,5 g HM)** Solution: 95% sat **NaCl** Starting volume: 145 ml **Atmosphere:**
Temperature: 25 °C Final volume: 118 ml **Ar / 0,03%CO2**

			static test					
	Ultrason. cleaning of 18,9 g (16,7 g HM) pwdr in 200 ml DIW	**Wash** (162 d)	**no pH control** 1. Sampling 19 days*	**no pH control** 2. Sampling 74 days*	**pH = 7** 3. Sampling 102 days*	**pH = 9** 4. Sampling 158 days*	**pH = 11** 5. Sampling 223 days*	**pH = 7 (end)** 6. Sampling 329 days*
Nuclide	0,45 µm -filtered		0.45 µm 1.8 nm	0.45 µm 1.8 nm	0.45 µm 1.8 nm	0.45 µm 1.8 nm	0.45 µm 1.8 nm	0.45 µm 1.8 nm'
RU106		2,30E-5	4,09E-5	4,39E-5	8,67E-5	8,88E-6	3,73E-5	4,40E-5
CS134		2,60E-4	6,63E-4	7,06E-4	8,97E-4	8,35E-4	9,04E-4	8,67E-4
CS137		2,60E-4	6,74E-4	6,98E-4	8,90E-4	8,38E-4	9,25E-4	8,85E-4
EU154		2,75E-5	2,73E-4	2,17E-4	3,60E-4	1,85E-6	1,61E-6	4,67E-4
EU155		2,51E-5	2,49E-4	1,94E-4	3,28E-4	1,40E-6	1,61E-6	4,13E-4
SB125		1,97E-5	1,51E-4	7,52E-5	1,68E-4	2,40E-4	3,19E-4	2,37E-5
SR90		1,38E-4	4,15E-4	2,99E-4	6,84E-4	4,65E-4	1,13E-4	9,05E-4
CE144		1,83E-5	1,75E-4	1,43E-4	1,20E-4	<4,02E-6	2,55E-6	4,08E-4
TC99		<8,46E-7	1,01E-4	4,38E-4	1,27E-3	9,44E-4	1,35E-3	1,29E-3
AG110M								
AM241		1,07E-5	1,33E-4	9,04E-5	1,25E-4	4,06E-7	4,71E-7	3,46E-4
AM243								
NP237		3,92E-6	2,02E-4	3,20E-4	7,40E-4	2,28E-4	2,28E-4	1,25E-3
NP239								
CM244								
CM242								
PU238		8,07E-7	1,50E-5	8,03E-6	1,74E-5	1,36E-6	5,32E-6	1,18E-5
PU239/40		7,58E-7	1,58E-5	8,54E-6	2,09E-5	1,43E-6	5,68E-6	1,22E-5
PU241		8,15E-7	1,24E-5	8,19E-6	1,86E-5	1,39E-6	5,17E-6	1,12E-5
U		1,02E-5	1,52E-4	1,85E-4	1,39E-4	1,86E-4	3,99E-4	3,23E-5
pHmeas+0,5		5,45	pH 5,51	pH 5,36				
Eh(mV)**		198	514 mV	217 mV	658 mV	48 mV	528 mV	643 mV

**Ehmeas + 208 mV

* time since start of the static test

TABLE 9: Effect of pH and CO_2 : Activity of leach solutions from spent fuel powder corrosion tests (Bq/ml)

Sample: **P 56(II) : 1,7 g (=1,5 g HM)** Solution: 95% sat **NaCl** Starting volume: 127 ml **Atmosphere: Ar/1%CO_2**

Temperature: 25 °C Final volume: 122 ml

			Ar-Atm.	static test												
	Ultrason. cleaning of 18,9 g (16,7 g HM) pwdr in 200 ml DIW		**Wash** (89 d)	**no pH control** 1. Sampling 15 days*		**no pH control** 2. Sampling 59 days*		**pH = 7** 3. Sampling 80 days*		**pH = 9** 4. Sampling 169 days*		**pH = 11** 5. Sampling 230 days*		**pH = 7 (end)** 6. Sampling 274 days*	
Nuclide	0,45 µm -filtered			0.45 µm	1.8 nm	0.45 µm	1.8 nm	0.45 µm	1.8 nm	0.45 µm	1.8 nm	0.45 µm	1.8 nm	0.45 µm	1.8 nm
RU106	6,92E+3	6,29E+3	1,12E+3	1,10E+3	1,07E+3	3,26E+3	3,70E+3	4,91E+3	5,28E+3	5,49E+3	5,69E+3	6,13E+3	5,72E+3	4,56E+3	5,35E+3
CS134	4,03E+6	5,11E+6	9,75E+4	6,57E+4	6,57E+4	1,79E+5	1,79E+5	2,03E+5	2,03E+5	3,43E+5	3,43E+5	4,51E+5	4,51E+5	4,67E+5	4,67E+5
CS137	6,03E+6	7,66E+6	5,90E+5	4,14E+5	4,14E+5	1,19E+6	1,19E+6	1,35E+6	1,35E+6	2,46E+6	2,46E+6	3,34E+6	3,34E+6	3,86E+6	3,86E+6
EU154	2,75E+2	2,85E+2	1,18E+2	3,36E+3	3,12E+3	9,63E+3	1,02E+4	6,81E+2	5,34E+2	1,02E+3	1,05E+3	2,24E+3	2,18E+3	1,24E+4	1,19E+4
EU155	1,50E+2	1,35E+2	4,06E+1	1,18E+3	1,09E+3	3,14E+3	3,30E+3	1,93E+2	1,53E+2	3,10E+2	3,59E+2	8,00E+2	7,56E+2	3,97E+3	3,83E+3
SB125	9,25E+2	8,14E+2	7,80E+2	2,01E+3	1,99E+3	4,94E+3	5,33E+3	2,03E+4	2,21E+4	4,52E+4	5,15E+4	3,57E+4	3,73E+4	3,63E+4	3,76E+4
SR90	8,88E+4	1,33E+5	1,31E+5	1,05E+5	1,07E+5	3,67E+5	3,92E+5	4,19E+5	5,65E+5	1,20E+6	1,23E+6	7,16E+5	7,56E+5	2,03E+6	2,09E+6
CE144	1,11E+3	9,99E+2	1,63E+1	4,97E+2	4,86E+2	9,25E+2	1,01E+3	7,93E+1	1,03E+2	1,14E+2	1,24E+2	<3,89E+1	<4,17E+1	<1,38E+2	<1,40E+2
TC99	<1,48E+0									4,97E+2	4,64E+2	5,24E+2	5,76E+2	5,27E+2	4,89E+2
AG110M				1,27E+1	8,49E+0										
AM241	3,26E+1	2,59E+1	2,11E+1	6,19E+2	5,74E+2	1,73E+3	1,83E+3	7,34E+1	5,92E+1	7,84E+1	7,94E+1	1,82E+2	2,12E+2	2,47E+3	2,38E+3
AM243	<3,70E-1	<3,70E-1													
NP237				1,09E-1	2,07E-1					4,15E+0	3,53E+0	4,45E+0	4,95E+0	6,51E+0	6,52E+0
NP239	<3,70E-1	<3,70E-1													
CM244	2,07E+2	2,22E+2													
CM242	5,92E+0	5,55E+0													
PU238	1,33E+2	1,25E+2		9,49E+1	9,64E+1	7,50E+2	7,65E+2	1,84E+2	1,20E+2	5,35E+3	5,21E+3	4,48E+3	4,43E+3	6,96E+2	3,26E+2
PU239/40	2,11E+1	2,00E+1		1,61E+1	1,66E+1	1,28E+2	1,29E+2	2,82E+1	2,02E+1	9,31E+2	8,97E+2	7,85E+2	7,48E+2	1,21E+2	5,78E+1
PU241	3,89E+3	3,74E+3		1,27E+3	1,46E+3	1,46E+4	1,50E+4	3,12E+3	2,10E+3	1,04E+5	9,91E+4	7,87E+4	7,80E+4	1,38E+4	6,52E+3
U (µg/ml)	*1,50E+1*									4,07E+2	4,12E+2	4,12E+2	4,33E+2	3,88E+2	3,75E+2
pHmeas+0,5			6,34	pH 5,34		pH 5,82									
Eh(mV)**			22mV	546 mV		259 mV		279 mV		197 mV		228 mV		648 mV	

**Ehmeas + 208 mV

* time since start of the static test

TABLE 10: Effect of pH and CO_2: Released fractions (FIAP) of nuclide inventories in spent fuel powder leachates

Sample: **P 56(II) : 1,7 g (=1,5 g HM)** Solution: 95% sat **NaCl** Starting volume: 127 ml **Atmosphere: Ar/1%CO_2**

Temperature: 25 °C Final volume: 122 ml

	Ar-Atm.			static test											
	Ultrason. cleaning of 18,9 g (16,7 g HM) pwdr in 200 ml DIW		**Wash** (89 d)	**no pH control** 1. Sampling 15 days*		**no pH control** 2. Sampling 59 days*		**pH = 7** 3. Sampling 80 days*		**pH = 9** 4. Sampling 169 days*		**pH = 11** 5. Sampling 230 days*		**pH = 7 (end)** 6. Sampling 274 days*	
Nuclide	0,45 µm -filtered			0.45 µm	1.8 nm	0.45 µm	1.8 nm	0.45 µm	1.8 nm	0.45 µm	1.8 nm	0.45 µm	1.8 nm	0.45 µm	1.8 nm
RU106	3,03E-5	3,41E-5	1,12E-3	7,01E-4	6,82E-4	2,23E-3	2,53E-3	3,23E-3	3,47E-3	4,47E-3	4,63E-3	5,29E-3	4,94E-3	5,20E-3	6,11E-3
CS134	1,25E-2	1,76E-2	1,48E-2	6,33E-3	6,33E-3	1,74E-2	1,74E-2	1,89E-2	1,89E-2	3,67E-2	3,67E-2	4,96E-2	4,96E-2	5,86E-2	5,86E-2
CS137	1,19E-2	1,52E-2	1,43E-2	6,36E-3	6,36E-3	1,74E-2	1,74E-2	1,90E-2	1,90E-2	3,71E-2	3,71E-2	5,03E-2	5,03E-2	5,83E-2	5,83E-2
EU154	8,65E-6	9,20E-6	5,85E-5	1,06E-3	9,82E-4	2,91E-3	3,09E-3	1,98E-4	1,55E-4	3,22E-4	3,32E-4	7,11E-4	6,92E-4	4,03E-3	3,87E-3
EU155	9,16E-6	8,61E-6	5,11E-5	9,42E-4	8,71E-4	2,44E-3	2,56E-3	1,44E-4	1,14E-4	2,54E-4	2,95E-4	6,63E-4	6,27E-4	3,46E-3	3,34E-3
SB125	7,53E-5	7,16E-5	2,12E-3	3,48E-3	3,44E-3	8,47E-3	9,14E-3	3,34E-2	3,64E-2	8,39E-2	9,56E-2	6,76E-2	7,07E-2	7,57E-2	7,85E-2
SR90	2,56E-4	3,87E-4	4,67E-3	2,38E-3	2,42E-3	7,91E-3	8,45E-3	8,67E-3	1,17E-2	2,67E-2	2,73E-2	1,59E-2	1,68E-2	4,52E-2	4,66E-2
CE144	5,50E-6	6,51E-6	4,47E-5	8,66E-4	8,47E-4	1,80E-3	1,96E-3	1,48E-4	1,92E-4	2,75E-4	2,99E-4	<1,01E-4	<1,09E-4	<5,17E-4	<5,24E-4
TC99	<2,59E-5									5,97E-2	5,57E-2	6,28E-2	6,90E-2	6,27E-2	5,81E-2
AG110M				3,82E-2	2,55E-2										
AM241	6,92E-6	5,15E-6	2,65E-5	4,93E-4	4,57E-4	1,28E-3	1,36E-3	5,23E-5	4,22E-5	5,85E-5	5,93E-5	1,34E-4	1,57E-4	1,75E-3	1,68E-3
AM243	<1,76E-6	<1,76E-6													
NP237				5,09E-4	9,66E-4					1,88E-2	1,60E-2	2,01E-2	2,24E-2	2,92E-2	2,93E-2
NP239	<1,76E-6	<1,76E-6													
CM244	5,60E-6	6,07E-6													
CM242	2,46E-6	3,74E-6													
PU238	4,81E-6	4,54E-6		2,51E-5	2,55E-5	1,88E-4	1,92E-4	4,43E-5	2,89E-5	1,38E-3	1,34E-3	1,15E-3	1,14E-3	1,78E-4	8,35E-5
PU239/40	4,87E-6	4,61E-6		2,63E-5	2,71E-5	1,98E-4	1,99E-4	4,18E-5	3,00E-5	1,48E-3	1,42E-3	1,24E-3	1,18E-3	1,90E-4	9,07E-5
PU241	5,86E-6	5,72E-6		1,67E-5	1,92E-5	1,84E-4	1,89E-4	3,77E-5	2,54E-5	1,36E-3	1,29E-3	1,03E-3	1,02E-3	1,83E-4	8,63E-5
U	1,92E-4									3,58E-2	3,63E-2	3,62E-2	3,80E-2	3,38E-2	3,27E-2
pHmeas+0,5			6,34	pH 5,34		pH 5,82									
Eh(mV)**			22mV	546 mV		259 mV		279 mV		197 mV		228 mV		648 mV	

**Ehmeas + 208 mV

* time since start of the static test

TABLE 11: Effect of pH and CO_2: Concentrations of radionuclides in leach solutions from spent fuel powder (mol/L)

Sample: **P 56(II) : 1,7 g (=1,5 g HM)** Solution: 95% sat **NaCl** Starting volume: 127 ml **Atmosphere: Ar/1%CO_2**
Temperature: 25 °C Final volume: 122 ml

	Ar-Atm.			static test											
	Ultrason. cleaning of 18,9 g (16,7 g HM) pwdr in 200 ml DIW		Wash (89 d)	no pH control 1. Sampling 15 days*		no pH control 2. Sampling 59 days*		pH = 7 3. Sampling 80 days*		pH = 9 4. Sampling 169 days*		pH = 11 5. Sampling 230 days*		pH = 7 (end) 6. Sampling 274 days*	
Nuclide	0,45 µm -filtered			0.45 µm	1.8 nm	0.45 µm	1.8 nm	0.45 µm	1.8 nm	0.45 µm	1.8 nm	0.45 µm	1.8 nm	0.45 µm	1.8 nm
RU106	1,3E-08	1,5E-08	2,87E-7	2,82E-7	2,74E-7	9,48E-7	1,08E-6	1,43E-6	1,54E-6	1,85E-6	1,92E-6	2,20E-6	2,05E-6	2,18E-6	2,55E-6
CS134	4,6E-06	6,5E-06	3,21E-6	2,16E-6	2,16E-6	6,27E-6	6,27E-6	7,11E-6	7,11E-6	1,29E-5	1,29E-5	1,75E-5	1,75E-5	2,08E-5	2,08E-5
CS137	4,4E-06	5,6E-06	3,10E-6	2,17E-6	2,17E-6	6,28E-6	6,28E-6	7,12E-6	7,12E-6	1,30E-5	1,30E-5	1,77E-5	1,77E-5	2,07E-5	2,07E-5
EU154	1,5E-10	1,6E-10	5,9E-10	1,69E-8	1,57E-8	4,93E-8	5,22E-8	3,48E-9	2,73E-9	5,31E-9	5,46E-9	1,17E-8	1,14E-8	6,71E-8	6,44E-8
EU155	1,6E-10	1,5E-10	5,2E-10	1,51E-8	1,39E-8	4,12E-8	4,33E-8	2,53E-9	2,01E-9	4,19E-9	4,85E-9	1,10E-8	1,03E-8	5,76E-8	5,56E-8
SB125	1,7E-10	1,6E-10	2,84E-9	7,31E-9	7,24E-9	1,88E-8	2,03E-8	7,73E-8	8,41E-8	1,82E-7	2,07E-7	1,47E-7	1,53E-7	1,66E-7	1,71E-7
SR90	4,4E-08	6,6E-08	4,69E-7	3,76E-7	3,83E-7	1,32E-6	1,41E-6	1,51E-6	2,03E-6	4,34E-6	4,44E-6	2,59E-6	2,74E-6	7,43E-6	7,65E-6
CE144	1,8E-09	2,1E-09	8,40E-9	2,56E-7	2,50E-7	5,61E-7	6,12E-7	4,81E-8	6,24E-8	8,36E-8	9,09E-8	<3,09E-8	<3,31E-8	<1,59E-7	<1,61E-7
TC99	<3,80E-9									8,33E-6	7,78E-6	8,79E-6	9,66E-6	8,84E-6	8,20E-6
AG110M		3,3E-36		4,65E-7	3,11E-7										
AM241	1,8E-10	1,3E-10	4,0E-10	1,19E-8	1,10E-8	3,26E-8	3,45E-8	1,38E-9	1,11E-9	1,45E-9	1,47E-9	3,33E-9	3,88E-9	4,36E-8	4,20E-8
AM243	<4,6E-11	<4,6E-11													
NP237				1,82E-8	3,46E-8					6,93E-7	5,89E-7	7,43E-7	8,26E-7	1,09E-6	1,09E-6
NP239	<6,8E-11	<6,8E-11													
CM244	3,1E-11	3,4E-11													
CM242	1,4E-11	2,1E-11													
PU238	2,9E-09	2,7E-09		1,40E-8	1,42E-8	1,11E-7	1,13E-7	2,72E-8	1,77E-8	7,91E-7	7,70E-7	6,63E-7	6,55E-7	1,03E-7	4,84E-8
PU239/40	2,9E-09	2,8E-09		1,46E-8	1,51E-8	1,16E-7	1,17E-7	2,57E-8	1,84E-8	8,47E-7	8,16E-7	7,14E-7	6,81E-7	1,10E-7	5,26E-8
PU241	3,5E-09	3,5E-09		9,33E-9	1,07E-8	1,08E-7	1,11E-7	2,31E-8	1,56E-8	7,79E-7	7,42E-7	5,92E-7	5,86E-7	1,06E-7	5,00E-8
U	9,7E-06														
pHmeas+0,5			6,34	pH 5,34		pH 5,82									
Eh(mV)**			22mV	546 mV		259 mV		279 mV		197 mV		228 mV		648 mV	

**Ehmeas + 208 mV

* time since start of the static test

TABLE 12: Effect of pH and CO_2: Incremental rates of radionuclides release from spent fuel powder (FIAP/d)

Sample: **P 56(II) : 1,7 g (=1,5 g HM)** Solution: 95% sat **NaCl** Starting volume: 127 ml **Atmosphere: Ar/1%CO_2**
Temperature: 25 °C Final volume: 122 ml

	Ar-Atm.		**static test**					
	Ultrason. cleaning of 18,9 g (16,7 g HM) pwdr in 200 ml DIW	**Wash** (89 d)	**no pH control** 1. Sampling 15 days*	**no pH control** 2. Sampling 59 days*	**pH = 7** 3. Sampling 80 days*	**pH = 9** 4. Sampling 169 days*	**pH = 11** 5. Sampling 230 days*	**pH = 7 (end)** 6. Sampling 274 days*
Nuclide	0,45 µm -filtered		0.45 µm 1.8 nm	0.45 µm 1.8 nm	0.45 µm 1.8 nm	0.45 µm 1.8 nm	0.45 µm 1.8 nm	0.45 µm 1.8 nm
RU106		1,26E-5	4,67E-5	3,48E-5	5,67E-5	1,69E-5	1,36E-5	
CS134		1,66E-4	4,22E-4	2,51E-4	1,45E-4	2,17E-4	2,12E-4	2,06E-4
CS137		1,60E-4	4,24E-4	2,51E-4	1,46E-4	2,21E-4	2,17E-4	1,81E-4
EU154		6,57E-7	7,05E-5	4,22E-5		1,58E-6	6,37E-6	7,55E-5
EU155		5,74E-7	6,28E-5	3,40E-5		1,37E-6	6,70E-6	6,36E-5
SB125		2,39E-5	2,32E-4	1,14E-4	1,22E-3	5,98E-4		1,84E-4
SR90		5,25E-5	1,59E-4	1,26E-4	6,90E-5	2,10E-4		6,66E-4
CE144		5,03E-7	5,78E-5	2,12E-5		1,56E-6		9,44E-6
TC99						6,71E-4	5,06E-5	
AG110M			2,55E-3					
AM241		2,97E-7	3,29E-5	1,80E-5		1,18E-7	1,24E-6	3,66E-5
AM243								
NP237			3,39E-5			2,11E-4	2,15E-5	2,07E-4
NP239								
CM244								
CM242								
PU238			1,67E-6	3,70E-6		1,50E-5		
PU239/40			1,75E-6	3,90E-6		1,62E-5		
PU241			1,11E-6	3,80E-6		1,49E-5		
U						4,02E-4	5,77E-6	
pHmeas+0,5		6,34	pH 5,34	pH 5,82				
Eh(mV)**		22mV	546 mV	259 mV	279 mV	197 mV	228 mV	648 mV

**Ehmeas + 208 mV

* time since start of the static test

TABLE 13: Activity of leach solutions from spent fuel powder corrosion tests (Bq/ml)

Sample:	**P 4 : 2,8 g (=2,4 g HM)**		Temperature: 25 °C		**Atmosphere: Ar/ 0,03%CO2**							
			Solution:Granite water (EGW) Starting volume: 200 ml Final volume: 174 ml						**Granite-bentonite water (GBW)** Starting volume: 203 ml Final volume: 187 ml			
			static test									
	Ultrason. cleaning of 18,9 g (16,7 g HM) pwdr in 200 ml DIW		Wash 55 days		1. Sampling 49 days*		2. Sampling 201 days*		3. Sampling 545 days*		4. Sampling 617 days*		5. Sampling 750 days*	
Nuclide	0,45 µm -filtered		0.45 µm	1.8 nm	0.45 µm	1.8 nm	0.45 µm	1.8 nm	0.45 µm	1.8 nm	0.45 µm	1.8 nm	0.45 µm	1.8 nm
RU106	6,92E+3	6,29E+3	1,36E+3	9,44E+2	5,47E+2	1,26E+2	1,52E+2	1,34E+2	8,21E+2					
CS134	4,03E+6	5,11E+6	3,34E+5	3,34E+5	7,68E+4	7,68E+4	2,21E+5	2,21E+5	1,73E+5	1,73E+5	5,23E+5	5,23E+5	5,33E+5	5,33E+5
CS137	6,03E+6	7,66E+6	1,58E+6	1,58E+6	3,69E+5	3,69E+5	1,23E+6	1,23E+6	1,23E+6	1,23E+6	3,87E+6	3,87E+6	4,48E+6	4,48E+6
EU154	2,75E+2	2,85E+2	8,64E+1	2,23E+1	1,23E+2	4,20E+0	3,05E+3	3,45E+1	5,14E+3	1,48E+1	3,93E+3	2,47E+3	1,04E+4	5,36E+3
EU155	1,50E+2	1,35E+2	3,17E+1	1,34E+1	4,68E+1	<1,5E+0	1,11E+3	1,82E+1	1,74E+3	4,32E+0	1,26E+3	7,90E+2	3,22E+3	1,64E+3
SB125	9,25E+2	8,14E+2	1,06E+4	1,26E+4	1,53E+4	1,60E+4	8,33E+3	8,07E+3	1,19E+4	1,01E+4	1,54E+3	1,52E+3	1,10E+3	8,38E+2
SR90	8,88E+4	1,33E+5	2,76E+5	9,04E+4	3,51E+4	1,45E+4	5,57E+4	2,79E+4	4,75E+4	2,57E+4	3,00E+6	3,28E+6	3,83E+6	2,99E+6
CE144	1,11E+3	9,99E+2	1,61E+1	6,50E+0	2,17E+1	<5,9E+0	7,07E+2	<5,4E+0	5,87E+2	<7,56E+0	<1,8E+2	<1,8E+2	<1,7E+2	<1,5E+2
TC99	<1,48E+0				5,70E+1	5,80E+1	5,33E+0	5,10E+0	5,08E+2	5,64E+2	1,23E+2	1,26E+2	2,40E+2	1,84E+2
AM241	3,26E+1	2,59E+1	<2,3E+0	<1,7E+0	6,00E+1	1,60E+0	9,65E+2	2,17E+0	1,96E+3	<1,99E+0	3,00E+2	1,72E+2	9,09E+2	4,53E+2
AM243	<3,70E-1	<3,70E-1												
NP237			1,51E+0	1,52E+0	2,18E-1	1,64E-1	1,46E-1	3,73E-2	4,81E-1	3,88E-1	4,32E+0	5,22E+0	8,41E+0	6,37E+0
NP239	<3,70E-1	<3,70E-1												
CM244	2,07E+2	2,22E+2			1,88E+2	3,67E+0	3,78E+3	1,25E+1						
CM242	5,92E+0	5,55E+0			3,31E-1	1,07E-2	8,37E+0	2,97E-2						
PU238	1,33E+2	1,25E+2	1,55E+2	4,97E+1	5,33E+2	2,73E+1	5,53E+3	4,93E+1	9,77E+3	9,29E+1	1,02E+3	1,10E+3	1,15E+3	8,46E+2
PU239/40	2,11E+1	2,00E+1	2,55E+1	8,04E+0	9,83E+1	5,77E+0	1,07E+3	1,07E+1	1,68E+3	1,59E+1	1,81E+2	1,88E+2	2,04E+2	1,45E+2
PU241	3,89E+3	3,74E+3	3,63E+3	1,15E+3	1,15E+4	7,50E+2	1,22E+5	1,23E+3	1,96E+5	1,87E+3	1,59E+4	1,83E+4	2,29E+4	1,64E+4
U (µg/ml)	*1,50E+1*		*3,35E+1*	*1,13E+1*	*1,28E+1*	*6,60E+0*	*4,07E+0*	*4,64E-1*	*4,07E+0*	*1,42E-1*	*8,52E-2*	*6,36E-2*	*7,03E-2*	*6,56E-2*
pHmeas			pH 7,34		pH 8,0		pH 7,96		pH 7,21		pH 7,42		pH 7,38	
Eh(mV)**			401 mV		422 mV		336 mV		379 mV		608 mV		298 mV	

**Ehmeas + 208 mV

* time since start of the static test

TABLE 14: Released fractions (FIAP) of radionuclide inventories in leachates from spent fuel powder

Sample:	P 4 : 2,8 g (=2,4 g HM)		Temperature: 25 °C				Atmosphere: Ar/ 0,03%CO2							
			Solution:Granite water (EGW) Starting volume: 200 ml Final volume: 174 ml								Granite-bentonite water (GBW) Starting volume: 203 ml Final volume: 187 ml			
			static test											
	Ultrason. cleaning of 18,9 g (16,7 g HM) pwdr in 200 ml DIW		Wash 55 days		1. Sampling 49 days*		2. Sampling 201 days*		3. Sampling 545 days*		4. Sampling 617 days*		5. Sampling 750 days*	
Nuclide	0,45 µm -filtered		0.45 µm	1.8 nm	0.45 µm	1.8 nm	0.45 µm	1.8 nm	0.45 µm	1.8 nm	0.45 µm	1.8 nm	0.45 µm	1.8 nm
RU106	3,03E-5	3,41E-5	4,55E-4	3,16E-4	2,44E-4	5,62E-5	6,32E-5	5,57E-5	5,62E-4					
CS134	1,25E-2	1,76E-2	1,40E-2	1,40E-2	5,33E-3	5,33E-3	1,64E-2	1,64E-2	1,59E-2	1,59E-2	5,89E-2	5,89E-2	6,33E-2	6,33E-2
CS137	1,19E-2	1,52E-2	2,24E-2	2,24E-2	5,42E-3	5,42E-3	1,70E-2	1,70E-2	1,62E-2	1,62E-2	5,97E-2	5,97E-2	6,40E-2	6,40E-2
EU154	8,65E-6	9,20E-6	2,47E-5	6,38E-6	3,64E-5	1,24E-6	8,39E-4	9,49E-6	1,41E-3	4,06E-6	1,28E-3	8,02E-4	3,20E-3	1,65E-3
EU155	9,16E-6	8,61E-6	2,18E-5	9,21E-6	3,41E-5	<1,1E-6	7,52E-4	1,23E-5	1,24E-3	3,07E-6	1,07E-3	6,70E-4	2,66E-3	1,35E-3
SB125	7,53E-5	7,16E-5	1,43E-2	1,70E-2	2,29E-2	2,39E-2	1,16E-2	1,12E-2	1,90E-2	1,62E-2	2,98E-3	2,95E-3	2,17E-3	1,65E-3
SR90	2,56E-4	3,87E-4	5,97E-3	1,96E-3	7,67E-4	3,17E-4	1,13E-3	5,67E-4	9,21E-4	4,99E-4	6,82E-2	7,46E-2	8,08E-2	6,31E-2
CE144	5,50E-6	6,51E-6	1,23E-5	4,96E-6	2,41E-5	<6,6E-6	7,31E-4	<5,6E-6	1,18E-3	<1,52E-5	<4,7E-4	<4,8E-4	<6,0E-4	<5,2E-4
TC99	<2,59E-5				6,87E-3	6,99E-3	5,98E-4	5,72E-4	5,33E-2	5,92E-2	1,51E-2	1,54E-2	2,70E-2	2,07E-2
AM241	6,92E-6	5,15E-6	<2,0E-6	<1,5E-6	4,89E-5	1,30E-6	7,32E-4	1,65E-6	1,28E-3	<1,30E-6	2,27E-4	1,30E-4	6,08E-4	3,03E-4
AM243	<1,76E-6	<1,76E-6												
NP237			6,87E-3	6,92E-3	9,93E-4	7,47E-4	6,18E-4	1,58E-4	1,91E-3	1,54E-3	2,00E-2	2,42E-2	3,57E-2	2,71E-2
NP239	<1,76E-6	<1,76E-6												
CM244	5,60E-6	6,07E-6			4,07E-5	7,94E-7	7,60E-4	2,51E-6						
CM242	2,46E-6	3,74E-6			4,19E-4	3,70E-5	9,88E-3	3,51E-5						
PU238	4,81E-6	4,54E-6	3,97E-5	1,27E-5	1,37E-4	7,01E-6	1,32E-3	1,18E-5	2,20E-3	2,09E-5	2,68E-4	2,89E-4	2,79E-4	2,05E-4
PU239/40	4,87E-6	4,61E-6	4,06E-5	1,28E-5	1,56E-4	9,18E-6	1,58E-3	1,58E-5	2,33E-3	2,20E-5	2,93E-4	3,04E-4	3,03E-4	2,15E-4
PU241	5,86E-6	5,72E-6	4,47E-5	1,42E-5	1,44E-4	9,42E-6	1,42E-3	1,44E-5	2,23E-3	2,13E-5	2,13E-4	2,45E-4	2,87E-4	2,05E-4
U	1,92E-4		2,96E-3	9,99E-4	1,13E-3	5,83E-4	3,34E-4	3,81E-5	3,13E-4	1,09E-5	7,65E-6	5,71E-6	5,80E-6	5,41E-6
Kr85											1,38E-2		6,74E-3	
pHmeas			pH 7,34		pH 8,0		pH 7,96		pH 7,21		pH 7,42		pH 7,38	
Eh(mV)**			401 mV		422 mV		336 mV		379 mV		608 mV		298 mV	

**Ehmeas + 208 mV

* time since start of the static test

TABLE 15: Concentrations of radionuclides in leach solutions from spent fuel powder corrosion tests (mol/L)

Sample:	**P 4 : 2,8 g (=2,4 g HM)**		Temperature: 25 °C		**Atmosphere: Ar/ 0,03%CO2**									
			Solution:Granite water (EGW) Starting volume: 200 ml Final volume: 174 ml						**Granite-bentonite water (GBW)** Starting volume: 203 ml Final volume: 187 ml					
			static test											
	Ultrason. cleaning of 18,9 g (16,7 g HM) pwdr in 200 ml DIW		Wash 55 days		1. Sampling 49 days*		2. Sampling 201 days*		3. Sampling 545 days*		4. Sampling 617 days*		5. Sampling 750 days*	
Nuclide	0,45 µm -filtered		0.45 µm	1.8 nm	0.45 µm	1.8 nm	0.45 µm	1.8 nm	0.45 µm	1.8 nm	0.45 µm	1.8 nm	0.45 µm	1.8 nm
RU106	1,3E-08	1,5E-08	1,88E-7	1,30E-7	1,01E-7	2,32E-8	2,80E-8	2,47E-8	2,66E-7					
CS134	4,6E-06	6,5E-06	4,90E-6	4,90E-6	1,87E-6	1,87E-6	6,19E-6	6,19E-6	6,39E-6	6,39E-6	2,03E-5	2,03E-5	2,38E-5	2,38E-5
CS137	4,4E-06	5,6E-06	7,85E-6	7,85E-6	1,90E-6	1,90E-6	6,39E-6	6,39E-6	6,51E-6	6,51E-6	2,06E-5	2,06E-5	2,40E-5	2,40E-5
EU154	1,5E-10	1,6E-10	4,06E-10	1,05E-10	5,97E-10	2,04E-11	1,48E-8	1,67E-10	2,66E-8	7,67E-11	2,06E-8	1,29E-8	5,63E-8	2,90E-8
EU155	1,6E-10	1,5E-10	3,57E-10	1,51E-10	5,59E-10	1,81E-11	1,33E-8	2,18E-10	2,33E-8	5,79E-11	1,72E-8	1,08E-8	4,67E-8	2,38E-8
SB125	1,7E-10	1,6E-10	3,08E-8	3,66E-8	4,93E-8	5,16E-8	2,69E-8	2,60E-8	4,71E-8	4,00E-8	6,33E-9	6,24E-9	5,02E-9	3,82E-9
SR90	4,4E-08	6,6E-08	9,66E-7	3,16E-7	1,24E-7	5,13E-8	1,97E-7	9,87E-8	1,71E-7	9,27E-8	1,09E-5	1,19E-5	1,40E-5	1,09E-5
CE144	1,8E-09	2,1E-09	3,72E-9	1,50E-9	7,28E-9	<2,0E-9	2,38E-7	<1,8E-9	4,10E-7	<5,28E-9	<1,4E-7	<1,4E-7	<1,9E-7	<1,7E-7
TC99	<3,80E-9				9,56E-7	9,73E-7	8,94E-8	8,55E-8	8,52E-6	9,46E-6	2,06E-6	2,11E-6	4,02E-6	3,09E-6
AM241	1,8E-10	1,3E-10	<4,9E-11	<3,7E-11	1,21E-9	3,21E-11	1,94E-8	4,36E-11	3,64E-8	<3,7E-11	5,49E-9	3,15E-9	1,61E-8	8,00E-9
AM243	<4,6E-11	<4,6E-11												
NP237			2,52E-7	2,54E-7	3,64E-8	2,74E-8	2,44E-8	6,23E-9	8,03E-8	6,48E-8	7,21E-7	8,71E-7	1,40E-6	1,06E-6
NP239	<6,8E-11	<6,8E-11												
CM244	3,1E-11	3,4E-11			2,16E-10	4,21E-12	4,34E-9	1,44E-11						
CM242	1,4E-11	2,1E-11												
PU238	2,9E-09	2,7E-09	2,27E-8	7,27E-9	7,82E-8	4,01E-9	8,12E-7	7,24E-9	1,44E-6	1,37E-8	1,51E-7	1,63E-7	1,71E-7	1,26E-7
PU239/40	2,9E-09	2,8E-09	2,32E-8	7,31E-9	8,94E-8	5,25E-9	9,73E-7	9,73E-9	1,53E-6	1,45E-8	1,65E-7	1,71E-7	1,86E-7	1,32E-7
PU241	3,5E-09	3,5E-09	2,55E-8	8,09E-9	8,25E-8	5,38E-9	8,76E-7	8,83E-9	1,46E-6	1,40E-8	1,20E-7	1,38E-7	1,76E-7	1,26E-7
U	9,7E-06		1,41E-4	4,75E-5	5,38E-5	2,77E-5	1,71E-5	1,95E-6	1,71E-5	5,97E-7	3,58E-7	2,67E-7	2,95E-7	2,76E-7
pHmeas			pH 7,34		pH 8,0		pH 7,96		pH 7,21		pH 7,42		pH 7,38	
Eh(mV)**			401 mV		422 mV		336 mV		379 mV		608 mV		298 mV	

**Ehmeas + 208 mV

* time since start of the static test

TABLE 16: Incremental rates of radionuclides release from spent fuel powder corrosion tests (FIAP/d)

Sample:	**P 4 : 2,8 g (=2,4 g HM)**	Temperature: 25 °C			**Atmosphere: Ar/ 0,03%CO2**		
			Solution:Granite water (EGW) Starting volume: 200 ml Final volume: 174 ml			**Granite-bentonite water (GBW)** Starting volume: 203 ml Final volume: 187 ml	
			static test				
	Ultrason. cleaning of 18,9 g (16,7 g HM) pwdr in 200 ml DIW	Wash 55 days	1. Sampling 49 days*	2. Sampling 201 days*	3. Sampling 545 days*	4. Sampling 617 days*	5. Sampling 750 days*
Nuclide	0,45 µm -filtered	0.45 µm 1.8 nm	0.45 µm 1.8 nm	0.45 µm 1.8 nm	0.45 µm 1.8 nm	0.45 µm 1.8 nm	0.45 µm 1.8 nm
RU106		8,3E-06	4,98E-6		1,46E-6		
CS134		2,5E-04	1,09E-4	7,49E-5	9,53E-7		6,34E-5
CS137		4,1E-04	1,11E-4	7,78E-5	3,78E-7	8,29E-4	6,28E-5
EU154		4,5E-07	7,43E-7	5,29E-6	1,80E-6	8,29E-4	1,51E-5
EU155		4,0E-07	6,96E-7	4,74E-6	1,53E-6		1,25E-5
SB125		2,6E-04	4,67E-4		2,35E-5		
SR90		1,1E-04	1,57E-5	2,66E-6		9,48E-4	1,29E-4
CE144		2,2E-07	4,91E-7	4,66E-6	1,42E-6	6,48E-6	1,23E-6
TC99			1,40E-4		1,53E-4	2,09E-4	9,73E-5
AM241		3,6E-08	9,98E-7	4,51E-6	1,72E-6	3,15E-6	2,98E-6
AM243							
NP237		1,2E-04	2,03E-5	-2,13E-6	3,84E-6	2,78E-4	1,28E-4
NP239							
CM244			8,30E-7	4,75E-6			
CM242			8,54E-6	6,24E-5			
PU238		7,2E-07	2,79E-6	7,84E-6	2,76E-6	3,73E-6	2,13E-7
PU239/40		7,4E-07	3,19E-6	9,44E-6	2,41E-6	4,07E-6	2,24E-7
PU241		8,1E-07	2,95E-6	8,47E-6	2,56E-6	2,95E-6	6,65E-7
U		5,4E-05	2,31E-5			1,06E-7	
pHmeas		pH 7,34	pH 8,0	pH 7,96	pH 7,21	pH 7,42	pH 7,38
Eh(mV)**		401 mV	422 mV	336 mV	379 mV	608 mV	298 mV

**Ehmeas + 208 mV

* time since start of the static test

TABLE 17: Long-term effect of iron: Activity of leach solutions from spent fuel pellet (Bq/ml)

Sample:	**K4 : 7,5 g (=6,6 g HM)**		Temperature: 25 °C				**Atmosphere: Ar**					
			Solution: 5m NaCl solution									
			Starting volume: 200 Final volume: 156 ml ml									
			static test (addition of 9,2 g Fe-powder)									
	Wash (200 ml-NaCl 5m) 31 days	Wash (200 ml NaCl 5m) 42 days	1. Sampling 50 days*		2. Sampling 112 days*		3. Sampling 207 days*		4. Sampling 438 days*		5. Sampling 1619 days*	
Nuclide	0,45 µm -filtered	0.45 µm	0.45 µm	1.8 nm	0.45 µm	1.8 nm	0.45 µm	1.8 nm	0.45 µm	1.8 nm	0.45 µm	1.8 nm'
RU106	5,33E+2	4,81E+2	<4,24E-1		<4,24E-1		<1,15E+1		<1,69E+1			
CS134	1,50E+6	8,03E+5	1,05E+6	1,12E+6	1,62E+6	1,72E+6	2,14E+6	2,18E+6	1,83E+6		6,06E+5	
CS137	1,92E+6	1,16E+6	1,95E+6	2,08E+6	2,85E+6	3,07E+6	4,01E+6	4,06E+6	3,67E+6		3,64E+6	
EU154	1,11E+2	1,70E+2	<4,24E-1		<4,24E-1		<1,15E+1		<7,04E+0		<1,27E+0	
EU155	5,55E+1	1,15E+2	<4,24E-1		<4,24E-1		<1,15E+1		<3,37E+0		<1,29E+0	
SB125	6,51E+2	1,63E+2	<4,24E-1		<4,24E-1		<1,15E+1		<1,26E+1		<7,38E+0	
SR90	4,70E+4	1,11E+4	2,12E+2		1,16E+3		1,70E+3		5,60E+3		4,97E+3	
CE144	2,59E+3	7,03E+2	<4,24E-1		<4,24E-1		<1,15E+1		<8,43E+0		<5,29E+0	
TC99	<1,48E+0										<3,23E-1	
AG110M	2,27E+2		<4,24E-1		<4,24E-1		<1,15E+1		<3,37E+0			
AM241	8,55E+1	3,03E+1	<4,24E-1		<4,24E-1		<4,03E+0		<4,27E+0		<1,12E+0	
AM243	1,30E+0	1,48E+0			<1,14E+0		<1,15E+0					
NP237	4,81E-2	3,70E-2									<5,63E-3	
NP239	2,59E-1	1,48E+0										
CM244	7,62E+1	1,81E+2	<2,29E-1		<2,29E-1		<2,29E-1		3,12E+0			
CM242	2,85E+0	4,44E+0					<0,00E+0		5,08E-2			
PU238	1,82E+2	4,22E+1	<2,54E-3	<2,22E-3	<2,54E-2	<2,22E-1	<2,64E-2		6,70E+0		<1,63E-1	
PU239/40	8,99E+1	5,44E+0	<2,54E-3	<2,22E-3	<2,54E-2	<1,48E-1	<2,64E-2				4,50E-2	
PU241	5,03E+3	1,27E+3										
U (µg/ml)	1,20E+0				9,16E-2		6,88E-2		1,37E-2		6,76E-3	
PHmeas+0,5	6,32	6,53	8,48		8		8,71		10,1		9,45	
Eh(mV)**	586	532	323		328		338		-132		71	

**Ehmeas + 208 mV

* time since start of the static test

'failed

TABLE 18: Long-term effect of iron: Released fractions of radionuclide inventories(FIAP) from spent fuel pellet

Sample:	**K4 : 7,5 g (=6,6 g HM)**		Temperature: 25 °C				**Atmosphere: Ar**					
			Solution: 5m NaCl solution									
			Starting volume: 200 ml Final volume: 156 ml									
			static test (addition of 9,2 g Fe-powder)									
	Wash (200 ml-NaCl 5m) 31 days	Wash (200 ml NaCl 5m) 42 days	1. Sampling 50 days*		2. Sampling 112 days*		3. Sampling 207 days*		4. Sampling 438 days*		5. Sampling 1619 days*	
Nuclide	0,45 µm -filtered	0.45 µm	0.45 µm	1.8 nm	0.45 µm	1.8 nm	0.45 µm	1.8 nm	0.45 µm	1.8 nm	0.45 µm	1.8 nm'
RU106	5,86E-6	6,55E-6	<7,80E-9		<7,37E-9		<1,88E-7		<3,47E-7			
CS134	1,17E-2	6,94E-3	1,06E-2	1,12E-2	1,53E-2	1,63E-2	1,91E-2	1,94E-2	1,76E-2		1,62E-2	
CS137	9,49E-3	5,76E-3	9,79E-3	1,05E-2	1,35E-2	1,46E-2	1,80E-2	1,82E-2	1,56E-2		1,55E-2	
EU154	8,79E-6	1,38E-5	<3,56E-8		<3,36E-8		<8,58E-7		<5,10E-7		<1,11E-7	
EU155	8,53E-6	1,84E-5	<7,23E-8		<6,83E-8		<1,74E-6		<5,09E-7		<2,86E-7	
SB125	1,33E-4	3,60E-5	<1,05E-7		<9,88E-8		<2,52E-6		<2,88E-6		<3,54E-6	
SR90	3,40E-4	8,10E-5	1,56E-6		8,06E-6		1,11E-5		3,48E-5		3,12E-5	
CE144	3,22E-5	1,15E-5	<1,02E-8		<9,68E-9		<2,47E-7		<2,47E-7		<2,56E-6	
TC99	<6,51E-5										<1,11E-5	
AG110M	2,82E-3		<1,12E-5		<1,06E-5		<2,71E-4		<1,14E-4			
AM241	4,56E-5	1,52E-5	<1,94E-7		<1,84E-7		<1,65E-6		<1,52E-6		<2,48E-7	
AM243	1,55E-5	1,77E-5			<1,29E-5		<1,22E-5				0,00E+0	
NP237	7,98E-5	6,14E-5									<7,29E-6	
NP239	3,09E-6	1,77E-5										
CM244	5,17E-6	1,25E-5	<1,60E-8		<1,51E-8		<1,43E-8		1,85E-7			
CM242	2,98E-6	7,51E-6							2,72E-7			
PU238	1,65E-5	3,84E-6	<2,3E-10	<2,0E-10	<2,19E-9	<1,92E-8	<2,14E-9		5,13E-7		<1,19E-8	
PU239/40	5,22E-5	3,16E-6	<1,47E-9	<1,29E-9	<1,39E-8	<1,22E-7	<1,36E-8				2,04E-8	
PU241	1,91E-5	4,90E-6										
U	3,87E-5				2,79E-6		1,97E-6		3,68E-7		1,70E-7	
Kr85									<1,19E-2		<4,52E-2	
pHmeas+0,5	6,32	6,53	8,48		8		8,71		10,1		9,45	
Eh(mV)**	586	532	323		328		338		-132		71	

**Ehmeas + 208 mV

* time since start of the static test

`failed

TABLE 19 : Long-term effect of iron: Concentrations of radionuclides in leachates from spent fuel pellet (mol/L)

Sample:	**K4 : 7,5 g (=6,6 g HM)**		Temperature: 25 °C				**Atmosphere: Ar**					
			Solution: 5m NaCl solution									
			Starting volume: 200 ml Final volume: 156 ml									
			static test (addition of 9,2 g Fe-powder)									
	Wash (200 ml-NaCl 5m) 31 days	Wash (200 ml NaCl 5m) 42 days	1. Sampling 50 days*		2. Sampling 112 days*		3. Sampling 207 days*		4. Sampling 438 days*		5. Sampling 1619 days*	
Nuclide	0,45 µm -filtered	0.45 µm	0.45 µm	1.8 nm	0.45 µm	1.8 nm	0.45 µm	1.8 nm	0.45 µm	1.8 nm	0.45 µm	1.8 nm
RU106	6,63E-9	7,41E-9	<8,8E-12		<8,8E-12		<2,4E-10		<4,7E-10			
CS134	1,12E-5	6,67E-6	1,01E-5	1,08E-5	1,56E-5	1,66E-5	2,07E-5	2,10E-5	2,03E-5		1,99E-5	
CS137	9,12E-6	5,54E-6	9,40E-6	1,01E-5	1,38E-5	1,48E-5	1,94E-5	1,96E-5	1,79E-5		1,91E-5	
EU154	3,96E-10	6,22E-10	<1,6E-12		<1,6E-12		<4,3E-11		<2,8E-11		<6,4E-12	
EU155	3,84E-10	8,28E-10	<3,3E-12		<3,3E-12		<8,8E-11		<2,7E-11		<1,6E-11	
SB125	7,87E-10	2,13E-10	<6,2E-13		<6,2E-13		<1,7E-11		<2,0E-11		<2,7E-11	
SR90	1,51E-7	3,60E-8	<6,9E-10		3,79E-9		5,56E-9		1,85E-8		1,78E-8	
CE144	2,68E-8	9,57E-9	<8,5E-12		<8,5E-12		<2,3E-10		<2,5E-10		<2,72E-9	
TC99	<2,48E-8										<5,42E-9	
AG110M	9,65E-8		<3,8E-10		<3,8E-10		<1,04E-8		<4,68E-9			
AM241	3,08E-9	1,02E-9	<1,3E-11		<1,3E-11		<1,2E-10		<1,2E-10		<2,1E-11	
AM243	1,04E-9	1,19E-9			<9,2E-10		<9,3E-10					
NP237	8,03E-9	6,18E-9									<9,4E-10	
NP239	3,11E-10	1,78E-9										
CM244	7,53E-11	1,81E-10	<2,3E-13		<2,3E-13	<0,00E+0	<2,3E-13		<3,2E-12			
CM242	4,34E-11	1,09E-10							<4,7E-12			
PU238	2,59E-8	6,02E-9	<3,6E-13	<3,2E-13	<3,6E-12	<3,2E-11	<3,8E-12		<9,6E-10		<2,4E-11	
PU239/40	8,18E-8	4,95E-9	<2,3E-12	<2,0E-12	<2,3E-11	<2,0E-10	<2,4E-11				<4,1E-11	
PU241	2,99E-8	7,68E-9										
U	5,04E-6				3,85E-7		2,89E-7		5,76E-8		2,84E-8	
pHmeas+0,5	6,32	6,53	8,48		8		8,71		10,1		9,45	
Eh(mV)**	586	532	323		328		338		-132		71	

**Ehmeas + 208 mV

* time since start of the static test

`failed

TABLE 20: Long-term effect of iron: Incremental release rates of radionuclides from spent fuel pellet (FIAP/d)

Sample:	**K4 : 7,5 g (=6,6 g HM)**		Temperature: 25 °C		**Atmosphere: Ar**		
			Solution: 5m NaCl solution				
			Starting volume: 200 ml Final volume: 156 ml				
			static test (addition of 9,2 g Fe-powder)				
	Wash (200 ml-NaCl 5m) 31 days	Wash (200 ml NaCl 5m) 42 days	1. Sampling 50 days*	2. Sampling 112 days*	3. Sampling 207 days*	4. Sampling 438 days*	5. Sampling 1619 days*
Nuclide	0,45 µm -filtered	0.45 µm	0.45 µm 1.8 nm	0.45 µm 1.8 nm	0.45 µm 1.8 nm	0.45 µm 1.8 nm	0.45 µm 1.8 nm
RU106	1,89E-7	1,56E-7	<1,6E-10		<1,90E-9	<7,4E-10	
CS134	3,77E-4	1,65E-4	2,11E-4	8,59E-5	4,96E-5		
CS137	3,06E-4	1,37E-4	1,96E-4	6,93E-5	5,48E-5		2,21E-7
EU154	2,84E-7	3,29E-7	<7,1E-10		<8,69E-9		
EU155	2,75E-7	4,38E-7	<1,45E-9		<1,76E-8		
SB125	4,30E-6	8,57E-7	<2,09E-9		<2,55E-8	<2,25E-9	<6,0E-10
SR90	1,10E-5	1,93E-6	3,12E-8	1,06E-7	3,74E-8	1,06E-7	
CE144	1,04E-6	2,74E-7	<2,0E-10		<2,50E-9	<6,7E-11	<1,96E-9
TC99	<2,10E-6						<9,38E-9
AG110M	9,10E-5		<2,25E-7		<2,75E-6		
AM241	1,47E-6	3,61E-7	<3,89E-9		<1,55E-8		
AM243	4,99E-7	4,21E-7		<2,08E-7	<3,4E-10		
NP237	2,58E-6	1,46E-6					<6,17E-9
NP239	9,97E-8	4,21E-7					
CM244	1,67E-7	2,96E-7	<3,2E-10		<4,0E-13	<7,4E-10	
CM242	9,61E-8	1,79E-7				1,18E-9	
PU238	5,33E-7	9,14E-8	<4,6E-12	<3,2E-11	<8,2E-13	2,21E-9	
PU239/40	1,68E-6	7,51E-8	<2,9E-11	<2,0E-10	<5,2E-12		1,7E-11
PU241	6,15E-7	1,17E-7					
U	1,25E-6			4,50E-8			
Kr85						1,99E-4	4,17E-5
pHmeas+0,5	6,32	6,53	8,48	8	8,71	10,1	9,45
Eh(mV)**	586	532	323	328	338	-132	71

**Ehmeas + 208 mV

* time since start of the static test

`failed

TABLE 21: Activity of leach solutions from spent fuel pellet corrosion tests (Bq/ml)

Sample:	**K9 : 7,4 g (=6,6 g HM)**		Temperature: 25 °C				**Atmosphere: Ar**					
			Solution: 5m NaCl solution									
			Starting volume: 200 ml									
			Final volume: 155 ml									
			static test									
	Wash (200 ml-NaCl 5m) 31 days	Wash (200 ml NaCl 5m) 42 days	1. Sampling 53 days*		2. Sampling 116 days*		3. Sampling 207 days*		4. Sampling 441 days*		5. Sampling 1624 days*	
Nuclide	0,45 µm -filtered	0.45 µm	0.45 µm	1.8 nm	0.45 µm	1.8 nm	0.45 µm	1.8 nm	0.45 µm	1.8 nm	0.45 µm	1.8 nm
RU106	5,51E+2	5,18E+2	1,18E+2	9,02E+1	2,41E+1		1,50E+2	1,90E+2	4,58E+1			
CS134	1,67E+6	1,36E+5	2,96E+5	2,93E+5	3,38E+5	3,74E+5	4,06E+5		7,33E+5		9,36E+5	9,36E+5
CS137	2,12E+6	1,86E+5	5,19E+5	5,18E+5	5,69E+5	6,33E+5	7,35E+5		1,38E+6		5,58E+6	5,58E+6
EU154	1,08E+2	1,81E+2	1,52E+2	9,88E+1	3,81E+1	8,73E+0	1,31E+1	<6,18E-1			<2,00E+0	<1,85E+0
EU155	6,03E+1	1,15E+2	8,85E+1	5,58E+1	2,54E+1		5,93E+0	<1,19E+0			<2,34E+0	<2,22E+0
SB125	5,14E+2	1,04E+2	1,14E+2	8,59E+1	4,23E+1	4,81E+1	1,74E+2	1,55E+2	2,20E+2		3,14E+2	3,33E+2
SR90	3,33E+4	2,48E+3	5,82E+3		1,06E+4		1,81E+4		3,67E+4		1,22E+5	1,23E+5
CE144	2,09E+3	9,99E+2	3,37E+1	2,49E+1	4,23E-1		<1,95E+0	<2,03E+0			<4,00E+0	<7,55E+0
TC99	<1,48E+0										3,84E+1	3,32E+1
AG110M	5,74E+1	5,18E+1	1,39E+2	1,12E+2			3,78E+2	3,71E+2	2,58E+2			
AM241	8,51E+1	2,22E+1	2,53E+1	1,12E+1	8,46E+0		8,05E+0	4,42E+0	<1,46E+0		<2,24E+0	<2,17E+0
AM243	<3,70E-1	<1,48E+0	<1,14E+0		2,62E+0		5,72E+0					
NP237	<3,70E-2	<3,70E-2	<4,21E-3		<4,23E-3						<7,34E-4	<7,40E-4
NP239	<3,70E-1	<1,48E+0	4,21E-1									
CM244	1,14E+2	2,68E+2	9,90E+1		2,62E+1		1,26E+1		3,57E-1			
CM242	4,55E+0	6,83E+0	8,01E-1									
PU238	1,39E+2	5,55E+1	2,74E+1	3,22E+1	1,13E+2	1,20E+2	3,59E+1		1,13E+1		2,17E-1	6,87E-1
PU239/40	4,44E+1	6,66E+0	5,06E+0	4,73E+0	1,61E+1	2,01E+1	5,04E+0		1,31E+0		5,63E-1	2,95E-1
PU241	3,58E+3	1,30E+3		6,39E+2		2,60E+3			1,13E+2		5,80E+1	6,36E+1
U (µg/ml)	*1,20E+0*				*5,72E-1*	*5,89E-1*	*8,01E-1*		*8,40E-1*		*3,57E-1*	*4,38E-2*
pHmeas+0,5	6,25	6,33	8,1		7,98		7,55		9,73		10,27	
Eh(mV)**	571	503	322		350		344		-7		479	

**Ehmeas + 208 mV

* time since start of the static test

TABLE 22: Released fractions (FIAP)of radionuclide inventories in leachates from spent fuel pellet

Sample:	**K9 : 7,4 g (=6,6 g HM)**		Temperature: 25 °C				**Atmosphere: Ar**					
			Solution: 5m NaCl solution									
			Starting volume: 200 ml									
			Final volume: 155 ml									
			static test									
	Wash (200 ml-NaCl 5m) 31 days	Wash (200 ml NaCl 5m) 42 days	1. Sampling 53 days*		2. Sampling 116 days*		3. Sampling 207 days*		4. Sampling 441 days*		5. Sampling 1624 days*	
Nuclide	0,45 µm -filtered	0.45 µm	0.45 µm	1.8 nm	0.45 µm	1.8 nm	0.45 µm	1.8 nm	0.45 µm	1.8 nm	0.45 µm	1.8 nm
RU106	6,15E-6	7,15E-6	2,20E-6	1,68E-6	4,25E-7		2,87E-6	1,62E-5	9,52E-7			
CS134	1,32E-2	1,19E-3	3,01E-3	2,98E-3	3,25E-3	3,59E-3	3,94E-3	1,83E-2	7,16E-3		2,52E-2	2,52E-2
CS137	1,06E-2	9,39E-4	2,65E-3	2,64E-3	2,74E-3	3,05E-3	3,35E-3	1,49E-2	5,93E-3		2,40E-2	2,40E-2
EU154	8,67E-6	1,49E-5	1,29E-5	8,41E-6	3,06E-6	7,03E-7	1,01E-6	<2,46E-5			<1,76E-7	<1,63E-7
EU155	9,39E-6	1,86E-5	1,53E-5	9,65E-6	4,14E-6		9,39E-7	<2,90E-5			<5,22E-7	<4,95E-7
SB125	1,07E-4	2,32E-5	2,84E-5	2,15E-5	9,99E-6	1,14E-5	4,08E-5	1,71E-4	5,10E-5		1,52E-4	1,61E-4
SR90	2,44E-4	1,83E-5	4,35E-5		7,47E-5		1,21E-4	3,84E-4	2,31E-4		7,72E-4	7,79E-4
CE144	2,64E-5	1,66E-5	8,26E-7	6,11E-7	9,79E-9		<5,10E-8	<4,30E-5			<1,95E-6	<3,68E-6
TC99	<6,59E-5										1,33E-3	1,15E-3
AG110M	7,23E-4	8,94E-4	3,74E-3	3,00E-3	1,07E-5		1,11E-2	1,27E-2	8,85E-3			
AM241	4,60E-5	1,12E-5	1,18E-5	5,19E-6	3,71E-6		3,21E-6	6,05E-5	<5,26E-7		<4,99E-7	<4,83E-7
AM243	<4,48E-6	<1,79E-5	<1,38E-5		3,00E-5		6,16E-5	8,40E-5				
NP237	<6,22E-5	<6,22E-5	<7,09E-6		<6,72E-6						<9,57E-7	<9,65E-7
NP239	<4,48E-6	<1,79E-5	5,10E-6									
CM244	7,83E-6	1,86E-5	7,01E-6		1,75E-6		7,99E-7	2,73E-5	2,14E-8			
CM242	4,83E-6	1,17E-5	2,71E-6									
PU238	1,28E-5	5,12E-6	2,53E-6	2,98E-6	9,91E-6	1,05E-5	2,97E-6	2,08E-5	8,76E-7		1,60E-8	5,07E-8
PU239/40	2,61E-5	3,92E-6	2,97E-6	2,78E-6	8,93E-6	1,12E-5	2,64E-6	3,27E-5	6,43E-7		2,57E-7	1,34E-7
PU241	1,38E-5	5,08E-6		2,55E-6					3,83E-7		2,13E-7	2,34E-7
U	3,92E-5				1,76E-5	1,82E-5	2,33E-5	6,25E-5	2,29E-5		9,03E-6	1,11E-6
Kr85									2,04E-3		1,57E-1	
pHmeas+0,5	6,25	6,33	8,1		7,98		7,55		9,73		10,27	
Eh(mV)**	571	503	322		350		344		-7		479	

**Ehmeas + 208 mV

* time since start of the static test

TABLE 23: Concentrations of radionuclides in leach solutions from spent fuel pellet (mol/L)

Sample: **K9 : 7,4 g (=6,6 g HM)** Temperature: 25 °C **Atmosphere: Ar**

Solution: 5m NaCl solution

Starting volume: 200 ml

Final volume: 155 ml

			static test									
	Wash (200 ml-NaCl 5m) 31 days	Wash (200 ml NaCl 5m) 42 days	1. Sampling 53 days*		2. Sampling 116 days*		3. Sampling 207 days*		4. Sampling 441 days*		5. Sampling 1624 days*	
Nuclide	0,45 µm -filtered	0.45 µm	0.45 µm	1.8 nm	0.45 µm	1.8 nm	0.45 µm	1.8 nm	0.45 µm	1.8 nm	0.45 µm	1.8 nm
RU106	6,86E-9	7,98E-9	2,46E-9	1,88E-9	5,02E-10	0,00E+0	3,60E-9	4,55E-9	1,27E-9			
CS134	1,25E-5	1,13E-6	2,85E-6	2,83E-6	3,26E-6	3,60E-6	4,19E-6	0,00E+0	8,13E-6		3,08E-5	3,08E-5
CS137	1,01E-5	8,90E-7	2,51E-6	2,50E-6	2,75E-6	3,06E-6	3,57E-6	0,00E+0	6,73E-6		2,93E-5	2,93E-5
EU154	3,85E-10	6,62E-10	5,74E-10	3,74E-10	1,44E-10	3,30E-11	5,05E-11	<2,38E-12			<1,01E-11	<9,33E-12
EU155	4,17E-10	8,28E-10	6,79E-10	4,29E-10	1,95E-10		4,68E-11	<9,42E-12			<2,99E-11	<2,84E-11
SB125	6,22E-10	1,35E-10	1,66E-10	1,25E-10	6,17E-11	7,01E-11	2,67E-10	2,37E-10	3,56E-10		1,14E-9	1,21E-9
SR90	1,07E-7	8,03E-9	1,90E-8	0,00E+0	3,46E-8		5,95E-8	0,00E+0	1,21E-7		4,37E-7	4,40E-7
CE144	2,16E-8	1,36E-8	6,77E-10	5,00E-10	8,49E-12		<4,70E-11	<4,90E-11			<2,06E-9	<3,89E-9
TC99	<2,48E-8										6,44E-7	5,57E-7
AG110M	2,44E-8	3,02E-8	1,26E-7	1,01E-7	3,84E-10		4,22E-7	4,15E-7	3,58E-7			
AM241	3,07E-9	7,49E-10	7,84E-10	3,46E-10	2,62E-10		2,40E-10	1,32E-10	<4,20E-11		<4,29E-11	<4,16E-11
AM243	<2,98E-10	<1,19E-9	<9,18E-10		2,12E-9		4,62E-9					
NP237	<6,18E-9	<6,18E-9	<7,04E-10		<7,06E-10						<1,23E-10	<1,24E-10
NP239	<4,44E-10	<1,78E-9	5,06E-10		0,00E+0							
CM244	1,13E-10	2,68E-10	1,01E-10		2,67E-11		1,29E-11		3,69E-13			
CM242	6,93E-11	1,68E-10	3,90E-11		0,00E+0				0,00E+0			
PU238	1,97E-8	7,92E-9	3,92E-9	4,61E-9	1,62E-8	1,72E-8	5,15E-9		1,62E-9		3,20E-11	1,01E-10
PU239/40	4,04E-8	6,06E-9	4,60E-9	4,30E-9	1,46E-8	1,83E-8	4,58E-9		1,19E-9		5,12E-10	2,68E-10
PU241	2,13E-8	7,86E-9		3,94E-9		1,60E-8			7,10E-10		4,26E-10	4,67E-10
U	5,04E-6				2,40E-6	2,47E-6	3,37E-6		3,53E-6		1,50E-6	1,84E-7
pHmeas+0,5	6,25	6,33	8,1		7,98		7,55		9,73		10,27	
Eh(mV)**	571	503	322		350		344		-7		479	

**Ehmeas + 208 mV

* time since start of the static test

TABLE 24 : Incremental rates of radionuclides release from spent fuel pellet corrosion tests (FIAP/d)

Sample: **K9 : 7,4 g (=6,6 g HM)** Temperature: 25 °C **Atmosphere: Ar**

Solution: 5m NaCl solution
Starting volume: 200 ml
Final volume: 155 ml

			static test				
	Wash (200 ml-NaCl 5m) 31 days	Wash (200 ml NaCl 5m) 42 days	1. Sampling 53 days*	2. Sampling 116 days*	3. Sampling 207 days*	4. Sampling 441 days*	5. Sampling 1624 days*
Nuclide	0,45 µm -filtered	0.45 µm	0.45 µm 1.8 nm	0.45 µm 1.8 nm	0.45 µm 1.8 nm	0.45 µm 1.8 nm	0.45 µm 1.8 nm
RU106	1,98E-7	1,70E-7	4,15E-8		2,71E-8		
CS134	4,25E-4	2,83E-5	5,68E-5	6,41E-6	9,65E-6	1,48E-5	1,53E-5
CS137	3,43E-4	2,24E-5	4,99E-5	3,82E-6	8,43E-6	1,19E-5	1,53E-5
EU154	2,80E-7	3,55E-7	2,44E-7				<1,49E-10
EU155	3,03E-7	4,44E-7	2,89E-7				<4,41E-10
SB125	3,44E-6	5,53E-7	5,37E-7		3,44E-7	5,46E-8	8,60E-8
SR90	7,88E-6	4,36E-7	8,20E-7	5,33E-7	5,56E-7	5,04E-7	4,61E-7
CE144	8,50E-7	3,95E-7	1,56E-8		<4,59E-10		<1,65E-9
TC99	<2,13E-6						1,12E-6
AG110M	2,33E-5	2,13E-5	7,05E-5		1,22E-4		
AM241	1,49E-6	2,68E-7	2,22E-7				
AM243	<1,44E-7	<4,26E-7	<2,60E-7	2,69E-7	3,67E-7		
NP237	<2,01E-6	<1,48E-6	<1,34E-7	<3,73E-10			<8,09E-10
NP239	<1,44E-7	<4,26E-7	9,62E-8				
CM244	2,53E-7	4,43E-7	1,32E-7				
CM242	1,56E-7	2,79E-7	5,12E-8				
PU238	4,12E-7	1,22E-7	4,78E-8	1,19E-7			
PU239/40	8,42E-7	9,32E-8	5,61E-8	9,71E-8			
PU241	4,44E-7	1,21E-7				1,64E-9	
U	1,26E-6			2,80E-7	7,32E-8	4,51E-9	
Kr85						1,12E-5	1,45E-4
pHmeas+0,5	6,25	6,33	8,1	7,98	7,55	9,73	10,27
Eh(mV)**	571	503	322	350	344	-7	479

**Ehmeas + 208 mV

* time since start of the static test

TABLE 25: Activity of leach solutions from spent fuel powder in the presence of iron powder (Bq/ml)

Sample:	P 3 : 2,6 g (=2,3 g HM)		Temperature: 25 °C		Atmosphere: Ar/ 0,03%CO2									
			Solution:Granite water (EGW) Starting volume: 200 ml Final volume: 173 ml								Solution:Granite-bentonite water (GBW) Starting volume: 208 ml Final volume: 193 ml			
			no Fe-addition		static test (addition of 2,6 g Fe-powder)									
	Ultrason. cleaning 18,9 g (16,7 g HM) pwdr in 200 ml DIW		Wash (EGW) 54 days		1. Sampling 50 days*		2. Sampling 196 days*		3. Sampling 545 days*		4. Sampling 617 days*		5. Sampling 750 days*	
Nuclide	0,45 µm -filtered		0.45 µm	1.8 nm	0.45 µm	1.8 nm	0.45 µm	1.8 nm	0.45 µm	1.8 nm	0.45 µm	1.8 nm	0.45 µm	1.8 nm
RU106	6,92E+3	6,29E+3	3,14E+3	4,09E+3	2,59E+3	2,53E+3	9,07E+1	9,37E+1	1,89E+1	1,39E+1	4,57E+1	4,46E+1	6,05E+0	
CS134	4,03E+6	5,11E+6	2,11E+5	2,11E+5	2,28E+4	2,28E+4	3,26E+4	3,26E+4	2,64E+4	2,64E+4	6,19E+3	6,19E+3	6,51E+3	
CS137	6,03E+6	7,66E+6	9,91E+5	9,91E+5	1,07E+5	1,07E+5	1,75E+5	1,75E+5	1,86E+5	1,86E+5	4,54E+4	4,54E+4	5,33E+4	
EU154	2,75E+2	2,85E+2	3,44E+1	2,75E+0	4,46E+1	<5,80E-1	<3,73E-1	<3,80E-1	<7,96E-1	<8,53E-1	<1,12E+0	<1,68E+0	<6,74E-1	
EU155	1,50E+2	1,35E+2	1,37E+1	<1,30E+0	1,53E+1	<6,30E-1	<7,03E-1	<6,77E-1	<1,08E+0	<1,08E+0	<2,25E+0	<2,77E+0	<1,94E+0	
SB125	9,25E+2	8,14E+2	6,65E+2	6,79E+2	2,79E+2	1,29E+2	<1,10E+0	<1,15E+0	<2,16E+0	<2,10E+0	<2,36E+0	<2,89E+0	<1,85E+0	
SR90	8,88E+4	1,33E+5	2,73E+4	2,16E+4	1,15E+4	6,29E+3	1,90E+4	1,66E+4	3,22E+4	2,53E+4	1,05E+5	1,15E+5	1,60E+5	
CE144	1,11E+3	9,99E+2	1,25E+1	<6,17E+0	1,36E+1	<2,31E+0	<2,21E+0	<2,14E+0	<3,10E+0	<3,07E+0	<7,41E+0	<8,18E+0	<5,34E+0	
TC99	<1,48E+0				6,30E+0	5,17E-1	<7,23E-2	<7,23E-2	1,01E+0	2,53E-1	3,06E-1	3,06E-1	3,02E-1	
AM241	3,26E+1	2,59E+1	1,10E+1	<1,13E+0	1,33E+1	<1,67E-2	2,00E-1	6,67E-2	<1,25E+0	<1,25E+0	<3,37E+0	<3,01E+0	<2,04E+0	
AM243	<3,70E-1	<3,70E-1			1,85E+0									
NP237			<1,31E-3	<1,31E-3	6,07E-3	<8,67E-4	<8,67E-4	<8,67E-4	<1,48E-3	<1,48E-3	0,00E+0	0,00E+0	4,38E-4	
NP239	<3,70E-1	<3,70E-1												
CM244	2,07E+2	2,22E+2			5,65E+1	3,33E-2	2,33E-1	1,23E-2						
CM242	5,92E+0	5,55E+0			6,67E-2	<4,26E-3	2,27E-2	<4,27E-3						
PU238	1,33E+2	1,25E+2	2,36E+1	2,30E-1	2,47E+1	<3,33E-2	3,00E-1	<3,33E-2	<3,30E-1	<3,30E-1	9,10E-2	4,51E-1	5,16E-2	
PU239/40	2,11E+1	2,00E+1	3,81E+0	3,70E-2	4,93E+0	<3,33E-2	5,67E-2	<3,33E-2	4,55E-2	6,82E-2	2,99E-1	2,17E-1	1,53E-2	
PU241	3,89E+3	3,74E+3	5,56E+2	6,98E+0	6,80E+2	<3,33E-2	<3,33E-2	<3,33E-2	<2,40E-3	<2,40E-3	0,00E+0	3,39E+0	5,65E+1	
U (µg/ml)	*1,50E+1*		3,00E-1	1,48E-1	2,20E-1	1,13E-2	4,80E-3	<4,00E-5	1,76E-2	1,02E-3	1,46E-2	1,03E-2	7,80E-3	
pHmeas			pH 7,8		pH 8,8		pH 10		pH 9,95		pH 9,51		pH 9,1	
Eh(mV)**			169 mV		408 mV		287 mV		-540 mV		101 mV		-440 mV	

**Ehmeas + 208 mV

* time since start of the static test

**failed

TABLE 26: Release fractions(FIAP) of radionuclide inventories in leach solutions from spent fuel powder

Sample:	**P 3 : 2,6 g (=2,3 g HM)**				Temperature: 25 °C						**Atmosphere: Ar/ 0,03%CO2**			
					Solution:Granite water (EGW) Starting volume: 200 ml Final volume: 173 ml						**:Granite-bentonite water (GBW)** Starting volume: 208 ml Final volume: 193 ml			
			no Fe-addition		**static test (addition of 2,6 g Fe-powder)**									
	Ultrason. cleaning 18,9 g (16,7 g HM) pwdr in 200 ml DIW		Wash (EGW) 54 days		1. Sampling 50 days*		2. Sampling 196 days*		3. Sampling 545 days*		4. Sampling 617 days*		5. Sampling 750 days*	
Nuclide	0,45 µm -filtered		0.45 µm	1.8 nm	0.45 µm	1.8 nm	0.45 µm	1.8 nm	0.45 µm	1.8 nm	0.45 µm	1.8 nm	0.45 µm	1.8 nm**
RU106	3,03E-5	3,41E-5	1,09E-3	1,43E-3	1,21E-3	1,18E-3	3,95E-5	4,08E-5	1,34E-5	9,83E-6	4,30E-5	4,19E-5	7,05E-6	
CS134	1,25E-2	1,76E-2	9,21E-3	9,21E-3	1,65E-3	1,65E-3	2,54E-3	2,54E-3	2,50E-3	2,50E-3	7,41E-4	7,41E-4	8,35E-4	
CS137	1,19E-2	1,52E-2	1,46E-2	1,46E-2	1,64E-3	1,64E-3	2,53E-3	2,53E-3	2,53E-3	2,53E-3	7,45E-4	7,45E-4	8,22E-4	
EU154	8,65E-6	9,20E-6	1,03E-5	8,20E-7	1,37E-5	<1,79E-7	<1,07E-7	<1,09E-7	<2,26E-7	<2,43E-7	<3,87E-7	<5,80E-7	<2,24E-7	
EU155	9,16E-6	8,61E-6	9,80E-6	<9,30E-7	1,16E-5	<4,78E-7	<4,99E-7	<4,80E-7	<7,95E-7	<7,95E-7	<2,03E-6	<2,50E-6	<1,73E-6	
SB125	7,53E-5	7,16E-5	9,33E-4	9,52E-4	4,35E-4	2,01E-4	<1,60E-6	<1,68E-6	<3,58E-6	<3,48E-6	<4,87E-6	<5,96E-6	<3,94E-6	
SR90	2,56E-4	3,87E-4	6,15E-4	4,87E-4	2,62E-4	1,43E-4	4,04E-4	3,53E-4	6,47E-4	5,08E-4	2,54E-3	2,78E-3	3,64E-3	
CE144	5,50E-6	6,51E-6	9,94E-6	<4,91E-6	1,57E-5	<2,67E-6	<2,39E-6	<2,32E-6	<6,42E-6	<6,36E-6	<2,10E-5	<2,32E-5	<2,04E-5	
TC99	<2,59E-5				7,91E-4	6,49E-5	<8,49E-6	<8,49E-6	1,10E-4	2,75E-5	3,99E-5	3,99E-5	3,67E-5	
AM241	6,92E-6	5,15E-6	9,76E-6	<1,00E-6	1,13E-5	<1,42E-8	1,59E-7	5,29E-8	<8,48E-7	<8,48E-7	<2,71E-6	<2,42E-6	<1,47E-6	
AM243	<1,76E-6	<1,76E-6			6,31E-5								0,00E+0	
NP237			<6,21E-6	<6,21E-6	2,88E-5	<4,11E-6	<3,84E-6	<3,84E-6	<6,07E-6	<6,07E-6			2,01E-6	
NP239	<1,76E-6	<1,76E-6												
CM244	5,60E-6	6,07E-6			1,27E-5	7,50E-9	4,91E-8	2,59E-9						
CM242	2,46E-6	3,74E-6			8,82E-5	<5,63E-6	2,81E-5	<5,28E-6						
PU238	4,81E-6	4,54E-6	6,29E-6	6,13E-8	6,61E-6	<8,91E-9	7,50E-8	<8,33E-9	<7,68E-8	<7,68E-8	2,55E-8	1,26E-7	1,35E-8	
PU239/40	4,87E-6	4,61E-6	6,32E-6	6,13E-8	8,17E-6	<5,52E-8	8,79E-8	<5,16E-8	6,52E-8	9,78E-8	5,15E-7	3,74E-7	2,45E-8	
PU241	5,86E-6	5,72E-6	7,12E-6	8,94E-8	8,89E-6	<4,4E-10	<4,1E-10	<4,1E-10	<2,8E-11	<2,8E-11		4,82E-8	7,64E-7	
U	1,92E-4		2,76E-5	1,36E-5	2,02E-5	1,04E-6	4,13E-7	<3,44E-9	1,40E-6	8,12E-8	1,40E-6	9,84E-7	6,94E-7	
Kr85											1,38E-3		1,42E-3	
pHmeas			pH 7,8		pH 8,8		pH 10		pH 9,95		pH 9,51		pH 9,1	
Eh(mV)**			169 mV		408 mV		287 mV		-540 mV		101 mV		-440 mV	

**Ehmeas + 208 mV

* time since start of the static test

**failed

TABLE 27: Concentrations of radionuclides in leach solutions from spent fuel powder(mol/L)

Sample:	P 3 : 2,6 g (=2,3 g HM)				Temperature: 25 °C				Atmosphere: Ar/ 0,03%CO2					
					Solution:Granite water (EGW) Starting volume: 200 ml Final volume: 173 ml						Granite-bentonite water (GBW) Starting volume: 208 ml Final volume: 193 ml			
			no Fe-addition		static test (addition of 2,6 g Fe-powder)									
	Ultrason. cleaning 18,9 g (16,7 g HM) pwdr in 200 ml DIW		Wash (EGW) 54 days		1. Sampling 50 days*		2. Sampling 196 days*		3. Sampling 545 days*		4. Sampling 617 days*		5. Sampling 750 days*	
Nuclide	0,45 µm -filtered		0.45 µm	1.8 nm	0.45 µm	1.8 nm	0.45 µm	1.8 nm	0.45 µm	1.8 nm	0.45 µm	1.8 nm	0.45 µm	1.8 nm**
RU106	1,3E-08	1,5E-08	4,33E-7	5,64E-7	4,77E-7	4,66E-7	1,67E-8	1,73E-8	6,12E-9	4,50E-9	1,64E-8	1,60E-8		
CS134	4,6E-06	6,5E-06	3,10E-6	3,10E-6	5,54E-7	5,54E-7	9,13E-7	9,13E-7	9,74E-7	9,74E-7	2,40E-7	2,40E-7	2,90E-7	
CS137	4,4E-06	5,6E-06	4,93E-6	4,93E-6	5,51E-7	5,51E-7	9,09E-7	9,09E-7	9,85E-7	9,85E-7	2,41E-7	2,41E-7	2,86E-7	
EU154	1,5E-10	1,6E-10	1,6E-10	1,3E-11	2,2E-10	2,8E-12	1,8E-12	1,8E-12	4,1E-12	4,4E-12	5,9E-12	8,8E-12	<1,04E-8	
EU155	1,6E-10	1,5E-10	1,5E-10	1,5E-11	1,8E-10	7,5E-12	8,4E-12	8,1E-12	1,4E-11	1,4E-11	3,1E-11	3,8E-11	<8,68E-9	
SB125	1,7E-10	1,6E-10	1,9E-9	2,0E-9	9,0E-10	4,2E-10	3,5E-12	3,7E-12	8,6E-12	8,3E-12	9,7E-12	1,2E-11	<1,37E-9	
SR90	4,4E-08	6,6E-08	9,56E-8	7,56E-8	4,07E-8	2,22E-8	6,72E-8	5,87E-8	1,16E-7	9,13E-8	3,80E-7	4,16E-7	3,88E-6	
CE144	1,8E-09	2,1E-09	2,89E-9	<1,43E-9	4,58E-9	<7,8E-10	<7,4E-10	<7,2E-10	<2,16E-9	<2,14E-9	<5,89E-9	<6,50E-9	<7,05E-8	
TC99	<3,80E-9				1,06E-7	8,67E-9	<1,21E-9	<1,21E-9	1,69E-8	4,24E-9	5,13E-9	5,13E-9	1,01E-6	
AM241	1,8E-10	1,3E-10	2,3E-10	2,4E-11	2,7E-10	3,4E-13	4,0E-12	1,3E-12	2,3E-11	2,3E-11	6,2E-11	5,5E-11	<2,81E-9	
AM243	<4,6E-11	<4,6E-11	0,00E+0	0,00E+0	1,49E-9									
NP237			<2,2E-10	<2,2E-10	<1,0E-9	<1,4E-10	<1,4E-10	<1,4E-10	<2,5E-10	<2,5E-10			3,71E-7	
NP239	<6,8E-11	<6,8E-11												
CM244	3,1E-11	3,4E-11			6,5E-11	3,8E-14	2,7E-13	1,4E-14						
CM242	1,4E-11	2,1E-11			4,5E-10	2,9E-11	1,5E-10	2,9E-11						
PU238	2,9E-09	2,7E-09	3,45E-9	3,4E-11	3,6E-9	4,9E-12	4,4E-11	4,9E-12	4,9E-11	4,9E-11	1,3E-11	6,7E-11	4,11E-8	
PU239/40	2,9E-09	2,8E-09	3,47E-9	3,4E-11	4,5E-9	3,0E-11	5,2E-11	3,0E-11	4,1E-11	6,2E-11	2,7E-10	2,0E-10	4,37E-8	
PU241	3,5E-09	3,5E-09	3,91E-9	4,9E-11	4,9E-9	2,4E-13	2,4E-13	2,4E-13	1,8E-14	1,8E-14	0,0E+0	2,5E-11	4,12E-8	
U	9,7E-06		1,26E-6	6,2E-7	9,2E-7	4,7E-8	2,0E-8	1,7E-10	7,4E-8	4,3E-9	6,1E-8	4,3E-8	1,34E-7	
pHmeas			pH 7,8		pH 8,8		pH 10		pH 9,95		pH 9,51		pH 9,1	
Eh(mV)**			169 mV		408 mV		287 mV		-540 mV		101 mV		-440 mV	

**Ehmeas + 208 mV

* time since start of the static test

**failed

TABLE 28: Incremental rates of radionuclides release from spent fuel powder (FIAP/d)

Sample:	**P 3 : 2,6 g (=2,3 g HM)**		Temperature: 25 °C		**Atmosphere: Ar/ 0,03%CO2**		
			Solution:Granite water (EGW) Starting volume: 200 ml Final volume: 173 ml			**Granite-bentonite water (GBW)** Starting volume: 208 ml Final volume: 193 ml	
		no Fe-addition	**static test (addition of 2,6 g Fe-powder)**				
	Ultrason. cleaning 18,9 g (16,7 g HM) pwdr in 200 ml DIW	Wash (EGW) 54 days	1. Sampling 50 days*	2. Sampling 196 days*	3. Sampling 545 days*	4. Sampling 617 days*	5. Sampling 750 days*
Nuclide	0,45 µm -filtered	0.45 µm 1.8 nm	0.45 µm 1.8 nm	0.45 µm 1.8 nm	0.45 µm 1.8 nm	0.45 µm 1.8 nm	0.45 µm 1.8 nm**
RU106		2,03E-5	2,41E-5			5,73E-7	
CS134		1,70E-4	3,29E-5	6,67E-6	3,43E-7	9,88E-6	1,08E-6
CS137		2,71E-4	3,27E-5	6,67E-6	4,51E-7	9,93E-6	9,59E-7
EU154		1,90E-7	2,75E-7			<5,16E-9	
EU155		1,82E-7	2,32E-7			<2,71E-8	
SB125		1,73E-5	8,70E-6		<5,98E-9	<6,49E-8	
SR90		1,14E-5	5,23E-6	1,07E-6	7,70E-7	3,39E-5	9,52E-6
CE144		1,84E-7	3,15E-7		<1,21E-8	<2,80E-7	<6,32E-9
TC99			1,58E-5		2,94E-7	5,32E-7	
AM241		1,81E-7	2,26E-7			<3,61E-8	
AM243			1,26E-6				
NP237		<1,15E-7	5,76E-7		<7,10E-9		1,50E-8
NP239							
CM244			2,55E-7				
CM242			1,76E-6				
PU238		1,17E-7	1,32E-7			3,4E-10	
PU239/40		1,17E-7	1,63E-7			6,87E-9	
PU241		1,32E-7	1,78E-7				5,70E-9
U		5,11E-7	4,05E-7		2,93E-9	1,86E-8	
			1,73E-8			1,87E-5	1,06E-5
pHmeas		pH 7,8	pH 8,8	pH 10	pH 9,95	pH 9,51	pH 9,1
Eh(mV)**		169 mV	408 mV	287 mV	-540 mV	101 mV	-440 mV

**Ehmeas + 208 mV

* time since start of the static test

**failed

APPENDIX 3 : Conditions and procedures of experiments conducted by Enresa

Appendix 3 summarizes the experimental procedures corresponding to the work packages:

II-1 Precipitation of spent UO_2 fuel and SIMFUEL

II-3 Coprecipitation U-Pu

SIMFUEL COPRECIPITATION TEST (WP-II.3):

Simfuel solution preparation

SIMFUEL solution was prepared by dissolving a SIMFUEL pellet in strong acid solution under oxidising conditions. The obtained SIMFUEL solution was dried and later redissolved in 6 N HCl. The chloride-SIMFUEL solution composition was analysed by ICP-MS; weight ratio is shown in TABLE 1

TABLE 1: Weight ratio Metal/Uranium (M/U) in acid SIMFUEL solutions

Element	*M/U*	*Element*	*M/U*
Sr	2.03 E-03	Pd	2.54 E-03
Y	6.80 E-04	Ba	3.62 E-03
Zr	5.19 E-03	La	2.16 E-03
Mo	5.03 E-03	Ce	8.78 E-03
Ru	6.24 E-04	Nd	9.06 E-03
Rh	7.03 E-04	U	1.00

Solid phases were precipitated from SIMFUEL solutions in NaCl solution by the experimental method described as follows. The coprecipitation experiments in granite-bentonite solution did not include any modification.

An aliquot of Chloride-SIMFUEL solution was added to carbonate free 5 m NaCl solution. The pH of this solution was adjusted to the selected pH value by addition of 0.1 N NaOH + 5 m NaCl carbonate free solution. Thereafter, the pH was maintained constant along the experiments and it was continuously measured by Ross electrode. Due to the precipitation reaction an acidification of the solution is produced. In order to maintain the pH constant along the experiments, it was adjusted to the selected value once per day, using a Metrohm titroprocessor Mod. 686, until no further NaOH addition was necessary to maintain the pH value.

Corrections for liquid junction potential were accomplished by calibration with solutions of known HCl activity with reference to the pH Pitzer´s convention. Measured pH value was corrected by using the following equation:

$$pH_{corr.} = pH_{meass.} + 0.25$$

TABLE 2 : Overview of initial experimental conditions for the SIMFUEL coprecipitation test in 5 m NaCl solution

Experimental code	*$[U]_{ini}$ (mol/kg)*	*$pH_{cor.}$*
PSIM-9	1.47 E-03	7.4
PSIM-10	1.32 E-03	
PSIM-13	1.33 E-03	
PSIM-14	1.25E-03	8.3
PSIM-15	9.37 E-04	
PSIM-3	7.50 E-04	
PSIM-6	8.39 E-04	9.3
PSIM-7	6.63 E-04	
PSIM-8	1.10 E-03	
PSIM-11	1.55 E-3	12
PSIM-12	1.55 E-3	

All experiments were performed at 25°C in sealed glass vessels. To avoid possible carbonate contamination, the gas volume of the glass vessel, in contact with the solution, was daily replaced with new N_2 gas by bubbling N_2 through the reactor vessel during at least one hour.

Samples of aqueous suspension were taken before and after pH adjustment and along the experiments. Aliquots were filtered through 0.22 µm pore size membranes and by ultrafiltration (nominal pore size 18 Å) in order to study the possible effect of colloids formation.

The initial experimental conditions for the SIMFUEL initial uranium concentration values were corrected by considering the dilution factor produced by the NaOH addition required for reaching the selected pH value. SIMFUEL coprecipitation experimental set performed in 5 m NaCl solutions is summarised TABLE 2.

TABLE 3 Overview of the initial experimental conditions for the SIMFUEL coprecipitation running test in GBW

Experimental code	*[U (initial) mol/kg*	*$pH_{exp.}$*
GPSIM1	3.4 E-03	9.6
GPSIM2	3.5 E-03	9.4
GPSIM4	3.3 E-03	8.8
GPSIM5	3.3 E-03	8.65
GPSIM6	3.0 E-03	8.4
GPSIM7	3.5 E-03	7.85
GPSIM8	3.5 E-03	7.3

TABLE 3 shows the initial experimental conditions for the SIMFUEL coprecipitation experiments performed in GBW.

U/PU COPRECIPITATION EXPERIMENTS (WP-II.3)

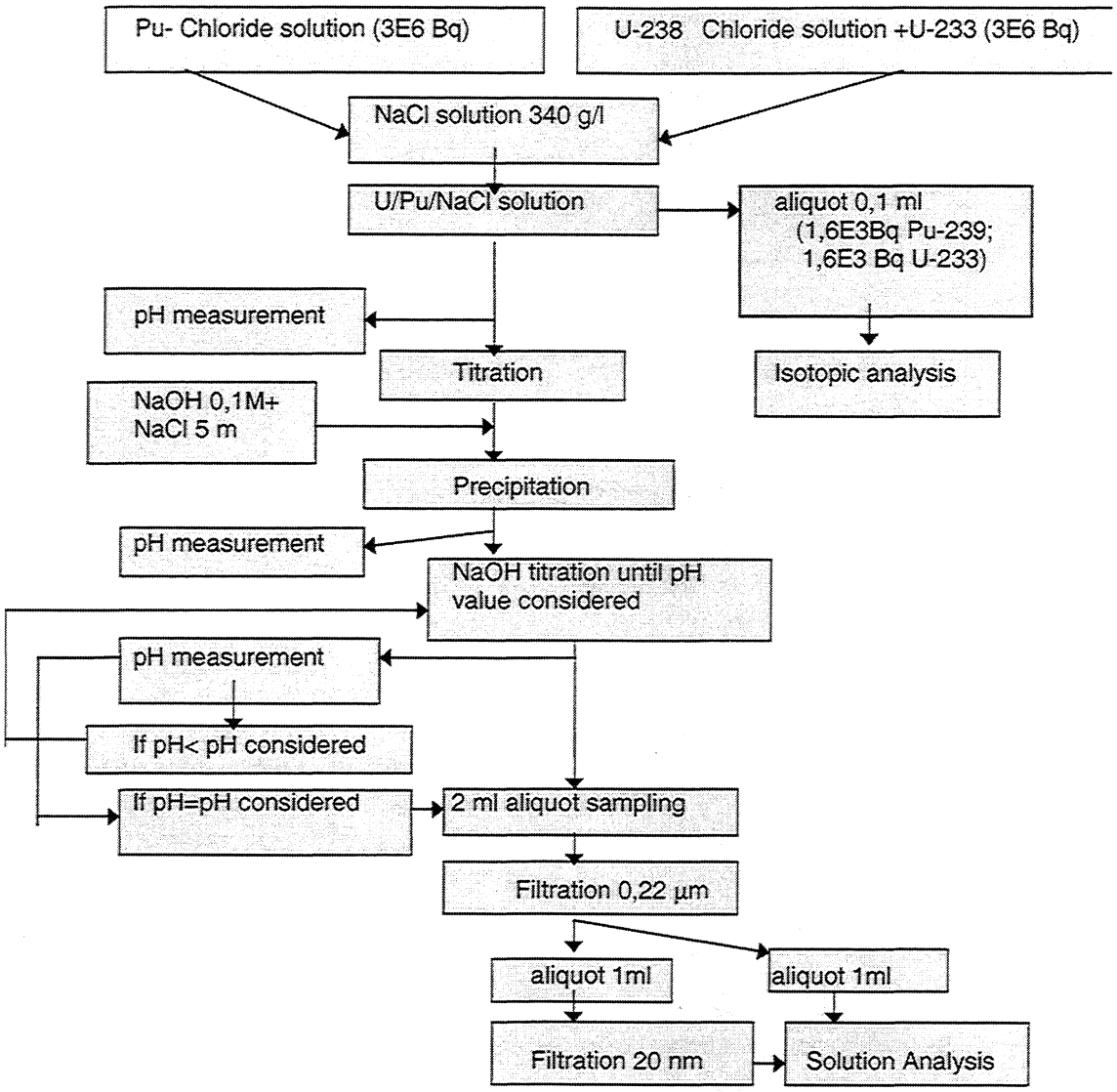

FIGURE 1 Coprecipitation: Experimental Procedure

The experimental procedure (summarised in FIGURE 1) is similar to the one described in detail for SIMFUEL coprecipitation experiments

The following previous steps were performed:

Isotopic analysis of the U-233 solution
Pu purification for Am and other impurities removal and isotopic analyses
Isotopic analysis of the Pu solution after the purification process
Development of analytical methods for Pu and U analysis

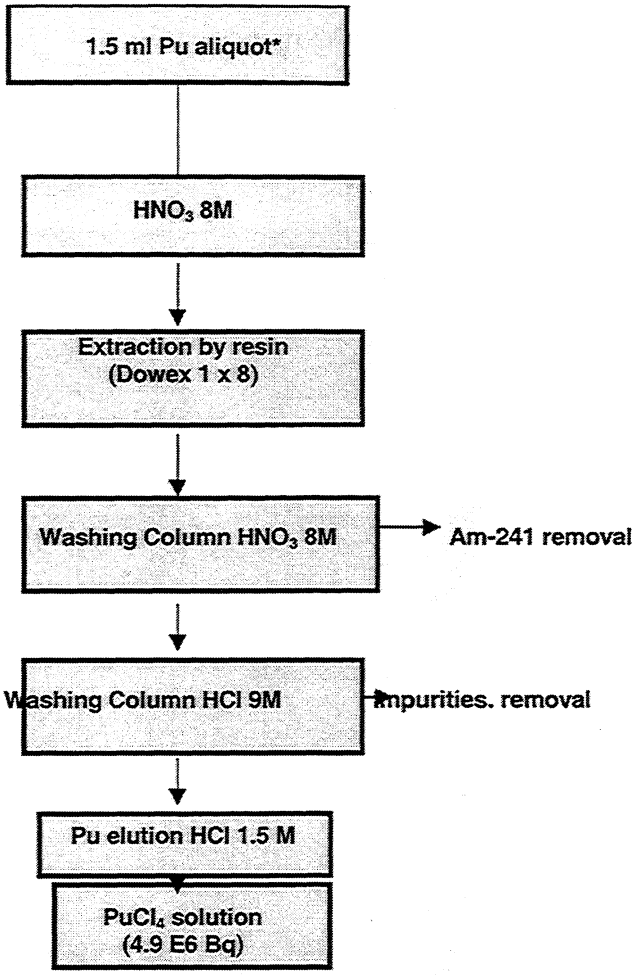

***Isotopic analysis of the initial Pu solution : ^{238}Pu 1.20E-4 (g/L), ^{239}Pu 1,60E0 (g/L), ^{240}Pu 1,30E-1 (g/L) and ^{241}Pu 3.85E-3 (g/L).**

FIGURE 2 The Pu purification method used for Am and other impurities removal

The Pu purification method used for Am and other impurities removal is summarised in FIGURE 2. Initial experimental conditions are shown in TABLE 4.

TABLE 4 Overview of the initial experimental conditions for the U/Pu coprecipitation test in 5m NaCl solutions

Experimental code	*$PH_{cor.}$*	*$[U]_{in.}$ (mol/kg H_2O)*	*[Pu] (mol/kg H_2O)*
Upu-2	5.6	2.72E-3	2.78E-5
Upu-3	7.5	4.98E-3	3.81E-5
Upu-4	7.3	2.17E-3	2.17E-5
Upu-5	9.1	3.69E-3	3.025E-5
Upu-6	9.2	5.78E-3	5.49E-5

Appendix 4 : Detailed conditions of experiments performed at VTT (WP I.4)

Materials

Unirradiated sintered polycrystalline UO_2 pellets and UO_2 powder were used in the experiments. The pellets had an average mass of 4.8 grams and a geometrical surface of $3.3 \cdot 10^{-4}$ m^2. A predissolution in synthetic groundwater was carried out for the pellets under anoxic conditions, in an attempt to remove a more soluble oxidized layer that might have been present on the surface due to the earlier manipulation of the pellets in air.

UO_2 powder (prepared by ABB Atom, Sweden) has a particle size of 0.7 μm, which results in a high specific surface area of 5.4 m^2/g (BET-method). The composition ratio O/U is 2.10 (gravimetric method). The powder has been treated with a mixture of nitrogen and air in order to stabilize it against spontaneous oxidation.

Metallic iron was added as iron chips (Baker Chemicals, reducing power as Fe 100.3 %).

SYNTHETIC GROUNDWATERS

Four types of synthetic groundwaters were used in the experiments. TABLE 1 gives the compositions. The saline and fresh (Allard) groundwaters were reference groundwaters within the site investigations for spent fuel disposal in Finland. The granite/bentonite groundwater (by Ciemat, Spain) simulated the effects of bentonite on spanish groundwater. The near-field groundwater simulated the effects of bentonite on saline groundwater.

The saline groundwater represents the groundwater found at a depth of 600 m in granitic bedrock. The composition was based on groundwater studies within the site investigations for spent fuel disposal in the Olkiluoto area. The saline Na-Ca-Cl water has a low alkalinity. The ionic strength is 0.5 M. The composition of the synthetic water was planned separately for air-saturated and anoxic (N_2 atmosphere) conditions with the help of EQ3/6 modelling and stability tests [97VUO]

The Allard groundwater is the reference groundwater for fresh groundwater conditions at great dephts in granitic bedrock. The composition was modified due to the stability problems of the original Allard groundwater both under air-saturated conditions and in N_2 atmosphere [98VUO/SNE]. The Ca, Mg, Si and carbonate contents were lowered in order to prevent the precipitation of calcite and silicate phases, and the loss of carbonate from solution.

The granite/bentonite groundwater by Ciemat [96MAR/MEL] simulates the effects of bentonite on spanish granitic groundwater. This saline synthetic groundwater has a high NO_3^- content (110 mg/l) compared with all the other groundwaters (TABLE 1).

The near-field groundwater simulates the effects of bentonite on saline groundwater (TDS= 67 g/l). It is very saline Na-Ca-Cl water with a low alkalinity. The ionic strength is 1.6 M. The composition was based on measured laboratory data on bentonite/saline groundwater interaction [98MUU/VUO].

REDOX CONDITIONS

The redox conditions included:

1) oxidizing, air-saturated conditions (p_{O2} = 0.2 atm, p_{CO2} = 0.0003 atm)

2) anaerobic conditions (N_2 atmosphere, O_2 < 1 ppm, $CO_2 \approx$ 0.1 ppm)

3) reducing conditions (N_2 atmosphere, low Eh, $CO_2 \approx$ 0.1 ppm)

The oxic experiments were carried out in polyethylene bottles. The bottles were kept loosely closed during dissolution periods in order to allow equilibrium with air in the aqueous phase.

The anoxic conditions of deep groundwater were simulated in an anaerobic glove box (Mecaplex, Braun) filled with nitrogen (adsorbers for O_2 and CO_2 : Cu catalyst and molecular sieve, respectively). The pellets were immersed in deaerated (with N_2) synthetic groundwater in polyethylene bottles inside the glove box. The oxygen concentration in the atmosphere of the box normally stays below 1 ppm (0.1...0.5 ppm). The carbon dioxide content is low, ≈ 0.1 ppm [97VUO/OLL]. The experimental vessels were kept tightly closed during the experiments.

An important parameter to be considered is the Eh of the aqueous phase. Under anaerobic (N_2) conditions, it may vary from slightly oxidizing to reducing depending on the composition of the gas phase (trace O_2 , H_2) and the composition of the aqueous phase. The complex formation of uranium with carbonate probably affects the relative stabilities of the oxidation states. This makes U(VI) stable in a more reducing redox regime than in the absence of carbonate, increasing solubility [91SKI]. Earlier UO_2 dissolution studies in synthetic groundwater (Allard) in N_2 atmosphere in the absence of reducing species have shown that dissolved uranium was mainly (> 90 %) at the U(VI) state [96OLL/OLI]. Obviously, the trace oxygen content in the atmosphere of the box is enough to cause slightly oxidizing conditions for uranium. The steady-state concentrations of uranium were nevertheless low ($2 \cdot 10^{-8}$ M).

The earlier tests in Allard and saline groundwater /Vuorinen et al. 1997/ have shown that lower Eh values can be achieved by the addition of reducing species, Fe^{2+}, S^{2-}, typically present in natural groundwaters, or metallic Fe to synthetic deaerated groundwater. The Eh values in the presence of these redox species ranged from -300 ... -200 mV (1 ppm Fe^{2+} , 1-5 ppm S^{2-}). The Eh value for deaerated synthetic groundwater in the absence of redox species fluctuates. Values from -20 ... +175 mV have been measured for synthetic groundwater after short periods (< 1 month) in the glove box. During longer periods in the box a trend towards lower Eh was observed.

The stability of the water chemistry (pH, Eh, S^{2-}, Fe^{2+}) in the experiments, as well as in parallel groundwater samples without UO_2 pellets, was followed during long dissolution periods (up to 300 days). FIGURE 1 gives the measured Eh and pH values as a function of time in a parallel sample of saline groundwater with 3 ppm S^{2-} during a follow-up period of 600 days. A platinum electrode (Yokogawa) was used as the redox electrode in combination with a Ag/AgCl reference electrode (Yokogawa). The reference electrode is filled with a gelled electrolyte solution. The sulphide content was decreased rapidly after the addition to synthetic groundwater, probably by reacting with trace oxygen left in the solution after deaeration with N_2, but remains rather stable afterwards, see TABLE 4, which gives the average values and deviations of all the S(-II) determinations carried out during the dissolution experiments in different aqueous phases. The determination was made using a standard spectrophotometric method (SFS 3038). The stability of redox conditions in synthetic groundwaters with S(-II) was shown also by the Eh and pH measurements. The scatter in the measured Eh was small, whereas in synthetic groundwaters with Fe(+II) as reducing species, there is more scatter in the measured Eh values.

ANALYTICAL METHODS

The uranium contents in the aqueous phase were analysed by ICP-MS. In Allard groundwater, the detection limit with the conventional nebulization method is low, 8.4·10-11 M. The sensitivity of this method is lowered by the salinity of synthetic groundwater. The sensitivity can be improved using a high efficiency sample nebulization device (Mistral). The detection limit of uranium in saline groundwater

(I= 0.5 M) is $2 \cdot 10^{-10}$ M with Mistral. There were, moreover, practical difficulties to use Mistral for saline groundwater samples, especially in the case of near-field groundwater (1.5 M), because of blocking of tubes.

For this reason a method for uranium separation, similar to the one used for U(VI) separation when analysing U oxidation states [96OLL], was tested, and used in the case of saline and near-field groundwater samples in the precipitation experiments. An anaerobic sample was first allowed to aerate in order to oxidize the U(IV) in the sample. A known amount of ^{233}U was added to the sample for yield determination. After this the sample was acidified to form chloride complexes of uranium. Hussonnois et al. [89HUS/GUI] have concluded that U(VI) is fixed at 100 % on the anionic resin with 4.5 M HCl medium. Subsequently, the U(VI) was recovered by elution with 0.1 M HCl. Finally, the concentration of uranium was determined with ICP-MS. The detection limit in 0.1 M HCl is at the same level as in Allard groundwater with low ionic strength.

The oxidation state of uranium in the anoxic dissolution experiments was determined using a method based on the separation of the tetravalent and hexavalent states by anion-exchange chromatography in HCl medium [98HUS/GUI, 96OLL]. Afterwards, the uranium contents of each of the fractions were measured with ICP-MS. A platinum electrode (Yokogawa) was used as redox electrode in combination with a Ag/AgCl reference electrode (Yokogawa).

The determination of the ferrous iron was made by a ferrozine method [79DIM].

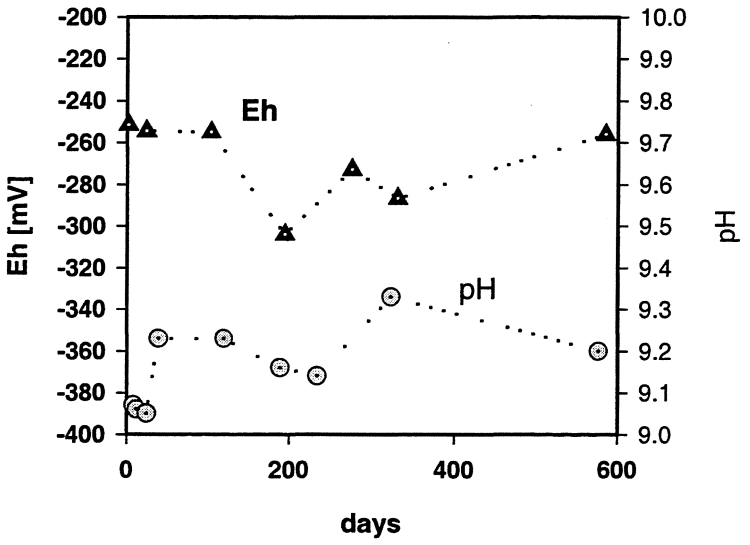

FIGURE 1. *The measured Eh and pH values in a parallel sample of saline groundwater with 3 ppm S(-II) during a follow-up period of 600 days under anaerobic conditions.*

TABLE 1 The compositions of the synthetic groundwaters.

	Saline granitic groundwater (air) /Vuorinen et al. 1997, 1998/		Saline granitic groundwater (N_2) (log p_{CO2} = -7) /Vuorinen et al. 1997, 1998/		Fresh granitic groundwater (air) /Allard et al. 1981/		Modified Allard groundwater (air) /Vuorinen and Snellman 1998/		Modified Allard groundwater (N_2) (log p_{CO2} = -4) /Vuorinen and Snellman 1998/		Granite/ bentonite groundwater (air) /Martínez et al. 1996/		Near-field groundwater (air) /Muurinen et al. 1996/		Near-field groundwater (N_2) (log p_{CO2} = -4) /Muurinen et al. 1996/	
	mg/l	*mmol/l*	*mg/l*	*mmol/l*	*mg/l*	*mmol/l*	*mg/l*	*mmol/l*	*mg/l*	*mmol/l*	*mg/l*	*mmol/l*	*mg/l*	*mmol/l*	*mg/l*	*mmol/l*
Na^+	4 800	209	4 800	209	52	2.3	52	2.3	52	2.3	3 750	163	22 700	987	22 700	987
Ca^{2+}	4 000	100	4 000	100	18	0.45	10	0.25	5.1	0.13	135	3.37	10 000	250	10 000	250
Mg^{2+}	56	2.3	55	2.3	4.3	0.18	2.8	0.12	0.7	0.03	600	24.7	700	29	700	29
Sr^{2+}	35	0.40	35	0.40	-	-	-	-	-	-	-	-	-			
K^+	21	0.54	21	0.54	3.9	0.10	3.9	0.10	3.9	0.10	20	0.5	200	5.1	200	5.1
HCO_3^-	10	0.16	-	-	123	2.01	91	1.5	65	1.07	27	0.44	8.5	0.14	4.8	0.08
SiO_2	2.5	0.04	-	-	8	0.13	2.9	0.05	1.7	0.028	8.3	0.14				
Br^-	105	1.31	105	1.31	-	-	-	-	-	-	15	0.19				
F^-	1.2	0.063	1.2	0.063	-	-	-	-	-	-	-	-				
I^-	0.9	0.007	0.9	0.007	-	-	-	-	-	-	-	-				
SO_4^{2-}	4.2	0.044	4.2	0.044	9.6	0.10	9.6	0.10	9.6	0.10	1500	15.6	1 200	12.5	1 200	12.5
B^{3+}	0.9	0.08	0.9	0.08	-	-	-	-	-	-	-	-				
Cl^-	14600	412	14600	412	58	1.6	47	1.3	52	1.5	6550	185	53 900	1 520	53 900	1 520
NO_3^-	-	-	-	-	-	-	-	-	-	-	110	1.77				
Ionic strength	0.5		0.5		0.004		0.004		0.004		0.25		1.6		1.6	
$pH_{theoretical}$	7.2		8.3		8.2		8.4		8.8		7.3		6.9		7.5	

TABLE 2. *The experimental conditions of the oxic, air-saturated dissolution tests (for synthetic groundwaters, see TABLE. 1).*

Solid	Synthetic groundwater	$pH_{measured}$*	S/V [m^{-1}]**	Duration [days]
UO_2 powder	Allard	8.4 (8.4)	1000	350
"	modified Allard	8.3 - 8.4 (8.3)	"	"
"	saline	7.0 - 7.1 (6.8)	"	"
"	granite/bentonite by Ciemat	7.5 (7.5)		"
"	near-field	6.6 - 6.8 (6.6)	"	204
UO_2 pellets	saline	7.0 - 7.1 (7.0-7.1)	0.66	702
"	"	"	1.98	"
"	"	"	19.8	"

* *pH_1 (pH_2): pH_1 and pH_2 measured at the beginning and at the end of the experiments, respectively*

** *S/V is based on geometric surface area*

TABLE 3. *The experimental conditions of the anoxic (N_2) dissolution experiments with UO_2 pellets in synthetic saline groundwater.*

Redox species addition	Eh [mV]*	pH measured**	S/V [m^{-1}]***	Duration [days]
none	-	8.0-8.1 (8.3)	0.66	300
1 ppm S(-II) 0.01 ppm Fe(+II)	-210	8.7 (8.8)	"	"
1 ppm Fe (+II)	-210	8.2 (8.0)	"	"
3 ppm S (-II)	-250	9.2 (9.2)	"	"
5 ppm S (-II)	-280	9.5 (9.5)	"	"
none	-	8.0-8.1 (8.0)	19.8	"
1 ppm S(-II) 0.01 ppm Fe(+II)	-210	8.7 (8.7)	"	"
metallic Fe (5 grams iron chips/ 50 ml of solution)	-	9.3 (8.8)	"	"
1 ppm S(-II) 0.01 ppm Fe(+II) metallic Fe (5 grams iron chips/50 ml of solution)	-	9.4 (8.9)	"	"

TABLE 4 *The experimental conditions of the anoxic (N_2) dissolution experiments with UO_2 pellets in modified Allard groundwater.*

Redox species addition	Eh [mV]*	pH measured**	S/V [m^{-1}]***	Duration [days]
none	-	8.8 (9.0)	0.66	400
1 ppm S(-II)	-250	9.0 (9.2)	"	"
3 ppm S (-II)	-290	9.2 (9.3)	"	"
5 ppm S (-II)	-310	9.4 (9.5)	"	"
1 ppm Fe(+II)	-220	8.7 (9.0)	"	"
none	-	8.8 (9.0)	19.8	300
3 ppm S(-II)	-200	9.2 (9.2)	"	200
metallic Fe 5 grams iron chips/ 50 ml of solution	-	9.5 (9.5)	"	200

* *Eh measured at the beginning of the experiments*

** *pH_1 (pH_2) measured at the beginning and at the end of the experiments, respectively*

*** *S/V is based on geometric surface area*

TABLE 5. *The stability of water chemistry in the UO_2 dissolution experiments under anoxic conditions.*

Redox species addition	Saline **S(-II), Fe(+II) [ppm]**	Saline **Eh [mV] pH**	Allard (modif.) **S(-II), Fe(+II) [ppm]**	Allard (modif.) **Eh [mV] pH**
1 ppm S(-II) (+0.01 ppm Fe(+II):saline)	**0.46 ± 0.04**	**-216 ± 5 8.69 ± 0.07**	**0.59 ± 0.02**	**-235 ± 16 9.08 ± 0.06**
3 ppm S(-II)	**1.99 ± 0.14**	**-265 ± 17 9.22 ± 0.06**	**2.01 ± 0.11**	**-275 ± 8 9.35 ± 0.06**
5 ppm S(-II)	**3.69 ± 0.11**	**-281 ± 16 9.56 ± 0.07**	**3.39 ± 0.12**	**-297 ± 10 9.45 ± 0.04**
1 ppm Fe(+II)	**0.87**	**-138 ± 68 8.05 ± 0.08**	**0.16 ± 0.04**	**-318 ± 114 8.79 ± 0.08**

TABLE 6. *The experimental conditions of the precipitation experiments.*

Synthetic groundwater **(see Appendix 4, Tab.1)**	pH	Eh measured [V]
modified Allard	**8.8**	**-0.25...-0.30**
modified Allard, 3 ppm S(-II)	**9.2**	**-0.27...-0.34**
modified Allard, met. Fe	**9.0**	**-0.45**
saline	**8.3**	**-0.30**
saline, 3 ppm S(-II)	9.2	-0.31
saline, met. Fe	8.4...8.8	-0.47
near-field	7.5	-0.31
near-field, 3 ppm S(-II)	7.5	-0.33
near-field, met. Fe	7.6...8.0	-0.48

APP 4-8 : ORIGINAL X-RAY PATTERN

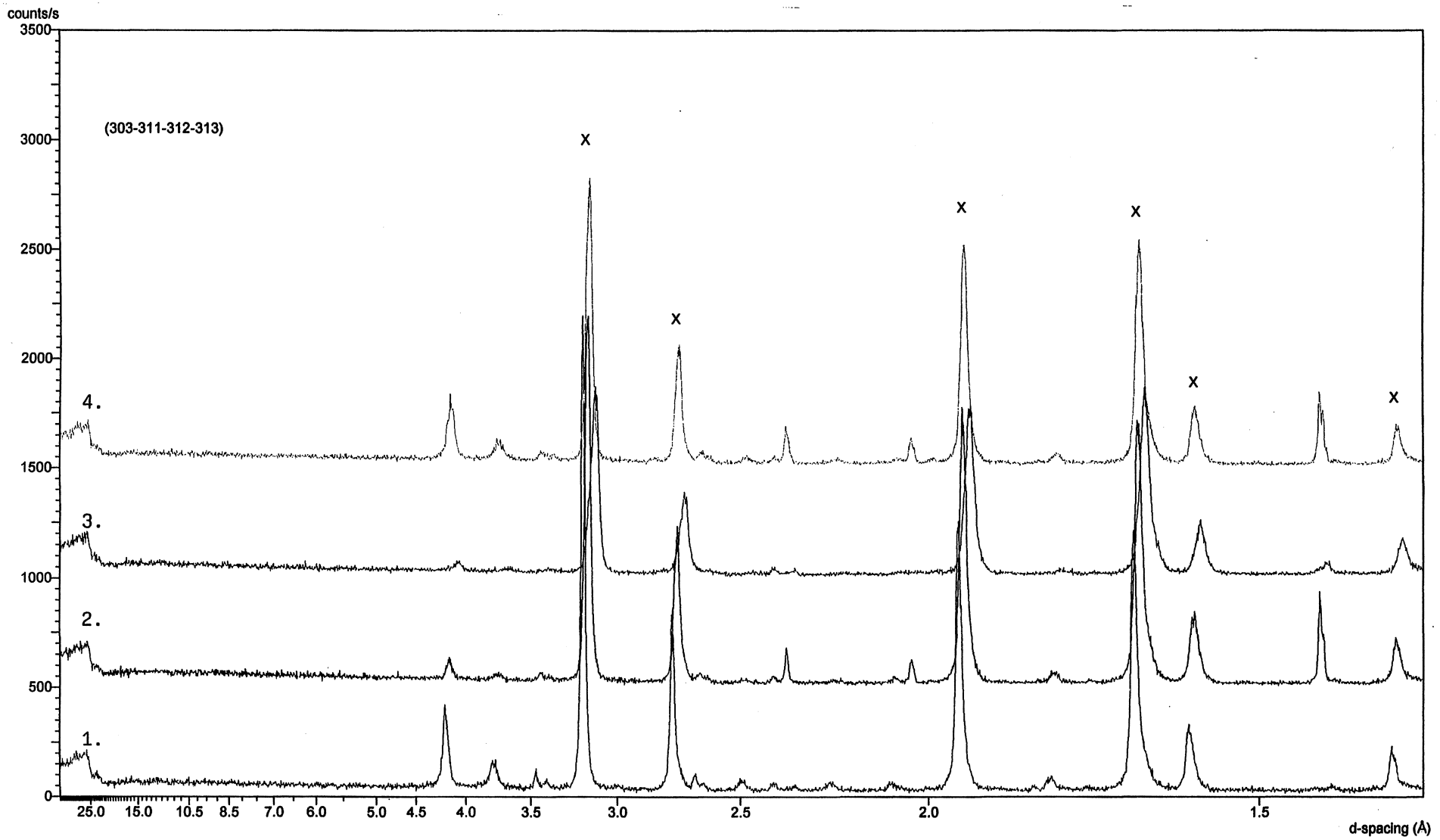

App. 4. *X-ray diffraction patterns obtained from UO_2 powder samples (on filters) after a contact time of 200 days in Allard (1, red), in modified Allard (2, green), in saline (3, violet) and in Spanish granite/bentonite (4, blue) groundwaters. The main peaks coming from UO_2 are marked with X.*

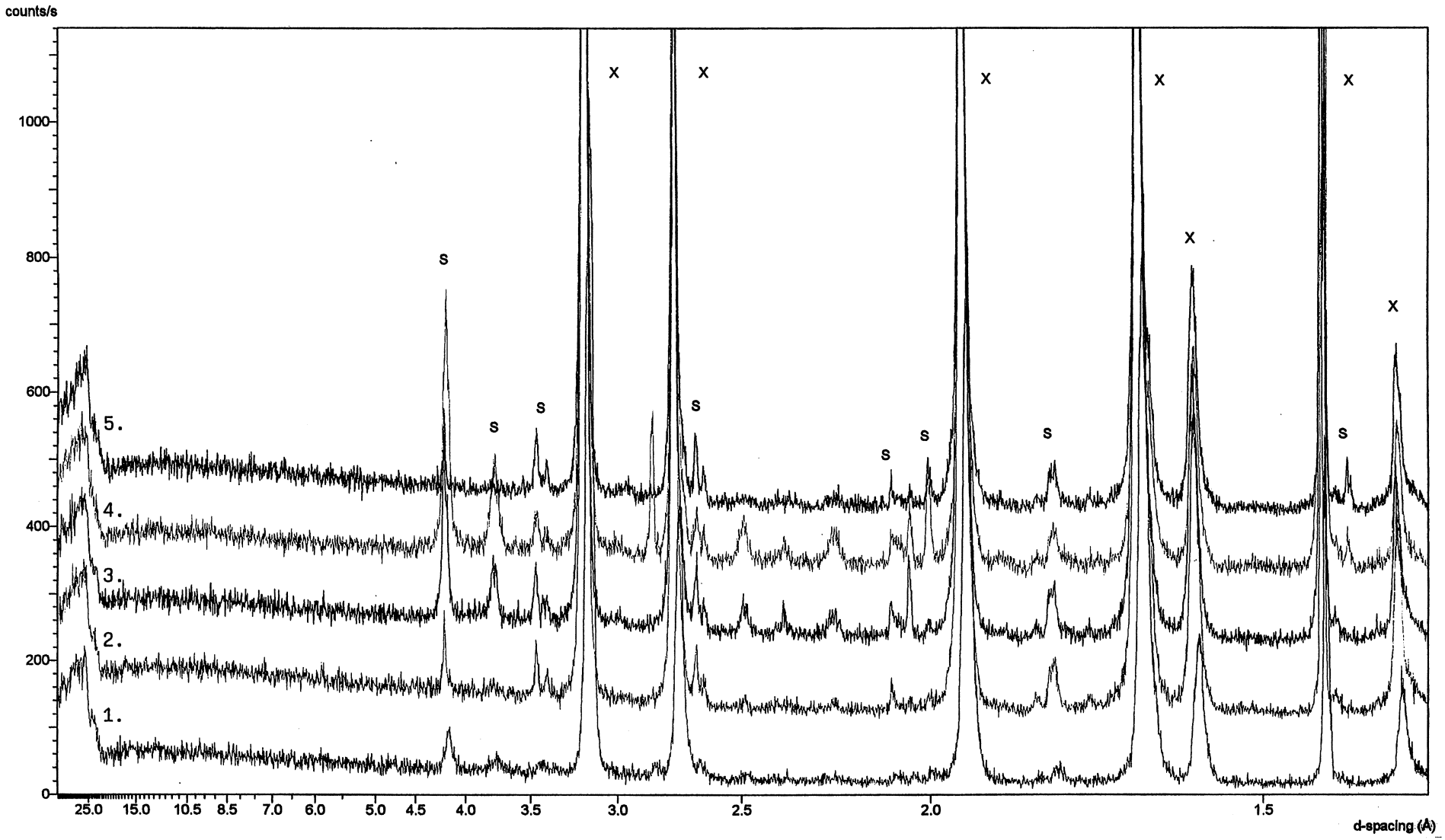

App. 5. X-ray diffraction patterns obtained from UO_2 powder samples (on filters) after a contact time of 1 year in Allard (2, green), modif. Allard (3, violet), saline (4, blue) and Spanish granite/bentonite (5, brown) groundwaters. The red one (1) shows the pattern obtained from the UO_2 powder sample before the contact with synthetic groundwater. The main peaks of UO_2 are marked with X. The peaks of a higher U oxide, U_3O_8 - UO_3 , are marked with S.

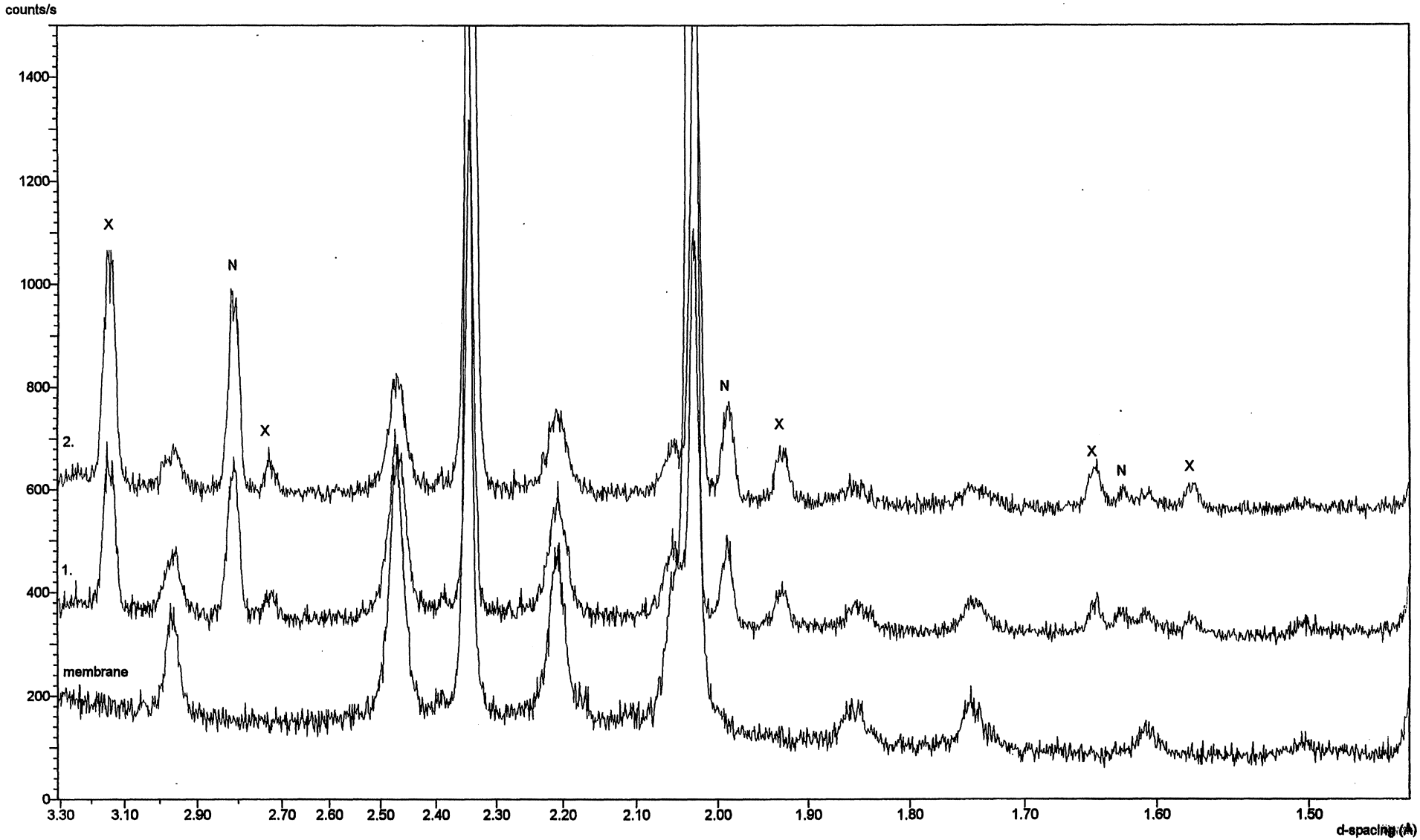

App. 6. X-ray diffraction patterns obtained from the U material retained on the membrane filter after the filtration of the aqueous phase at the end of the UO_2 dissolution experiments (S/V= 19.8 m^{-1}) in anaerobic (1, green) and reducing (2, violet) saline groundwater. The main peaks coming from $UO_2 - U_4O_9$ are marked with X. The peaks coming from the residual NaCl on the filter caused by the evaporation of saline solution are marked with N.

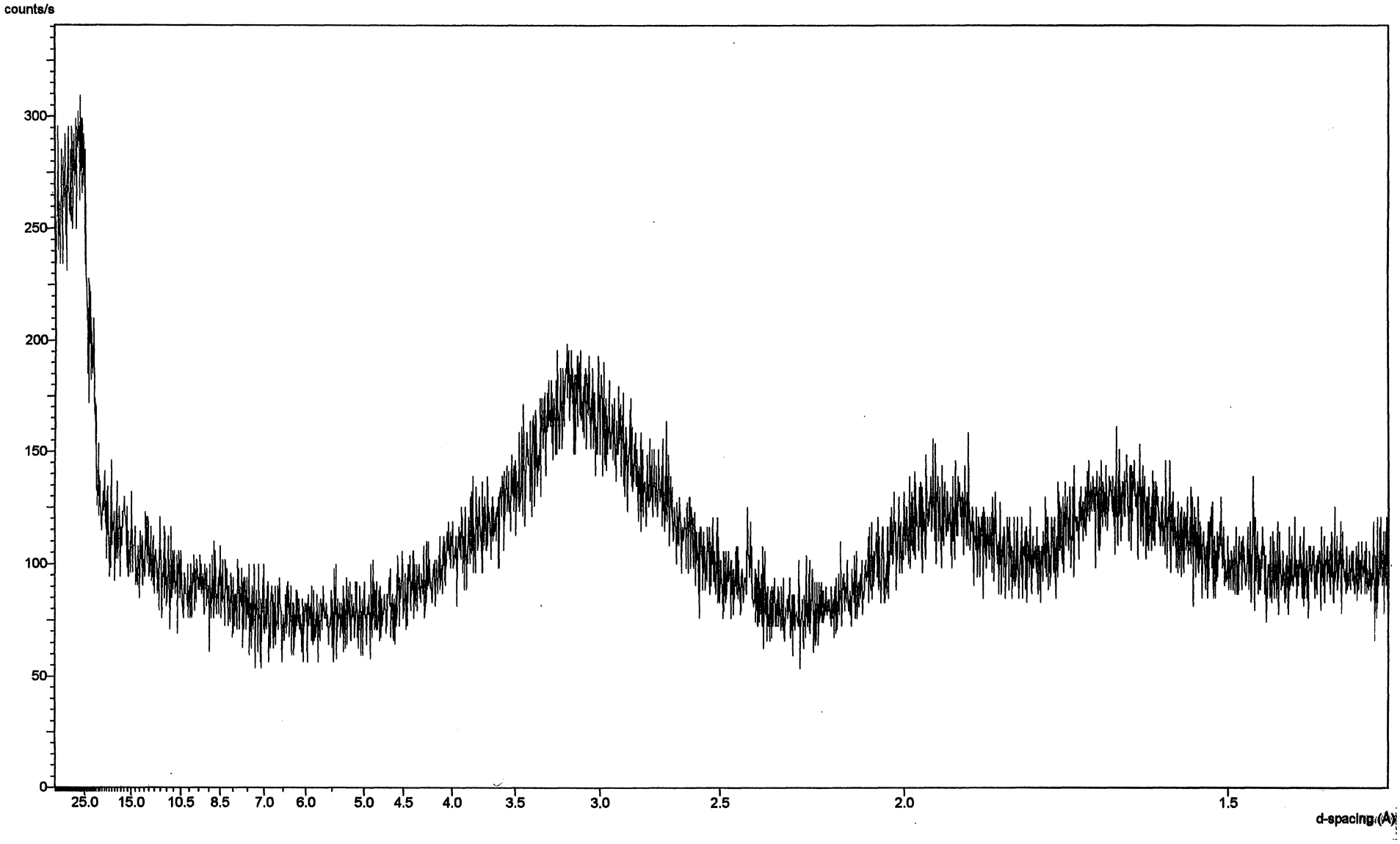

App. 7. X-ray diffraction pattern obtained from the U solid material, $UO_2 - U_3O_7$, after an ageing time of 40 days in the oversaturation experiment in Allard (modif.) groundwater under anoxic conditions.

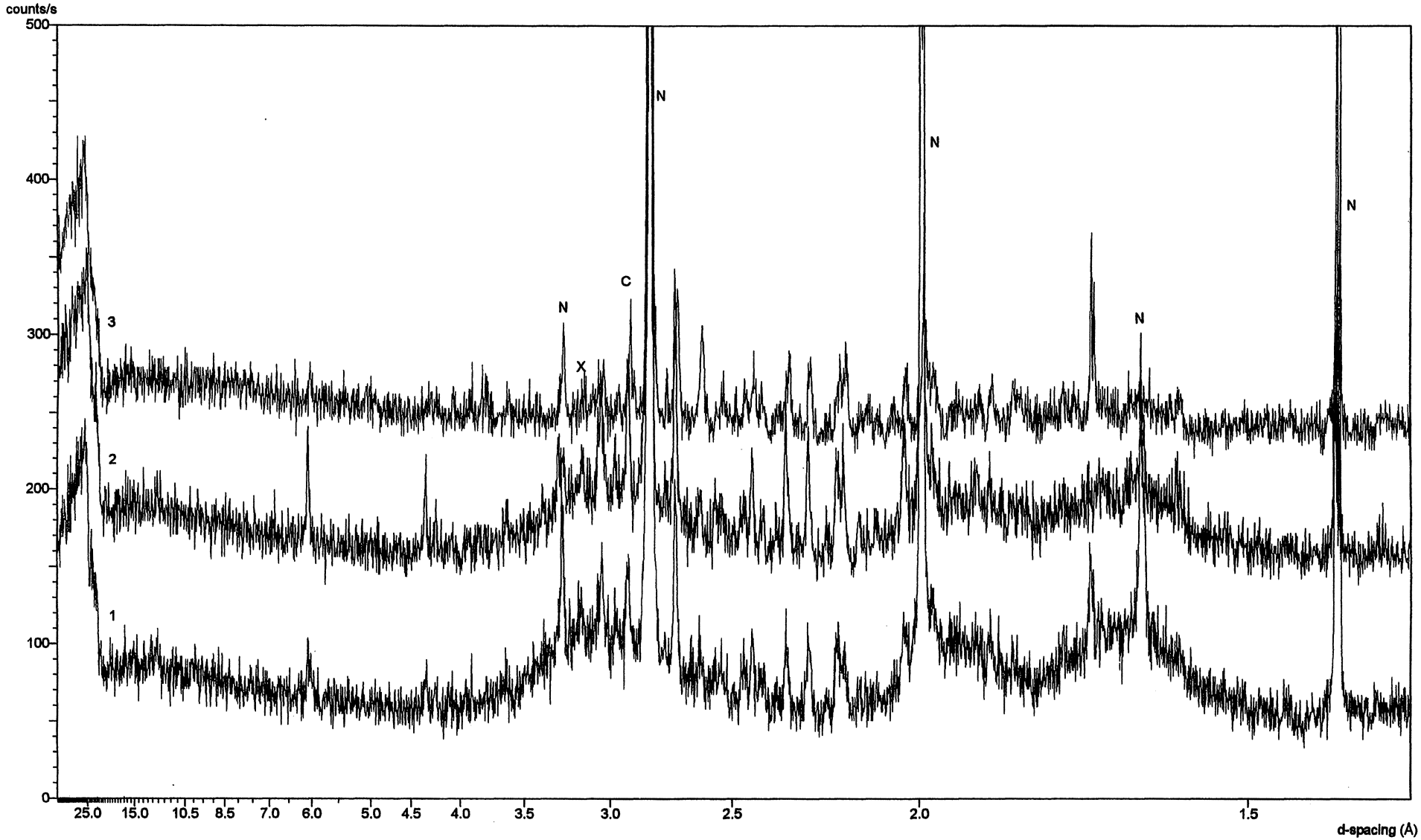

App. 8. X-ray diffraction patterns obtained from the U solid phases after an ageing time of 30 days in the oversaturation experiments in anoxic saline (1, green), saline (met. Fe)(2, red) and very saline near-field (3, blue) groundwaters. The main peaks coming from UO_2-U_4O_9 are marked with X and the main peaks coming from an impure U(IV) oxide (possibly Sr- or $CaUO_3$) are marked with C. The peaks coming from the residual NaCl on the solid sample caused by the evaporation of saline solution are marked with N.

Appendix 5 : Detailed conditions and results of experiments performed at CEA (WP III)

TABLEs with original measurement results, calculated results, materials compositions and further descriptions for integral test (CEA, WP III.3)

ANNEX 1 SAMPLE ANALYSIS PROCEDURE

Liquid Samples

Alpha Spectrometry

The analyses were performed using an *Enertec 7184* single-channel alpha spectrometer equipped with an *Enertec IPE-450-100-BB Ch Alpha* low-noise passivated implanted-junction silicon detector, coupled with an *Enertec 7183* microprocessor-driven multichannel analyzer. Samples were prepared by depositing 0.5 ml of solution on a 30 mm diameter stainless steel disk and evaporating it. The thickness of the resulting deposits resulted in self-absorption and significant uncertainty on the measured results. In order to minimize the statistical measurement error, the analysis time was adjusted according to the source activity. A counting time of 100 000 seconds was used for our samples. This technique was used to determine the following isotopes: $^{239+240}Pu$, $^{238}Pu+^{241}Am$ and ^{244}Cm

Gamma Spectrometry

To determine the isotopes: ^{60}Co, $^{106}Ru+^{106}Rh$, ^{125}Sb, ^{134}Cs, ^{137}Cs, ^{144}Ce, ^{154}Eu and ^{241}Am a gamma spectrometer was used with a N type pure Ge diode detector, an *Ortec 572* amplifier and an *Enertec 7183* multichannel analyzer. The test solution volume was always 50 ml; if the sample volume was not sufficient, it was dilluted. A counting time of about 3600 seconds ensured reliable statistical results.

Determination of ^{90}Sr

The dissolved ^{90}Sr was determined by radiochemical separation and β counting. The fission products other than cesium and strontium were precipitated as hydroxides by adding NH_4OH. After filtering the solution, nonradioactive yttrium was added to precipitate the yttrium contained in the sample. Strontium was separated by liquid-liquid extraction in the organic phase by thenoyl-trifluoroacetone (TTA), then stripped in the aqueous phase with 3M nitric acid. The solution was then evaporated on a cupel constituting the source, and the strontium was determined by β counting using an *NU-20* multiple detector, considering the ingrowth of ^{90}Y. The contamination by other β-emitting fission products was estimated at less than 1%.

ICP–AES and ICP/MS

The ICP/AES Jobin Yvon JY 66P spectrometer was used to determine Mo, Tc, Zr, U, Nd Mg, Na, Ca, K, Si, Al. To determine ^{88}Sr, ^{99}Tc, ^{237}Np, ^{238}U, ^{137}Cs, $^{106}Ru+^{106}Rh$, ^{241}Am, ^{244}Cm and ^{240}Pu in the spent and ^{88}Sr, ^{89}Y, ^{90}Zr, ^{95}Mo, ^{101}Ru, ^{103}Rh, ^{108}Pd, ^{138}Ba, ^{139}La, ^{140}Ce, ^{146}Nd and ^{238}U in SIMFUEL solutions, the ICP–MS *VG Elemental PlasmaQuad II+* mass spectrometer was used together with an *SX300* quadrupole filter and a *Meinhardt* nebulizer. If possible, isobaric interferences were mitigated by subtracting the contributions of each isotope based

on the isotopic abundance as determined by radionuclide inventory calculations. Semi-quantitative analyses yielded the approximate concentrations of the desired elements (± 30%) in order to prepare a suitable calibration range for quantitative analysis and to match the dilution factor of each sample. Quantitative analyses were carried out on the first and last weekly samples collected for each type of fuel; quantitative analyses were also performed on all the other solutions for one experiment with clay and one experiment with granite. Matrix effects were corrected by adding an internal standard, consisting of an element not found in the solution. For the SIMFUEL leachates we used ^{115}In for spent fuel ^{166}Ho.

Eh

The redox potential of the supernatant was measured at the end of each SIMFUEL leaching experiment, using a Ag/AgCl reference electrode in 3M KCl (+190 mV_{SHE}). The measurement was carried out immediately after removal of the leaching pot cover and as close as possible to the fuel in order to minimize the effect of rapid solution reoxidation by oxygen diffusion.

Solid Samples

For lack of a suitable $\beta\gamma$ characterization capability, only pure α-contaminated materials were examined. As the environmental materials had been rinsed in acid, examination in that condition was unnecessary.

Only leached SIMFUEL specimens were analyzed by SEM and characterized by X-ray microanalysis using en EDS probe. After drying, a sample holder from each environment (granite and clay) was opened in a fume chamber to remove some SIMFUEL particles (agglomerated within the clay in that sample). The specimens were attached to a sample holder with double-sided adhesive tape, covered with a carbon deposit and placed in the SEM chamber.

ANNEX 2, RECOVERING THE ACTIVITY FIXED ON THE ENVIRONMENTAL MATERIALS

The activity released by the fuel during leaching were found distributed into three fractions:
activity in solution, in the form of dissolved or colloidal species,
activity sorbed on the leaching system components (sample holder and leaching pot),
activity fixed on the environmental materials.

The first two fractions were easily recovered in the weekly solution samples and by final rinsing of the system components. Recovering the third fraction, however, was more difficult depending on the nature of the environmental materials. While acid rinsing was sufficient to desorb most of the activity fixed on the surface, it was not possible to recover the activity trapped in the foliated structure of the clay, which first had to be eliminated: we opted for alkaline melting.

Preliminary tests were carried out to assess the effectiveness of rinsing the environmental materials, separating the clay from the sand and alkaline melting of the clay. In these tests we used a spent fuel leachate obtained during another study, for which the chemical composition had been determined. Two leaching pots were prepared, one containing granite and the other a sand/clay mixture; each contained an empty sample holder. The leachant was added to each pot in quantities sufficient to ensure thorough wetting of the environmental materials. The pots were then heated to 90°C and maintained for two months.

At the end of the test period, the pots were allowed to cool to room temperature before sampling and analyzing the supernatant. Each sample holder and leaching pot was rinsed for 24 hours with 1M nitric acid; the environmental materials were also rinsed for 24 hours with 1M nitric acid. The sand/clay mixture was placed in suspension by stirring and the clay was separated from the sand by settling. The clay was then transferred to a fume chamber and allowed to dry before pulverization. It was next transferred to a glove box to prepare a mixture 2 g of K_2CO_3 with 0.2 g of clay. The mixture was transferred to a platinum crucible and heated to 980°C for 30 minutes in an electric oven in another glove box. The melted mixture was mixed with 20 ml of 68% *Prolabo* "Normapur" nitric acid, then diluted to one liter in Milli-Q double-distilled water..

The test findings were as follows:

About 80% of the initial activity was recovered with granite.

The glove boxes in which the clay samples were prepared and the oven itself resulted in strontium and actinide contamination on the same order of magnitude as the concentrations of these elements in the sample.

Since the actinide concentrations were near the detection limit of our equipment (α spectrometer, ICP-MS), the measurement errors were very significant.

The results of alkaline melting with potassium carbonate were not sufficiently reproducible, and the specimen was not always fully etched.

We therefore modified the experimental protocol for the environmental materials in the integral experiments by installing a clean oven in the fume chamber for alkaline melting, and by using *Prolabo* lithium tetraborate ($Li_2B_4O_7$) as a more aggressive melting agent.

TABLE 1. *Chemical composition of Boom clayey groundwater*

Species	Chemical composition of reference at 16°C ($mol.L^{-1}$)	Theoretical chemical composition target ($mol.L^{-1}$)
Na^+	$1,8\times10^{-2}$ to $1,9\times10^{-2}$	$1,6\times10^{-2}$
K^+	$1,3\times10^{-4}$ to $1,4\times10^{-4}$	$2,7\times10^{-4}$
Ca^{2+}	$1,0\times10^{-4}$ to $1,3\times10^{-4}$	$1,4\times10^{-4}$
Mg^{2+}	$7,0\times10^{-5}$ to $1,6\times10^{-4}$	$1,0\times10^{-4}$
Fe	$2,2\times10^{-5}$ to $8,2\times10^{-5}$	-
Al^{3+}	$2,4\times10^{-5}$ to $3,3\times10^{-5}$	-
HCO_3^-	$1,2\times10^{-2}$ to $1,4\times10^{-2}$	$1,5\times10^{-2}$
Cl^-	$7,6\times10^{-4}$ to $9,8\times10^{-4}$	$1,0\times10^{-3}$
F^-	$1,9\times10^{-4}$ to $2,3\times10^{-4}$	$1,9\times10^{-4}$
SO_4^{2-}	$2,8\times10^{-5}$ to $6,3\times10^{-5}$	$1,1\times10^{-4}$
pH	8,7 to 9,7	8,7 to 9,7
Eh	-300 to –250 mV_{ENH}	-350 to –300 mV_{ENH}

TABLE 2. *Chemical composition of clayey water synthesized for Simfuel and spent fuel leaching experiments*

Species	Chemical composition ($mol.L^{-1}$)				
	Chemical composition theoretical aiming	Simfuel tank B pots 3and 4 as synthesized	Simfuel tank B pots 3and 4 end of leaching	Spent Fuel tank D pots 3and 4 as synthesized	Spent Fuel tank D pots 3and 4 end of leaching
Mg^{2+}	$1,0\times10^{-4}$	$1,0\times10^{-4}$	$0,9\times10^{-4}$	$1,0\times10^{-4}$	$1,0\times10^{-4}$
K^+	$2,7\times10^{-4}$	$3,1\times10^{-4}$	$3,0\times10^{-4}$	$2,8\times10^{-4}$	$3,0\times10^{-4}$
Ca^{2+}	_	$9,8\times10^{-5}$	$6,1\times10^{-5}$	$9,9\times10^{-5}$	$5,9\times10^{-5}$
Na^+	$1,6\times10^{-2}$	$1,7\times10^{-2}$	$1,6\times10^{-2}$	$1,6\times10^{-2}$	$1,6\times10^{-2}$
SO_4^{2-}	$1,1\times10^{-4}$	$1,4\times10^{-4}$	$0,9\times10^{-4}$	$1,1\times10^{-4}$	$1,0\times10^{-4}$
Cl^-	$1,0\times10^{-3}$	$0,9\times10^{-3}$	$1,0\times10^{-3}$	$1,1\times10^{-3}$	$1,0\times10^{-3}$
F^-	$1,7\times10^{-4}$	$< 0,5\times10^{-4}$	$1,6\times10^{-4}$	$1,9\times10^{-4}$	$1,7\times10^{-4}$
HCO_3^-	$1,5\times10^{-2}$	$< 0,02\times10^{-2}$	$1,4\times10^{-2}$	$1,7\times10^{-2}$	$1,5\times10^{-2}$
pH	8,7 à 9,7	7,77	8,63	8,81	8,76
Rb	$1,5\times10^{-2*}$	$1,6\times10^{-2**}$	$1,5\times10^{-2}$	$1,5\times10^{-2}$	$1,5\times10^{-2}$

*Rb calculée avec : *[Ca^{2+}] = 0 et ** [F^-] = 0,5 10^{-4}*

***TABLE 3.** Chemical composition of granitic groundwater*

Species	Chemical composition of reference at 90°C ($mol.L^{-1}$)	Theoretical chemical composition target ($mol.L^{-1}$)
Si_{total}	$1,10\times10^{-3}$	$1,10\times10^{-3}$
H_4SiO_4	$4,14\times10^{-4}$	$4,14\times10^{-4}$
C_{total}	$4,70\times10^{-4}$	$4,70\times10^{-4}$
HCO_3^-	$4,20\times10^{-4}$	$4,20\times10^{-4}$
Na^+	$4,14\times10^{-3}$	$4,14\times10^{-3}$
K^+	$5,10\times10^{-5}$	$5,10\times10^{-5}$
Ca^{2+}	$6,00\times10^{-5}$	$6,00\times10^{-5}$
Al^{3+}	$4,20\times10^{-5}$	$4,20\times10^{-5}$
Cl^-	$2,90\times10^{-3}$	$2,90\times10^{-3}$
F^-	$3,00\times10^{-4}$	$3,00\times10^{-4}$
Mg, Sr, Li, B, Rb, Cs, Cd, Br, Mn, Fe, Ni	$< 1,00\times10^{-5}$	-
pH	8,7 to 9,7	8,7 to 9,7
Eh	-350 to -300 mV_{ENH}	-350 to -300 mV_{ENH}
log (PCO_2)	-3,61	-

***TABLE 4.** Chemical composition of granitic water synthesized for Simfuel and spent fuel leaching experiments*

Species	Chemical composition ($mol.L^{-1}$)				
	Chemical composition theoretical aiming	Simfuel tank A pots 1and 2 as synthesized	Simfuel tank A pots 1and 2 end of leaching	Spent Fuel tank C pots 1and 2 as synthesized	Spent Fuel tank C pots 1and 2 end of leaching
K^+	$5,10\times10^{-5}$	$5,70\times10^{-5}$	$6,80\times10^{-5}$	$5,90\times10^{-5}$	$6,70\times10^{-5}$
Ca^{2+}	$6,00\times10^{-5}$	$6,90\times10^{-5}$	$8,50\times10^{-5}$	$6,60\times10^{-5}$	$6,40\times10^{-5}$
Na^+	$4,14\times10^{-3}$	$4,15\times10^{-3}$	$4,32\times10^{-3}$	$4,10\times10^{-3}$	$4,24\times10^{-3}$
Al^{3+}	$4,20\times10^{-5}$	$1,10\times10^{-5}$	$0,50\times10^{-5}$	$1,60\times10^{-5}$	$0,40\times10^{-5}$
Si	$1,10\times10^{-3}$	$1,10\times10^{-3}$	$1,00\times10^{-3}$	$1,10\times10^{-3}$	$1,00\times10^{-3}$
Cl^-	$2,90\times10^{-3}$	$2,80\times10^{-3}$	$2,90\times10^{-3}$	$2,90\times10^{-3}$	$3,00\times10^{-3}$
F^-	$3,00\times10^{-4}$	$3,00\times10^{-4}$	$3,10\times10^{-4}$	$2,20\times10^{-4}$	$3,30\times10^{-4}$
HCO_3^-	$4,20\times10^{-4}$	$6,50\times10^{-4}$	$15,00\times10^{-4}$	$< 0,3\times10^{-4}$	$5,20\times10^{-4}$
pH	8,7 à 9,7	7,64	8,13	7,56	7,77
Rb	$1,40\times10^{-4}$	$1,80\times10^{-4}$	$3,60\times10^{-4}$	$1,20\times10^{-4}$	$1,20\times10^{-4}$

***TABLE 5.** Grinding and screening results for Gravelines 3+2 fuel (60GWd/t_{HM})*

Experimental conditions	(g ± 0,1g)	(%)
Initial fuel weight fragments	26,3	
Number of grinding and sreening cycles	5	
Fraction < 50 µm	13,3	50,7
Fraction 50 to 250 µm	11	41,9
Fraction > 250 µm	0,6	2,3
Unrecovered fraction	1,3	5,1

***TABLE 6.** Spent fuel leaching test solution analysis samples and methods*

Samples	Treatments	Analyses
Sampling 1, 3, 5, 7, 9, 11	filtration(*)	pH, α/γ spectro., β counting, ICP-AES
Sampling 2, 4, 6, 8, 10, 12	filtration(*)	ICP-MS
Filter rinse 1, 3, 5, 7, 9, 11 (HNO_3 1M)	-	α/γ spectro., β counting, ICP-AES
Filter rinse 2, 4, 6, 8, 10, 12 (HNO_3 1M)	-	ICP-MS
Final Supernatent Leachate	filtration(*) ultrafiltration(**) filtration(*) ultrafiltration(**)	α/γ spectro., β counting, ICP-AES α/γ spectro., β counting, ICP-AES ICP-MS ICP-MS
Vessel Rinse (HNO_3 1M)	- -	α/γ spectro., β counting, ICP-AES ICP-MS
Fuel Sample Holder Rinse (Milli-Q water)	filtration(*) filtration(*)	α/γ spectro., β counting, ICP-AES ICP-MS
Environmental Materials Rinse (HNO_3 1M)	filtration(*) filtration(*)	α/γ spectro., β counting, ICP-AES ICP-MS
Alkaline melting (for clay material only)	- -	α/γ spectro., β counting, ICP-AES ICP-MS

(*) : 0.45µm filter, (**) : 10000 Da

TABLE 6. *Simfuel leaching test solution analysis samples and methods*

Samples	Treatments	Analyses
Sampling 1 to 12	filtration(*)	pH, ICP-MS
Filter Rinse 1 to 12 (HNO_3 1M)	_	ICP-MS
Final Supernatent Leachate	 filtration(*) ultrafiltration(**)	Eh ICP-MS ICP-MS
Vessel Rinse (HNO_3 1M)	_	ICP-MS
Fuel Sample Holder Rinse (Milli-Q water)	filtration(*)	ICP-MS
Environmental Materials Rinse (HNO_3 1M)	filtration(*)	ICP-MS
Alkaline melting (for clay material only)	_	ICP-MS

(*) : 0.45µm filter, (**) : 10000 Da

TABLE 7. Gravelines 3+2 preleaching leachates: cumulative fractions of inventory released into aqueous solutions.

Contact time (d)		1	5	8	7	14	13	22	21	49
Cumulative contact time (d)		1	6	14	21	35	48	70	91	140
^{90}Sr		2,7E-04	4,0E-04	6,5E-04	7,2E-04	8,7E-04	9,4E-04	1,1E-03	1,2E-03	1,3E-03
	error	*4,0E-05*	*4,6E-05*	*6,1E-05*	*6,4E-05*	*6,8E-05*	*7,0E-05*	*7,4E-05*	*7,6E-05*	*7,9E-05*
^{125}Sb		<7,1E-04	<8,7E-04	<9,2E-04	<1,1E-03	<1,2E-03	<1,3E-03	<1,5E-03	<1,7E-03	<1,7E-03
	error	*1,1E-04*	*1,1E-04*	*1,1E-04*	*1,1E-04*	*1,1E-04*	*1,2E-04*	*1,2E-04*	*1,3E-04*	*1,3E-04*
^{134}Cs		4,2E-03	5,1E-03	5,4E-03	5,6E-03	5,9E-03	6,0E-03	6,2E-03	6,4E-03	6,6E-03
	error	*2,1E-04*	*2,2E-04*	*2,2E-04*	*2,2E-04*	*2,2E-04*	*2,2E-04*	*2,2E-04*	*2,2E-04*	*2,2E-04*
^{137}Cs		5,3E-03	6,3E-03	6,7E-03	7,0E-03	7,3E-03	7,5E-03	7,7E-03	7,9E-03	8,3E-03
	error	*3,7E-04*	*3,9E-04*	*3,9E-04*	*3,9E-04*	*3,9E-04*	*3,9E-04*	*3,9E-04*	*3,9E-04*	*3,9E-04*
$^{239}Pu+^{240}Pu$		5,9E-06	6,8E-06	1,1E-05	1,6E-05	1,9E-05	2,3E-05	2,8E-05	2,9E-05	4,1E-05
	error	*1,8E-06*	*1,8E-06*	*2,2E-06*	*2,9E-06*	*3,0E-06*	*3,4E-06*	*3,7E-06*	*3,7E-06*	*5,4E-06*
$^{238}Pu+^{241}Am$		6,8E-06	8,5E-06	1,6E-05	2,4E-05	2,9E-05	3,5E-05	3,8E-05	3,9E-05	5,7E-05
	error	*6,8E-07*	*7,1E-07*	*1,0E-06*	*1,4E-06*	*1,5E-06*	*1,7E-06*	*1,7E-06*	*1,7E-06*	*2,5E-06*
^{244}Cm		1,1E-05	2,1E-05	4,2E-05	6,6E-05	9,2E-05	9,8E-05	1,0E-04	1,1E-04	1,3E-04
	error	*7,8E-07*	*1,1E-06*	*1,9E-06*	*1,4E-06*	*1,5E-06*	*1,7E-06*	*1,7E-06*	*1,7E-06*	*2,5E-06*
U		4,7E-05	1,3E-04	2,1E-04	2,9E-04	2,1E+07	4,7E-04	4,9E-04	5,4E-04	5,9E-04
	error	*1,4E-06*	*2,9E-06*	*3,9E-06*	*4,9E-06*	*6,5E-06*	*6,8E-06*	*6,9E-06*	*7,1E-06*	*7,2E-06*
Nd		2,6E-05	6,1E-05	1,2E-04	1,7E-04	5,8E-03	2,7E-04	<3,0E-04	<3,2E-04	<3,6E-04
	error	*2,9E-06*	*5,1E-06*	*8,9E-06*	*1,1E-05*	*1,5E-05*	*1,5E-05*	*dl*	*dl*	*dl*
Tc		<5,3E-04	<1,0E-03	<1,1E-03	<1,3E-03	<1,5E-03	<1,8E-03	<2,1E-03	<2,3E-03	<2,4E-03
Mo		1,9E-04	<2,5E-04	<3,2E-04	<3,7E-04	<4,5E-04	<6,3E-04	<9,6E-04	<1,1E-03	<1,1E-03
Zr		1,5E-05	2,8E-05	5,5E-05	6,4E-05	1,5E-05	9,6E-05	<1,1E-04	<1,2E-04	<1,4E-04
	error	*1,5E-06*	*2,0E-06*	*3,5E-06*	*3,8E-06*	*4,4E-06*	*4,6E-06*	*dl*	*dl*	*dl*

dl : detection limit

TABLE 8. *Gravelines 3+2 spent fuel integral leaching experiments: cumulative fraction of inventory released in aqueous phase of weekly samples.*

Clay/Granitic Groundwater													
Sampling n°		1	2	3	4	5	6	7	8	9	10	11	12	Final
Time (days)		7	5	7	9	7	7	7	7	7	7	7	7	7
Cumulative time (days)		7	12	19	28	35	42	49	56	63	70	77	84	91
Sampling volume (mL)		10,9	9,5	8,3	10,4	9,2	10	11,7	10,4	10,3	10,2	12,6	11,1	
^{90}Sr		3,2E-05	3,2E-05	2,9E-05	2,8E-05	2,8E-05	2,7E-05	2,7E-05	2,8E-05	2,8E-05	2,9E-05	2,9E-05	3,0E-05	3,2E-05
	Error	*5,2E-06*	*4,1E-06*	*3,1E-06*	*2,6E-06*	*2,2E-06*	*2,0E-06*	*1,8E-06*	*1,8E-06*	*1,8E-06*	*1,7E-06*	*1,7E-06*	*1,7E-06*	*1,8E-06*
^{134}Cs		2,2E-04	2,3E-04	2,2E-04	2,1E-04	2,1E-04	2,2E-04	2,2E-04	2,4E-04	2,5E-04	2,5E-04	2,6E-04	2,6E-04	2,5E-04
	Error	*1,6E-05*	*1,3E-05*	*1,0E-05*	*8,8E-06*	*7,6E-06*	*7,2E-06*	*6,8E-06*	*6,7E-06*	*6,6E-06*	*6,5E-06*	*6,3E-06*	*5,8E-06*	*5,5E-06*
^{137}Cs		2,2E-04	2,3E-04	2,2E-04	2,1E-04	2,1E-04	2,2E-04	2,2E-04	2,4E-04	2,5E-04	2,5E-04	2,6E-04	2,6E-04	2,5E-04
	Error	*1,8E-05*	*1,5E-05*	*1,2E-05*	*1,0E-05*	*8,7E-06*	*8,2E-06*	*7,7E-06*	*7,7E-06*	*7,6E-06*	*7,4E-06*	*7,2E-06*	*6,7E-06*	*6,3E-06*
$^{239+240}Pu$		4,1E-08	3,4E-08	2,2E-08	3,3E-08	4,6E-08	4,5E-08	4,3E-08	4,4E-08	4,3E-08	5,2E-08	6,3E-08	6,1E-08	5,7E-08
	Error	*2,1E-08*	*1,3E-08*	*6,7E-09*	*1,1E-08*	*1,5E-08*	*1,3E-08*	*1,0E-08*	*9,0E-09*	*8,1E-09*	*1,1E-08*	*1,4E-08*	*1,1E-08*	*9,0E-09*
$^{238}Pu+^{241}Am$		2,3E-08	1,7E-08	8,9E-09	9,7E-09	1,1E-08	1,1E-08	1,1E-08	1,2E-08	1,2E-08	1,3E-08	1,4E-08	1,5E-08	1,7E-08
	Error	*7,1E-09*	*4,1E-09*	*1,8E-09*	*1,8E-09*	*1,9E-09*	*1,9E-09*	*1,9E-09*	*1,9E-09*	*1,9E-09*	*1,9E-09*	*2,0E-09*	*2,1E-09*	*2,2E-09*
^{244}Cm		<3,7E-09	<3,0E-09	<2,0E-09	<2,1E-09	<2,3E-09	<2,4E-09	<2,5E-09	<2,7E-09	<2,9E-09	<3,0E-09	<3,2E-09	<3,4E-09	<3,5E-09
	Error													
Mo		1,0E-03	1,2E-03	1,3E-03	1,2E-03	1,1E-03	1,2E-03	1,2E-03	1,2E-03	1,2E-03	1,2E-03	1,3E-03	1,3E-03	1,3E-03
	Error	*2,1E-04*	*2,1E-04*	*2,0E-04*	*1,6E-04*	*1,2E-04*	*1,1E-04*	*1,1E-04*	*9,8E-05*	*8,9E-05*	*9,0E-05*	*9,0E-05*	*9,0E-05*	*9,1E-05*
^{238}U		5,0E-07	5,2E-07	5,1E-07	4,7E-07	6,5E-07	8,4E-07	7,3E-07	5,9E-07	6,0E-07	6,1E-07	6,1E-07	6,2E-07	1,0E-06
	Error	*5,5E-08*	*4,7E-08*	*3,8E-08*	*3,0E-08*	*4,3E-08*	*5,6E-08*	*3,7E-08*	*2,4E-08*	*2,4E-08*	*2,4E-08*	*2,3E-08*	*2,3E-08*	*5,6E-08*

Granite/Granitic Groundwater													
Sampling n°		1	2	3	4	5	6	7	8	9	10	11	12	Final
Time (days)		7	5	7	9	7	7	7	7	7	7	7	7	7
Cumulative time (days)		7	12	19	28	35	42	49	56	63	70	77	84	91
Sampling volume (mL)		9,7	10,7	10,1	11,7	9,7	6,2	9,6	6,5	10,7	11,8	12,5	13,5	
^{90}Sr		3,3E-05	2,8E-05	2,2E-05	2,3E-05	2,4E-05	2,3E-05	2,2E-05	2,3E-05	2,4E-05	2,4E-05	2,4E-05	2,8E-05	3,4E-05
	Error	*5,2E-06*	*3,7E-06*	*2,2E-06*	*2,0E-06*	*1,9E-06*	*1,7E-06*	*1,5E-06*	*1,6E-06*	*1,6E-06*	*1,5E-06*	*1,5E-06*	*1,8E-06*	*2,2E-06*
^{134}Cs		2,0E-04	2,3E-04	2,5E-04	2,8E-04	3,0E-04	2,9E-04	2,6E-04	2,9E-04	3,1E-04	3,2E-04	3,4E-04	3,3E-04	3,2E-04
	Error	*1,4E-05*	*1,3E-05*	*1,3E-05*	*1,2E-05*	*1,2E-05*	*9,6E-06*	*7,5E-06*	*8,0E-06*	*8,5E-06*	*8,4E-06*	*8,4E-06*	*7,5E-06*	*6,8E-06*
^{137}Cs		2,0E-04	2,3E-04	2,5E-04	2,8E-04	3,1E-04	2,9E-04	2,7E-04	2,9E-04	3,1E-04	3,2E-04	3,5E-04	3,4E-04	3,3E-04
	Error	*1,6E-05*	*1,5E-05*	*1,5E-05*	*1,4E-05*	*1,4E-05*	*1,1E-05*	*8,7E-06*	*9,3E-06*	*9,8E-06*	*9,8E-06*	*1,0E-05*	*8,7E-06*	*8,0E-06*
$^{239+240}Pu$		8,3E-08	6,2E-08	3,4E-08	3,6E-08	3,8E-08	3,9E-08	4,0E-08	4,2E-08	4,3E-08	4,5E-08	4,7E-08	6,1E-08	7,9E-08
	Error	*4,2E-08*	*2,5E-08*	*1,0E-08*	*1,1E-08*	*1,1E-08*	*1,1E-08*	*1,1E-08*	*1,1E-08*	*1,1E-08*	*1,1E-08*	*1,1E-08*	*1,4E-08*	*2,0E-08*
$^{238}Pu+^{241}Am$		1,5E-08	1,4E-08	1,3E-08	1,3E-08	1,3E-08	1,5E-08	1,8E-08	1,8E-08	1,9E-08	1,8E-08	1,8E-08	2,2E-08	2,7E-08
	Error	*4,6E-09*	*3,7E-09*	*2,8E-09*	*2,3E-09*	*2,0E-09*	*2,3E-09*	*2,8E-09*	*2,6E-09*	*2,4E-09*	*2,1E-09*	*1,9E-09*	*2,5E-09*	*3,4E-09*
^{244}Cm		3,2E-08	3,2E-08	3,0E-08	2,7E-08	2,2E-08	2,6E-08	3,0E-08	3,2E-08	3,3E-08	3,1E-08	2,9E-08	3,3E-08	3,9E-08
	Error	*1,0E-08*	*8,1E-09*	*6,3E-09*	*4,5E-09*	*3,2E-09*	*3,7E-09*	*4,3E-09*	*4,3E-09*	*4,3E-09*	*3,6E-09*	*3,2E-09*	*3,7E-09*	*4,4E-09*
Mo		3,3E-03	3,4E-03	3,5E-03	3,6E-03	3,7E-03	3,7E-03	3,5E-03	3,9E-03	4,2E-03	4,3E-03	4,3E-03	4,4E-03	4,5E-03
	Error	*6,9E-04*	*6,0E-04*	*5,1E-04*	*4,5E-04*	*4,0E-04*	*3,5E-04*	*3,0E-04*	*3,3E-04*	*3,6E-04*	*3,4E-04*	*3,2E-04*	*3,1E-04*	*2,9E-04*
^{238}U		1,2E-06	1,1E-06	1,0E-06	8,4E-07	8,0E-07	7,3E-07	7,5E-07	7,8E-07	7,7E-07	7,7E-07	7,7E-07	7,6E-07	1,5E-06
	Error	*1,3E-07*	*1,0E-07*	*7,3E-08*	*4,8E-08*	*4,2E-08*	*3,8E-08*	*3,8E-08*	*3,8E-08*	*3,8E-08*	*3,7E-08*	*3,7E-08*	*3,7E-08*	*9,2E-08*

To be continued on next page...

TABLE 8 (continuation). **Gravelines 3+2 spent fuel integral leaching experiments: cumulative fraction of inventory released in aqueous phase of weekly samples.**

Clay/Clayey Groundwater													
Sampling n°		1	2	3	4	5	6	7	8	9	10	11	12	Final
Time (days)		5	7	9	7	7	7	7	7	7	7	7	7	7
Cumulative time (days)		5	12	21	28	35	42	49	56	63	70	77	84	91
Sampling volume (mL)		9	8,1	8,9	9,6	9,8	13	11,3	8,9	9,8	12,9	10,7	12,2	
^{90}Sr		5,1E-05	3,9E-05	2,3E-05	2,4E-05	2,4E-05	2,5E-05	2,5E-05	2,6E-05	2,7E-05	2,8E-05	2,9E-05	2,9E-05	2,9E-05
	Error	*8,2E-06*	*5,0E-06*	*2,2E-06*	*2,1E-06*	*2,1E-06*	*2,0E-06*	*1,9E-06*	*1,9E-06*	*1,9E-06*	*1,9E-06*	*1,9E-06*	*1,9E-06*	*1,9E-06*
^{134}Cs		1,5E-04	1,4E-04	1,2E-04	1,3E-04	1,3E-04	1,3E-04	1,4E-04	1,5E-04	1,5E-04	1,6E-04	1,7E-04	1,6E-04	1,6E-04
	Error	*1,0E-05*	*8,2E-06*	*6,0E-06*	*5,4E-06*	*4,8E-06*	*4,5E-06*	*4,2E-06*	*4,1E-06*	*4,0E-06*	*4,0E-06*	*4,0E-06*	*3,7E-06*	*3,4E-06*
^{137}Cs		1,5E-04	1,4E-04	1,3E-04	1,3E-04	1,3E-04	1,4E-04	1,4E-04	1,5E-04	1,5E-04	1,6E-04	1,7E-04	1,7E-04	1,6E-04
	Error	*1,2E-05*	*9,4E-06*	*7,0E-06*	*6,3E-06*	*5,6E-06*	*5,2E-06*	*4,9E-06*	*4,8E-06*	*4,6E-06*	*4,6E-06*	*4,7E-06*	*4,3E-06*	*4,0E-06*
$^{239+240}Pu$		4,1E-08	3,2E-08	2,0E-08	2,1E-08	2,3E-08	2,9E-08	3,5E-08	3,5E-08	3,3E-08	3,5E-08	3,7E-08	4,3E-08	5,0E-08
	Error	*2,1E-08*	*1,3E-08*	*6,0E-09*	*6,1E-09*	*6,1E-09*	*7,8E-09*	*9,1E-09*	*7,9E-09*	*6,7E-09*	*6,8E-09*	*6,9E-09*	*8,4E-09*	*1,0E-08*
$^{238}Pu+^{241}Am$		1,9E-08	1,5E-08	9,9E-09	1,0E-08	1,1E-08	1,1E-08	1,2E-08	1,2E-08	1,1E-08	1,2E-08	1,4E-08	1,4E-08	1,4E-08
	Error	*5,8E-09*	*3,8E-09*	*1,9E-09*	*1,8E-09*	*1,7E-09*	*1,7E-09*	*1,6E-09*	*1,5E-09*	*1,4E-09*	*1,5E-09*	*1,7E-09*	*1,6E-09*	*1,6E-09*
^{244}Cm		3,7E-09	6,9E-09	1,0E-08	8,2E-09	5,5E-09	6,2E-09	7,0E-09	8,2E-09	9,5E-09	9,1E-09	8,6E-09	8,9E-09	9,4E-09
	Error	*1,2E-09*	*1,9E-09*	*2,7E-09*	*1,7E-09*	*8,0E-10*	*8,7E-10*	*9,5E-10*	*1,1E-09*	*1,3E-09*	*1,1E-09*	*8,9E-10*	*9,1E-10*	*9,2E-10*
Mo		2,7E-03	3,3E-03	3,8E-03	4,5E-03	5,4E-03	5,7E-03	6,0E-03	6,4E-03	6,6E-03	6,9E-03	7,3E-03	7,6E-03	7,8E-03
	Error	*5,7E-04*	*5,9E-04*	*6,1E-04*	*6,7E-04*	*7,4E-04*	*6,7E-04*	*6,1E-04*	*5,9E-04*	*5,7E-04*	*5,5E-04*	*5,4E-04*	*5,2E-04*	*5,0E-04*
^{238}U		3,7E-06	3,2E-06	2,5E-06	1,7E-06	1,6E-06	1,6E-06	1,7E-06	1,9E-06	2,0E-06	2,2E-06	2,1E-06	1,9E-06	7,2E-06
	Error	*4,1E-07*	*2,9E-07*	*1,8E-07*	*9,7E-08*	*9,5E-08*	*9,3E-08*	*9,5E-08*	*9,8E-08*	*1,0E-07*	*1,1E-07*	*9,7E-08*	*9,4E-08*	*6,0E-07*

Granite/Clayey Groundwater														
Sampling n°		1	2	3	4	5	6	7	8	9	10	11	12	Final
Time (days)		7	5	7	9	7	7	Not done	14	7	7	7	7	7
Cumulative time (days)		7	12	19	28	35	42		56	63	70	77	84	91
Sampling volume (mL)		11,9	10,8	11,3	9,3	10,6	8,9		14,6	9,9	10,4	13,5	12,8	
^{90}Sr		5,6E-06	6,7E-06	7,7E-06	8,8E-06	9,6E-06	1,0E-05	Nd	1,1E-05	1,1E-05	1,3E-05	1,5E-05	1,6E-05	1,6E-05
	Error	*8,9E-07*	*8,9E-07*	*8,8E-07*	*8,9E-07*	*8,8E-07*	*8,6E-07*		*7,8E-07*	*7,6E-07*	*8,6E-07*	*9,8E-07*	*9,5E-07*	*9,2E-07*
^{134}Cs		6,9E-05	9,5E-05	1,2E-04	1,3E-04	1,4E-04	1,6E-04	Nd	1,7E-04	2,0E-04	2,1E-04	2,2E-04	2,3E-04	2,4E-04
	Error	*4,9E-06*	*5,6E-06*	*6,4E-06*	*6,0E-06*	*5,6E-06*	*5,8E-06*		*6,0E-06*	*6,3E-06*	*6,3E-06*	*6,2E-06*	*5,8E-06*	*5,3E-06*
^{137}Cs		6,8E-05	9,5E-05	1,2E-04	1,4E-04	1,4E-04	1,6E-04	Nd	1,8E-04	2,0E-04	2,1E-04	2,3E-04	2,4E-04	2,4E-04
	Error	*5,5E-06*	*6,5E-06*	*7,4E-06*	*7,0E-06*	*6,4E-06*	*6,7E-06*		*7,0E-06*	*7,4E-06*	*7,3E-06*	*7,3E-06*	*6,9E-06*	*6,4E-06*
$^{239+240}Pu$		4,1E-08	3,5E-08	2,4E-08	2,5E-08	2,7E-08	2,9E-08	Nd	3,0E-08	3,3E-08	3,4E-08	3,6E-08	6,9E-08	1,1E-07
	Error	*2,1E-08*	*1,4E-08*	*7,1E-09*	*7,2E-09*	*7,2E-09*	*7,3E-09*		*7,3E-09*	*7,4E-09*	*7,5E-09*	*7,5E-09*	*2,1E-08*	*3,6E-08*
$^{238}Pu+^{241}Am$		8,1E-09	9,8E-09	1,1E-08	1,4E-08	1,6E-08	1,8E-08	Nd	1,8E-08	2,0E-08	2,1E-08	2,2E-08	3,5E-08	5,0E-08
	Error	*2,5E-09*	*2,5E-09*	*2,5E-09*	*2,8E-09*	*3,1E-09*	*3,0E-09*		*2,7E-09*	*2,6E-09*	*2,6E-09*	*2,7E-09*	*5,7E-09*	*9,0E-09*
^{244}Cm		3,7E-09	4,2E-09	4,4E-09	7,6E-09	1,1E-08	1,3E-08	Nd	1,5E-08	1,7E-08	1,8E-08	1,8E-08	3,2E-08	4,8E-08
	Error	*1,2E-09*	*1,1E-09*	*9,5E-10*	*1,7E-09*	*2,5E-09*	*2,6E-09*		*2,7E-09*	*2,9E-09*	*2,6E-09*	*2,4E-09*	*5,8E-09*	*9,4E-09*
Mo		3,9E-03	4,8E-03	5,6E-03	6,0E-03	6,3E-03	6,8E-03	Nd	6,9E-03	7,5E-03	7,9E-03	8,3E-03	9,0E-03	9,7E-03
	Error	*8,2E-04*	*8,3E-04*	*8,4E-04*	*7,8E-04*	*7,2E-04*	*7,1E-04*		*6,6E-04*	*6,5E-04*	*6,4E-04*	*6,3E-04*	*6,7E-04*	*7,0E-04*
^{238}U		1,8E-06	1,8E-06	1,7E-06	1,4E-06	1,5E-06	1,6E-06	nd	1,4E-06	1,4E-06	1,4E-06	1,4E-06	1,3E-06	5,1E-06
	Error	*2,0E-07*	*1,6E-07*	*1,2E-07*	*8,2E-08*	*8,2E-08*	*8,2E-08*		*6,9E-08*	*6,7E-08*	*6,6E-08*	*6,6E-08*	*6,6E-08*	*4,2E-07*

TABLE 9. *Gravelines 3+2 spent fuel integral leaching experiments: fission products and actinide concentrations (**mol·l**$^{-1}$) in weekly samples in the different media*

Clay/Granitic Groundwater														
Sampling n°		1	2	3	4	5	6	7	8	9	10	11	12	Final
Time (days)		7	5	7	9	7	7	7	7	7	7	7	7	7
Cumulative time (days)		7	12	19	28	35	42	49	56	63	70	77	84	91
^{90}Sr		4,6E-09		2,4E-09		1,4E-09		8,1E-10		7,3E-10		5,7E-10		6,3E-10
Sr		8,3E-09		4,4E-09		2,6E-09		1,5E-09		1,3E-09		1,0E-09		1,1E-09
	Error	*1,2E-09*		*6,6E-10*		*3,9E-10*		*2,2E-10*		*2,0E-10*		*1,5E-10*		*1,7E-10*
^{134}Cs		5,2E-10		3,1E-10		2,0E-10		1,6E-10		1,4E-10		1,2E-10		3,8E-11
Cs		1,2E-07		6,8E-08		4,4E-08		3,4E-08		3,0E-08		2,6E-08		8,3E-09
	Error	*6,9E-09*		*4,1E-09*		*2,6E-09*		*2,1E-09*		*1,8E-09*		*1,5E-09*		*5,0E-10*
^{238}U			2,8E-08		1,6E-08		3,3E-08		5,1E-09		4,4E-09		2,7E-09	3,1E-08
U			2,8E-08		1,6E-08		3,3E-08		5,2E-09		4,5E-09		2,8E-09	3,2E-08
	Error		*2,8E-09*		*1,6E-09*		*3,3E-09*		*5,2E-10*		*4,5E-10*		*2,8E-10*	*3,2E-09*
^{239}Pu		<1,8E-11		3,6E-12		1,2E-11		6,7E-12		3,6E-12		1,0E-11		3,6E-12
Pu		<3,8E-11		7,6E-12		2,5E-11		1,4E-11		7,6E-12		2,1E-11		7,6E-12
	Error	*1,9E-11*		*3,8E-12*		*1,3E-11*		*6,9E-12*		*3,8E-12*		*1,1E-11*		*3,8E-12*
^{244}Cm		<4,1E-14		<8,2E-15		<8,2E-15		<8,2E-15		<8,2E-15		<8,2E-15		<8,2E-15
Cm		<3,6E-14		<7,3E-15		<7,3E-15		<7,3E-15		<7,3E-15		<7,3E-15		<7,3E-15
	Error													
Mo		1,1E-06		1,0E-06		5,1E-07		4,1E-07		2,0E-07		2,0E-07		2,0E-07
	Error	*1,1E-07*		*1,0E-07*		*5,1E-08*		*4,1E-08*		*2,0E-08*		*2,0E-08*		*2,0E-08*

Granite/Granitic Groundwater														
Sampling n°		1	2	3	4	5	6	7	8	9	10	11	12	Final
Time (days)		7	5	7	9	7	7	7	7	7	7	7	7	7
Cumulative time (days)		7	12	19	28	35	42	49	56	63	70	77	84	91
^{90}Sr		4,7E-09		1,6E-09		1,1E-09		5,5E-10		6,8E-10		4,0E-10		1,4E-09
Sr		8,4E-09		2,9E-09		2,0E-09		9,8E-10		1,2E-09		7,2E-10		2,6E-09
	Error	1,3E-09		4,4E-10		3,0E-10		1,5E-10		1,8E-10		1,1E-10		3,9E-10
^{134}Cs		4,7E-10		4,1E-10		3,5E-10		1,6E-10		2,0E-10		1,9E-10		7,4E-11
Cs		1,0E-07		9,0E-08		7,8E-08		3,5E-08		4,5E-08		4,2E-08		1,6E-08
	Error	6,2E-09		5,4E-09		4,7E-09		2,1E-09		2,7E-09		2,5E-09		9,8E-10
^{238}U			6,0E-08		2,0E-08		5,4E-09		7,0E-09		4,4E-09		2,0E-09	5,1E-08
U			6,1E-08		2,0E-08		5,4E-09		7,1E-09		4,4E-09		2,0E-09	5,2E-08
	Error		6,1E-09		2,0E-09		5,4E-10		7,1E-10		4,4E-10		2,0E-10	5,2E-09
^{239}Pu		3,6E-11		<3,6E-12		3,6E-12		3,6E-12		<3,6E-12		3,6E-12		1,5E-11
Pu		7,6E-11		<7,6E-12		7,6E-12		7,6E-12		<7,6E-12		7,6E-12		3,0E-11
	Error	*3,8E-11*		*3,8E-12*		*3,8E-12*		*3,8E-12*		*3,8E-12*		*3,8E-12*		*1,5E-11*
^{244}Cm		3,6E-13		2,1E-13		4,7E-14		1,1E-13		1,1E-13		2,3E-14		1,1E-13
Cm		3,2E-13		1,8E-13		4,1E-14		9,7E-14		9,7E-14		2,1E-14		9,7E-14
	Error	*9,5E-14*		*5,5E-14*		*1,2E-14*		*2,9E-14*		*2,9E-14*		*6,2E-15*		*2,9E-14*
Mo		3,7E-06		2,6E-06		1,7E-06		1,0E-06		1,4E-06		1,0E-06		7,2E-07
	Error	*3,7E-07*		*2,6E-07*		*1,7E-07*		*1,0E-07*		*1,4E-07*		*1,0E-07*		*7,2E-08*

To be continued on next page...

TABLE 9 (continuation). **Gravelines 3+2 spent fuel integral leaching experiments: fission products and actinide concentrations ($mol \cdot l^{-1}$) in weekly samples in the different media**

Clay/Clayey Groundwater														
Sampling n°		1	2	3	4	5	6	7	8	9	10	11	12	Final
Time (days)		5	7	9	7	7	7	7	7	7	7	7	7	7
Cumulative time (days)		5	12	21	28	35	42	49	56	63	70	77	84	91
^{90}Sr		7,3E-09		1,3E-09		1,0E-09		7,1E-10		6,3E-10		6,3E-10		4,8E-10
Sr		1,3E-08		2,3E-09		1,8E-09		1,3E-09		1,1E-09		1,1E-09		8,6E-10
	Error	*2,0E-09*		*3,5E-10*		*2,8E-10*		*1,9E-10*		*1,7E-10*		*1,7E-10*		*1,3E-10*
^{134}Cs		3,5E-10		1,9E-10		1,3E-10		1,0E-10		8,8E-11		8,3E-11		3,7E-11
Cs		7,6E-08		4,1E-08		3,0E-08		2,3E-08		1,9E-08		1,8E-08		8,1E-09
	Error	*4,6E-09*		*2,5E-09*		*1,8E-09*		*1,4E-09*		*1,2E-09*		*1,1E-09*		*4,8E-10*
^{238}U			1,7E-07		2,1E-08		1,2E-08		2,1E-08		3,3E-08		8,1E-10	3,6E-07
U			1,8E-07		2,1E-08		1,2E-08		2,1E-08		3,3E-08		8,2E-10	3,7E-07
	Error		*1,8E-08*		*2,1E-09*		*1,2E-09*		*2,1E-09*		*3,3E-09*		*8,2E-11*	*3,7E-08*
^{239}Pu		<1,8E-11		<3,6E-12		<3,6E-12		6,7E-12		3,6E-12		3,6E-12		7,3E-12
Pu		<3,8E-11		<7,6E-12		<7,6E-12		1,4E-11		7,6E-12		7,6E-12		1,5E-11
	Error	*1,9E-11*		*3,8E-12*		*3,8E-12*		*6,9E-12*		*3,8E-12*		*3,8E-12*		*7,6E-12*
^{244}Cm		<4,1E-14		9,6E-14		1,5E-14		2,3E-14		4,0E-14		1,5E-14		1,6E-14
Cm		<3,6E-14		8,5E-14		1,3E-14		2,1E-14		3,5E-14		1,3E-14		1,5E-14
	Error	*1,1E-14*		*2,5E-14*		*4,0E-15*		*6,2E-15*		*1,1E-14*		*4,0E-15*		*4,4E-15*
Mo		3,1E-06		3,2E-06		3,8E-06		2,9E-06		2,5E-06		2,2E-06		1,7E-06
	Error	*3,1E-07*		*3,2E-07*		*3,8E-07*		*2,9E-07*		*2,5E-07*		*2,2E-07*		*1,7E-07*

Granite/Clayey Groundwater														
Sampling n°		1	2	3	4	5	6	7	8	9	10	11	12	Final
Time (days)		5	7	9	7	7	7		14	7	7	7	7	7
Cumulative time (days)		5	12	21	28	35	42		56	63	70	77	84	91
^{90}Sr		7,9E-10		7,5E-10		7,1E-10		nd		5,3E-10		7,4E-10		6,3E-10
Sr		1,4E-09		1,3E-09		1,3E-09				9,5E-10		1,3E-09		1,1E-09
	Error	*2,1E-10*		*2,0E-10*		*1,9E-10*				*1,4E-10*		*2,0E-10*		*1,7E-10*
^{134}Cs		1,6E-10		2,1E-10		1,7E-10		nd		1,8E-10		1,7E-10		1,2E-10
Cs		3,6E-08		4,5E-08		3,7E-08				4,0E-08		3,8E-08		2,6E-08
	Error	*2,1E-09*		*2,7E-09*		*2,2E-09*				*2,4E-09*		*2,3E-09*		*1,6E-09*
^{238}U			9,3E-08		3,2E-08		3,1E-08	nd	1,3E-08		6,1E-09		1,8E-10	2,5E-07
U			9,4E-08		3,3E-08		3,1E-08		1,4E-08		6,1E-09		1,8E-10	2,6E-07
	Error		*9,4E-09*		*3,3E-09*		*3,1E-09*		*1,4E-09*		*6,1E-10*		*1,8E-11*	*2,6E-08*
^{239}Pu		1,8E-11		3,6E-12		3,6E-12		nd		3,6E-12		3,6E-12		3,0E-11
Pu		3,8E-11		7,6E-12		7,6E-12				7,6E-12		7,6E-12		6,3E-11
	Error	*1,9E-11*		*3,8E-12*		*3,8E-12*				*3,8E-12*		*3,8E-12*		*3,2E-11*
^{244}Cm		4,1E-14		3,1E-14		8,6E-14		nd		9,6E-14		7,0E-14		3,3E-13
Cm		3,6E-14		2,8E-14		7,6E-14				8,5E-14		6,2E-14		2,9E-13
	Error	*1,1E-14*		*8,4E-15*		*2,3E-14*				*2,6E-14*		*1,9E-14*		*8,7E-14*
Mo		4,4E-06		4,3E-06		3,4E-06		nd		2,7E-06		2,5E-06		2,8E-06
	Error	*4,4E-07*		*4,3E-07*		*3,4E-07*				*2,7E-07*		*2,5E-07*		*2,8E-07*

TABLE 10. *SIMFUEL integral leaching experiments : Distribution (%) of elements in solution, in colloid (2 nm < ∅ < 0,45 µm) or dissolved form*

		Clay/Granitic Groundwater		Granite/Granitic Groundwater		Clay/Clayey Groundwater		Granite/Clayey Groundwater	
		Dissolved form	colloid	Dissolved form	colloid	Dissolved form	colloid	Dissolved form	colloid
Sr		15	85	15	85	16	84	12	88
	Minimum	*16*	*84*	*16*	*84*	*18*	*82*	*13*	*87*
	Maximum	*13*	*87*	*13*	*87*	*15*	*85*	*11*	*89*
Mo		39	61	15	85	16	84	12	88
	Minimum	*43*	*57*	*16*	*84*	*17*	*83*	*13*	*87*
	Maximum	*35*	*65*	*13*	*87*	*14*	*86*	*11*	*89*
Ba		19	81	31	69	16	84	3	97
	Minimum	*21*	*79*	*35*	*65*	*17*	*83*	*3*	*97*
	Maximum	*17*	*83*	*28*	*72*	*14*	*86*	*3*	*97*
U		11	89	14	86	19	81	12	88
	Minimum	*2*	*98*	*15*	*85*	*21*	*79*	*13*	*87*
	Maximum	*20*	*80*	*12*	*88*	*17*	*83*	*11*	*89*

TABLE 11. *SIMFUEL integral leaching experiments : Cumulative fraction of inventory released in the aqueous phase of weekly samples.*

Clay/Granitic Groundwater													
Sampling n°	1	2	3	4	5	6	7	8	9	10	11	12	Final
Time (days)	5	7	9	7	7	7	7	7	7	7	7	7	7
Cumulative time (days)	5	12	21	28	35	42	49	56	63	70	77	84	91
Sampling volume (mL)	8,6	8,6	9,4	10,2	10,8	11,3	10,5	10,8	11,3	11,1	11,6	11,8	
Sr	8,9E-2	1,1E-1	1,4E-1	1,4E-1	1,6E-1	1,8E-1	1,9E-1	2,1E-1	2,2E-1	2,4E-1	2,5E-1	2,7E-1	2,7E-1
Error	*5,3E-3*	*5,9E-3*	*6,4E-3*	*5,7E-3*	*5,9E-3*	*5,8E-3*	*5,5E-3*	*6,0E-3*	*5,5E-3*	*5,5E-3*	*5,6E-3*	*5,5E-3*	*5,2E-3*
Mo	1,4E-3	1,4E-3	1,6E-3	2,0E-3	2,0E-3	2,1E-3	2,2E-3	2,3E-3	2,4E-3	2,4E-3	2,4E-3	2,4E-3	2,3E-3
Error	*8,5E-5*	*7,3E-5*	*7,1E-5*	*8,4E-5*	*7,2E-5*	*6,2E-5*	*6,1E-5*	*5,7E-5*	*5,6E-5*	*4,9E-5*	*4,5E-5*	*4,3E-5*	*4,1E-5*
Ba	8,2E-3	9,1E-3	1,1E-2	1,1E-2	1,4E-2	1,5E-2	1,7E-2	1,9E-2	2,1E-2	2,3E-2	2,4E-2	2,7E-2	3,5E-2
Error	*4,9E-4*	*4,7E-4*	*5,3E-4*	*4,5E-4*	*5,1E-4*	*5,0E-4*	*5,3E-4*	*5,5E-4*	*5,6E-4*	*6,0E-4*	*5,7E-4*	*6,1E-4*	*9,7E-4*

Granite/Granitic Groundwater													
Sampling n°	1	2	3	4	5	6	7	8	9	10	11	12	Final
Time (days)	7	7	5	7	9	7	7	7	7	7	7	7	7
Cumulative time (days)	7	14	19	26	35	42	49	56	63	70	77	84	91
Sampling volume (mL)	10,1	10,5	9,8	10,3	9,6	13,3	12,4	10,7	10,7	11,8	11,8	11,3	
Sr	9,4E-3	9,8E-3	1,1E-2	2,1E-2	2,5E-2	2,3E-2	2,1E-2	2,9E-2	2,5E-2	3,1E-2	2,8E-2	2,8E-2	3,0E-2
Error	*5,6E-4*	*4,9E-4*	*4,7E-4*	*9,5E-4*	*1,0E-3*	*7,4E-4*	*5,4E-4*	*8,5E-4*	*5,5E-4*	*7,7E-4*	*5,6E-4*	*5,3E-4*	*5,5E-4*
Mo	6,0E-3	6,8E-3	7,3E-3	7,6E-3	7,8E-3	8,0E-3	8,8E-3	9,1E-3	9,5E-3	9,6E-3	1,0E-2	1,0E-2	1,0E-2
Error	*3,6E-4*	*3,5E-4*	*3,1E-4*	*2,8E-4*	*2,5E-4*	*2,3E-4*	*2,3E-4*	*2,2E-4*	*2,1E-4*	*2,0E-4*	*2,0E-4*	*2,0E-4*	*1,8E-4*
Ba	5,4E-3	7,4E-3	6,7E-3	8,1E-3	9,0E-3	9,5E-3	1,2E-2	1,1E-2	1,4E-2	1,4E-2	1,7E-2	1,5E-2	1,8E-2
Error	*3,2E-4*	*3,8E-4*	*2,8E-4*	*3,1E-4*	*3,1E-4*	*3,0E-4*	*3,7E-4*	*2,9E-4*	*3,9E-4*	*3,3E-4*	*4,3E-4*	*2,9E-4*	*3,7E-4*

Clay/Clayey Groundwater													
Sampling n°	1	2	3	4	5	6	7	8	9	10	11	12	Final
Time (days)	7	7	7	5	7	9	7	7	7	7	7	7	7
Cumulative time (days)	7	14	21	26	33	42	49	56	63	70	77	84	91
Sampling volume (mL)	9,7	8,3	9,7	4,8	8,2	6,1	9,7	10,6	10	9,8	10,8	11,4	
Sr	6,1E-2	6,9E-2	7,0E-2	7,5E-2	7,5E-2	7,9E-2	8,0E-2	8,5E-2	9,0E-2	9,3E-2	9,6E-2	9,9E-2	1,0E-1
Error	*3,7E-3*	*3,5E-3*	*3,1E-3*	*2,9E-3*	*2,6E-3*	*2,5E-3*	*2,4E-3*	*2,3E-3*	*2,3E-3*	*2,2E-3*	*2,1E-3*	*2,0E-3*	*2,0E-3*
Mo	2,9E-3	3,9E-3	3,0E-3	3,5E-3	3,0E-3	3,1E-3	3,0E-3	2,9E-3	3,1E-3	3,1E-3	3,2E-3	3,2E-3	3,3E-3
Error	*1,7E-4*	*2,0E-4*	*1,2E-4*	*1,3E-4*	*9,5E-5*	*9,0E-5*	*7,8E-5*	*7,2E-5*	*7,4E-5*	*6,8E-5*	*6,8E-5*	*6,6E-5*	*6,5E-5*
Ba	4,2E-3	6,0E-3	7,1E-3	7,8E-3	8,5E-3	9,7E-3	1,1E-2	1,2E-2	1,3E-2	1,5E-2	1,6E-2	1,7E-2	2,2E-2
Error	*2,5E-4*	*3,2E-4*	*3,3E-4*	*3,2E-4*	*3,3E-4*	*3,5E-4*	*3,8E-4*	*3,8E-4*	*3,9E-4*	*4,2E-4*	*4,1E-4*	*4,4E-4*	*6,3E-4*

Granite/Clayey Groundwater													
Sampling n°	1	2	3	4	5	6	7	8	9	10	11	12	Final
Time (days)	7	7	7	5	7	9	7	7	7	7	7	7	7
Cumulative time (days)	7	14	21	26	33	42	49	56	63	70	77	84	91
Sampling volume (mL)	9,9	10,7	9,9	11,2	10,7	7,9	10,2	10,4	9,1	10,1	10,5	10,5	
Sr	7,6E-3	6,4E-3	6,5E-3	6,3E-3	6,7E-3	6,9E-3	6,8E-3	7,0E-3	7,3E-3	7,5E-3	7,7E-3	8,0E-3	9,5E-3
Error	*4,6E-4*	*3,1E-4*	*2,6E-4*	*2,2E-4*	*2,1E-4*	*1,9E-4*	*1,7E-4*	*1,7E-4*	*1,7E-4*	*1,7E-4*	*1,6E-4*	*1,6E-4*	*2,1E-4*
Mo	1,3E-2	1,4E-2	1,4E-2	1,6E-2	1,7E-2	1,8E-2	1,9E-2	2,0E-2	2,1E-2	2,1E-2	2,2E-2	2,3E-2	2,4E-2
Error	*7,5E-4*	*7,0E-4*	*6,0E-4*	*5,8E-4*	*5,6E-4*	*5,5E-4*	*5,2E-4*	*5,0E-4*	*4,8E-4*	*4,8E-4*	*4,5E-4*	*4,5E-4*	*4,4E-4*
Ba	1,2E-3	2,3E-3	2,6E-3	3,3E-3	4,4E-3	4,3E-3	5,2E-3	5,2E-3	6,4E-3	7,8E-3	7,7E-3	7,8E-3	1,8E-2
Error	*7,5E-5*	*1,2E-4*	*1,2E-4*	*1,4E-4*	*1,8E-4*	*1,4E-4*	*1,7E-4*	*1,5E-4*	*1,9E-4*	*2,4E-4*	*2,0E-4*	*1,8E-4*	*7,5E-4*

TABLE 12. Simfuel leach rates published in the literature

Simfuel Composition (at%)	Particle Size	Mode	Leaching duration (days)	T (°C)	Leachant	pH	P_{O2}	Carbonates ($mol.L^{-1}$)	Other	Leaching Rate ($mg.m^{-2}.j^{-1}$)	Reference
3	pellet	sequential	~270	25	Allard	8,2	Under air	$2,0\ 10^{-3}$		valeur	Bruno *et al.* [Erreur! Signet non défini.,Erreur! Signet non défini.]
3	pellet	static	~167	25	GroundWater	7,5	0,97 atm	$2,75\ 10^{-3}$		moyenne	
6	pellet	sequential	~270	25	Allard	8,2	Under air	$2,0\ 10^{-3}$		0,008	
6	pellet	static	~167	25	GroundWater	7,5	0,97 atm	$2,75\ 10^{-3}$			
3	pellet	flow		25	Allard	8,2	Under air	$2,0\ 10^{-3}$		0,80	
3	pellet	flow		25	Allard	8,2	Under air	$2,0\ 10^{-3}$		1,35	
6	pellet	flow		25	Allard	8,2	Under air	$2,0\ 10^{-3}$		0,61	
3	pellet	flow		25	GroundWater	7,5	0,97 atm	$2,75\ 10^{-3}$		0,84	
6	pellet	flow		25	GroundWater	7,5	0,97 atm	$2,75\ 10^{-3}$		1,58	
6	pellet	flow		25	GroundWater	7,5	0,97 atm	$2,75\ 10^{-3}$		1,25	
6	pellet	sequential	300	30	Allard	8,2	< 1 ppm	$2,0\ 10^{-3}$		0,08*	Ollila [Erreur! Signet non défini.]
6	pellet	sequential	300	30	Allard	8,2	< 1 ppm	$2,0\ 10^{-3}$	$FeCl_2$	0,04*	
6	Grains 50-250 µm	quasi static	77	90	Granitic GW	8,1	$Ar/H_2/CO_2$	$1,6\ 10^{-3}$	Clay/Sand mixture + Fe	0,04	Our work
6	Grains 50-250 µm	quasi static	77	90	Granitic GW	8,1	$Ar/H_2/CO_2$	$1,6\ 10^{-3}$	Granite + Fe	0,01	*mean apparent*
6	Grains 50-250 µm	quasi static	77	90	Clayey GW	8,8	$Ar/H_2/CO_2$	$1,4\ 10^{-2}$	Clay/Sand mixture + Fe	0,01	*leaching rates*
6	Grains 50-250 µm	quasi static	77	90	Clayey GW	8,8	$Ar/H_2/CO_2$	$1,4\ 10^{-2}$	Granite + Fe	*0,0001***	

determined from a graphic reading* * very low correlation (r^2=0,45)*

TABLE 13. *Gravelines 3+2 spent fuel (60 GWd/t_{HM}) activity and mass inventories calculated by CESAR code after 2797 days of cooling (01/01/1997).*

Actinides					Fission Products			
Element	Isotope	α Specific Activity (Bq/g_u)	β Specific Activity (Bq/g_u)	Specific Mass (g/t_u)	Element	Isotope	β Specific Activity (Bq/g_u)	Specific Mass (g/t_u)
Ra	244	2,663E+03		4,509E-07	Se	79	2,157E+04	8,372E+00
Th	228	2,665E+03		8,787E-05	Kr	85	3,477E+08	2,395E+01
Th	229	3,452E-02		4,386E-06	Rb	87	1,364E+00	4,307E+02
Th	230	4,850E+00		6,494E-03	Sr	86	_	8,802E-01
Th	232	8,204E-06		2,022E-03	Sr	88	_	6,012E+02
Pa	231	1,709E+00		9,702E-04	Sr	89	0,000E+00	0,000E+00
Pa	233	0,000E+00	2,34E+04	3,053E-05	Sr	90	3,800E+09	7,530E+02
U	232	3,084E+03		3,895E-03	Y	90	3,801E+09	1,888E-01
U	233	1,420E+00		3,978E-03	Y	91	1,566E-04	1,726E-13
U	234	4,801E+04		2,106E+02	Zr	93	1,184E+05	1,273E+03
U	235	3,970E+02		4,965E+03	Zr	95	4,115E-03	5,177E-12
U	236	1,472E+04		6,303E+03	Nb	95	9,132E-03	6,312E-12
U	237	0,000E+00	1,26E+05	4,171E-05	Mo	95	_	1,340E+03
U	238	1,126E+04		9,093E+05	Mo	96	_	1,260E+02
Np	237	2,345E+04		8,990E+02	Mo	97	_	1,469E+03
Np	238	0,000E+00	2,18E+03	2,277E-07	Mo	98	_	1,554E+03
Np	239	0,000E+00	2,75E+06	3,204E-04	Mo	100	_	1,759E+03
Pu	236	8,924E+03		4,539E-04	Tc	99	9,124E+05	1,455E+03
Pu	238	3,365E+08		5,314E+02	Ru	103	0,000E+00	0,000E+00
Pu	239	1,372E+07		6,045E+03	Ru	106	1,513E+08	1,233E+00
Pu	240	2,741E+07		3,252E+03	Rh	106	1,513E+08	1,145E-06
Pu	241	1,258E+05	5,13E+09	1,347E+03	Pd	107	8,826E+03	4,643E+02
Pu	242	1,930E+05		1,367E+03	Ag	110m	2,521E+06	1,434E-02
Pu	244	3,108E-02		4,736E-02	Cd	113	1,596E-09	1,268E-01
Am	241	8,566E+07		6,758E+02	Cd	113m	1,697E+06	1,973E-01
Am	242m	2,182E+03	4,59E+05	1,277E+00	In	115	4,459E-07	1,938E+00
Am	243	2,750E+06		3,738E+02	Sn	121	9,884E+05	2,791E-05
Cm	242	4,329E+05		3,533E-03	Sn	121m	2,853E+05	6,409E-01
Cm	243	2,245E+06		1,320E+00	Sn	123	1,651E+01	5,431E-08
Cm	244	4,585E+08		1,532E+02	Sn	126	4,486E+04	4,273E+01
Cm	245	9,773E+04		1,545E+01	Sb	124	0,000E+00	0,000E+00
Cm	246	3,294E+04		2,886E+00	Sb	125	6,486E+07	1,698E+00
Cm	247	2,109E-01		6,143E-02	Sb	126	4,486E+04	1,451E-05
Cm	248	1,639E+00		1,180E-02	Te	123	1,035E-07	9,624E-03
Bk	249	2,469E-02	3,96E+01	6,413E-07	Te	127	1,003E+01	1,027E-10
Cf	249	5,317E+01		3,509E-04	Te	127m	2,457E-01	2,933E-08
Cf	250	1,622E+02		4,009E-05	I	129	2,122E+03	3,249E+02
Cf	251	1,712E+00		2,917E-05	Cs	134	9,940E+08	2,076E+01
Cf	252	7,793E+01		3,929E-06	Cs	135	3,042E+04	7,141E+02
					Cs	137	6,017E+09	1,877E+03
					Ce	144	4,460E+07	3,787E-01
					Pr	144	4,460E+07	1,595E-05
					Pm	147	9,188E+08	2,678E+01
					Pm	148m	0,000E+00	0,000E+00
					Sm	151	1,993E+07	2,047E+01
					Eu	152	7,885E+05	1,208E-01
					Eu	154	3,466E+08	3,551E+01
					Eu	155	3,066E+08	1,782E+01
					Tb	160	1,366E-04	3,270E-13

TABLE 14. *Gravelines 3+2 spent fuel (60 GWd/tHM) activity and mass inventories calculated by CESAR for exploitation of preleaching test results (cf. grey cells data)*

Date	01/01/96	01/07/96	01/01/97
Cooling time	2431	2614	2797
Inventory	calculated	extrapolated	calculated
Radionuclide Activity inventory ($Bq.g_U^{-1}$)			
^{90}Sr	$3,89\times10^{9}$	$3,85\times10^{9}$	$3,80\times10^{9}$
^{125}Sb	$8,33\times10^{7}$	$7,41\times10^{7}$	$6,49\times10^{7}$
^{134}Cs	$1,39\times10^{9}$	$1,19\times10^{9}$	$9,94\times10^{8}$
^{137}Cs	$6,16\times10^{9}$	$6,09\times10^{9}$	$6,02\times10^{9}$
$^{239+240}Pu$	$4,11\times10^{7}$	$4,11\times10^{7}$	$4,11\times10^{7}$
$^{238}Pu^{+241}Am$	$4,17\times10^{8}$	$4,19\times10^{8}$	$4,22\times10^{8}$
^{244}Cm	$4,76\times10^{8}$	$4,68\times10^{8}$	$4,59\times10^{8}$
Element Mass inventory ($\mu g.g_U^{-1}$)			
Mo	6248	6248	6248
Tc	1455	1455	1455
Zr	6576	6585	6594
U	920806	920808	920810
Nd	7506	7507	7507

TABLE 15. *Mass inventory of Simfuel (6 at%)*

Elements of addition	Simulated elements	Specific chemical composition ($g/100g_U$)		
		As fabricated	Measured	
			mean value	σ
Ba	Ba	0,24 ± 0,02	0,225	0,015
Ce	Ce, Pu	1,46 ± 0,02	1,660	0,080
La	La, Am, Cm	0,25 ± 0,02	0,270	0,020
Mo	Mo	0,47 ± 0,02	0,460	0,070
Sr	Sr	0,10 ± 0,02	0,965	0,015
Y	Y	0,06 ± 0,02	0,280	0,020
Zr	Zr	0,48 ± 0,02	N.D.	N.D.
Rh	Rh	0,06 ± 0,02	0,530	0,060
Pd	Pd	0,24 ± 0,02	0,095	0,005
Ru	Ru, Tc	0,44 ± 0,02	0,064	0,009
Nd	Nd, Pr, Pm, Sm	0,83 ± 0,02	0,540	0,040

TABLE 16. Gravelines 3+2 preleaching: leachates analysis results

Contact time (days)	1	5	8	7	14	13	22	21	49
Cumulative contact time (days)	1	6	14	21	35	48	70	91	140
Leachant Volume (mL)	93,8	89,0	91,3	85,5	68,0	101,3	97,8	100,9	90,1
Remaining Leachate Volume (mL)	7,3	6,4	14,9	7,8	12,3	8,0	14,4	13,1	0,0
				Activity (Bq/mL)					
^{90}Sr	1,07E+05	6,20E+04	1,10E+05	4,69E+04	8,75E+04	3,62E+04	6,60E+04	3,55E+04	6,30E+04
^{125}Sb	< 5,42E+03	< 1,76E+03	< 5,12E+02	1,42E+03	1,11E+03	1,26E+03	1,55E+03	1,17E+03	< 8,90E+02
^{134}Cs	5,17E+05	1,56E+05	5,12E+04	4,02E+04	4,80E+04	2,01E+04	2,52E+04	1,93E+04	3,92E+04
^{137}Cs	3,36E+06	9,30E+05	3,09E+05	2,57E+05	3,07E+05	1,30E+05	1,58E+05	1,22E+05	2,57E+05
$^{239}Pu+^{240}Pu$	2,50E+01	6,00E+00	1,70E+01	3,00E+01	1,70E+01	2,00E+01	2,00E+01	6,00E+00	5,70E+01
^{244}Cm	5,35E+02	5,65E+02	1,08E+03	1,51E+03	1,90E+03	5,48E+02	2,14E+02	2,18E+02	1,48E+03
$^{238}Pu + ^{241}Am$	2,92E+02	1,00E+02	3,21E+02	4,60E+02	3,22E+02	3,03E+02	1,48E+02	4,60E+01	8,34E+02
				Elementary Concentrations (mg/L)					
U	4,51	8,42	8,3	10,57	17,85	6,41	2,77	4,51	5,12
Nd	0,02	0,03	0,05	0,05	0,09	0,03	< 0,02	0,02	0,03
Tc	< 0,08	< 0,08	0,02	0,03	0,05	0,05	0,05	0,03	< 0,02
Mo	0,12	< 0,05	< 0,05	< 0,05	0,07	0,12	0,21	0,1	< 0,05
Zr	0,01	0,01	0,02	0,01	0,02	0,01	< 0,01	< 0,01	< 0,01

TABLE 17. Gravelines 3+2 spent fuel integral leaching experiments: filtered and ultrafiltered supernatant solution analysis results

Medium	**Clay/Granitic Groundwater**		**Granite/Granitic Groundwater**		**Clay/Clayey Groundwater**		**Granite/Clayey Groundwater**	
Supernatant Treatment	filtered	ultrafitered	filtered	ultrafitered	filtered	ultrafitered	filtered	ultrafitered
				Activity (Bq/mL)				
^{90}Sr	295	257,5	336	339	224	271,5	296	288
^{60}Co	< 0,8	< 0,9	< 1,3	< 1,2	< 0,8	< 0,9	< 1,6	< 1,1
^{106}Ru	< 35,5	< 34,5	< 24	< 48,5	< 36	< 35,5	< 124	< 125
^{125}Sb	< 16	< 16	35	43	18	25	< 30	< 30
^{134}Cs	240	242	473	484	235	245	764	790
^{137}Cs	1850	1870	3620	3670	1780	1810	5890	5990
^{144}Ce	< 15	< 15	< 21	< 21	< 15	< 15	< 27	< 27
^{154}Eu	< 4	< 4	< 6	< 6	< 4	< 4	< 8	< 8
^{241}Am	< 30	< 30	< 42	< 42	< 30	< 29	< 53	< 53
$^{239+240}Pu$	< 0,006	0,012	0,024	0,018	0,012	0,006	0,05	0,006
$^{238}Pu+^{241}Am$	0,031	0,02	0,07	0,024	0,018	0,024	0,21	0,12
^{244}Cm	0,006	< 0,006	0,08	0,006	0,012	< 0,006	0,24	0,018
				Elementary Concentration (mg/L)				
Mo	< 0,02	< 0,02	0,07	0,07	0,17	0,17	0,27	0,28
Tc	< 0,02	< 0,02	< 0,02	< 0,02	< 0,02	< 0,02	< 0,02	< 0,02
Zr	0,02	< 0,01	< 0,01	< 0,01	< 0,01	< 0,01	< 0,01	< 0,01
U	< 0,08	< 0,08	< 0,08	< 0,08	< 0,08	0,09	0,08	0,08
Nd	< 0,02	< 0,02	< 0,02	< 0,02	< 0,02	< 0,02	< 0,02	< 0,02
				Isotope Concentration (µg/L)				
^{88}Sr	154	163	182	179	100	119	555	754
^{99}Tc	< 1	< 1	< 1	< 1	< 1	< 1	< 1	< 1
^{237}Np	< 1	< 1	< 1	< 1	< 1	< 1	< 1	< 1
^{238}U	3,7	3,9	6,1	5,9	42,9	40,2	30,3	29,8
^{240}Pu	< 1	< 1	< 1	< 1	< 1	< 1	< 1	< 1

TABLE 18. *Gravelines 3+2 spent fuel integral leaching experiments: weekly samples analysis results.*

Clay/Granitic Groundwater													
Sampling n°	1	2	3	4	5	6	7	8	9	10	11	12	Final
Time (days)	7	5	7	9	7	7	7	7	7	7	7	7	7
Cumulative time (days)	7	12	19	28	35	42	49	56	63	70	77	84	91
Sampling Volume (mL)	10,9	9,5	8,3	10,4	9,2	10	11,7	10,4	10,3	10,2	12,6	11,1	
						Activity(Bq/mL)							
^{90}Sr	2155	1652,5	1150	912,5	675	527,75	380,5	360,75	341	304,25	267,5	281,25	295
^{60}Co	< 3,0	< 2,8	< 2,5	< 2,3	< 2,0	< 2,0	< 2,0	< 2,0	< 2,0	< 1,8	< 1,5	< 1,2	< 0,8
^{106}Ru	< 175	< 155	< 136	< 122	< 108	< 100	< 93	< 91	< 89	< 85	< 81	< 58	< 36
^{125}Sb	< 81	< 72	< 63	< 57	< 51	< 48	< 44	< 43	< 42	< 40	< 38	< 27	< 16
^{134}Cs	3350	2670	1990	1630	1270	1135	1000	943	886	818	750	495	240
^{137}Cs	23300	18750	14200	11645	9090	8070	7050	6730	6410	5845	5280	3565	1850
^{144}Ce	< 76	< 66	< 56	< 52	< 48	< 45	< 41	< 40	< 39	< 38	< 36	< 26	< 15
^{154}Eu	< 21	< 19	< 17	< 15	< 13	< 12	< 11	< 11	< 11	< 11	< 10	< 7	< 4
^{241}Am	< 148	< 132	< 115	< 104	< 92	< 87	< 81	< 80	< 79	< 74	< 69	< 50	< 30
$^{239+240}Pu$	< 0,03	0,018	0,006	0,013	0,02	0,0155	0,011	0,0085	0,006	0,0115	0,017	0,0115	<0,006
$^{238}Pu+^{241}Am$	0,17	0,091	0,012	0,016	0,02	0,0185	0,017	0,017	0,017	0,02	0,023	0,027	0,031
^{244}Cm	< 0,030	< 0,018	< 0,006	< 0,006	< 0,006	< 0,006	< 0,006	< 0,006	< 0,006	< 0,006	< 0,006	< 0,006	0,006
						Elementary Concentration (mg/L)							
Mo	0,11	0,105	0,1	0,075	0,05	0,045	0,04	0,03	0,02	0,02	< 0,02	< 0,02	< 0,02
Tc	< 0,02	< 0,02	< 0,02	< 0,02	< 0,02	< 0,02	< 0,02	< 0,02	< 0,02	< 0,02	< 0,02	< 0,02	< 0,02
Zr	0,05	< 0,03	< 0,01	< 0,01	< 0,01	< 0,01	< 0,01	< 0,01	< 0,01	< 0,01	< 0,01	< 0,02	0,02
U	< 0,08	< 0,08	< 0,08	< 0,08	< 0,08	< 0,08	< 0,08	< 0,08	< 0,08	< 0,08	< 0,08	< 0,08	< 0,08
Nd	< 0,02	< 0,02	< 0,02	< 0,02	< 0,02	< 0,02	< 0,02	< 0,02	< 0,02	< 0,02	< 0,02	< 0,02	< 0,02
						Isotope Concentration (µg/L)							
^{88}Sr	611	596	581	566	415	264	258	252	246	240	231	222	308
^{99}Tc	< 1	< 1	< 1	< 1	< 1	< 1	< 1	< 1	< 1	< 1	< 1	< 1	< 1
^{237}Np	< 1	< 1	< 1	< 1	< 1	< 1	< 1	< 1	< 1	< 1	< 1	< 1	< 1
^{238}U	7,98	6,56	5,14	3,72	5,75	7,78	4,502	1,224	1,135	1,046	0,847	0,648	7,46
^{240}Pu	< 1	< 1	< 1	< 1	< 1	< 1	< 1	< 1	< 1	< 1	< 1	< 1	< 1
Granite/Granitic Groundwater													
Sampling n°	1	2	3	4	5	6	7	8	9	10	11	12	Final
Time (days)	7	5	7	9	7	7	7	7	7	7	7	7	7
Cumulative time (days)	7	12	19	28	35	42	49	56	63	70	77	84	91
Sampling Volume (mL)	9,7	10,7	10,1	11,7	9,7	6,2	9,6	6,5	10,7	11,8	12,5	13,5	
						Activity(Bq/mL)							
^{90}Sr	2185	1475	765	647,5	530	393	256	288,5	321	254	187	429,5	672
^{60}Co	< 3,0	< 2,8	< 2,5	< 2,8	< 3,0	< 2,8	< 2,5	< 2,5	< 2,5	< 2,5	< 2,5	< 1,9	< 1,3
^{106}Ru	< 168,0	< 161	< 153,3	< 149	< 144,0	< 120	< 96,5	< 103	< 109,0	< 106	< 102,5	< 63	< 24,0
^{125}Sb	88	< 80	< 72	< 70	< 67	< 56	< 45	< 49	< 52	< 51	< 49	< 42	35
^{134}Cs	2990	2800	2610	2440	2270	1650	1030	1170	1310	1260	1210	841,5	473
^{137}Cs	20900	19800	18700	17500	16300	11850	7400	8400	9400	9065	8730	6175	3620
^{144}Ce	< 72	< 70	< 68	< 66	< 63	< 53	< 43	< 46	< 48	< 48	< 47	< 34	< 21
^{154}Eu	< 20	< 20	< 19	< 19	< 18	< 15	< 12	< 13	< 14	< 14	< 13	< 10	< 6
^{241}Am	< 141	< 137	< 133	< 129	< 124	< 104	< 84	< 89	< 94	< 92	< 90	< 66	< 42
$^{239+240}Pu$	0,06	0,033	< 0,006	0,006	0,006	0,006	0,006	0,006	< 0,006	0,006	0,006	0,015	0,024
$^{238}Pu+^{241}Am$	0,11	0,085	0,06	0,047	0,034	0,0455	0,057	0,0515	0,046	0,0345	0,023	0,0465	0,07
^{244}Cm	0,260	0,205	0,150	0,092	0,034	0,057	0,080	0,08	0,080	0,0485	0,017	0,0485	0,080
						Elementary Concentration (mg/L)							
Mo	0,36	0,305	0,25	0,21	0,17	0,135	0,1	0,12	0,14	0,12	0,10	0,085	0,07
Tc	< 0,04	< 0,03	< 0,02	< 0,02	< 0,02	< 0,02	< 0,02	< 0,02	< 0,02	< 0,02	< 0,02	< 0,02	< 0,02
Zr	0,04	< 0,03	< 0,01	< 0,01	< 0,01	< 0,01	< 0,01	< 0,01	< 0,01	< 0,01	< 0,01	< 0,01	< 0,01
U	< 0,08	< 0,08	< 0,08	< 0,08	< 0,08	< 0,08	< 0,08	< 0,08	< 0,08	< 0,08	< 0,08	< 0,08	< 0,08
Nd	< 0,02	< 0,02	< 0,02	< 0,02	< 0,02	< 0,02	< 0,02	< 0,02	< 0,02	< 0,02	< 0,02	< 0,02	< 0,02
						Isotope Concentration (µg/L)							
^{88}Sr	62,9	61,0	59,1	57,2	52,8	48,4	48,0	47,6	33,7	19,8	22,5	25,2	364,0
^{99}Tc	< 1	< 1	< 1	< 1	< 1	< 1	< 1	< 1	< 1	< 1	< 1	< 1	< 1
^{237}Np	< 1	< 1	< 1	< 1	< 1	< 1	< 1	< 1	< 1	< 1	< 1	< 1	< 1
^{238}U	19,0	14,3	9,5	4,8	3,0	1,3	1,5	1,7	1,4	1,0	< 1	< 1	12,2
^{240}Pu	< 1	< 1	< 1	< 1	< 1	< 1	< 1	< 1	< 1	< 1	< 1	< 1	< 1

Extrapolated data

To be continued on next page ...

TABLE 18 (continuation). **Gravelines 3+2 spent fuel integral leaching experiments: weekly samples analysis results.**

Clay/Clayey Groundwater													
Sampling n°	1	2	3	4	5	6	7	8	9	10	11	12	Final
Time (days)	5	7	9	7	7	7	7	7	7	7	7	7	7
Cumulative time (days)	5	12	21	28	35	42	49	56	63	70	77	84	91
Sampling Volume (mL)	9	8,1	8,9	9,6	9,8	13	11,3	8,9	9,8	12,9	10,7	12,2	
Activity(Bq/mL)													
^{90}Sr	3425	2015	605	542,75	480,5	406,5	332,5	315,25	298	297,75	297,5	260,75	224
^{60}Co	< 3,0	< 2,5	< 2,0	< 2,0	< 2,0	< 2,0	< 2,0	< 2,0	< 2,0	< 2,0	< 2,0	< 1,4	< 0,8
^{106}Ru	< 142,5	< 128	< 112,5	< 104	< 95,5	< 89	< 83,0	< 80	< 76,5	< 76	< 75,5	< 56	< 36,0
^{125}Sb	< 68	< 59	< 49	< 46	< 42	< 40	< 37	< 36	< 34	< 34	< 34	< 26	18
^{134}Cs	2220	1705	1190	1025,5	861	762	663	613,5	564	546	528	381,5	235
^{137}Cs	15600	12110	8620	7410	6200	5485	4770	4410	4050	3970	3890	2835	1780
^{144}Ce	< 58	< 52	< 46	< 42	< 37	< 36	< 34	< 33	< 32	< 32	< 31	< 23	< 15
^{154}Eu	< 17	< 15	< 13	< 12	< 11	< 11	< 10	< 10	< 9	< 9	< 9	< 7	< 4
^{241}Am	< 123	< 107	< 91	< 84	< 77	< 73	< 69	< 65	< 61	< 61	< 61	< 46	< 30
$^{239+240}Pu$	< 0,03	< 0,018	< 0,006	< 0,006	< 0,006	< 0,009	0,011	0,0085	0,006	0,006	0,006	0,009	0,012
$^{238}Pu+^{241}Am$	0,14	0,087	0,034	0,0315	0,029	0,026	0,023	0,017	0,011	0,017	0,023	0,0205	0,018
^{244}Cm	< 0,03	0,05	0,070	0,0405	0,011	0,014	0,017	0,023	0,029	0,02	0,011	0,0115	0,012
Elementary Concentration (mg/L)													
Mo	0,3	0,305	0,31	0,34	0,37	0,325	0,28	0,26	0,24	0,225	0,21	0,19	0,17
Tc	< 0,04	< 0,03	< 0,02	< 0,02	< 0,02	< 0,02	< 0,02	< 0,02	< 0,02	< 0,02	< 0,02	< 0,02	< 0,02
Zr	0,06	< 0,04	< 0,01	< 0,01	< 0,01	< 0,01	< 0,01	< 0,01	< 0,01	< 0,01	< 0,01	< 0,01	< 0,01
U	0,77	< 0,43	< 0,08	< 0,08	< 0,08	< 0,08	< 0,08	< 0,08	< 0,08	< 0,08	< 0,08	< 0,08	< 0,08
Nd	< 0,02	< 0,02	< 0,02	< 0,02	< 0,02	< 0,02	< 0,02	< 0,02	< 0,02	< 0,02	< 0,02	< 0,02	< 0,02
Isotope Concentration (µg/L)													
^{88}Sr	410	356	302	248	220	192	167	142	144	147	138	130	199
^{99}Tc	< 1	< 1	< 1	< 1	< 1	< 1	< 1	< 1	< 1	< 1	< 1	< 1	< 1
^{237}Np	< 1	< 1	< 1	< 1	< 1	< 1	< 1	< 1	< 1	< 1	< 1	< 1	< 1
^{238}U	59,3	41,2	23,1	5,0	3,9	2,8	3,9	4,9	6,4	7,8	4,0	< 1	85,8
^{240}Pu	< 1	< 1	< 1	< 1	< 1	< 1	< 1	< 1	< 1	< 1	< 1	< 1	< 1

Granite/Clayey Groundwater													
Sampling n°	1	2	3	4	5	6	7	8	9	10	11	12	Final
Time (days)	5	7	9	7	7	7		14	7	7	7	7	7
Cumulative time (days)	5	12	21	28	35	42		56	63	70	77	84	91
Sampling Volume (mL)	11,9	10,8	11,3	9,3	10,6	8,9	Not done	14,6	9,9	10,4	13,5	12,8	
Activity(Bq/mL)													
^{90}Sr	371,5	361	350,5	341,75	333	312		270	249	298,75	348,5	322,25	296
^{60}Co	< 2,5	< 2,3	< 2,0	< 2,0	< 2,0	< 2,3		< 2,8	< 3,0	< 2,8	< 2,5	< 2,1	< 1,6
^{106}Ru	< 104,0	< 110	< 115,0	< 109	< 102,0	< 103		< 105	< 105,5	< 102	< 99,0	< 81	< 62,0
^{125}Sb	241	< 152	63	< 55	< 47	< 47		< 48	< 48	< 48	< 47	< 39	< 30
^{134}Cs	1040	1180	1320	1205	1090	1107,5		1142,5	1160	1130	1100	932	764
^{137}Cs	7220	8380	9540	8620	7700	7880		8240	8420	8205	7990	6940	5890
^{144}Ce	< 43	< 46	< 49	< 47	< 44	< 45		< 46	< 46	< 45	< 44	< 36	< 27
^{154}Eu	< 12	< 13	< 13	< 13	< 12	< 12		< 13	< 13	< 13	< 12	< 10	< 8
^{241}Am	< 85	< 91	< 96	< 91	< 86	< 87		< 88	< 88	< 88	< 87	< 70	< 53
$^{239+240}Pu$	< 0,03	0,018	0,006	0,006	0,006	0,006		0,006	0,006	0,006	0,006	0,028	0,05
$^{238}Pu+^{241}Am$	0,06	0,0585	0,057	0,063	0,069	0,065		0,056	0,051	0,051	0,051	0,1305	0,21
^{244}Cm	< 0,03	0,0265	0,023	0,043	0,063	0,065		0,068	0,070	0,0605	0,051	0,1455	0,240
Elementary Concentration (mg/L)													
Mo	0,43	0,425	0,42	0,375	0,33	0,313		0,278	0,26	0,25	0,24	0,255	0,27
Tc	< 0,04	< 0,03	< 0,02	< 0,02	< 0,02	< 0,02		< 0,02	< 0,02	< 0,02	< 0,02	< 0,02	< 0,02
Zr	< 0,02	< 0,02	< 0,01	< 0,01	< 0,01	< 0,01		< 0,01	< 0,01	< 0,01	< 0,01	< 0,01	< 0,01
U	0,13	< 0,11	< 0,08	< 0,08	< 0,08	< 0,08		< 0,08	< 0,08	< 0,08	< 0,08	< 0,08	0,08
Nd	< 0,02	< 0,02	< 0,02	< 0,02	< 0,02	< 0,02		< 0,02	< 0,02	< 0,02	< 0,02	< 0,02	< 0,02
Isotope Concentration (µg/L)													
^{88}Sr	145	125	105	84	66	47		23	26	29	17	4,9	1110
^{99}Tc	1,8	1,5	1,2	< 1	< 1	< 1		< 1	< 1	< 1	< 1	< 1	< 1
^{237}Np	< 1	< 1	< 1	< 1	< 1	< 1		< 1	< 1	< 1	< 1	< 1	< 1
^{238}U	29,5	22,2	15,0	7,7	7,5	7,4		3,2	2,3	1,4	< 1	< 1	60
^{240}Pu	2,4	1,6	< 1	< 1	< 1	< 1		< 1	< 1	< 1	< 1	< 1	< 1

☐ *Extrapolated data*

TABLE 18. *Gravelines 3+2 spent fuel integral leaching experiments: filter rinsing solution analysis results*

Clay/Granitic Groundwater												
Sampling n°	1	2	3	4	5	6	7	8	9	10	11	12
Time (days)	7	5	7	9	7	7	7	7	7	7	7	7
Cumulative time (days)	7	12	19	28	35	42	49	56	63	70	77	84
Activity (Bq/mL)												
^{90}Sr	84	44,4	4,8	4,10	3,4	2,23	1,05	0,96	0,875	0,82	0,77	0,72
^{60}Co	< 1,0	< 0,75	< 0,5	< 0,65	< 0,8	< 0,80	< 0,8	< 0,90	< 1,0	< 1,00	< 1,0	< 1,00
^{106}Ru	< 34,5	< 20,65	< 6,8	< 7,15	< 7,5	< 7,25	< 7,0	< 6,75	< 6,5	< 6,75	< 7,0	< 7,25
^{125}Sb	< 16,0	< 9,20	< 2,4	< 2,65	< 2,9	< 2,65	< 2,4	< 2,70	< 3,0	< 2,35	< 1,7	< 1,05
^{134}Cs	268	136,7	5,3	5,3	5,2	4,8	4,3	4,9	5,5	3,8	2,03	0,30
^{137}Cs	1860	944,5	29	32,5	36	31	26	28,5	31	19,5	8	8
^{144}Ce	< 15,0	< 8,9	< 2,8	< 2,8	< 2,8	< 2,8	< 2,8	< 2,8	< 2,8	< 2,4	< 2,0	< 1,60
^{154}Eu	< 4,0	< 2,4	< 0,8	< 0,8	< 0,8	< 0,8	< 0,8	< 0,8	< 0,8	< 0,8	< 0,7	< 0,65
^{241}Am	< 29,0	< 17,0	< 4,9	< 5,4	< 5,9	< 5,9	< 5,8	< 5,6	< 5,3	< 5,2	< 5,0	< 4,85
$^{239+240}Pu$	0,028	0,018	0,007	0,017	0,027	0,019	0,01	< 0,009	< 0,007	< 0,007	0,007	0,007
$^{238}Pu+^{241}Am$	0,82	0,42	0,02	0,027	0,033	0,026	0,019	0,023	0,027	0,024	0,02	0,016
^{244}Cm	2,38	< 1,19	< 0,007	< 0,007	< 0,007	< 0,009	0,01	0,015	0,02	0,017	0,013	0,009
Elementary Concentration (mg/L)												
Mo	< 0,05	< 0,04	< 0,02	< 0,02	< 0,02	< 0,02	< 0,02	< 0,02	< 0,02	< 0,02	< 0,02	< 0,02
Tc	< 0,02	< 0,02	< 0,02	< 0,02	< 0,02	< 0,02	< 0,02	< 0,02	< 0,02	< 0,02	< 0,02	< 0,02
Zr	< 0,01	< 0,01	< 0,01	< 0,01	< 0,01	< 0,01	< 0,01	< 0,01	< 0,01	< 0,01	< 0,01	< 0,01
U	< 0,08	< 0,08	< 0,08	< 0,08	< 0,08	< 0,08	< 0,08	< 0,08	< 0,08	< 0,08	< 0,08	< 0,08
Nd	< 0,02	< 0,02	< 0,02	< 0,02	< 0,02	< 0,02	< 0,02	< 0,02	< 0,02	< 0,02	< 0,02	< 0,02
Isotope Concentration (µg/L)												
^{88}Sr	1,62	2,16	2,70	3,24	2,39	1,54	2,43	3,32	2,84	2,36	1,78	1,21
^{99}Tc	< 1	< 1	< 1	< 1	< 1	< 1	< 1	< 1	< 1	< 1	< 1	< 1
^{237}Np	< 1	< 1	< 1	< 1	< 1	< 1	< 1	< 1	< 1	< 1	< 1	< 1
^{238}U	< 1	< 1	< 1	< 1	< 1	< 1	< 1	< 1	< 1	< 1	< 1	< 1
^{240}Pu	< 1	< 1	< 1	< 1	< 1	< 1	< 1	< 1	< 1	< 1	< 1	< 1

Granite/Granitic Groundwater												
Sampling n°	1	2	3	4	5	6	7	8	9	10	11	12
Time (days)	7	5	7	9	7	7	7	7	7	7	7	7
Cumulative time (days)	7	12	19	28	35	42	49	56	63	70	77	84
Activity (Bq/mL)												
^{90}Sr	26	22	18	14,25	10,5	9,00	7,5	34,25	61	38,50	16	-6,50
^{60}Co	< 0,8	< 0,85	< 0,9	< 0,90	< 0,9	< 0,85	< 0,8	< 0,95	< 1,1	< 1,05	< 1,0	< 0,95
^{106}Ru	< 12,0	< 15,25	< 18,5	< 17,75	< 17,0	< 14,25	< 11,5	< 19,50	< 27,5	< 21,25	< 15,0	< 8,75
^{125}Sb	< 5,0	< 6,50	< 8,0	< 7,50	< 7,0	< 6,00	< 5,0	< 9,00	< 13,0	< 10,00	< 7,0	< 4,00
^{134}Cs	18	37,5	57	58,0	59	41,5	24	99,0	174	112,0	50	-12,00
^{137}Cs	126	280,5	435	420,5	406	291	176	718	1260	804,5	349	8
^{144}Ce	< 4,0	< 3,1	< 2,2	< 2,2	< 2,1	< 3,6	< 5,0	< 9,0	< 13,0	< 10,0	< 7,0	< 4,00
^{154}Eu	< 1,0	< 1,6	< 2,2	< 2,2	< 2,1	< 1,8	< 1,5	< 2,8	< 4,0	< 3,0	< 2,0	< 1,00
^{241}Am	< 8,0	< 11,5	< 15,0	< 15,0	< 15,0	< 12,5	< 10,0	< 17,0	< 24,0	< 18,5	< 13,0	< 7,50
$^{239+240}Pu$	0,006	0,01	0,013	0,021	0,028	0,029	0,03	0,05	0,07	0,045	0,02	-0,005
$^{238}Pu+^{241}Am$	0,04	0,027	0,013	0,022	0,03	0,026	0,22	0,76	1,3	0,73	0,16	-0,41
^{244}Cm	0,08	0,05	0,02	0,06	0,09	0,6	1,11	4,16	7,2	3,92	0,64	-2,64
Elementary Concentration (mg/L)												
Mo	< 0,05	< 0,04	0,03	< 0,03	< 0,02	< 0,02	< 0,02	< 0,02	< 0,02	< 0,02	< 0,02	< 0,02
Tc	< 0,02	< 0,02	< 0,02	< 0,02	< 0,02	< 0,02	< 0,02	< 0,02	< 0,02	< 0,02	< 0,02	< 0,02
Zr	< 0,01	< 0,01	< 0,01	< 0,01	< 0,01	< 0,01	< 0,01	< 0,01	< 0,01	< 0,01	< 0,01	< 0,01
U	< 0,08	< 0,08	< 0,08	< 0,08	< 0,08	< 0,08	< 0,08	< 0,08	< 0,08	< 0,08	< 0,08	< 0,08
Nd	< 0,02	< 0,02	< 0,02	< 0,02	< 0,02	< 0,02	< 0,02	< 0,02	< 0,02	< 0,02	< 0,02	< 0,02
Isotope Concentration (µg/L)												
^{88}Sr	2,11	2,06	2,01	1,97	1,83	1,69	1,47	1,25	2,34	3,42	3,06	2,7
^{99}Tc	< 1	< 1	< 1	< 1	< 1	< 1	< 1	< 1	< 1	< 1	< 1	< 1
^{127}I	< 1	< 1	< 1	< 1	< 1	< 1	< 1	< 1	< 1	< 1	< 1	< 1
^{237}Np	< 1	< 1	< 1	< 1	< 1	< 1	< 1	< 1	< 1	< 1	< 1	< 1
^{238}U	< 1	< 1	< 1	< 1	< 1	< 1	< 1	< 1	< 1	2,12	1,12	< 1
^{239}Pu	< 1	< 1	< 1	< 1	< 1	< 1	< 1	< 1	< 1	< 1	< 1	< 1
^{240}Pu	< 1	< 1	< 1	< 1	< 1	< 1	< 1	< 1	< 1	< 1	< 1	< 1

TABLE 19 (continuation). **Gravelines 3+2 spent fuel integral leaching experiments: filter rinsing solution analysis results**

Clay/Clayey Groundwater												
Sampling n°	1	2	3	4	5	6	7	8	9	10	11	12
Time (days)	7	5	7	9	7	7	7	7	7	7	7	7
Cumulative time (days)	7	12	19	28	35	42	49	56	63	70	77	84
Activity (Bq/mL)												
^{90}Sr	128,5	65,45	2,4	1,68	0,955	0,65	0,335	1,47	2,6	3,35	4,1	4,85
^{60}Co	< 0,9	< 0,90	< 0,9	< 0,95	< 1,0	< 0,90	< 0,8	< 0,80	< 0,8	< 0,90	< 1,0	< 1,10
^{106}Ru	< 24,0	< 15,00	< 6,0	< 6,13	< 6,3	< 6,75	< 7,3	< 7,00	< 6,8	< 8,13	< 9,5	< 10,88
^{125}Sb	< 11,0	< 6,75	< 2,5	< 2,35	< 2,2	< 2,10	< 2,0	< 2,30	< 2,6	< 3,05	< 3,5	< 3,95
^{134}Cs	123	63,7	4,4	3,5	2,5	2,5	2,4	3,7	5	8,5	12	15,50
^{137}Cs	857	442,5	28	20,5	13	12,5	12	20	28	55,5	83	8
^{144}Ce	< 10,0	< 6,4	< 2,8	< 2,6	< 2,4	< 2,5	< 2,5	< 2,5	< 2,5	< 3,2	< 3,8	< 4,45
^{154}Eu	< 3,0	< 1,9	< 0,7	< 0,7	< 0,7	< 0,7	< 0,7	< 0,8	< 0,8	< 0,9	< 1,0	< 1,10
^{241}Am	< 21,0	< 13,3	< 5,5	< 5,3	< 5,0	< 4,8	< 4,5	< 4,9	< 5,3	< 6,4	< 7,5	< 8,60
$^{239+240}Pu$	0,02	0,02	0,02	< 0,015	< 0,0095	0,011	0,013	0,013	0,013	0,042	0,07	0,098
$^{238}Pu+^{241}Am$	0,65	0,34	0,02	0,02	0,019	0,02	0,02	0,02	0,02	0,033	0,046	0,059
^{244}Cm	3,2	1,60	0,007	0,008	0,01	0,022	0,033	0,027	0,02	0,07	0,11	0,15
Elementary Concentration (mg/L)												
Mo	< 0,05	< 0,04	< 0,02	< 0,02	< 0,02	< 0,02	< 0,02	< 0,02	< 0,02	< 0,02	< 0,02	< 0,02
Tc	< 0,02	< 0,02	< 0,02	< 0,02	< 0,02	< 0,02	< 0,02	< 0,02	< 0,02	< 0,02	< 0,02	< 0,02
Zr	< 0,01	< 0,01	< 0,01	< 0,01	< 0,01	< 0,01	< 0,01	< 0,01	< 0,01	< 0,01	< 0,01	< 0,01
U	< 0,08	< 0,08	< 0,08	< 0,08	< 0,08	< 0,08	< 0,08	< 0,08	< 0,08	< 0,08	< 0,08	< 0,08
Nd	< 0,02	< 0,02	< 0,02	< 0,02	< 0,02	< 0,02	< 0,02	< 0,02	< 0,02	< 0,02	< 0,02	< 0,02
Isotope Concentration (µg/L)												
^{88}Sr	1,47	1,48	1,50	1,52	1,57	1,63	1,19	0,75	1,63	2,50	1,79	1,08
^{99}Tc	< 1	< 1	< 1	< 1	< 1	< 1	< 1	< 1	< 1	< 1	< 1	< 1
^{127}I	< 1	< 1	< 1	< 1	< 1	< 1	< 1	< 1	< 1	< 1	< 1	< 1
^{237}Np	< 1	< 1	< 1	< 1	< 1	< 1	< 1	< 1	< 1	< 1	< 1	< 1
^{238}U	< 1	< 1	< 1	< 1	< 1	< 1	< 1	2,06	1,57	1,08	1,52	1,96
^{239}Pu	< 1	< 1	< 1	< 1	< 1	< 1	< 1	< 1	< 1	< 1	< 1	< 1
^{240}Pu	< 1	< 1	< 1	< 1	< 1	< 1	< 1	< 1	< 1	< 1	< 1	< 1

Granite/Clayey Groundwater												
Sampling n°	1	2	3	4	5	6	7	8	9	10	11	12
Time (days)	7	5	7	9	7	7		14	7	7	7	7
Cumulative time (days)	7	12	19	28	35	42		56	63	70	77	84
Activity (Bq/mL)												
^{90}Sr	114	88,5	63	38,75	14,5	20,13	nd	31,38	37	26,50	16	5,50
^{60}Co	< 0,9	< 0,95	< 1,0	< 0,75	< 0,5	< 0,63	nd	< 0,88	< 1,0	< 0,90	< 0,8	< 0,70
^{106}Ru	< 33,0	< 30,25	< 27,5	< 21,25	< 15,0	< 17,25	nd	< 21,75	< 24,0	< 19,75	< 15,5	< 11,25
^{125}Sb	< 15,0	< 14,00	< 13,0	< 10,00	< 7,0	< 8,25	nd	< 10,75	< 12,0	< 9,50	< 7,0	< 4,50
^{134}Cs	215	192,0	169	106,0	43	64,00	nd	106,00	127	88,5	50	11,50
^{137}Cs	1510	1356	1202	757,5	313	451,75	nd	729,25	868	607,5	347	8
^{144}Ce	< 14,0	< 13,0	< 12,0	< 9,5	< 7,0	< 8,00	nd	< 10,00	< 11,0	< 9,0	< 7,0	< 5,00
^{154}Eu	< 4,0	< 3,8	< 3,5	< 2,8	< 2,0	< 2,25	nd	< 2,75	< 3,0	< 2,5	< 2,0	< 1,50
^{241}Am	< 27,0	< 25,5	< 24,0	< 18,5	< 13,0	< 15,00	nd	< 19,00	< 21,0	< 17,0	< 13,0	< 9,00
$^{239+240}Pu$	0,04	0,027	0,013	0,01	0,007	0,016	nd	0,024	0,02	0,017	0,013	0,09
$^{238}Pu+^{241}Am$	0,26	0,22	0,17	0,13	0,08	0,07	nd	0,07	0,07	0,07	0,06	0,05
^{244}Cm	0,54	0,52	0,49	0,33	0,16	0,25	nd	0,33	0,29	0,18	0,07	-0,04
Elementary Concentration (mg/L)												
Mo	< 0,05	< 0,04	0,02	< 0,02	< 0,02	< 0,02	nd	< 0,02	< 0,02	< 0,02	< 0,02	< 0,02
Tc	< 0,02	< 0,02	< 0,02	< 0,02	< 0,02	< 0,02	nd	< 0,02	< 0,02	< 0,02	< 0,02	< 0,02
Zr	< 0,01	< 0,01	0,01	< 0,01	< 0,01	< 0,01	nd	< 0,01	< 0,01	< 0,01	< 0,01	< 0,01
U	< 0,08	< 0,16	0,24	< 0,16	< 0,08	< 0,08	nd	< 0,08	< 0,08	< 0,08	< 0,08	< 0,08
Nd	< 0,02	< 0,02	< 0,02	< 0,02	< 0,02	< 0,02	nd	< 0,02	< 0,02	< 0,02	< 0,02	< 0,02
Isotope Concentration (µg/L)												
^{88}Sr	15,712	11,12	6,528	1,936	1,454	< 1	nd	5,28	3,536	1,792	1,192	< 1
^{99}Tc	< 1	< 1	< 1	< 1	< 1	< 1	nd	< 1	< 1	< 1	< 1	< 1
^{237}Np	< 1	< 1	< 1	< 1	< 1	< 1	nd	< 1	< 1	< 1	< 1	< 1
^{238}U	6,743	5,08	3,417	1,754	3,747	5,74	nd	2,68	1,133	< 1	< 1	< 1
^{240}Pu	< 1	< 1	< 1	< 1	< 1	< 1	nd	< 1	< 1	< 1	< 1	< 1

Extrapolated data

TABLE 20. *Gravelines 3+2 spent fuel tests: solution analysis results for material rinse, alkaline melting, pot rinse and sample-holder rinse*

	Clay/Granitic Groundwater				Granite/Granitic Groundwater			
	Material Rinse	Alkaline Melting[(1)]	Pot Rinse	Sample-holder Rinse	Material Rinse	Alkaline Melting[(1)]	Pot Rinse	Sample-holder Rinse
Activity (Bq/mL)								
^{90}Sr	15200	9,5	1095	8	6700		131,5	45
^{60}Co	< 3,0	< 0,3	< 1,4	< 0,8	< 3		< 0,6	< 0,8
^{106}Ru	< 126,5	< 4,85	51,5	< 13	< 111		< 17,5	< 16
^{125}Sb	< 57	< 2,3	< 24	< 6,5	< 52		34	26
^{134}Cs	3020	11	496	31	2480		57	42
^{137}Cs	23000	89	3790	231	18800		431	310
^{144}Ce	69	< 2,3	< 23	< 6	< 48		< 8	< 7
^{154}Eu	602	< 0,7	52	< 1,6	96		< 4	< 2,3
^{241}Am	< 110	< 4,7	< 44	< 12	95		< 15	< 13
$^{239+240}Pu$	4,7	2,5	14	0,006	3,6		0,5	< 0,006
$^{238}Pu+^{241}Am$	215	2,6	82	0,011	54		9,4	0,88
^{244}Cm	912	0,16	79	0,017	99		15	2,8
Elementary Concentration (mg/L)								
Mo	< 0,2	< 0,1	0,05	0,02	< 0,15		0,06	< 0,02
Tc	< 0,02	< 0,03	< 0,02	< 0,02	< 0,02		< 0,02	< 0,02
Zr	< 0,10	0,012	0,02	< 0,01	< 0,1		0,01	< 0,01
U	< 0,25	< 0,08	0,51	< 0,08	< 0,25		0,45	< 0,08
Nd	1,35	< 0,03	0,1	< 0,02	1,35		< 0,02	< 0,02
Isotope Concentration (µg/L)								
^{88}Sr	5220	19,58	748	14,58	2740		131,2	36,8
^{99}Tc	< 10	< 10	< 10	< 1	< 10		< 10	< 1
^{237}Np	< 10	< 10	< 10	< 1	< 10		< 10	< 1
^{238}U	2940	27,4	452	0,994	8880		458	21,8
^{240}Pu	< 10	< 10	< 10	< 1	< 10		< 10	< 1

	Clay/Clayey Groundwater				Granite/Clayey Groundwater			
	Material Rinse	Alkaline Melting[1]	Pot Rinse	Sample-holder Rinse	Material Rinse	Alkaline Melting[1]	Pot Rinse	Sample-holder Rinse
Activity (Bq/mL)								
^{90}Sr	11250	3,5	58	38,5	7300		96,5	33,5
^{60}Co	< 2,5	< 0,4	< 0,8	< 0,7	< 2,3		< 0,8	< 1
^{106}Ru	< 101	< 2,4	< 16	< 13	< 113,5		< 20	< 14
^{125}Sb	< 47	< 1	14	20	< 53		50	61
^{134}Cs	2060	1	42	26	2580		66	31
^{137}Cs	15600	9	308	194	19500		496	232
^{144}Ce	< 45	< 1	< 7	< 6	< 50		< 9	< 6
^{154}Eu	363	< 0,3	< 2	< 1,5	130		< 3	< 1,7
^{241}Am	< 90	< 2,1	< 13	< 11	< 98		< 17	< 12
$^{239+240}Pu$	4,9	0,09	0,25	0,01	13		0,14	0,023
$^{238}Pu+^{241}Am$	83	0,26	2,9	0,09	138		3,1	0,14
^{244}Cm	524	0,05	3,0	0,14	133		7,4	0,017
Elementary Concentration (mg/L)								
Mo	< 0,02	< 0,1	0,06	0,05	0,05		7,9	0,02
Tc	< 0,02	< 0,03	< 0,02	< 0,02	< 0,02		< 0,02	< 0,02
Zr	< 0,01	0,014	< 0,01	< 0,01	< 0,01		0,02	< 0,01
U	< 0,25	< 0,08	0,14	< 0,08	< 0,25		0,8	< 0,08
Nd	< 0,1	< 0,03	< 0,02	< 0,02	< 0,1		0,02	< 0,02
Isotope Concentration (µg/L)								
^{88}Sr	6140	7,16	45,8	21,6	2320		147,6	19,06
^{99}Tc	< 10	< 10	< 10	< 1	< 10		< 10	< 1
^{237}Np	< 10	< 10	< 10	< 1	< 10		< 10	< 1
^{238}U	2500	< 10	155	31,6	9540		810	7,08
^{240}Pu	< 10	< 10	< 10	< 1	< 10		< 10	< 1

[1]: *only for clay*

TABLE 21 *SIMFUEL integral leaching experiments: filtered and ultrafiltered supernatant solution analysis results*

Medium	**Clay/Granitic Groundwater**		**Granite/Granitic Groundwater**		**Clay/clay Groundwater**		**Granite/Clay Groundwater**	
Supernatant Treatment	filtered	ultrafiltered	filtered	ultrafiltered	filtered	ultrafiltered	filtered	ultrafiltered
Sr	1612	238	139	20	592	96	70	8,5
Y	< 2	< 2	< 2	< 2	< 2	< 2	< 2	< 2
Zr	< 2	< 2	< 2	< 2	< 2	< 2	< 2	< 2
Mo	23,4	9,2	153	23	53	8,2	572	68
Ru	< 2	< 2	< 2	< 2	< 2	< 2	< 2	< 2
Rh	< 2	< 2	< 2	< 2	< 2	< 2	< 2	< 2
Pd	< 2	< 2	< 2	< 2	< 2	< 2	< 2	< 2
Ba	936	176	298	93	616	97	772	24
La	< 2	< 2	< 2	< 2	< 2	< 2	< 2	< 2
Ce	2,2	< 2	3,4	< 2	< 2	< 2	< 2	< 2
Nd	2,7	< 2	2,6	< 2	< 2	< 2	< 2	< 2
U	32	28	2728	370	58	10,9	152	18

TABLE 22. *SIMFUEL integral leaching experiments:weekly sample analysis results.*

Clay/Granitic Groundwater													
Sampling n°	1	2	3	4	5	6	7	8	9	10	11	12	Final
Time (days)	5	7	9	7	7	7	7	7	7	7	7	7	7
Cumulative time (days)	5	12	21	28	35	42	49	56	63	70	77	84	91
Sampling volume (mL)	8,6	8,6	9,4	10,2	10,8	11,3	10,5	10,8	11,3	11,1	11,6	11,8	
Isotope Concentration (µg/L)													
^{88}Sr	2384	2636	2828	2440	2464	2372	2132	2336	2056	2012	1988	1880	1612
^{89}Y	< 2	< 2	< 2	< 2	< 2	< 2	< 2	< 2	< 2	< 2	< 2	< 2	< 2
^{90}Zr	< 2	< 2	< 2	< 2	< 2	< 2	< 2	< 2	< 2	< 2	< 2	< 2	< 2
^{95}Mo	174	147	141	165	136	110	105	91	86	62	46	37	23
^{101}Ru	< 2	< 2	< 2	< 2	< 2	< 2	< 2	< 2	< 2	< 2	< 2	< 2	< 2
^{103}Rh	< 2	< 2	< 2	< 2	< 2	< 2	< 2	< 2	< 2	< 2	< 2	< 2	< 2
^{108}Pd	2,2	< 2	< 2	< 2	< 2	< 2	< 2	< 2	< 2	< 2	< 2	< 2	< 2
^{138}Ba	512	480	532	444	500	476	496	504	504	544	496	528	936
^{139}La	< 2	< 2	< 2	< 2	< 2	< 2	< 2	< 2	< 2	< 2	< 2	< 2	< 2
^{140}Ce	< 2	< 2	< 2	< 2	< 2	< 2	< 2	< 2	< 2	< 2	< 2	< 2	2,2
^{146}Nd	< 2	< 2	< 2	< 2	< 2	< 2	< 2	< 2	< 2	< 2	< 2	< 2	2,7
^{238}U	25	< 2	< 2	7,7	< 2	< 2	< 2	< 2	< 2	< 2	< 2	< 2	32

Granite/Granitic Groundwater													
Sampling n°	1	2	3	4	5	6	7	8	9	10	11	12	Final
Time (days)	7	7	5	7	9	7	7	7	7	7	7	7	7
Cumulative time (days)	7	14	19	26	35	42	49	56	63	70	77	84	91
Sampling volume (mL)	10,1	10,5	9,8	10,3	9,6	13,3	12,4	10,7	10,7	11,8	11,8	11,3	
Isotope Concentration (µg/L)													
^{88}Sr	252	214	198	420	448	301	177	343	161	287	150	118	139
^{89}Y	< 2	< 2	< 2	< 2	< 2	< 2	< 2	< 2	< 2	< 2	< 2	< 2	< 2
^{90}Zr	< 2	< 2	< 2	< 2	< 2	< 2	< 2	< 2	< 2	< 2	< 2	< 2	< 2
^{95}Mo	744	692	604	520	436	384	376	316	299	252	244	238	153
^{101}Ru	< 2	< 2	< 2	< 2	< 2	< 2	< 2	< 2	< 2	< 2	< 2	< 2	< 2
^{103}Rh	< 2	< 2	< 2	< 2	< 2	< 2	< 2	< 2	< 2	< 2	< 2	< 2	< 2
^{108}Pd	< 2	< 2	< 2	< 2	< 2	< 2	< 2	< 2	< 2	< 2	< 2	< 2	< 2
^{138}Ba	337	390	268	301	298	272	343	234	363	277	386	190	298
^{139}La	< 2	< 2	< 2	< 2	< 2	< 2	< 2	< 2	< 2	< 2	< 2	< 2	< 2
^{140}Ce	< 2	< 2	< 2	< 2	< 2	< 2	< 2	< 2	< 2	< 2	< 2	< 2	3,4
^{146}Nd	< 2	< 2	< 2	< 2	< 2	< 2	< 2	< 2	< 2	< 2	< 2	< 2	2,6
^{238}U	< 2	< 2	< 2	< 2	46	< 2	< 2	< 2	< 2	< 2	< 2	< 2	2728

To be continued on next page...

TABLE 22 (continuation). **SIMFUEL integral leaching experiments: weekly sample analysis results.**

Clay/Clayey Groundwater													
Sampling n°	1	2	3	4	5	6	7	8	9	10	11	12	Final
Time (days)	7	7	7	5	7	9	7	7	7	7	7	7	7
Cumulative time (days)	7	14	21	26	33	42	49	56	63	70	77	84	91
Sampling volume (mL)	9,7	8,3	9,7	4,8	8,2	6,1	9,7	10,6	10	9,8	10,8	11,4	
Isotope Concentration (μg/L)													
^{88}Sr	1652	1528	1312	1196	1072	1016	912	868	816	748	680	612	592
^{89}Y	< 2	< 2	< 2	< 2	< 2	< 2	< 2	< 2	< 2	< 2	< 2	< 2	< 2
^{90}Zr	< 2	< 2	< 2	< 2	< 2	< 2	< 2	< 2	< 2	< 2	< 2	< 2	< 2
^{95}Mo	357	408	235	244	162	145	113	90	95	72	71	59	53
^{101}Ru	< 2	< 2	< 2	< 2	< 2	< 2	< 2	< 2	< 2	< 2	< 2	< 2	< 2
^{103}Rh	< 2	< 2	< 2	< 2	< 2	< 2	< 2	< 2	< 2	< 2	< 2	< 2	< 2
^{108}Pd	< 2	< 2	< 2	< 2	< 2	< 2	< 2	< 2	< 2	< 2	< 2	< 2	< 2
^{138}Ba	264	326	334	314	330	349	372	362	373	396	379	404	616
^{139}La	< 2	< 2	< 2	< 2	< 2	< 2	< 2	< 2	< 2	< 2	< 2	< 2	< 2
^{140}Ce	< 2	< 2	< 2	< 2	< 2	< 2	< 2	< 2	< 2	< 2	< 2	< 2	< 2
^{146}Nd	< 2	< 2	< 2	< 2	< 2	< 2	< 2	< 2	< 2	< 2	< 2	< 2	< 2
^{238}U	< 2	< 2	< 2	< 2	< 2	< 2	< 2	< 2	< 2	< 2	< 2	< 2	58

Granite/Clayey Groundwater													
Sampling n°	1	2	3	4	5	6	7	8	9	10	11	12	Final
Time (days)	7	7	7	5	7	9	7	7	7	7	7	7	7
Cumulative time (days)	7	14	21	26	33	42	49	56	63	70	77	84	91
Sampling volume (mL)	9,9	10,7	9,9	11,2	10,7	7,9	10,2	10,4	9,1	10,1	10,5	10,5	
Isotope Concentration (μg/L)													
^{88}Sr	204	132	105	81	74	63	49	44	44	42	39	37	70
^{89}Y	< 2	< 2	< 2	< 2	< 2	< 2	< 2	< 2	< 2	< 2	< 2	< 2	< 2
^{90}Zr	< 2	< 2	< 2	< 2	< 2	< 2	< 2	< 2	< 2	< 2	< 2	< 2	< 2
^{95}Mo	1544	1404	1152	1088	1008	964	868	820	744	712	636	616	572
^{101}Ru	< 2	< 2	< 2	< 2	< 2	< 2	< 2	< 2	< 2	< 2	< 2	< 2	< 2
^{103}Rh	< 2	< 2	< 2	< 2	< 2	< 2	< 2	< 2	< 2	< 2	< 2	< 2	< 2
^{108}Pd	< 2	< 2	< 2	< 2	< 2	< 2	< 2	< 2	< 2	< 2	< 2	< 2	< 2
^{138}Ba	8	127	120	142	176	131	169	134	180	232	184	150	772
^{139}La	< 2	< 2	< 2	< 2	< 2	< 2	< 2	< 2	< 2	< 2	< 2	< 2	< 2
^{140}Ce	< 2	< 2	< 2	< 2	< 2	< 2	< 2	< 2	< 2	< 2	< 2	< 2	< 2
^{146}Nd	< 2	< 2	< 2	< 2	< 2	< 2	< 2	< 2	< 2	< 2	< 2	< 2	< 2
^{238}U	< 2	5,2	< 2	< 2	< 2	< 2	< 2	< 2	< 2	< 2	< 2	< 2	152

***TABLE 23**. SIMFUEL integral leaching experiments: filter rinsing solution analysis results*

Clay/Granitic Groundwater												
Sampling n°	1	2	3	4	5	6	7	8	9	10	11	12
Time (days)	5	7	9	7	7	7	7	7	7	7	7	7
Cumulative time (days)	5	12	21	28	35	42	49	56	63	70	77	84
Sampling volume (mL)	8,6	8,6	9,4	10,2	10,8	11,3	10,5	10,8	11,3	11,1	11,6	11,8
Isotope Concentration (µg/L)												
^{88}Sr	80,4	27,4	11,3	12,8	8,8	14,1	8,0	20,8	15,6	16,1	18,0	32,4
^{89}Y	6,7	< 2	< 2	< 2	< 2	< 2	< 2	< 2	< 2	2,9	< 2	3,6
^{90}Zr	< 2	< 2	< 2	< 2	< 2	< 2	< 2	< 2	< 2	5,4	< 2	2,2
^{95}Mo	6	7	4	6	3	5	5	5	6	2	5	6
^{101}Ru	< 2	< 2	< 2	< 2	< 2	< 2	< 2	< 2	< 2	< 2	< 2	< 2
^{103}Rh	< 2	< 2	< 2	< 2	< 2	< 2	< 2	< 2	< 2	< 2	< 2	< 2
^{108}Pd	< 2	< 2	< 2	< 2	< 2	< 2	< 2	< 2	< 2	< 2	< 2	< 2
^{138}Ba	155,6	22,3	19,6	14,0	11,7	22,9	29,2	32,8	49,2	72,8	43,2	115,2
^{139}La	17,4	< 2	< 2	< 2	< 2	< 2	< 2	2,6	< 2	4,8	4,8	6,8
^{140}Ce	34,9	< 2	< 2	< 2	< 2	< 2	< 2	5,0	2,2	8,7	10,2	14,5
^{146}Nd	20,8	< 2	< 2	< 2	< 2	< 2	< 2	4,9	2,4	4,8	4,6	8,8
^{238}U	58,4	18,3	< 2	84,8	< 2	< 2	7,5	68,8	< 2	< 2	< 2	< 2

Granite/Granitic Groundwater												
Sampling n°	1	2	3	4	5	6	7	8	9	10	11	12
Time (days)	7	7	5	7	9	7	7	7	7	7	7	7
Cumulative time (days)	7	14	19	26	35	42	49	56	63	70	77	84
Sampling volume (mL)	10,1	10,5	9,8	10,3	9,6	13,3	12,4	10,7	10,7	11,8	11,8	11,3
Isotope Concentration (µg/L)												
^{88}Sr	47,2	17,9	11,1	37,6	24,2	24,6	13,5	43,2	10,5	130,0	9,6	8,3
^{89}Y	4,6	< 2	< 2	2,6	< 2	< 2	< 2	4,7	< 2	13,0	< 2	< 2
^{90}Zr	< 2	< 2	< 2	< 2	< 2	< 2	< 2	< 2	< 2	< 2	< 2	< 2
^{95}Mo	18,3	21,2	15,7	12,1	10,4	14,7	10,4	10,4	7,0	10,3	13,4	12,1
^{101}Ru	< 2	< 2	< 2	< 2	< 2	< 2	< 2	< 2	< 2	< 2	< 2	< 2
^{103}Rh	< 2	< 2	< 2	< 2	< 2	< 2	< 2	< 2	< 2	< 2	< 2	< 2
^{108}Pd	< 2	< 2	< 2	< 2	< 2	< 2	< 2	< 2	< 2	< 2	< 2	< 2
^{138}Ba	85,2	40,4	28,4	57,6	41,2	26,0	298,4	89,2	26,0	148,8	35,2	59,6
^{139}La	4,9	< 2	< 2	2,4	< 2	< 2	< 2	5,3	< 2	20,0	< 2	< 2
^{140}Ce	10,4	2,8	< 2	4,9	3,3	2,5	< 2	11,0	< 2	41,2	< 2	3,1
^{146}Nd	6,3	2,6	< 2	2,6	3,1	< 2	< 2	6,4	< 2	23,7	< 2	< 2
^{238}U	< 2	< 2	< 2	< 2	< 2	< 2	< 2	133,2	< 2	32,1	< 2	< 2

To be continued on next page...

TABLE 23 (continuation). **SIMFUEL integral leaching experiments: filter rinsing solution analysis results**

Clay/Clayey Groundwater												
Sampling n°	1	2	3	4	5	6	7	8	9	10	11	12
Time (days)	7	7	7	5	7	9	7	7	7	7	7	7
Cumulative time (days)	7	14	21	26	33	42	49	56	63	70	77	84
Sampling volume (mL)	9,7	8,3	9,7	4,8	8,2	6,1	9,7	10,6	10	9,8	10,8	11,4
Isotope Concentration (µg/L)												
^{88}Sr	106,4	9,2	6,6	8,8	17,9	6,5	9,0	6,5	5,8	8,4	10,4	6,0
^{89}Y	2,5	< 2	< 2	< 2	< 2	< 2	< 2	< 2	< 2	< 2	< 2	< 2
^{90}Zr	< 2	< 2	< 2	< 2	< 2	< 2	< 2	< 2	< 2	< 2	< 2	< 2
^{95}Mo	23	4,8	4,8	6,0	6,3	5,2	3,8	4,3	988	7,3	7,0	4,8
^{101}Ru	< 2	< 2	< 2	< 2	< 2	2,2	< 2	< 2	< 2	< 2	< 2	< 2
^{103}Rh	< 2	< 2	< 2	< 2	< 2	< 2	< 2	< 2	< 2	< 2	< 2	< 2
^{108}Pd	< 2	< 2	< 2	< 2	< 2	< 2	< 2	< 2	< 2	< 2	< 2	< 2
^{138}Ba	42,8	7,08	11,3	13,8	13,1	7,4	28,4	20,9	10,5	11,4	17,0	27,9
^{139}La	5,0	< 2	< 2	< 2	< 2	< 2	< 2	< 2	< 2	< 2	< 2	< 2
^{140}Ce	9,3	< 2	< 2	< 2	< 2	< 2	< 2	< 2	< 2	< 2	< 2	< 2
^{146}Nd	6,0	< 2	< 2	< 2	< 2	< 2	< 2	< 2	< 2	< 2	< 2	< 2
^{238}U	< 2	< 2	< 2	7,2	< 2	< 2	< 2	5,8	< 2	< 2	< 2	< 2

Granite/Clayey Groundwater												
Sampling n°	1	2	3	4	5	6	7	8	9	10	11	12
Time (days)	7	7	7	5	7	9	7	7	7	7	7	7
Cumulative time (days)	7	14	21	26	33	42	49	56	63	70	77	84
Sampling volume (mL)	9,9	10,7	9,9	11,2	10,7	7,9	10,2	10,4	9,1	10,1	10,5	10,5
Isotope Concentration (µg/L)												
^{88}Sr	11,2	11,3	5,8	7,2	9,9	5,3	5,3	7,6	5,5	11,2	3,8	3,2
^{89}Y	< 2	< 2	< 2	< 2	< 2	< 2	< 2	< 2	< 2	< 2	< 2	< 2
^{90}Zr	< 2	< 2	< 2	< 2	< 2	< 2	< 2	< 2	< 2	< 2	< 2	< 2
^{95}Mo	31,2	38,0	24,2	36,9	16,6	21,6	17,0	15,9	17,7	14,5	27,2	20,0
^{101}Ru	< 2	< 2	< 2	< 2	< 2	< 2	< 2	< 2	< 2	< 2	< 2	< 2
^{103}Rh	< 2	< 2	< 2	< 2	< 2	< 2	< 2	< 2	< 2	< 2	< 2	< 2
^{108}Pd	< 2	< 2	< 2	< 2	< 2	< 2	< 2	< 2	< 2	< 2	< 2	< 2
^{138}Ba	6,7	13,3	7,1	7,8	12,1	6,5	8,6	7,5	6,8	31,8	20,9	35,7
^{139}La	< 2	< 2	< 2	< 2	< 2	< 2	< 2	< 2	< 2	< 2	< 2	< 2
^{140}Ce	< 2	< 2	< 2	< 2	< 2	< 2	< 2	< 2	< 2	< 2	< 2	< 2
^{146}Nd	< 2	< 2	< 2	< 2	< 2	< 2	< 2	< 2	< 2	< 2	< 2	< 2
^{238}U	< 2	< 2	< 2	< 2	58,8	< 2	< 2	< 2	< 2	< 2	< 2	< 2

TABLE 24. *SIMFUEL integral leaching experiments: solution analysis results for material rinse, alkaline melting, pot rinse and sample-holder rinse*

	Clay/Granitic Groundwater				Granite/Granitic Groundwater			
	Material Rinse	Alkaline Melting[1]	Pot Rinse	Sample-holder Rinse	Material Rinse	Alkaline Melting[1]	Pot Rinse	Sample-holder Rinse
^{88}Sr	7600	6,68	132,6	19,1	1960		17,6	4,4
^{89}Y	880	4,08	13,8	< 1	4140		61	< 1
^{90}Zr	42,9	19,86	6,36	< 1	134		18,0	< 1
^{95}Mo	< 25	14,3	12,22	1,602	150		125	39,4
^{101}Ru	< 25	< 1	< 1	< 1	< 50		< 1	< 1
^{103}Rh	< 25	< 1	< 1	< 1	< 50		< 1	< 1
^{108}Pd	< 25	< 1	< 1	< 1	< 50		< 1	< 1
^{138}Ba	14500	14,44	189,2	17,5	2800		12,4	11,7
^{139}La	2635	3,26	27,2	< 1	1910		31	< 1
^{140}Ce	5400	6,68	55,8	< 1	5080		78,2	< 1
^{146}Nd	2845	2,88	29,2	< 1	3040		41,4	< 1
^{238}U	2085	6,36	86	< 1	19400		1026	18,3

	Clay/Clayey Groundwater				Granite/Clayey Groundwater			
	Material Rinse	Alkaline Melting[1]	Pot Rinse	Sample-holder Rinse	Material Rinse	Alkaline Melting[1]	Pot Rinse	Sample-holder Rinse
^{88}Sr	8660	4,6	340	4535	3200		42	3900
^{89}Y	820	4,2	59	2785	9050		91,2	2755
^{90}Zr	< 50	20,6	7	3530	< 250		30,4	18150
^{95}Mo	< 50	3,9	59,8	2575	515		454	3385
^{101}Ru	< 50	< 1	< 1	262,5	< 250		< 1	266
^{103}Rh	< 50	< 1	< 1	148,5	< 250		< 1	158
^{108}Pd	< 50	< 1	< 1	950	< 250		< 1	520
^{138}Ba	18500	22,2	1152	18800	2170		62,8	15900
^{139}La	2230	3,2	161,6	11500	3580		48,8	12350
^{140}Ce	4510	6,1	324	79050	10050		121,2	84950
^{146}Nd	2460	2,8	167,8	43300	6150		64,2	46700
^{238}U	1030	2,8	122,2	92500	51000		918	72500

Appendix 6: Original test data obtained by ITU

ELEMENT CONCENTRATION IN SOLUTION MEASURED BY ICP-MS IN THE DIFFERENT SAMPLES (TABLES 1-6).

Tab. 1: Composition of the samples obtained from the experiment with a MOX fuel with a burn-up of 12 GWd/tU. Concentrations are given in ng/mL of the element.

	1 day	8 days	45 days	135 days	315 days
Se		0.65	3.68	8.93	
Rb	189.82	504.48	1432.42	1317.30	888.90
Sr	15.66	23.10	62.79	61.90	57.81
Y	0.49		2.61	0.97	0.78
Zr	8.76	29.63			
Mo	30.18	162.57	29.86		
Tc	0.24			0.49	
Ru	0.81	0.64		1.35	
Rh					
Pd	1.01			25.26	4.05
Pd	1.38				
Ag	7.10		7.84	104.31	20.73
Cd	122.50	191.21	28.18	20.23	9.35
Sn	1.82		6.53	6.09	
Sb		3.71		15.63	9.00
Sn	1.08	3.98	7.70	8.38	1.92
I	6.57	40.93	35.62	1589.12	96.62
Te	1.61	3.24	15.29		2.23
Cs	12335	30690	84543	83188	32207
Ba	446.37	1601.58	5010.13	6319.76	3136.14
La		6.95	2.09	5.85	4.89
Ce	0.18	3.52		13.87	5.94
Pr	0.10	0.69		5.85	1.37
Nd	2.39	1.42		41.87	
Pm	0.15	1.16		2.92	3.91
Sm	2.61	8.27	9.33	17.41	24.43
Eu	0.23	0.54	1.81	7.90	2.60
Gd				0.77	3.38
Np	0.93	0.51			
U	188.45	188.35	252.82	102.75	75.44
Pu	1.53	25.56		26.63	47.80
Am	0.13			13.82	4.20
Cm				2.01	

Tab. 2: Composition of the samples obtained from the experiment with a MOX fuel with a burn-up of 20 GWd/tU. Concentrations are given in ng/mL of the element.

	1 day	8 days	45 days	135 days	315 days
Se				4.17	
Rb	903.66	916.58	1053.66	284.84	140.60
Sr		97.27	99.13	59.26	20.97
Y	4.22	10.32	2.08	13.81	14.63
Zr	2263.70				
Mo	5682.04	46.54	55.23		
Tc	4.22				
Ru			2.88		0.56
Rh					
Pd				7.66	1.33
Pd				2.80	0.65
Ag		14.12		45.36	33.65
Cd	1586.69	1829.56	1457.57	1215.35	251.50
Sn		40.73		18.49	1.85
Sb				13.83	2.33
Sn				1.21	1.56
I	104.27	117.93	91.33	1769.42	145.00
Te		15.89	6.62		0.53
Cs	72389.27	102156.9	110284.9	25530.99	3792.70
Ba	7319.69	16556.52	16681.41	7329.65	1329.49
La	25.34	109.15	30.18	175.54	82.51
Ce	129.99	422.46	359.45	710.17	316.40
Pr	30.03	54.84	30.70	115.38	76.47
Nd	67.64	181.56	81.41	338.81	196.97
Pm	8.91	24.98	16.13	51.78	26.48
Sm	41.89	77.57	102.22	237.74	142.69
Eu		9.43	6.63	15.98	9.93
Gd	0.74	12.83	6.56	20.19	12.28
Np	2.08		0.47		1.05
U	320.11	172.91	307.53	80.40	198.30
Pu	143.64	930.80	918.10	560.13	158.90
Am	43.68	147.27	96.27	224.20	248.51
Cm	1.13	1.00	0.26	6.83	4.68

Tab. 3: Composition of the samples obtained from the experiment with a MOX fuel with a burn-up of 25 GWd/tU. Concentrations are given in ng/mL of the element.

	1 day	8 days	45 days	135 days	315 days
Se			3.64		2.85
Rb	230.89	866.88	975.37	351.22	254.92
Sr	43.35	73.85	91.36	30.88	33.37
Y	0.71	0.55	2.58		0.30
Zr	12.30			7.45	
Mo	142.58	22.53	27.41		
Tc			1.03		
Ru	7.19				
Rh	0.47				
Pd	1.22		10.71	10.86	
Pd			10.27		
Ag	2.60	7.73		34.05	15.35
Cd	150.82	1019.28	370.80	245.59	174.07
Sn			25.83		
Sb		1.11	8.28	14.70	0.82
Sn	1.74		6.35	9.01	1.93
I	146.03	294.13	185.23	3978.64	208.48
Te	3.30	0.70			0.43
Cs	29239	97448	104206	35688	12127
Ba	1940	7757	10016	5321	1924
La	4.01	1.10	8.78	20.95	1.64
Ce	4.03	19.90	115.66	96.41	11.69
Pr		5.52	13.43	8.90	1.16
Nd	7.96	5.08	60.21	20.89	2.75
Pm	0.47	0.55	3.62	6.81	0.26
Sm			46.12	23.38	7.66
Eu		6.39	5.38	6.06	1.77
Gd			1.63	0.82	0.35
Np	0.21				
U	261.27	66.16	227.03	71.00	26.93
Pu	14.62	12.67	658.67	141.74	22.10
Am	3.84	6.98	59.85	22.22	5.53
Cm			0.78	1.26	0.06

Tab. 4: Composition of the samples obtained from the experiment with a UO_2 fuel with a burn-up of 30 GWd/tU. Concentrations are given in ng/mL of the element.

	1 day	8 days	45 days	135 days	315 days
Se			0.47		
Rb	30.07	14.44	56.32	28.99	27.02
Sr	10.08	3.06	32.24	9.82	24.32
Y	0.15	0.07	0.03		0.07
Zr	12.95	2.55	2.08		0.61
Mo	31.32	9.67	4.43		2.45
Tc	1.88	0.35	1.84		
Ru	2.15	0.20	0.72	0.08	
Rh	1.14	0.01	0.05		
Pd	0.37		0.40		0.19
Pd	0.84	0.14	0.73		0.25
Ag	36	26	115	7	16
Cd	7.09	2.35	5.47	1.29	1.58
Sn	1.58	0.70	0.65	6.37	2.53
Sb	6.26	5.07	8.50	7.03	4.09
Sn	0.04		0.13	0.42	0.15
I	1.70	0.59	1.60	101.07	7.38
Te	0.32	0.06	0.30		0.62
Cs	1410	791	2918	1423	785
Ba	131	52	289	87	592
La	0.21		0.08	0.14	0.82
Ce	2.02	0.88	1.62	3.49	1.44
Pr	0.49	0.25	0.54	2.04	0.21
Nd	1.56	0.72	2.22	4.34	0.95
Pm	0.20	0.10	0.10	0.51	0.11
Sm	0.63	0.35	0.23	3.79	0.25
Eu	0.07	0.03		0.39	0.31
Gd	0.06	0.03		0.67	0.10
Np	0.94	0.50	1.72		0.13
U	403.52	120.18	287.78	31.34	32.70
Pu	2.09	0.96	2.41	4.51	4.00
Am	0.38	0.30	0.21	3.73	1.27
Cm	0.02		0.01	0.52	0.07

Tab. 5: Composition of the samples obtained from the experiment with a UO_2 fuel with a burn-up of 50 GWd/tU. Concentrations are given in ng/mL of the element.

	1 day	8 days	45 days	135 days	315 days
Se		0.45		3.97	
Rb	84.08	74.66	89.96	77.95	81.8
Sr	12.59	6.15	26.17	27.69	39.92
Y	0.32	0.16	0.15		0.39
Zr	38.09	4.80	2.03	2.35	
Mo	66.02	16.60	23.61		
Tc	2.76	0.48	0.72		
Ru	3.57	1.12	0.72		0.27
Rh	0.76	0.11	0.28	0.51	
Pd			1.90	4.33	0.23
Pd	0.68	0.17	0.32		0.23
Ag	8.96	5.77	2.60	12.46	10.3
Cd	14.32	0.68	0.79	3.89	0.62
Sn	3.09	6.06			3.44
Sb	31.44	15.84	28.23	19.17	5.68
Sn			0.45	1.88	
I	3.02	6.37	18.65	521.84	14.47
Te	0.60	0.59	0.33		0.66
Cs	6145.60	5817.58	6831.08	6707.36	3253.50
Ba	245.17	136.04	302.07	381.02	637
La	0.56		0.13		1.55
Ce	1.89	1.25	1.60	2.87	2.54
Pr	1.07	0.40	0.64		0.68
Nd	2.95	1.00	2.36	10.94	2.46
Pm	0.46	0.27	0.10		0.31
Sm		1.83	1.77	7.48	0.33
Eu	0.09		0.16		0.59
Gd	0.19		0.20		
Np	1.48	0.46	0.67		0.59
U	801.36	142.34	515.05	88.18	103.38
Pu	3.03	1.34	1.53	7.12	7.36
Am	0.22	0.08	0.03		0.31
Cm		0.01	0.04	0.13	0.16

Tab. 6: Composition of the samples obtained from the experiment with a UO_2 fuel with a burn-up of 50 GWd/tU and two series of defects. Concentrations are given in ng/mL of the element.

	1 day	8 days	45 days	135 days	315 days
Se	0.02		0.06		
Rb	16.36	28.75	35.42	272.42	159.9
Sr	14.69	4.17	44.24	47.34	67.07
Y	0.11	0.22	0.86		0.27
Zr	8.06	5.40	3.31		0.51
Mo	29.70	24.55	17.38	48.26	18.5
Tc	2.85	2.47	5.29	2.82	
Ru	0.45	0.19	0.81		
Rh	0.34	0.12	1.13		
Pd	1.10	0.12	4.35	5.83	0.32
Pd	1.31	0.08	2.80		0.22
Ag	6.84	8.56	26.19	7.19	19.2
Cd	19.12	2.63	4.30	2.62	3.74
Sn		1.48	2.36		1.91
Sb	9.96	5.18	13.26	9.68	0.94
Sn		0.03		3.80	
I		0.56	0.80	136.02	10.97
Te	0.07	0.25	0.41	2.33	1.51
Cs	675	1867	2286	18362	7940
Ba	61.91	58.37	345.99	1134.20	1429
La			1.78		1.96
Ce	0.36	1.10	3.47		3.61
Pr	0.15	0.34	1.56		0.41
Nd	0.47	1.52	5.53	2.76	1.76
Pm	0.05	0.13	0.61		0.36
Sm	0.16	0.35	2.23	5.03	2.95
Eu	0.02	0.07	0.34	0.62	1.36
Gd			0.17		
Np	0.36	0.58	2.65	1.68	0.69
U	173.04	443.22	1866.80	845.30	149.88
Pu	0.59	0.85	0.96	0.45	1.58
Am		0.03	0.04		0.26
Cm			0.01	0.51	

Potentiostatic measurements on UO_2 (FIGURES 1-4)

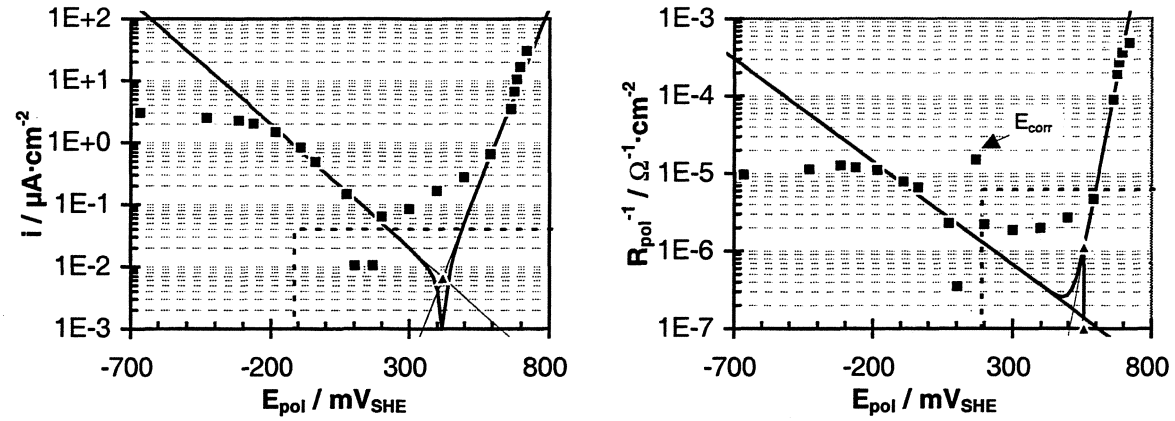

Fig. 1: Potentiostatic polarisation curves obtained from unirradiated UO_2 in air saturated 95% saturated NaCl solution (T = 22°C, C(O_2) = 7.4 ppm, initial pH 7.1, tpol = 10 min, A_{el} = 0.478 cm^2, d_{el} = 1.5 mm).

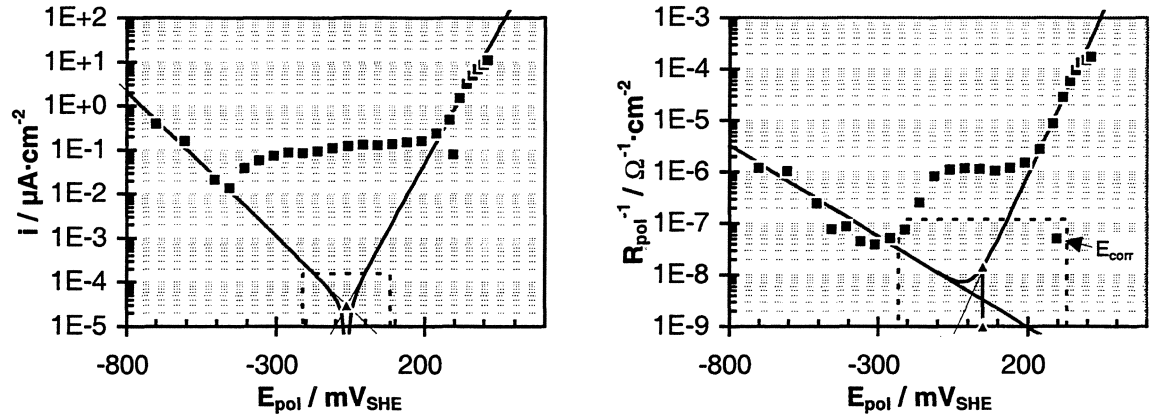

Fig. 2: Potentiostatic polarisation curves obtained from unirradiated UO_2 in N_2-purged synthetic groundwater (T = 23°C, p(O_2) < 1 mbar, initial pH 8.4, tpol = 10 min, A_{el} = 0.478 cm^2, d_{el} = 1 mm).

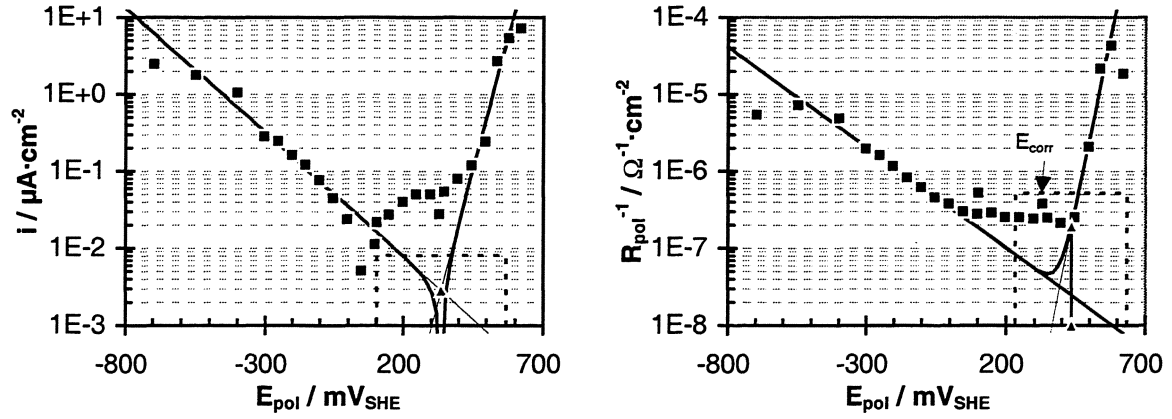

Fig. 3: Potentiostatic polarisation curves obtained from unirradiated UO_2 in N_2-purged synthetic groundwater (T = 60°C, p(O_2) < 1 mbar, initial pH 7.4, tpol = 20 min, A_{el} = 0.478 cm^2, d_{el} = 0.9 mm).

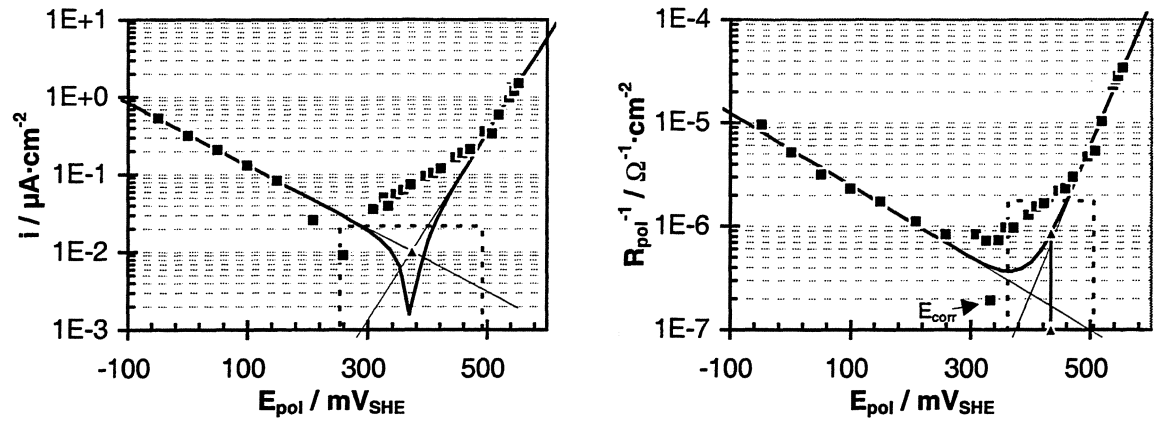

Fig. 4: Potentiostatic polarisation curves obtained from unirradiated UO_2 in N_2-purged synthetic groundwater ($T = 60°C$, $p(O_2) < 1$ mbar, initial pH 7.7, tpol = 60 min, $A_{el} = 0.478\ cm^2$, $d_{el} = 1$ mm).

OPEN CIRCUIT POTENTIALS (FIGURES 5-15)
UNIRRADIATED UO_2

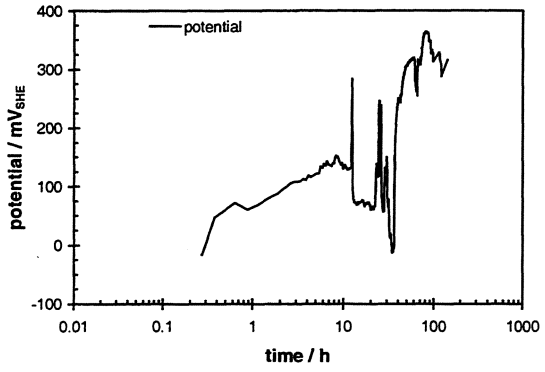

Fig. 5: Open circuit potential of unirradiated UO_2 at 60°C in N_2-purged synthetic groundwater ($^{max}E_{corr} = 364\ mV_{SHE}$, $C(O_2) = 0.05$ ppm, initial pH 7.7)

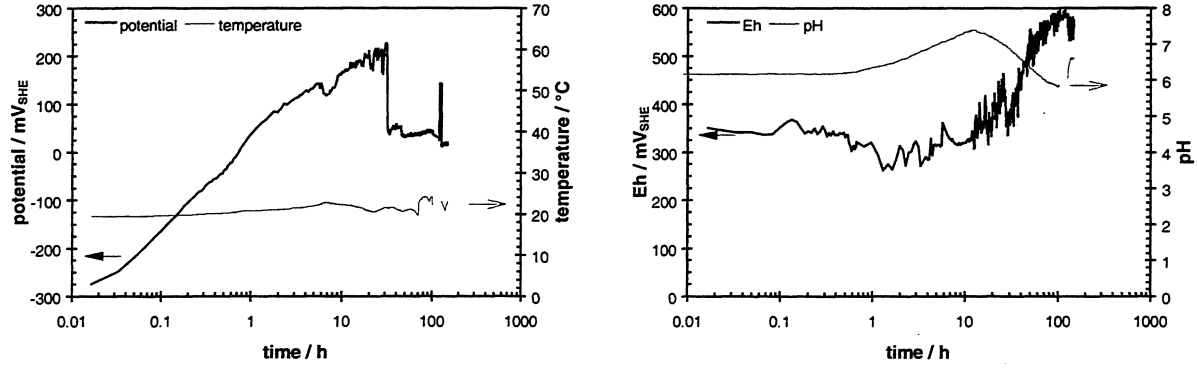

Fig. 6: Open circuit potential of unirradiated UO_2 and related temperature, pH and Eh data at 22°C in 95% saturated NaCl solution ($^{max}E_{corr} = 226\ mV_{SHE}$)

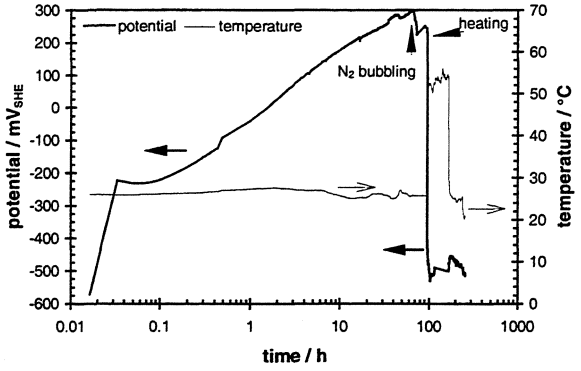

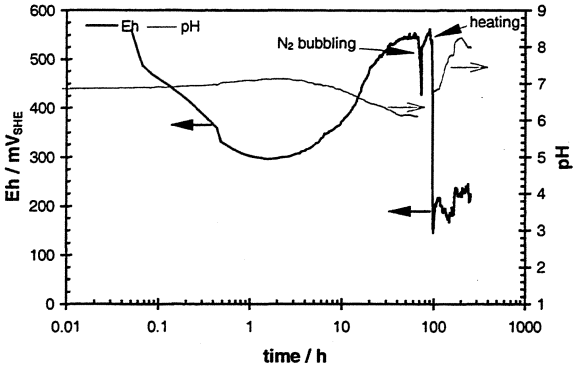

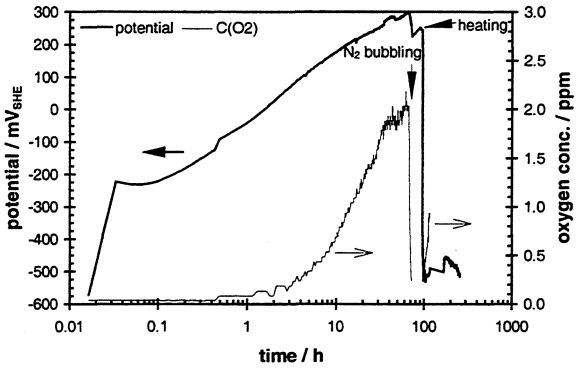

Fig. 7: Open circuit potential of unirradiated UO_2, related temperature, pH, Eh and oxygen concentration data in 95% saturated NaCl solution ($^{max}E_{corr}$ = 299 mV_{SHE})

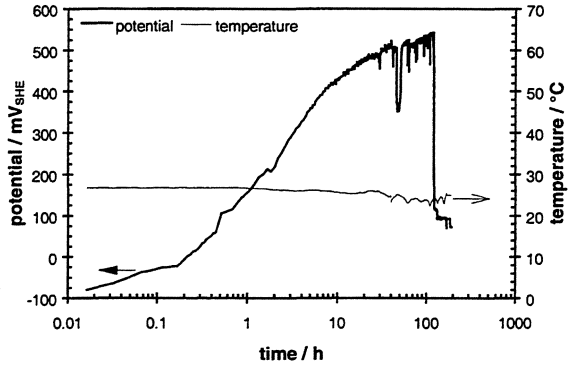

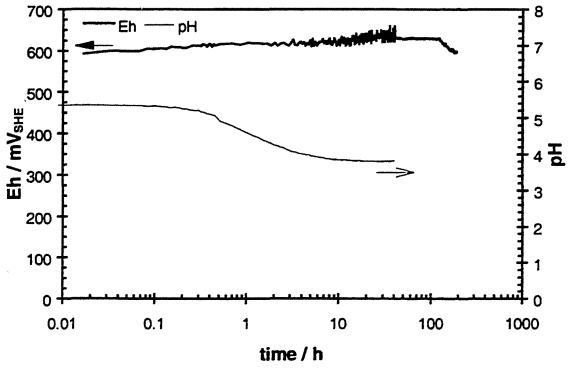

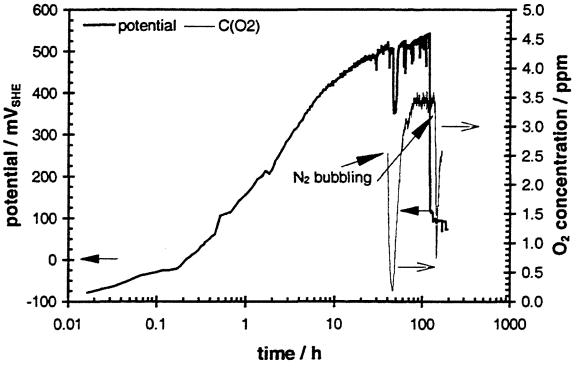

Fig. 8: Open circuit potential of unirradiated UO_2, related temperature, pH, Eh and oxygen concentration data in 95% saturated NaCl solution ($^{max}E_{corr}$ = 543 mV_{SHE})

SPENT FUEL

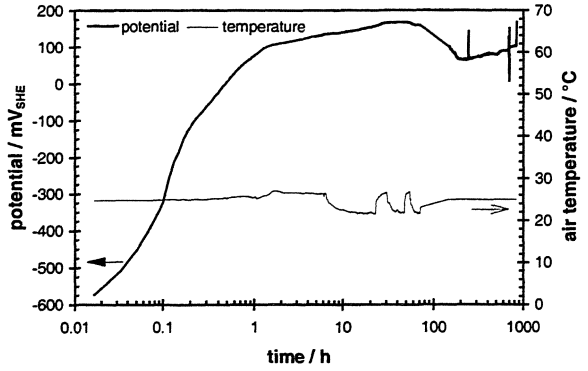

Fig. 9: Open circuit potential of used UO_2 fuel B2 (burn-up: 31.5 GWd/t) and related temperature, in synthetic ($^{max}E_{corr}$ = 168 mV_{SHE}, T: 22 – 28°C, $C(O_2)$ < 2 ppm, initial pH 8)

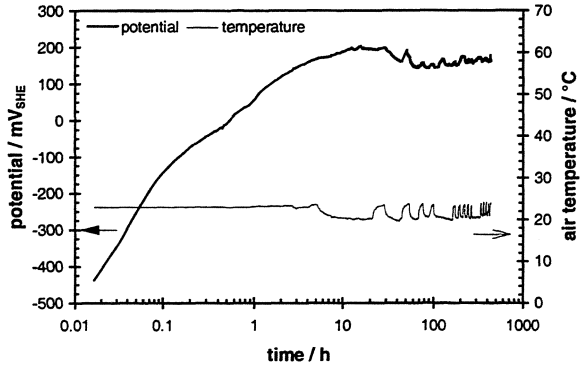

Fig. 10: Open circuit potential of used UO_2 fuel B2 (burn-up: 31.5 GWd/t) and related temperature, in synthetic groundwater ($^{max}E_{corr}$ = 204 mV_{SHE}, T: 20 – 25°C, $C(O_2)$ < 2 ppm, initial pH 7.6)

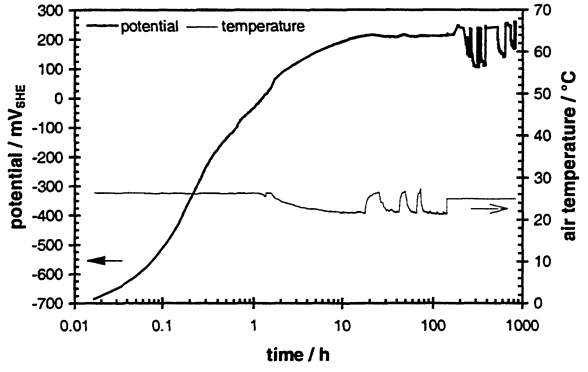

Fig. 11: Open circuit potential of used UO_2 fuel B3 (burn-up: 45.2 GWd/t) and related temperature, in synthetic groundwater ($^{max}E_{corr}$ = 260 mV_{SHE}, T: 22 – 28°C, $C(O_2)$ < 2 ppm, initial pH 8)

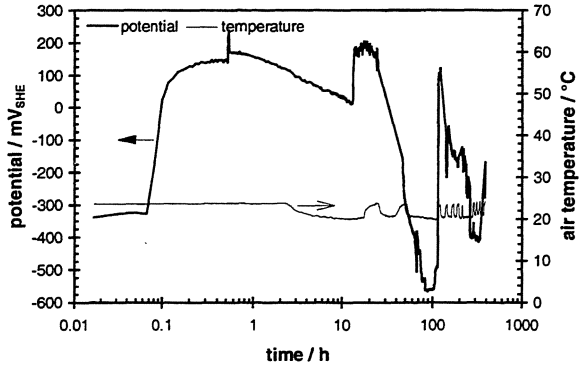

Fig. 12: Open circuit potential of used UO_2 fuel B4 (burn-up: 53.1 GWd/t) and related temperature, in synthetic groundwater ($^{max}E_{corr}$ = 239 mV_{SHE}, T: 22 – 25°C, $C(O_2)$ < 2 ppm, initial pH 7.6)

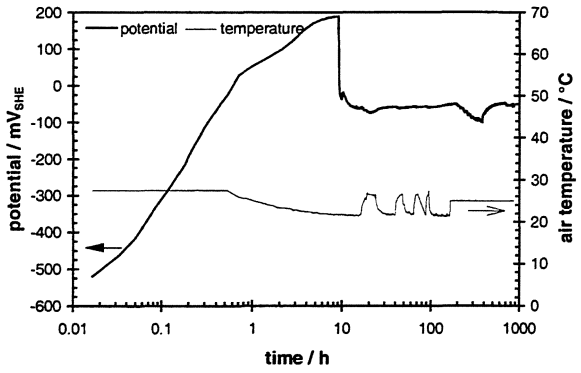

Fig. 13: Open circuit potential of used UO_2 fuel B4 (burn-up: 53.1 GWd/t) and related temperature, in 95% saturated NaCl solution ($^{max}E_{corr}$ = 190 mV_{SHE}, T: 22 – 28°C, $C(O_2)$ < 2 ppm, initial pH 7.2)

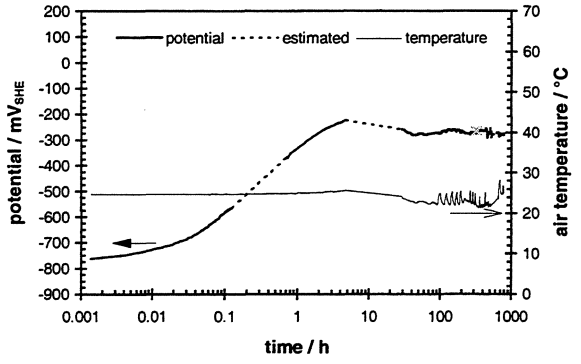

Fig. 14: Open circuit potential of used MOX fuel (burn-up: 21.1 GWd/t) and related temperature, in 95% saturated NaCl solution ($^{max}E_{corr}$ = -256 mV_{SHE}, T: 22 – 28°C, $C(O_2)$ < 2 ppm, initial pH 7.2)

BASE METALS

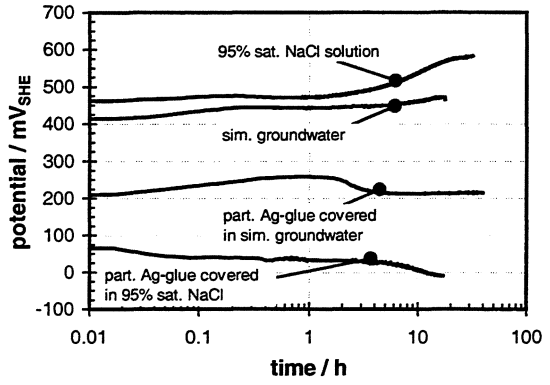

Fig. 15: Open circuit potentials of gold coated brass (MS58) in chloride containing media

CALCULATED FUEL COMPOSITIONS OF FUELS USED FOR LEACHING EXPERIMENTS AND ELECTROCHEMICAL MEASUREMENTS (ITU DATA)

Tab. 7: ORIGEN calculation of UO_2 fuel composition (burn-up 31.5 GWd/t)

Mass-number	Element E1	E2	E3	Fuel type: UO_2, B2 (31.5 GWd/tU) calculated content of isotope E1 $g \cdot t^{-1}_{fuel}$	calculated content of isotope E2 $g \cdot t^{-1}_{fuel}$	calculated content of isotope E3 $g \cdot t^{-1}_{fuel}$
80	Se			12.82		
82	Se	Kr		31.39	0.67	
83	Kr			38.79		
84	Kr			105.6		
85	Kr	Rb		12.78	107.9	
86	Kr			180.1		
87	Rb			239.5		
88	Sr			329.3		
89	Y			442.2		
90	Sr	Zr		417.7	122.8	
91	Zr			571.8		
92	Zr			620.4		
93	Zr			681.4		
94	Zr			738		
95	Mo			735.1		
96	Zr	Mo		767.6	27.38	
97	Mo			761.1		
98	Mo			784.2		
99	Tc			798.3		
100	Mo	Ru		892.5	47.15	
101	Ru			744.1		
102	Ru			728.8		
103	Rh			438.6		
104	Ru	Pd		501.2	208.8	
105	Pd			240.5		
106	Pd			438.2		
107	Pd			195.8		
108	Pd			122.3		
109	Ag			65.95		
110	Pd	Cd		39.9	37.54	
111	Cd			19.9		
112	Cd			9.33		
113	Cd			0.22		
114	Cd			11.16		
115	In			1.14		
116	Cd	Sn		4.55	2.05	
117	Sn			3.94		
118	Sn			3.31		
119	Sn			3.47		
120	Sn			3.43		
121	Sb			3.46		
122	Sn			4.74		
123	Sb			4.19		
124	Sn	Te		8.23	0.09	
125	Sb	Te		0.74	9.74	
126	Sn	Te		20	0.56	
127	I			44.82		
128	Te	Xe		83.07	2.77	
129	I			170.2		
130	Te	Xe		343	0.35	
131	Xe			397.3		
132	Xe			1046		
133	Cs			1022		
134	Xe	Cs	Ba	1448	6.58	209.9
135	Cs			191.1		
136	Xe	Ba		2351	15.38	
137	Cs	Ba		932.7	262	
138	Ba			1231		
139	La			1152		
140	Ce			1192		
141	Pr			1067		
142	Ce	Nd		1071	16.06	
143	Nd			777.1		
144	Nd			1250		
145	Nd			651.3		
146	Nd			636.1		
147	Pm	Sm		9.86	155.3	
148	Nd	Sm		341.1	121.9	
149	Sm			8.42		
150	Nd	Sm		163.2	358.4	
151	Sm			39.47		
152	Sm			90.23		
153	Eu			110.8		
154	Sm	Eu	Gd	31.16	16.31	21.13
155	Eu	Gd		1.12	3.35	
156	Gd			63.34		
158	Gd			11.93		
234	U			143.2		
235	U			8382		
236	U			4407		
237	Np			412.9		
238	U	Pu		945600	112.5	
239	Pu			4635		
240	Pu			2049		
241	Pu	Am		536.9	335.3	
242	Pu			296.9		
243	Am			67.01		
244	Cm			12.46		
245	Cm			0.97		
246	Cm			0.11		

Element	calculated content of element $g \cdot g^{-1}_{fuel}$
Se	4.42E-05
Rb	3.47E-04
Sr	7.47E-04
Y	4.42E-04
Zr	3.50E-03
Mo	3.20E-03
Tc	7.98E-04
Ru	2.02E-03
Rh	4.39E-04
Pd	1.25E-03
Ag	6.60E-05
Cd	8.27E-05
Sn	4.92E-05
Sb	8.39E-06
I	2.15E-04
Te	4.36E-04
Cs	2.15E-03
Ba	1.72E-03
La	1.15E-03
Ce	2.26E-03
Pr	1.07E-03
Nd	3.83E-03
Pm	9.86E-06
Sm	8.05E-04
Eu	1.28E-04
Gd	9.98E-05
Np	4.13E-04
U	9.59E-01
Pu	7.63E-03
Am	4.02E-04
Cm	1.35E-05

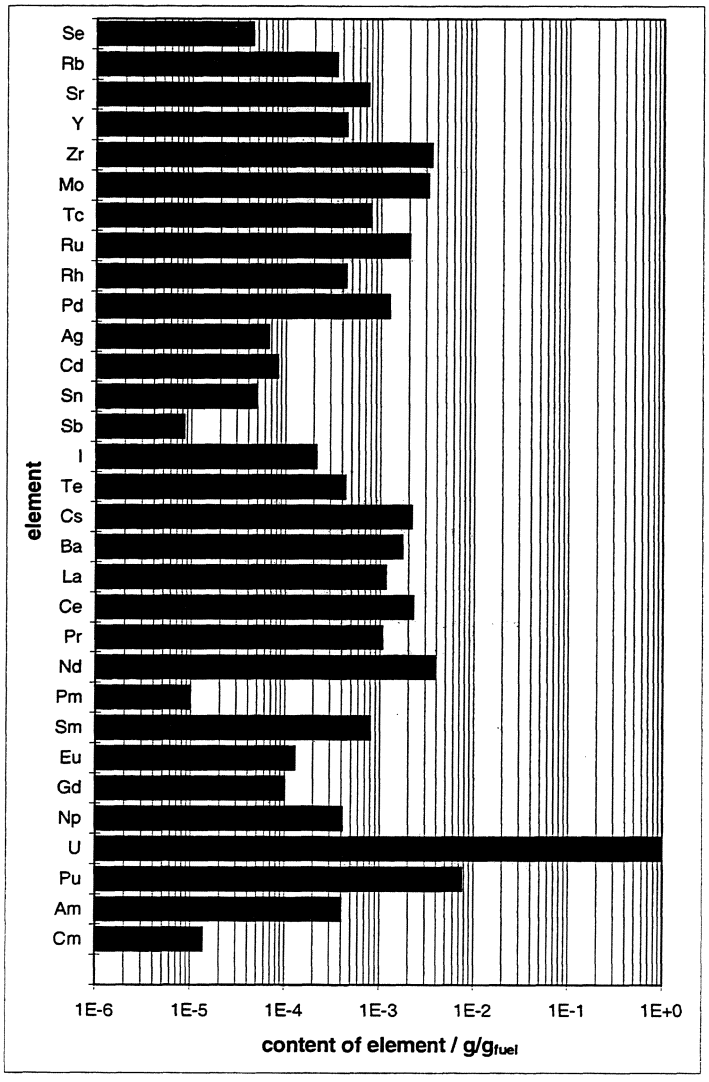

Tab. 8: ORIGEN calculation of UO_2 fuel composition (burn-up 45.7 GWd/t).

Mass-number	Element			Fuel type: UO_2, B3 (45.7 GWd/tU)		
	E1	E2	E3	calculated content of isotope E1 $g \cdot t^{-1}_{fuel}$	calculated content of isotope E2 $g \cdot t^{-1}_{fuel}$	calculated content of isotope E3 $g \cdot t^{-1}_{fuel}$
80	Se			17.82		
82	Se	Kr		43	1.42	
83	Kr			44.18		
84	Kr			150		
85	Kr	Rb		16.92	143.3	
86	Kr			237.7		
87	Rb			315.4		
88	Sr			432.3		
89	Y			578		
90	Sr	Zr		545.8	161.2	
91	Zr			756.4		
92	Zr			835.6		
93	Zr			921.9		
94	Zr			1024		
95	Mo			998.6		
96	Zr	Mo		1076	62.66	
97	Mo			1079		
98	Mo			1132		
99	Tc			1118		
100	Mo	Ru		1295	109.4	
101	Ru			1072		
102	Ru			1115		
103	Rh			568.6		
104	Ru	Pd		820.9	451.2	
105	Pd			329.4		
106	Pd			860.5		
107	Pd			359		
108	Pd			226.9		
109	Ag			101.2		
110	Pd	Cd		75.88	100.7	
111	Cd			37.65		
112	Cd			17.33		
113	Cd			0.24		
114	Cd			19.62		
115	In			1.3		
116	Cd	Sn		7.25	4.07	
117	Sn			6.35		
118	Sn			5.34		
119	Sn			5.53		
120	Sn			5.43		
121	Sb			5.25		
122	Sn			7.6		
123	Sb			6.37		
124	Sn	Te		13.1	0.15	
125	Sb	Te		1.2	15.76	
126	Sn	Te		32.34	0.96	
127	I			70.95		
128	Te	Xe		127	7.26	
129	I			258.5		
130	Te	Xe		501.6	0.63	
131	Xe			472.1		
132	Xe			1662		
133	Cs			1313		
134	Xe	Cs	Ba	2090	13.84	439
135	Cs			231.6		
136	Xe	Ba		3523	28.32	
137	Cs	Ba		1357	380.2	
138	Ba			1763		
139	La			1634		
140	Ce			1709		
141	Pr			1504		
142	Ce	Nd		1519	37.38	
143	Nd			901.3		
144	Nd			1928		
145	Nd			861.5		
146	Nd			955.1		
147	Pm	Sm		9.8	150.2	
148	Nd	Sm		491.5	167.9	
149	Sm			10.34		
150	Nd	Sm		246.7	555.9	
151	Sm			52.08		
152	Sm			122		
153	Eu			183.5		
154	Sm	Eu	Gd	51.57	66.49	43.17
155	Eu	Gd		2.17	6.48	
156	Gd			179.4		
158	Gd			23.57		
234	U			110.8		
235	U			3715		
236	U			4843		
237	Np			666.6		
238	U	Pu		933400	264.9	
239	Pu			4732		
240	Pu			2489		
241	Pu	Am		758.5	468.8	
242	Pu			693.4		
243	Am			250		
244	Cm			81.38		
245	Cm			8.47		
246	Cm			1.69		

B3 (45.7 GWd/tU)	
Element	calculated content of element $g \cdot g^{-1}_{fuel}$
Se	6.08E-05
Rb	4.59E-04
Sr	9.78E-04
Y	5.78E-04
Zr	4.78E-03
Mo	4.57E-03
Tc	1.12E-03
Ru	3.12E-03
Rh	5.69E-04
Pd	2.30E-03
Ag	1.01E-04
Cd	1.83E-04
Sn	7.98E-05
Sb	1.28E-05
I	3.29E-04
Te	6.45E-04
Cs	2.92E-03
Ba	2.61E-03
La	1.63E-03
Ce	3.23E-03
Pr	1.50E-03
Nd	5.42E-03
Pm	9.80E-06
Sm	1.11E-03
Eu	2.52E-04
Gd	2.53E-04
Np	6.67E-04
U	9.42E-01
Pu	8.94E-03
Am	7.19E-04
Cm	9.15E-05

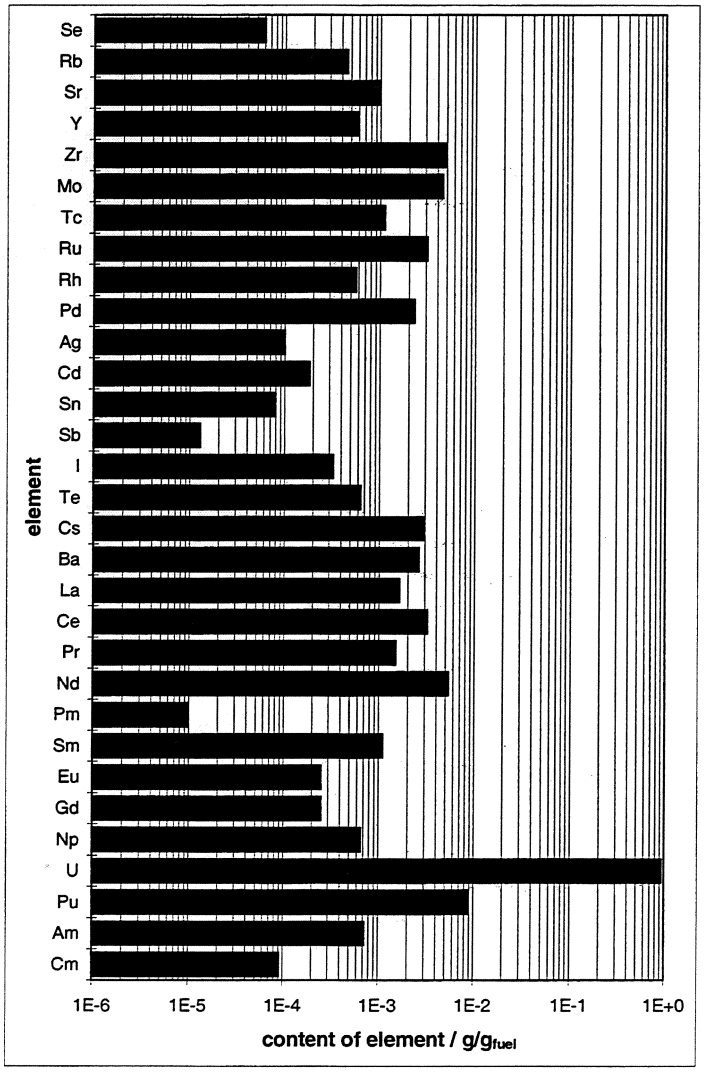

Tab. 9: ORIGEN calculation of UO_2 fuel composition (burn-up 53.1 GWd/t).

Mass-number	Element			Fuel type: UO_2, B4 (53.1 GWd/tU) calculated content of isotope E1	calculated content of isotope E2	calculated content of isotope E3
	E1	E2	E3	$g \cdot t^{-1}_{fuel}$	$g \cdot t^{-1}_{fuel}$	$g \cdot t^{-1}_{fuel}$
80	Se			20.22		
82	Se	Kr		48.35	1.89	
83	Kr			44.32		
84	Kr			171.4		
85	Kr	Rb		17.22	159.2	
86	Kr			260.9		
87	Rb			345.7		
88	Sr			472.6		
89	Y			630.3		
90	Sr	Zr		577.6	193.9	
91	Zr			830.2		
92	Zr			929.8		
93	Zr			1027		
94	Zr			1160		
95	Mo			1095		
96	Zr	Mo		1227	109.9	
97	Mo			1236		
98	Mo			1313		
99	Tc			1262		
100	Mo	Ru		1507	155.8	
101	Ru			1240		
102	Ru			1336		
103	Rh			562		
104	Ru	Pd		1017	676.1	
105	Pd			537.2		
106	Pd			981.4		
107	Pd			465.2		
108	Pd			295		
109	Ag			117.8		
110	Pd	Cd		99.96	152.7	
111	Cd			50.98		
112	Cd			22.79		
113	Cd			0.24		
114	Cd			25		
115	In			1.29		
116	Cd	Sn		8.87	5.42	
117	Sn			7.814		
118	Sn			6.588		
119	Sn			6.759		
120	Sn			6.63		
121	Sb			6.21		
122	Sn			9.319		
123	Sb			7.527		
124	Sn	Te		16.01	0.33	
125	Sb	Te		1.19	19.84	
126	Sn	Te		39.84	1.28	
127	I			84.27		
128	Te	Xe		152	11.28	
129	I			308.3		
130	Te	Xe		586.2	0.81	
131	Xe			483.8		
132	Xe			2027		
133	Cs			1401		
134	Xe	Cs	Ba	2412	14.88	606.2
135	Cs			433		
136	Xe	Ba		3957	54.6	
137	Cs	Ba		1540	482.3	
138	Ba			2036		
139	La			1875		
140	Ce			1966		
141	Pr			1720		
142	Ce	Nd		1736	57.71	
143	Nd			911.6		
144	Nd			2320		
145	Nd			952.3		
146	Nd			1132		
147	Pm	Sm		7.77	152.2	
148	Nd	Sm		569.1	279.7	
149	Sm			6.949		
150	Nd	Sm		293.5	580.6	
151	Sm			53.47		
152	Sm			129.4		
153	Eu			210		
154	Sm	Eu	Gd	64.91	40.55	43.17
155	Eu	Gd		2.66	8.17	
156	Gd			333		
158	Gd			34.46		
234	U			33.73		
235	U			2113		
236	U			4659		
237	Np			745.5		
238	U	Pu		927400	380.6	
239	Pu			4696		
240	Pu			2605		
241	Pu	Am		799.6	515.6	
242	Pu			902		
243	Am			395.5		
244	Cm			165.1		
245	Cm			19.35		
246	Cm			5.14		

B4 (53.1 GWd/tU)	
Element	calculated content of element $g \cdot g^{-1}_{fuel}$
Se	6.86E-05
Rb	5.05E-04
Sr	1.05E-03
Y	6.30E-04
Zr	5.37E-03
Mo	5.26E-03
Tc	1.26E-03
Ru	3.75E-03
Rh	5.62E-04
Pd	3.05E-03
Ag	1.18E-04
Cd	2.61E-04
Sn	9.84E-05
Sb	1.49E-05
I	3.93E-04
Te	7.60E-04
Cs	3.39E-03
Ba	3.18E-03
La	1.88E-03
Ce	3.70E-03
Pr	1.72E-03
Nd	6.24E-03
Pm	7.77E-06
Sm	1.27E-03
Eu	2.53E-04
Gd	4.19E-04
Np	7.46E-04
U	9.34E-01
Pu	9.38E-03
Am	9.11E-04
Cm	1.90E-04

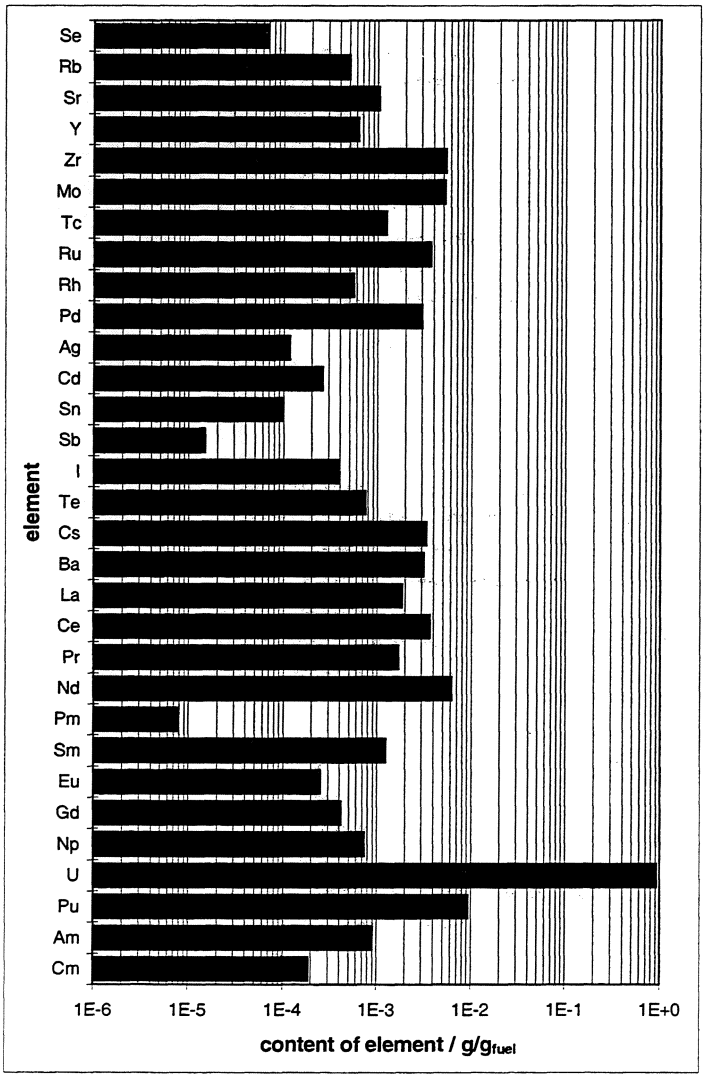

Tab. 10: ORIGEN calculation of MOX composition (21.1 GWd/tU)

Mass-number	Element			Fuel type: MOX (21.1 GWd/tU) calculated content of isotope E1 $g \cdot t^{-1}_{fuel}$	calculated content of isotope E2 $g \cdot t^{-1}_{fuel}$	calculated content of isotope E3 $g \cdot t^{-1}_{fuel}$
	E1	E2	E3			
80	Se			6.9		
81	Br			10.7		
82	Se	Kr		14.3	0.3	
83	Kr			21.4		
84	Kr			38.9		
85	Kr	Rb		5.9	37.9	
86	Kr			64.1		
87	Rb			80.6		
88	Sr			112.6		
89	Y			142.9		
90	Sr	Zr		148.7	28.9	
91	Zr			208.3		
92	Zr			252.4		
93	Zr			323.9		
94	Zr			357.1		
95	Mo			405		
96	Zr	Mo		433.2	3.738	
97	Mo			465.4		
98	Mo			501.4		
99	Tc			527.7		
100	Mo	Ru		601.4	12.65	
101	Ru			535.6		
102	Ru			558.2		
103	Rh			556.7		
104	Ru	Pd		557	49.74	
105	Pd			484.4		
106	Pd	Ru		432.3	2.888	
107	Pd			329.9		
108	Pd			237.1		
109	Ag			140.5		
110	Pd	Cd		71.01	14.79	
111	Cd			34.29		
112	Cd			15.71		
113	Cd			0.7365		
114	Cd			17.31		
115	In	Sn		3.786	0.1898	
116	Cd	Sn		4.624	1.74	
117	Sn			4.478		
118	Sn			4.535		
119	Sn			4.628		
120	Sn			4.638		
121	Sb			4.739		
122	Sn			4.996		
123	Sb			5.711		
124	Sn	Te		7.049	0.05513	
125	Sb	Te		2.122	11.33968	
126	Sn	Te		20.56	0.5628	
127	I			49.58		
128	Te	Xe		84.82	0.5709	
129	I			150.8		
130	Te	Xe		264.4	2.3	
131	Xe			393.7		
132	Xe			633.1		
133	Cs			796.1		
134	Xe	Cs	Ba	905.6	2.295	21.19
135	Cs			555.9		
136	Xe	Ba		1164	13.68	
137	Cs	Ba		672	126.2	
138	Ba			738.6		
139	La			719.8		
140	Ce			712		
141	Pr			665.7		
142	Ce	Nd		634.3	2.682	
143	Nd			553.1		
144	Nd	Ce		546.4	0.8274	
145	Nd			400.5		
146	Nd			349.7		
147	Pm	Sm		33.09	198.8	
148	Nd	Sm		232.2	41.4	
149	Sm			5.998		
150	Nd	Sm		137.4	173.3	
151	Sm	Eu		31.93	1.684	
152	Sm	Eu		137.9	0.14	
153	Eu			69.95		
154	Sm	Eu	Gd	40.07	5.078	3.8
155	Eu	Gd		5.055	7.273	
156	Gd			32.33		
158	Gd			19.81		
159	Tb			3.948		
160	Gd			1.883		
234	U			7.252		
235	U			5126		
236	U			268.8		
237	Np			48.64		
238	U	Pu		9.20E+05	143.3	
239	Pu			23110		
240	Pu			13330		
241	Pu	Am		7674	3459	
242	Pu	Am		3883	11.93	
243	Am	Cm		429.9	0.5038	
244	Cm			35.02		
245	Cm			0.7691		
246	Cm			0.02271		

Element	MOX (21.1 GWd/tU) calculated content of element $g \cdot g^{-1}_{fuel}$
Se	2.12E-05
Br	1.07E-05
Rb	1.18E-04
Sr	2.61E-04
Y	1.43E-04
Zr	1.60E-03
Mo	1.98E-03
Tc	5.28E-04
Ru	1.67E-03
Rh	5.57E-04
Pd	1.60E-03
Ag	1.41E-04
Cd	8.75E-05
Sn	5.28E-05
Sb	1.26E-05
I	2.00E-04
Te	3.61E-04
Cs	2.03E-03
Ba	9.00E-04
La	7.20E-04
Ce	1.35E-03
Pr	6.66E-04
Nd	2.22E-03
Pm	3.31E-05
Sm	6.29E-04
Eu	8.19E-05
Gd	6.51E-05
Tb	3.95E-06
Np	4.86E-05
U	9.25E-01
Pu	4.81E-02
Am	3.90E-03
Cm	3.63E-05

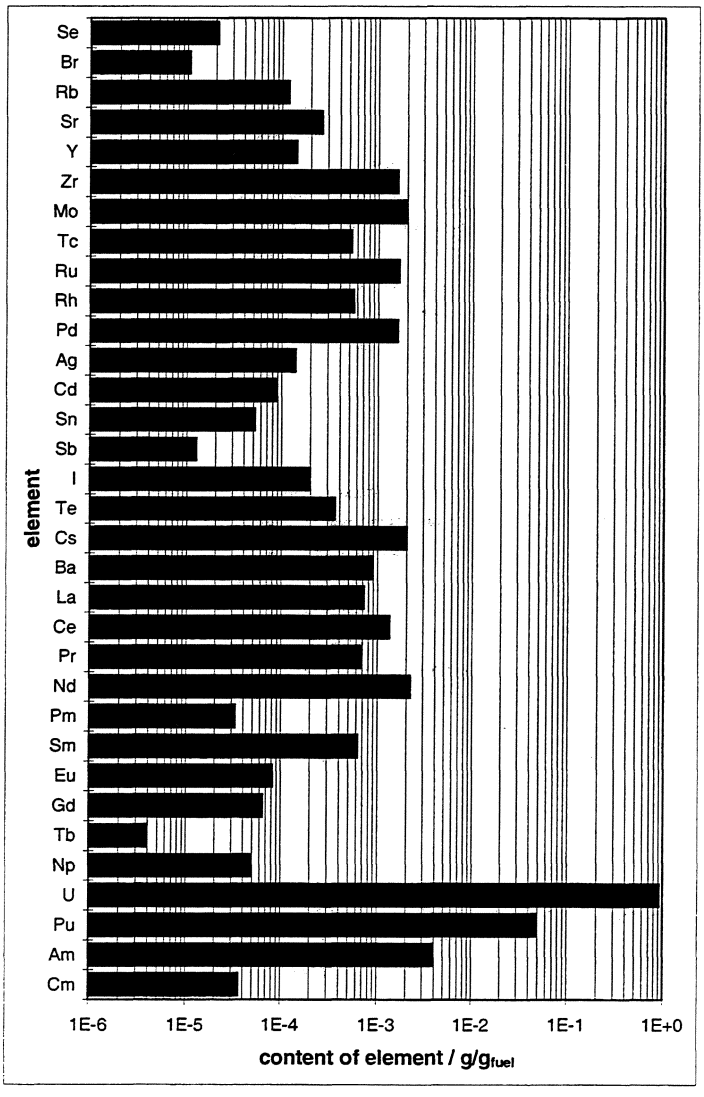

Appendix 7: Original test data obtained by SCK·CEN

FIRST TEST SERIES

***TABLE 1** : Uranium concentrations of the media in the test containers during the washing steps*

medium	start date	washing date (= sampling date)	contact time (days)	accumulated duration (days)	sample nr	U conc (µg/l)	U conc (mol/l)	mol U /m²/day	total U washed off (µg)
RIC	97-03-26	97-03-28	2	2	RIC970320-1/U2/v/1	15700	6,6E-05	3,3E-05	628
RIC	97-03-26	97-04-01	4	6	RIC970320-1/U2/v/2	2220	9,3E-06	2,3E-06	717
RIC	97-03-26	97-04-04	3	9	RIC970320-1/U2/v/3	559	2,3E-06	7,8E-07	739
RIC	97-03-26	97-04-07	3	12	RIC970320-1/U2/v/4	200	8,4E-07	2,8E-07	747
RIC	97-03-26	97-04-11	4	16	RIC970320-1/U2/v/5	144	6,1E-07	1,5E-07	753
RIC	97-03-26	97-04-14	3	19	RIC970320-1/U2/v/6	86	3,6E-07	1,2E-07	756
RIC	97-03-26	97-04-21	7	26	RIC970320-1/U2/v/7	*70*	*3,0E-07*	*4,2E-08*	759
RIC	97-03-26	97-04-28	7	33	RIC970320-1/U2/v/8	*70*	*3,0E-07*	*4,2E-08*	762
RIC	97-03-26	97-05-13	15	48	RIC-1/U2/v/9	151	6,3E-07	**4,2E-08**	768
RIC	97-03-26	97-05-21	8	56	RIC-1/U2/v/10	*104*	*4,4E-07*	*5,5E-08*	772
RIC	97-03-26	97-05-28	7	63	RIC-1/U2/v/11	*91*	*3,8E-07*	*5,5E-08*	776
RIC	97-03-26	97-06-04	7	70	RIC-1/U2/v/12	*91*	*3,8E-07*	*5,5E-08*	779
RIC	97-03-26	97-06-13	9	79	RIC-1/U2/v/13	*117*	*4,9E-07*	*5,5E-08*	784
RIC	97-03-26	97-06-20	7	86	RIC-1/U2/v/14	91,1	3,8E-07	5,5E-08	788
RIC	97-03-26	97-06-20	7	86	RIC-2/U2/v/14	102	4,3E-07	6,1E-08	
SCW	97-03-26	97-03-28	2	2	SCW970226-1/U2/v/1	19700	8,3E-05	4,1E-05	788
SCW	97-03-26	97-04-01	4	6	SCW970226-1/U2/v/2	3600	1,5E-05	3,8E-06	932
SCW	97-03-26	97-04-04	3	9	SCW970226-1/U2/v/3	1200	5,0E-06	1,7E-06	980
SCW	97-03-26	97-04-07	3	12	SCW970226-1/U2/v/4	703	3,0E-06	9,8E-07	1008
SCW	97-03-26	97-04-11	4	16	SCW970226-1/U2/v/5	731	3,1E-06	7,7E-07	1037
SCW	97-03-26	97-04-14	3	19	SCW970226-1/U2/v/6	548	2,3E-06	7,7E-07	1059
SCW	97-03-26	97-04-21	7	26	SCW970226-1/U2/v/7	*239*	*1,0E-06*	*1,4E-07*	1069
SCW	97-03-26	97-04-28	7	33	SCW970226-1/U2/v/8	*239*	*1,0E-06*	*1,4E-07*	1078
SCW	97-03-26	97-05-13	15	48	SCW-1/U2/v/9	513	2,2E-06	1,4E-07	1099
SCW	97-03-26	97-05-21	8	56	SCW-1/U2/v/10	*152*	*6,4E-07*	*8,0E-08*	1105
SCW	97-03-26	97-05-28	7	63	SCW-1/U2/v/11	*133*	*5,6E-07*	*8,0E-08*	1110
SCW	97-03-26	97-06-04	7	70	SCW-1/U2/v/12	*133*	*5,6E-07*	*8,0E-08*	1116
SCW	97-03-26	97-06-13	9	79	SCW-1/U2/v/13	*171*	*7,2E-07*	*8,0E-08*	1123
SCW	97-03-26	97-06-20	7	86	SCW-1/U2/v/14	133	5,6E-07	**8,0E-08**	1128
SCW	97-03-26	97-06-20	7	86	SCW-2/U2/v/14	192	8,1E-07	1,2E-07	
SCWHA	97-03-26	97-03-28	2	2	SCWHA970304-1/U2/v/1	17200	7,2E-05	3,6E-05	688
SCWHA	97-03-26	97-04-01	4	6	SCWHA970304-1/U2/v/2	3220	1,4E-05	3,4E-06	817
SCWHA	97-03-26	97-04-04	3	9	SCWHA970304-1/U2/v/3	948	4,0E-06	1,3E-06	855
SCWHA	97-03-26	97-04-07	3	12	SCWHA970304-1/U2/v/4	541	2,3E-06	7,6E-07	876
SCWHA	97-03-26	97-04-11	4	16	SCWHA970304-1/U2/v/5	376	1,6E-06	3,9E-07	891
SCWHA	97-03-26	97-04-14	3	19	SCWHA970304-1/U2/v/6	138	5,8E-07	1,9E-07	897
SCWHA	97-03-26	97-04-21	7	26	SCWHA-1/U2/5/v	207	8,7E-07	1,2E-07	905
SCWHA	97-03-26	97-04-28	7	33	SCWHA970327-1/U2/v/8	*92*	*3,9E-07*	*5,5E-08*	909
SCWHA	97-03-26	97-05-13	15	48	SCWHA-1/U2/v/9	197	8,3E-07	5,5E-08	917
SCWHA	97-03-26	97-05-21	8	56	SCWHA-1/U2/v/10	*99*	*4,2E-07*	*5,2E-08*	921
SCWHA	97-03-26	97-05-28	7	63	SCWHA-1/U2/v/11	*87*	*3,7E-07*	*5,2E-08*	924
SCWHA	97-03-26	97-06-04	7	70	SCWHA-1/U2/v/12	*87*	*3,7E-07*	*5,2E-08*	928
SCWHA	97-03-26	97-06-13	9	79	SCWHA-1/U2/v/13	*112*	*4,7E-07*	*5,2E-08*	932
SCWHA	97-03-26	97-06-20	7	86	SCWHA-1/U2/v/14	86,9	3,7E-07	**5,2E-08**	936
SCWHA	97-03-26	97-06-20	7	86	SCWHA-2/U2/v/14	211	8,9E-07	2,3E-08	
SCWHA\C	97-03-21	97-03-25	4	4	SCWHA\C970210-1/U2/v/1	1830	7,7E-06	1,9E-06	73
SCWHA\C	97-03-21	97-03-28	3	7	SCWHA\C970210-1/U2/v/2	1280	5,4E-06	1,8E-06	124
SCWHA\C	97-03-21	97-04-01	4	11	SCWHA\C970210-1/U2/v/3	1060	4,5E-06	1,1E-06	167
SCWHA\C	97-03-21	97-04-04	3	14	SCWHA\C970210-1/U2/v/4	811	3,4E-06	1,1E-06	199
SCWHA\C	97-03-21	97-04-07	3	17	SCWHA\C970210-1/U2/v/5	680	2,9E-06	9,5E-07	226
SCWHA\C	97-03-21	97-04-09	2	19	SCWHA\C970210-1/U2/v/6	525	2,2E-06	1,1E-06	247
SCWHA\C	97-03-21	97-04-11	2	21	SCWHA\C970210-1/U2/v/7	447	1,9E-06	9,4E-07	265
SCWHA\C	97-03-21	97-04-14	3	24	SCWHA\C970210-1/U2/v/8	461	1,9E-06	6,5E-07	284
SCWHA\C	97-03-21	97-04-21	7	31	SCWHA\C970210-1/U2/v/9	*240*	*1,0E-06*	*1,4E-07*	293
SCWHA\C	97-03-21	97-04-28	7	38	SCWHA\C970210-1/U2/v/10	*240*	*1,0E-06*	*1,4E-07*	303
SCWHA\C	97-03-21	97-05-13	15	53	SCWHA\C-1/U2/v/11	514	2,2E-06	**1,4E-07**	324
SCWHA\C	97-03-21	97-05-21	8	61	SCWHA\C-1/U2/v/12	*311*	*1,3E-06*	*1,6E-07*	336
SCWHA\C	97-03-21	97-05-28	7	68	SCWHA\C-1/U2/v/13	*272*	*1,1E-06*	*1,6E-07*	347
SCWHA\C	97-03-21	97-06-03	6	74	SCWHA\C-1/U2/5/v/14	233	9,8E-07	1,6E-07	356
SCWHA\C	97-03-21	97-06-03	6	74	SCWHA\C-2/U2/5/v/14	248	1,0E-06	1,7E-07	

The values in italic are interpolations of the measured values. The 95% probability interval is within 15%.

***TABLE 2** : Uranium concentration, pH, Eh of the media in the first test series (solubility tests)*

medium	duration (days)	filtration	sample nr	U (µg/l)	U (mol/l)	pH	Eh (mV SHE)	sample nr	U (µg/l)	U (mol/l)	pH	Eh (mV SHE)
RIC	3	YM30	RIC-1/U2/1	14,3	6,0E-08	9,0		RIC-2/U2/1	27,3	1,1E-07	8,8	
RIC	10	YM30	RIC-1/U2/2	25,1	1,1E-07	9,0		RIC-2/U2/2	36,8	1,5E-07	9,1	
RIC	45	YM30	RIC-1/U2/3	295	1,2E-06	9,1	-150	RIC-2/U2/3	56	2,4E-07	9,0	-140
RIC	45	YM100	RIC-1/U5/3	124	5,2E-07	9,1	-150	RIC-2/U5/3	56,7	2,4E-07	9,0	-140
RIC	123	YM30	RIC-1/U2/4	3160	1,3E-05	9,8	267	RIC-2/U2/4	3010	1,3E-05	9,0	296
RIC	123	45µ	RIC-1/U45/4	4140	1,7E-05	9,8	267	RIC-2/U45/4	4500	1,9E-05	9,0	296
RIC	139	YM30	RIC-1/U2/5			8,1	306					
RIC	168	YM30	RIC-1/U2/6			8,3	-71					
RIC	180	YM30	RIC-1/U2/7	5997	2,5E-05	8,1						
SCW	3	YM30	SCW-1/U2/1	49,7	2,1E-07	8,6		SCW-2/U2/1	51,6	2,2E-07	8,8	
SCW	10	YM30	SCW-1/U2/2	87,6	3,7E-07	8,9		SCW-2/U2/2	85,8	3,6E-07	9,2	
SCW	46	YM30	SCW-1/U2/3	151	6,3E-07	9,7	189	SCW-2/U2/3	142	6,0E-07	9,8	182
SCW	46	YM100	SCW-1/U5/3	150	6,3E-07	9,7	189	SCW-2/U5/3	140	5,9E-07	9,8	182
SCW	123	YM30	SCW-1/U2/4	28400	1,2E-04	9,8	252	SCW-2/U2/4	18200	7,6E-05	9,7	287
SCW	123	45µ	SCW-1/U45/4	27500	1,2E-04	9,8	252	SCW-2/U45/4	17400	7,3E-05	9,7	287
SCW	139	YM30	SCW-1/U2/5			8,2	360					
SCW	168	YM30	SCW-1/U2/6			8,3	-76					
SCW	180	YM30	SCW-1/U2/7	20700	8,7E-05	8,1						
SCWHA	3	YM30	SCWHA-1/U2/1	19,2	8,1E-08	8,8		SCWHA-2/U2/1	39	1,6E-07	8,7	
SCWHA	10	YM30	SCWHA-1/U2/2	71,4	3,0E-07	9,0		SCWHA-2/U2/2	37,9	1,6E-07	9,1	
SCWHA	45	YM30	SCWHA-1/U2/3	96,3	4,0E-07	8,9	-112	SCWHA-2/U2/3	114	4,8E-07	9,1	-119
SCWHA	45	YM100	SCWHA-1/U5/3	98,6	4,1E-07	8,9	-112	SCWHA-2/U5/3	109	4,6E-07	9,1	-119
SCWHA	123	YM30	SCWHA-1/U2/4	1330	5,6E-06	8,9	246	SCWHA-2/U2/4	3870	1,6E-05	9,8	217
SCWHA	123	45µ	SCWHA-1/U45/4	2430	1,0E-05	8,9	246	SCWHA-2/U45/4	4710	2,0E-05	9,8	217
SCWHA	139	YM30	SCWHA-1/U2/4			8,2	308					
SCWHA	168	YM30	SCWHA-1/U2/5			8,2	-87					
SCWHA	180	YM30	SCWHA-1/U2/6	1285	5,4E-06	8,2						
SCWHA\C	2	YM30	SCWHA\C-1/U2/1	51,7	2,2E-07	8,4	-106	SCWHA\C-2/U2/1	80,1	3,4E-07	8,4	-80
SCWHA\C	10	YM30	SCWHA\C-1/U2/2	132	5,5E-07	8,2		SCWHA\C-2/U2/2	146	6,1E-07	8,4	
SCWHA\C	31	YM30	SCWHA\C-1/U2/3	182	7,6E-07	8,5		SCWHA\C-2/U2/3	176	7,4E-07	8,6	
SCWHA\C	31	YM100	SCWHA\C-1/U5/3	202	8,5E-07	8,6		SCWHA\C-2/U5/3	203	8,5E-07	8,6	
SCWHA\C	58	YM30	SCWHA\C-1/U2/4	185	7,8E-07	8,6	-74	SCWHA\C-2/U2/4	149	6,3E-07	8,6	-83
SCWHA\C	139	YM30	SCWHA\C-1/U2/5	717	3,0E-06	7,7	278	SCWHA\C-2/U2/5	880	3,7E-06	7,7	272
SCWHA\C	139	45µ	SCWHA\C-1/U45/5	2160	9,1E-06	7,7	278	SCWHA\C-2/U45/5	3280	1,4E-05	7,7	272
SCWHA\C	188	YM30	SCWHA\C-1/U2/6	823	3,5E-06	7,74>8, 26	93					
SCWHA\C	227					8,2						
SCWHA\C	240	YM30	SCWHA\C-1/U2/7	800	3,4E-06	8,2	39					

SECOND TEST SERIES

TABLE 3: :Predissolution results (container SCW-3)

medium	start date	washing date (= sampling date)	contact time (days)	accumulated duration (days)	sample nr	U conc (µg/l)	U conc (mol/l)	mol U /l/day = mol U /m²/day	total U washed off(µg)	pH	Eh(mV/ E_{SHE}
SCW	98-02-02	98-02-04	2	2	SCW-3/U45/v/1	35500	1,49E-04	7,46E-05	1420	8,08	192
SCW	98-02-02	98-02-06	2	4	SCW-3/U45/v/2	5020	2,11E-05	1,05E-05	1620,8	8,11	266
SCW	98-02-02	98-02-09	3	7	SCW-3/U45/v/3	2130	8,95E-06	2,98E-06	1706	8,14	89
SCW	98-02-02	98-02-13	4	11	SCW-3/U45/v/4	1310	5,50E-06	1,38E-06	1758,4	8,14	206
SCW	98-02-02	98-02-16	3	14	SCW-3/U45/v/5	800	3,36E-06	1,12E-06	1790,4	8,17	233
SCW	98-02-02	98-02-20	4	18	SCW-3/U45/v/6	773	3,25E-06	8,12E-07	1821,32	8,13	
SCW	98-02-02	98-02-23	3	21	SCW-3/U45/v/7	450	1,89E-06	6,30E-07	1839,32	8,16	269
SCW	98-02-02	98-02-27	4	25	SCW-3/U45/v/8	485	2,04E-06	5,09E-07	1858,72	8,14	184
SCW	98-02-02	98-03-02	3	28	SCW-3/U45/v/9	319	1,34E-06	4,47E-07	1871,48	8,1	269
SCW	98-02-02	98-03-06	4	32	SCW-3/U45/v/10	337	1,42E-06	3,54E-07	1884,96	8,1	228
SCW	98-02-02	98-03-09	3	35	SCW-3/U45/v/11	207	8,70E-07	2,90E-07	1893,24	8,2	276
SCW	98-02-02	98-03-13	4	39	SCW-3/U45/v/12	236	9,92E-07	2,48E-07	1902,68	8,18	274
SCW	98-02-02	98-03-16	3	42	SCW-3/U45/v/13	167	7,02E-07	2,34E-07	1909,36	8,19	99
SCW	98-02-02	98-03-19	3	45	SCW-3/U45/v/14	144	6,05E-07	2,02E-07	1915,12	8,2	257
SCW	98-02-02	98-03-24	5	50	SCW-3/U45/v/15	193	8,11E-07	1,62E-07	1922,84	8,15	266
SCW	98-02-02	98-03-27	3	53	SCW-3/U45/v/16	139	5,84E-07	1,95E-07	1928,4	8,22	279
SCW	98-02-02	98-03-31	4	57	SCW-3/U45/v/17	151	6,34E-07	1,59E-07	1934,44	8,15	293
SCW	98-02-02	98-04-03	3	60	SCW-3/U45/v/18	129	5,42E-07	1,81E-07	1939,6	8,26	288
SCW	98-02-02	98-04-06	3	63	SCW-3/U45/v/19	119	5,00E-07	1,67E-07	1944,36	8,17	256
SCW	98-02-02	98-04-10	4	67	SCW-3/U45/v/20	120	5,04E-07	1,26E-07	1949,16	8,12	293
SCW	98-02-02	98-04-14	4	71	SCW-3/U45/v/21	110	4,62E-07	1,16E-07	1953,56	8,18	291
SCW	98-02-02	98-04-20	6	77	SCW-3/U45/v/22	144	6,05E-07	1,01E-07	1959,32	8,19	245
SCW	98-02-02	98-04-23	3	80	SCW-3/U45/v/23	91	3,82E-07	1,27E-07	1962,96	8,25	293
SCW	98-02-02	98-04-27	4	84	SCW-3/U45/v/24	102	4,29E-07	1,07E-07	1967,04	8,17	261
SCW	98-02-02	98-04-30	3	87	SCW-3/U45/v/25	87	3,66E-07	1,22E-07	1970,52	8,2	259
SCW	98-02-02	98-05-04	4	91	SCW-3/U45/v/26	94	3,95E-07	9,87E-08	1974,28	8,16	301
SCW	98-02-02	98-05-08	4	95	SCW-3/U45/v/27	87	3,66E-07	9,14E-08	1977,76	8,12	259
SCW	98-02-02	98-05-11	3	98	SCW-3/U45/v/28	73	3,07E-07	1,02E-07	1980,68	8,19	85
SCW	98-02-02	98-05-15	4	102	SCW-3/U45/v/29	84	3,53E-07	8,82E-08	1984,04	8,19	79
SCW	98-02-02	98-05-20	5	107	SCW-3/U45/v/30	90	3,78E-07	7,56E-08	1987,64	8,17	64
SCW	98-02-02	98-05-25	5	112	SCW-3/U45/v/31	87	3,66E-07	7,31E-08	1991,12	8,15	239
SCW	98-02-02	98-05-28	3	115	SCW-3/U45/v/32	49	2,06E-07	6,86E-08	1993,08	8,17	207
SCW	98-02-02	98-06-02	5	120	SCW-3/U45/v/33	67	2,82E-07	5,63E-08	1995,76	8,22	223
SCW	98-02-02	98-06-08	6	126	SCW-3/U45/v/35	48	2,02E-07	3,36E-08	1997,68	8,2	246
SCW	98-02-02	98-06-15	7	133	SCW-3/U45/v/37	53	2,23E-07	3,18E-08	1999,8	8,11	235
SCW	98-02-02	98-06-22	7	140	SCW-3/U45/v/38	94	3,95E-07	5,64E-08	2003,56	8,23	234
SCW	98-02-02	98-06-26	4	144	SCW-3/U45/v/39					8,27	224
SCW	98-02-02	98-06-29	7	147	SCW-3/U45/v/40	56	2,35E-07	3,36E-08	2005,8	8,25	235
SCW	98-02-02	98-07-03	4	151	SCW-3/U45/v/41					8,17	-
SCW	98-02-02	98-07-06	3	154	SCW-3/U45/v/42	45	1,89E-07	6,30E-08	2007,6	8,12	-
SCW	98-02-02	98-07-09	3	157	SCW-3/U45/v/43					8,24	-
SCW	98-02-02	98-08-04	26	183	SCW-3/U45/v/44	155	6,51E-07	2,50E-08	2013,8	8,2	-
SCW	98-02-02	98-08-07	3	186	SCW-3/U45/v/45					8,22	-
SCW	98-02-02	98-08-10	3	189	SCW-3/U45/v/46	33	1,39E-07	4,62E-08	2015,12	8,24	-
SCW	98-02-02	98-08-13	3	192	SCW-3/U45/v/47					8,22	-
SCW	98-02-02	98-08-17	4	196	SCW-3/U45/v/48	35	1,47E-07	3,68E-08	2016,52	8,22	-
SCW	98-02-02	98-08-21	4	200	SCW-3/U45/v/49					8,21	-
SCW	98-02-02	98-08-28	7	207	SCW-3/U45/v/50	43	1,81E-07	2,58E-08	2018,24	8,14	-

TABLE 4 : Predissolution results (container SCWHA-3)

medium	start date	washing date (= sampling date)	contact time (days)	accumulated duration (days)	sample nr	U conc (µg/l)	U conc (mol/l)	mol U /l/day = mol U /m²/day	total U washed off(µg)	pH	Eh(mV E_{SHE})
SCWHA	98-02-02	98-02-04	2	2	SCWHA-3/U45/v/1	33800	1,42E-04	7,10E-05	1352	8,06	68
SCWHA	98-02-02	98-02-06	2	4	SCWHA-3/U45/v/2	6280	2,64E-05	1,32E-05	1603,2	8,09	266
SCWHA	98-02-02	98-02-09	3	7	SCWHA-3/U45/v/3	2370	9,96E-06	3,32E-06	1698	8,13	74
SCWHA	98-02-02	98-02-13	4	11	SCWHA-3/U45/v/4	1180	4,96E-06	1,24E-06	1745,2	8,2	194
SCWHA	98-02-02	98-02-16	3	14	SCWHA-3/U45/v/5	765	3,21E-06	1,07E-06	1775,8	8,15	230
SCWHA	98-02-02	98-02-20	4	18	SCWHA-3/U45/v/6	708	2,97E-06	7,44E-07	1804,12	8,12	-
SCWHA	98-02-02	98-02-23	3	21	SCWHA-3/U45/v/7	413	1,74E-06	5,78E-07	1820,64	8,12	272
SCWHA	98-02-02	98-02-27	4	25	SCWHA-3/U45/v/8	406	1,71E-06	4,26E-07	1836,88	8,19	182
SCWHA	98-02-02	98-03-02	3	28	SCWHA-3/U45/v/9	258	1,08E-06	3,61E-07	1847,2	8,15	103
SCWHA	98-02-02	98-03-06	4	32	SCWHA-3/U45/v/10	240	1,01E-06	2,52E-07	1856,8	8,12	229
SCWHA	98-02-02	98-03-09	3	35	SCWHA-3/U45/v/11	166	6,97E-07	2,32E-07	1863,44	8,19	278
SCWHA	98-02-02	98-03-13	4	39	SCWHA-3/U45/v/12	185	7,77E-07	1,94E-07	1870,84	8,17	276
SCWHA	98-02-02	98-03-16	3	42	SCWHA-3/U45/v/13	122	5,13E-07	1,71E-07	1875,72	8,17	101
SCWHA	98-02-02	98-03-19	3	45	SCWHA-3/U45/v/14	120	5,04E-07	1,68E-07	1880,52	8,19	255
SCWHA	98-02-02	98-03-24	5	50	SCWHA-3/U45/v/15	169	7,10E-07	1,42E-07	1887,28	8,13	268
SCWHA	98-02-02	98-03-27	3	53	SCWHA-3/U45/v/16	123	5,17E-07	1,72E-07	1892,2	8,22	278
SCWHA	98-02-02	98-03-31	4	57	SCWHA-3/U45/v/17	122	5,13E-07	1,28E-07	1897,08	8,14	292
SCWHA	98-02-02	98-04-03	3	60	SCWHA-3/U45/v/18	104	4,37E-07	1,46E-07	1901,24	8,23	290
SCWHA	98-02-02	98-04-06	3	63	SCWHA-3/U45/v/19	96	4,03E-07	1,34E-07	1905,08	8,16	258
SCWHA	98-02-02	98-04-10	4	67	SCWHA-3/U45/v/20	107	4,50E-07	1,12E-07	1909,36	8,11	289
SCWHA	98-02-02	98-04-14	4	71	SCWHA-3/U45/v/21	99	4,16E-07	1,04E-07	1913,32	8,18	289
SCWHA	98-02-02	98-04-20	6	77	SCWHA-3/U45/v/22	145	6,09E-07	1,02E-07	1919,12	8,17	238
SCWHA	98-02-02	98-04-23	3	80	SCWHA-3/U45/v/23	81	3,40E-07	1,13E-07	1922,36	8,24	292
SCWHA	98-02-02	98-04-27	4	84	SCWHA-3/U45/v/24	112	4,71E-07	1,18E-07	1926,84	8,18	265
SCWHA	98-02-02	98-04-30	3	87	SCWHA-3/U45/v/25	83	3,49E-07	1,16E-07	1930,16	8,19	260
SCWHA	98-02-02	98-05-04	4	91	SCWHA-3/U45/v/26	95	3,99E-07	9,98E-08	1933,96	8,17	301
SCWHA	98-02-02	98-05-08	4	95	SCWHA-3/U45/v/27	86	3,61E-07	9,03E-08	1937,4	8,12	250
SCWHA	98-02-02	98-05-11	3	98	SCWHA-3/U45/v/28	67	2,82E-07	9,38E-08	1940,08	8,2	84
SCWHA	98-02-02	98-05-15	4	102	SCWHA-3/U45/v/29	79	3,32E-07	8,30E-08	1943,24	8,19	71
SCWHA	98-02-02	98-05-20	5	107	SCWHA-3/U45/v/30	102	4,29E-07	8,57E-08	1947,32	8,16	60
SCWHA	98-02-02	98-05-25	5	112	SCWHA-3/U45/v/31	108	4,54E-07	9,08E-08	1951,64	8,18	240
SCWHA	98-02-02	98-05-28	3	115	SCWHA-3/U45/v/32	58	2,44E-07	8,12E-08	1953,96	8,3	205
SCWHA	98-02-02	98-06-02	5	120	SCWHA-3/U45/v/33	81	3,40E-07	6,81E-08	1957,2	8,17	229
SCWHA	98-02-02	98-06-08	6	126	SCWHA-3/U45/v/35	50	2,10E-07	3,50E-08	1959,2	8,2	240
SCWHA	98-02-02	98-06-15	7	133	SCWHA-3/U45/v/37	59	2,48E-07	3,54E-08	1961,56	8,1	234
SCWHA	98-02-02	98-06-22	7	140	SCWHA-3/U45/v/38	94	3,95E-07	5,64E-08	1965,32	8,24	232
SCWHA	98-02-02	98-06-26	4	144	SCWHA-3/U45/v/39					8,27	251
SCWHA	98-02-02	98-06-29	7	147	SCWHA-3/U45/v/40	67	2,82E-07	4,02E-08	1968	8,24	237
SCWHA	98-02-02	98-07-03	4	151	SCWHA-3/U45/v/41					8,18	-
SCWHA	98-02-02	98-07-06	3	154	SCWHA-3/U45/v/42	46	1,93E-07	6,44E-08	1969,84	8,08	-
SCWHA	98-02-02	98-07-09	3	157	SCWHA-3/U45/v/43					8,2	-
SCWHA	98-02-02	98-08-04	26	183	SCWHA-3/U45/v/44	169	7,10E-07	2,73E-08	1976,6	8,22	-
SCWHA	98-02-02	98-08-07	3	186	SCWHA-3/U45/v/45					8,16	-
SCWHA	98-02-02	98-08-10	3	189	SCWHA-3/U45/v/46	34	1,43E-07	4,76E-08	1977,96	8,19	-
SCWHA	98-02-02	98-08-13	3	192	SCWHA-3/U45/v/47					8,16	-
SCWHA	98-02-02	98-08-17	4	196	SCWHA-3/U45/v/48	39	1,64E-07	4,10E-08	1979,52	8,18	-
SCWHA	98-02-02	98-08-21	4	200	SCWHA-3/U45/v/49					8,2	-
SCWHA	98-02-02	98-08-28	7	207	SCWHA-3/U45/v/50	53	2,23E-07	3,18E-08	1981,64	815	-

TABLE 5 : Predissolution results (container RIC-3)

medium	start date	washing date (= sampling date)	contact time (days)	accumulated duration (days)	sample nr	U conc (µg/l)	U conc (mol/l)	mol U /l/day = mol U /m²/day	total U washed off(µg)	pH	Eh(mV/ E_{SHE})
RIC	98-02-02	98-02-04	2	2	RIC-3/U45/v/1	36900	1,55E-04	7,75E-05	1476	8,1	200
RIC	98-02-02	98-02-06	2	4	RIC-3/U45/v/2	7620	3,20E-05	1,60E-05	1780,8	8,07	254
RIC	98-02-02	98-02-09	3	7	RIC-3/U45/v/3	2130	8,95E-06	2,98E-06	1866	8,11	100
RIC	98-02-02	98-02-13	4	11	RIC-3/U45/v/4	1130	4,75E-06	1,19E-06	1911,2	8,19	197
RIC	98-02-02	98-02-16	3	14	RIC-3/U45/v/5	564	2,37E-06	7,90E-07	1933,76	8,17	234
RIC	98-02-02	98-02-20	4	18	RIC-3/U45/v/6	619	2,60E-06	6,50E-07	1958,52	8,16	
RIC	98-02-02	98-02-23	3	21	RIC-3/U45/v/7	418	1,76E-06	5,85E-07	1975,24	8,16	267
RIC	98-02-02	98-02-27	4	25	RIC-3/U45/v/8	365	1,53E-06	3,83E-07	1989,84	8,25	189
RIC	98-02-02	98-03-02	3	28	RIC-3/U45/v/9	236	9,92E-07	3,31E-07	1999,28	8,16	279
RIC	98-02-02	98-03-06	4	32	RIC-3/U45/v/10	265	1,11E-06	2,78E-07	2009,88	8,11	250
RIC	98-02-02	98-03-09	3	35	RIC-3/U45/v/11	180	7,56E-07	2,52E-07	2017,08	8,21	277
RIC	98-02-02	98-03-13	4	39	RIC-3/U45/v/12	211	8,87E-07	2,22E-07	2025,52	8,18	277
RIC	98-02-02	98-03-16	3	42	RIC-3/U45/v/13	133	5,59E-07	1,86E-07	2030,84	8,18	101
RIC	98-02-02	98-03-19	3	45	RIC-3/U45/v/14	130	5,46E-07	1,82E-07	2036,04	8,19	263
RIC	98-02-02	98-03-24	5	50	RIC-3/U45/v/15	206	8,66E-07	1,73E-07	2044,28	8,16	265
RIC	98-02-02	98-03-27	3	53	RIC-3/U45/v/16	135	5,67E-07	1,89E-07	2049,68	8,24	275
RIC	98-02-02	98-03-31	4	57	RIC-3/U45/v/17	169	7,10E-07	1,78E-07	2056,44	8,16	292
RIC	98-02-02	98-04-03	3	60	RIC-3/U45/v/18	144	6,05E-07	2,02E-07	2062,2	8,21	288
RIC	98-02-02	98-04-06	3	63	RIC-3/U45/v/19	107	4,50E-07	1,50E-07	2066,48	8,18	259
RIC	98-02-02	98-04-10	4	67	RIC-3/U45/v/20	121	5,08E-07	1,27E-07	2071,32	8,12	290
RIC	98-02-02	98-04-14	4	71	RIC-3/U45/v/21	113	4,75E-07	1,19E-07	2075,84	8,17	290
RIC	98-02-02	98-04-20	6	77	RIC-3/U45/v/22	133	5,59E-07	9,31E-08	2081,16	8,2	238
RIC	98-02-02	98-04-23	3	80	RIC-3/U45/v/23	84	3,53E-07	1,18E-07	2084,52	8,24	292
RIC	98-02-02	98-04-27	4	84	RIC-3/U45/v/24	101	4,24E-07	1,06E-07	2088,56	8,17	267
RIC	98-02-02	98-04-30	3	87	RIC-3/U45/v/25	79	3,32E-07	1,11E-07	2091,72	8,2	266
RIC	98-02-02	98-05-04	4	91	RIC-3/U45/v/26	92	3,87E-07	9,66E-08	2095,4	8,17	302
RIC	98-02-02	98-05-08	4	95	RIC-3/U45/v/27	80	3,36E-07	8,40E-08	2098,6	8,11	256
RIC	98-02-02	98-05-11	3	98	RIC-3/U45/v/28	73	3,07E-07	1,02E-07	2101,52	8,17	87
RIC	98-02-02	98-05-15	4	102	RIC-3/U45/v/29	73	3,07E-07	7,67E-08	2104,44	8,18	76
RIC	98-02-02	98-05-20	5	107	RIC-3/U45/v/30	83	3,49E-07	6,97E-08	2107,76	8,19	61
RIC	98-02-02	98-05-25	5	112	RIC-3/U45/v/31	76	3,19E-07	6,39E-08	2110,8	8,17	238
RIC	98-02-02	98-05-28	3	115	RIC-3/U45/v/32	47	1,97E-07	6,58E-08	2112,68	8,2	203
RIC	98-02-02	98-06-02	5	120	RIC-3/U45/v/33	64	2,69E-07	5,38E-08	2115,24	8,24	190
RIC	98-02-02	98-06-08	6	126	RIC-3/U45/v/35	53	2,23E-07	3,71E-08	2117,36	8,17	250
RIC	98-02-02	98-06-15	7	133	RIC-3/U45/v/37	40	1,68E-07	2,40E-08	2118,96	8,12	227
RIC	98-02-02	98-06-22	7	140	RIC-3/U45/v/38	81	3,40E-07	4,86E-08	2122,2	8,24	221
RIC	98-02-02	98-02-26	4	144	RIC-3/U45/v/39					8,22	208
RIC	98-02-02	98-06-29	3	147	RIC-3/U45/v/40	46	1,93E-07	6,44E-08	2124,04	8,23	235
RIC	98-02-02	98-07-03	4	151	RIC-3/U45/v/41					8,15	-
RIC	98-02-02	98-07-06	3	154	RIC-3/U45/v/42	36	1,51E-07	5,04E-08	2125,48	8,17	-
RIC	98-02-02	98-07-09	3	157	RIC-3/U45/v/43					8,15	-
RIC	98-02-02	98-08-04	26	183	RIC-3/U45/v/44	161	6,76E-07	2,60E-08	2131,92	8,24	-
RIC	98-02-02	98-08-07	3	186	RIC-3/U45/v/45					8,22	-
RIC	98-02-02	98-08-10	3	189	RIC-3/U45/v/46	25	1,05E-07	3,50E-08	2132,92	8,24	-
RIC	98-02-02	98-08-13	3	192	RIC-3/U45/v/47					8,24	-
RIC	98-02-02	98-08-17	4	196	RIC-3/U45/v/48	29	1,22E-07	3,05E-08	2134,08	8,24	-
RIC	98-02-02	98-08-21	4	200	RIC-3/U45/v/49					8,22	-
RIC	98-02-02	98-08-28	7	207	RIC-3/U45/v/50	43	1,81E-07	2,58E-08	2135,8	8,18	-

TABLE 6 : *Predissolution results (container SCWHA\C-3)*

medium	start date	washing date (= sampling date)	contact time (days)	accumulated duration (days)	sample nr	U conc (µg/l)	U conc (mol/l)	mol U /l/day = mol U /m²/day	total U washed off(µg)	pH	Eh(mV/ E_{SHE})
SCWHA\C	98-06-19	98-06-22	3	3	SCWHA\C-3/U45/v/1	5580,00	2,34E-05	7,82E-06	223	7,54	259
SCWHA\C	98-06-19	98-06-26	4	7	SCWHA\C-3/U45/v/2	177,00	7,44E-07	1,86E-07	230	7,71	247
SCWHA\C	98-06-19	98-06-29	3	10	SCWHA\C-3/U45/v/3	25,00	1,05E-07	3,50E-08	231	8,26	18
SCWHA\C	98-06-19	98-07-03	4	14	SCWHA\C-3/U45/v/4	8,00	3,36E-08	8,40E-09	232	8,39	30
SCWHA\C	98-06-19	98-07-06	3	17	SCWHA\C-3/U45/v/5	7,40	3,11E-08	1,04E-08	232	8,27	-
SCWHA\C	98-06-19	98-07-09	3	20	SCWHA\C-3/U45/v/6	13,00	5,46E-08	1,82E-08	232	8,10	-
SCWHA\C	98-06-19	98-08-04	26	46	SCWHA\C-3/U45/v/7	12,00	5,04E-08	1,94E-09	233	8,09	-
SCWHA\C	98-06-19	98-08-07	3	49	SCWHA\C-3/U45/v/8	13,00	5,46E-08	1,82E-08	233	8,11	-
SCWHA\C	98-06-19	98-08-10	3	53	SCWHA\C-3/U45/v/9	12,00	5,04E-08	1,68E-08	234	8,25	-
SCWHA\C	98-06-19	98-08-13	3	56	SCWHA\C-3/U45/v/10	60,00	2,52E-07	8,40E-08	236	8,51	-
SCWHA\C	98-06-19	98-08-17	4	60	SCWHA\C-3/U45/v/11	68,00	2,86E-07	7,14E-08	239	8,20	-
SCWHA\C	98-06-19	98-08-21	4	63	SCWHA\C-3/U45/v/12	4,00	1,68E-08	4,20E-09	239	8,33	-
SCWHA\C	98-06-19	98-09-21	31	94	SCWHA\C-3/U45/v/13	3,99	1,68E-08	5,41E-10	239	8,46	-
SCWHA\C	98-06-19	98-09-24	3	97	SCWHA\C-3/U45/v/14	0,96	4,03E-09	1,34E-09	239	8,16	-
SCWHA\C	98-06-19	98-09-29	5	102	SCWHA\C-3/U45/v/15	6,30	2,65E-08	5,29E-09	240	8,26	-
SCWHA\C	98-06-19	98-10-02	3	105	SCWHA\C-3/U45/v/16	6,10	2,56E-08	8,54E-09	240	8,14	-
SCWHA\C	98-06-19	98-10-05	3	108	SCWHA\C-3/U45/v/17	3,20	1,34E-08	4,48E-09	240	8,18	-
SCWHA\C	98-06-19	98-10-08	3	111	SCWHA\C-3/U45/v/18	7,40	3,11E-08	1,04E-08	240	8,50	-
SCWHA\C	98-06-19	98-10-13	5	116	SCWHA\C-3/U45/v/19	5,50	2,31E-08	4,62E-09	241	8,21	-
SCWHA\C	98-06-19	98-10-16	3	119	SCWHA\C-3/U45/v/20	7,00	2,94E-08	9,80E-09	241	8,11	-
SCWHA\C	98-06-19	98-10-19	3	122	SCWHA\C-3/U45/v/21	3,80	1,60E-08	5,32E-09	241	8,15	
SCWHA\C	98-06-19	98-10-23	4	126	SCWHA\C-3/U45/v/22	3,70	1,55E-08	3,89E-09	241	8,19	

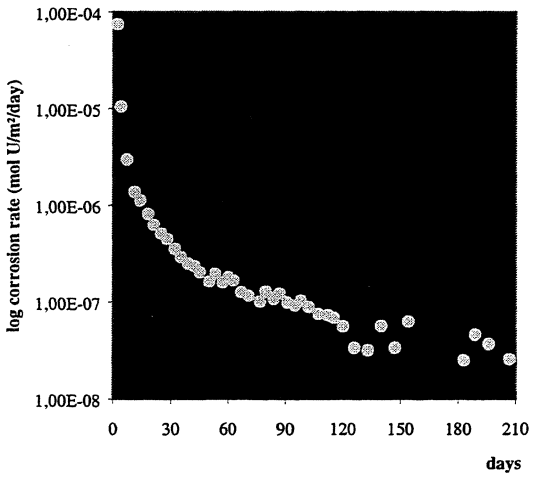

GURE 1 *: Predissolution of container SCW-3 'CW water)*

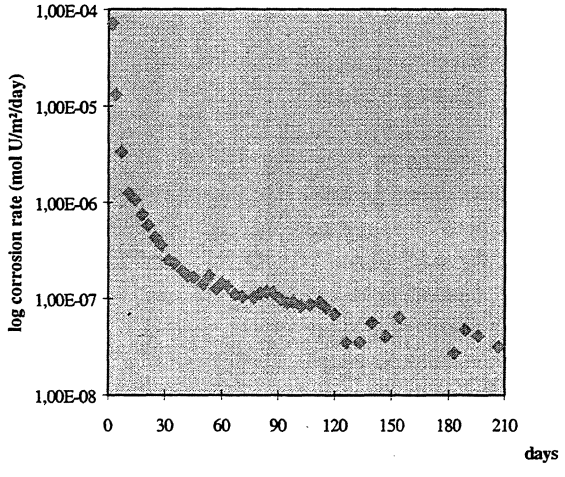

FIGURE 2 *: Predissolution of container SCWHA-(SCW water)*

TABLE 7 : *Uranium concentration, pH, Eh of the media in the second test series (solubility tests)*

medium	start date	sampling date	leaching duration (days)	sample	U conc (µg/l)	U conc (mol/l)	mol U /m²/day	total U washed off (µg)	pH	Eh (mV/E_{SHE})
RIC-3	98-08-28	98-08-28	0	RIC-3/U2/5/0	4,40	1,85E-08	-	0,35	8,45	-188
RIC-3	98-08-28	98-08-31	3	RIC-3/U2/5/3	40,00	1,68E-07	5,60E-08	1,78	8,50	-177
RIC-3	98-08-28	98-09-03	6	RIC-3/U2/5/6	56,00	2,35E-07	3,92E-08	2,42	8,43	-152
RIC-3	98-08-28	98-09-07	10	RIC-3/U2/5/10	70,20	2,95E-07	2,95E-08	2,88	8,26	-159
RIC-3	98-08-28	98-09-10	13	RIC-3/U2/5/13	74,10	3,11E-07	2,39E-08	3,03	8,26	-161
RIC-3	98-08-28	98-09-22	25	RIC-3/U2/5/25	26,80	1,13E-07	4,50E-09	1,14	8,25	-123
RIC-3	98-08-28	98-10-08	41	RIC-3/U2/5/41	12,40	5,21E-08	1,27E-09	0,56	8,40	-246
RIC-3	98-08-28	98-11-10	74	RIC-3/U2/5/74	3,27	1,37E-08	1,86E-10	0,20		
RIC-4	98-08-28	98-08-28	0	RIC-4/U2/5/0	5,00	2,10E-08	-	0,40	8,31	-205
RIC-4	98-08-28	98-08-31	3	RIC-4/U2/5/3	45,00	1,89E-07	6,30E-08	2,00	8,61	-184
RIC-4	98-08-28	98-09-03	6	RIC-4/U2/5/6	51,00	2,14E-07	3,57E-08	2,24	8,51	-160
RIC-4	98-08-28	98-09-07	10	RIC-4/U2/5/10	60,10	2,53E-07	2,53E-08	2,47	8,45	-171
RIC-4	98-08-28	98-09-10	13	RIC-4/U2/5/13	61,30	2,58E-07	1,98E-08	2,52	8,42	-175
RIC-4	98-08-28	98-09-22	25	RIC-4/U2/5/25	17,90	7,52E-08	3,01E-09	0,78	8,27	-140
RIC-4	98-08-28	98-10-08	41	RIC-4/U2/5/41	4,53	1,90E-08	4,64E-10	0,25	8,18	-271
RIC-4	98-08-28	98-11-10	74	RIC-4/U2/5/74	4,15	1,74E-08	2,36E-10	0,23		
SCWHA-3	98-08-28	98-08-28	0	SCWHA-3/U2/5/0	2,90	1,22E-08	-	0,23	8,60	-184
SCWHA-3	98-08-28	98-08-31	3	SCWHA-3/U2/5/3	65,00	2,73E-07	9,10E-08	2,72	8,47	-182
SCWHA-3	98-08-28	98-09-03	6	SCWHA-3/U2/5/6	76,00	3,19E-07	5,32E-08	3,16	8,31	-154
SCWHA-3	98-08-28	98-09-07	10	SCWHA-3/U2/5/10	91,30	3,84E-07	3,84E-08	3,66	8,15	-159
SCWHA-3	98-08-28	98-09-10	13	SCWHA-3/U2/5/13	94,30	3,96E-07	3,05E-08	3,78	8,15	-162
SCWHA-3	98-08-28	98-09-22	25	SCWHA-3/U2/5/25	108,00	4,54E-07	1,82E-08	4,33	8,18	-137
SCWHA-3	98-08-28	98-10-08	41	SCWHA-3/U2/5/41	112,00	4,71E-07	1,15E-08	4,49	8,12	-166
SCWHA-3	98-08-28	98-11-10	74	SCWHA-3/U2/5/74	134,00	5,63E-07	7,61E-09	5,37		
SCWHA-4	98-08-28	98-08-28	0	SCWHA-4/U2/5/0	2,60	1,09E-08	-	0,21	8,58	-188
SCWHA-4	98-08-28	98-08-31	3	SCWHA-4/U2/5/3	49,00	2,06E-07	6,86E-08	2,06	8,63	-176
SCWHA-4	98-08-28	98-09-03	6	SCWHA-4/U2/5/6	62,00	2,61E-07	4,34E-08	2,58	8,50	-166
SCWHA-4	98-08-28	98-09-07	10	SCWHA-4/U2/5/10	75,50	3,17E-07	3,17E-08	3,03	8,19	-165
SCWHA-4	98-08-28	98-09-10	13	SCWHA-4/U2/5/13	80,80	3,39E-07	2,61E-08	3,24	8,23	-168
SCWHA-4	98-08-28	98-09-22	25	SCWHA-4/U2/5/25	95,30	4,00E-07	1,60E-08	3,82	8,21	-144
SCWHA-4	98-08-28	98-10-08	41	SCWHA-4/U2/5/41	102,00	4,29E-07	1,05E-08	4,09	8,34	-180
SCWHA-4	98-08-28	98-11-10	74	SCWHA-4/U2/5/74	104,00	4,37E-07	5,91E-09	4,17		
SCW-3	98-08-28	98-08-28	0	SCW-3/U2/5/0	2,60	1,09E-08	-	0,21	8,54	-188
SCW-3	98-08-28	98-08-31	3	SCW-3/U2/5/3	56,00	2,35E-07	7,84E-08	2,34	8,65	-177
SCW-3	98-08-28	98-09-03	6	SCW-3/U2/5/6	69,00	2,90E-07	4,83E-08	2,86	8,54	-167
SCW-3	98-08-28	98-09-07	10	SCW-3/U2/5/10	85,30	3,58E-07	3,58E-08	3,42	8,36	-171
SCW-3	98-08-28	98-09-10	13	SCW-3/U2/5/13	92,10	3,87E-07	2,98E-08	3,69	8,32	-173
SCW-3	98-08-28	98-09-22	25	SCW-3/U2/5/25	105,00	4,41E-07	1,76E-08	4,21	8,18	-137
SCW-3	98-08-28	98-10-08	41	SCW-3/U2/5/41	107,00	4,50E-07	1,10E-08	4,29	8,14	-172
SCW-3	98-08-28	98-11-10	74	SCW-3/U2/5/74	113,00	4,75E-07	6,42E-09	4,53		
SCW-4	98-08-28	98-08-28	0	SCW-4/U2/5/0	1,40	5,88E-09	-	0,11	8,45	-180
SCW-4	98-08-28	98-08-31	3	SCW-4/U2/5/3	74,00	3,11E-07	1,04E-07	3,02	8,35	-171
SCW-4	98-08-28	98-09-03	6	SCW-4/U2/5/6	93,00	3,91E-07	6,51E-08	3,78	8,26	-157
SCW-4	98-08-28	98-09-07	10	SCW-4/U2/5/10	117,00	4,92E-07	4,92E-08	4,69	8,21	-171
SCW-4	98-08-28	98-09-10	13	SCW-4/U2/5/13	119,00	5,00E-07	3,85E-08	4,77	8,17	-165
SCW-4	98-08-28	98-09-22	25	SCW-4/U2/5/25	139,00	5,84E-07	2,34E-08	5,57	8,22	-114
SCW-4	98-08-28	98-10-08	41	SCW-4/U2/5/41	131,00	5,50E-07	1,34E-08	5,25	8,43	-184
SCW-4	98-08-28	98-11-10	74	SCW-4/U2/5/74	127,00	5,34E-07	7,21E-09	5,09		

medium	start date	sampling date	leaching duration (days)	sample	U conc (µg/l)	U conc (mol/l)	mol U /m²/day	total U washed off (µg)	pH	Eh (mV/E_{SHE})
SCWHA\C-3	98-10-23	98-10-23	0	SCWHA\C980415/U2/1	8,02	3,37E-08		0,64	10,1	-420
SCWHA\C-3	98-10-23	98-10-26	3	SCWHA\C-3/U2/5/3	114,00	4,79E-07	1,60E-07	4,88	10,3	-295
SCWHA\C-3	98-10-23	98-10-30	7	SCWHA\C-3/U2/5/7	264,00	1,11E-06	1,58E-07	10,88	8,6	-251
SCWHA\C-3	98-10-23	98-10-30	11	SCWHA\C-3/U2/5/11	278	1,17E-06	1,.06E-07	11,44	8,7	-211
SCWHA\C-3	98-10-23	98-10-30	17	SCWHA\C-3/U2/5/17	284	1,19E-06	7,02E-07	11.68	8.8	-223
SCWHA\C-3	98-10-23	98-11-23	31	SCWHA\C-3/U2/5/31	353,00	1,48E-06	4,78E-08	14,44	7,9	-196
SCWHA\C-4	98-10-23	98-10-23	0	SCWHA\C980415/U2/1	8,02	3,37E-08		0,64	10,1	-421
SCWHA\C-4	98-10-23	98-10-26	3	SCWHA\C-4/U2/5/3	84,40	3,55E-07	1,18E-07	3,70	10,2	-291
SCWHA\C-4	98-10-23	98-10-30	7	SCWHA\C-4/U2/5/7	306,00	1,29E-06	1,84E-07	12,56	8,6	-246
SCWHA\C-4	98-10-23	98-11-03	11	SCWHA\C-4/U2/5/11	308,00	1,29E-06	1,18E-07	12,64	8,80	-208
SCWHA\C-4	98-10-23	98-11-09	17	SCWHA\C-4/U2/5/17	290,00	1,22E-06	7,17E-08	11,92	8,8	-221
SCWHA\C-4	98-10-23	98-11-23	31	SCWHA\C-4/U2/5/31	350,00	1,47E-06	4,74E-08	14,32	7,9	-189

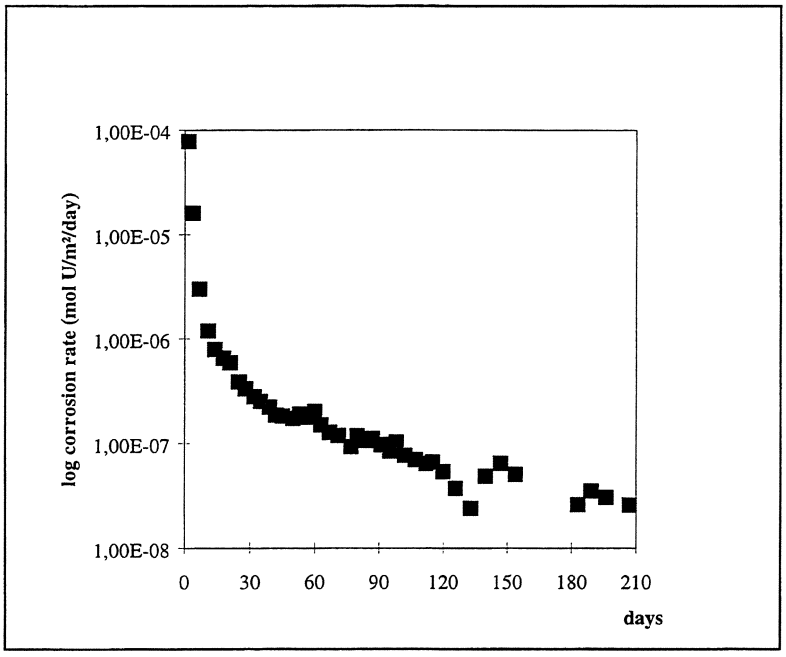

***FIGURE 3** : Predissolution of container RIC-3 (SCW water)*

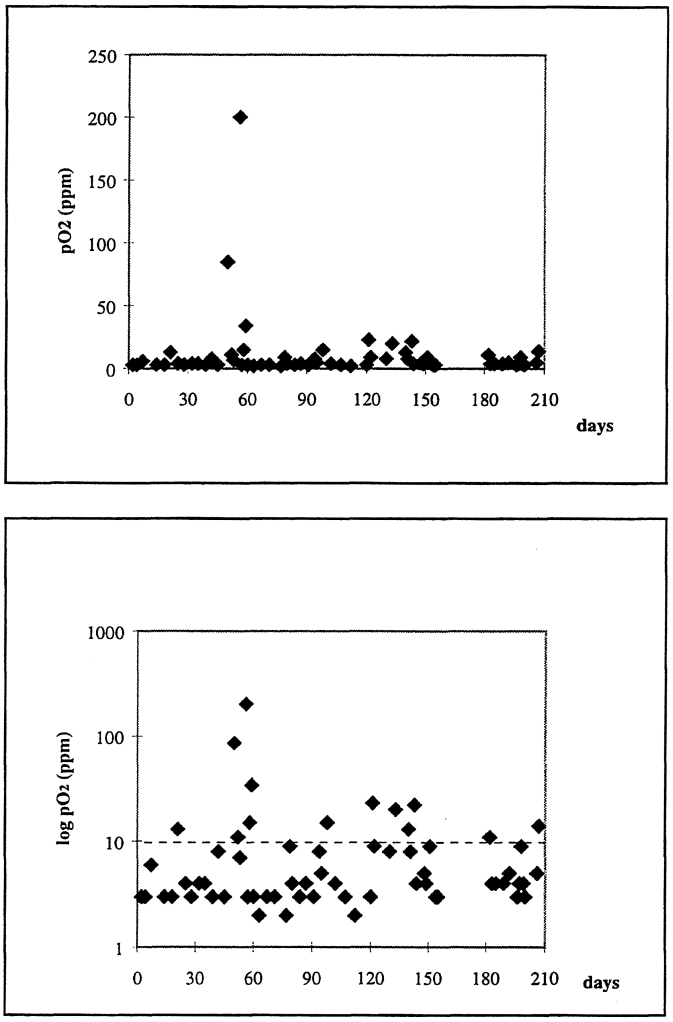

***FIGURE 4** : Oxygen partial pressure in Ar/CO_2 glove box during predissolution stage*

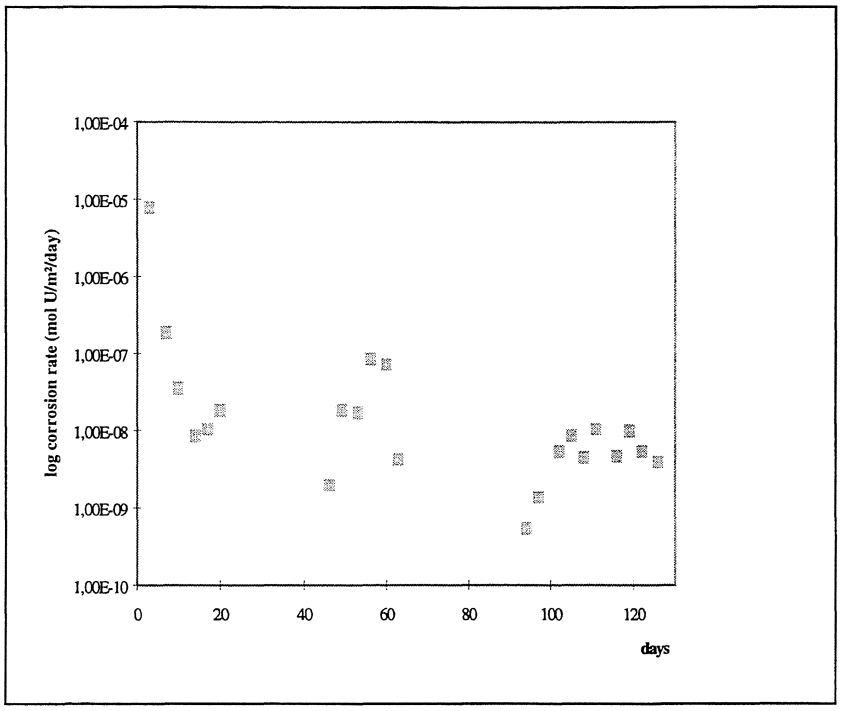

***FIGURE 5** : Predissolution of container SCWHA\C-3 (SCW\C water)*

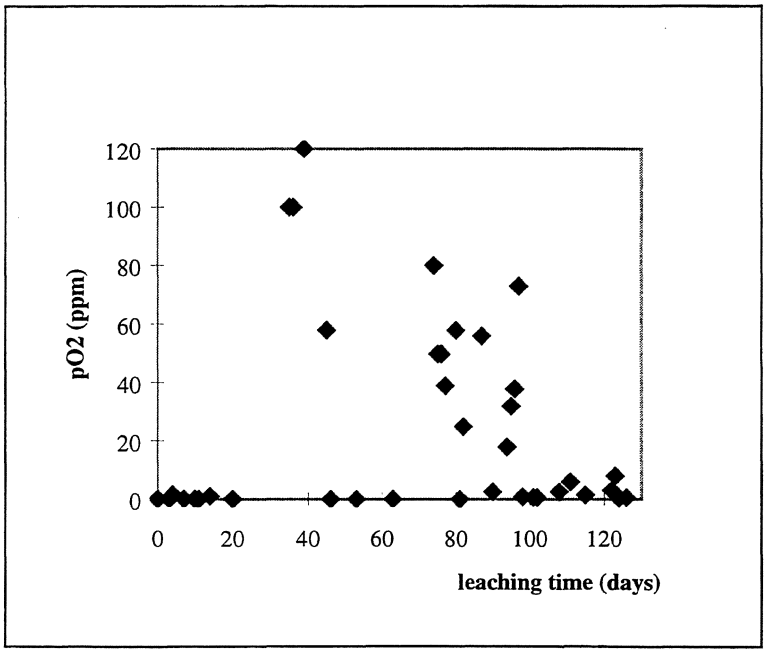

***FIGURE 6** : Oxygen partial pressure in Ar glove box during predissolution stage*

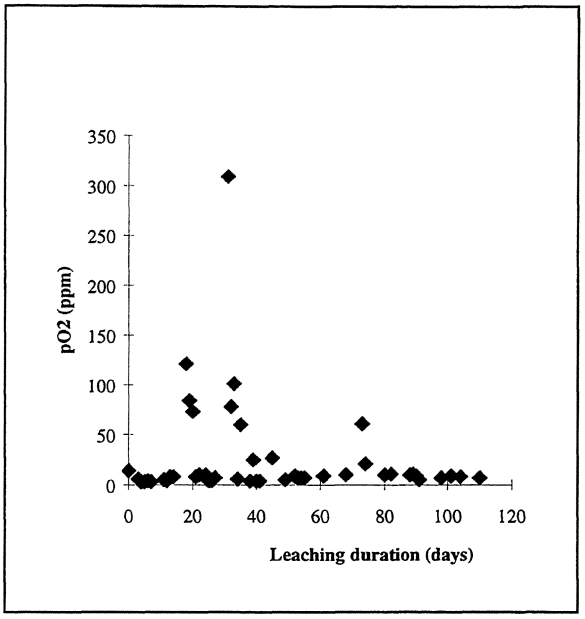

***FIGURE 7** : Oxygen partial pressure in Ar/CO_2 glove box during dissolution tests.*

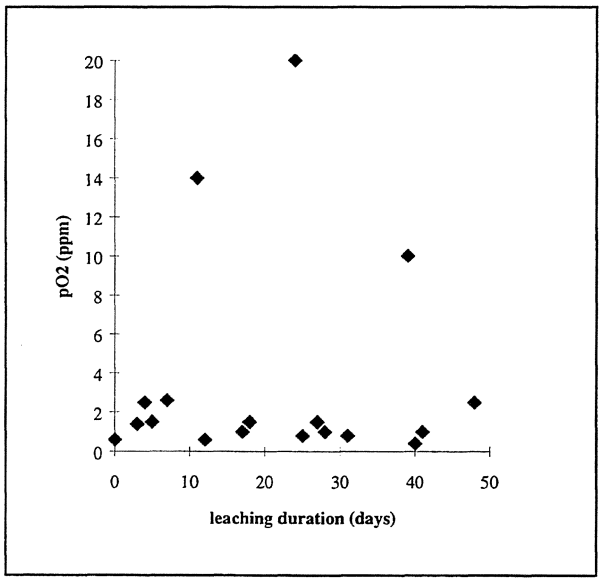

***FIGURE 8** : Oxygen partial pressure in Ar glove box during dissolution tests.*

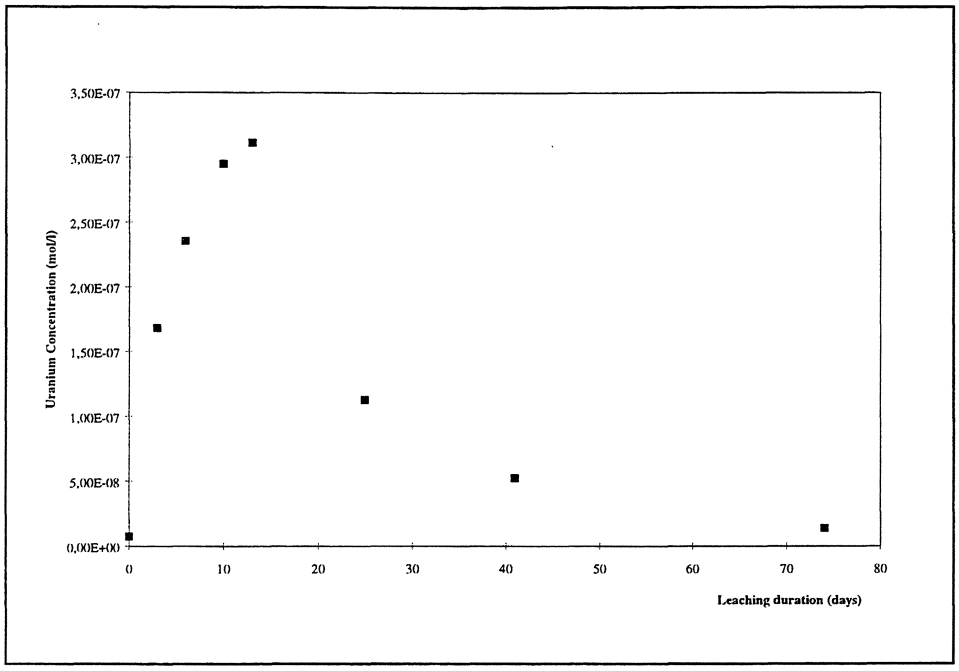

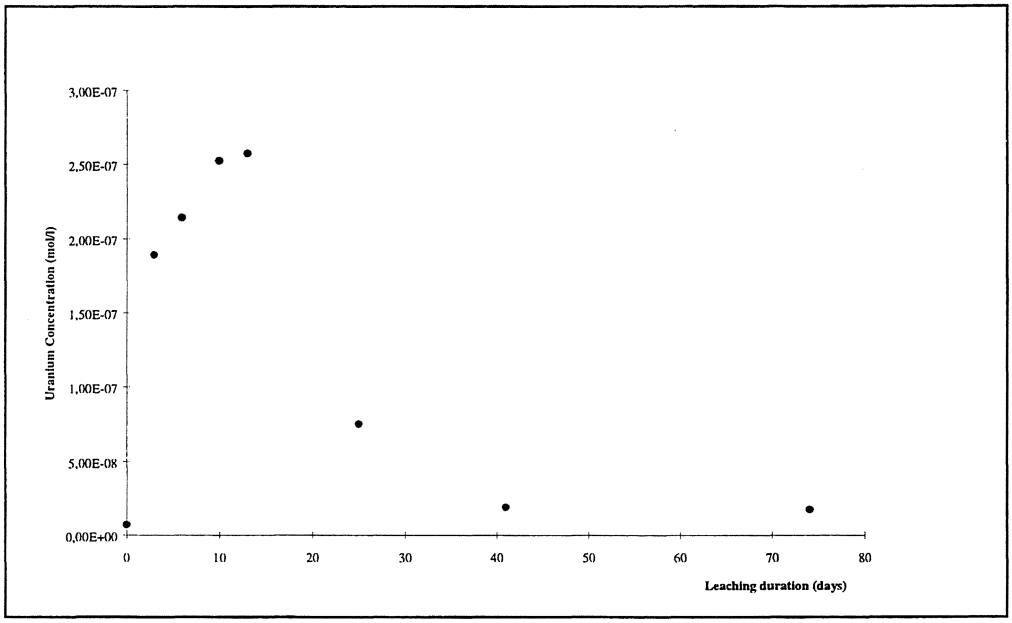

FIGURE 9 *: Uranium results medium without carbonate a- container RIC-3 ; b- container RIC-4*

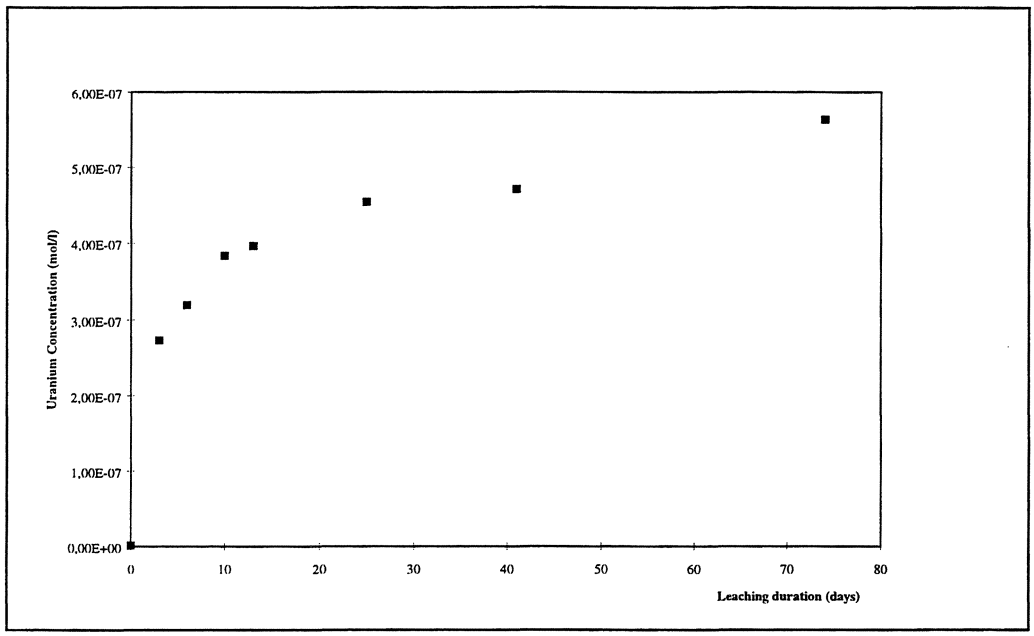

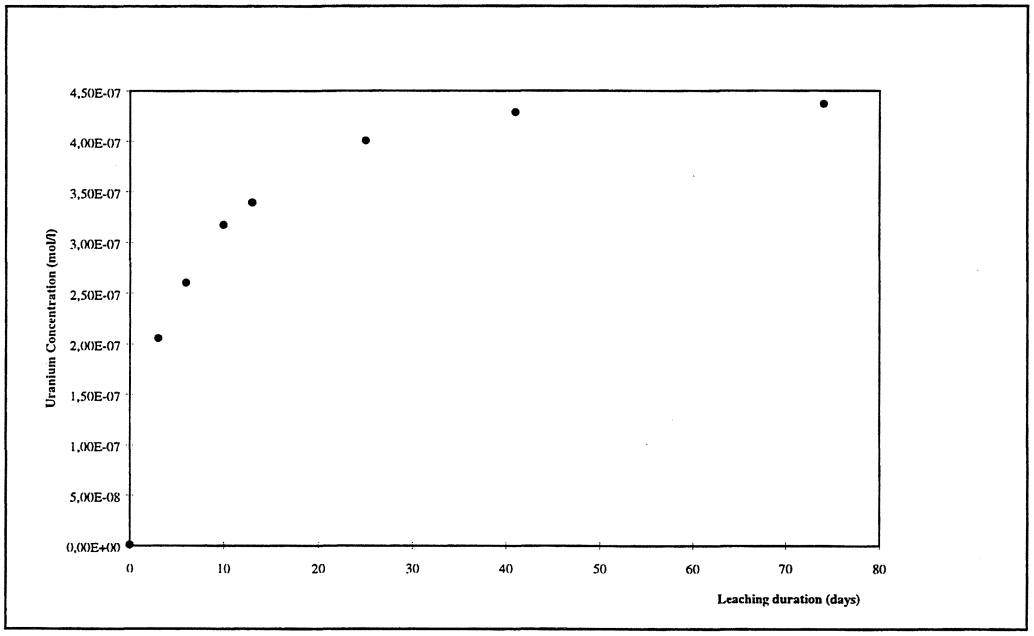

***FIGURE 10** : Uranium results medium without carbonate a- container SCWHA-3 ; b- container SCWHA-4*

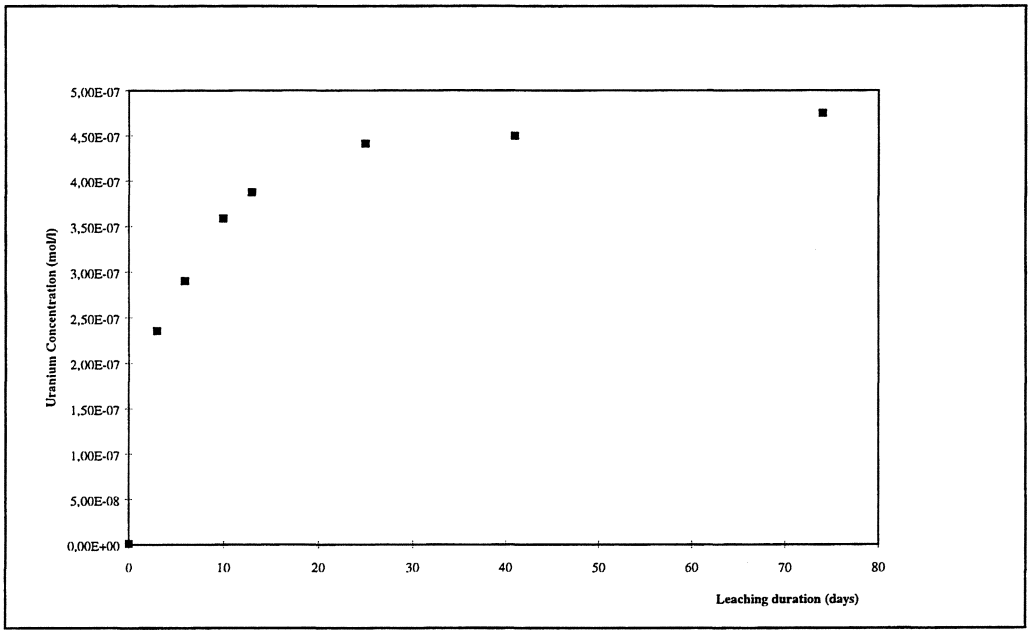

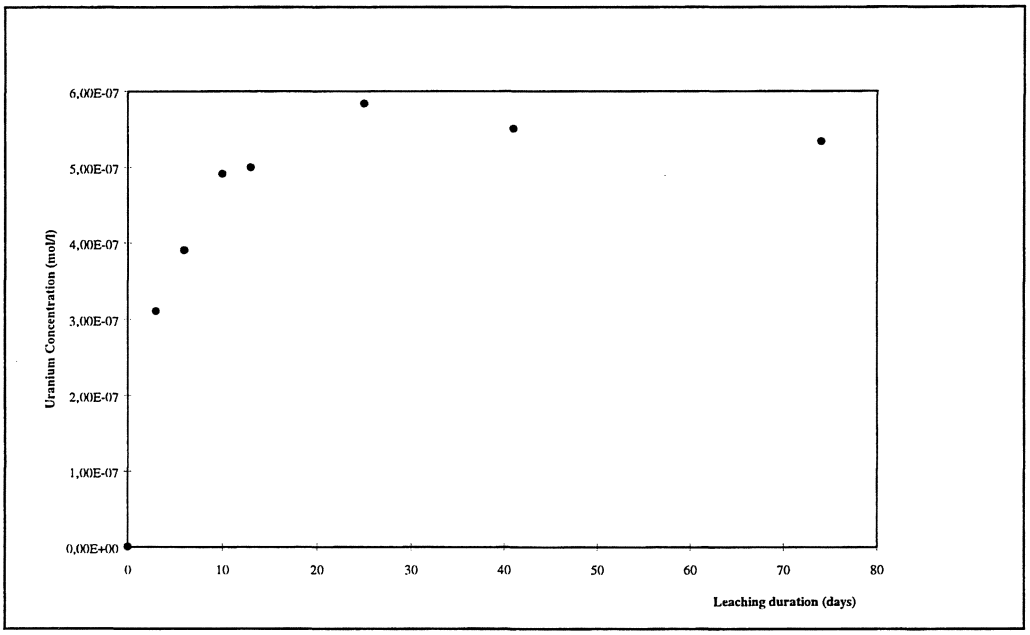

***FIGURE 11** : Uranium results medium without carbonate above- container SCW-3 ; below- container SCW-4*

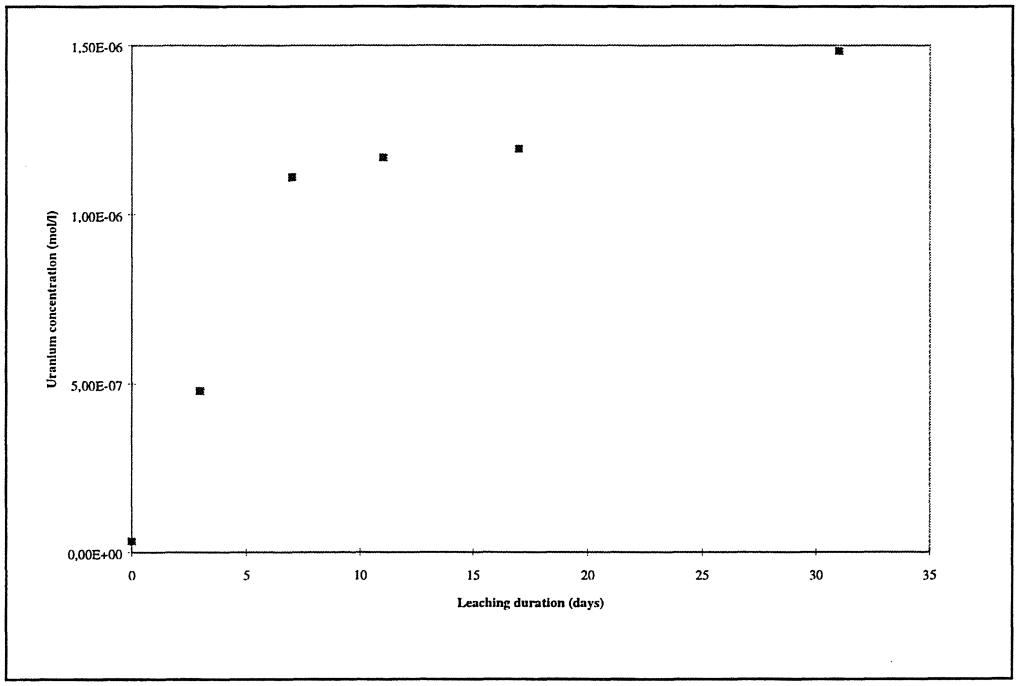

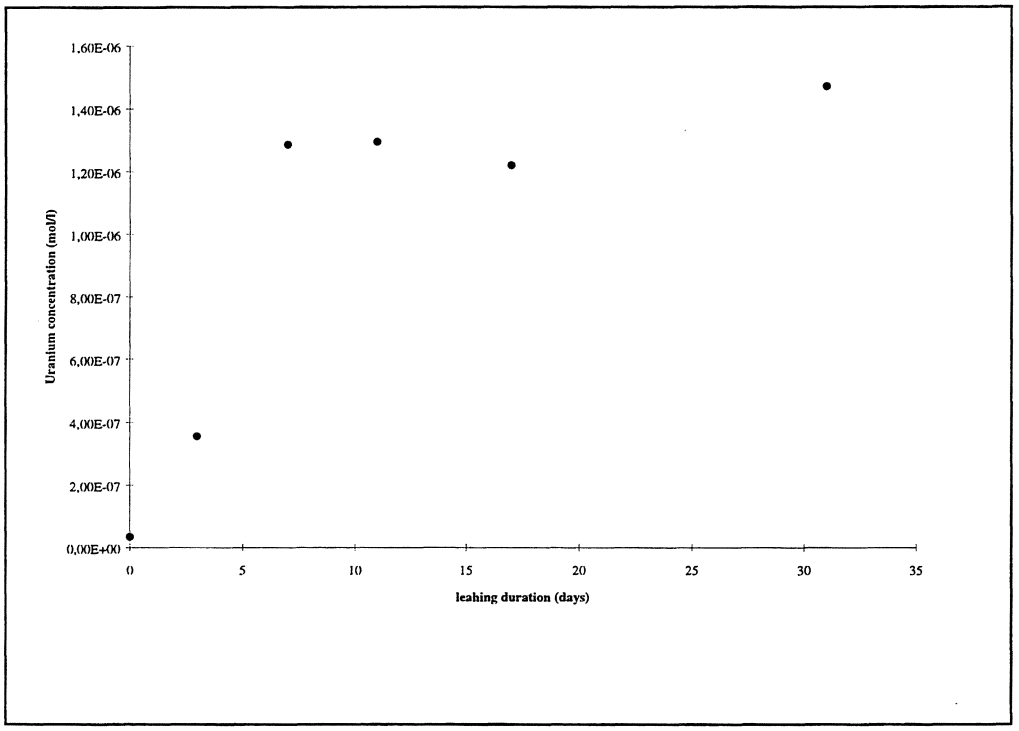

***FIGURE 12** : Uranium results medium without carbonate above- container SCWHA\C-3 ; below- container SCWHA\C-4*

Appendix 8: Symbols used by FUB and original test data obtained by FUB

EXPLICATION OF SYMBOLS USED:

b	reciprocal slope of lnj=f(E) curve
F	Faraday constant
$\Delta G_a^{0\#}$	standard free activation enthalpy
j_0	exchange current density
j_a	partial anodic current density
j_k	partial cathodic current density
k_a^0	maximum velocity constant of anodic process
k_k^0	maximum velocity constant of cathodic process
k_a	velocity constant of anodic process
k_k	velocity constant of cathodic process
$\tilde{k}$	constant
k^*	proportional factor
$\hat{k}$	constant
R	general gas constant
T	Kelvin temperature
z	amount of electrochemical valence
α	transfer coefficient
Γ_{red}	moles of reduced species per unit area
Γ_{ox}	moles of oxidised species per unit area
η_D	overvoltage of transfer reaction
φ_{Me}	inner potential of metal
$\Delta\varphi$	Galvani voltage
$\Delta\varphi_B$	Galvani voltage of reference electrode
$\Delta\varphi_{rev}$	Galvani voltage at equilibrium
φ_L	inner potential of solution
S_{ox}	Oxidised form of the relevant species
S_{red}	reduced form of the relevant species
n	number of electrons exchanged in the redox process
$\tilde{a}(S_{red})$	activity of the reduced form at equilibrium (rational scale)
$\tilde{a}(S_{ox})$	activity of the oxidised form at equilibrium (rational scale)
$\tilde{a}(e^-)$	activity of the electrons at equilibrium (rational scale)
K	thermodynamical equilibrium constant
μ_i^I	chemical potential of species i in phase I
μ_i^{II}	chemical potential of species i in phase II
$\tilde{\mu}_i^I$	electrochemical potential of species i in phase I
$\tilde{\mu}_i^{II}$	electrochemical potential of species i in phase II
z_i	number of electrical unit charges of species i
φ^I	Galvani potential of phase I
φ^{II}	Galvani potential of phase II
α	transfer factor
E, E_{app}	Potential, applied
E_{gl}	electrode potential at equilibrium
E_{corr}	free corrosion potential (rest potential)
m	stoechiometrical factor of H^+ activity or slope of lnj = f(E) curve
ε_{Diff}	diffusion potential
$\varepsilon_{Kontakt}$	contact potential
I_0	current amplitude in EIS
Φ	phase shift in EIS

Z	impedance
R_{pol}	polarization resistance
R_{bulk}	resistance of bulk electrode
R_{Ω}	ohm's resistance
C_{dl}	double layer capacitance
C_{bulk}	capacitance of bulk electrode

TABLE 1 Corrosion on Ti99.8Pd and Zircaloy-4 at applied potential in sat. NaCl

Potential (mV)	Zircaloy-4 (25°C) Rate (µm/a)	Ti99.8Pd (25°C) Rate (µm/a)	Zircaloy-4 (55°C) Rate (µm/a)	Ti99.8Pd (55°C) Rate (µm/a)
-1500	0.08			
-1200	0.1			
-1100	1.32			
-1000	0.12			
-900	0.05			
-600	0.146			
-300	0.14			
-100	0.4			
0	5.1			
300	17533			
600	74467			
900	117450			
-1000		0.6		
-500		2.8		
-250		5.3		
0		0.5		
500		0.8		
-1500			0.25495	
-1300			8.57469	
-1100			0.19841	
-900			0.134415	
-600			0.012895	
-300			0.03955	
0			0.046	
150			1275	
300			60766	
600			211715	
-1000				1.4
-500				2
-250				1.1
0				0.6
500				1.4

TABLE 2 Original data for relation between applied potential versus corrosion rate (FIGURE I.6-31)

uncorr. val.		KMnO4	K2Cr207	Potential, applied		correct. val.
g/m²·d		g/m²·d	g/m²·d	mV / SHE		g/m²·d
0				-1800		
0				-1300		
0				-800		
0				-300		
0				200		
0				300		
0				400		
0				500		
7.8615				600		
				640		
				652		
				660		
				680		
				682		
11.0061				700		
				743		
				720		
				740		
				743		
				760		
				780		
31.446				800		
				815		
				830		
				850		
44.0244				900		
				910		
				950		
100.6272				1000		
99.0549				1100		
136.7901				1200		
160.3746				1300		
242.1342				1400		
251.568				1500		
388.3581				1600		
361.629				1700		
526.7205				1800		
476.4069				1900		
597.474				2000		
597.474				2100		
732.6918				2200		
		646.2153		719		
		58.64679		649		
		6.383538		590		
				756		

			487.4	734		
			298.7	700		
			36.9	658		
				-1433		0
				-1280		0
				-787		0
				-297		0
				200		0
				300		0
				400		0
				500		0
				600		7.9
				665		11
				681		31.5
				682		44.1
				731		100.6
				759		99.1
				767		136.8
				791		160.4
				791		242.1
				771		251.6
				792		388.4
				809		361.6
				813		526.7
				851		476.4
				841		597.5
				897		597.5
				944		732.7

TABLE 2 Original data for relation between corrosion potential versus corrosion rate ("calibration curve") (FIGURE I.6-32)

Pot mV (SHE)		log cor.rate	log cor.rate		log.cor.rate
		Redox sys.	E2		E1
637	Chlorine:	1.7847025			
720	Bromine:	2.6589409			
734	$KMnO_4$:	2.8844284			
743	$K_2Cr_2O_7$:	2.953179			
577					0.8955129
645					1.6437009
674					2.0027229
408	BPW,pH3,air:	-1.39794			
345	BPW,pH9,air:	-1.886057			
639.1			1.64365		
650.7			1.9001486		
664.7			2.0548428		
669.8			2.0339864		
200			-3.564474		

TABLE 3 Original data for relation between corrosion potential versus corrosion rate in presence and absence of carbonate ("calibration curve") (FIGURE I.6-36)

Pot mV(SHE)	log. cor. rate with 0.1M Carb.	log. cor. rate with 0.01M Carb.
349	-0.575009	
397	0.0641929	
436	0.7757927	
458	1.2887387	
467	1.5820591	
497	1.6935022	
511	1.8266378	
526	1.9536324	
544	2.0262749	
554	2.1403975	
555	2.2188812	
470		0.3241861
490		0.6252161
504		0.9262461
519		1.2784286
534		1.3655787
548		1.4703141
563		1.5794586
582		1.6464054
602		1.7865841
649		1.6666087
663		1.7043973
687		1.8427
732		1.8427
742		2.0231561
762		2.2326711

TABLE 3 Original data for relation between corrosion potential versus corrosion rate ("calibration curve") at various temperatures (FIGURE I.6-37)

Pot. mV (SHE)		log cor. rate at 5°C
470		-2.37478
519.9		-1.89766
569.9		-1.63442
619		-0.6266
668		-0.31409
709.5		0.421096
724.6		1.05254
734		1.321135

Appendix 9: Details of radiolysis modelling data used by STUDSVIK

TABLE 1 Rate constants, $dm^3 \cdot mol^{-1} \cdot s^{-1}$ in deionized water (EU 18)

NO	REACTION					RATE CONSTANT	
1	OH	+H2	= H	+H2O		K(1)= 3.400E+07 *	
2	OH	+H2O2	= HO2	+H2O		K(2)= 2.700E+07 *	
3	OH	+O2-	= O2	+OH-		K(3)= 1.000E+10 *	
4	OH	+HO2	= H2O	+O2		K(4)= 7.100E+09 *	
5	OH	+OH	= H2O2			K(5)= 5.500E+09 *	
6	OH	+OH-	= H2O	+O-		K(6)= 1.200E+10 *	
7	OH	+HO2-	= HO2	+OH-		K(7)= 7.500E+09 *	
8	OH	+H	= H2O			K(8)= 7.000E+09 *	
9	OH	+E-	= OH-			K(9)= 3.100E+10 *	
10	OH	+O-	= HO2-			K(10)= 1.800E+10 *	
11	O-	+H2O	= OH	+OH-		K(11)= 1.700E+06 *	
12	E-	+O2	= O2-			K(12)= 1.900E+10 *	
13	E-	+H2O2	= OH	+OH-		K(13)= 1.100E+10 *	
14	E-	+O2-	= HO2-	+OH-	-H2O	K(14)= 1.300E+10 *	
15	E-	+H+	= H			K(15)= 2.300E+10 *	
16	E-	+H2O	= H	+OH-		K(16)= 1.900E+01 *	
17	E-	+HO2-	= O-	+OH-		K(17)= 3.500E+09 *	
18	E-	+E-	= H2	+OH-	+OH-	K(18)= 5.500E+09 *	
19	E-	+HO2	= HO2-			K(19)= 2.000E+10 *	
20	E-	+H	= H2	+OH-	-H2O	K(20)= 2.500E+10 *	
21	H	+HO2	= H2O2			K(21)= 2.000E+10 *	
22	H	+H2O2	= H2O	+OH		K(22)= 9.000E+07 *	
23	H	+OH-	= E-	+H2O		K(23)= 2.200E+07 *	
24	H	+O2	= HO2			K(24)= 2.100E+10 *	
25	H	+O2-	= HO2-			K(25)= 2.000E+10 *	
26	H	+H	= H2			K(26)= 7.800E+09 *	
27	HO2	+O2-	= O2	+HO2-		K(27)= 9.600E+07 *	
28	HO2	+HO2	= H2O2	+O2		K(28)= 8.400E+05 *	
29	HO2		= H+	+O2-		K(29)= 8.000E+05 *	
30	H+	+O2-	= HO2			K(30)= 5.000E+10 *	
31	H+	+HO2-	= H2O2			K(31)= 2.000E+10 *	
32	H2O2		= H+	+HO2-		K(32)= 3.560E-02 *	
33	H+	+OH-	= H2O			K(33)= 1.430E+11 *	
34	H2O		= H+	+OH-		K(34)= 2.599E-05 *	
35	O2-	+O2-	= HO2-	+O2	-H+	K(35)= 1.800E+09 *	H+
36	UO2	+OH	= UO3H			K(36)= 4.000E+08 *	
37	UO2	+H2O2	= UO3H	+OH		K(37)= 2.000E-02 *	
38	UO2	+HO2	= UO3H	+H2O2	-H2O	K(38)= 2.000E+08 *	
39	UO2	+O2-	= UO3H	+HO2-	-H2O	K(39)= 2.000E+08 *	
40	UO3H	+UO3H	= UO3	+UO2	+H2O	K(40)= 3.000E+00 *	
41	UO3H	+OH	= UO3	+H2O		K(41)= 8.000E+08 *	
42	UO3H	+E-	= UO2	+OH-		K(42)= 5.000E+08 *	
43	UO3H	+H2O2	= UO3	+H2O	+OH	K(43)= 2.000E-02 *	
44	UO3H	+O2-	= UO3	+HO2-		K(44)= 2.000E+08 *	
45	UO3H	+O2-	= UO2	+OH-	+O2	K(45)= 4.000E+08 *	
46	UO3H	+HO2	= UO3	+H2O2		K(46)= 4.000E+08 *	
47	UO3	+E-	= UO3H	+OH-	-H2O	K(47)= 5.000E+07 *	
48	UO3	+O2-	= UO3-	+O2		K(48)= 4.000E+06 *	
49	UO3-	+H2O	= UO3H	+OH-		K(49)= 1.000E+01 *	
50	UO3H	+H	= UO2	+H2O		K(50)= 4.500E+06 *	
51	UO3	+H	= UO3H			K(51)= 4.500E+05 *	
52	UO3	+HO2	= UO3H	+O2		K(52)= 4.000E+06 *	
53	O2		= O2D			K(53)= 4.000E-03 *	
54	H2		= H2D			K(54)= 1.000E-02 *	
55	H2O2		= H2O2D			K(55)= 3.000E-03 *	
56	H2O2		= H2O	+O		K(56)= 1.000E-03 *	
57	O	+O	= O2			K(57)= 1.000E+09 *	
58	UO3		= UO3D			K(58)= 4.000E-05 *	
59	UO2	+O2	= UO3H	+HO2	-H2O	K(59)= 1.000E-04 *	

TABLE 1 (continued)

NO	REACTION	RATE CONSTANT
60	UO3H +O2 = UO3 +HO2	K(60)= 1.000E-04 *
61	UO2 = UO2D	K(61)= 7.000E-02 *
62	UO2D = UO2	K(62)= 7.000E-09 *

TABLE 2 Rate constants in 5 m NaCl solutions, $dm^3 \cdot mol^{-1} \cdot s^{-1}$ (EU 129)

NO	REACTION						RATE CONSTANT		
1	OH	+H2	= H	+H2O			K(1)=	3.400E+07	*
2	OH	+H2O2	= HO2	+H2O			K(2)=	2.700E+07	*
3	OH	+O2-	= O2	+OH-			K(3)=	1.000E+10	*
4	OH	+HO2	= H2O	+O2			K(4)=	7.100E+09	*
5	OH	+OH	= H2O2				K(5)=	5.500E+09	*
6	OH	+OH-	= H2O	+O-			K(6)=	1.200E+10	*
7	OH	+HO2-	= HO2	+OH-			K(7)=	7.500E+09	*
8	OH	+H	= H2O				K(8)=	7.000E+09	*
9	OH	+E-	= OH-				K(9)=	3.100E+10	*
10	OH	+O-	= HO2-				K(10)=	1.800E+10	*
11	O-	+H2O	= OH	+OH-			K(11)=	1.700E+06	*
12	E-	+O2	= O2-				K(12)=	1.900E+10	*
13	E-	+H2O2	= OH	+OH-			K(13)=	1.100E+10	*
14	E-	+O2-	= HO2-	+OH-	-H2O		K(14)=	1.300E+10	*
15	E-	+H+	= H				K(15)=	2.300E+10	*
16	E-	+H2O	= H	+OH-			K(16)=	1.900E+01	*
17	E-	+HO2-	= O-	+OH-			K(17)=	3.500E+09	*
18	E-	+E-	= H2	+OH-	+OH-		K(18)=	5.500E+09	*
19	E-	+HO2	= HO2-				K(19)=	2.000E+10	*
20	E-	+H	= H2	+OH-	-H2O		K(20)=	2.500E+10	*
21	H	+HO2	= H2O2				K(21)=	2.000E+10	*
22	H	+H2O2	= H2O	+OH			K(22)=	9.000E+07	*
23	H	+OH-	= E-	+H2O			K(23)=	2.200E+07	*
24	H	+O2	= HO2				K(24)=	2.100E+10	*
25	H	+O2-	= HO2-				K(25)=	2.000E+10	*
26	H	+H	= H2				K(26)=	7.800E+09	*
27	HO2	+O2-	= O2	+HO2-			K(27)=	9.600E+07	*
28	HO2	+HO2	= H2O2	+O2			K(28)=	8.400E+05	*
29	HO2		= H+	+O2-			K(29)=	8.000E+05	*
30	H+	+O2-	= HO2				K(30)=	5.000E+10	*
31	H+	+HO2-	= H2O2				K(31)=	2.000E+10	*
32	H2O2		= H+	+HO2-			K(32)=	3.560E-02	*
33	H+	+OH-	= H2O				K(33)=	1.430E+11	*
34	H2O		= H+	+OH-			K(34)=	2.599E-05	*
35	O2-	+O2-	= HO2-	+O2	-H+		K(35)=	1.800E+09	* H+
36	UO2	+OH	= UO3H				K(36)=	4.000E+08	*
37	UO2	+CL2-	= UO3H	+HCL	+CL-	-H2O	K(37)=	4.000E+08	*
38	UO2	+HCLO	= UO3H	+CL			K(38)=	4.000E-03	*
39	UO2	+H2O2	= UO3H	+OH			K(39)=	2.000E-02	*
40	UO2	+HO2	= UO3H	+H2O2	-H2O		K(40)=	2.000E+08	*
41	UO2	+O2-	= UO3H	+HO2-	-H2O		K(41)=	2.000E+08	*
42	UO3H	+UO3H	= UO3	+UO2	+H2O		K(42)=	3.000E+00	*
43	UO3H	+OH	= UO3	+H2O			K(43)=	8.000E+08	*
44	UO3H	+CL2-	= UO3	+HCL	+CL-		K(44)=	8.000E+08	*
45	UO3H	+HCLO	= UO3	+CL	+H2O		K(45)=	4.000E-03	*
46	UO3H	+E-	= UO2	+OH-			K(46)=	5.000E+08	*
47	UO3H	+H2O2	= UO3	+H2O	+OH		K(47)=	2.000E-02	*
48	UO3H	+O2-	= UO3	+HO2-			K(48)=	2.000E+08	*
49	UO3H	+O2-	= UO2	+OH-	+O2		K(49)=	4.000E+08	*
50	UO3H	+HO2	= UO3	+H2O2			K(50)=	4.000E+08	*
51	UO3	+E-	= UO3H	+OH-	-H2O		K(51)=	5.000E+07	*
52	UO3	+O2-	= UO3-	+O2			K(52)=	4.000E+06	*
53	UO3-	+H2O	= UO3H	+OH-			K(53)=	1.000E+01	*
54	UO3H	+H	= UO2	+H2O			K(54)=	4.500E+06	*
55	UO3	+H	= UO3H				K(55)=	4.500E+05	*

TABLE 2. CONTINUED

NO	REACTION						RATE CONSTANT	
56	UO3	+HO2	= UO3H	+O2			K(56)=	4.000E+06 *
57	O2		= O2D				K(57)=	4.000E-03 *
58	H2		= H2D				K(58)=	1.000E-02 *
59	H2O2		= H2O2D				K(59)=	3.000E-03 *
60	H2O2		= H2O	+O			K(60)=	1.000E-03 *
61	O	+O	= O2				K(61)=	1.000E+09 *
62	UO3		= UO3D				K(62)=	4.000E-05 *
63	UO2	+O2	= UO3H	+HO2	-H2O		K(63)=	1.000E-04 *
64	UO3H	+O2	= UO3	+HO2			K(64)=	1.000E-04 *
65	UO2		= UO2D				K(65)=	7.000E-02 *
66	UO2D		= UO2				K(66)=	7.000E-08 *
67	OH	+CL-	= CLOH-				K(67)=	4.300E+09 *
68	OH	+HCLO	= CLO	+H2O			K(68)=	9.000E+09 *
69	OH	+HCLO2	= CLO2	+H2O			K(69)=	6.300E+09 *
70	E-	+CL	= CL-	+H2O			K(70)=	1.000E+10 *
71	E-	+CL2-	= CL-	+CL-	+H2O		K(71)=	1.000E+10 *
72	E-	+CLOH-	= CL-	+OH-	+H2O		K(72)=	1.000E+10 *
73	E-	+HCLO	= CLOH-				K(73)=	7.200E+09 *
74	E-	+CL2	= CL2-				K(74)=	1.000E+10 *
75	E-	+CL3-	= CL2-	+CL-			K(75)=	1.000E+10 *
76	E-	+HCLO2	= CLO	+OH-			K(76)=	2.500E+09 *
77	E-	+HCLO3	= CLO2	+OH-			K(77)=	4.000E+04 *
78	H	+CL	= CL-	+H+			K(78)=	1.000E+10 *
79	H	+CL2-	= CL-	+CL-	+H+		K(79)=	8.000E+09 *
80	H	+CLOH-	= CL-	+H2O			K(80)=	1.000E+10 *
81	H	+CL2	= CL2-	+H+			K(81)=	7.000E+09 *
82	H	+HCLO	= CLOH-	+H+			K(82)=	2.000E+09 *
83	H	+CL3-	= CL2-	+CL-	+H+		K(83)=	1.000E+10 *
84	HO2	+CL2-	= CL-	+HCL	+O2		K(84)=	4.000E+09 *
85	HCL		= CL-	+H+			K(85)=	5.000E+05 *
86	HO2	+CL2	= CL2-	+H+	+O2		K(86)=	1.000E+09 *
87	HO2	+CL3-	= CL2-	+HCL	+O2		K(87)=	1.000E+09 *
88	O2-	+CL2-	= CL-	+CL-	+O2		K(88)=	1.200E+10 *
89	O2-	+HCLO	= CLOH-	+O2			K(89)=	7.500E+06 *
90	H2O2	+CL2-	= HCL	+HCL	+O2-		K(90)=	1.400E+05 *
91	H2O2	+CL2	= HO2	+CL2-	+H+		K(91)=	1.900E+02 *
92	H2O2	+HCLO	= HCL	+H2O	+O2		K(92)=	1.700E+05 *
93	OH-	+CL2-	= CLOH-	+CL-			K(93)=	7.300E+06 *
94	OH-	+CL2	= HCLO	+CL-			K(94)=	2.160E+08 *
95	H+	+CLOH-	= CL	+H2O			K(95)=	2.100E+10 *
96	H2O	+CL2O2	= HCLO	+HCLO2			K(96)=	5.000E+02 *
97	H2O	+CL2O2	= O2	+HCLO	+HCL		K(97)=	1.000E+02 *
98	H2O	+CL2O	= HCLO	+HCLO			K(98)=	1.000E+02 *
99	H2O	+CL2O4	= HCLO2	+HCLO3			K(99)=	5.000E+02 *
100	H2O	+CL2O4	= HCLO	+HCL	+O4		K(100)=	1.000E+02 *
101	O4		= O2	+O2			K(101)=	1.000E+05 *
102	CL-	+CL	= CL2-				K(102)=	2.100E+10 *
103	CL-	+CLOH-	= CL2-	+OH-			K(103)=	9.000E+04 *
104	CL-	+HCLO	= CL2	+OH-			K(104)=	1.000E-04 *
105	CL-	+CL2	= CL3-				K(105)=	1.000E+04 *
106	CLOH-		= OH	+CL-			K(106)=	6.100E+09 *
107	CL2-		= CL	+CL-			K(107)=	1.100E+05 *
108	CL2-	+CL2-	= CL3-	+CL-			K(108)=	7.000E+09 *
109	CL3-		= CL2	+CL-			K(109)=	5.000E+04 *
110	CLO	+CLO	= CL2O2				K(110)=	1.500E+10 *
111	CLO2	+CLO2	= CL2O4				K(111)=	1.000E+05 *
112	CL2O2	+HCLO2	= HCLO3	+CL2O			K(112)=	1.000E+05 *
113	HCLO		= CLO-	+H+			K(113)=	1.000E+02 *
114	H+	+CLO-	= HCLO				K(114)=	1.000E+10 *

TABLE 3 G-Values

	α	β, γ **Normal**	**Phase 1**	β, γ **corrected***
OH	0.24	2.67	2.31	3.85
E-	0.06	2.66	2.28	3.19
H	0.21	0.55	0.50	0.60
H_2	1.3	0.45	0.57	0.52
H_2O_2	0.985	0.72	0.76	0.29
H+	0.06	2.76	2.36	3.29
OH-	0	0.1	0.08	0.10
HO_2	0.22	0	0.03	0
$-H_2O$	2.71	6.87	7.72	7.72

Corrected for seavenging in spur and direct effect in 5 m NaCl solution

TABLE 4 G-values proposed by Kelm and Bohnert for strong salt solutions

Species	β, γ (from ref 4, 5)	α	Mixed ratiation 14.7% α, 85.3% β, γ
H_2O_2	0.11	0.23	0.128
H_2	0.63	1.52	0.761
H	0.85	0.26	0.762
e^-	3.35	0.06	2.866
OH	0.31	0.06	2.866
OH-	1.58	2.08	1.654
H^+	0.00	0.00	0.000
Cl^-	-9.86	-3.76	-8963
Cl_2^-	4.93	0.00	4.205
H_2O	-5.46	-3.31	-5.144
$ClOH^-$	0.00	0.55	0.081
Cl_3^-	0.00	1.07	0.157
HO_2	0.00	0.05	0.007

TABLE 5 Rates for generation of radiolysis gases and fuel alteration during spent fuel dissolution. Summary of experimental results from Granbow et al (96GRA/LOI, 95LOI/GRA)

Sample	Solution	Gas generation rate 10^{-7} mol • g^{-1} • d		Fuel alteration rate 10^{-9} mol UO_2• g^{-1} • d^{-1}	HP/FA*
		H_2	O_2		
Pellet	DIW	1.2	0.9 6.43.0		
Pellet	NaCl**	1.9	0.8	2.0	15
Powder	NaCl	2.6	? 23 2.4		
Pellet	NaCl/Fe[x]	10.5	<0.1	0.05	u.a

* Hydrogen production/fuel alteration
** 95 % saturated
x iron powder

TABLE 6 Additional G-values because of diffusion (molecules/100 eV)

Calc no	Phase No	ΔC in 100 d			G (to be used in next phase)		
		O_2D	H_2D	H_2O_2D	O_2	H_2	H_2O_2
EU11	1	1.44E-3*	1.34	0.47	1.01E-5	9.5E-3	3.3E-3
EU12	2	6.13E-11	4.03E-3	4.066E-6	6.8E-6	4.5E-5	4.5E-8
EU18	1	6.1E-4	1.31	0.172	4.3E-6	9.2E-3	1.21E-3
EU19	2	4.7E-11	4.6E-3	4.0E-6	5.2E-13	5.1E-5	4.4E-8
EU21	2		4.6E-3			5.1E-5	

* read as 1.44·10-3

TABLE 7 Calculation of radiolysis caused by a fuel pellet in deionized water.

Calc no	Phase	Concentrations after 200 d						
		H_2	H_2O_2	O_2	H_2D	O_2D	UO_3D	
EU11	1	3.9E-6	4.2E-6	1.00E-8			1.73	Original kD* used
EU12	2	1.09E-5	3.2E-8	3.1E-13				
EU13	2	1.20E-5	1.03E-5	1.60E-5				$G(H_2D)$ removed
EU14	2	1.00E-5	6.2E-6	9.5E-6				All G(D) removed
EU15	1	2.3E-3	7.6E-8	2.6E-12			2.3E-3	no diffusion
EU16	1	7.7E-6	8.6E-6	2.7E-8			2.66	O_2D, H_2O_2D removed kH_2D 50%
EU17	1	1.52E-5	8.5E-6	2.6E-8			2.62	O_2D, H_2O_2D removed kH_2D 25%
EU18	1	1.52E-5	6.6E-6	1.79E-8	2.6	1.23E-3	2.274	All kD 25%
EU19	2	1.25E-5	3.1E-8	2.3E-13				
EU20	3	1.84E-6	9.9E-7	1.43E-6	1.20E-4	5.9E-5		No diffusion from phase 2
EU21	2	1.24E-5	3.1E-8	2.3E-13				O_2D, H_2O_2D, removed
EU22	3	1.79E-6	9.4E-7	1.35E-6	1.17E-4	5.6E-5		Phase 3 incl diff of H_2
EU23	3	6.7X10-6	1.9E-5	3.0E-5	4.4E-4	1.24E-3		EU20 but $(O2D)_0 = 1.037E^{-3}$
EU24	3	2.5E-6	1.9E-6	2.9E-6	1.62E-4	1.18E-4		EU20 but $O2D10^{-4}$ ml/min
EU25	3	4.5E-6	8.2E-6	1.28E-5	3.0E-4	5.3E-4		EU20 but $O2D\ 10^{-3}$ ml/min
EU26	1	3.5E-5	8.1E-5	8.2E-6	6.1	0.56	0.82	EU18 but 9520 Gy/h α
EU27	1	1.2E-5	4.3E-6	3.5E-9	2.1	2.4E-4	1.84	EU26 but 9520 Gy/h β

* kD = rate constant for diffusion

TABLE 8 Calculation of radiolysis effects caused by a fuel pellet in a 5 m NaCl solution. pH8. Dose rate 9520 Gy/h (mixed radiation)

	Concentrations at 200 d, mol·cm^{-3}						Conc at 400 d	Corr rate μg·cm^{-2}·d^{-1}		Comments
EU no	H_2O_2	O_2	$HClO_3$	UO_3H	ClO_3	UO_3D	UO_3D	0-200 d	0-400 d	
83	1.8E-6	1.2E-9	~0	1.0E-4	3.4E-3	2.36	4.73	9.6	9.6	Corr scavenging in spur
84	1.6E-6	1.0E-9	~0	1.0E-4	3.4E-3	2.37	4.75	9.6	9.6	Corr scavenging + direct effect
124	1.6E-6	1.0E-9	4.2E-9	1.0E-4	3.4E-3	2.37	4.75	9.6	9.6	G-values from EU84 mechanism from EU123
125	1.1E-6	6.5E-9	3.1E-5	1.1E-4	5.1E-3	3.53	7.07	14.3	14.3	Kelm's G-values, mech. From EU123
129	1.1E-6	6.5E-9	3.1E-5	1.1E-4	5.1E-3	3.53	7.07	14.3	14.3	As EU125, but $k_{38}=k_{45}$=4E-3 (was 1E-2)
130	2.8E-8	1.6E-5	0.29	4.1E-5	7.8E-4	0.53	1.08	2.1	2.2	As EU129, but $k_{37}=k_{44}$=1E4 (RE w Cl_2^-)
131	7.9E-7	4.0E-6	4.0E-4	1.2E-4	4.3E-3	3.02	6.00	12.2	12.2	As EU129, but $k_{37}=k_{44}$=1E6 (RE w Cl_2^-)
132	3.0E-8	1.5E-5	0.22	5.6E-5	1.4E-4	0.93	1.9	3.8	3.8	As EU129, but $k_{37}=k_{44}$=1E5 (RE w Cl_2^-)
133	1.4E-7	9.1E-6	1.0E-2	9.7E-5	3.4E-3	2.32	4.63	9.4	9.4	As EU129, but $k_{37}=k_{44}$=5E5 (RE w Cl_2^-)
134	5.2E-8	1.2E-5	6.6E-2	8.3E-5	2.7E-3	1.85	3.69	7.5	7.5	As EU129, but $k_{37}=k_{44}$=3E5 (RE w Cl_2^-)

Re 37 and 44 are reactions of U-species with Cl^-_2

TABLE 9 Corrosion rates of UO_2 in deionized water and in 5 m NaCl solutions.

Time, d	ΔC(UO_3D) mol·dm^{-3}	Corrosion rate ug·cm^{-2}·d^{-1}
Deionized water, calc. no 18 K2		
0-200	2.28	9.6
513-1604	12.44	9.6
5 m NaCl solution, Calc no 129 K9		
0-200	3.53	14.3
514-1697	20.9	14.3

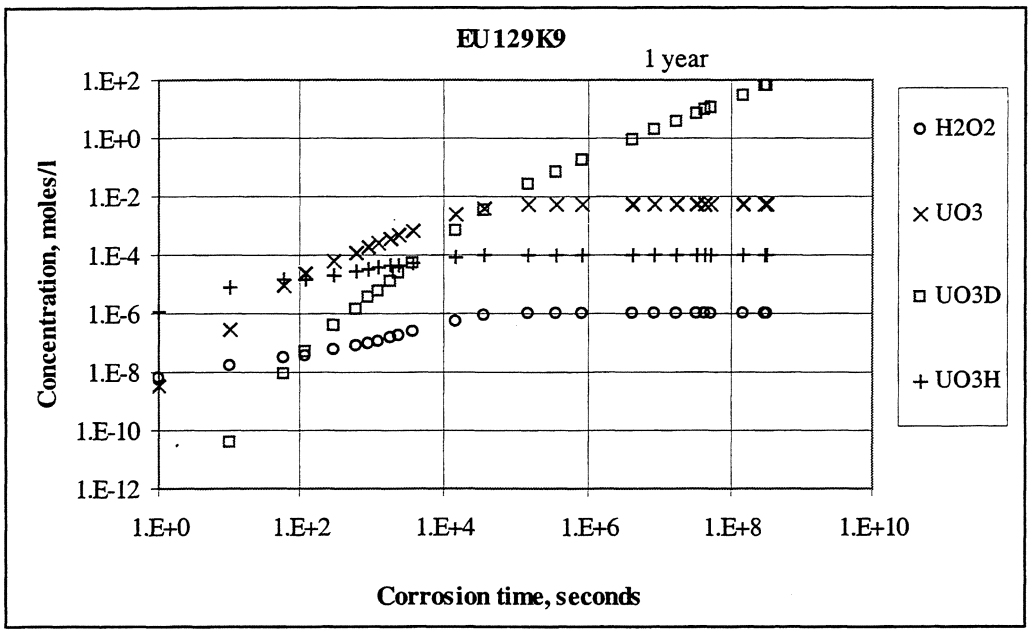

FIGURE 1 Radiolysis in phase 3 (surface layer with β,γ radiation). 5 m NaCl solution.

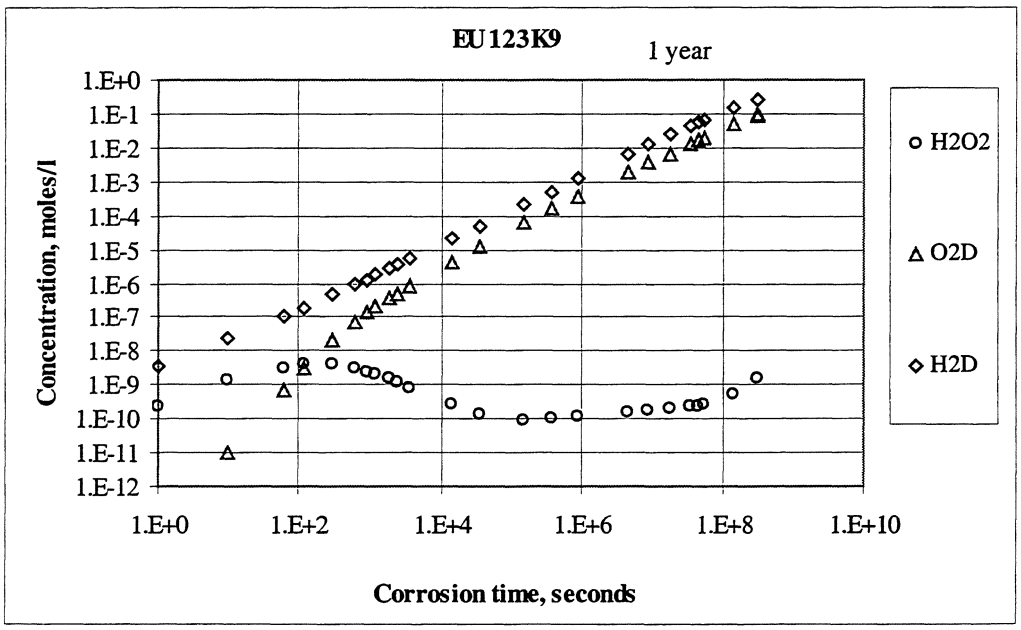

FIGURE 2 Radiolysis in phase 3 (surface layer with β,γ radiation). 5 m NaCl solution.